From Mock-ups to Artworks: Development and Application of Specific Analytical Methodologies

Clarimma Sessa

From Mock-ups to Artworks: Development and Application of Specific Analytical Methodologies

Clarimma Sessa

Programa de Doctorat:

Química Analítica del Medi Ambient i la Pol·lució

From Mock-ups to Artworks: Development and Application of Specific Analytical Methodologies

Memòria presentada per na

Clarimma Sessa

Per tal d'optar al títol de Doctora per la Universitat de Barcelona

Sra. Clarimma Sessa

Barcelona, 18 de setembre de 2014

El Dr. **Jose Francisco García**, professor titular del Departament de Química Analítica de la Universitat de Barcelona

FA CONSTAR:

que el present treball d'investigació ha estat realitzat per la Sra. Clarimma Sessa al Departament de Química Analítica de la Universitat de Barcelona sota la seva direcció.

Dr. Jose Francisco García

Barcelona, 18 de setembre de 2014

Table of contents

Acronyms

APB	Adhesive plastic bag
BSE	Backscattered electrons
FTIR	Fourier transform infrared spectroscopy
FT-Raman	Fourier transform Raman spectroscopy
ICP-MS	Inductively coupled plasma mass spectrometry
ICP-OES	Inductively coupled plasma optical emission spectroscopy
IRR	Infrared-reflectography
MA-rFTIR	Macroscopic Fourier transform infrared in reflection mode
mid-IR FORS	Mid infrared fibre optic reflectance spectroscopy
NIR	Near-infrared spectroscopy
p.s.	Particle size
PCA	Principal component analysis
PLS-DA	Partial least square – discriminant analysis
SE	Secondary electrons
SEM-EDS	Scanning electron microscopy coupled with energy dispersive X-ray spectroscopy
SMIRR	Scanning multispectral IR reflectography
SNV	Standard normal variate algorithm
WDS	Wavelength dispersive spectroscopy
XRA	X-ray micro-analysis
XRF	X-ray fluorescence
XRR	X-ray radiography

Objectives

The main scope of this doctoral project was the evaluation of micro- and non-destructive techniques applied to artwork characterization. The need to study capabilities and limitations of these techniques arises from their increased use in the field of Cultural Heritage, without sufficient previous evaluation.

The investigation path was planned aiming at the development of specific analytical methods. The methods were tested using mock-ups of known composition, followed by their application to real artworks. Oil paintings, photographs and a large metal alloy object were investigated as representatives of three important artwork categories.

The specific objectives were:

i. Determination of the detection limit and reproducibility of techniques such as scanning electron microscopy (SEM) coupled with energy-dispersive X-ray spectroscopy (EDS) probe and Fourier-transform infrared spectroscopy in transmission mode (micro-FTIR) and with remote set-up (midIR-FORS). Special attention was paid to the capacities of the latter technique as its non-destructive qualifies for the examination of unique artworks. The value of multivariate methods for midIR-FORS spectra modelling and interpretation was also in the focus of investigation.

ii. Study of the composition and structure of six portraits of the early years of the Pablo Picasso's artistic production using non-destructive techniques.

iii. Investigation of the degradation process of silver photographs based on the determination of the sulphur content by means of X-ray fluorescence (XRF).

iv. Determination of the composition of the metal alloys used to cast the different parts of the San Lorenzo Pulpit and to establish their historical relationship according to their composition. In order to be able to find this relationship, it was necessary to evaluate the contribution of the different sources of dispersion in the measurement of the concentration of the elements contained in the samples and, thus, define an optimal procedure for the determination of the concentration of major and minor components of the metal alloy.

Chapter 1

A vision of Artworks through their materials

The application of the micro and non-destructive techniques to the investigation of Cultural Heritage

Context

This introductory chapter is intended to provide a quick overview of the material properties aspect of the artwork types investigated in the present thesis. Special attention is paid to those physical-chemical features that have an influence on the analytical process as well as on the obtainable information. The presented topics are wide and complex fields, so that the effort has been invested to summarize and discuss only those aspects that are useful to better understand the results and the discussion presented in the next chapters. First, an explanation of the structure and possible material types encountered in each artwork is presented and, then, a brief outline is given of the analytical techniques and the multivariate method employed to manage the obtained data. The advantages and limitation of both non- and micro-destructive techniques when applied to artwork characterization will be discussed based on the available literature.

1.1 Artworks structure

1.1.1 Oil paintings: structure and materials

The main type of artwork investigated in chapter 2 and 3 will be the oil painting. According to Giorgio Vasari (1511-1574) in his *Lives of the Artists* (*Le vite dei più eccelenti pittori, scultori e architetti*, Firenze, 1550), the technique of oil painting, as used untill today with few technical modifications, was invented in Europe around 1410 by Jan van Eyck (1390 - 1441)[1]. The most importat achievement was the development of a stable siccative oil (mainly linseed oil) as the binder of mineral pigments[2].

A painting should be considered as a complex laminated structure (Figure 1). The support, its ground, and its layers of colour are overlapped in accordance with the physical and chemical rules that determine its stability[3]. The most common *support* is a canvas (linen, cotton or other textiles) stretched and fixed on a *framework*, a rigid structure typically made of wood. On the canvas a layer named *preparation* can be applied, commonly based on animal glue and gypsum, although more/the most modern commercial preparations show a rather variable composition. This layer has the purpose to make the surface suitable to paint application and to reduce the volumetric variation of the support, which can be caused by temperature and humidity fluctuations, or mechanical stress. An additional layer named "*imprimitura"/ground* may be also applied. It means a fine and small grain size material, in some cases pigmented, used with the aim to give more intensity to the superficial colours. The paint layer is a plastic film with a thickness of approximately a micron/few microns, where pigment or dye, organic or inorganic, natural or synthetic, are mixed with a binder. Finally, a coating/varnish (natural or synthetic resins) may be applied on the surface to protect or finish the aesthetical appearance of the surface.

The binder is defined as a liquid or semi-liquid substance that provides cohesion, keeps the pigment within the coating, protects them from deterioration, and ensures the adhesion on the substrate. The type of binder commonly serves to classify the artistic technique, for example, proteinaceous binders are distinctive of tempera and the lipid-based binder is characteristic of oil paintings. The oil used is commonly linseed, poppy, nut oil[4], etc, although linseed oil is the most common one due to its siccative properties.

Instead, pigments are coloured compounds, which are not soluble in the vehicle/binder and are mostly inorganic, although they can also have organic origin, e.g. some types of copper phtalocyanine[5] or madder lake. This definition permits to distinguish pigments from

dyes/colorants that are water-soluble and mostly organic.[5,6] In order to make these organic compounds insoluble in the media, they usually are precipitated onto an alumina substrate.

Another term that will be employed in the following is filler. It is an inert, usually white or slightly coloured substance, insoluble in the medium. The difference between filler and pigment lies in the purpose for which it is used. A filler is not a colorant but it is used to increase the volume/bulk as well as to modify the optical or technical properties of the material[7]. Fillers commonly found are sulphates, quartz, clays, carbonates, etc.

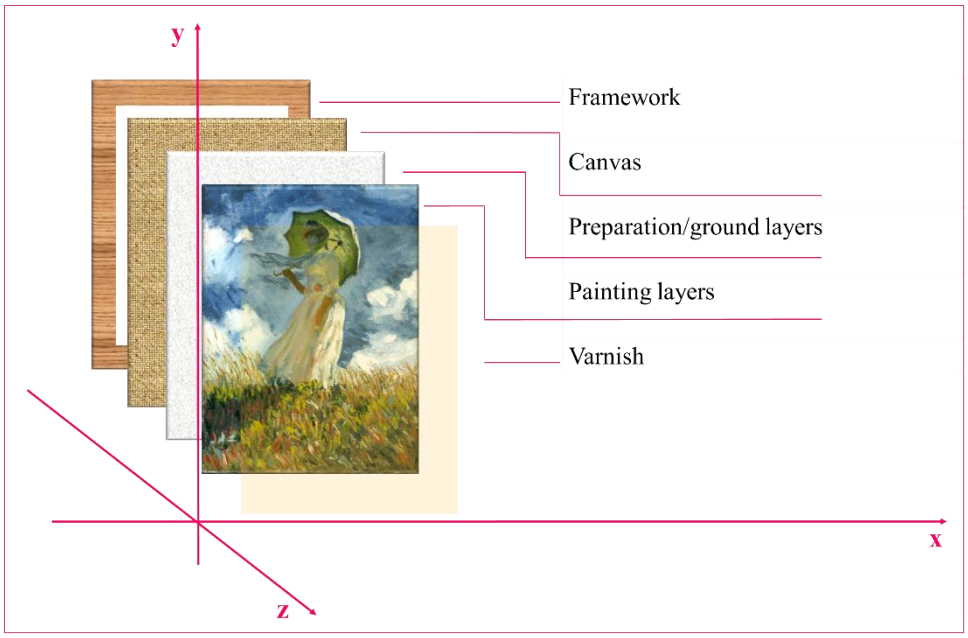

Figure 1. Structure of an oil painting on canvas. The subject of the painting is the "Essai de figure en plein-air: Femme à l'ombrelle tournée vers la gaucheen", C. Monet 1886, Musée d'Orsay, Paris. Reproduction made by the artist Alfonso Rodriguez.

Paint layer and material distribution

The paint layers present, although they are very thin, a high heterogeneity. This is easily understood if the different steps of the creation process of an oil paint are considered. Figure 2 demonstrates some of the phases documented by the artist A. Rodriguez when he painted the reproduction presented above in Figure 1. When the preparation layer is completely dry, the canvas is ready for the application of the paint. In some cases, a sketch is drawn as guide for the representation (Figure 2 – layer 1). The manual procedure to prepare the oil paints includes the amalgamation of each pigment and the oil until they create a viscous paste. Furthermore, different colours could be blended to obtain a broad scale of shades and hues (Figure 2 – oil preparation). The paint is applied on the substrate, generally by brush or palette knife, superposing different layer one over the other and/or covering the surface with different paint colours, which in some cases partially overlap. As consequence of this

process, the distribution of the material across surface (x/y dimension) and in depth (z dimension) (Figure 2 – cross-section) is complex and influenced by many factors. Thus, from an analytical point of view, the paint layers are the most complex part of a painting to be characterized.

As matter of fact, the paint layers may present two levels of heterogeneity: macro and micro level:

Micro level or short distance (in depth and across surface) describes when apparently monochromatic areas are composed of different superposed layers or one layer created by mixing together two or more compounds[8].

Macro level or large distance (across the surface) denotes when areas that appear similar to simple visual inspection reveal the use of two or more compounds[9].

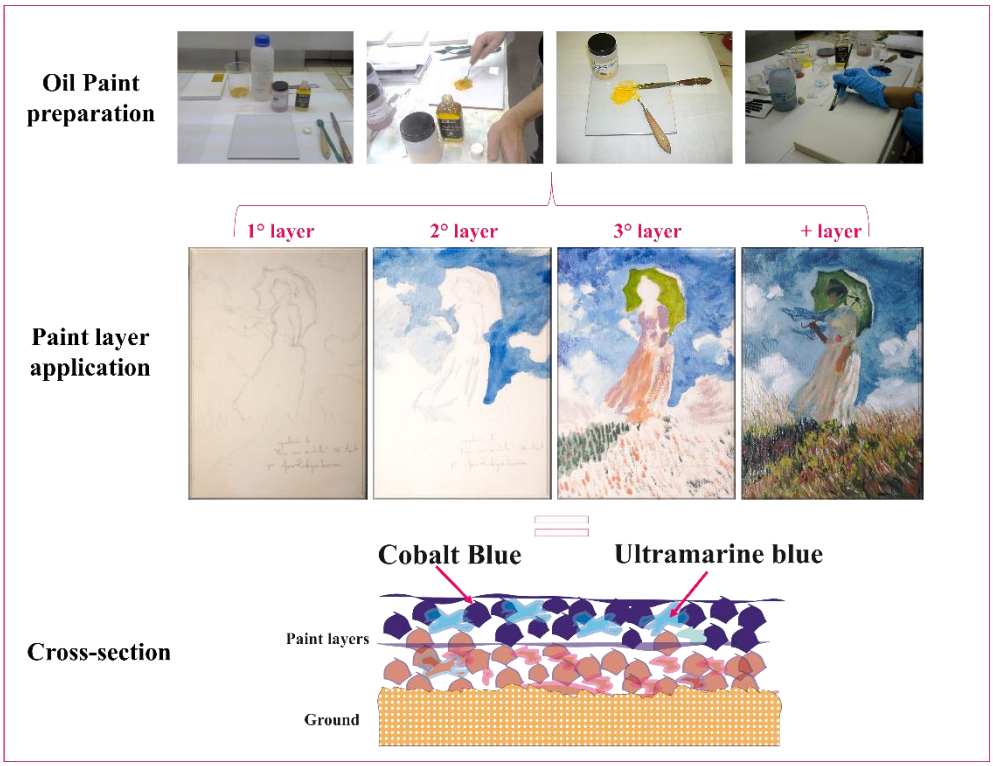

Figure 2. Oil paint creation process from the oil paint preparation to the painting.

Pigments

Among the components of paint layers, the used pigments, their composition, and their distribution are extremely important for artwork investigation purposes. In fact, their chemical nature and their physical distribution establish the rules of the conservation/restoration treatments that can be performed. Most of them may be used as dating-marker, due to their progressive introduction into the colour market and/or artistic

field. Natural pigments have been known since prehistoric time, but, starting from the fortuitous synthesis of Prussian blue in 1704, the discovery and production of new pigments has dramatically increased[10,11].

Furthermore, the mapping of these compounds permits the investigation of the studio practice of a specific artist as well as the identification of non-original materials in order to reveal retouches or forgeries[12]. The following part gives a brief introduction to the fundamental properties of this type of pigment when dispersed in a medium

Fundamental properties

Pigments are crystalline substances that have a definite internal structure in which the atoms occur in specific proportions and are arranged in an ordered geometric pattern. All crystalline materials present one of the seven crystallographic system distinguished by the symmetry of the crystalline form (Cubic, Tetragonal, Rhombic, Hexagonal, Monoclinic, etc.). The unit cell is the smallest three dimensional block, which is defined by the length of the axes (a, b, c) and the angles between them (α, β, γ)[13]. The crystalline structure is characteristic of every pigment and determine its physical and chemical properties.

Particle size

A particle is the individual unit that can have any shape or structure. The particle size can be classified as *very fine* (<0.3 μm), *fine* (1.0-0.3 μm), *medium* (3-1 μm), *large* (10-3 μm), *coarse* (10-3 μm), *very coarse* (< 40 μm). Although, in some cases classification is not as strict. In natural pigments for example, such as ochre and natural earth, particle size and their distribution is not uniform[13]. Furthermore, different particles can be joined together to form aggregates, agglomerates or flocculates. The last case is referred to agglomerate that are in suspension in the pigment-binder system[7]. Shape and morphology of the particles are used as diagnostic parameters for pigment identification by using optical microscopy.

The density of a powdered or granulated material is the mass per volume (1 g/cm^3). For modern industrial pigments, normally the *apparent density* and *tamped volume* are measured. Further information is available in the ISO 787, which specifies a general method for determining those parameters after tamping of a sample of pigment or extender. The density is important because it may influence the distribution in the binder of one or more pigments determining a layer's internal structure.

The particle size and shape influence the hiding power, tinting strength and colour of the paint. All these terms will be further explained below. The small, uniform particle size of modern pigments results in higher tinting strength and pure colour. In contrast, the larger

size and heterogeneous shapes of the traditional pigments'particles offers the artist a greater variety of shades. They are typically more transparent, allowing more light to pass through the layers of paint and be reflected from the ground, thereby increasing its apparent luminosity (Figure 2). For example, the crystalline hematite of about one micron size has a characteristic violet tint differing from the bright red colour of hematite with sub-micron particles[14].

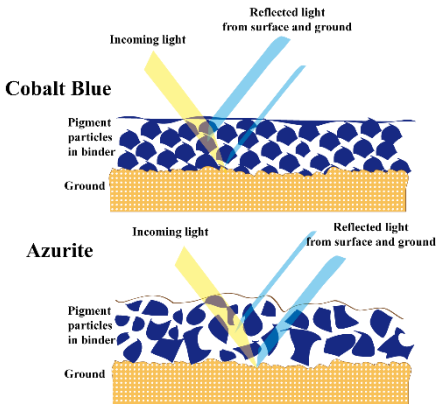

Figure 3. Influence of the particle size on hiding power and tinting strength.

Binder-pigment interaction

Particularly interesting is the interaction of the pigment with the binder, compatibility and effect on binder drying. These effects have to be considered when a pigment is applied in oil or other mediums. Thus, appropriate pigments for each binder are historically defined as mentioned in several handbooks about painting techniques[3]. The interaction between an oil and the pigment implies complex processes further explained elsewhere[4,15–19]. Nevertheless, it is interesting to mention that pigments have a fundamental role on the velocity of the oil paint film drying process. It is also important to highlight that each pigment has an oil absorption capacity that is defined as the volume of oil required to form a coherent and putty-like mass with 100 g pigment under specified condition[7].

Stability properties

Other important properties of pigments are the stability properties, i.e. resistance toward light, weather, heat, chemicals and retention of gloss. These are properties that have great importance for the conservation status assessment of a chromatic layer and may determine the resistance of the artefact along time. The appropriate atmosphere conditions have to be considered in order to prevent conservation issues[20].

Optical properties

The colour is the fundamental property of an artistic pigment and arises from the transmission or absorption of light. Photons that strikes a pigmented film can be directly reflected without entering or can be absorbed, refracted, reflected and scattered before reaching again the surface and leaving the material as reflection beam[21]. These phenomena are controlled by the crystal structure and chemical composition of the material[13]. The following part provides a brief review of the principal effects that may occur when light interacts with a paint layer.

Refraction

Refraction is defined as the change of the direction of the path of photons when they pass from one medium into another. The propagation of the beam through a transparent medium is described by the refractive index n, which is defined as the ratio of the velocity of light in free space c to the velocity of light in the medium v according to:

$$n = \frac{c}{v}, \tag{1}$$

According to Snell's law, when light travelling through a medium of refractive index n_1 encounters and enters a medium of refractive index n_2, then the light beam is bent through an angle given by the following equation:

$$\frac{\sin i}{\sin r} = \frac{n_1}{n_2}, \tag{2}$$

where, i is the angle of incidence and r is the angle of refraction. The refraction angle depends on the wavelength[22]. In a painting layer, the refractive angle increases as the difference between n of binder and n of pigment increases. A large refractive angle determines a high hiding power of the paint film. Pigments with high n have a high hiding power, while a binder with a high n makes the painting layer transparent.

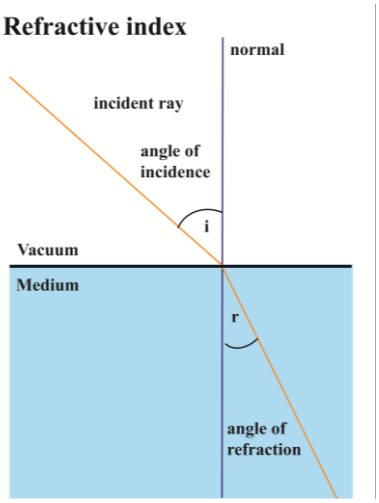

Figure 4. Refractive index scheme. ®Encyclopaedia Britannica.

Reflection

The external reflection of the beam due to the interaction with a smooth and shiny plane, which reflects the light at an angle equal to the angle of incidence, can be named surface or specular reflection[23]. Reflection and transmission of electromagnetic waves at an interface depend on both the absorption index (k) and refractive index (n) (Figure 4) and follow the Fresnel equation[21]:

$$R_s = \frac{(n-1)^2+k^2}{(n+1)^2+k^2} \quad (3)$$

When pigments are of very small particle size and have about the same refractive index as the binder in which they are dispersed, the photon are not deflected from their path and the layer appears transparent.

Absorption

When the photons of a light beam interact with atoms or molecules, the radiation can be partially absorbed. There is a number of mechanisms such as atomic vibration and rotation, molecular orbital and charge transfer that cause absorption of light at a determined wavelengths. Absorption is ruled by the combined Lambert-Beer law, which is expressed as:

$$A = \log\frac{I_0}{I} = \varepsilon c l \ , \quad (4)$$

where the proportionality constant ε is the absorptivity of the material, c the concentration and l the thickness. The absorption is the responsible of the pigments colour.

Scattering

Light that enters the paint layer is typically scattered several times before it either exits layer or is absorbed. This reflection of scattered photons in a volume is called *bulk reflection*. As aforementioned, pigments are not dissolved in the system. They exist as a suspension/dispersion as tiny suspended particles that have the ability to scatter as well as absorb light. The amount of scattering is a function of the difference in the refractive index of the pigment and the suspending medium, of the particle size and the wavelength of the incident light[24]. The theory that explains the phenomenon of scattering is the Kubelka-Munk theory[25]. It is based on the fact that the optical properties of a film, which absorbs and scatters light, may be described by two constants: the absorption coefficient *K* and the scattering coefficient *S*. Each beam is attenuated by absorption and scatter losses, but is also reinforced

by the scattering losses of the respective opposite beam[7]. For an "infinitely thick" layer, the Kubelka-Munk equation may be written as:

$$f(R_\infty) = \frac{(1-R_\infty)^2}{2R_\infty} = \frac{K}{S} = \frac{2.303ac}{S} \quad (5)$$

where R_∞, is the absolute reflectance of the layer; S is the scattering coefficient; K is the molar absorption coefficient[26];a is the absorptivity; and c the analyte concentration[25]. The amount and the angular distribution of scattered light depend on the particle size, refractive index, and concentration of the pigment. The absorption coefficient K obeys Beer's law, even at high pigment volume concentrations and it is proportional to it. When the concentration increases, the distance between the pigment particles decreases, , which leads to a higher probability for an interaction and the single particles may diminish the scattered light power[13]. Thus, the relation between S and concentration c is linear only at low concentrations and remain below the linear value at high concentration. When the scattering is due to the interaction of light with a rough surface, the phenomenon is named *diffuse reflection*[21,25,27].

All the aforementioned phenomena influence the hiding power and transparency, tinting strength or lightening power of the pigment and the medium. The *hiding power* is defined as the thickness of an applied paint film on a contrasting surface at which it disappeared, while the transparency of a pigmented system denotes its low ability to scatter light. The *tinting strength* is a measure of a colorant to confer colour to a light scattering material by virtue of its absorption. It is related not only to particle size and structure but also to some extent to particle size distribution[7]. The same property of a white pigment can be defined lightening power, in terms of its ability to increase the reflectance of an absorbing (black or coloured) medium by meansof its scattering power[7].

Chemical properties

The classical and more practical way to classify pigments is based on their colour, according to most of the sources consulted[7,13,28,29]. A brief overview on the pigments that will be mentioned in the following chapters is presented below.

White pigments/Fillers

Nonselective light scattering causes the optical effect. In this case scattering is higher than absorption[7,24].

Lead white. This name is normally used to identify two different pigments and two related minerals. The first is lead carbonate (neutral lead carbonate - $PbCO_3$, fine particle size (p.s.)),

which is the synthetic analogue of the mineral cerussite (fine to coarse p.s., n=1.94-2.09), and the second is lead carbonate hydroxide (basic lead carbonate - $PbCO_3.Pb(OH)_2$, fine to medium p.s.), which is the synthetic analogue of the mineral cerussite (fine to coarse p.s., n=1.94-2.09), and the second is the lead carbonate hydroxide (basic lead carbonate - $PbCO_3.Pb(OH)_2$, fine to medium p.s.) that is the synthetic analogue of Hydrocerussite[30]. The lead carbonate hydroxide has been produced since antiquity, although it normally is found mixed with the neutral lead carbonate because the manufacturing conditions in some cases were difficult to control. In fact, overheating may cause a high proportion of the neutral form or other lead oxides.

Zinc white. The principal compound produced with the name of white zinc is the Zn (II) oxide (ZnO, particles fine or very fine, n=1.95-2.1). It has been known since ancient times as residue of the brass production that includes the smelting of copper and zinc carbonate. It was first promoted as water colour by Winsor and Newton in 1830, but was not popular for oil painting due to its limited drying capacity and the low hiding power. After 1840, when the French or indirect industrial process for zinc oxide production was optimized, its usability in oil paint was improved because it was sold mixed with a pre-polymerized siccative oil. It has been described as very common in painting after 1850. It is also documented that it was normally mixed with lead white and/or barite/barium sulphate or as a lightening agent in coloured pigments by the manufacturers[30].

Zinc white, lead white and titanium white were the main white pigment commercially available in the mid- to late twentieth century[30]. Although zinc white is stable to light several studies have demonstrate that it tends to saponify the fatty acid components of siccative oils[31], This process is facilitated by very fine particles[32,33].

Titanium white. The main compound designed with this name is the synthetic titanium (IV) oxide pigments (TiO_2 – moderate to coarse p.s, n=2.55-2.73). It was not produced until 1921 when American and Norwegian companies began to develop its production for painting. It presents excellent hiding power and twice the opacity of pure lead white. In its natural form cassiterite can be found with minerals including quartz, wolframite, tourmaline, topaz, fluorite and micas[13].

Barium sulphate. Synthetic barium sulphate ($BaSO_4$) has been used since the earlier nineteenth century as white pigment[34–36], but mostly as an extender[37–39]. The natural analogue mineral is baryte.

Calcium carbonate. The mineral form of calcium carbonate is calcite ($CaCO_3$). Different origins and forms are documented, such as chalk, coral, eggshell and oyster shell[13]. It was used as a white pigment as well as extender and its use is widely cited in literature. It is available in nature as secretion of many marine invertebrates (natural precipitation) and it has been produced without interruption during modern times. Calcium carbonate presents mainly the crystal structure of the mineral calcite (trigonal, n=1.48-1.66, from fine to medium p.s.).

Kaolin. In some cases used as synonym for the mineral form kaolinite, it presents as common composition $Al_4[Si_4O_{10}](OH)_8$ derived from weathering of feldspars (n=1.53-1.57, polycrystalline particles in plates and lamellar aggregate)[30]. It is normally associated to natural ochre pigments[21].

Quartz. It is a silicon dioxide mineral (SiO_2, n= 1.54-1.55, variable p.s.), and generally serves as filler or substrate for dyes, because it is very stable. It is a white substance, although it can appear with a variety of colours depending of the impurities contained.

Alumina. It is the name commonly attributed to aluminium oxide Al_2O_3.

Black pigments

In the case of black pigments, the absorption is much higher than the scattering.

Carbon based black pigments include any pigment that contain elemental carbon. Carbon black is a generic term, often being used as a synonym for lamp black, compound based on sooting flame. However, with the same term it can be referred to vegetable black or black earths (carbonaceous clay)[40].

The **Bone black** is a mixture of organic and inorganic compounds. It has been demonstrated that the inorganic phase is based on mineral hydroxyapatite, which includes calcium phosphate, calcium carbonate, calcium fluoride and calcium hydroxide; while the organic part, when it remains, is composed mostly by collagen and a small amount of lipid. It may also include other C-based compounds. This inorganic component is predominantly crystalline, though may be present in amorphous forms[41]. The variety produced by burn ivory is named ivory black. This type of coke black is documented since ancient time. They are very stable in acid and alkaline medium and have high hiding power.

Fe based black pigments (see also natural red earths). The literature uses the name Mars pigments or black oxide. These terms are used as synonym for synthetic iron oxide

pigments[3]. The natural mineral magnetite (Fe_3O_4) shows poor tinting strength and it was considered not of interest by the pigment industry[7].

An unambiguous identification of black pigments used in art and archaeology remains a challenge owing to the variety of sources and manufacturing processes used in their preparation[42]. However, *Vila et al.* proposed a method to differentiate between originals and non-original artistic prints based on the characterization of contemporary black printing inks using infrared spectroscopy[43].

Coloured pigments

For coloured pigment the absorption of the light is selective and dependent on the wavelength[24].

Blue pigments

Prussian blue is considered the first modern synthetic pigment. It was synthetized in 1704. Afterwards, its production as artists' pigment became extremely widespread. Even few years after its discovery it was used in a painting by Watteau (Gilles, 1718-1719 - Paris, Musée du Louvre, Comediens italiens, 1719-20 – Washington, National Gallery of Art) [10,11]. Its common formula is $KFe[FeCN_6]$ and $Fe[FeCN_6]_3$, although the modern formulation is better described as $M^I Fe^{III} Fe^{II}(CN)_{6\,n} H_2O$, where M^I is a ion such as potassium (K^+), ammonium (NH_4^-) or sodium (Na^+). It has a refractive index n of 1.56 and presents very fine particles although it forms a very variable aggregates from fine to coarse. Pure Prussian blue is extremely light fast while it strongly fades when mixed with a white pigment, especially with lead white or zinc oxide[44].

Ultramarine blue ($Na_{6-10}Al_6Si_6O_{24}S_{2-4}$, n=1.5-1.54) was first synthetized in 1824[45]. Since then, it was used as substitute for its expensive natural homologue "*lapis lazuli*". The natural form was produced grinding the mineral Lazurite, employed since ancient time. The chemical composition of both substances is similar, although the natural form presents more impurities and bigger and more irregular particles. It has a good hiding power and can be used in several kinds of media due to its stability. The natural pigment was first imported to Europe through the port of Venice from the ancient quarries of Badakhshan (now Afghanistan)[46]. Lately, studies by *Miliani* and *Smith et al.* have demonstrated that it is possible to distinguish the natural form by infrared spectroscopy detecting the entrapment of carbon dioxide in its crystalline structure[47,48]. One of the most important pigments of the history, lapis lazuli was the principal blue pigment used by Michelangelo in the famous sky

of the "The Last Judgment" fresco, deeply studied by *Ballirano et al.*[49], which tried to determine the possible provenance of the original materials.

Cobalt blue is a mixture of oxide of cobalt and aluminium ($CoO.Al_2O_3$, n=1.69-1.70, from large to very coarse p.s.). Its tinting strength is not particularly high, although it was often employ because of its stability. In literature is often named Thenard's blue in honour of Louis Jacques Thénard, one of the first scientist to publish his experiments with cobalt and alumina between 1803 and 1804, after which the substance was used as an artists' pigment. However, the use of cobalt compounds in ceramics and glass making goes back to the ancient time. It was a very common pigment in nineteenth-century painting and nowadays it is still in use. An extensive study has been performed by *Bacci et al.* for the non-destructive identification of cobalt based pigment by fibre optics reflectance spectroscopy (FORS)[50]. The variety named **Cobalt blue dark** produced by ® Kremer Pigmente GmbH & Co. is composed by a silicate matrix($(Co,Zn)_2SiO_4$). On the other hand, the so-called **Cerulean blue** is a cobalt tin oxide (Co-Sn-oxide). Its origin is not clear but some sources mention that it has been synthetized since 1805, but its production was improved only in 1860[51]. A study published by *Mahon and Centeno* has demonstrated its use in a painting by John Singer Sargent, dated 1883-84[52].

Copper phtalocyanine blue. The first CuPc pigment ($C_{32}H_{16}CuN_8$, n<1.66, very fine p.s.) was patented in 1928, by the Scottish Prof. Patrick Linstead and his co-workers, who elucidated the structure of this new class of compounds in 1933-34. The archives of artists' colours makers, such as product catalogues and colour charts, are the earliest sources proving the use of CuPc blue in artists' colours[30]. In England, the artistic material supplier Winsor & Newton first proposed an oil colour based on phthalo blue in 1937, under the name Winsor Blue. It has been used extensively by 20th century artists, including R. Lichtenstein, P. Delvaux, W. Kandinsky, Y. Klein, S. Francis, E. Kelly and B.Newman and Picasso[53,54]. In a recent study, *Defeyt and Strivay* have reviewed the the CuPc pigment possibly found in contemporary art, focusing on the suggestion of conservation treatments for these compounds. They are high performance pigments, with remarkable light- fastness and are insoluble in most of solvents, except, in aromatic solvents[55]. They have a low hiding power and are normally admixed with other pigments[56].

Yellow pigments

Yellow ochre is a naturally available earth pigments forming either as the direct weathering of iron-rich ore deposits or as soils. The principal colouring matter is the iron hydroxide

goethite ($\alpha - FeOOH$) although it can be associated with other minerals such a less common yellow iron oxide lepidocrite ($\gamma - FeOOH$), clay, feldspars and carbonate depending on the geological sources. The various shades are determined by several factors: the average size of crystallites and the corresponding dispersion; their proportion with respect to the presence of other chemical components such as aluminosilicate materials (kaolinite, quartz, manganese oxide, etc.) and other minor components (calcite, gypsum, etc.)[14,57].They can be burnt to produce brown, red and violet shades due to the oxidation to iron (III). It is a very stable class of pigments and was one of the earliest to be used and has been identified often in roman mural paintings[58,59]. Very important sources of this mineral were located in France. Thus, in some cases it is named French yellow ochre. *Hradil et al.* has published a very extensive review focus on crystallographic characterization of ochre and other natural and synthetic earth pigment[14]. Furthermore, *Balakhnina et al.* have deeply studied the influence of the yellow ochre in the drying process of linseed oil by means of the infrared spectral changes[60].

Strontium chromate ($SrCrO_4$) it is also known as strontium yellow and ultramarine yellow. It is commonly named lemon yellow. It has been used by many artists, such as Matisse and Bonnard[61].

Cadmium yellow (n~2.53-2.51, very fine p.s.) is part of the cadmium sulphide and selenides group. The compounds, part of this class, show shades ranging from yellow to red. The generic composition is based on cadmium, sulphur and selenium ($Cd(S,Se)$) giving a range of yellow through orange to red pigment. In some cases zinc or mercury ($(Cd,Hg)S$ or $(Cd,Zn)S$) may be introduced in the formulation to obtain a varieties of orange and brown shades. Synthetic yellow cadmium was commercially available only in the 1840s and it was extensively used in oil and watercolour, although the first compounds presented some problem of stability when exposed to light and humidity[30,62]. An example of photo-induced degradation of Cd-based pigments has been demonstrated to be the cause of the discolouring, fading and darkening on a painting by Henry Matisse[63]. These pigments were rapidly adopted by the Impressionists and are commonly used by contemporary artists[64]. *Cesaratto et al.* recently published a method for their characterization based on their time-resolved luminescence properties[65].

Chrome yellow ($PbCrO_4$). When chrome yellow was first introduced as a pigment in the early part of the nineteenth century, it provided a bright, opaque yellow on the artists' palette. However, its original form was photo-sensitive and tends to darkened. *Monico et al.* published an extensive study focused on the degradation process of lead chromate in

paintings by Vincent van Gogh using spectroscopic techniques[66]. In the handbook *Handbuch der Ölmalerei* in 1910 Bouvier declared that it was often admixed with Prussian blue (Berliner blue) to create green shades[67]. This pigment mixture is commonly call chrome green. The same mixture is still used to produce chromium green at industrial scale[7].

Green pigments

Cu arsenite (n=1.55-1.749, amorphous) includes a large variety of compounds although and it is generally associated with Scheele's green. This pigment has been considered as mixture of different compounds but is mostly reported by the formula $Cu(AsO_2)_2$. It was synthesised by the Swedish chemist C.W. Scheele in 1775. The detection of Scheele's green on a miniature believed to be medieval, together with other synthetic pigment, allowed *Burgio et al.* to establish that they were forgeries painted around the end of the nineteenth and the beginning of the twentieth century[68].

Chrome oxide (Cr_2O_3, mean n= 2.5, very fine up to fine p.s.) is an opaque gloomy green pigment. It is not common because it is expensive compared with the others green greens, terms employed to define mixtures of yellow and blue colours. The first evidence of its use has been found in a painting by Turned dated 1810[69]. A study of *Nel et al.* has stressed the difficulties in the detection of the pigment by XRD because often it is mixed with amorphous extenders matrices[70].

Malachite (n=1.65-1.91) is a basic copper carbonate mineral ($Cu_2CO_3(OH)_2$, n=1.65-1.9). It is a secondary mineral formed in oxidised areas of copper ore deposit and is commonly associated with the less abundant azurite. When grinded to a fine particle size it becomes transparent, which is why it is generally used as pigment in very coarse size[13]. It was used since antiquity.

Green earths (see also red natural earths) are natural green pigments based on the mixture of the clay minerals glauconite and celadonite.

Red pigments

Natural red earths (see also Yellow ochre). They are classified by *Eastaugh et al.* based on the increasing of the manganese content in Ochres (Mn<5%), Siennas (Mn>5%) and Umbers (Mn 5-20%)[30]. Used since ancient time, their continually increasing importance is based on their non-toxicity, chemical stability and the wide variety of colours ranging from yellow, orange, red, brown to black. The difference between natural and synthetic earths is well defined by their crystalline structure[7]. Natural reds are of different provenance (e.g. Persian

Red, Spanish Red), but their colour is always given by the presence of hematite (α-Fe_2O_3 above 90%)[14]. Hematite, Iron Oxide, English Red and Venetian Red are terms that will be found in the present thesis as synonyms for red ochre. The terminology defining naturally occurring and synthetic red iron (III) oxide pigments is extremely confusing with many terms being indiscriminately applied to both varieties, or transferred to a synthetic variety when naturally occurring varieties were exhausted. Venetian red, for example, was reputed to have originally used to describe a naturally occurring source (now exhausted) of red ochre from Venice (or Verona) and was subsequently applied to the synthetic pigment because the colour was reproduced. English red was historically one of the numerous terms used to describe red ochre[30]. Nowadays, for example, Kremer Pigmente GmbH & Co proposes in its catalogue a large variety of Fe-based pigments with different names and some changes in their composition depending on the shades.

Red lead or lead oxide ($2PbO.PbO_2$ or Pb_3O_4)[71] is the synthetic analogue of the mineral minium. Red lead may be formed when litharge (PbO) is heated to temperatures over 316° C (600° F). It generally contains some litharge (from 2% to 15%) and reacts quite readily with drying oils. Red lead pigmented oils must be used quickly or they will dry. Films formed from red lead and oil become brittle. A large review on the mechanism of interaction between lead oxides or other Pb-based compounds and linseed oil has been published by *Tumosa and Mecklenburg*[19].

Vermilion is the synthetic analogue of the natural mineral cinnabar ($\alpha - HgS$). Its use goes back to the Greeks. Since then it was described as photo-sensitive. Several studies stressed the problem of darkening of this pigment on different kinds of artworks and the mechanism of degradation is still under investigation[72]. As occur for its yellow analogue, specifics study have been dedicated to cases of degradation on manuscripts as well as in wallpaintings[73,74].

Cadmium red (see also Cd yellow). This pigment was first commercialized in 1910, although it had been mentioned in a patent granted already in 1892[30]. The composition can be a cadmium sulphide selenide (CdS_xCdSe), pure cadmium selenide ($CdSe$) or cadmium mercury sulphides (CdS_xHgS).

1.1.2 Salt print photographs: Conservation issues

The field and history of photographs is broad and complex. In this section, a brief excursus will be presented on the origin, structure and stability properties of the specific case of silver salted print images, which is the subject of investigation in chapter 4.

In 1834-35 W.H. *Fox Talbot* (1800-1877) started to experiment and produce the first photographs on paper with silver chloride as sensitizer, fixed before with sodium chloride and finally adopting a sodium thiosulfate (Hypo). He is usually considered the inventor of the salted print images, although other important achievements prior to his work are documented[75]. A very large body of photographic works, writings, exhibitions, and patents make him one of the most important researchers in the history of photographs. He also invented the calotype process, changing his formula to use silver iodide, which was more sensitive than silver chloride and permitted shorter exposure times[76]. This process was then partially modified by *Gustave Le Gray* (1820-1884), who introduced the dry waxed paper (1851)[77]. It was a treatment that involved the use of wax to prepare the paper-support prior to the application of iodide, especially used for French papers as they were sized with starches and were not suitable for the process.[76] *Le Gray* began his career in 1842 and is one of the most noted photographers that were using the salt print process together with *David Octavius Hill* (1802-1870) and *Robert Adamson* (1821-1848). The latter two photographers worked at Edinburgh and produced several calotype and salt print works between 1843-47[78]. The subjects were variable, although the portraits are the most famous. The production of salt print continues, with different variations and discoveries, approximately until the middle of the 1850s.

Process

The method to produce salt prints images described by *Stulik*[75] and *Lavédrine*[79] involves several steps. The first important step is the choice of a suitable ***paper.*** The quality of the paper used as support of the image has great importance[79] on the photographic process as it influences its physiochemical properties, in terms of matrix compounds and surface roughness/smoothness. The photographic paper base must be free of photoactive impurities such as iron and lignin or other metals. In order to obtain grade of purity, the paper was originally made from cotton rags, and then substituted at the beginning of nineteen century by purified wood pulp. These factors influenced the stability and the final esthetical appearance of the work. The paper was normally *"sized"*, which means that it was treated with gelatin or starches to limit the absorption of chemicals used and prevent them from sinking into the paper fiber weft and improve the image quality. Most papers are pre-sized.[80] During the process the paper is soaked in a salt solution - *salting* - generally from sodium chloride and dried. Then, it is brushed with abundant coating of silver nitrate solution and dried in subdued light – *sensitizing*. Afterwards, it is exposed under a negative using an UV source or direct sunlight (print-out process) - *exposure*. Once the image became dark the

excess of silver nitrate is removed by water – *washing*. Then, the image was fixed by a sodium thiosulphate solution – *image fixing* - and immersed for a variable time in water to chemically reduce the light-sensitive salts[80] - developing process. The image forming material can be unprotected or it can be coated with a layer of organic coating or varnish – *coating.*[75,81] A scheme of the process and photograph structure is presented in Figure 5.

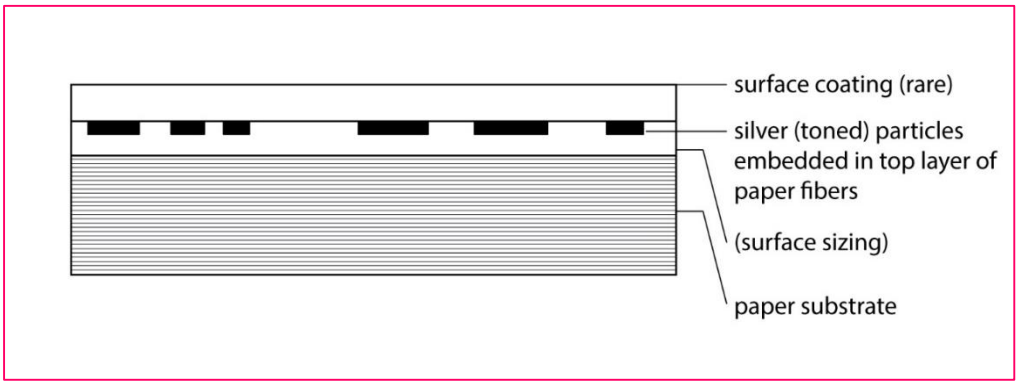

Figure 5. Simplified scheme of a salt print image cross-section[75].

Structure

The resulting images have a characteristic matte appearance, although this aspect often is not enough to recognise the type of photographs with a simple visual examination. On microscopic scale, this kind of image presents the deposition of photochemical reduced silver particles (around 0.5 µm in diameter) on the top or partially retained in the fibre interstices[82]. The grade of heterogeneity of the silver deposition is appreciable even at low magnification (Figure 6). Thus, the silver is the main component of the photograph, although the elemental composition of this type of photographs can be more complex. The simple paper may incorporate several impurities, such as metals for example due to residues or intentionally added during the production process[83]. Other elements could be introduced by contamination, due to the conjunction of pollutant with moisture and heat. All these components may trigger reaction mechanisms during the revelation process or/and degradation phenomena.

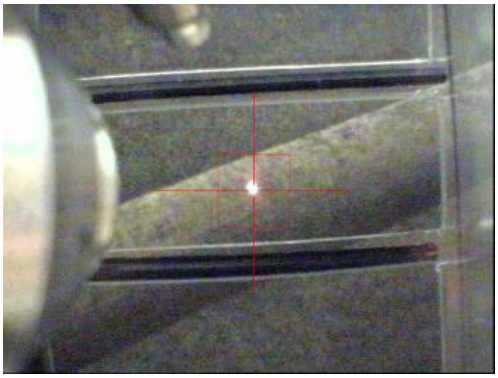

Figure 6. Microphotograph of a salt print image that shows the heterogeneity of silver deposition.

Stability

The main factors that influence the long-term stability of the silver images are water, air pollutants, heat, light, the processing, and particle size. The first four are related to the conservation conditions at which the artwork is stored or/and exhibited to, whereas the latter two depend on the procedure followed by the artist. Therefore, it is extremely important to investigate the physicochemical features of the photographs with the aim to establish specific conservation guidelines[84]. The mechanism of degradation and the possible causes are complex and strictly depending on the history of each artwork. Although, based on the literature available, the most frequently mentioned factors of degradation, manifested as fading and discoloration, are residues of sulphur attributed to the fixing step or/and the contact of the image with the pollutant H_2S in presence of humidity/moisture and heat. This was also the conclusion of the first report written in 1855 after the experiments of the committee organized by the Photographic Society of London to investigate the causes of fading in positive photographic pictures on paper. Several articles have been published between 1855 and 1991 on the topic. They are collected in the publication edited by *Norris and Gutierrez*[85]. Most of the investigators agree that oxidising agents and sulphur sensitization results in the formation of silver sulphide on the surface of the silver halide crystals, but there is no agreement on the exact function of this compound.[82] The oxidation and migration of silver caused by environmental oxidizing atmosphere is also considered, but only for local blemish and discoloration. Due to the complexity of the topic and the general necessity to clear all the variables that may influence this kind of phenomena a the further explication of possible reaction mechanisms and causes of degradation is left to more specialized handbooks.[76,82]

1.1.3 Cast bronze object: structure and composition

The investigation of the metal alloy composition, structure, and technology of an artefact may provide insight into its origin in terms of provenance, historic context, and authenticity, as well as contribute to the assessment of the conservation state. As metals played a significant role in society throughout the ages, the humans strongly experimented by alloying or mixing them with other elements with the aim to improve the properties of the materials, depending on their use and the available technology[86,87]. For example, through metallurgical procedures, melting points can be lowered, leading to final products of enhanced hardness; other characteristics, such as strength, workability and resistance to corrosion can be similarly improved[88].

In the periodic table, 87 elements are classified as metals, most of which are naturally available in its metallic form, either pure or as an alloy. From this point, the terms *alloy* and *alloying* will be used as a deliberate mixture of one or more metals.

The most common alloys founded in ancient object are essentially binary and ternary mixtures of copper, gold, silver, iron, lead, arsenic, antimony and tin in different proportions with possible addition of nickel, platinum and mercury[89].

Due to the large variety of combinations and the complexity of the metallographic aspects related to each possibility, we will focused on copper-based alloys, particularly on cast bronzes, as main topic of the chapter 5 of the present thesis.

The ease of reducing copper from its ore has guaranteed to copper and its alloys a long history, lasting thousands of years and nowadays continue to be important for the high electrical and thermal conductivity, the ease to form/cast and corrosion resistance[90].

Under the UNS (unified numbering system), the term bronze (C90200-C95900) applies to a broad class of alloys in which the principal alloying element is neither zinc nor nickel[91].

There are four broad categories of bronzes:

- tin bronzes;
- leaded and high leaded tin bronzes;
- nickel-tin bronzes;
- aluminium bronzes.

The first two categories, together with arsenic, antimony bronzes and brasses, are the most common copper alloy encountered in archaeological and artistic object[92–97].

Metals and alloys

Metals can be described as an aggregation of atoms connected with metallic bonds and, when in the solid form, considered as lattice of positive ions surrounded by a cloud of delocalized

electrons. The crystal structure of a solid metal refers to the internal structure or arrangement of the atoms in an ordered, repeating three-dimensional pattern.

Several types of lattice structures may be possible, such as Close-Packed Hexagonal (CPH), Face-Centred Cubic (FCC), Body-Centred Cubic (BCC), Rhombohedral (R), Body-Centred tetragonal (BCT), etc. The FCC structure is characteristic of copper, lead, silver, other native metals, R structure of arsenic, antimony, and bismuth while BCT arrangement is distinctive of tin[89]. Normal metallic objects are polycrystalline, which means they consist of an aggregate of many very small crystals called grains.

Structure of casting alloys

Metals can be *cast* or *worked.* These two terms identify the main ways to create a metal object. As *working* are defined all those actions such as annealing, drawing, engraving, filing, cold/hot working, machining, piercing, etc. that permit to transform and model the artefact. Instead, the *casting* is the operation of pouring metal into sand, plaster or other moulds and allowing it to solidify[89,98]. Cast objects could be finally worked to finish details and decorations.

In literature, several casting and working techniques are documented. A casting procedure may imply the use of an *open*, *two* or *multi piece moulds*. The action to cast a part attached to an already existing object or component is defined as *casting on*. S*lush casting* is considered the method in which metal is spun in the mould with the aim to create a thin shall. Finally, the *lost-wax* procedure means casting from a wax model covered with a clay mould. After pouring the molten alloy and the wax is molten out, the metal fills the space and acquires the shape of the lost model. A more detailed description of these techniques are available elswhere[91]. As example, the bell casting is one of the most complicated and laborious procedure. A simplified schema is presented in Figure 7.

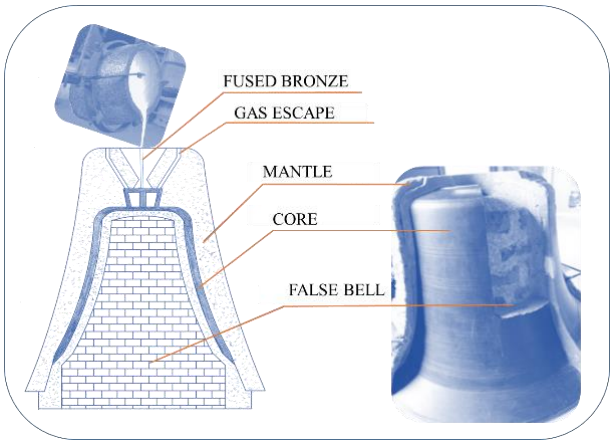

Figure 7. Structure of a mould use to bell casting.

The casting procedure is crucial for the formation of the micro and macro structure of an alloy/object and may lead to segregation phenomena.

Segregation is defined as any variation from uniform distribution of the chemical elements in the alloy[99,100]. It depends on the distribution of the melts/solutes between the solid and the liquid phase during freezing[90]. Different types of segregations may arise during the casting procedure that have consequence in macro or micro scale structure.

Micro-segregation is a result of dendritic solidification and implies segregation of impurities between the dendrite arms. The formation of dendritic is defined as the random growing of crystals in the alloy as effect of the cooling process (Figure 9). Starting from a central body (primary arm), ramifications tend to develop approximately in perpendicular direction (secondary and tertiary arms) and the shape of the crystal changes into a tree-like[101]. The crystals grow until connecting each other and the rate at which the metal in cooled and the presence of impurities influence their size. It is a segregation of the solute elements over distances of approximately dendrite arm spacing (Figure 8), i.e. in the order of hundreds of μm or less[102]. It is possible to inspect several micrographs of copper alloy microstructures sections on the web site of the Copper development association Inc[103].

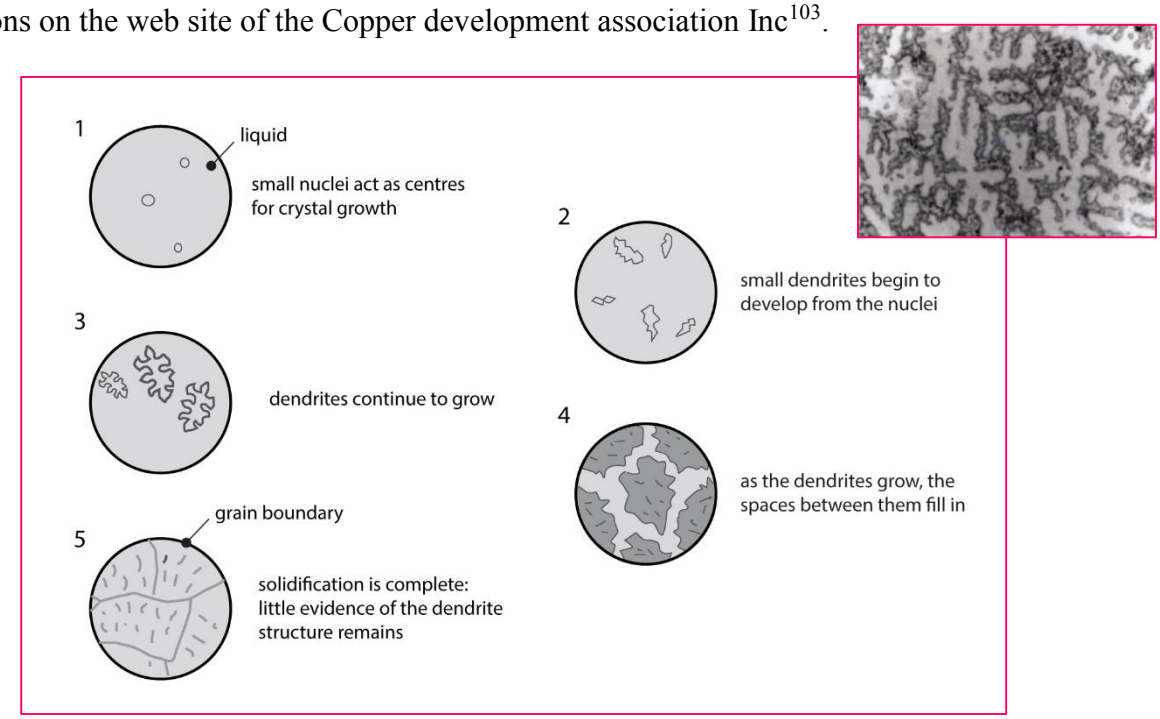

Figure 8. a) Scheme of dendrites growing process; b) Micrograph section of a Tin bronze[89]

Depending on the amount and nature of the alloying constituent present, the remaining fluid in the inter-dendritic spaces will solidify to form different phases of the specific alloy system[104]. A phase is considered as a homogeneous portion of a system that has uniform physical and chemical features. The faster is the rate of cooling, the smaller are the dendrites.

A micro-segregation phenomenon that often arises in impure metals or alloys if one of the constituents has a lower melting point then the others. E.g. in an Cu/Sn-based alloy, the copper that has higher melting point (1083 °C) solidifies first and the dendrite arm will be richer in Cu, while the external part will be rich in Sn because of its lower melting point (232°C). Consequently, a compositional gradientis present from the inner region and external part of the dendrite (coring)[89].

Macro-segregation refers to variations in composition that occur in alloy castings in scale from several millimeters to centimeters or even meters[105]. This phenomenon includes *Normal, Inverse* and *Gravity segregation.*

The *Normal segregation* occurs in slowly cooled casting. The first crystals to separate from the molten alloy during solidification are rich in the higher melting point alloy and occupy a position close to the mould face.

The *Inverse segregation* has opposite direction and it is frequently found in alloys that have been rapidly cooled from the molten state. The constituent with the lower melting point is concentrated towards the outside of the ingot along with the primary crystals of the higher melting point alloy and its concentration decreases as the centre of the ingot is approached. This macro-segregation may produce sort of coating on the object[105–107].

Gravity segregation is caused by the tendency of the densest component to sink in the alloy melt, e.g. the lead in a Cu-Sn system. Theoretically, the lead is expected to concentrate in the lower part of the mould. With the regard to this type of segregation *Craddock et al.* studied the relation between lead concentration and the position on which mould/object was positioned during casting. They achieved interesting information about the procedure followed by west African smiths[108].

An important factor influencing the structure of an alloy is the relation of the temperature and the mutual solubility of the different components. Phase diagrams are used to predict which phases should be present in the alloy at equilibrium. Although, it is important to bear in mind that diagrams usually refer to very slowly cooled melts, which rarely is true for archaeological materials[89]. For more details, phase diagrams are available in the *ACerS-NIST Phase Equilibria Diagrams Database*[109]. For further discussion about diagrams and the possible phases presented in a metal alloy the reader is referred to more specific manuals[91].

In the context of this thesis, it is enough to consider that when two or more metals are mixed together they may show complete or partial solid solubility or be insoluble. Thus, the

coexisting phases will influence the structures derived and, consequently, their physical and mechanical properties as well as the spatial distribution of the elements across the object depth.

As examples, tin in copper is a case of partial solubility; while lead results as totally immiscible in the same system. Thus, in the last case the lead is supposed to appear as globules or finely dispersed among dendrites depending on the cooling rate of the casting procedure[89,110].

Cooling curves

One of the most important physical properties of the metal that have to be cosidered in a casting alloy design is the *melting point*. Each pure substance shows a characteristic cooling curve. A simple example is presented in Figure 9. Plotting the temperature of the lead versus time it is possible to obtain the cooling curve that shows the melting point of the element considered and the freezing plateau.

With alloys the behaviour of the curve will change and the range over which solidification occurs depends on the proportions of the elements. As an example, it is interesting to see how the presence of lead can lower the melting point of an alloy. Hence, a lower temperature has to be reach and the technology used to produce an object may be simplified

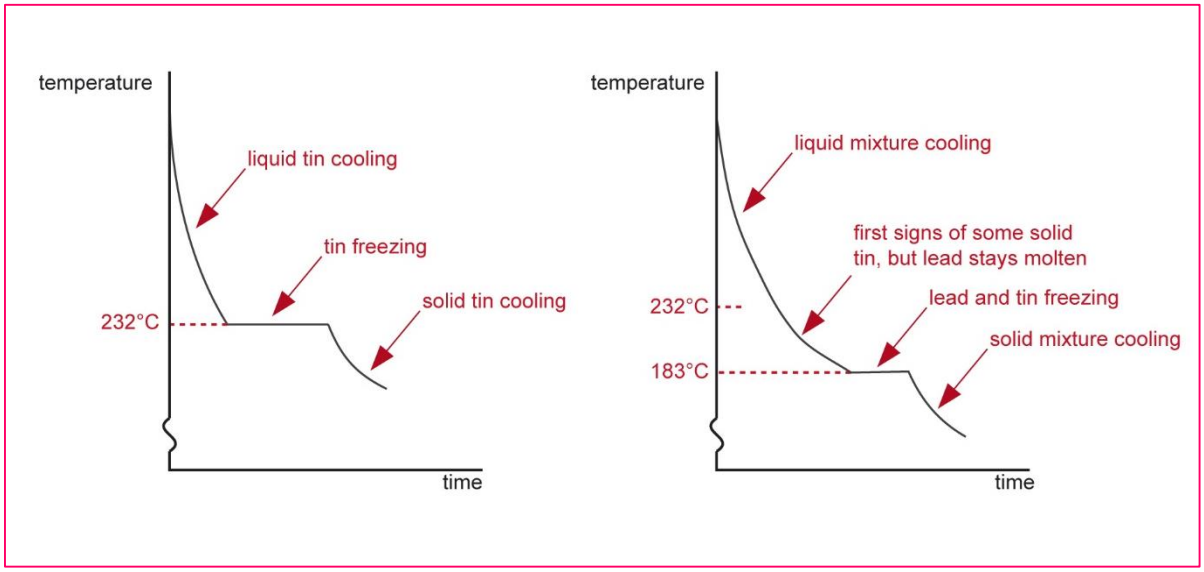

Figure 9. Cooling curve of Tin and Tin-lead alloys.

The number of phases, their proportions, and their spatial arrangement influence the microstructure of an alloy and consequently its properties. The mechanical feature of a

material are normally established by means of standard procedure (e.g. Brinell or Vicker test) that permit to test:

- *strength (elastic and plastic deformation);*
- *inelasticity;*
- *elastic properties;*
- *tensile properties (yield point, yield stress, ductility, resilience, toughness;*
- *true stress and strain;*
- *elastic recovery during plastic deformation;*
- *compressive, shear, and torsional deformation.*

In particular, tensile properties indicate how the material will react to forces being applied in tension and determines the capacity of the material to be plastically deformed/worked (malleability) and how the material can be stretched (ductility), while hardness establishes the resistance to plastic deformation (e.g., a local dent or scratch)[91].

These properties are especially important when an alloy is designed with the aim to create an artefact because they influence the resistance and conservation of the object along time, as well as permit the artist to deform the metal and to obtain the aesthetical result desired.

Considering all the phenomena and factors described above, it becomes clear which difficulties an artist/smith has to overcome to obtain the object designed and how the heterogeneity of the material can be explained.

1.2 Analytical techniques: Fundamentals and application in conservation science

The structures of oil paintings, photographs as well as metal objects described above suggest a high grade of heterogeneity that should be considered when analytical techniques have to be applied. The limited number of available samples due to the necessity to preserve the physical integrity of valuable and unique objects results in a compromise between the quality of the results and the impact of the analytical process on the artwork. The following section presents the techniques that have been employed in the different case studies in the present thesis. After a brief description of the fundamentals of the techniques, the discussion will focus on their advantages and limitations. Finally, some cases of application based on the literature are cited as examples.

1.2.1 Subsurface testing

The complex path of an artefact investigation starts generally with non-destructive global testing methods. The first step is an accurate analysis with visible radiation that permits to recognize and understand the visual choices and the *modus operandi* of the artist. Visual analysis addresses an artwork's formal elements, visual attributes such as colours, lines, textures. Nevertheless, subsurface layers may include underdrawings, subjacent painting layers, and alterations, and in a growing number of cases, conservators have discovered abandoned compositions on paintings, illustrating artists' practice of reusing a canvases or panels, leaving layers that visible light cannot reach. The interest to discover what the artists have hidden, or/and the concern about the real conservation state of the materials, led to a continuous development of new technologies that permit to access to the inner structure of a Cultural Heritage artifacts[111]. The standard methods used for this purpose still are the infrared reflectography and X-ray radiography. The images acquired by means of these techniques will be key tools in the study of easel paintings in chapter 3.

These techniques are based on the selective penetration of radiation at different wavelengths, near-infrared light and X-rays, through the structure of the object and the capacity of the material to reflect or absorb the radiation. Figure 10 shows the penetration power of each type of radiation depending on the relative wavelength.

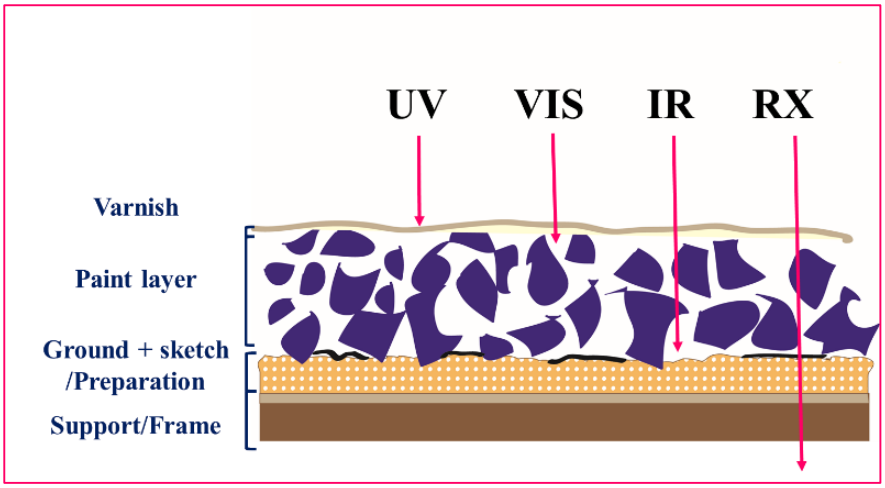

Figure 10. Scheme of the penetration of each type radiation in paint structure.

X-ray radiography (XRR)

X-rays are a form of the electromagnetic radiation (0.01 to 10 nm), that are produced when fast moving electrons interact with matter. The spectrum obtained is composed of two

overlapped spectra: the characteristic spectrum at discrete energies (see XRF section) and a general spectrum with continuous range of energies, also named Bremsstrahlung. This effect is generated through the deceleration of high-energy electrons when they strike the electron cloud and the nuclei of atoms in the sample. The Bremsstrahlung spectrum is the phenomenon used in x-ray radiography[112].

Characteristic X-rays/Planck's equation: $E_x = h \cdot \nu = h \cdot \frac{c}{\lambda} = \Delta E_{kin} = E_{kin}(i) - E_{kin}(f)$ (6)

Bremsstrahlung: $E_{max} - E_{kin}(i)$ (7)

where λ = wavelength of the radiation; c = speed of light; h = Planck's constant; E = Energy of the radiation measured in kilo-electron volts

The radiographic image (XRI) is determined by the x-ray absorption of painting components (pigments and support), and by their concentration and their thickness. The absorption, according to Lambert-Beer's law (eq.4), depends on the material irradiated (absorption coefficient μ) and increases proportionally with the atomic number (Z) of the elements irradiated. The equation of the progressive attenuation of the beam can be expressed as:

$I(d) = I_0 \cdot e^{-\mu d}$ More depth more abs (8)

where $I(d)$ is the intensithy at depth, d, I_0 the intensity of the incident beam, and μ the linear attenuation coefficient.

The mass absorption coefficient, μ/ρ, is a function of the atomic number of the absorber (Z) and the energy (E) of the incident X-ray[113]:

$\mu = kZ^3/E^3$ (9)

As mentioned before, pigments may include in their formulation elements that are very heavy, such as lead, as well as very light ones like carbon. The differences in their Z number are expressed in the XRI in a grey scale. The high-density areas will appear white and bright, while points with lighter elements will appear black. The acquisition of a good quality XRI is a complex combination of several parameters, which have to be optimized. Two of those are current (intensity) and voltage. The first will have effect on the time required for the acquisition of the image, and the second, more important one will establish the energy of the X-ray, consequently their penetration (minor λ). The differences in attenuation coefficients should be maximized by choice of energy as in the following example assuming equal thickness of the two materials:

E.g. $\frac{I_{Cu}(d)}{I_{Pb}(d)} = e^{(\mu_{Pb} - \mu_{Cu}) \cdot d}$ (10)

Furthermore, the geometrical set-up has to be established to avoid or minimize the detection of the scattered rays that may cause artefacts in the image[112]. In Figure 11 is presented a simplified scheme of an X-Ray instrumentation. Although, X-ray radiography is a very useful tool to understand the structure of a painting or other artefacts, it is important to keep in mind that the images that result are the projection of a three-dimensional structure onto a two-dimensional plane, XR plate or 2D screen[112]. New technologies have dramatically improved the quality and the readability of XR images. Tomographic imaging or full-field 3d imaging by means of synchrotron radiation are two of the methods reviewed by *Janssens et al.*[111] that permit to improved XRI acquisition and interpretation.

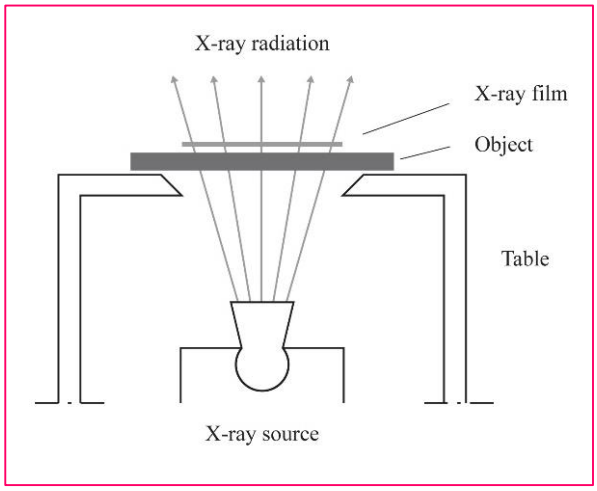

Figure 11. Scheme of the instrumentation for X-ray radiography

Infrared-reflectography (IRR)

An infrared reflectography set-up is basically composed of an halogen lamp, which emits light in the visible and near-infrared spectrum (800–2.300 nm, little variations in the range depend on the equipment available) and a detector, normally a CCD camera with appropriate filters. The IR source due to its wavelength has a limited penetration in depth. It crosses the pictorial layer and is reflected/scattered on the base or the preparation layer of the artwork (see scheme in Figure 12)[114]. The reflected radiation captured is transformed by the camera in a visible image[111]. In IRR the differences in material distribution are expressed in a grey scale. Unlike in XRI, the white areas correspond to the high scattering capacity compounds, while darker zones suggest infrared absorbing materials. IRR is suitable for the study of underdrawings that consist of infrared absorbing materials, such as carbon black, on reflective chalk or gypsum grounds, as normally found in paintings. However, many paints contain infrared absorbing pigments that hinder the distinction between the underdrawings/underneath layers from the covering paint layers[111]. Conventional IRR is

performed in wideband modality, i.e., by acquiring the image in the large near-infrared (NIR) band, determined by the spectral range of the device. The images obtained are difficult to interpret and need an accurate visual supervision. To overcome in part this limitation, *Daffara et al.* have developed, at the National Institute of Optics (INOA, Italy), a scanning multispectral infrared reflectography (SMIRR) device that allowed to simultaneously collect a set of raster images at different wavelengths in the NIR range of 800–2.300 nm. The information obtained is organized in a tensor and the images at different wavelengths may be managed separately[115]. Further technical information is available in chapter 3 were different IRR images acquired with this system are presented.

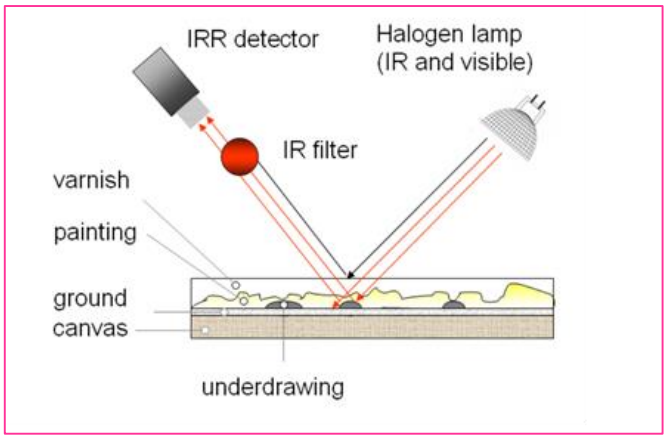

Figure 12. Scheme of a NIR reflectography set-up.

1.2.2 Fourier transform Infrared Spectroscopy (FTIR)

Fundamental

The infrared spectroscopy is based on changes in the vibrational energy of molecules due to the absorption of IR radiation. The infrared radiation belong to the spectral range between visible and microwave radiation. This range can be divided in three parts:

- Near IR (NIR) → 14.000 – 4.000 cm^{-1}
- Mid IR (MIR) → 4.000 – 500 cm^{-1}
- Far IR (FIR) → 500 – 20 cm^{-1}

According to Planck's law (Eq. 6), all regions in the electromagnetic spectrum can be described by energy E that is directly proportional to frequency. Since frequency is inversely proportional to wavelength, it follows that energy of electromagnetic radiation and wavelength are also inversely related. In the context of infrared spectroscopy, wavelengths are measured in “wavenumbers", which have the units cm^{-1} (wavenumber, $\bar{\upsilon} = 1/\lambda$ where wavelength is expressed in centimeters). One of the advantages of wavenumber over

wavelength units is that they are directly proportional to energy[23]. Thus, a transition that requires greater energy will occur at a higher wavenumber. The energy of IR radiation is too low to affect the electrons within an atom. Instead, IR radiation does correspond to the energy required for translational, rotational, and vibrational energy transitions. Since a molecule's movements is unique to its structure, the measurement of these transitions makes IR a powerful tool for compound characterization[23].

According to Hooke's law, which explains the approximation to the harmonic oscillator model, we can express the fundamental vibrational frequency of a molecular ensemble with the equation:

$$\nu = \frac{1}{2\pi c}\sqrt{\frac{k}{\mu}} \qquad (11)$$

where ν = fundamental vibration frequency, k = force constant, and μ = reduced mass. The reduced mass, $\mu = m_1 m_2 / m_1 + m_2$, where m_1 and m_2 are the component masses for the chemical bond under consideration[116]. However, deviations from the ideal harmonic model have to be considered when transitions at high levels of absorbed energy occur.

The interactions of infrared radiation with matter may be understood in terms of changes in molecular dipoles associated with vibrations and rotations. The number of movement is established/described by the degrees of freedom (3N-6 or 3N-5 for non-linear and linear molecules, respectively). The possible rotations are classified in two main categories of *stretching* (ν) and *bending* (δ) vibrations (Figure 13). The term *stretching* defines changes in inter-atomic distance along bond axis, while *bending* denotes the change in the angle between two bonds. There are four types of bend: rocking, scissoring, wagging, and twisting. Some bonds can stretch in-phase (symmetrical stretching) or out-of-phase (asymmetric stretching), as shown in Figure 14.

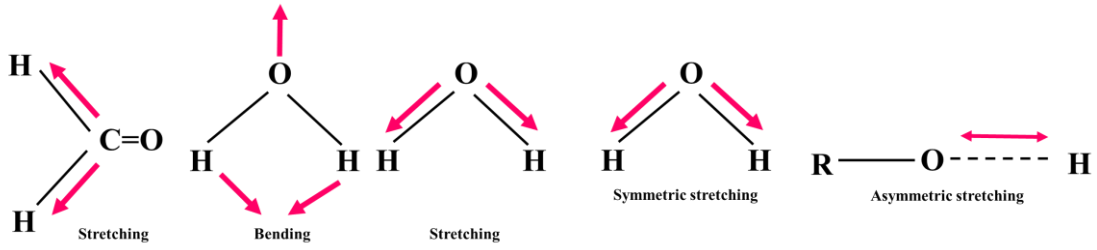

Figure 13. a) Stretching and banding vibration; b) Symmetric and asymmetric stretching vibration.

The terms *in-plane* and *out-of-plane* bending vibrations are used to define the plan in which atoms bonded can move, which are respectively in the plane of the molecule and perpendicular to the plane, respectively, as illustrated in Figure 14.

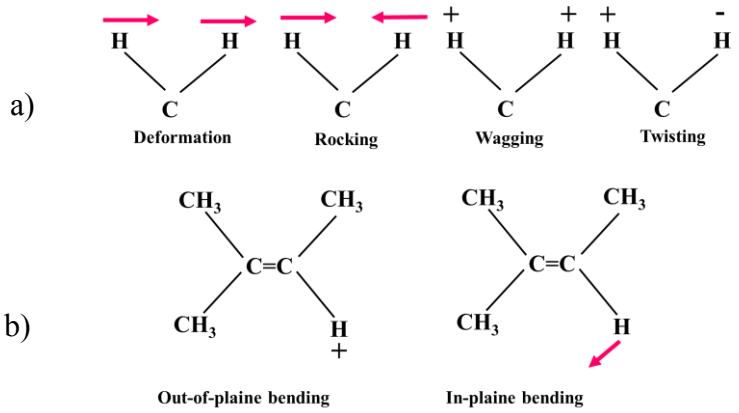

Figure 14. a) Different type of bending vibration; b) Out-of-plain and in-plane banding vibration.

An important remark in this context is that only the vibrations that imply a change on the dipole moment of the molecule are active in the IR region. Thus, they will appear as an absorption band in the IR spectrum. Furthermore, the theoretical number of the possible vibration may be modified by many factors that result in important changes to the spectra and may hinder the band assignment. A reduction in the number of absorption bands can be attributed to the degeneracy, where two vibrational modes may occur at identical frequencies, overlapping, or weak absorptions, or vibrational modes that occur at wavenumbers outside of the instrument range[23]. The number of observed bands may be increased due to overtones and combination modes. The overtones are multiples of the fundamental absorption frequency. As transitions that extend beyond the first quantum level (to the second, third, fourth, etc.), which give rise to weaker absorptions, they are influenced by anharmonicity, which must be taken into account when assessing the frequency of these higher frequency vibrations[116]. In addition, the combination bands arise when two fundamental bands absorbing for example at $\bar{\upsilon}_1$ and $\bar{\upsilon}_2$ absorb energy simultaneously. The resulting band will appear at $(\bar{\upsilon}_1 + \bar{\upsilon}_2)$ wavenumbers[117]. A further discussion on theoretical and experimental aspects of vibrational combination bands and overtones has been published by *Jakob and Persson*[118].

A dramatic improvement in infrared spectrometer technology was the introduction of the Fourier Transform infrared (FTIR) equipment. In particular, FTIR spectroscopy is based on

the idea of the interference of radiation between two beams to yield an interferogram. The simultaneous measurements of the entire spectral range is possible by the introduction of the Michelson interferometer, which consists of two perpendicularly plane mirrors, one of which can be moved in a direction perpendicular to the plane, and a beam splitter. The beam splitter is made of a material that transmits and reflects light in equal proportions. The two beams reflects back to the beam splitter from the mirrors and interfere constructively or destructively according to the optical path difference produced by the moving mirror.[119]. The distance recorded between the two beams and consequently their frequencies are finally converted by the mathematical method of Fourier-transformation, [117] which permits to obtain the infrared spectrum. The advantages of a FTIR system are the high signal noise ratio, high signal-to-noise ratio, high resolution, and very short recording times.

Transmission Methods

Transmission spectroscopy is the oldest and most straightforward infrared method[117] exhibiting a high signal-to-noise ratio and offering the possibility to better interpret the obtained spectra. In this case, the infrared beam passes through the sample. The intensity of the signal obtained is the intensity of the incident beam without the component absorbed by the molecules, a function of the wavelength, which is used as fingerprint of the molecules. According to the Lambert-Beer law (Eq.4) the absorption is directly proportional to the thickness (l), absorptivity (ε) and the concentration (c) of the material.

The measurement set-up can be different depending on the nature of the sample and the information needed. There are two general methods for the examination of solid samples with transmission infrared spectroscopy: one uses alkali halide discs and the other one films.

The use of alkali halide discs involves mixing, grinding and homogenizing a properly weighted sample with a dry alkali halide powder transparent to infrared radiation. The particles produced have to be smaller than the wavelength of IR radiation (5 μm) [23]. The KBr salt is the most commonly used halide powder. Finally, the powder is pressed in a pellet with a thickness of 2 mm and an approximate diameter of 13 mm, which can be reduced down to 0.5-1.5 mm for micropellets. Usually the sample needed accounts for about 2-3% in weight with regard to the salt quantity. For analysis, a sample pellet is placed in a pellet holder and inserted directly into the sample compartment of the IR spectrometer. For macro samples, the area of analysis may cover the entire salt pellet, while for samples to be analyzed

on a micro spectrometer the area of analysis may be only 1 x 1 mm^2 or less[23]. It is important to obtain a uniform thickness across the pellet and a homogeneous distribution of the sample particles with the aim to avoid scattering phenomena and incorrect interpretation of the spectra. Clearly, interferences due to contamination or hydration of the pellet have to be avoided.

In case of microanalysis of films, performed using a spectrometer equipped with an optical microscope, the sample is extracted by means of a scalpel. It is placed between two industrial-grade diamonds, aligned in a steel compression cell and pressed. Infrared radiation from the spectrometer is focused onto a sample placed on one diamond window and controlled by a microscope x –y stage. The microscope permits to select the areas to be analyzed and to focalize the beam. The sample needs to be about 100µm x 100µm. The transmission method is micro-destructive, because it is necessary to extract the sample, and punctual, due to the very narrow and focused infrared beam used. This characteristic make it difficult to obtain representative results (Figure 15).

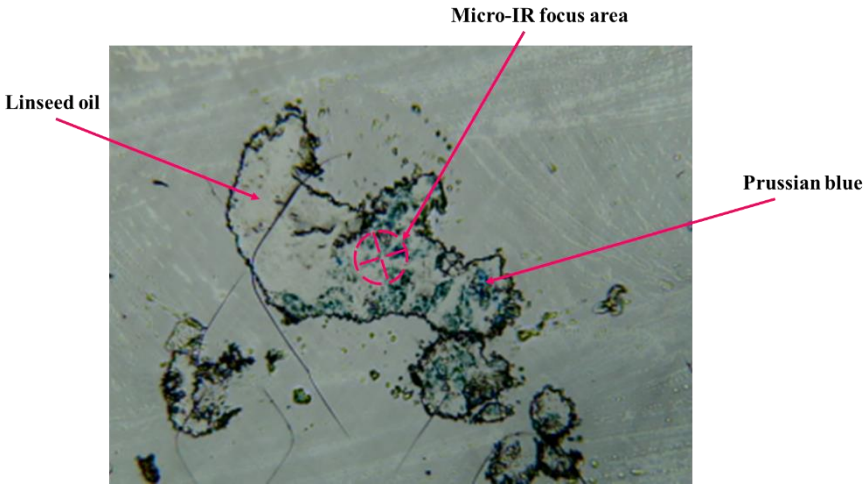

Figure 15. Magnification of a sample of oil paint layer pressed using a diamond cell.

Reflection Methods

Reflection methods can be divided into two categories: *internal* and *external reflectance*. In the first category, *internal reflectance* measurements can be applied by using an attenuated total reflectance cell in contact with the sample. In the second category, *external reflectance* measurements involve an infrared beam reflected directly from the sample surface, which permits to acquire mid-infrared spectra without any contact with the analyzed surface.

The techniques used for experiment in chapter 2 and 3 of the present thesis belong to the second category. The two different set-ups employed were mid-infrared fiber optic reflectance (midIR-FORS) and a macroscopic Fourier transform infrared scanning in reflection mode (MA-rFTIR). The spectra obtained depend on two type of reflection: specular and diffuse.

Specular reflection

As aforementioned, the specular, also called surface reflection, is the radiation emitted from a flat surface with the same angle as the incident beam. When the reflective surface is a bulk absorbing material, the reflection spectrum is ruled by Fresnel's law (Eq.3)[120]. It is important to keep in mind that the refractive index changes with wavelengths. Two types of spectral distortion are observable in infrared spectra due to this phenomenon: derivative-like and/or inverted (so-called reststrahlen) bands. When absorbing samples with absorption index - $k<1$ (most organic molecules including polymers) are analysed, the resulting spectra may present bands with derivative features. Instead, reststrahlen bands appear due to the strong signal from materials with $k\gg1$ (most inorganic salts, nitrates, carbonates, sulphates, phosphates)[21,120]. It is possible to convert the bands of a specular spectrum in a pseudo-transmittance signal applying a Kramers-Kronig algorithm, which permits to calculate both absorption (k) and refractive index (n) and correct the spectra. Further explanation of the mathematical method are presented elsewhere[121].

Diffuse reflection

The bulk or diffuse reflection is the radiation that penetrates into the sample and then emerges at all angles after suffering multiple reflections and refractions by the sample particles[122]. As the phenomenon is related to absorption processes, the spectra obtained are quite similar to those obtained in transmission mode, although they present some shifts on the absorption wavenumbers and differences on the relative band intensities[21].

Band intensity depends on scattering. The *Rayleigh scattering law* can be considered when the scattering center (e.g. pigment particle size of 0.1 μm) is much smaller than the light beam (infrared radiation 3-11 μm). In this case, the scattering cross-section, defined as the area of collision, will vary with the wavelength proportionally to λ^{-4}. Thus, shorter wavelengths are scattered more strongly than longer wavelengths. As scattering causes attenuation of a light beam in an analogous way to absorption[22], it can be explained by the intensification of low wavenumber bands with respect to the high wavenumber side region

of the spectra. The lower the absorption coefficient is, the higher is the penetration in depth of diffuse radiation. This means that the bands that normally show a weak absorption in transmission mode (small absorption coefficient) in reflectance spectra present higher intensity, due the larger volume crossed and the number of scattering phenomena produced [21]. This is the reason for the use of overtone bands used as characteristic signal in reflectance spectra because they are not affected by distortions or interferences[123].

A diffuse reflectance spectrum can be corrected applying the Kubelka–Munk algorithm (Eq.5). The corrected spectrum demonstrates a linear relationship between band intensity and the sample concentration. This allows a comparison with transmission spectra that are usually recorded in absorbance units[25]. The algorithm is based on assumptions[27,124] that in a realistic sample are not always accomplished, such as the homogeneity. Thus, the correction has to be considered as an approximation.

As both types of reflection can be simultaneously manifested in an infrared spectra acquired in reflection mode, the aforementioned algorithms can be applied only in specific cases or spectral ranges. Otherwise, the bands will be distorted and lead to erroneous assignment. Nevertheless, the spectra are rather difficult to interpret. The measurement condition (e.g. geometrical set-up, technological details) and special data treatments method have to be optimized with the aim to reduce interferences and achieve higher signal-to-noise ratios.

Application

In 2001 *Casadio and Toniolo* published a chronological survey on the analytical application of infrared spectroscopy to the material characterization of polychrome works of art and archaeology over forty years[125]. Since then the technologies have been dramatically improved and the use of infrared has become a routine method in cultural heritage investigation.

The infrared spectrometers provide, nowadays, very high signal-to-noise ratio. New developments permit the acquisition of high quality mapping of areas relatively extensive. A large number of spectra can be acquired with a high spatial resolution in short time. Despite the high quality information achieved, the need to extract material from artwork is an important limit of these techniques. The analyzed material is loss in the process and in some cases is not representative of the entire object or area investigated. For this reason, non-destructive techniques were more and more improved, employed and progressively adapted to satisfy the needs of this specific field[126]. The inconvenience of spectral distortions have been overcome by the possibility to obtain a large number of measurements without any sampling or contact with the artwork surface. The information about organic and

inorganic substances distributed across the entire surface of the object investigated without limitation of the measurements number constitutes an important benefit.

The two principal systems used to collect the reflected radiation are a fiber optic probes (midIR-FORS) or a frontal reflection modules incorporated into a compact FTIR spectrometer (MA-rFTIR) (Figure 16).

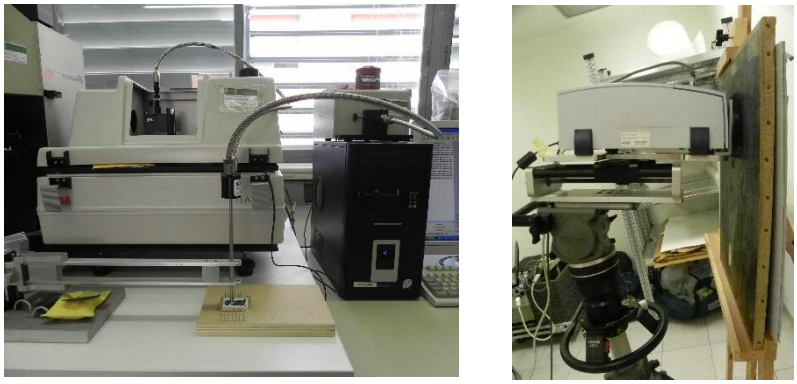

Figure 16. Remote IR spectrometer a) midIR-FORS; b) MA-rFTIR.

One of the first documented uses of fiber probes has been performed at the National Gallery of London for colour monitoring in the late 1970s. Then, some years later *Bacci et al.* published the first review about this tool describing it as very versatile and useful for in-situ application[127]. The mid infrared fiber probe is normally made of chalcogenide glass, which allows the collection of spectra in a wavenumber range from 6000/4000 to 900 cm^{-1}, except between 2200 and 2050 cm^{-1} region where the Se–H stretching absorbs. Other materials can be used depending on the spectral range of interest. The fibers interferences hinder the reading of the spectra and may cause loss of information because of the overlapping with signals of the sample. However, the use of the fiber probe is preferred when the location of the point to be analyzed is difficult to reach with other set-ups (e.g. 3D object as statues). Compact version of the spectrometer equipped with fibers are available suitable for *in situ* measurements campaigns.

On the other hand,, MA-rFTIR set-up permits to enlarge the spectral range and record spectra with higher signal-to-noise ratio. The spectrometer incorporates a a deuterated triglycine sulphate (DTGS) detector, which is less sensitive than a mercury cadmium telluride (MCT) detector, but it can operate at room temperature, making it more useful for in situ measurements[128].

The infrared reflectance spectroscopy, due to the capacity to detect organic and inorganic compounds, covers several aspects of the artistic material analysis, from degradation mechanisms[129] to investigations of the studio practice[36,130], and has been applied to a wide

set of materials, such as paintings (pigments/dye and binders)[21,131–134], metals, photographs[135,136], paper (e.g. manuscripts, prints)[137–139] etc.

A common conservation issue, for example, is the formation of metal soap due to the creation of a complex between metals contained in pigments and fatty acids of the siccative oil present in the polychrome layers. These compounds can result in white crystal formations that erupt through the paint surface and may lead to detachments and loss of material. Both, micro- and non-destructive infrared spectroscopy have been successfully employed for the identification of oxalates[33] on easel[140] and wall paintings[141]. *Monico et al.* have demonstrated that infrared reflection profiles of metal-oxalates are characterized by derivative-like and/or inverted features, apart from combinations or overtone bands, which can be in part correct by the Kramers-kronig algorithm. The publication stresses the utility of the mid-IR reflectance technique to identify the carboxylate nature and origin, and to map its presence across the artwork surface[142]. The knowledge acquired allows the design of appropriate conservation strategies for storage or treatment of vulnerable paintings.

Nevertheless, the mid-infrared spectroscopy is commonly used to identify pigments, dyes and binders. *Miliani et al.* have extensively studied pigment reference sample as well as real artworks by means of reflectance spectra[21].

Despite of its utility for artwork characterization, this technique has many limitations. First of all, the distortions that affect the spectra hinder the interpretation and assignation of the characteristic bands. As mentioned before, the distortions are caused by the chemical features of the surface investigated, but also by many physical factors, such as the roughness of the analyzed surface. Indeed, even the painting surfaces that appear rather flat may presents irregularities (Figure 17). Another important limitation is the sensitivity. Due to the shift of the principal band numbers and the distortions, only general information about organic compounds can be achieved. This is the case for siccative oils, whose spectra do not show significant differences between different types (linseed, poppy etc). However, *Miliani et al.* have demonstrated that mathematical correction of the signals of organic compounds in NIR range show slightly differences[143].

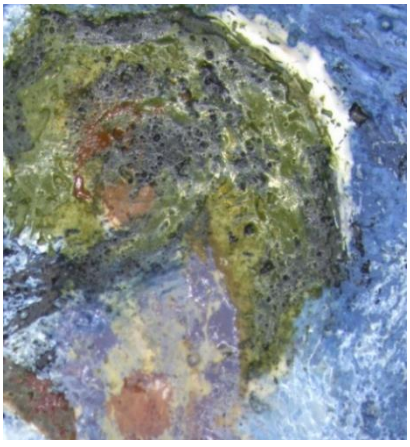

Figure 17. Rough surface possibly find in oil painting.

1.2.3 X-Ray fluorescence (XRF)

Fundamental

X-ray fluorescence is based on the emission of secondary X-rays by matter that has been excited by primary X-rays of a specific energy. When an inner shell electron is displaced by collision with a primary electron, an outer shell electron may fall into the inner shell to reestablish the proper charge balance in its orbitals following an ionization event (photoelectric absorption process). The time period between the excitation and the emission is called the lifetime of the excited state. For the lower atomic number elements, this lifetime increases to such an extent that there is a significant probability that a second electron can be ejected from the atom before the first vacancy is filled. By the emission of an x-ray photon, the ionized atom returns to ground state[144]. Each element has many energy levels and therefore many potential vacancy-filling mechanisms. Because the atomic structure of each element is different, each element will emit different X-rays at characteristic energies. The system of labels is explained in Figure 18 where the first letter (K,L,M) stands for the shell in which the vacancy is filled and the second one (α, β, γ, δ) the level from which the substitute electron drops down. The energy difference between adjacent electron shells becomes less, progressing outward from the nucleus. It follows that the energy released upon electron transitions between adjacent shells in the outer shells is less than that released for inner shell transitions. That means, for a given atom, that Mα radiation will be of lower energy than Lα radiation, which in return will be of lower energy than Kα radiation[113].

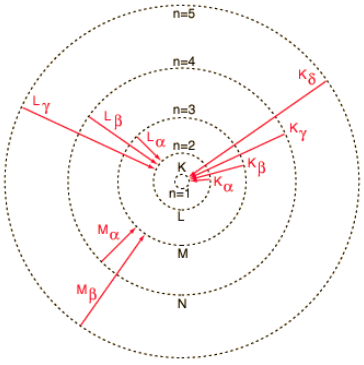

Figure 18. Shell atom scheme.

The XRF analysis are completely non-destructive and the measurements are acquired with a distance of about one cm or less from the surface of the sample, depending on the geometrical setup of the spectrometer and the optimal focus beam conditions. The instruments, generally, allow to detect only elements with Z<15 (P). In order to achieve a high determination quality an accurate calibration by acquiring a spectrum of a known element(s) should be assured. The calibration step is more reliable if performed with elements of approximately the same Z number as the sample to be analyzed due to the matrix interferences.

XRF technique is commonly used for qualitative analysis, although with appropriate standards quantitative or semi-quantitative analysis may be performed. In quantitative XRF analysis it is important to keep in mind that the efficiency of X-ray detection decreases proportionally with the Z number, as their element-specific X-rays are partially or completely absorbed by the air. This problem can be partly solved by applying a helium flush.

The measured intensities not only depend on the analyte concentration but also on accompanying elements (matrix), sample type (shape, thickness and heterogeneity) and measurement conditions such as setup geometry of the spectrometer, spectral distribution of the ionizing radiation and the efficiency of detection systems[145]. Thus, several parameters have to be considered, such as acquisition time, acceleration voltage and probe current, direct or indirect radiation, dead time as well as the acquisition time.

Absorption is usually the biggest factor that must be considered in the measurement of compositions by X-ray microanalysis. The detection of a specific element is possible if the energy of the primary beam is sufficiently high to permit the ionization of the atoms. The minimum energy needed for each element is determined by the *absorption edge* of the specific element, defined as the energy equal to the binding energy of an electron shell (K, L, M, etc.) in the absorber[146]. Therefore, the voltage setting, which determines the energy of the X-ray source, is a fundamental parameter to be considered. Instead, the current probe influences the number of X-rays emitted by the samples, and consequently, the intensity of the detected signal.

The efficiency of the detection of the X-rays emitted is a characteristics of the detector available. The processing of an X-ray event by the detector and its associated electronics takes a finite amount of time[147]. Dead time is the time that the detector needs before being ready to count a new X-ray event. This phenomenon should be considered when concentration/intensity ratio has to be compared between samples, although, normally this correction is done automatically by currently available instruments[148]. Furthermore, sum peaks may appear in the spectra as result of the simultaneous arrival of two photons to the detector. This situation just occurs under high count rate conditions[149].

The acquisition time mostly influences the detection of light elements, as the probability of a X-ray emission decreases with the decrease of Z number. Longer acquisition times permit

to increase the number of counts collected for each peak being measured and to minimize the impact of random fluctuations present in the spectral background.

The intensity of a specific element is influenced by the matrix in which it is included. When matrix elements emit characteristic radiation of slightly higher energy than the energy of analyte absorption edge, the analyte is excited to emit characteristic radiation in addition to that excited directly by the X-ray source. Thus, an enhancement of X-ray radiation may occur in the specimen. The primary and secondary absorption occur as the elements in the specimen absorb the primary and characteristic radiation, respectively[145]. Numerous methods for matrix correction, both empirical and theoretical, have been proposed for quantitative XRF analysis and are further explained elsewhere[145,150]. However, the more practical and effective method to minimize matrix effect is the preparation of thin samples. For these samples, matrix effects are not observed under certain measurement conditions and linear relationship between radiation intensity and analyte concentration is observed (Figure 18)[151].

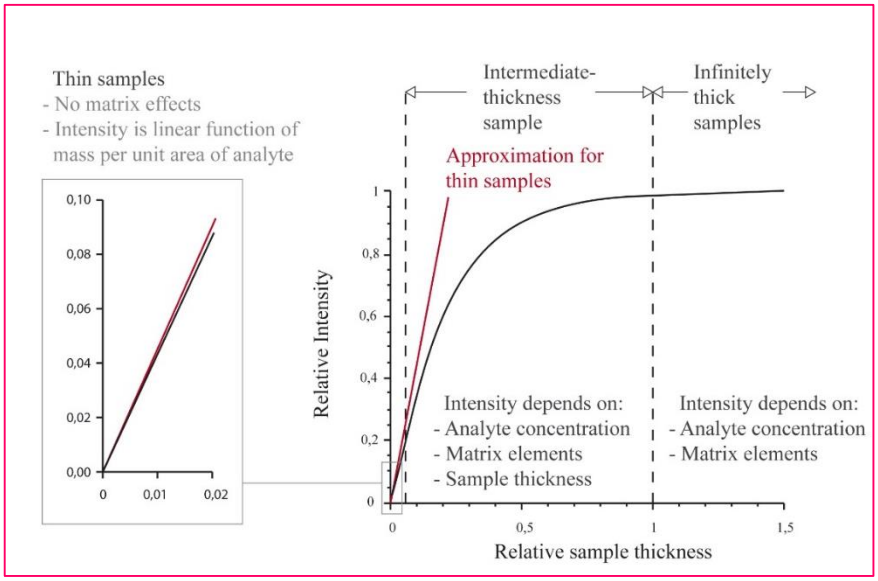

Figure 19. The general division of the sample in XRF analysis[145].

Application

The XRF is one of the most commonly used technique to analyze elemental composition in conservation science field. Being non-destructive, fast and versatile are qualities that make of XRF an optimal technique for the investigation of valuable artefacts of a large varieties of types[152] like paintings[153–156], glasses[157], photographs[136], metal object[136,158,159], wall-paper[160], prints[161] etc. New instruments, easy to operate, and intuitive software permit to obtain very useful information about the elemental composition and material distribution

across the object. A large number of measurements can be performed respecting the physical integrity of the artwork. Both, bench and portable instruments are available and allow the analysis of 2D or 3D objects of different dimension. The main limitations in the application of XRF for artwork investigation purposes are:

Limited sensitivity to low Z elements. Indeed, most of the materials analyzed are composed of light elements, such as C, Na, Mg, Al, Si, P, S and Cl;

Penetration power. Most of the artefact present complex layer-structure and the distribution in depth of the element cannot be definitely determined. Only a meticulous evaluation of the distribution across the surface of all elements and the additional use of complementary surface techniques permit a good approximation of the stratigraphy reconstruction;

Spectra interpretation. The physical features of the surfaces, the heterogeneity and the aforementioned layer-structure of the objects result in very complex spectra, not easily interpretable. The limited resolution of the spectra, in some cases, does not permit to resolve peaks with identical, or nearly identical, emission energies (e.g. mixture of pigments containing Ba Lα and Ti Kα lines or Co Kα and Fe Kβ, Pb Mα and S Kα). Furthermore, for high counts signals from heavy elements (e.g. Pb based metal alloys) may cause sum peaks that can lead to misleading interpretation[162].

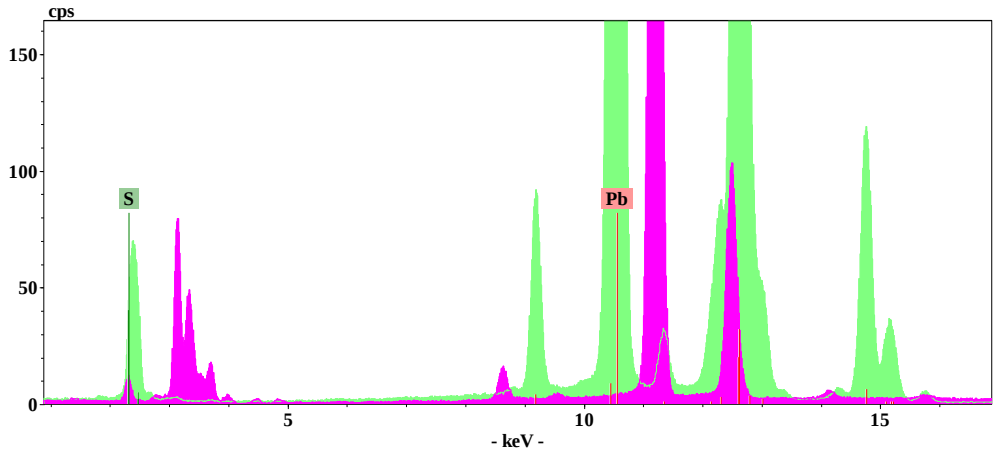

Figure 20. Overlapping of the S K and Pb M lines in XRF spectra of pigment references. Cadmium sulphide (green trace) and Lead Carbonate (magenta trace).

XR source interferences. The material used as target to produce the primary X-ray (XR source) produces its own discrete emission lines, which may coincide or be partially overlapped with the emission lines proper of the samples. (W or Rh tube). For example, the energetic line of the Hg are partially overlapped with the signal of the W source (Lα 9.9890). In this case, the less intense (Lβ 11.8240) has to be evaluated. Thus, the detection limit of the instrument for this element increases.

Object position set-up. The irradiation geometry is usually not optimal, especially for 3D objects. Although, new instruments are rather versatile and are equipped with led-focal

systems and cameras that permit to localize the point analyzed and to control the reproducibility of the measurements condition;

Calibration. The matrices investigated are complex to reproduce and normally unknown. Thus, the creation of adequate standards for quantitative analysis is often no possible. Nowadays, great efforts are undertaken to create mock-ups of known composition that could permit a better evaluation of the results obtained on different objects;

Reproducibility of the results. The variability of measurement conditions and data treatments methods hinder the comparison between data acquired in different laboratories. It is interesting to mention that a series of round-robin tests (proficiency tests) have been conducted bi-annually since 2002. As explained by *Namowicz et al*., in 2008 a set of thirteen mock-ups, consisting of both modern and traditional pigments on canvas, were analyzed by different laboratories. The test results show that the average percentage of respondents who correctly identified the key elements present in all 11 painted samples was 65%, while the average percentage of participants who provided correct interpretations of the results was only 40%[162]. Thus, the necessity to establish standard working practices and further understanding of the application of X-ray fluorescence spectroscopy was emphasized.

1.2.4 Scanning electron microscopy (SEM) coupled with Energy dispersive X-Ray spectroscopy (EDS)

Fundamental

Scanning electron microscopy (SEM) with Energy Dispersive X-Ray Analysis (EDS) is based on an electron beam that is scanned across a sample's surface. When the electrons strike the sample, different signals are generated in response. The detection of specific signals produces an image or reveals a sample's elemental composition. The three signals that provide the most relevant information in SEM are the reflection of secondary and backscattered electrons and the emission of X-rays.

Secondary electrons (SE) = Topography (superficial features)

The electrons of the sample that leave the atom with a very low kinetic energy (≥50eV) are called secondary electrons. Due to their low energy only the SE emitted by the superficial atoms of the sample are detected (<10 nm). Thus, the production of SE is strictly related to the topography of the sample. A high-resolution contrast image (spatial resolution higher than 50 Å) can be obtained because of the small diameter of the primary electron beam, and the magnification can reach 500,000x, depending on the instrument.

Backscattered electrons (BSE) = Composition and morphology (shape and size of the sample's particles)

Backscattered electrons are defined as the incident electrons that are elastically scattered by the specimen's atomic nuclei or by outer shell electrons of similar energy through an angle of more than 90°. During the collision, the electrons lose a negligible part of their energy (≤50eV) and are deflected in a wide range of angles. The production of BE depends on the atomic number (Z) of the elements encountered in the sample[163]. Elements with higher atomic numbers have more positive charges on the nucleus, and as a result, more electrons are backscattered, causing a higher signal. The image produced is the result of the contrast between the average of Z number of light (dark areas) and heavy (white areas) elements. The electrons are emitted from a certain depth in the sample, thus the spatial resolution obtained in the image is lower than the one obtained by secondary electrons. X-rays can derive from deeper in the sample than both, secondary and backscattered electrons.

X-ray micro-analysis (XRA) = elemental composition

The SEM is usually equipped with a probe that permits to measure the energies of characteristic X-rays produced due to the impact of the high energy electron beam. X-rays are generated as a result of the ejection of shell electron (low energy) by an energetic electron beam. X-rays may also be used to form maps or line profiles, showing the elemental distribution on a sample surface. These X-rays can be analyzed by either wavelength dispersive (WDS) or energy dispersive methods (EDS). WDS system permits to detect X-rays scattered off the sample based on their characteristic wavelengths. This is done by diffracting the X-rays through an analyzer crystal according to Bragg's Law[113]. The angle can be changed in order to measure elements sequentially, or multiple crystals and detectors may be arrayed around a sample for simultaneous analysis. On the other hand, the EDS system converts the energies detected in a proportional electronic signal and can provide rapid qualitative or even, with adequate standards, quantitative analysis of the elemental composition[113]. The W/EDS technique is only capable of detecting elements with $Z \geq 6$, over carbon, due to the beryllium window that permit to maintain the vacuum, but filters the X-rays emitted over this edge. The not-conductive samples have to be coated with a thin layer of electrically conductive material. The commonly used methods of coating are high voltage sputtering and evaporation. For cold sputtering, a range of coating materials such as gold (Au), gold-palladium (Au-Pd), chromium (Cr), silver (Ag), etc. may be used, while carbon is used for evaporation[164]. The spectral resolution may be different depending on the system. It is defined as the width of the peak, in eV, measured at half of the peak height (FWHM -

full width at half maximum). The smaller the resolution value, the more easily an elemental line is distinguished from other nearby X-ray line intensities. For WDS the resultion depends on the crystal and optics design, particularly collimation, as well as spacing and positional reproducibility, while for EDS it is established by the resolution of the detector. Although WDS has higher resolution (R~20-5 eV) than EDS bench set-ups (Si detector R ~129-145 eV), they are the most commonly used because they are less expensive[165].

Application

As stressed by *Schreiner at. al.,* since 1962, due to the possibility to obtain simultaneously and fast useful information about the surface topography and elemental composition distribution across very small samples made SEM-EDS one of the most commonly used and broadly available analytical tools in science conservation. Although, unlike non-invasive methods of analysis, it requires a sample to be taken. Furthermore, since the artistic materials tend to be nonconductive they need to be coated, which in some cases is not recommendable due to its irreversibility[166]. The dimensions of the sample have to be about 1mm x 100µm x 100µm and it has to be compatible with vacuum. However, some systems, like environmental scanning electron microscope (ESEM) allows examining non-conducting samples without the usual coatings by the application of a low pressure water vapour (approximately 1 Torr) in the sample chamber[167]. Due to the vacuum system, SEM/EDS enables the analysis of Na, Mg, Al and Si, which are main constituents of many artistic materials, such as earth pigments or glasses, but cannot be detected by XRF. The study of real artworks is limited by sampling opportunities; for example, paintings in good condition may not offer the opportunity to remove even the smallest flake or fragment of material, which is the minimum necessary for SEM examination. Despite these inconveniences, SEM –EDS is often used due to the possibility to study cross-sections of layer-structured materials and to obtain the elemental distribution for each layer. Furthermore, using BSE images particle size, shape, and distribution of different phases, can be established and by means of SE images changes in morphology of specific surfaces, due to e.g. degradation processes, can be investigated[167]. Such examinations provide in many cases sufficient information about the structure of the paint layers, the grain size and grain size distribution of the various pigments as well as information about varnish layers or organic binding media.

1.2.5 Inductively coupled plasma optical emission spectroscopy (ICP-OES)

The *ICP-OES* is an analytical technique that is part of the wide branch of the Optic Atomic spectroscopy. The principle of the technique is based on the release of the excess energy as

electromagnetic radiation when atoms are excited, due to thermic or electric energy absorption, caused by collision with other particles.

The spectra obtained are the result of the emissions by the excited atoms and are proportional to the energetic transitions between atom shells. The emission lines depend on the atomic structure, thus they are discrete and characteristic of each element. Furthermore, the intensity emitted is directly proportional to the concentration of the analysed element. Indeed, quantitative analysis is possible thanks to a calibration function achieved by the analysis of reference materials, which permit to establish the relation between the detected signal and the concentration of the analyte present in the samples. The mechanism of formation of ions in *ICP-OES* is a plasma discharge, in particular *Inductively coupled plasma*[168], which can be defined as a gaseous electrically conductive mixture that contains a high concentration of cations and electrons. In this case, an electron flow generated by the application of an intense electromagnetic field is converted into an argon gas flowing through the torch.

1.2.6 Inductively coupled plasma mass spectrometry (ICP-MS)

The ICP-MS use the aforementioned high temperature plasma to generate positively charged ions. The sample, introduced generally in liquid form is vaporized, atomized and ionized. When it finally arrives to approximately 6000-7000 K, it exists as exited atoms and ions, representing the elemental composition of the sample. ICP-MS is used mainly for detection of positive ions, although also negative ions are produced. Since the transportation of the latter ones is different most commercially used instruments are not designed to measure them[168]. Once the gas-phase ions have been produced, they need to be separated according to their masses, which have to be determined. The physical property of ions that is measured by a mass analyser is their mass-to-charge ratio (m/z) rather than their mass alone[169]. This characteristic permits isotope detection. Their abundance is determined by the detector, which converts the ions into electrical signals.

Application

The ICP-OES and ICP-MS are widely used in cultural heritage investigation, mainly in archaeology for metal object characterization[94,170–175]; although they imply the extraction of material from the artwork and the later dissolution of the sample. However, their use, when possible, allows the determination of a large number of elements even at low concentrations simultaneously and with high accuracy. The method is well developed and only a small amount of sample is needed for performing an analysis[170]. Indeed, the main advantages are

the low detection limit (lower for ICP-MS), the high sensitivity, and the calibration (matrix effect).

The possibility to calibrate the instrument is the key for the analytical process. It is the aspect that creates the major problem when a non-destructive approach is performed, like in the XRF quantification procedure. In addition, many other sources of errors must be also considered when an analytical method is applied, in order to know the accurancy of the results.

However, the analytical method is not exempt of errors and sources of dispersion. One of the critical steps is the sampling, which has to be optimize to limit the damage to the object, but at the same time preserving the representativity of the results and maximizing the recovery of the bulk sample. Afterwards, the sample treatment has to be performed in the most accurate manner to avoid loss of material. For this aspect, the measure of the weight is the most difficult step for the small amount of material handled. Then, for the dissolution step suitable acids have to be found that allow the total dissolution of the sample avoiding interferences during the instrument measurement. Before this step, the calibration curves have to be established selecting the element standard and the dilution factor to have an approximation as close as possible to the sample matrix. The measurement phases are also delicate. Even, the introduction of the liquid sample can be a source of dispersion and the specialized manuals go further in the explanation of the optimal set-up depending on the type of solution introduced [169,176]. However, the measurement errors can be reduced by using the internal standard method.

The high sensitivity of the technique is most useful in the cultural heritage due to the possibility to compare material within and between objects, establishing relations and patterns of distribution. A common example is the comparison between metal source/ore and metal object to determine their origin and cultural/historic context. For example, of *Chikwendu et al.* conducted an extensive study of Nigerian sources of copper, lead and tin with the main scope to identify the origin of important metal artefacts produced in the same areas. However, this study presents a high grade of uncertainty due to the high variability of the elemental concentrations, generally influenced by many factor[93].

1.3 Data treatment and multivariate methods

The most important advantage of the non-destructive analytical techniques is the possibility to acquire a large number of spectra with the aim to obtain representative results of the composition across the artwork surface. In consequence, a large and complex volume of data

is produced. Thus, the interpretation and the management of such information became very demanding due to the number of variables and relations to be analyzed. In this case, a multivariate approach is suggested. The most widely applied multivariate methods are Principal Component Analysis (PCA) and Partial Least Square regression (PLS). In the last decades their use in science conservation field has drastically increased. These methods will be employed in this thesis for midIR-FORS spectra (Chapter 2) and ICP-OES/MS data (Chapter 5) analysis. In both cases, they were key tools to facilitate and improve data observation and to establish/find trends and patterns.

1.3.1 Pre-processing

The data sets are complex and generally present noise and interferences that could be detrimental for mathematical treatment. All information not needed for data interpretation should be reduced to avoid misleading results. Thus, after creating a first matrix with all the variables to be analyzed, it is important to apply pre-treatment algorithms to optimize the data set. The selection of the algorithm depends on the nature of the data. Indeed, the FORS spectra are affected by many distortions and present variability not strictly related to the chemical composition of the specimen. Hence, the treatment of the data should/could include several steps.

Matrix reduction/variable selection

First, the model should be simplified removing the data affected by high noise and interferences. For example, the more evident interferences due to the use of calcogenite fibers, which absorb in the mid- and far-infrared regime, are the strong signals of the Se–H stretching (2200-2050, $\leq$ 900 cm^{-1}). Therefore, the first step, before applying multivariate method, is to cut off this range of wavenumbers, which the models could interpret as important due to the magnitude of the signal. Practically, once the signals attributed to the fiber are identified, a new spectra matrix can be created eliminating the wavenumber ranges/channels where these signal are located

Smoothing

The random noise that affect the data obtained from chemical spectrum analyzers can be reduced maintaining the shape and height of waveform peaks by applying some correction algorithms as for example Savizky-Golay smoothing algorithm, which was used in this work. When a series of the data contains equally spaced values $f_i \equiv f(t_i)$, where $t_i \equiv t_0 + i\Delta$

for some constant sample spacing Δ and i = ... − 2, −1, 0, 1, 2,..., the simplest type of digital filter replaces each data value f_i by a linear combination g_i of itself and some number of nearby neighbors:

$$g_i = \sum_{n=n_L}^{n_R} C_n f_i + n \quad (12)$$

where n_L is the number of points used "to the left" of a data point i, i.e. before, while n_R is the number used to the right, i.e., later[177]. The data "window" and the polynomial order have to be established in a previous step (e.g 5 points, order 0).

In case of reflectance spectra, the number of points should be carefully selected to assure that combination bands – generally very small peaks, which are important for material characterization – are not eliminated.

Standard normal variate algorithm (SNV)

The SNV is one of the algorithms designed to reduce the (physical) variability between samples due to scatter, in order to minimise the multiplicative interferences of this effect and the change of light distance [178]. It permits also to adjust baseline shifts between samples conserving relative intensity between the absorption bands of the all spectra[179–181]. The increase of signal intensity that is normally observed when a component with a higher reflectivity is detected is reduced.

SNV uses the equation: $x_{Snv} = (x_{i,k} - \bar{x}_i)/STD$ (13)

where x_{Snv} is the transformed element, $x_{i,k}$ is the original element and $\overline{x_i}$ is the mean of spectrum i. k=1,2,…,m, where m is the number of variables in the spectra, and i=1,2,…,n, where n is the number validation sets. Normalization as suggested by *Rinnan et al.* normalization can be used at both ends of differentiated or baseline correction, although it is easier to assess the effect of normalization if it is done prior to any other operation.[182]

Base line correction

The spectra measured by using remote techniques usually involve large baseline variations. A base line algorithm can be applied to subtract a polynomial baseline offset from the spectra

Normally, the first treatments to be considered are Mean centering and Autoscale. These two pre-processing methods revealed to be not useful/effective for FORS spectra treatment because they did not allow an improvement of the data. However, they were successfully applied to the ICP-OES/MS.

Mean centering

It is applied by subtracting the mean value of the data set from every component of the data set, that corresponds to the common part of the spectra, e. g. the oil binding in measurements acquired on oil paintings. It permits to obtain a more simple and interpretable regression model[183].

Autoscaling

The autoscaling procedure uses both mean centering and variance scaling and helps to remove useless variation. The formula applied to the autoscale treatment is expressed as:

$$\boldsymbol{X} = \frac{\boldsymbol{X}-\bar{\boldsymbol{X}}}{\boldsymbol{SD}(\boldsymbol{X})} \qquad (14)$$

The autoscaling permits to compare data evaluating variability and neglecting their difference in terms of magnitude. This method was not used for FORS spectra due to the magnification of the noise.

1.3.2 Principal Component Analysis (PCA)

PCA is an orthogonal linear transformation (change of the base) whose main objective is to simplify the description of the data set. This method permits to extract the most important information, reducing the original data set to few variables (principal components, PCs).[184] The PCs may be defined as mathematical variables that describe the main directions of data variance, so, they are the axes of the new base (Figure 21).

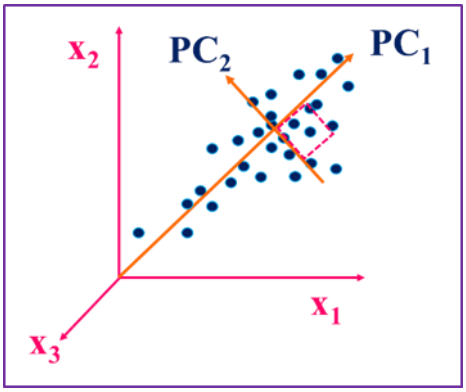

Figure 21. Graphical representation of the Principal component space.[185]

The experimental matrix notation can be expressed as **X** (structure + noise) = **T** $\mathbf{P^T}$ + **E**, where the *Loadings* $\mathbf{P^T}$ (projections) can be defined as the relationships between original variables and the principal components (e.g. $\mathbf{t_1}=\mathbf{x_1p_{11}}+\mathbf{x_2p_{21}}$, loadings of the original variables in first PC, $\mathbf{t_1}$). Instead, the *Scores* (Targets) **T** are the relationships between the samples in the space defined by the principal components. Finally, **E** is the experimental error or unexplained variances. The result of PCA are two types of information, the *scores* that are the values of the original variable in the new database, which

are normally represented as a plot that shows a map of sample on PCs space, and the *loadings* that represents the weights assigned to each original variable to form the new one (score). In the score plots, the shorter is the distance between scores, the more similar are the samples. In consequence, they are represented as groups named *clusters* (marked with circular line in the score plot of Figure 23). The identification/interpretation of the principal components, which imply the simultaneous analysis of both 'loadings' and 'scores' plots (Figure 23), permits to understand trends, patterns and outliers in the data. Further information about the method are available elsewhere.[184] Each PC explains a certain percentage of the variance of the original date.

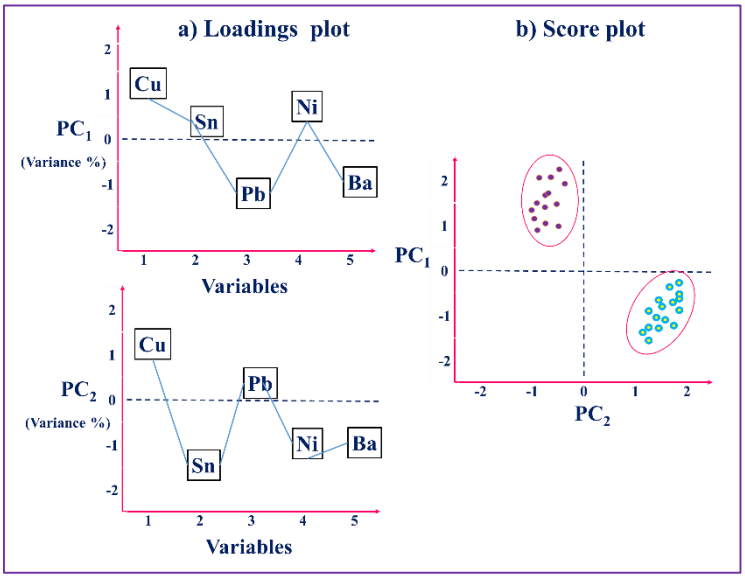

Figure 22. a) Loading plot; b) score plot PC1 vs.PC2

1.3.3 Partial Least Square (PLS)

PLS is based on the same principle of component selection as PCA with the difference that it is used as method for multivariate calibration. Indeed, it searches, unlike PCA, for a set of components (called *latent vectors*) that explain simultaneously X and Y with the constraint that these components explain as much as possible of the covariance between X and Y. Thus, PLS finds components from X that are also relevant for Y. It is followed by a regression step where the analysis of X is used to predict Y[186]. When several dependent data are available for calibration, two approaches can be used in PLS regression: either the classes are calibrated for one at a time (PLS1), or properties are calibrated at once (PLS2). Instead, Partial least squares Discriminant Analysis (PLS-DA) is a variant used when the Y permits to assign a category to each variable, normally using a 0-1 code that shows if it is or is not present in a certain component[187]. This method is similar to the cluster analysis in PCA, which attributes the sample to a certain category. However, in PLS-DA the main difference is the possibility to identify the belonging to more than one category at the same time, and thus, distinguish the individual components (included in the calibration) of a sample mixture.

1.6 References

1. Vasari, G. *Le vite de piu eccelenti pittori, scultori e architetti*. (1550).

2. Mills, J. S. & White, R. *The Organic chemistry of museum objects*. (Butterworth-Heinemann, 1994).

3. Mayer, R. *The Artist's handbook of Materials&Techniques*. 1–761 (1991).

4. Grehk, T. M., Berger, R. & Bexell, U. Investigation of the drying process of linseed oil using FTIR and ToF-SIMS. *J. Phys. Conf. Ser.* **100,** 012019 (2008).

5. Herbst, W. & Hunger, K. *Industrial Organic Pigments*. (WILEY-VCH Verlag, 2004).

6. Hunger, K. *Industrial Dyes Chemistry, Properties, Applications*. (Wiley-VCH).

7. Buxbaum, G. & Pfaff, G. *Industrial inorganic pigments*. (Wiley-VCH, 2005).

8. Ball, P., Lanza, L. & Vicentini, P. *Colore: una biografia*. (Bureau Biblioteca Univ. Rizzoli, 2004).

9. M.Bacci. Non invasive instrumentation for detection and colour control of paintings and art works. *Archeometriai Mühely* **46-50,** (2006).

10. Berrie, B. H. Prussian Blue. In: West Fitzhugh, E. (ed.), Artists' Pigment: A Handbook of Their History and Characteristics. *Artist. Pigment A Handb. Their Hist. Charact.* **3,** 191–217 (1997).

11. Bartoll, J. The early use of Prussian blue in paintings. in *9th Int. Conf. NDT Art* 25–30 (2008).

12. Miliani, C. *et al.* Original and fake blue pigments from the Church of San Francesco in Montefalco painted by Benozzo Gozzoli: a spectroscopic approach. in *Sixth Infrared Raman Users Gr. Conf.* 213–219 (Il Prato, 2005).

13. Eastaugh, N., Siddall, R., Walsh, V. & Chaplin, T. *Pigment compendium Optical Microscopy of Historical Pigments*. 415 (2004).

14. Hradil, D., Grygar, T., Hradilová, J. & Bezdička, P. Clay and iron oxide pigments in the history of painting. *Appl. Clay Sci.* **22,** 223–236 (2003).

15. van, der W. Microspectroscopic analysis of traditional oil paint (MolArt; 7), PhD Thesis. *Univ. Amsterdam* 32–34 (2002).

16. Lazzari, M. & Chiantore, O. Drying and oxidative degradation of linseed oil. **65,** 303–313 (1999).

17. Weerd, J. Van Der, Loon, A. Van & Boon, J. J. FTIR Studies of the Effects of Pigments on the Aging of Oil FTIR on Studies the Aging of the Effects of Oil of Pigments. **50,** 3–22 (2012).

18. Berg, J. D. J. van den. Analytical chemical studies on traditional linseed oil paints. *Univ. Amsterdam* (2002).

19. Tumosa, C. S. & Mecklenburg, M. F. The influence of lead ions on the drying of oils. *Rev. Conserv.* **6,** 39–49 (2005).

20. Schaeffer, T. T. *Effects of Light on Materials in research in conservation*. (2001).

21. Miliani, C., Rosi, F., Daveri, A. & Brunetti, B. Reflection infrared spectroscopy for the non-invasive in situ study of artists' pigments. *Appl. Phys. A Mater. Sci. Process.* **106,** 295–307 (2012).

22. Fox, M. *Optical Properties of Solids*. 262 (2007).

23. Derrick, M. R., Stulik, D. & Landry, J. M. *Infrared Spectroscopy in conservation Science Scientific tools for conservation*. (The Getty Conservation Institute, 1999).

24. Johnston-feller, R. *Color Science in the Examination of Museum Objects Nondestructive Procedures*. (2001).

25. Van Nimmen, E. *et al.* FT-IR spectroscopy of spider and silkworm silks. Part I. Different sampling techniques. *Vib. Spectrosc.* **46,** 63–68 (2008).

26. V., B. & Torrent, J. Kubelka-Munk theory to study the influence of iron oxides on soil colour. *J. soil Sci.* **37,** 499–510 (1986).

27. M. Milosevic, S. L. B. A Review of FT-IR Diffuse Reflection Sampling Considerations. *Appl. Spectrosc.* **37,** 347–364 (2002).

28. Vahur, S., Teearu, A. & Leito, I. ATR-FT-IR spectroscopy in the region of 550-230 cm-1 for identification of inorganic pigments. *Spectrochim. Acta. A. Mol. Biomol. Spectrosc.* **75,** 1061–72 (2010).

29. VAHUR, S. Expanding the possibilities of ATR-FT-IR spectroscopy in determination of inorganic pigments. (2010).

30. Eastaugh, N., Siddall, RuthWalsh, V. & Chaplin, T. *Pigment Compendium: A Dictionary of Historical Pigments*. 202 (Elsevier, 2006).

31. Otero, V. *et al.* Characterisation of metal carboxylates by Raman and infrared spectroscopy in works of art. *J. Raman Spectrosc.* n/a–n/a (2014). doi:10.1002/jrs.4520

32. Keune, K. Binding medium, pigments and metal soaps characterised and localised in paint cross-sections (MolArt; 11), PhD Thesis. *Univ. Amsterdam* 1–7 (2005).

33. Robinet, L. & Corbeil, M. The Characterization of Metal Soaps. *Stud. Conserv.* **48,** 23–40 (2003).

34. Arrizabalaga, I., Gómez-Laserna, O., Aramendia, J., Arana, G. & Madariaga, J. M. Determination of the pigments present in a wallpaper of the middle nineteenth century: The combination of mid-diffuse reflectance and far infrared spectroscopies. *Spectrochim. Acta. A. Mol. Biomol. Spectrosc.* **124C,** 308–314 (2014).

35. Rosi, F. *et al.* A non-invasive XRF study supported by multivariate statistical analysis and reflectance FTIR to assess the composition of modern painting materials. *Spectrochim. Acta Part A Mol. Biomol. Spectrosc.* **71,** 1655–1662 (2009).

36. Miliani, C., Rosi, F., Burnstock, A., Brunetti, B. G. G. & Sgamellotti, A. Non-invasive in-situ investigations versus micro-sampling: a comparative study on a Renoirs painting. *Appl. Phys. A* **89,** 849–856 (2007).

37. Kuckova, S., Hynek, R., Nemec, I., Kodicek, M. & Jehlicka, J. Critical comparison of spectrometric analyses of non-mineral blue dyes and pigments used in artworks. *Sect. Title Hist. Educ. Doc.* **44,** 963–967 (2012).

38. Burnstock, A., Reissner, E., Richardson, C. & Berg, K. J. Van Den. Inorganic Materials from Paintings and Watercolours By Paul Cézanne from The Courtauld Gallery Using two Methods of Non-Invasive Portable XRF with Light Microscopy and SEM / EDX Spectroscopy. in *9th Int. Conf. NDT Art, Jerusalem Isr. 25-30 May 2008* 25–30 (2008).

39. Haswell, R., Carlyle, L. & Mensch, K. T. J. Original Paper Van Gogh ' s Painting Grounds : Quantitative Determination of Bulking Agents (Extenders) Using SEM = EDX. **167,** 163–167 (2006).

40. Lake, S. *et al. Artists' Pigments A handbook of their history and chractacteristics. Vol. 4*. 224 (2007).

41. Hedges, R. E. M. A Review of Current Approaches in the Pretreatment of Bone. *Radiocarbon* **34,** 279–291 (1992).

42. Tomasini, E. P., Halac, E. B., Reinoso, M., Di Liscia, E. J. & Maier, M. S. Micro-Raman spectroscopy of carbon-based black pigments. *J. Raman Spectrosc.* **43,** 1671–1675 (2012).

43. Vila, A., Ferrer, N. & García, J. F. Chemical composition of contemporary black printing inks based on infrared spectroscopy: basic information for the characterization and discrimination of artistic prints. *Anal. Chim. Acta* **591,** 97–105 (2007).

44. Samain, L. *et al.* Fading of modern Prussian blue pigments in linseed oil medium. *J. Anal. At. Spectrom.* **26,** 930 (2011).

45. Hamerton, I., Tedaldi, L. & Eastaugh, N. A systematic examination of colour development in synthetic ultramarine according to historical methods. *PLoS One* **8,** e50364 (2013).

46. Plesters, J. Ultramarine blue, Natural and Artificial. *Artist. Pigment. A Handb. Their Hist. Charact.* **2,** 37–65 (1993).

47. Miliani, C., Daveri, A., Brunetti, B. G. & Sgamellotti, A. CO2 entrapment in natural ultramarine blue. *Chem. Phys. Lett.* **466,** 148–151 (2008).

48. Smith, G. D. & Robert, K. I. The presence of trapped carbon dioxide in lapis lazuli and its potential use in geo-sourcing natural ultramarine pigment. **10,** 415–421 (2009).

49. Ballirano, P. & Maras, A. Mineralogical characterization of the blue pigment of Michelangelo's fresco "The Last Judgment."*Amarican Mineral.* **91,** 997–1005 (2006).

50. Bacci, M. & Picollo, M. Non-Destructive Spectroscopic Detection of Cobalt (II) In Paintings and Glass. *Stud. Conserv.* **41,** 136–144 (1996).

51. Rose, F. & Woringer, P. *Die mineralfarben und die durch mineralstoffe erzeugten färbungen*. 395 (O. Spanner, 1916).

52. Mahon, D., Centeno, S. & Robinson, E. Study of John Singer Sargent ' s Pierre Gautreau Portrait of Madame Pierre Gautreau. *Metrop. MUSEUM J.* **40,** (2005).

53. Vandenabeele, P., Hardy, A., Edwards, H. G. M. & Moens, L. Evaluation of a Principal Components-Based Searching Algorithm for Raman Spectroscopic Identification of Organic Pigments in 20th Century Artwork. *Appl. Spectrosc.* **55,** 525–533 (2001).

54. Lottici, P. P. μ-Raman pigments analysis of a painting with the signature "Picasso."in *B. Abstr. RAA-2011 6th Int. Congr. Appl. Raman Spectrosc. (Parm, 5-8 Settembre 2011)* 175–176 (Timeo, 2011). at <http://books.google.de/books?id=oPgAywAACAAJ>

55. Defeyt, C. & Strivay, D. PB15 as 20th and 21st Artists' Pigments:Conservation Concerns. *e-Preserv. Sci.* **11,** 6–14 (2014).

56. Defeyt, C. *et al.* Contribution to the identification of α-, β- and ε-copper phthalocyanine blue pigments in modern artists' paints by X-ray powder diffraction, attenuated total reflectance micro-fourier transform infrared spectroscopy and micro-Raman spectroscopy. *J. Raman Spectrosc.* **43,** 1772–1780 (2012).

57. Manuel, P., Ruis, I., Andrikopoulos, K. S., Ramos, P. M. & Ruisánchez, I. Micro-Raman and X-ray fluorescence spectroscopy data fusion for the classification of ochre pigments. *Talanta* **75,** 926–936 (2008).

58. Aliatis, I. *et al.* Green pigments of the Pompeian artists' palette. *Spectrochim. Acta. A. Mol. Biomol. Spectrosc.* **73,** 532–8 (2009).

59. Mazzocchin, G. a, Agnoli, F., Mazzocchin, S. & Colpo, I. Analysis of pigments from Roman wall paintings found in Vicenza. *Talanta* **61,** 565–72 (2003).

60. Balakhnina, I. a., Brandt, N. N., Kimberg, Y. S., Rebrikova, N. L. & Chikishev, a. Y. Variations in the IR spectra of yellow ochre due to mixing with binding medium and drying. *J. Appl. Spectrosc.* **78,** 183–188 (2011).

61. Kühn, H. & Curran, M. in *Artist. Pigment A Handb. Their Hist. Charact. Vol.1* (Feller, R. L.) 187–218 (1986).

62. Van der Snickt, G. *et al.* Characterization of a degraded cadmium yellow (CdS) pigment in an oil painting by means of synchrotron radiation based X-ray techniques. *Anal. Chem.* **81,** 2600–10 (2009).

63. Mass, J. *et al.* The photodegradation of cadmium yellow paints in Henri Matisse's Le Bonheur de vivre (1905–1906). *Appl. Phys. A* **111,** 59–68 (2013).

64. Fiedler, I. & Bayard, M. *Artists' pigments : a handbook of their history and characteristics Vol.1*. 65–108. (in Artists' Pigments: A Handbook of Their History and Characteristics, Cambridge University Press and National Gallery of Art, Cambridge, 1986, pp. 65–108.I. Fiedler and M. Bayard, in Artists' Pigments: A Handbook of Their History and Characteristics, ed., 1986).

65. Cesaratto, A. *et al.* Analysis of cadmium-based pigments with time-resolved photoluminescence. *Anal. Methods* **6,** 130–138 (2014).

66. Monico, L. *et al.* Degradation process of lead chromate in paintings by Vincent van Gogh studied by means of spectromicroscopic methods. 3. Synthesis, characterization, and detection of different crystal forms of the chrome yellow pigment. *Anal. Chem.* **85,** 851–9 (2013).

67. Bouvier, P. L. *Handbuch der Ölmalerei*. 48,63 (1910).

68. Burgio, L., Clark, R. J. H. & Hark, R. R. Spectroscopic investigation of modern pigments on purportedly medieval miniatures by the Spanish Forger. *J. Raman Spectrosc.* **40,** 2031–2036 (2009).

69. Newman. in *Artist. Pigment. A Handb. their Hist. Charact. Vol. 3* (W.FitzHugh., ed. E.) (1997).

70. Nel, P., Lau, D., Hay, D. & Wright, N. Non-destructive micro-X-ray diffraction analysis of painted artefacts: Determination of detection limits for the chromium oxide–zinc oxide matrix. *Nucl. Inst.and Methods Phys. Res. B* **251,** 489–495 (2006).

71. in *Artist. Pigment. A Handb. Their Hist. Charact. Vol.1* (FitzHugh, E. W.) 109–139 (1986).

72. Keune, K. & Boon, J. J. Analytical imaging studies clarifying the process of the darkening of vermilion in paintings. *Anal. Chem.* **77,** 4742–50 (2005).

73. Miguel, C., Claro, A., Goncalves, A. P., Muralha, V. S. F. & Melo, M. J. A study on red lead degradation in a medieval manuscript Lorvao Apocalypse (1189). *J. Raman Spectrosc.* **40,** 1966–1973 (2009).

74. Aze, S., Vallet, J.-M., Baronnet, A. & Grauby, O. The fading of red lead pigment in wall paintings: tracking the physico-chemical transformations by means of complementary micro-analysis techniques. *Eur. J. Mineral.* **18,** 835–843 (2006).

75. Stulik, D. C. & Kaplan, A. The Atlas of Analytical Signatures of Photographic Processes SALT PRINT. *Getty Conserv. Inst.* 1–19 (2013).

76. *Focal Encyclopedia of Photography*. 30–36 (2007).

77. Barro, L. & Kennedy, N. W. Gustave Le Gray's Salted Paper Prints. in *Trienn. Meet. ICOM Comm. Conserv.* **2,** 533–540 (2005).

78. Eremin, K., Tate, J. & Berry, J. in *Conserv. Sci.* (Townsend, J. H., Eremin, K. & Adriaens, A.) (2003).

79. Lavédrine, B. Photographs of the past. Process and Preservation. 340 (2009).

80. Vila, A. *et al.* Understanding the gum dichromate process in pictorialist photographs : A literature review and technical study. *Stud. Conserv.* **58,** (2013).

81. Stulik, D. C. & Herant P. Khanjian. in *Conserv. Sci.* (Joyce H. Townsend, Katherine Eremin, A. A. (eds)) 188–194 (2003).

82. Haist, G. *Modern Photographic Processing: v. 1*. 559–663 (2000).

83. Herring, R. *Paper & paper making, ancient and modern.* 100 (1856).

84. Weaver, G. A Guide to Fiber-Base Gelatin Silver Print Condition and Deterioration.

85. *Issues in The Conservation of photographs*. (2010).

86. Goffer, Z. *Archaeological Chemistry, John*. (1980).

87. Walaszek, D. *et al.* Metallurgical and chemical characterization of copper alloy reference materials within laser ablation inductively coupled plasma mass spectrometry: Method development for minimally-invasive analysis of ancient bronze objects. *Spectrochim. Acta Part B At. Spectrosc.* **79-80,** 17–30 (2013).

88. Bugoi, R., Constantinescu, B., Popescu, A. D. & Munnik, F. Archaeometallurgical Studies of Bronze Age Objects from the Romanian Cultural Heritage. *Rom. Reports Phys.* **65,** 1234–1245 (2013).

89. Scott, D. A. *Metallography and Microstructure of Ancient and Historic Metals*. 1–155 (1991).

90. Campbell, J. *Complete Casting Handbook : Metal Casting Processes, Techniques and Design*. 1–1130 (2011).

91. Davis, J. R. *Handbook: Copper and Copper Alloys*. 652 (2001).

92. Scott, D. A. *Metallography and Microstructure of Ancient and Historic Metals*. (1991).

93. Chikwendu, V. E., Craddok, P. T., Farquhar, R. M., Shaw, T. & Umeji, A. C. Nigerian Sourses of Copper, Lead and Tin for The Igbo-Ukwu Bronzes. *Archaeometry* **31,** 27–36 (1989).

94. Young, M. L. *et al.* Matisse to Picasso: a compositional study of modern bronze sculptures. *Anal. Bioanal. Chem.* **395,** 171–84 (2009).

95. Ospitali, F. *et al.* The characterization of Sn-based corrosion products in ancient bronzes: a Raman approach. *J. Raman Spectrosc.* **43,** 1596–1603 (2012).

96. Source, R. E. S. Development of Bronze Casting in Italy at the End of the Quattrocento. *Metrop. Museum J.* **16,** 87–116 (2014).

97. Quintero, H. Physico-Chemical Research of Cultural Heritage Materials Using Microanalytical Methods. (2009).

98. Taşliçukur, Z., Altuğ, G. S. ., Polat, Ş., Atapek, Ş. . H. & Türedi, E. A Microstructural Study on CuSn10 Bronze Produced by Sand and Investment Casting Techniques. in *Met. 2012* (2012).

99. Munnik, F., Sjöland, K. A., Vittiglio, G., Ingelbrecht, C. & Wätjen, U. Nuclear microprobe study of metal segregation in quaternary bronze. *Nucl. Instruments Methods Phys. Res. Sect. B Beam Interact. with Mater. Atoms* **158,** 281–286 (1999).

100. Halvaee, a & Talebi, a. Effect of process variables on microstructure and segregation in centrifugal casting of C92200 alloy. *J. Mater. Process. Technol.* **118,** 122–126 (2001).

101. Weinberg, F. & Chalmers, B. Further Observations on Dendritic Growth in Metals. *Can. J. Phys.* **30,** 488–502

102. GUNGOR, M. N. A Statistically Significant Experimental Technique for Investigating Microsegregation in Cast Alloys. *Metall. Trans.* **20A,** 2529–2533 (1989).

103. Copper development association. at <http://www.copper.org/resources/properties/microstructure/>

104. Pisarek, B. P. Model of Cu-Al-Fe-Ni Bronze Crystallization. *Arch. Foundry Eng.* **13,** 72–79 (2013).

105. Beckermann, C. in *Encycl. Mater. Sci. Technol.* 4733–4738 (Elsevier, 2001). doi:10.1016/B0-08-043152-6/00824-X

106. Fink, C. G. & Kopp, A. H. Ancient Egyptian Antimony Plating on Copper Objects: A Rediscovered Ancient Egyptian Craft. *Metrop. Museum Stud.* **4,** 163–167 (1933).

107. Youdelis, W. V. Inverse segregation in aluminum-copper alloys. (1956).

108. Craddock, P. T. & Picton, J. Medieval Copper Alloy Production and West African Bronze Analyses - PART II. *Archaeometry* **28,** 3–32 (1986).

109. NIST Standard Reference Database. at <http://www.nist.gov/srd/nist31.cfm>

110. Hughes, M. J., Northover, J. P. & Staniaszek, B. E. P. Problems in the Analysis of Leaded Bronze Alloys In Ancient Artefact. *Oxford J. Archaeol.* **1,** 359–364 (1982).

111. Janssens, K., Dik, J., Cotte, M. & Susini, J. Photon-Based Techniques for Nondestructive Subsurface Analysis of Painted Cultural Heritage Artifacts. *Acc. Chem. Res.* **43,** 814 (2009).

112. Lang, J. & Middleton, A. *Radiography of Cultural Material*. 1–19 (Elsevier Butterworth-Heinemann, 2005).

113. Friel, J. J. *X-ray and image analysis in electron microscopy*. 97 (1995).

114. Van Asperen de Boer, J. R. Infrared reflectography: a method for the examination of paintings. *Appl. Opt.* **7,** 1711–4 (1968).

115. Daffara, C., Pampaloni, E., PEZZATI, L., Barucci, M. & FONTANA, R. Scanning multispectral IR reflectography SMIRR: an advanced tool for art diagnostics. *Acc. Chem. Res.* **43,** 847–56 (2010).

116. Coates, J. in *Encycl. Anal. Chem.* (Meyers, R. A.) 10815–10837 (John Wiley& Sons Ltd, 2000).

117. Stuart, B. & Preface, S. *Infrared Spectroscopy: Fundamentals and Applications*. *Infrared Spectrosc. Fundam. Appl.* **8,** 1–13 (2004).

118. Jakob, P. & Persson, B. N. J. Infrared spectroscopy of overtones and combination bands. *J. Chem. Phys.* **109,** 8641 (1998).

119. Ferrer, N. in *Handb. Instrum. Tech. Mater. Chem. Biosci. Res.* 1–3 (2012).

120. Griffiths, P. R. & Haseth, J. A. *"Fourier Transform Infrared Spectrometry" 2ed*. *"Fourier Transform Infrared Spectrom. Second Ed. P. R. Griffiths J. A. Haseth Wiley-Interscience, New York, April 2007 ISBN-13 978-0-471-19404-0* 277–279 (Wiley, 2007).

121. Search, H., Journals, C., Contact, A., Iopscience, M. & Address, I. P. Kramers-Kronig analysis of reflection data. *Appl. Phys.* **16,** (1965).

122. Fuller, M. P. & Griffiths, P. R. Diffuse Reflectance Measurements by Infrared Fourier Transform Spectrometry. *Anal. Chem.* **50,** 1906–1910 (1978).

123. Rosi, F. *et al.* On the use of overtone and combination bands for the analysis of the CaSO4-H2O system by mid-infrared reflection spectroscopy. *Appl. Spectrosc.* **64,** 956–963 (2010).

124. Yang, L. & Kruse, B. Revised Kubelka–Munk theory. I. Theory and application. *Opt. Soc. Am. A* **21,** 1933–1941 (2004).

125. Casadio, F. & Toniolo, L. The analysis of polychrome works of art: 40 years of infrared spectroscopic investigations. *J. Cult. Herit.* **2,** 71–78 (2001).

126. Aucouturier, M. & Darque-Ceretti, E. The surface of cultural heritage artefacts: physicochemical investigations for their knowledge and their conservation. *Chem. Soc. Rev.* **36,** 1605–21 (2007).

127. Bacci, M. Fibre optics applications to works of art. *Proc. 2nd Eur. Conf. Opt. Chem. Sensors Biosens.* **29,** 190–196 (1995).

128. Legrand, S., Alfeld, M., Vanmeert, F., De Nolf, W. & Janssens, K. Macroscopic Fourier transform infrared scanning in reflection mode (MA-rFTIR), a new tool for chemical imaging of cultural heritage artefacts in the mid-infrared range. *Analyst* **139,** 2489–98 (2014).

129. Kahrim, K. *et al.* The application of in situ mid-FTIR fibre-optic reflectance spectroscopy and GC–MS analysis to monitor and evaluate painting cleaning. *Spectrochim. Acta Part A Mol. Biomol. Spectrosc.* **74,** 1182–1188 (2009).

130. Miliani, C. *et al.* In situ non-invasive investigation on the painting techniques of early Meissen Stoneware. *Spectrochim. Acta Part A Mol. Biomol. Spectrosc.* **73,** 587–592 (2009).

131. Rosi, F. *et al.* Non-invasive identification of organic materials in wall paintings by fiber optic reflectance infrared spectroscopy: a statistical multivariate approach. *Anal. Bioanal. Chem.* **395,** 2097–2106 (2009).

132. Ploeger, R., Scalarone, D., Chiantore, O. & Surfaces, N. Non-Invasive Mid-Infrared Fibre Optic Reflectance Spectroscopy Analysis of Painted Glass Magic Lantern Plates. in *9th Int. Conf. NDT Art, Jerusalem Isr. 25-30 May 2008* 25–30 (2008).

133. Salvadó, N. *et al.* Identification of copper-based green pigments in Jaume Huguet's Gothic altarpieces by Fourier transform infrared microspectroscopy and synchrotron radiation X-ray diffraction. *J. Synchrotron Radiat.* **9,** 215–222 (2002).

134. Joseph, E. *et al.* Performance evaluation of mapping and linear imaging FTIR microspectroscopy for the characterisation of paint cross sections. *Anal. Bioanal. Chem.* **396,** 899–910 (2010).

135. Christensen, M. C. FT-IR Techniques for studying the composition and degradation of Photographic Materials. 1–14 (2007).

136. Vila, A. & Centeno, S. FTIR, Raman and XRF identification of the image materials in turn of the 20th century pigment-based photographs. *Microchem. J.* **106,** 255–262 (2013).

137. Buti, D., Rosi, F., Brunetti, B. G. & Miliani, C. In-situ identification of copper-based green pigments on paintings and manuscripts by reflection FTIR. *Anal. Bioanal. Chem.* **405,** 2699–711 (2013).

138. Bruni, S., Caglio, S., Guglielmi, V. & Poldi, G. The joined use of n.i. spectroscopic analyses – FTIR, Raman, visible reflectance spectrometry and EDXRF – to study drawings and illuminated manuscripts. *Appl. Phys. A* **92,** 103–108 (2008).

139. Delaney, J. K. *et al.* Use of imaging spectroscopy, fiber optic reflectance spectroscopy, and X-ray fluorescence to map and identify pigments in illuminated manuscripts. *Stud. Conserv.* **59,** 91–101 (2014).

140. Bacci, M. *et al.* Detection of alteration products in artworks by non-destructive spectroscopic analysis. in *MRS Proceedings, 352* **352,** 153–159 (1995).

141. Nevin, A. *et al.* The identification of copper oxalates in a 16th century Cypriot exterior wall painting using micro FTIR, micro Raman spectroscopy and Gas Chromatography-Mass Spectrometry. *J. Cult. Herit.* **9,** 154–161 (2008).

142. Monico, L., Rosi, F., Miliani, C., Daveri, A. & Brunetti, B. G. Non-invasive identification of metal-oxalate complexes on polychrome artwork surfaces by reflection mid-infrared spectroscopy. *Spectrochim. Acta. A. Mol. Biomol. Spectrosc.* **116,** 270–80 (2013).

143. Vagnini, M. *et al.* FT-NIR spectroscopy for non-invasive identification of natural polymers and resins in easel paintings. *Anal. Bioanal. Chem.* **395,** 2107–18 (2009).

144. Chemistry, A. & Dr . Alan RyderMermet, K. XRF Spectroscopy. 1–19

145. *X-Ray Spectroscopy*. 142 (InTech, 2012). doi:10.5772/1422

146. NPL (Nationa physical Laboratory). Tables of Physical & Chemical Constants 4.2.1 X-ray absorption edges, characteristic X-ray lines and fluorescence yields. *Kaye Laby Online version 1.0* (1995). at <www.kayelaby.npl.co.uk>

147. Janssens, K. in *Handb. Spectrosc.* (Gauglitz, G. & Vo-Dinh, T.) 366–420 (2003).

148. Rousseau, R. M. Detection Limit and Estimate of Uncertainty of Analytical XRF Results. *rigaku J.* **18,** 33–47 (2001).

149. Espen, P. J. M. v.; Janssens, K. *In Handbook of X-ray Spectrometry*. 224 (1993).

150. *Handbook of Practical X-Ray Fluorescence Analysis*. 16–17 (2006).

151. Barrett, T., Shannon, R., Wade, J. & Lang, J. in *Stud. Archaeol. Sci. Handheld XRF Art Archaeol.* (Shugar, A. N. & L. Mass, J.) 191 – 214 (2012).

152. Janssens, K. *et al.* Use of Microscopic XRF for Non-destructive Analysis in Art and Archaeometry. **91,** 73–91 (2000).

153. Ricci, C. *et al.* The Perugino's palette: integration of an extendedin situ XRF study by Raman spectroscopy. *J. Raman Spectrosc.* **35,** 616–621 (2004).

154. Šmit, Ž., Janssens, K., Proost, K. & Langus, I. Confocal μ-XRF depth analysis of paint layers. *Nucl. Instruments Methods Phys. Res. Sect. B Beam Interact. with Mater. Atoms* **219-220,** 35–40 (2004).

155. Van de Voorde, L. *et al.* Non-destructive in situ study of “Mad Meg” by Pieter Bruegel the Elder using mobile X-ray fluorescence, X-ray diffraction and Raman spectrometers. *Spectrochim. Acta Part B At. Spectrosc.* **97,** 1–6 (2014).

156. Rosi, F., Miliani, C., Borgia, I., Brunetti, B. & Sgamellotti, A. Identification of nineteenth century blue and green pigments by in situ x-ray fluorescence and micro-Raman spectroscopy. *J. Raman Spectrosc.* **35,** 610–615 (2004).

157. Jembrih-Simbürger, D. *et al.* The colour of silver stained glass - analytical investigations carried out with XRF, SEM/EDX, TEM, and IBA. *J. Anal. At. Spectrom.* **17,** 321–328 (2002).

158. Smith, Dylan (National Gallery of Art, Washington, D. The application of alloy analysis to questions of attribution: Giovanni Francesco Susini and the workshop of Gianbologna. in *Met. 2010 - Proceedings Interim Meet. ICOM-CC Met. Work. Gr.* (Mardikian, Paul; Chemello, Claudia; Watters, Christopher; Hull, P.) 256–263 (2010).

159. Šatović, D., Desnica, V. & Fazinić, S. Use of portable X-ray fluorescence instrument for bulk alloy analysis on low corroded indoor bronzes. *Spectrochim. Acta Part B At. Spectrosc.* **89,** 7–13 (2013).

160. Castro, K., Pérez-Alonso, M., Rodríguez-Laso, M. D., Etxebarria, N. & Madariaga, J. M. Non-invasive and non-destructive micro-XRF and micro-Raman analysis of a decorative wallpaper from the beginning of the 19th century. *Anal. Bioanal. Chem.* **387,** 847–60 (2007).

161. Striova, J. *et al.* Non-destructive and non-invasive analyses shed light on the realization technique of ancient polychrome prints. *Spectrochim. Acta. A. Mol. Biomol. Spectrosc.* **73,** 539–45 (2009).

162. Namowicz, C., Trentelman, K. & Mcglinchey, C. XRF of Cultural Heritage Materials: Round-Robin IV - Paint On Canvas. *Powder Diffr.* **24,** 124–129 (2009).

163. Cortadellas, N., Fernández, E. & Garcia, A. in *Handb. Instrum. Tech. Mater. Chem. Biosci. Res.* (Seoane, J. R. & Llovet Ximenes, X.) (Centres Científics i Tecnològics. Universitat de Barcelona, 2012). at <http://diposit.ub.edu/dspace/handle/2445/32166>

164. Sarkar, S. L., Aimin, X. & Jana, D. *Handbook of Analytical Techniques in Concrete Science and Technology*. *Handb. Anal. Tech. Concr. Sci. Technol.* 231–274 (Elsevier, 2001).

165. Goldstein, J. *Scanning electron microscopy and X-ray microanalysis*. (Springer, 2003).

166. House, S., History, T. N. & Road, C. Scanning electron microscopy techniques for imaging materials from paintings. 202–231 (2000).

167. Schreiner, M., Melcher, M. & Uhlir, K. Scanning electron microscopy and energy dispersive analysis : applications in the field of cultural heritage. *Anal. Bioanal. Chem.* **387,** 737–747 (2007).

168. Thomas, R. TUTORIAL A Beginner ’ s Guide to ICP-MS. *Spectrosc. Tutor.* **16,** 26–28 (2001).

169. Hoffmann, E. de & Stroobant, V. *Mass Spectrometry*. 243–271 (2007).

170. Trampuž Orel, N. & Drglin, T. ICP-AES comparative study of some Late Bronze Age hoards: Evidence for low impurity bronzes in the Eastern Alps. *Nucl. Instruments Methods Phys. Res. Sect. B Beam Interact. with Mater. Atoms* **239,** 44–50 (2005).

171. Smith, K., Horton, K., Watling, R. J. & Scoullar, N. Detecting art forgeries using LA-ICP-MS incorporating the in situ application of laser-based collection technology. *Talanta* **67,** 402–13 (2005).

172. Zupan, J., Klemenc, S. & Budic, B. Statistical evaluation of data obtained by inductively coupled plasma atomic emission spectrometry (ICP-AES) for archaeological copper ingots 1. *Anal. Chim. Acta* **389,** 141–150 (1999).

173. De Wannemacker, G., Vanhaecke, F., Moens, L., Van Mele, A. & Thoen, H. Lead isotopic and elemental analysis of copper alloy statuettes by double focusing sector field ICP mass spectrometry. *J. Anal. At. Spectrom.* **15,** 323–327 (2000).

174. Young, M. L., Casadio, F., Marvin, J., Chase, W. T. & Dunand, D. C. An Ancient Chinese Bronze Fragment Re-Examined after 50 Years: Contributions from Modern and Traditional Techniques. *Archaeometry* **6,** 1015–1043 (2010).

175. Holley, E. a., James McQuillan, a., Craw, D., Kim, J. P. & Sander, S. G. Mercury mobilization by oxidative dissolution of cinnabar (α-HgS) and metacinnabar (β-HgS). *Chem. Geol.* **240,** 313–325 (2007).

176. Gaines, P. Sample Introduction for ICP-MS.

177. Description, S. in *Numer. RECIPES C ART Sci. Comput.* 650–655 (1992).

178. Azzouz, T., Puigdomenech, A., Aragay, M. & Tauler, R. Comparison between different data pre-treatment methods in the analysis of forage samples using near-infrared diffuse reflectance spectroscopy and partial least-squares multivariate calibration method. *Anal. Chim. Acta* **484,** 121–134 (2003).

179. Muehlethaler, C., Massonnet, G. & Esseiva, P. The application of chemometrics on Infrared and Raman spectra as a tool for the forensic analysis of paints. *Forensic Sci. Int.* **209,** 173–182 (2011).

180. Fearn, T., Riccioli, C., Garrido-Varo, A. & Guerrero-Ginel, J. E. On the geometry of SNV and MSC. *Chemom. Intell. Lab. Syst.* **96,** 22–26 (2009).

181. Rinnan, Å. *et al.* Chapter 2 - Data Pre-processing. *Infrared Spectrosc. Food Qual. Anal. Control* 29–50 (2009). doi:10.1016/B978-0-12-374136-3.00002-X

182. Rinnan, Ä., Berg, F. Van Den & Engelsen, S. B. Review of the most common pre-processing techniques for near-infrared spectra. **28,** (2009).

183. *Handbook of Near-Infrared Analysis, Third Edition*. 208–210 (2007).

184. Massart, L. & Vandeginste, B. *Handbook of Qualimetrics Part A/B*. 519–556 (1991).

185. Tauler, R. Introduction to Chemometrics. (2011).

186. Abdi, H. Partial least squares regression and projection on latent structure regression (PLS Regression). *John Wiley Sons, Inc* (2010). doi:10.1002/wics.051

187. Galtier, O. *et al.* Comparison of PLS1-DA, PLS2-DA and SIMCA for classification by origin of crude petroleum oils by MIR and virgin olive oils by NIR for different spectral regions. *Vib. Spectrosc.* **55,** 132–140 (2011).

Chapter 2

Evaluation of micro- and non-destructive analytical techniques for oil painting investigation.

Context

This chapter collect three articles focused on the evaluation of analytical techniques when applied for artwork characterization purposes. Two micro-destructive techniques, SEM-EDS and micro-FTIR and the non-destructive midIR-FORS have been tested, in terms of detection limit and reproducibility. Moreover, it have been discussed the use and utility of multivariate method, such as PCA and PLS-DA, as complementary tools for reflectance spectra management.

2.1 Determination of detection limits for SEM-EDS and m-FTIR analysis of artwork

Anal Bioanal Chem (2011) 400:2241–2251
DOI 10.1007/s00216-011-4881-y

ORIGINAL PAPER

Determination of detection limits for SEM-EDS and m-FTIR analysis of artwork

C. Sessa · A. Vila · J. F. García

Received: 28 December 2010 / Revised: 1 March 2011 / Accepted: 7 March 2011 / Published online: 14 April 2011

Abstract Scanning electron microscopy and energy-dispersive X-ray spectroscopy (SEM-EDS) and micro-Fourier transform infrared (m-FTIR) spectroscopy are two of the primary analytical techniques used for the characterisation of artwork (Casadio and Toniolo, *J. Cult. Herit.* 2:71–78, 2001; Bruni et al., *Vibr. Spectrosc.* 20:15–25, 1999; Bouchard et al., *e-Preserv. Sci*. 6:27–37, 2009). Despite wide application of these techniques, no studies have been performed to evaluate their detection limits for this type of analysis. The characterisation of minor components used in a piece of art is important because these components may provide key information about the process of creation and answer questions regarding conservation and restoration (Casadio and Toniolo, *J. Cult. Herit.* 2:71–78, 2001; Bicchieri et al., *Spectrochim. Acta B At. Spectrosc.* 56:915–922, 2001). This study focused on easel paintings. Several mock-ups were prepared, and the painting layers were created with binary mixtures of three different blues (Prussian blue, phthalocyanine blue and ultramarine blue). Blue pigments have been used extensively in many art pieces and several studies have described problems related to their determination in low concentrations (Bouchard et al., *e-Preserv. Sci*. 6:27–37, 2009; Bicchieri et al., *Spectrochim. Acta B At. Spectrosc.* 56:915–922, 2001; Osticiolia et al., *Spectrochim. Acta A Mol. Biomol. Spectrosc.* 73:525–531, 2009; Giaccai, *Mater. Res. Soc. Symp. Proc.* 1047:233–242, 2008; Lutzenberger and Stege, *e-Preserv. Sci.* 6:89–100, 2009). This study indicated that the minimum concentrations at which the presence of the minor pigment is detected in at least half of the determinations performed are between 0.9% and 1.5% for phthalocyanine blue, between 0.8% and 1.3% for Prussian blue and between 0.3% and 1% for ultramarine blue with SEM-EDS; with m-FTIR spectroscopy, the minimum concentrations are between 0.9% and 1.5% for phthalocyanine blue, 2.4% or more for Prussian blue and 19% or more for ultramarine blue. The concentrations measured for some pigments were high and may result in errors in the description of the composition of a piece of art. The use of complementary techniques may address this limitation. On the basis of these results, the application of analytical procedures that include replicate determinations and analyses of areas of 100×100 μm^2 or greater and exclude single determinations are recommended to more accurately describe the material composition of a work of art.

Keywords Fourier transform infrared · Scanning electron microscopy and energy-dispersive X-ray spectroscopy · Detection limit · Paintings · Heterogeneity · Ultramarine blue · Prussian blue · Phthalocyanine blue

C. Sessa · J. F. García (✉)
Departament de Química Analítica, Facultat de Química,
Universitat de Barcelona,
Diagonal 647,
08028 Barcelona, Spain
e-mail: jfgarcia@ub.edu

A. Vila
Department of Scientific Research,
The Metropolitan Museum of Art,
1000 Fifth Avenue,
New York, NY 1002, USA

Introduction

The application of two analytical techniques, scanning electron microscopy and energy-dispersive X-ray spectros-

copy (SEM-EDS) and micro-Fourier transform infrared (m-FTIR) spectroscopy, to the study of art pieces has been used to provide a general overview of their material characteristics. These techniques are generally available at museums and other institutions that study objects of cultural heritage. When necessary, their results are complemented by other atomic or molecular spectroscopy or chromatographic analytical techniques.

SEM-EDS and m-FTIR spectroscopy are complementary techniques that provide information about elemental and organic and inorganic molecular composition. However, despite the widespread use of these techniques, no studies have been performed to determine their limits of detection in artwork analysis. Thus, the objective of this study was to establish the detection limits for the determination of pigments by SEM-EDS and m-FTIR spectroscopy when these techniques are applied to the characterisation of oil easel paintings.

Modern colourants are becoming increasingly important targets of art-technological research with respect to questions of studio practice and authenticity. Consequently, full identification of all organic and inorganic colorants/ pigments and fillers in painting micro-samples has become a challenging task [7, 8]. The painting layers in this study were completed with binary mixtures of three different blues [Prussian blue (PB), phthalocyanine blue (Pht) and synthetic ultramarine blue (UM)]; however, the information obtained for these pigments can be applied to address the expected limitations of these techniques when used to study this type of art.

Blue is a colour that has been included in art compositions since ancient times. This continuous use highlights the importance of blue pigments in the evolution of art history because they reflect the search to find new materials with equivalent or new chromatic properties that are more widely available and have improved chemical stability. Azurite, lapis lazuli (natural ultramarine) and Egyptian blue were the most important blue pigments in antiquity. Since the eighteenth century, chemical developments have yielded new, cheaper alternatives that include synthetics blues: PB (1710) [6, 9, 10], UM (1828) [5, 8, 9, 11] and Pht (1935) [9, 12, 13]. Several studies on these pigments have been published recently, and some reports stress the difficulties related to their identification when they are included in mixtures and at low concentrations [3–6]. Another difficulty related to the identification of these materials is the ambiguous labelling of some pigments in current use that has no relation to their chemical composition [8].

From an analytical point of view, the selected pigments have different detection characteristics in both techniques as well as different particle sizes. In SEM-EDS, PB and UM have higher signals per mass unit than Pht. In m-FTIR spectroscopy, the intensity of the signal obtained per mass unit for the vibration selected is higher for Pht and UM than for PB; fingerprint spectra obtained from PB and Pht do not or only partially overlap the oil spectrum, whereas the fingerprint spectrum of UM totally overlaps the oil spectrum. In addition, the particle size decreases in the order PB to UM to Pht [14, 15], and this variation permits the evaluation of the influence of the microheterogeneity on the results obtained.

As the typology of artwork is varied, for example paintings, sculptures, paper, textile and archaeological materials, and each type possesses a specific composition and matrix, we focused this study on one of the most common types: oil easel paintings. For this purpose, mock-ups of oil easel paintings on canvas with binary pigment mixtures of known composition were prepared, and SEM-EDS and m-FTIR spectroscopy techniques were employed to determine the concentrations of PB, Pht and UM present. In addition, the amount of minor pigment in the binary mixtures was chosen to more accurately establish the detection limit interval as well as to prepare a series of proportions with the major component of the binary mixture that would produce colour changes observable with the naked eye.

Experimental

Materials

A detailed description of the pigments used in this study is presented in Table 1. The medium was a polymerised linseed oil (reference 368) purchased from Jacques Blockx in Barcelona (Spain). A commercial canvas on a stretcher,

Table 1 Description of pigments

Pigment	Commercial name	Reference	Manufacturer	Country of purchase	General formula
Pht	Heliogenblau	23050	Kremer	Germany	$C_{32}H_{15}N_8Cu$
PB	Miloriblu	45200	Kremer	Germany	$NH_4Fe[Fe(CN)_6]$
UM	Ultramarine Blue Dark	45010	Kremer	Germany	$3Na_2O{\cdot}3Al_2O_3{\cdot}6SiO_2{\cdot}2Na_2S$

Pht phthalocyanine blue, *PB* Prussian blue, *UM* synthetic ultramarine blue

prepared with a white ground (16 cm×22 cm), was used as the support.

Instrumentation

Scanning electron microscopy and energy-dispersive X-ray spectroscopy

Analyses were carried out with a Cambridge Instruments Stereoscan 360 scanning electron microscope, equipped with an INCA Energy 200 microanalysis apparatus. Spectra were recorded under the following conditions: 20 kV, 1 nA and a 20–35-mm distance from sample to detector.

Fourier transform infrared spectroscopy

Analyses were performed with a Bomem MB-120 Fourier transform infrared spectrometer equipped with a Spectra-Tech Analytical Plan microscope with a diamond cell as a sample holder. The spectrometer has a KBr beam splitter and a glow bar source. The microscope has its own mercury cadmium telluride detector refrigerated with liquid nitrogen. Spectra were recorded between 4,000 and 350 cm^{-1} with a resolution of 4 cm^{-1}, and with accumulation of 100 scans. Measurements were done in transmission mode. The results were processed with GRAMS-32.

Procedure

Oil painting mock-up preparation

The percentage of linseed oil required for each pigment was established empirically to obtain a viscous paint. Owing to the pigment grain size and form, the oil absorption of each pigment is different. From the results obtained in this step (percentage of oil necessary for each pigment to obtain a viscous paste), paintings with different binary mixtures of pigment were prepared (Table 2).

During the preparation of the viscous paste, an inert volatile solvent (white spirit) was used to make the paint more flexible and easier to work with on the canvas surface. Once the paint paste had been prepared, two layers of paint were applied on the prepared canvas white ground. The drying time was 2 weeks between each application of layer and the total drying time was 1 month for all layers.

Sampling and measurement

Scanning electron microscopy and energy-dispersive X-ray spectroscopy Small samples (200 μm×200 μm×50 μm), which were extracted from the mock-up painting surface, were sufficient to perform SEM-EDS analyses. The

Table 2 Concentrations and proportions of pigments in canvas paintings

PB+Pht				Pht+PB				PB+UM			
PB (pigment/ oil wt%)	Pht (pigment/ oil wt%)	PB (pigment/ pigment wt%)	Pht (pigment/ pigment wt%)	Pht (pigment/ oil wt%)	PB (pigment/ oil wt%)	Pht (pigment/ pigment wt%)	PB (pigment/ pigment wt%)	PB (pigment/ oil wt%)	UM (pigment/ oil wt%)	PB (pigment/ pigment wt%)	UM (pigment/ pigment wt%)
32.1	0.3	99	1	24.2	0.2	99	1	32.2	0.3	99	1
31.3	0.9	97	3	26.4	0.8	97	3	31.8	1.0	97	3
30.7	1.5	95	5	26.7	1.3	95	5	31.4	1.6	95	5
30.1	2.4	93	7	26.7	2.1	93	7	30.8	2.5	93	7
28.5	3.4	89	11								
25.1	6.2	80	20	25.9	6.5	80	20	27.7	6.9	80	20
20.3	10.2	67	33	23.5	15.5	67	33	24.2	12.1	67	33
15	15	50	50	15	15	50	50	19	19	50	50

samples were removed from the painting with a microsurgery scalpel. Subsequently, the samples were deposited on carbon adhesive stuck on stubs of aluminium and then re-covered by carbon.

Three samples from different locations on each painting were extracted to check sample reproducibility. Five different points of each sample from a preestablished regular geometrical scheme were analysed with four differently sized areas (10×10, 20×20, 50×50 and 100×100 μm^2) to evaluate the material reproducibility and homogeneity.

Fourier transform infrared spectroscopy Extraction of small particles (100 μm×100 μm) from the painted surface was carried out with a microsurgery scalpel. Manipulation was performed under a magnification lens (×50). Owing to the minimal size of the extracted fragments and the potential heterogeneity of the material, five samples were removed from each painting to ensure representative results.

With use of the infrared microscope, each of these small samples was placed on the diamond cell and pressed to obtain a layer as thin as possible to facilitate infrared radiation transmission. The diameter of the radiation beam that passed through the sample was 100 μm.

Detection

Scanning electron microscopy and energy-dispersive X-ray spectroscopy The INCA Energy 200 software identifies the element automatically when the signal is 3 times higher than the standard deviation of the background noise [11].

Fourier transform infrared spectroscopy To identify peaks, GRAMS/32 uses an algorithm that performs slope-based edge detection with "tangent baseline" peak edge refinement. The raw edges are first detected on either side of a peak where the absolute value of the slope exceeds a minimum. The edge slope is automatically determined by the software, using a setting of 0 to prevent peak rejection.

Expert detection Expert or non-automatic detection is an attempt to improve the results obtained by the automatic detection procedure. In the former case, the criterion to determine the existence of an element or compound consists of observation by the analyst of the presence of a signal at the energy or frequency corresponding to the element or band selected. This criterion requires that the analyst is aware of the potential presence of the pigment and, therefore, of the element or absorption band. Material characterisation of artwork is often an open problem, but sometimes there is some information, even from preliminary optical observations, about materials that may be found in the object. In these cases, expert detection can be applied.

Parameters

The heterogeneity parameter used in this study was the mean of the relative standard deviations (mRSD) of the series of measurements performed for each area analysed.

The intensity ratio (minor component vs. major component) of the representative elements of both pigments included in the layer was calculated from the spectra obtained in each measurement. For each sample and area of each pigment mixture at the selected proportion, the mean, the standard deviation and the relative standard deviation (RSD) of the five measurements performed were calculated. From these data, the mRSD is calculated as the mean of the three RSD values obtained from the series of five measurements obtained for each sample and area. When the paint layer includes a single pigment, the procedure for the mRSD calculation is the same, but the ratio of the relevant elements detected in the pigment composition (PB, K/Fe; UM, Si/Al; and Pht, Cl/Cu) is used.

The detection limit of 0.5 (DL0.5) is defined as the minimum concentration at which the signal related to the presence of the element or compound is detected in at least half of the measurements performed.

Results and discussion

This section is organised by technique, describing first SEM-EDS and then m-FTIR spectroscopy, and for each technique, the detection limits achieved and the dispersion observed are discussed as functions of the automatic or expert detection procedure that was used.

Previous knowledge concerning the material characteristics of artwork or knowledge generated by the analysis of a piece may provide information about the potential presence of some defined components in specific paint layers. In these cases, the use of spot analysis on some samples is especially useful to confirm this hypothesis. Conversely, when there is no special information available about the sample, and a general approach to the composition is required, area analysis favours the integration of the volume analysed of all components included in the layer and yields more representative information.

The detection limit used to compare the different detection capabilities was established following the DL0.5 criterion.

Scanning electron microscopy and energy-dispersive X-ray spectroscopy analysis

The signals obtained by SEM-EDS depend on several factors, including the composition and formula of the pigments, the relationship between the number of atoms of the chemical element monitored versus the mass of the pigment, the concentration of pigment in the paint layer, the particle size and distribution behaviour of the pigment on the paint layer and the energy of radiation detected

The experimental procedure was performed on a series of paint layers of known composition (see "Experimental") that include binary mixtures of pigments. The mixtures included one pigment with a high value for the relationship between the number of atoms of the monitored chemical element versus the molecular mass of the pigment (NAH), PB, and one pigment with a low value for this relationship (NAL), Pht; the second mixture included two pigments with a high value (NAH), PB and UM.

For each painting considered, three samples were taken and four areas of different sizes from each sample were analysed (10×10, 20×20, 50×50 and 100×100 μm^2). For each sample and area, five measurements were performed. These series of data permitted a preliminary approach to the determination of the detection limit and were representative of the results obtained under different measurement conditions.

Detection

Pure pigments The pigments used in this study were supplied by Kremer, who describes their composition as $NH_4Fe[Fe(CN)_6]$ for PB, $3Na_2O{\bullet}3Al_2O_3{\bullet}6SiO_2{\bullet}2Na_2S$ for UM and $C_{32}H_{15}N_8Cu$ for Pht. However, the results obtained in the SEM-EDS analysis (using an area of 100×100 μm^2 and five replicate measurements) are partially in disagreement with this information.

For PB, potassium was detected with a K/Fe peak intensity ratio of 0.719±0.014; this indicates that the pigment has another component, probably $KFe[Fe(CN)_6]$. Thus, the amount of iron was around half of that expected.

For UM, the Si/Al signal ratio should be around 1 according to the formula indicated by Kremer ($3Na_2O{\bullet}3Al_2O_3{\bullet}6SiO_2{\bullet}2NaS$); however, the experimental value is 2.460±0.092. We have no explanation for this difference; the presence of additional compounds is clearly indicated, and the silicon signal is approximately double that expected.

For Pht, the supplier indicates that in addition to the formula ($C_{32}H_{15}N_8Cu$), there are 0.5 chlorine atoms per copper phthalocyanine molecule. The analysis performed here shows that the Cu/Cl intensity ratio is 0.444±0.009, which is the inverse of the expected proportion, and the copper signal is probably much lower than that indicated by the Kremer information.

According to the supplier's information, the relationship between the number of atoms of the monitored chemical element versus the mass of the pigments is 7.0×10^{-3} mol Fe atoms per gram of pigment for PB, 6.0×10^{-3} mol Si atoms per gram of pigment for UM, and 1.7×10^{-3} mol Cu atoms per gram of pigment for Pht. These values indicate that ratio of the number of atoms of the monitored chemical element versus the mass of the pigments is higher for PB and UM than for Pht.

With regard to the particle size of the different pigments and their grouping in the paint layers, a preliminary approach based on SEM-EDS images indicates that PB is composed of particles quite isolated in the paint layer, with sizes in the range of 35–75 μm, UM is composed of fine particles, 10–15 μm, continuously distributed in the paint layer and Pht shows uniform and light distribution over the entire paint layer without the clear presence of particles [14–16].

On the basis of the above information, the discussion of SEM-EDS has been divided into two parts focused on the detection or non-detection of the minor element (by using automatic or expert identification) and on the evaluation of the dispersion of the values obtained, which is an indicator of the heterogeneity of the pigment distribution on the paint layer (and consequently on the probability of pigment being detected).

Mixtures The presence of the pigments was monitored by detection of iron for PB, copper for Pht and silicon for UM. The results obtained when paint layers included a mixture of two pigments, one with a NAH (PB) and one with a NAL (Pht), are presented first.

For the mixture of PB (major component) plus Pht (minor component), the relative success in the identification for a total of 15 determinations (three samples and five measurements each) for different areas using automatic and expert detection is shown in Fig. 1. The same results for the inverse mixture of Pht (major component) plus PB (minor component) are shown in Fig. 2. As expected, the number of positive identifications increases when the concentration of the components increases.

For the mixture of PB (major component) plus Pht (minor component), the DL0.5 for Pht is in the range from 6.3 to 10.2% in automatic detection mode, whereas it decreases to 0.94–1.3% in expert mode. For the reverse pair, Pht (major component) and PB (minor component), the DL0.5 for PB is between 6.5 and 15.5% in automatic mode and in the range from 0.8 to 1.5% with the expert procedure (Table 3). The use of expert mode clearly improves the detection limit that is achieved; however, the application of this procedure requires that the analyst is

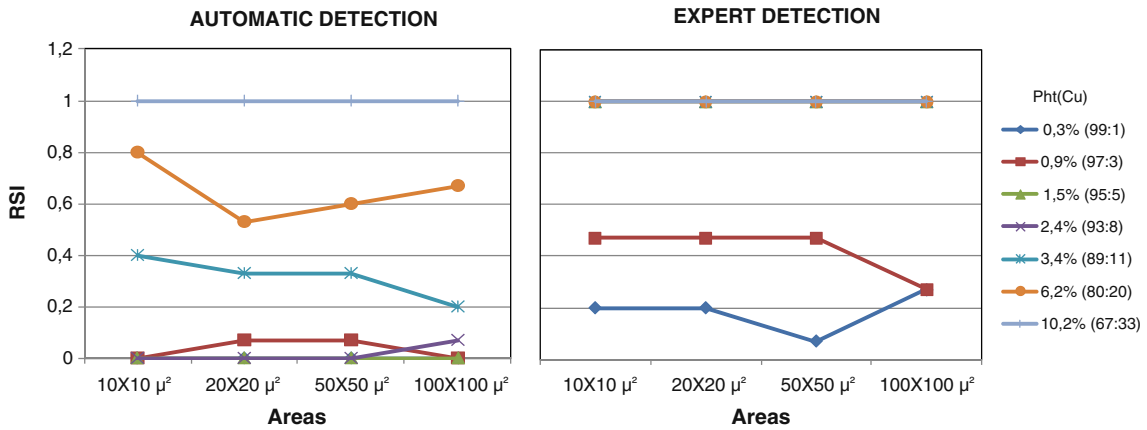

Fig. 1 Automatic and expert detection for the mixture of Prussian blue (major component) plus phthalocyanine blue (minor component). *RSI* relative success in the identification, *Pht* phthalocyanine blue

aware of the presence of a second pigment in the mixture. The limits that were achieved using automatic detection, around 6.5–15.5%, are considered quite high for material characterisation studies because they correspond to a mass ratio between the two pigments in the mixture of 67:33–80:20, and the introduction of a second component in this proportion by the artist is always intentional and should be detected in material analysis. When expert detection is applied, the DL0.5 that was achieved corresponds to lower proportions; in this case, the proportions are in the range from 97:3 to 95:5.

For the mixture of two pigments with NAH, PB (major component) plus UM (minor component), the detection limits that were achieved were between 1.6 and 2.5% in automatic mode and below 0.32% in expert mode (Fig. 3 and Table 3).

Again, application of the expert criterion improves the limits that are obtained. The differences in the values achieved for the detection limit can be related to the ratio between the number of atoms and the mass of pigment. Thus, the pigment with NAH, UM, has a lower detection limit. The difference between the limits obtained for UM and PB can be explained by the higher content of silica and the lower content of iron observed in the previous analysis of the pure pigments.

On the basis of these results, the area that was selected for the analysis had no influence on the values of the DL0.5 for any pigment, mixture or detection procedure. This behaviour indicates that the distribution of the pigment on the paint layer has a secondary influence, and this is discussed in the following section.

Distribution

Another key factor in the characterisation of artwork is the intrinsic heterogeneity in the distribution of the constituent materials. In the characterisation of the paint layers, this distribution depends on the artist's procedure and also on the physical and chemical properties of the raw materials used. The heterogeneity of the distribution was evaluated using three samples, four areas (10×10, 20×20, 50×50, 100×100 μm^2) and five determinations for each sample and area using automatic and expert detection.

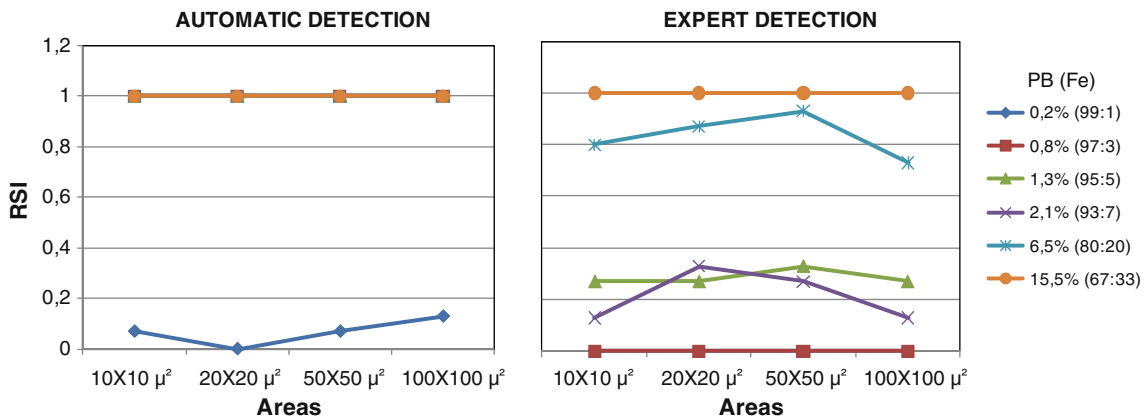

Fig. 2 Automatic and expert detection for the mixture of phthalocyanine blue (major component) plus Prussian blue (minor component). *PB* Prussian blue

Table 3 Detection limits for pigments in scanning electron microscopy and energy-dispersive X-ray spectroscopy analysis

	Automatic	Expert
PB+Pht	6.2–10.2% (80:20/67:33)	0.9–1.5% (97:3/95:5)
Pht+PB	6.5-15.5% (80:20/67:33)	0.8–1.3% (97:3/95:5)
PB+UM	1.6–2.5% (95:5/93:7)	0.3–1% (99:1/97:3)

The heterogeneity parameter value (mRSD) provides information on the dispersion of the intensity signals of the two representative elements of the mixed pigments. For layers prepared with a single pigment, the mRSD provides information about the minimum dispersion when this pigment is included in the paint layer.

Pure pigments

The first approach to determine the heterogeneity of pigment distribution in a paint layer was the evaluation of the behaviour of pure pigments. The results obtained for the mRSD are shown in Fig. 4 and Table 4.

To avoid the influence of other factors such as insufficient material in an area, we focused on the largest area (100×100 μm^2), and the minimum dispersion expected for any binary mixture was consistently around 10–15% for all cases.

Mixtures

Four factors have a significant influence on the dispersion of the intensity ratios that were detected: the concentration of the minor pigment, the number of atoms of the monitored element versus the molecular mass of the pigment, the particle size of the pigment and the size of the area analysed. To minimise the variability introduced by the two former factors, the discussion focuses on the mixtures with sufficient amounts of the minor pigment (2.1–2.4% or greater) to avoid determination of its distribution by the limited amount of pigment in the paint layer.

For any series, considerable variability in the mRSD values below the concentration limit of 2.1–2.4% can be observed. Up to this value, the mRSD values follow a convergent process as the concentration of the minor components increases. In addition, for any value in this range, the dispersion for the largest area (100×100 μm^2) is relatively constant and yields the minimum value of any area considered (20–33%). These mRSD values indicate that a higher dispersion occurs for mixtures than for pure pigments and, perhaps more importantly, that lower dispersion corresponds to those pigments (UM and PB) with lower detection limits. Thus, a NAH seems to be a more important factor for reproducibility than the particle size of the pigment analysed.

The results obtained using SEM-EDS analysis indicate that a general approach to the determination of sample composition necessitates the application, when possible, of replicate analysis of areas of at least 100×100 μm^2 to improve reproducibility. The detection limit also improves when the analyst is aware of the potential presence of a compound, and expert detection is used.

Micro-Fourier transform infrared spectroscopy analysis

In addition to the factors indicated previously for SEM-EDS, the signals obtained in m-FTIR spectroscopy also depend on the absorption intensity of the selected vibration versus the mass of the pigment and on the overlapping of the selected peak by other component bands present in the paint layer.

The pigments in this study show very specific vibrational bands that can be used as markers. The band observed at 1,010 cm^{-1} is assigned to the asymmetric stretching mode of the silicate group (Si–O–Si) in UM [8, 17, 18], and PB exhibits one band at 2,090 cm^{-1} that is very characteristic of

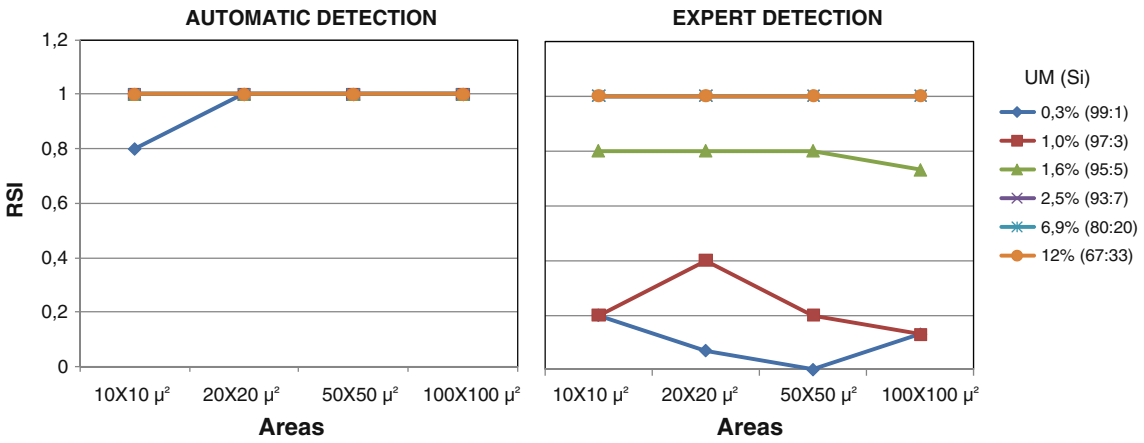

Fig. 3 Automatic and expert detection for the mixture of Prussian blue (major component)+ultramarine blue (minor component). *UM* ultramarine blue

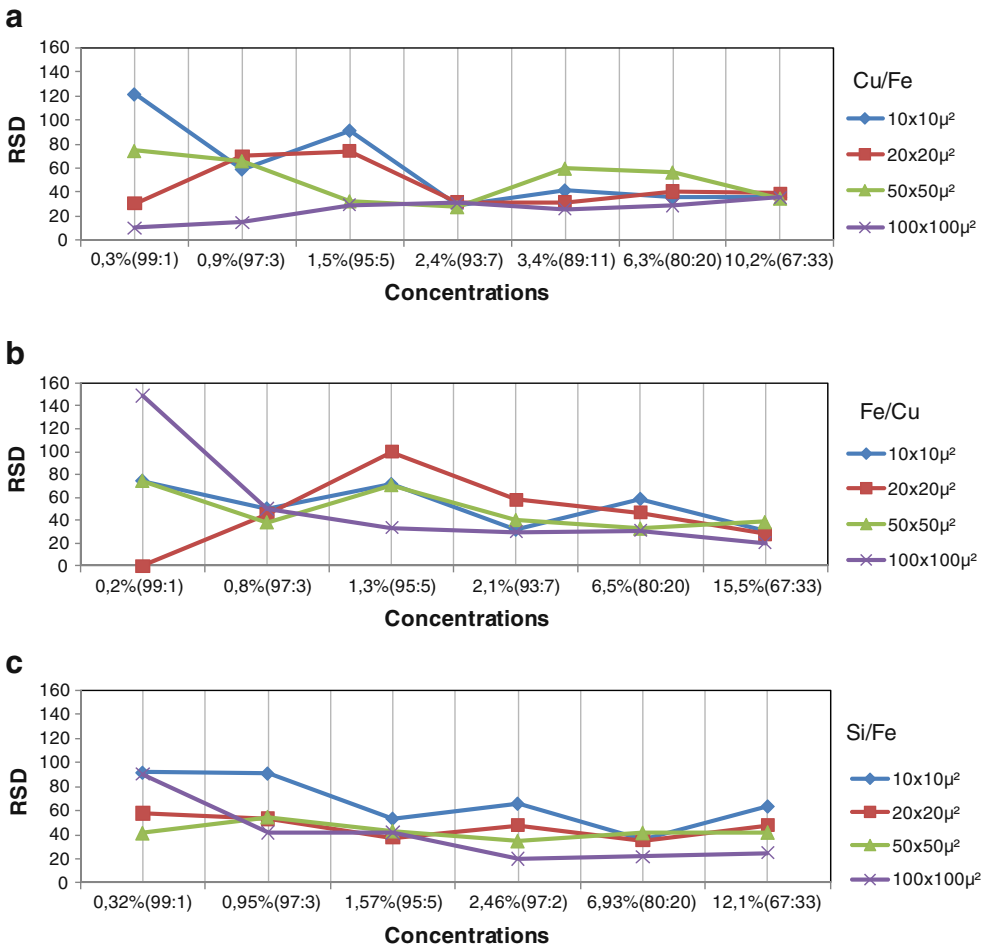

Fig. 4 Mean of the relative standard deviations for the intensity ratios of **a** Cu/Fe, **b** Fe/Cu and **c** Si/Fe

CN^- stretching [8, 17]. Pht is an organic pigment with several characteristic bands in the 1,500-1,000-cm^{-1} range; in this case, the signals at 1,505 cm^{-1} and 1,332 cm^{-1} were selected as markers [8, 9, 17]. The binary mixtures that were analysed included pigments with signals that overlapped to different degrees on the linseed oil spectrum—not overlapped PB (2,090 cm^{-1}), slightly overlapped Pht (1,505 cm^{-1}), partially overlapped Pht (1,332 cm^{-1}) and totally overlapped UM (1,010 cm^{-1})—and signals with different absorption intensities were also observed: higher for UM (1,010 cm^{-1}) and Pht (1,332 cm^{-1} approximately double that at 1,505 cm^{-1}) than for PB (2,090 cm^{-1}) (Figs. 5, 6).

For each of the pigments, determination of the absorption intensities of the selected bands by mass unit was performed by measuring the area of the peaks obtained by analysing KBr micropellets with weighed amounts of pigment. For each paint layer, five samples were extracted and analysed independently. Automatic detection and expert detection were used to recognise the presence of the marker bands.

Detection

Mixtures For the mixture of Pht (major component) plus PB (minor component), where the representative band of

Table 4 Heterogeneity distribution of the major elements in the pure pigments

	mRSD					
	Pigment/oil wt%	Pigment/pigment wt%	10×10 µm²	20×20 µm²	50×50 µm²	100×100 µm²
PB (K/Fe)	32.4	100	13.1	15.5	11.3	14
UM (Si/Al)	47.7	100	7.6	16	5.4	9.9
Pht (Cl/Cu)	20.1	100	16	47.7	30.9	9.6

mRSD mean of the relative standard deviations

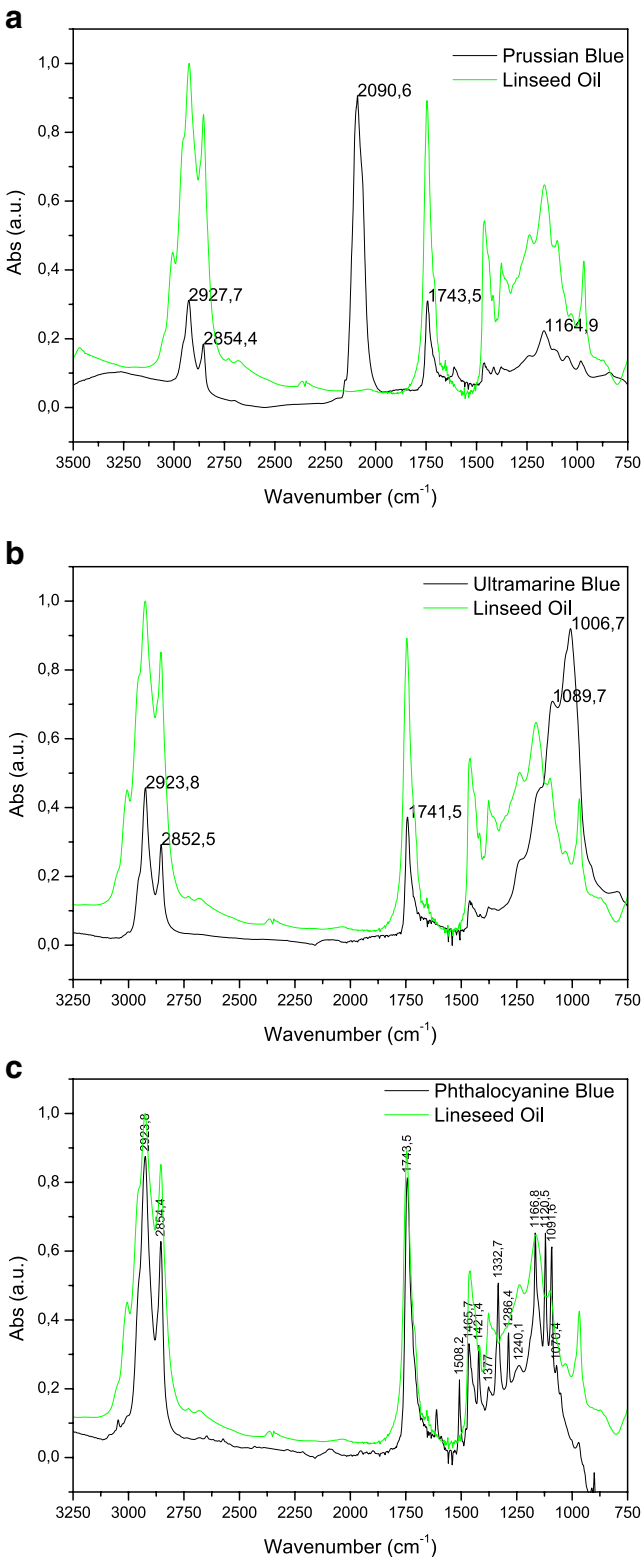

Fig. 5 Fourier transform mid-infrared spectra of the oil binder and pure pigments for **a** Prussian blue, **b** phthalocyanine blue and **c** ultramarine blue

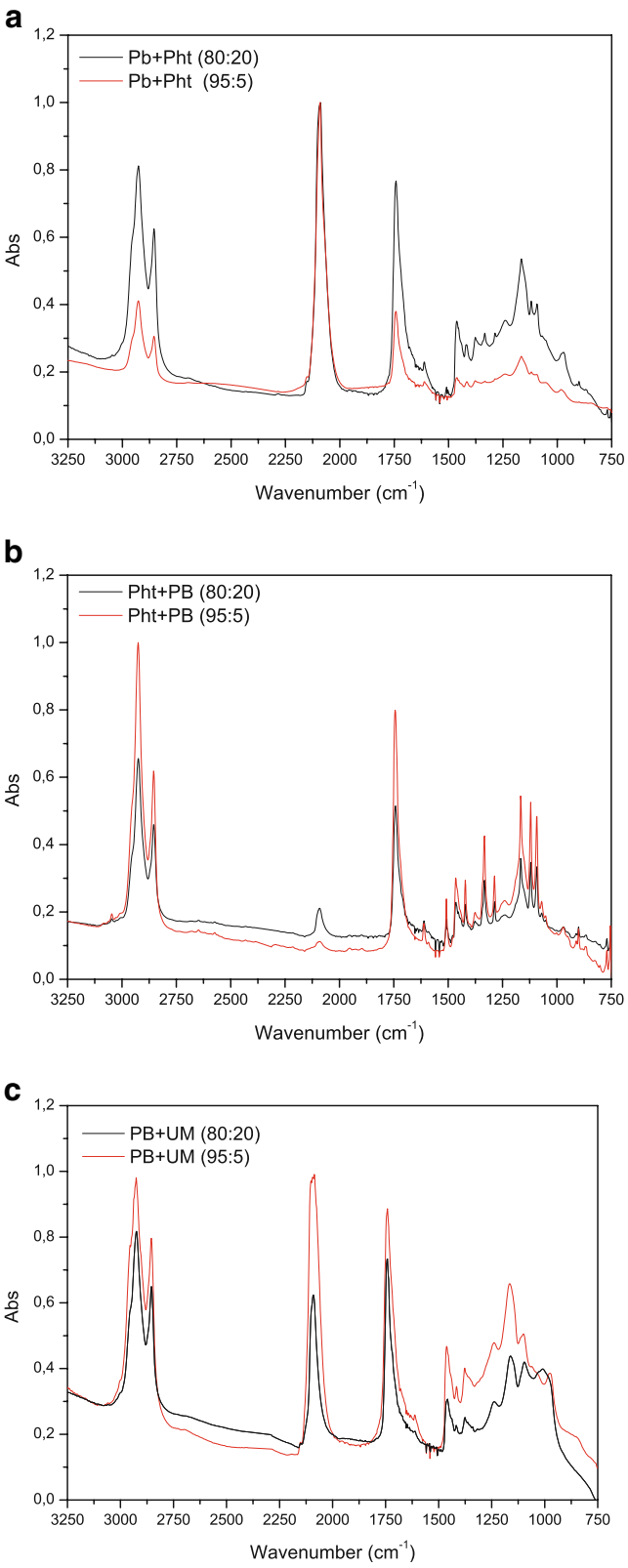

Fig. 6 Fourier transform mid-infrared spectra for the pigments in the mixture with oil binder at proportions of 80:20 and 95:5 for **a** Prussian blue plus phthalocyanine blue, **b** phthalocyanine blue+Prussian blue and *c* Prussian blue+ultramarine blue

Table 5 Detection limits for pigments in micro-Fourier transform infrared spectroscopy

	Automatic	Expert
PB (2,090 cm^{-1})	≤0.24% (99:1)	≤0.24 % (99:1)
Pht (1,505 cm-^{1})	6.2-10.2% (80:20/67:33)	6.2-10.2% (80:20/67:33)
Pht (1,332 cm^{-1})	2.4–3.4% (93:7/89:11)	0.9–1.5% (97:3/95:5)
UM (1,089 cm^{-1})	≥19% (50:50)	≥19% (50:50)

the minor component (2,090 cm^{-1}) is not overlapped, the signal was detected in all of the analyses and at almost all concentrations; the DL0.5 values in the automatic and expert modes were the lowest assessed, at 0.24%, which corresponds to a proportion of 99:1 for the two modes (Tables 4 and 5).

When the degree of overlap increases slightly, PB (major component) plus Pht (minor component, 1,505 cm^{-1}), or the overlap becomes partial, PB (major component) plus Pht (minor component, 1,332 cm^{-1}), the number of positive identifications at low concentrations decreases. The DL0.5 values achieved for the band at 1,505 cm^{-1} in both automatic and expert modes are between 10.2% and 6.3%, which correspond to the proportion range from 67:33 to 80:20 between these pigments. However, when the marker band is partially overlapped (1,332 cm^{-1}), the DL0.5 value improves to 3.4–2.4% and 1.5–0.9% in the automatic and expert modes, respectively, which corresponds to mass proportions of 93:7–89:11 and 93:7–95:5. This observation can be explained by accounting for the higher intensity of the absorption at 1,332 cm^{-1} compared to that at 1,505 cm^{-1}; this factor is enough to compensate for the influence of the partial band overlap.

For the mixture of PB (major component) plus UM (minor component, 1,089 cm^{-1}), in which the band of UM is totally hidden by the linseed oil peaks, the pigment signal cannot be detected in any case, neither in automatic mode nor in expert mode. The DL0.5 value is worse than the higher concentration considered for UM (19%), which corresponds to a 50:50 mass ratio between these pigments.

From these results, the use of expert mode to detect the marker bands clearly yields detection limits similar to or better than those obtained using automatic mode; however, the improvement is not as significant as that observed for the SEM-EDS results.

As expected for m-FTIR spectroscopy analysis, the detection limit depends on the extent of overlap with the selected bands. The presence of a binding medium in all of the paint layers introduces a potential interference for detection of the pigments. With use of m-FTIR spectroscopy with a diamond cell, this effect could be overcome if the radiation beam is focused on a segregated pigment particle. However, this approach implies some knowledge of the sample composition, but this is not always the situation, especially for a minor pigment in a mixture. When the overlap is not total, the absorptivity of the monitored band by mass unit is a secondary factor that determines the detection limit that can be achieved.

Similar to SEM-EDS analysis, the size of the pigment particles does not influence the detection limits determined.

Distribution

Mixtures In m-FTIR spectroscopy, the heterogeneity of the distribution of pigment in the paint layers was evaluated using the RSD values of the peak intensity ratios of the series of five independent determinations performed for each mixture and composition. The mixtures included Pht (major component) plus PB (minor component) and PB (major component) plus Pht (minor component) but not PB (major component) plus UM (minor component) owing to the lack of signal detected for UM. In both mixtures of Pht plus PB, the peaks considered for the ratio were PB (2,090 cm^{-1}) and Pht (1,505 and 1,332 cm^{-1}).

As in SEM-EDS, only mixtures with a concentration of the minor component up to 2.1–2.4% would be considered

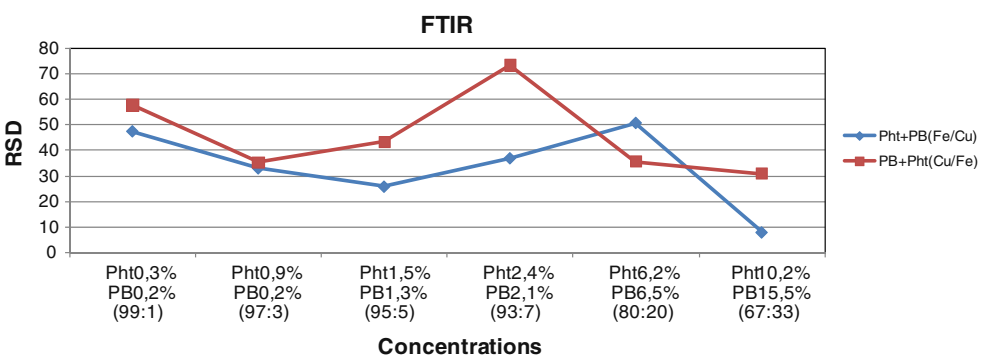

Fig. 7 Mean of the relative standard deviations for the intensity ratios of Cu/Fe and Fe/Cu. *FTIR* Fourier transform infrared, *Pht* phthalocyanine blue, *PB* Prussian blue

to acquire sufficient signals. The results obtained from these analyses are shown in Fig. 7.

Similar explanations of these results for m-FTIR spectroscopy and for SEM-EDS can be made. When the pigment concentration increases, up to 2.1–2.4%, dispersion decreases and the RSD values range from 7 to 33%. Dispersion seems to be lower for pigments that do not experience overlap of the representative peak (PB) and that experience partial overlap but have relatively high absorption (Pth, 1,332 cm^{-1}); these characteristics also imply lower detection limits in both cases. As in the SEM-EDS study, particle size is not relevant, and the most important overall factor influencing the reproducibility is the net signal obtained for the representative peak. Interestingly, the RSD values for SEM-EDS and m-FTIR spectroscopy are quite similar and probably reflect how the pigments are distributed in the paint layers.

Conclusions

This systematic study concerning the detection limits achieved by the two most commonly used techniques, SEM-EDS and micro-FTIR spectroscopy, for material characterisation of artwork indicates that:

- Detection limits for some pigments in both techniques are high for material characterisation purposes. This situation may result in an erroneous description of artwork composition. The use of spot analysis or complementary techniques may aid in overcoming this limitation.
- Detection limits critically depend on the intensity of the signal registered (SEM-EDS, m-FTIR spectroscopy) and the band overlap (m-FTIR spectroscopy). Particle size does not seem to be a relevant factor for the detection limit.
- The reproducibility of results and the probability of detecting the minor pigment depend on the area of the sample analysed (SEM-EDS) and on the number of replicates performed. Thus, for the purpose of general knowledge, large areas (at least 100×100 μm^2) and several replicates are recommended to improve the results obtained.
- Expert detection rather than automatic detection of the peaks is also highly recommended, especially for SEM-EDS; however, expert application depends on the information previously available or deduced from the piece of art. Sometimes this information is not sufficient to identify the presence of all minor compounds.

Acknowledgements The authors wish to recognise Ramon Fontarnau (who died in 2008, SCT-UB) for his help throughout the years in the application of SEM-EDS to the study of artwork. He introduced us to this technique, and he patiently eased all of our doubts about the technique and the problematic cases that have been studied. With the support of people like Ramon, research becomes a pleasant activity. The authors also wish to thank N. Ferrer (SCT-UB) for her kind advice in the use and interpretation of the infrared spectroscopy data as well as Costanza Miliani (University of Perugia). Finally, the authors are grateful for financial support from the Spanish Ministerio de Educación y Ciencia for this study (HAR2008-03849/ARTE).

References

1. Casadio F, Toniolo L (2001) J Cult Herit 2J Cult Herit:71–78
2. Bruni S, Cariatia F, Casadio F, Toniolo L (1999) Vibr Spectrosc 20:15–25
3. Bouchard M, Rivenc R, Menke C (2009) e-Preserv Sci 6:27–37
4. Bicchieri M, Nardone M, Russo PA, Sodo A, Corsi M, Cristoforetti G, Palleschi V, Salvetti A, Tognoni E (2001) Spectrochim Acta Part B Atom Spectrosc 56:915–922
5. Osticiolia I, Mendesa NFC, Nevinc A, Gild FPSC, Becuccia M, Castelluccia E (2009) Spectrochim Acta A Mol Biomol Spectrosc 73:525–531
6. Giaccai J (2008) Mater Res Soc Symp Proc 1047:233–242
7. Lutzenberger K, Stege H (2009) e-Preserv Sci 6:89–100
8. Silva CE, Silva LP, Edwards HGM, de Oliveira LFC (2006) Anal Bioanal Chem 386:2183–2191
9. Clark RJH (2002) C R Chem 5:7–20
10. Berrie BH (1997) In West Fitzhugh E (ed), Artists' pigments: a handbook of their history and characteristics, vol 3. National Gallery of Art, Washington, pp 191–217
11. Plesters J (1993) In Roy A (ed) Artists' pigments: a handbook of their history and characteristics, vol 2. National Gallery of Art, Washington, pp 37–65
12. Zollinger H Colour chemistry, syntheses, properties and applications of organic dyes and pigments, 3rd edn. Wiley-VCH, Weinheim, pp 140–160
13. Quillen Lomax S, Learner T (2006) J Am Inst Conserv 45:107–125
14. Dupuis G, Menu M (2006) Appl Phys A Mater Sci Process 83:469–474
15. Eastaugh N, Walsh V, Chaplin T, Siddal R (2004) Pigments compendium: optical microscopy of historical pigments. Elsevier, Oxford, p 45, 113–115, 121–123
16. Schmidt CM, Walton MS, Trentelman K (2009) Anal Chem 81 (20):8513–8518
17. Vila A, Ferrer N, Garcia JF (2007) Anal Chim Acta 588:96–107
18. Desnica V, Furic K, Schreiner M (2004) e-Preserv Sci 1:15–21

2.2 Evaluation of MidIR fibre optic reflectance: Detection limit reproducibility and binary mixture discrimination.

Spectrochimica Acta Part A: Molecular and Biomolecular Spectroscopy 115 (2013) 617–628

Contents lists available at SciVerse ScienceDirect

Spectrochimica Acta Part A: Molecular and Biomolecular Spectroscopy

journal homepage: www.elsevier.com/locate/saa

Evaluation of MidIR fibre optic reflectance: Detection limit, reproducibility and binary mixture discrimination

Clarimma Sessa, Héctor Bagán, José Francisco García *

Departament de Química Analítica, Universitat de Barcelona, Diagonal 645, E-08028 Barcelona, Spain

HIGHLIGHTS

- Detection limits for all the pigments are high for artworks characterisation purposes.
- Physical features of the artworks are important for characterisation using MidIR-FORS.
- Results dispersion is mainly affected by heterogeneity of the paint layers.
- Data pre-treatments reduce the instrumental/procedure variability.
- PCA and MidIR-FORS are able to discriminate between binary mixtures of oil paints.

GRAPHICAL ABSTRACT

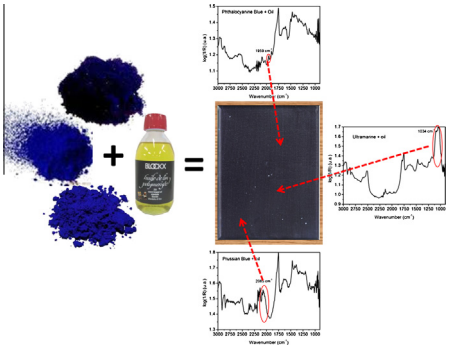

ARTICLE INFO

Article history:
Received 22 February 2013
Received in revised form 10 June 2013
Accepted 24 June 2013
Available online 3 July 2013

Keywords:
MidIR-FORS
FTIR
Paintings
Ultramarine blue
Prussian blue
Phthalocyanine blue

ABSTRACT

MidIR fibre optic reflectance (MidIR-FORS) is a promising analytical technique in the field of science conservation, especially because it is non-destructive. Another advantage of MidIR-FORS is that the obtained information is representative, as a large amount of spectral data can be collected. Although the technique has a high potential and is almost routinely applied, its quality parameters have not been thoroughly studied in the specific application of analysis of artistic materials.

The objective of this study is to evaluate the instrumental capabilities of MidIR-FORS for the analysis of artwork materials in terms of detection limit, reproducibility, and mixture characterisation. The study has been focused on oil easel painting and several paints of known composition have been analysed. Paint layers include blue pigments not only because of their important role along art history, but also because their physical and spectroscopic characteristics allow a better evaluation of the MidIR-FORS capabilities.

The results of the analysis indicate that MidIR-FORS supplies a signal affected by different factors, such as the optical, morphological and physical properties of the surface, in addition to the composition of materials analysed.

Consequently, the detection limits established are relatively high for artistic objects (Prussian blue – PB 2.1–6.5%; Phthalocyanine blue - Pht 6.3–10.2%; synthetic Ultramarine blue – UM 12.1%) and may therefore lead to an incomplete description of the artwork.

Reproducibility of the technique over time and across surface has been determined. The results show that the major sources of dispersion are the heterogeneity of the pigments distribution, physical features, and band shape distortions. The total dispersion is around 4% for the most intense bands (oil) and increases up to 26% when weak or overlapped bands are considered (PB, Pht, UM). The application of

* Corresponding author. Tel.: +34 934021281; fax: +34 934021233.
E-mail address: jfgarcia@ub.edu (J.F. García).

http://dx.doi.org/10.1016/j.saa.2013.06.088

different pre-treatments (cutoff of fibres absorption, Savizky–Golay smoothing algorithm, polynomial baseline offset, Standard Normal Variate algorithm – SNV) to the raw spectra allows improving these results to maximum values of 15%.

Finally, the capabilities of PCA and MidIR-FORS to discriminate between binary mixtures were tested. The results demonstrate that it is possible to differentiate mixtures depending on the range of concentration of their components, within specific limits of detection.

Introduction

An important characteristic of the artworks is their material heterogeneity [1]. The increase of the number of determinations is a common option to improve the representativity of the information obtained, but this approach is not favourable as it stands against the preservation of the physical integrity of these important objects [2].

Accordingly, science conservation fields are currently focusing on the development of non-invasive methods [3–7] to complement the classical techniques SEM–EDX, micro-FTIR, chromatographic, etc. [5,8,9].

The Mid-IR fibre optics coupled with Fourier transform infrared bench (MidIR-FORS) permits the performance of non-invasive reflection measurements. It is a promising technique, routinely applied [2] but its quality parameters, such as detection limit and reproducibility, have not been studied thoroughly for the specific application of artistic materials analysis [6,10]. It is important to underline that characterisation of minor components used in a piece of art is extremely useful, because these components may provide key information about the creation process and answer questions regarding conservation and restoration [3,5,11,12]. However, the use of a non-destructive technique such as MidIR-FORS implies some limitations. The signal obtained with Fourier infrared spectroscopy analysing a paint layer depends on the composition and concentration of the pigments and the binder, the absorption intensity, and the degree of overlap of the selected vibrations bands [13]. Moreover, the signal obtained with reflectance arrangement also depends on the particle size, the distribution of the pigments, the morphological and physical properties of the surface analysed [14], and the angle of the incident light as the penetration depth of the beam in the paint layer. Due to all of these factors, the main shortcoming of the technique is that reflection mode spectra can present odd distortions of band shape, position and intensity, implying that the interpretation of reflection spectra of unknown heterogeneous materials could be challenging [2,15].

Because of the non-destructiveness of the MidIR-FORS, a large amount of data could be obtained but the provided information is not easily interpretable. Accordingly, chemometric methods may be helpful tools to extract the information included in the recorded spectra. Among these methods, principal component analysis (PCA) allows reduction of the dimensionality of a series of data by transforming the set of original variables into a simplified group of variables named principal components (PCs), which represent the relevant information [1,10,16].

The objective of this study is to evaluate the instrumental capabilities of MidIR-FORS in the analysis of artwork in terms of detection limit, reproducibility, and capabilities to discriminate binary mixtures of inorganic pigments and colorants.

Despite of the general purpose of this study, the work has been focused on one of the most common types of artworks: oil easel paintings. The pigments included in the paint layers are blue and they have been selected not only by their historical use, but also because they present different physical, morphological and optical properties, as well as detection characteristics [13]. These factors permit to evaluate some of the variables that can affect the quality of spectra acquired.

Blue is a colour that has been included in art compositions since ancient times. This continuous use highlights the importance of blue pigments in the evolution of art history because they reflect the search to find new materials with equivalent or new chromatic properties that are more widely available and with a higher chemical stability. Azurite, lapis lazuli (natural ultramarine) and Egyptian blue were the most important blue pigments in antiquity. Since the eighteenth century chemical developments have yielded new, cheaper alternatives that include synthetic blues: Prussian blue (PB) [17–20] (1706), Ultramarine blue (UM) [17,21,22] (1828) and Phthalocyanine blue (Pht) [17,23,24] (1935). Several studies on these pigments have been published, and some reports stress the difficulties related to their identification when they are included in mixtures at low concentrations [11,13].

The information obtained for these pigments can be applied to address the expected limitations of MidIR-FORS when used to study other types of art objects [2].

Experimental

Materials

Pigments used in this study are presented in Table 1. The medium was a polymerised linseed oil purchased from Jacques Blockx trademark in Barcelona (Spain). A commercial canvas on a stretcher, prepared with a white ground (dimension 16 × 22 cm), was used as support.

Instrumentation

MidIR-FORS

Reflection FTIR spectra were recorded using a BOMEM MB^{-1}20 Fourier transform infrared spectrometer equipped with a Remspec mid-infrared fibre optic sampling probe. The spectrometer has a KBr beam splitter, a Glowbar source and a mercury cadmium telluride (MCT) detector refrigerated with liquid nitrogen.

The fibre optic probe is a bifurcate cable containing 19 chalcogenide glass fibres, each one with a diameter of 500 μm, seven of which carry the infrared radiation from the source to the sample, while the others 12 collect the radiation reflected off the surface.

The chalcogenide glass fibres allow the acquisition of spectra from 4000 to 900 cm^{-1}, except in the 2200–2050 cm^{-1} region due to the Se–H stretching absorption of the fibres. All FORS spectra were recording with 200 scans at a spectral resolution of 4 cm^{-1}.

Micro-FTIR

Analyses were performed with the same BOMEM MB120 Fourier transform infrared spectrometer equipped with a Spectra-Tech Analytical Plan microscope with a diamond cell as a sample holder. Spectra were recorded between 4000 and 350 cm^{-1} with a resolution of 4 cm^{-1} and an accumulation of 100 scans. Measurements were performed in transmission mode.

Infrared imaging

Reflection FTIR Imaging was performed with a Thermo iN10 MX spectrometer with a MCT detector. A computer controlled *x*–*y*

Table 1
Description of pigments.

Acronym	Pigment	Commercial name	Ref.	Manufacturer	Purchased	General formula
Pht	Phthalocyanine blue	Heliogenblau	23,050	Kremer	Germany	$C_{32}H_{15}N_8Cu$
PB	Prussian blue	Milori Blau	45,200	Kremer	Germany	$NH_4Fe[Fe(CN)_6]$
UM	Synthetic Ultramarine blue	Ultramarine blue dark	45,010	Kremer	Germany	$3Na_2O{\cdot}3Al_2O_3{\cdot}6SiO_2{\cdot}2Na_2S$

stage enabled scanning of the sample spot by spot according to the selected area. Reflection measurements were collected with an objective aperture of 150 μm, a step size of 150 μm, a spectral resolution of 4 cm^{-1} in a spectral range of 4000–675 cm^{-1}, accumulating 4 scans. The dimension of the mapping area was 4.5 mm^2 equivalents to 1024 spectra.

Procedure

Oil paintings preparation

The painting layers were completed with binary mixtures of three different blues [Prussian blue (PB), Phthalocyanine blue (Pht) and synthetic Ultramarine blue (UM)]. Due to the pigment grain size, form, and composition, the oil absorbed by each pigment is different. Thus, the percentage of linseed oil required to obtain a viscous paint for each pigment was established empirically. From the results obtained in the previous step, paintings with different binary mixtures of pigment were prepared (Table 2).

During the preparation of the viscous paint, an inert volatile solvent (White Spirit) was used to make the paint more flexible and easier to work with on the canvas surface. Once the paint was pasted, two layers of paint were applied on the prepared canvas white ground. The drying time was 2 weeks between each of the layers and a total drying time of 2 months for all layers.

Sampling and measurement

MidIR-FORS. The fibre optic probe was held perpendicular to the sample surface by a mechanical arm. The distance between the probe and the surface remained fixed at approximately 4 mm. The area investigated was around 20 mm^2 depending on the probe diameter.

The total reflectance R (from combined diffuse and specular components) was measured using the spectrum collected from an aluminium mirror as background. The spectrum intensity unit is defined as a pseudo absorbance A' obtained from R by $A' = \log(1/R)$.

Micro-FTIR. Extraction of small particles (approximately 1×1 mm) from the painted surface was performed with a micro-surgery scalpel. Manipulation was performed under a magnification lens (50×). Five samples were removed from each painting. Using the infrared microscope, each one of these small samples was placed on the diamond cell and pressed to obtain a layer as thin as possible to facilitate transmission of infrared radiation. The diameter of the radiation beam that passed through the sample was 100 μm. The measurement performed was focused in the centre of the diamond cell.

Infrared imaging. Measurements were performed on two strips cut from the mock-up with the paint layers of PB + UM5050% and PB + Pht5050% mixtures.

Experimental set-up

Using MidIR-FORS, five spectra for each mock-up were acquired across the surface, changing the analytical conditions such as point (following a grid line) and day on which the spectra were collected.

(I) Same day at the same point (D = P=) – repetitivity.
(II) Same day at a different point (D = P≠) – reproducibility across surface.
(III) Different day at the same point (D ≠ P=) – reproducibility along time.
(IV) Different day at a different point (D ≠ P≠) – reproducibility.

Principal component analysis (PCA)

PCA was applied. The statistical treatment of the spectra was implemented in Matlab PLS_toolbox_652 from Eigenvector RI.

Detection – parameters and data treatments

The detection limit 0.5 (DL0.5) is defined as the minimum concentration at which the signal related to the presence of the compound is detected in at least half of the measurements performed. The evaluation of the limit was established applying only a baseline correction as a common data treatment, while no other pre-treatments were applied to avoid misunderstanding in the interpretation of spectra. However, as verification, the values were calculated before and after the pre-treatments described, and no changes in the values were observed.

The dispersion parameter used in this study is the mean of the Relative Standard Deviations (mRSD) of the series of measurements performed for each analysed surface calculated with the following formula:

$$\mathrm{mRSD} = \frac{\sum_i^{\mathrm{n}} \left(\frac{\sqrt{\frac{\sum_j^m \left(H_{ij} - \overline{H}_i\right)^2}{m-1}}}{\overline{H}_i} \times 100 \right)}{\mathrm{n}}$$

Table 2
Concentrations and proportions of pigments in canvas paintings.

PB + Pht				Pht + PB				PB + UM			
PB	Pht	PB	Pht	Pht	PB	Pht	PB	PB	UM	PB	UM
(Pigment/total wt%)		(Pigment/pigment wt%)		(Pigment/total wt%)		(Pigment/pigment wt%)		(Pigment/total wt%)		(Pigment/pigment wt%)	
32.1	0.3	99	1	24.2	0.2	99	1	32.2	0.3	99	1
31.3	0.9	97	3	26.4	0.8	97	3	31.8	1.0	97	3
30.7	1.5	95	5	26.7	1.3	95	5	31.4	1.6	95	5
30.1	2.4	93	7	26.7	2.1	93	7	30.8	2.5	93	7
25.1	6.2	80	20	25.9	6.5	80	20	27.7	6.9	80	20
20.3	10.2	67	33	23.5	15.5	67	33	24.2	12.1	67	33
15	15	50	50	15	15	50	50	19	19	50	50

where $H_{i,j}$ is the height of the selected band of the spectrum, j is the spectrum analysed, i is the sample analysed, m is the total number of spectra analysed in each sample and n is the total number of samples analysed.

The height of the bands selected as the marker of each pigment was established by using MATLAB.

Before applying principal component analysis, the data set was processed using pre-treatment methods. As the first step, the wavelengths that correspond to the signal of the strong fibres absorption were cut off. The spectra were smoothed using the Savizky–Golay smoothing algorithm [25] (5 point filter, order of the polynomial 0, no derivative correction) and normalised by the Standard Normal Variate algorithm (SNV) [16]. SNV uses the following equation: $x_{Snv} = (x_{i,k} - \bar{x}_i)/\mathrm{STD}$; where x_{SNV} is the transformed element, $x_{i,k}$ is the original element, $\bar{x}_i$ is the mean of spectra i, $k = 1, 2, \ldots, m$, m is the number of variables in the spectra, and $i = 1, 2, \ldots, n$, where n is the number of the validation sets.

Finally, a baseline algorithm was applied to subtract a polynomial baseline offset from the spectra.

Results and discussion

A preliminary step in this study was the analysis of the spectra to establish the marker band for each pigment. The detection limits achieved for MidIR-FORS were subsequently compared with the micro-FTIR. Starting from those limits, a study of the reproducibility of the FORS signal was performed focusing on the factors that may introduce dispersion of the data. Finally, PCA analysis was applied to evaluate the capability of this statistic method to discriminate among the different binary mixtures.

MidIR-FORS

Marker bands

The marker bands have been chosen as an indication of the presence of the pigment in the paint layer. All of the selected bands are characteristic, presenting different relative intensities and overlapping-levels with the absorption bands of the binder or the absorption signal of the fibres that constitute the probe.

The marker band chosen in the spectrum of the PB correspond to the CN^- stretching (Fig. 1a). This band is slightly shifted to 2085 cm^{-1}, though it is partially overlapped by the Se–H stretching absorption of the fibres and it shows a medium intensity. In the case of the Pht, it was used as a marker one of the two combination bands at 1959 (marker) and 1895 cm^{-1} that appear in the spectrum collected in the reflectance mode (Fig. 1b).

The spectrum of the UM shows characteristic bands in the 1150–950 cm^{-1} (1034 cm^{-1} as marker) range due to the overlapping between the stretching of Si—O—Si and Si—O—Al. In the reflectance-mode spectrum two combination bands also appear at 1958 and 1797 cm^{-1} that are not considered because their absorption is too weak (Fig. 1c).

The binary mixtures that were analysed included pigments with signals that generate different intensities and different degrees of overlap (Table 3) between them and the linseed oil spectrum.

Detection limit – MidIR-FORS

Once the characteristic bands were selected, the detection limit used to compare the different techniques was established following the DL0.5 criteria.

For the mixture of Pht (major component) plus PB (minor component), where the representative band of the minor component (2085 cm^{-1}) is slightly overlapped with the S–H stretching, the signal was detected in almost all of the analyses and concentrations; the DL0.5 values were established between 2.1% and 6.5%, corresponding to a proportion of the pigments ranging between 93:7 and 80:20.

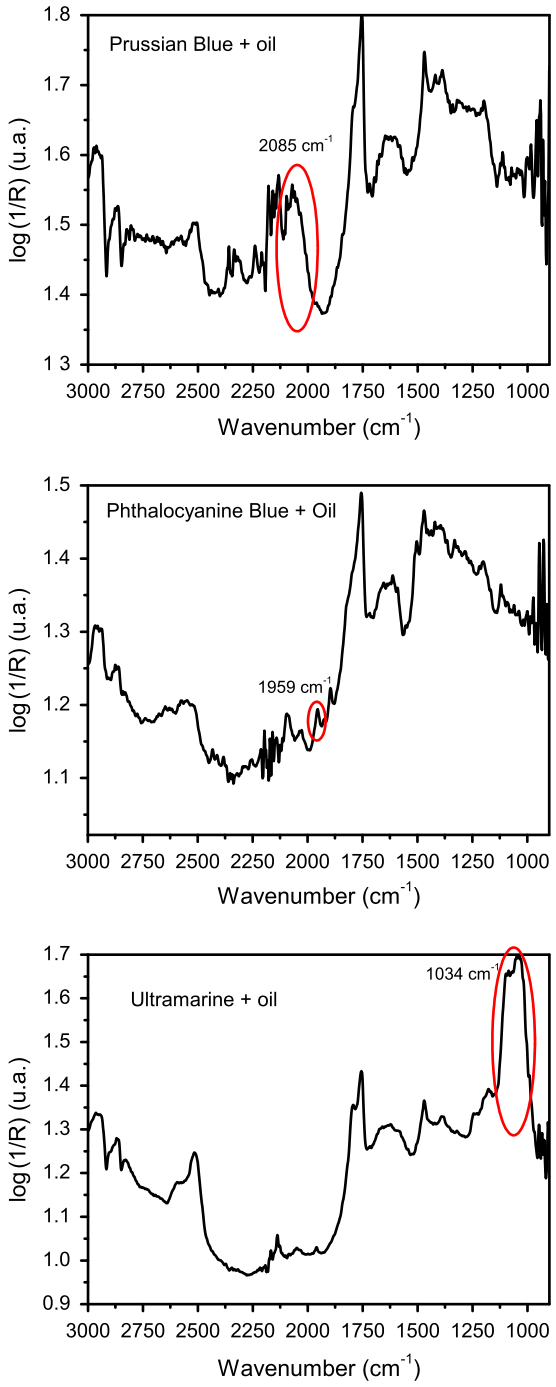

Fig. 1. MidIR-FORS spectra of the oil binder and pure pigments for (a) Prussian blue, (b) Phthalocyanine blue and (c) Ultramarine blue.

When the relative intensity decreases, in the case of PB (major component) plus Pht (minor component), the number of positive identifications at low concentrations also decrease. The DL0.5 values achieved for the band at 1959 cm^{-1} are between 6.3% and 10.2% (80:20/67:33).

For the mixture of PB (major component) plus UM (minor component, 1034 cm^{-1}), the UM band can be detected only at a concentration of 12.1%, which corresponds to a 67:33 mass ratio of the pigments. At 50:50 proportions, the intensity of 1034 cm^{-1} band is below expectations. This behaviour could be explained

Table 3
Description of the "marker" bands.

Pigment	Characteristic bands (cm^{-1})	Relative intensity	Overlap with oil/fibre absorption	Particle size (μm)
Pht	1959	*w*	Slightly/no	<1
PB	2085	*m*	No/yes	75–35
UM	1034	*s*	Yes/no	15–10
Oil	1750	*s*	No/no	–

with so-called inverted or "Reststrahlen bands" that appear as a result of specular reflectance [15]. This component of the radiation is reflected directly from the surface of the grains and has no absorptive interaction with the sample. Derivative-shaped peaks or apparent absorbance dips ("Reststrahlen bands") appear at very strong molecular vibration bands (such as Si—O) in the 1200–400 cm^{-1} region [26].

To verify the presence of the inverted band a reflection FTIR imaging mapping of a selected area of the PB + UM5050% painting has been recorded. Although this technique uses a reflection mode it provides spectra with a higher signal/noise ratio with respect to the MidIR-FORS arrangement because of the absence of the fibres noise factor.

As can be seen in Fig. 2, when the Kramer–Kronig algorithm [24,27] is applied to the UM spectra to correct for the specular component, the infrared imaging mapping shows a clearer presence of the pigment across the surface. Once demonstrated that the detection problem of the UM is the inversion of the marker band, it is important to underline that in MidIR-FORS spectra both specular and diffuse components of the reflected light are present, as consequence of surface roughness [28]. Thus, no corrections can be applied and the spectra are much more difficult to interpret [5,29–33].

Detection limits obtained for all of the pigments are high for material characterisation purposes. This situation may result in an erroneous description of artwork composition and presents an important drawback in the study of the creative process of the artist.

The FTIR mode commonly used for characterisation purposes is the transmission mode. For that reason it is interesting to compare it with the reflectance technique to understand better how the detection limit may change.

By comparing the results of the MidIR-FORS with the results obtained with the micro-FTIR (Table 4), the increase in the values for the reflectance mode can be observed. In both techniques the identification of the absorption band was established following the same criteria; thus, it is possible to explain this behaviour by the low signal/noise ratio, the distortions that affect the reflectance spectra, and the heterogeneous distribution of the pigment across the surface. Fig. 3 shows the mapping of the PB and Pht mixture (50:50%) considering the Pht marker band. It can be observed that the heterogeneity in the distribution of the pigments is larger than expected, taking into account only the particle size. This behaviour could be related to different arrangements of the particles in the paint layer during the drying process.

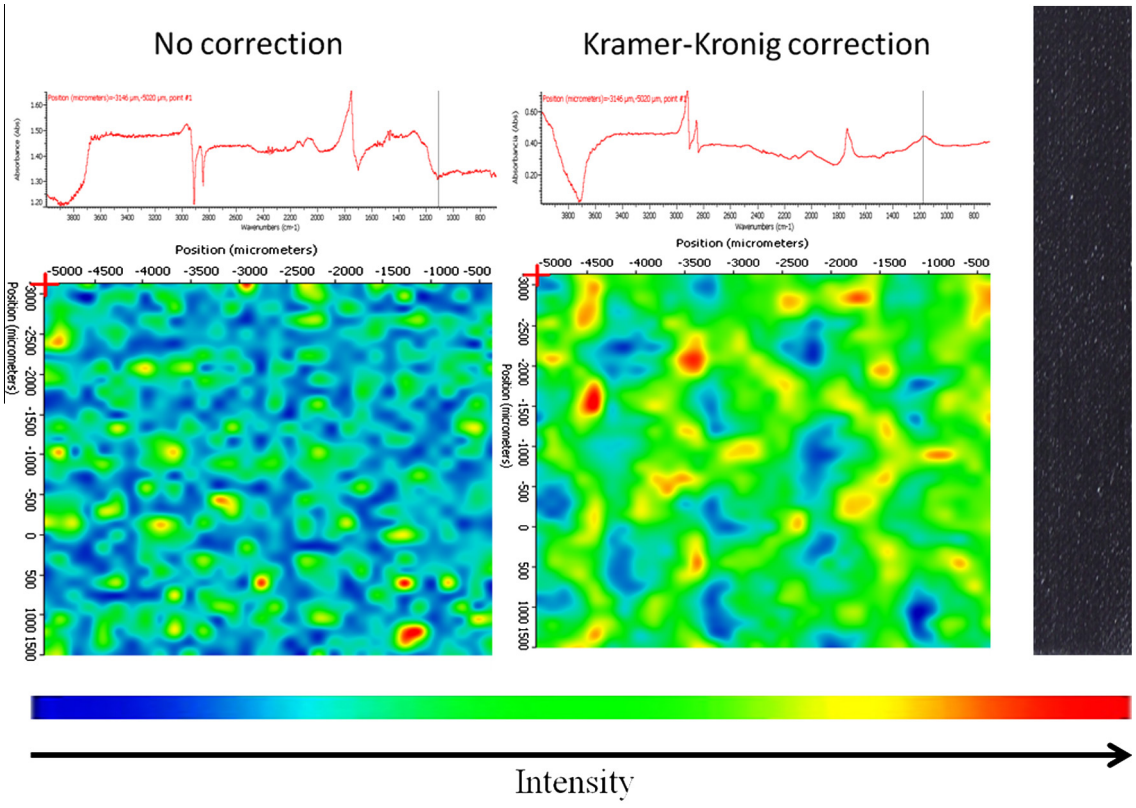

Fig. 2. FTIR false colour plot of PB + UM5050% painting – peak area map of Ultramarine marker band (1034 cm^{-1}): (a) raw spectrum and mapping, and (b) spectrum and mapping corrected by Kramer–Kronig algorithm.

Table 4
Detection limits for pigments in MidIR-FORS vs. micro-FTIR.

Pigment	MidIR-FORS		Micro-FTIR	
	(Pigment/total wt%)	(Pigment/pigment wt%)	(Pigment/total wt%)	(Pigment/pigment wt%)
Pht	6.3–10.2	80:20/67:33	0.9–1.5	97:3/95:5
PB	2.1–6.5	93:7/80:20	⩽0.24	99:1
UM	12.1	67:33	⩾19	50:50

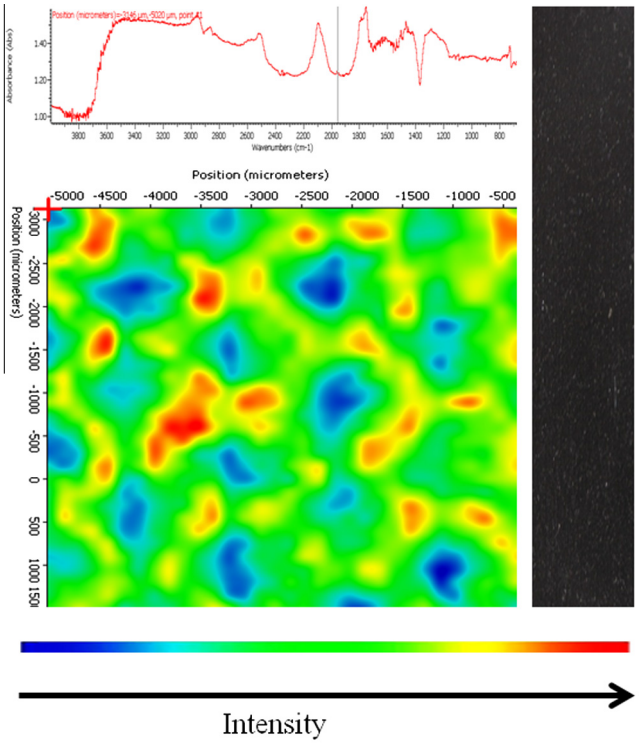

Fig. 3. FTIR false colour plot of PB + Pht5050% painting – peak area map of Phthalocyanine marker band (peak area map of 1959 cm^{-1}): raw spectrum and mapping.

Reproducibility

The next step in this experiment was to study the reproducibility of the technique. The spectra collected have many sources of variability. These sources of variability can be grouped into two classes depending on the origin: instrument (instability) and painting layers (physical–chemical features).

Fig. 4 shows a scheme of the reproducibility study arrangement that explains how the dispersion factors have been investigated and connected with the analysis condition changes.

For this study of reproducibility only mixtures with concentrations of minor component upon the detection limit were considered.

Due to the high variability of the results, discussion was performed based on the average values of the data.

The reproducibility study was performed, firstly, using the raw spectra as usually performed and, afterwards, using the processed spectra, with the aim to investigate the effect of the pre-treatments on the data set reproducibility.

Instrumental reproducibility. The stability of the instrumental stability can be estimated by considering the C=O band (s) of the linseed oil (1750 cm^{-1}), which is present in the mixtures in high and quite constant proportion in all the paint layers. The results obtained for the repetitivity – evaluating series of measurements

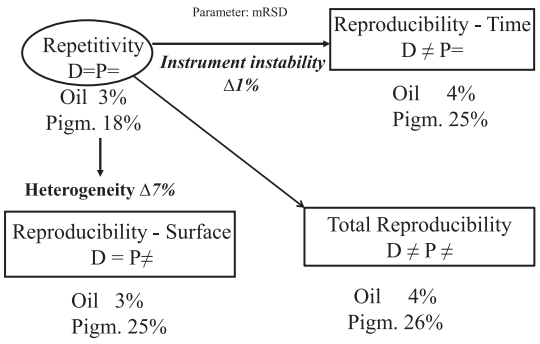

Fig. 4. Diagram of the reproducibility for MidIR-FORS row spectra.

acquired on the same day at the same point across the surface (D = P=) – show that the relative dispersion for the oil band intensity (mRSD) is 3%. When the day changes (D ≠ P=) the variation increase a bit up to 4%. These two values cannot be considered different and they lead to the conclusion that the instrumental reproducibility is approximately 3–4%. This dispersion is a quite low, which means that the analysis may be performed on different days without significant variation in the response of the equipment.

Paint reproducibility – paint layers heterogeneity. Several factors will be taken into account to discuss the reproducibility of measurements across the painting surface: intensity and degree of overlap of bands, particle size and distribution of pigments in the paint layers.

The dispersion of the results may be evaluated by comparing the dispersion obtained for the pigment signals vs. the dispersion of the linseed oil signal under constant analysis conditions (D = P=). The results show (Fig. 5) an increase of the total mean repetitivity parameter in RSD from a value of 3% for the oil to up to 18% for the pigments considered together. Observing the repetitivity of the three pigments and binder it is interesting to notice that the values of mRSD are higher for the pigment with the band-marker characterised by lower intensity, such as the Pht – 17%, compared to the UM and oil – 3% – which shows a higher intensity. In the case of the PB, which has an intermediate intensity, the dispersion rose to 20% due to the overlapping of the S–H stretching band with the marker band.

Second, the dispersion across the paint surface was considered. For this purpose, the results presented above (D = P=) were compared to the results obtained for measurements acquired on the same day but at different points across the surface of the mock-up (reproducibility across surface – D = P≠). In this case, the total dispersion increased to up to 25%, with a difference of 7% that may be attributed to the heterogeneity of the distribution of the pigment across the paint layer. Comparing the repetitivity values of pigments (D = P=) with those obtained for reproducibility across surface (D = P≠), the dispersion clearly increases in all the cases (UM Δ12%, PB Δ9%, Pht Δ4%).

The higher dispersion value for PB (particle diameter ~35 μm) than for Pht (homogeneous distribution aspect in SEM image analysis – organic nature) may be due to the larger particle size

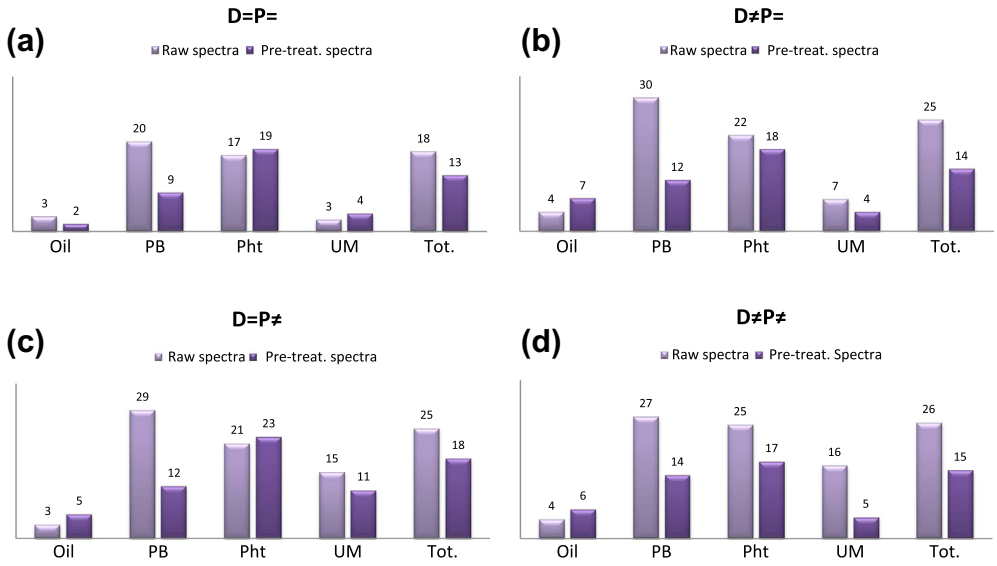

Fig. 5. Bar chart of the results obtained by MidIR-FORS without and with the application of pre-treatment to the raw data. (a) Bar chart of repetitivity (D = P=), (b) reproducibility over time (D ≠ P=), (c) reproducibility across the surface (D = P≠), and (d) total reproducibility (D ≠ P≠).

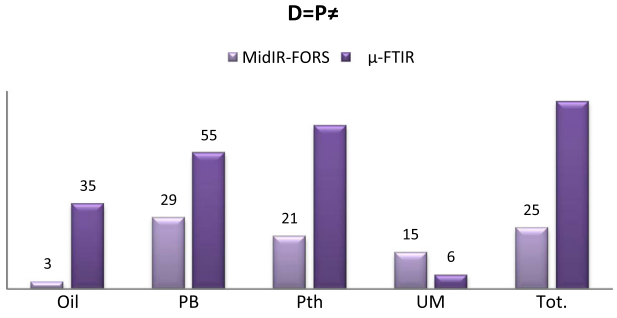

Fig. 6. Bar chart of the results for the reproducibility across the surface obtained by MidIR-FORS vs. Micro-FTIR.

of the first pigment relative to the second pigment that produces a more heterogeneous distribution of the PB pigment. The increase of the UM dispersion may be attributed to changes in roughness of the surface, which leads to variation of the signal reflection and distortion of the marker band, as it was discussed in detection limit section.

Furthermore, reproducibility along time has been studied when just the day of measurement changes (D ≠ P=). It is possible to notice that the variation on procedure conditions have low influence on the more intense bands (oil and UM), although it is an important dispersion factor when the band is overlapped with the signal/noise of the fibres (PB – D = P = 20% – D ≠ P = 30%). One possible explanation for the slight increase of the UM could be related to changes in the analysis procedure, such as slightly different position of the probe.

The values obtained for all the pigments support the importance of the particle size and the morphological features of the surface analysed as reasons of measurements variability.

The total dispersion (D ≠ P≠) achieved is approximately 3% for the oil and 26% for the pigments. The value for the pigments is quite elevated, although all the identifications are above the detection limit. Each compound shows the dispersion values of the factor established as critical for each pigment's properties and marker band features (UM – changes in probe position and band distortions – P≠; PB – heterogeneity and overlapping – D ≠; Pht – low relative band intensity – D≠).

Pre-treated spectra reproducibility. Reflection spectra are affected by many factors that contribute to making the extraction of the

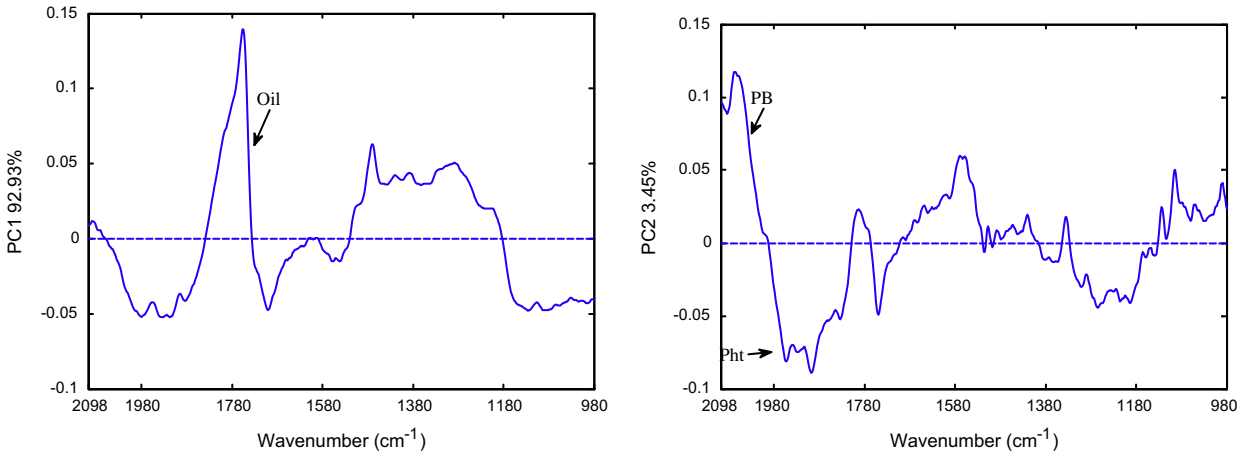

Fig. 7. Loading plot of the PCA model: (a) PCs1; and (b) PCs2.

composition information more difficult. To reduce these contributing factors and to facilitate signal identification pre-treatment methods were applied to the spectra. As the first step, the wavelengths that correspond to the strong fibres absorption (2200–2050 cm^{-1} and $\geqslant$ 900 cm^{-1}) were cut off and the Savizky–Golay smoothing algorithm [34] was used to reduce the noise. The SNV algorithm was applied to minimise the multiplicative interferences of scatter and the change of light distance. SNV corrects both multiplicative and additive scatter effects [16,35]. To remove slope variations on an individual spectrum basis, each object is treated independently. Finally, it was applied a baseline to better evaluate the changes in the intensity of the bands chosen. Mean centring and autoscaling were not used because no improvements on the discrimination between mixtures were observed when applied; on the contrary, the noise was amplified when these treatments were included.

Pre-processing led to a decrease in the offset between the spectra, and the data became visibly more linear depending on the concentration of the pigments.

The total dispersion after pre-processing data decreased approximately 5 percentage points when the day of the analysis is the same (D = P≠, D = P=) and11 percentage point when the day of measurement also change (D ≠ P=, D ≠ P≠). These pre-treatments reduce the remaining major sources of dispersion, such as procedure variability. Only the dispersion relative to the heterogeneity of the distribution of compound remains the same/, as shown by the fact that total dispersion of D = P≠ became equal to D ≠ P≠ and, for those measurement conditions the values are higher than D = P=.

Another important comment associated with the data treatment is that the order the increase of the dispersion follows the order of the relative intensity of the band chosen for each pigment (Oil, UM, PB and Pht).

MidIR-FORS vs. micro-FTIR – reproducibility. Comparing the reproducibility of MidIR-FORS vs. micro-FTIR – D = P≠ (Fig. 6) – the values of mRSD that correspond to the oil band increase to up to 35%. The important increase in the dispersion may be due to the reduced number of samples taken in a highly heterogeneous artwork and/or to the sample manipulation in the measurement process with micro-FTIR. Thus, when the sample is pressed on the diamond cell and the components are dispersed across the cell area, reproducibility will depend on the material distribution with regard to the infrared radiation point and on the thickness of the layer. Furthermore, the largest areas analysed by FORS (approximately 2×2 mm^2 – area of the probe) compared with the 100×100 μm^2 area of the micro-FTIR beam has – like in the case of the sampling – a strong influence on the dispersion obtained,

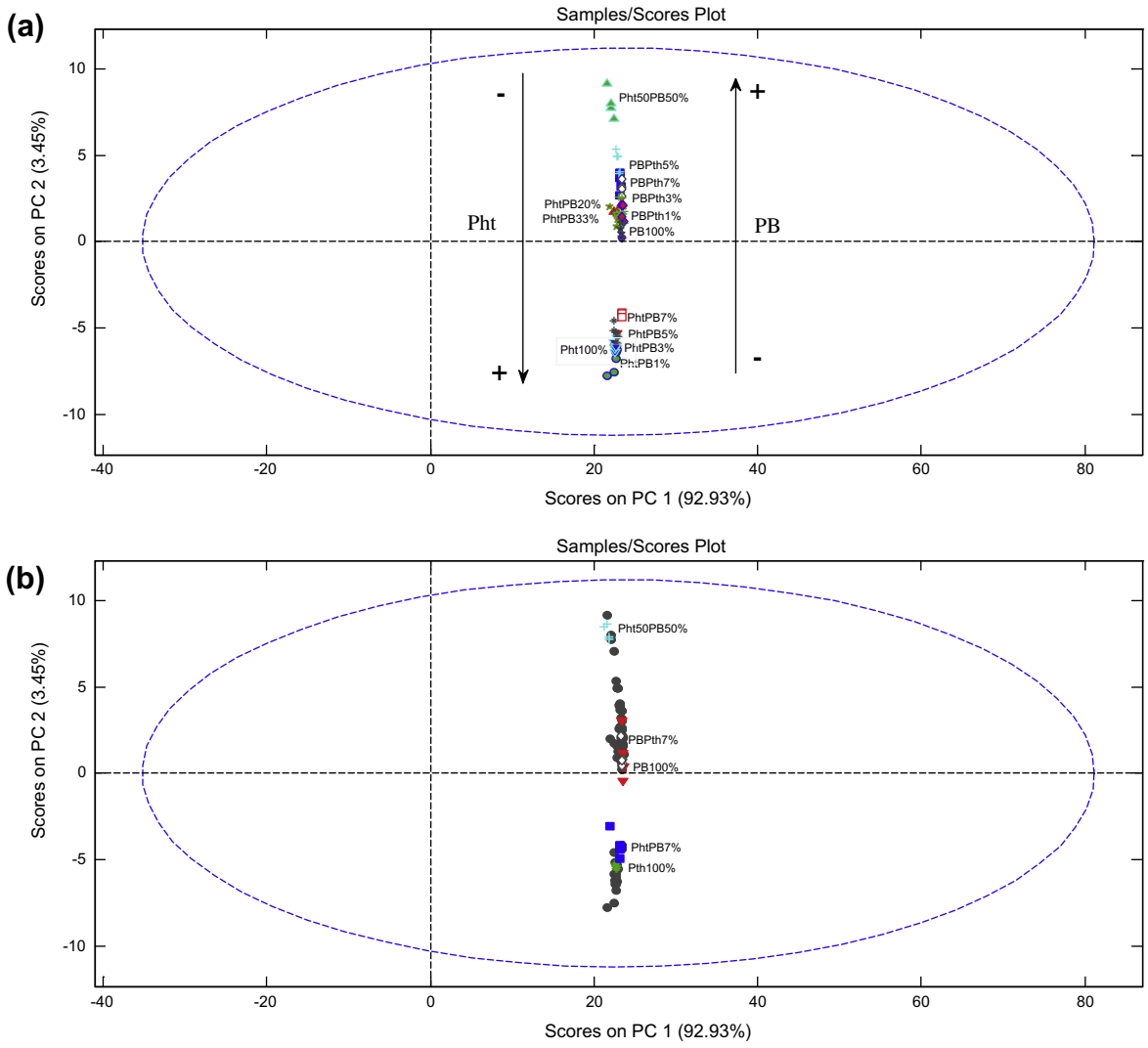

Fig. 8. Score plot of the PC2 vs. PC3 calculated for: (a) PB minor component mixture data set; and (b) Pth minor component mixture data set.

due to the high heterogeneity of the artwork. The same behaviour may be observed in the case of the pigments (PB 55%, Pht 66%) except for the UM, for which the characteristic band result more easy identifiable in transmission mode.

Micro-FTIR produces high-quality spectra and is useful for the characterisation of artistic materials, although the results indicate variability and dispersion, which may be reduced by performing replicates and by the experience of the analyst selecting the cell point where the material of interest is located. However, replicates option is limited due to the restrictions on taking a high number of samples from an artwork. Other options like the use of micro-FTIR imaging can be used to improve the results, but with the same limitation of reduced surface analysed [36].

Principal component analysis (PCA)

Finally, to identify and quantify different mixtures a statistical treatment, principal component analysis (PCA), was applied to the data.

This method was applied to the matrix data set composed on spectra collected on the paintings created with PB + Pth and PB + UM mixture (5 spectra for each proportion of the D = P = and D = P ≠ conditions). The range of wavenumbers considered was between 2090 and 900 cm^{-1}, where the marker bands are located. Before using the spectra matrix, pre-treatments, such as cut off of fibres absorption, Savizky–Golay smoothing algorithm, polynomial baseline offset and Standard Normal Variate algorithm – SNV were applied.

PB+Pth mixture. In the calibration step, spectra acquired in D = P = conditions were used. Three Principal Components (PCs) were selected due to the fact that these explain more than 98% of the total variance.

Analysing the loadings plots of the PCs selected, it is possible to observe that the corresponding to the PC1 (Var.92.93%) focuses the main variance to the carbonyl band of the linseed oil (Fig. 7a). On the other hand the PC2 (3.45%) gives positive contribution to the marker band of PB (stretching of the CN^-ion at 2090 cm^{-1}) and negative contribution to the marker band of Pht (combination bands at 1959 and 1895 cm^{-1}) (Fig. 7b). The loading of the PC3 (1.41%) has difficult physical interpretation.

In Fig. 8a the PC1–PC2 score plot is reported, and the image shows large clustered groups indicating that the first component

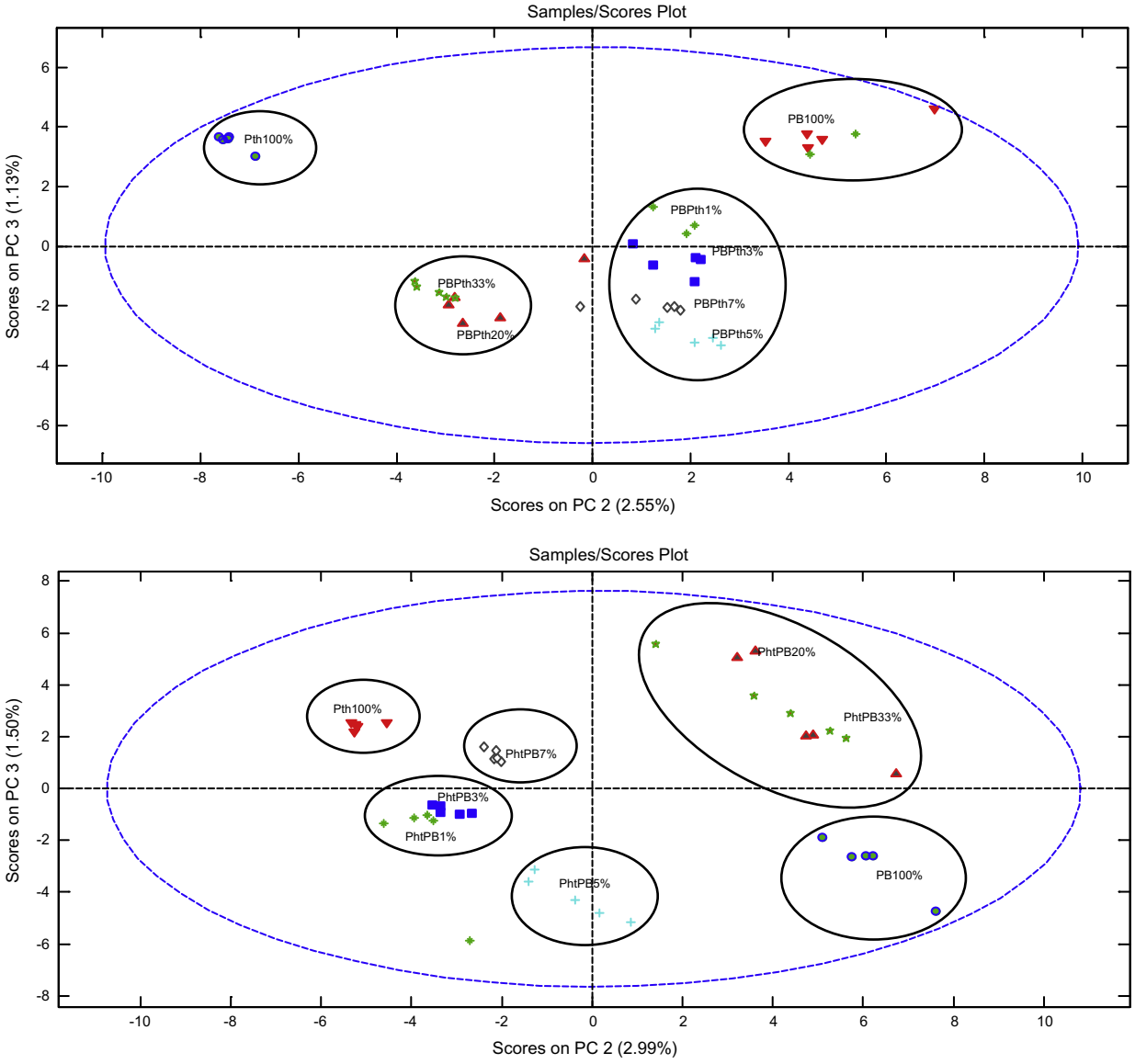

Fig. 9. Score plot of the PC2 vs. PC3 calculated for: (a) Pth minor component mixture data set; and (b) PB minor component mixture data set.

does not play an important role in the differentiation of the mixtures because the image was related to the oil and not to the pigments. For the PC2, the score represents a linear behaviour that explains the increase/decrease of the PB and Pht in the mixtures, following the loading interpretation where the increase of the Pht concentration tends toward negative values, and the increase of the PB concentration tends to positive score values.

The presence or absence of the marker band and the variability of the intensity of the stretching of the CN^-ion allows the separation of the score into three clusters. The two principal clusters (Pht 100 to Pht + PB7% and PB100% to PB + Pht 7%) discriminate among the mixtures depending on the major proportion of one pigment with respect to the other. The third cluster identification corresponds to the mixture of PB + Pht at 5050%.

The calibration model was validate with spectra acquired in D = P≠ condition. The validation score plot shows a good agreement with the calibration values (Fig. 8b) for the proportions Pht 100%, Pht + PB 8%, PB 100%, PB + Pht 7% and PB + Pht5050%. Despite of it is possible to observe a distribution in the clusters that reflect the variability of the signal due to the change of the points analysed.

To improve the discrimination capacity of the model, the score values of the PC3 were also considered. To better visualize the results obtained two plots of the two halves of the series of spectra acquired are presented (Fig. 9). In both cases, three PCs were selected presenting similar loadings plots as in the general model.

The PC2 and PC3 plots (Fig. 9) show a partial discrimination of the mixtures. These results demonstrate the difficulty to quantify the composition of the pigments but also that a differentiation between ranges of concentrations is possible, which could be useful for a global evaluation of the mixture composition.

Furthermore, it is interesting to notice that, for both pigments, the model permits a differentiation of the clusters even at the concentrations corresponding to the detection limit.

In fact, in Fig. 9a where the Pht is the minor component, it can be seen that the mixtures are discriminated starting from the proportion of Pht 20–33%. However, when the PB is the minor compound (Fig. 9b), those differentiations begin at a proportion of PB 5–7%.

The validation of the model using the spectra acquired in the D = P≠ analysis condition, yields a good agreement in the score values of the new spectra with regard to the ones obtained in the model. The result indicates a satisfying match of the new scores with the concentration cluster established with the first model.

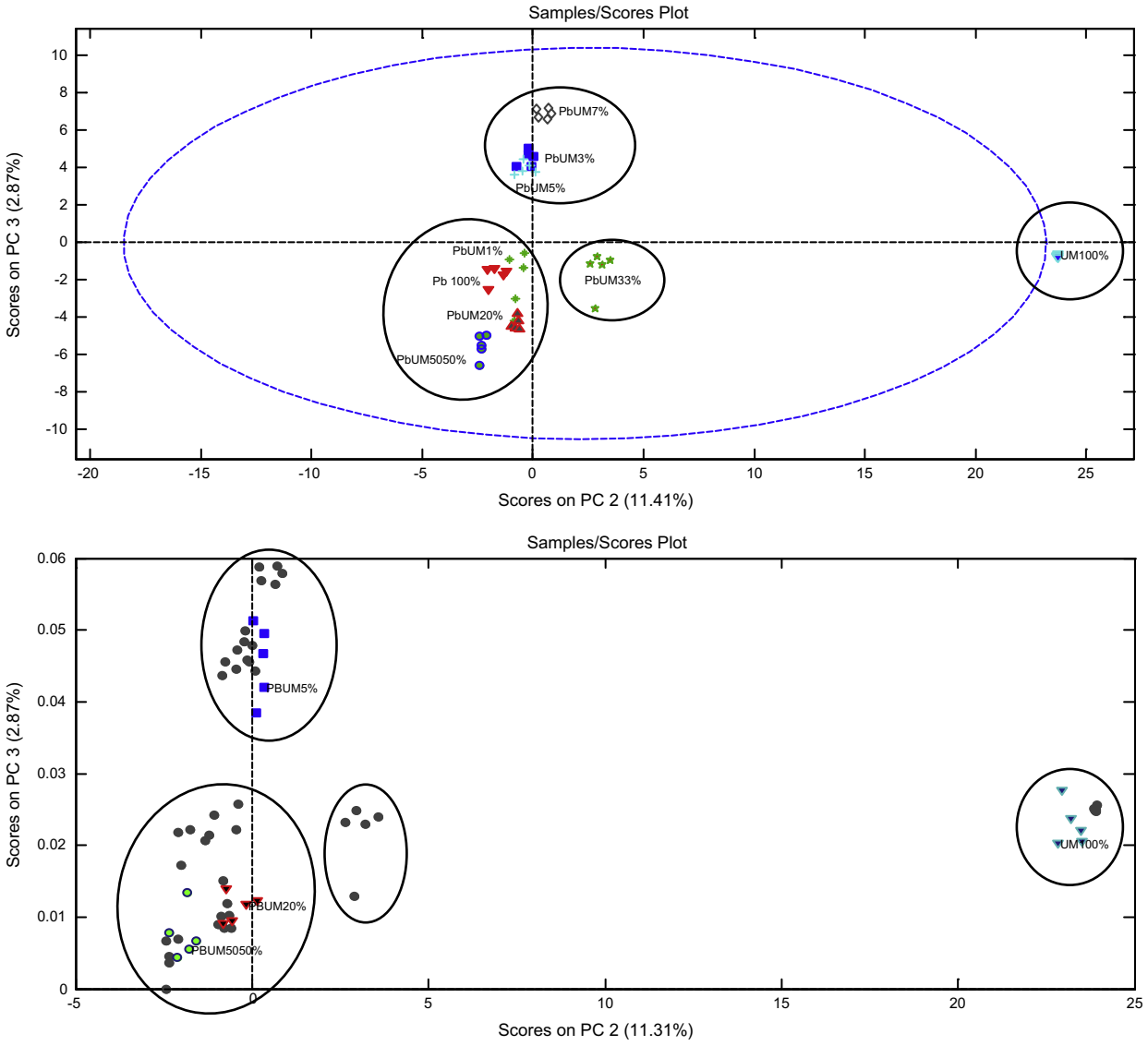

Fig. 10. Score plot of the PC2 vs. PC3 calculated for "UM minor component mixture" data set: (a) calibration model and (b) validation model.

The same procedure above was applied to the spectra of the PB + UM mixture. Three PCs were selected (98% of the total variance). In this case, the score plot (Fig. 10a) shows four principal clusters. The first one identifies the spectra where the 1034 cm^{-1} band of the UM is not present (PB100% and PB + UM1%) or probably inverted (PB + UM20% and PB + UM5050%); the second one corresponds to mixtures where the UM pigment is present in low concentrations (PB + UM3% – 5% – 7%); and the third is in concomitance of the detection limit (PB + UM33%). The last cluster corresponds to the pure pigment, whose spectrum presents a very definite marker band. The model has been validated with spectra acquired in D = P≠ condition (mixtures PB + UM5% – 20% – 50% – 100%). The new scores match the corresponding cluster (Fig. 10b).

According to the results obtained, the application of PCA to the MidIR-FORS spectra allows the differentiation of the binary mixtures according to the concentration range. This differentiation is achieved even at concentrations close to the detection limit due to the fact that the PCA model considers the variability of the full spectra and not only a characteristic band as usually performed.

Conclusions

For material characterisation of artworks, this study focusing on the detection limit and the reproducibility achieved by the MidIR-FORS spectroscopy indicates that:

- Detection limits for all the pigments are high for artworks material characterisation purposes. This situation may result in an erroneous description of object composition. Use of a complementary analytical technique to complete the information obtained by MidIR-FORS is recommended.
- Physical features (roughness of the surface, thickness of paint layers, etc.) of the artwork are significant issues to consider when using MidIR-FORS for characterisation, because those factors have an important effect on the quality of the reflectance spectra and are the cause of the high detection limits.
- The dispersion of the results due to the instrumental/procedure reproducibility is quite low, indicating that reflectance analysis can be performed on different days without a significant variation of the response of the instrumentation.
- The main factors that can affect the dispersion of the results obtained by MidIR-FORS are the heterogeneity of the paint layers, the signal intensity of the representative bands selected, the particle size and the distribution of the pigments, and the level of overlap of the marker bands with the signal of the binder or of the fibres.
- Data pre-treatment and variable selection provided the optimal results for infrared analysis. Pre-treatments permit to reduce the procedure variability remaining mainly the variability due to the heterogeneity of the paint layer analysed. This study underlines that the use of Standard Normal Variate algorithm (SNV) together with removal of the noisy variables by a selection of the wavelengths are responsible for the major improvement of the spectra data set.
- PCA and MidIR-FORS methods are able to discriminate between different mixtures of oil paints on canvas according to the concentration range of the pigments included and within their detection limits.

Acknowledgments

The authors wish to thank N. Ferrer (SCT-UB) for her kind advice on the use and interpretation of the infrared spectroscopy. The authors are grateful for financial support from the Spanish Ministerio de Educación y Ciencia for this study (HAR2011-29654 2011–2013 and PhD Grant FPU/AP2009-2575).

References

[1] A. Sarmiento, M. Pérez-Alonso, M. Olivares, K. Castro, I. Martínez-Arkarazo, L. Fernández, J. Madariaga, Classification and identification of organic binding media in artworks by means of Fourier transform infrared spectroscopy and principal component analysis, Anal. Bioanal. Chem. 399 (2011) 3601–3611.
[2] C. Miliani, F. Rosi, A. Daveri, B. Brunetti, Reflection infrared spectroscopy for the non-invasive in situ study of artists' pigments, Appl. Phys. A: Mater Sci. Process. 106 (2012) 295–307.
[3] M. Bacci, S. Baronti, A. Casini, P. Castagna, R. Linari, A. Orlando, M. Picollo, B. Radicati, Detection of alteration products in artworks by non-destructive spectroscopic analysis, Mater. Res. Soc. Symp. Proc. 352 (1995) 153–159.
[4] T. Poli, O. Chiantore, M. Nervo, A. Piccirillo, Mid-IR fiber-optic reflectance spectroscopy for identifying the finish on wooden furniture, Anal. Bioanal. Chem. 400 (2011) 1161–1171.
[5] F. Casadio, L. Toniolo, The analysis of polychrome works of art: 40 years of infrared spectroscopic investigations, J. Cultural Heritage 2 (2001) 71–78.
[6] M. Bacci, M. Fabbri, M. Picollo, S. Porcinai, Non-invasive fibre optic Fourier transform-infrared reflectance spectroscopy on painted layers: Identification of materials by means of principal component analysis and Mahalanobis distance, Anal. Chim. Acta 446 (2001) 15–21.
[7] M. Bacci, R. Chiari, S. Porcinai, B. Radicati, Principal component analysis of near-infrared spectra of alteration products in calcareous samples: an application to works of art, Chem. Intellig. Lab. Syst. 39 (1997) 115–121.
[8] F. Rosi, A. Daveri, C. Miliani, G. Verri, P. Benedetti, F. Piqué, B. Brunetti, A. Sgamellotti, Non-invasive identification of organic materials in wall paintings by fiber optic reflectance infrared spectroscopy: a statistical multivariate approach, Anal. Bioanal. Chem. 395 (2009) 2097–2106.
[9] G. Dupuis, M. Menu, Quantitative evaluation of pigment particles in organic layers by fibre-optics diffuse-reflectance spectroscopy, Appl. Phys. A: Mater. Sci. Process. 80 (2005) 667–673.
[10] F. Rosi, V. Manuali, C. Miliani, B.G. Brunetti, A. Sgamellotti, T. Grygar, D. Hradil, Raman scattering features of lead pyroantimonate compounds. Part I: XRD and Raman characterization of $Pb_2Sb_2O_7$ doped with tin and zinc, J. Raman Spectrosc. 40 (2009) 107–111.
[11] S. Kuckova, I. Nemec, R. Hynek, J. Hradilova, T. Grygar, Analysis of organic colouring and binding components in colour layer of art works, Anal. Bioanal. Chem. 382 (2005) 275–282.
[12] C. Miliani, C. Ricci, F. Rosi, I. Borgia, B. Brunetti, A. Sgamellotti, Original and fake blue pigments from the church of S. Francesco in Montefalco painted by Benozzo Gozzoli: a spectroscopic approach, in: Proceedings of IRUG6 Conference, 2004.
[13] C. Sessa, A. Vila, J.F. Garcia, Determination of detection limits for SEM–EDS and m-FTIR analysis of artwork, – analytical and bioanalytical chemistry, Anal. Bioanal. Chem. 400 (2011) 2241–2251.
[14] E. Van Nimmen, K. De Clerck, J. Verschuren, K. Gellynck, T. Gheysens, J. Mertens, L. Van Langenhove, FT-IR spectroscopy of spider and silkworm silks: Part I. Different sampling techniques, Vib. Spectrosc. 46 (2008) 63–68.
[15] F. Rosi, A. Federici, B.G. Brunetti, A. Sgamellotti, S. Clementi, C. Miliani, Multivariate chemical mapping of pigments and binders in easel painting cross-sections by micro IR reflection spectroscopy, Anal. Bioanal. Chem. 399 (2011) 3133–3145.
[16] C. Muehlethaler, G. Massonnet, P. Esseiva, The application of chemometrics on Infrared and Raman spectra as a tool for the forensic analysis of paints, Forensic Sci. Int. 209 (2011) 10.
[17] R.J.H. Clark, Pigment identification by spectroscopic means: an arts/science interface, C. R. Chim. 5 (2002) 7–20.
[18] J. Giaccai, Pigment analysis of two Thai banner paintings, Mater. Res. Soc. Symp. Proc. 1047 (2008).
[19] B.H. Berrie, Prussian Blue. in: E. West Fitzhugh (Ed.), Artists' Pigment: A Handbook of Their History and Characteristics, Artists' Pigment: A Handbook of Their History and Characteristics, vol. 3, 1997, pp. 191–217.
[20] S. Kuckova, R. Hynek, I. Nemec, M. Kodicek, J. Jehlicka, Critical comparison of spectrometric analyses of non-mineral blue dyes and pigments used in artworks, Surf. Interface Anal. 44 (2012) 963–967.
[21] J. Plesters, Ultramarine blue, Natural and Artificial, Artists' Pigments: A Handbook of Their History and Characteristics, vol. 2, 1993, pp. 37–65.
[22] I. Osticioli, N.F.C. Mendes, A. Nevin, F.P.S.C. Gil, M. Becucci, E. Castellucci, Analysis of natural and artificial ultramarine blue pigments using laser induced breakdown and pulsed Raman spectroscopy, statistical analysis and light microscopy, Spectrochim. Acta Part A: Mol. Biomol. Spectrosc. 73 (2009) 525–531.
[23] S.Q. Lomax, Phthalocyanine and quinacridone pigments: their history, properties and use, Rev. Conserv. 6 (2005) 19–29.
[24] H. Zollinger, Color Chemistry: Synthesis, Properties and Applications of Organic Dyes and Pigments, VCH, Weinheim, VCH, Weinheim, 2004, pp. 140–160.
[25] A. Savitzky, M.J.E. Golay, Smoothing and differentiation of data by simplified least squares procedures, Anal. Chem. 36 (1964) 1627–1639.
[26] J. Madejová, FTIR techniques in clay mineral studies, Vib. Spectrosc. 31 (2003) 1–10.

[27] J. Workman, The Handbook of Organic Compounds NIR, IR, Raman, and UV–Vis Spectra Featuring Polymers and Surfactants, vol. 3, Academic Press, 2001.
[28] R.J.D. Tilley, Light and Colour, in: Anonymous Colour and the Optical Properties of Materials, John Wiley & Sons, Ltd., 2010, pp. 1–48.
[29] S. Bruni, F. Cariati, F. Casadio, L. Toniolo, Spectrochemical characterization by micro-FTIR spectroscopy of blue pigments in different polychrome works of art, Vib. Spectrosc. 20 (1999) 15–25.
[30] A. van Loon, Color Changes and Chemical Reactivity in Seventeenth-Century Oil Paintings (MolArt; 14), PhD Thesis, University of Amsterdam, 2008, pp. 24–32.
[31] d.W. van, Microspectroscopic Analysis of Traditional Oil Paint (MolArt; 7), PhD Thesis, University of Amsterdam, 2002, pp. 32–34.
[32] B. Harbecke, Application of Fourier's allied integrals to the Kramers–Kronig transformation of reflectance data, Appl. Phys. A 40 (1986) 151–158.
[33] K. Keune, Binding Medium, Pigments and Metal Soaps Characterised and Localised in Paint Cross-Sections (MolArt; 11), PhD Thesis, University of Amsterdam, 2005, pp. 1–7.
[34] M.P. Seah, W.A. Dench, Smoothing and the signal-to-noise ratio of peaks in electron spectroscopy, J. Electron Spectrosc. Relat. Phenom. 48 (1989) 43–54.
[35] Å. Rinnan, L. Nørgaard, F.v.d. Berg, J. Thygesen, R. Bro, S.B. Engelsen, Chapter 2 – data pre-processing (2009) 29–50.
[36] T. Poli, O. Chiantore, A. Giovagnoli, A. Piccirillo, FTIR imaging investigation in MIR and in an enlarged MIR–NIR spectral range, Anal. Bioanal. Chem. Issue 9 (402) (2012) p2977.

2.3 Influence of composition and roughness on the pigment mapping of paintings using mid-infrared fiberoptics reflectance spectroscopy (mid-IR FORS) and multivariate calibration

Anal Bioanal Chem
DOI 10.1007/s00216-014-8091-2

RESEARCH PAPER

Influence of composition and roughness on the pigment mapping of paintings using mid-infrared fiberoptics reflectance spectroscopy (mid-IR FORS) and multivariate calibration

Clarimma Sessa · Héctor Bagán · Jose Francisco García

Received: 6 June 2014 / Revised: 29 July 2014 / Accepted: 4 August 2014

Abstract Mid-infrared fiberoptics reflectance spectroscopy (mid-IR FORS) is a very interesting technique for artwork characterization purposes. However, the fact that the spectra obtained are a mixture of surface (specular) and volume (diffuse) reflection is a significant drawback. The physical and chemical features of the artwork surface may produce distortions in the spectra that hinder comparison with reference databases acquired in transmission mode. Several studies attempted to understand the influence of the different variables and propose procedures to improve the interpretation of the spectra. This article is focused on the application of mid-IR FORS and multivariate calibration to the analysis of easel paintings. The objectives are the evaluation of the influence of the surface roughness on the spectra, the influence of the matrix composition for the classification of unknown spectra, and the capability of obtaining pigment composition mappings. A first evaluation of a fast procedure for spectra management and pigment discrimination is discussed. The results demonstrate the capability of multivariate methods, principal component analysis (PCA), and partial least squares discrimination analysis (PLS-DA), to model the distortions of the reflectance spectra and to delimitate and discriminate areas of uniform composition. The roughness of the painting surface is found to be an important factor affecting the shape and relative intensity of the spectra. A mapping of the major pigments of a painting is possible using mid-IR FORS and PLS-DA when the calibration set is a palette that includes the potential pigments present in the artwork mixed with the appropriate binder and that shows the different paint textures.

Keywords Pigments · mid-IR FORS · Roughness · Oil paintings · Artwork characterization · PCA · PLS-DA

Introduction

A common aim in the study of artwork is to obtain representative information about the composition and structure of a piece without damaging it. Remote spectroscopic techniques are good candidates for this purpose, and mid-infrared fiberoptics reflectance spectroscopy (mid-IR FORS) is especially suitable because of its capability to provide information about the pigments and binders, both inorganic and organic, included in the superficial layers [1–3].

However, the application of mid-IR FORS to actual artwork for composition identification has been difficult because the spectra obtained are a mixture of surface (specular) and volume (diffuse) reflection. The absorption coefficients, refractive indexes, and scattering coefficients of the layers, as well as the optical geometry of the incident/reflected radiation determine the contribution of both reflection components and, consequently, the changes introduced in the spectrum [4, 5]. Distortions in the shape, intensity, and wavelength of the absorption bands hinder the interpretation of the spectra based on comparison with those available from reference databases obtained in transmission mode [6].

Thus, the mid-IR FORS spectra for polychrome artworks will be related to the chemical composition of the surface layers (pigments and binders) as well as the physical aspects of these layers (morphology and distribution). In this study, the chalcogenide glass fibers set-up hinder beyond the legibility of the spectra. This set-up does not permit the detection of those compounds that present characteristic bands in the

Electronic supplementary material The online version of this article (doi:10.1007/s00216-014-8091-2) contains supplementary material, which is available to authorized users.

C. Sessa · H. Bagán · J. F. García (✉)
Analytical Chemistry Department, University of Barcelona,
Martí i Franquès 1, 08028 Barcelona, Spain
e-mail: jfgarcia@ub.edu

Published online: 28 August 2014

range of absorption of the fibers (range between 2200 and 2050 cm^{-1} and low wavenumber region).

Several studies have attempted to understand the influence of the different variables and propose procedures to improve the interpretation of the spectra. For this purpose, it is especially interesting to consider the influence of the surface roughness on the spectral distortions. Some studies have explicitly evaluated the effect of surface roughness on the characterization of stones [7, 8], whereas other works have focused on the changes induced by different painting techniques in wall paintings [9] or by the finish on wooden furniture [10]. All of these studies have revealed variations that could be related to the implicit roughness changes. Evidence of the influence of roughness is also found in near infrared (NIR) reflectance studies [11]. In all cases, the spectral distortions are significant. However, only few studies investigating this issue for easel painting can be found in the available literature [12, 13].

Previous studies have attempted to overcome the difficulties related to the interpretation of the distorted spectra obtained by mid-IR FORS using multivariate calibration methods [principal component analysis (PCA) and partial least squares analysis (PLS)] [1, 3, 9, 14]. These studies have shown the critical importance of a calibration set composed of standards that include all variables responsible for the distortions that are present in the samples [11, 15, 16]. In particular, it is recommended that standards and samples have the same composition matrix [9, 17].

Furthermore, as observed in previous experiments, pretreatments are a key step previous to the multivariate method application. Indeed, pretreatments permit reducing the variability in the spectra due to the analysis procedure remaining mainly the variability attributable to the heterogeneity of the paint layer [3]. Thus, in this study several pretreatments were applied to the spectra matrix with the aim to optimize the data set.

It this study, a palette with a composition similar to the one of the analyzed painting was used to obtain a better approximation to the matrix of the painting reproductions. First, PCA was applied for uniform areas discrimination. Second, the identification of the composition of single spots was extended to the whole paint area to obtain pigment mappings applying mid-IR FORS and PLS-DA, as previously performed using other spectroscopic techniques, such as mid-IR in attenuated total reflectance (ATR) mode [18] and micro Fourier transform infrared (FTIR) reflectance [19]. The method was validated by comparing the predicted composition with the one described in the artist's notes and the results obtained with a screening method.

This article strives to contribute to the application of mid-IR FORS to the identification of pigment composition of easel painting by assessing a fast methods for spectra management to obtain pigment composition mappings and by studying the influence of roughness on mid-IR FORS measurements using a multivariate approach.

This study was performed by analyzing two reference palettes and two oil paintings inspired by P. Mondrian's "Composition with red, blue, and yellowish-green" and by Matisse's "Blue nude II". The mock-ups were painted by the artist Alfonso Rodríguez using materials and technique coherent with the epoch of the original paintings.

Experimental

Materials

Palette/reference paints

Palette 1 was prepared by applying single pigments (Kremer Pigmente GmbH and Co. KG Hauptstr. 41 – 47 DE 88317 Aichstetten, Germany) (Table 1) mixed with linseed oil (Jacques Blockx Fils s.a. Le Tombeu, 10 4550 Nandrin, Belgique) by brush on a wood/canvas tablet. Preliminarily the support was ground with a thin preparation layer of a rabbit glue solution saturated with calcium carbonate (Fig. 1a). Palette 2 includes the same series of pigments as palette 1 (Table 1) also mixed with pre-polymerized linseed oil and extended on commercial canvas ground with two preparation layers (Fig. 1b).The paint layers of this palette present different textures. The surface was divided into three strips on which paint in one brush layer, in two brush layers, and as one thick palette/knife application was applied. The latter area exhibits the roughest surface. The mock-ups have not be refinished with varnish layers to avoid interferences in infrared spectra.

Paintings

The artist Alfonso Rodriguez painted two oil paintings on commercial canvas at reduced scale (16×22 cm) preliminary ground with two preparation layers, as in palette 2. The paintings are inspired by P. Mondrian's "Composition with red, blue, and yellowish-green" (*RBY*) (1920) and H. Matisse's "Blue nude II" (*BN II*) (1952).

The artist used the raw materials listed above, which are compatible with 20th century artworks [1, 20–23]. The artist provided a detailed documentation of the pigments contained in each layer and the procedure. A diagram of the two paintings is presented in Fig. 2a and b. The two miniatures show two levels of difficulty in terms of mixture complexity. *BN II* is created with four mono-pigment layers and three areas with mixtures of three blue pigments in different proportion. In *RBY*, the artist painted each area with complex mixtures. These two paintings were used as two cases of increasing difficulty to test the methods presented in this study. The composition of the two paintings is shown in Tables 2 and 3. The information provided was used to validate the prediction.

Table 1 Pigments used on the palette and paintings. The information supplied by the producer is presented: name, description, reference number. The elementary composition determined by XRF is also reported

Pigments	Description	Element comp. Mayor	Element comp. Minor	Ref.	Pigments	Description	Ref.	Element comp. Mayor	Element comp. Minor
Cadmium Yellow	Cadmium sulfide (CdS)+cadmium selenide (CdSe) in varying proportion	Cd, Se, Zn	S	21060	Cadmium Red	Cadmium sulfide (CdS)+ cadmium selenide (CdSe) in varying proportion	21130	Cd, Se	S,Zn
French Ochre	Natural yellow earth $SiO_2+Al_2O_3+Fe_2O_3$	Fe	K, Ti, Cr, Zn, As	40010	Prussian Blue	Iron hexacyanoferrate KFe[Fe (CN)6].H2O	45200	Fe	K
Titanium white	Titanium dioxide	Ti	P, Fe	46280	Phthalocyanine Blue	Copper phthalocyanine blue C32H15N8Cu	23050	Cu	Cl, Fe, K
White lead	Basic lead carbonate 2PbCO3•Pb(OH)2	Pb		46000	Ultramarine Blue, dark	Sodium-aluminium-sulfo-silicate 3Na2O.3Al2O3.6SiO2.2Na2S	45010	Ca	Al, Si, S, Ti
Zinc White	Pure zinc oxide	Zn		46300	Cobalt blue, dark	$(Co,Zn)_2SiO_4$	45700	Co, Zn	S, Ba,Fe
Hematite	Iron(III) oxide	Fe		48650	Cobalt Cerulean Blue	Co-Sn-oxide	45730	Co	Sn, Cr, Fe,Zn
Iron Oxide	Anhydrous iron(III)-oxide	Fe	Ti, Cr, Mn, Cu	48120	Malachite, synthetic	basic copper carbonate CuCO3*Cu(OH)2	44400	Cu	Ca, Fe
English Red	Limestone powder / calcium carbonate+Iron oxide	Fe	Cr, Mn, Cu	40545	Ivory black	Burnt animal bone black	47200	Ca	P, Fe
Venetian Red	Iron oxide	Fe	Cr, Mn, Cu	40510	Preparation layer	Calcium Carbonate		Ca	Fe

Instrumentation

Mid-IR FORS

Reflection FTIR spectra were recorded using a BOMEM MB-120 Fourier transform infrared spectrometer equipped with a Remspec mid-infrared fiberoptic sampling probe. The spectrometer includes a KBr beam splitter, a Glowbar source, and a mercury cadmium telluride (MCT) detector refrigerated with liquid nitrogen. Spectra were recorded with 200 scans at a spectral resolution of 4 cm^{-1}.

The fiberoptic probe is a bifurcate cable containing 19 chalcogenide glass fibers, each one with a diameter of 500 μm. Seven of these fibers carry the infrared radiation from the source to the sample, while the other 12 collect the radiation reflected off the surface. The chalcogenide glass fibers allow spectra to be acquired from 4000 to 900 cm^{-1}, except in the 2200–2050 cm^{-1} region attributable to the Se-H stretching absorption of the fibers [24].

Measurement conditions

Mid-IR FORS

The fiberoptic probe was held perpendicular to the sample surface by a mechanical arm. The distance between the probe and the surface was approximately 4 mm. The investigated area was 20 mm^2, which is related to the probe diameter.

The total reflectance R (from combined diffuse and specular components) was measured using the spectrum collected from an aluminium mirror as background. The spectrum intensity unit is defined as a pseudo-absorbance A' obtained from R by A'=log (1/R).

A series of five measurements was performed for each oil color on palette 1, and 10 on palette 2; 10 measurements were performed on a single spot for each uniform area across the painting. Moreover, 88 points were analyzed across the painting surface following a coordinate stencil, which permits each spectrum to be mapped to an x/y coordinate on the painting surface. The stencil allows the creation of a composition map (Figs. 8 and 9). The range of considered wavelengths was between 3500 and 900 cm^{-1}, except the range between 2200 and 2050 cm^{-1}, because of the fiber absorption.

Experimental setup

Principal component analysis (PCA) and partial least squares discrimination analysis (PLS-DA)

PCA and PLS-DA were implemented using MATLAB and the PLS_toolbox_703 from Eigenvector RI.

PCA

PCA allows the reduction of the dimensionality of a data series by transforming the set of original variables (in this case, wave numbers) into another group of reduced variables, called principal components (PCs), containing the relevant information of the original variables. Moreover, PCA aids in the interpretation of data, showing features that remain hidden in the visual examination of the spectra. PCA has been applied to different data matrixes composed by the spectra that were acquired on the palette and different points across the painting surface, with the aim of evaluating the capability of the technique to differentiate between pigments and discriminate uniform areas (zones with similar composition and roughness).

PLS-DA

The prediction of the composition across the painting surface was performed using PLS-DA. PLS-DA is a PLS model developed to predict the class assignment of each sample [25–27]. PLS-DA is conducted using an exclusive binary coding scheme with one bit per class. The resulting class assignment is expressed in terms of a value from 0 to 1. Using this result matrix, a determined pigment class is assigned to each sample/spectrum in the data matrix. These values are normally distributed around 0 when the prediction is "not being in a class" and are close to 1 when the prediction is "being in a class" [28]. Negative values can be obtained in the "not being in a class" attribution due to the characteristics of the mathematical algorithm of the method. Evaluating the results of the training set, a mean threshold of +0.2 was established to reduce false positive class attribution according with the mean error obtained. On the other hand, zero and negative values were established as no class attribution. This method was previously applied to the prediction of pigment composition; however, for different techniques and only to identify pigments in single-component layer [28, 29].

For the study of the pigment distribution across the two paintings, *BN II* and *RBY*, three calibration models (blue, white/yellow and red) were created with the spectra that had been acquired on the paint references of palette 2. These models were applied to the different uniform areas after a visual evaluation of color and surface appearance.

Data pretreatment

Before applying PCA and PLS, different pretreatments were applied to the data set to remove some of the large amount of variability from the reflectance spectra. The influence of the different pretreatment on the spectra matrix has been studied elsewhere [3]. As first steps, the wavelengths that correspond to the signal of the strong fiber absorption (2200–2050 cm^{-1} and ≤900 cm^{-1}) were cut off, and the Savitzky-Golay smoothing algorithm [30–32] (15-point filter, 0-order polynomial, no derivative correction) was applied to reduce the noise. These two steps permit reducing the strong signal and variations that do not have any significance for the pigments/compounds

Fig. 1 (**a**) Reference paints on a wood tablet; (**b**) commercial canvas with reference paints applied on three areas reproducing different textures

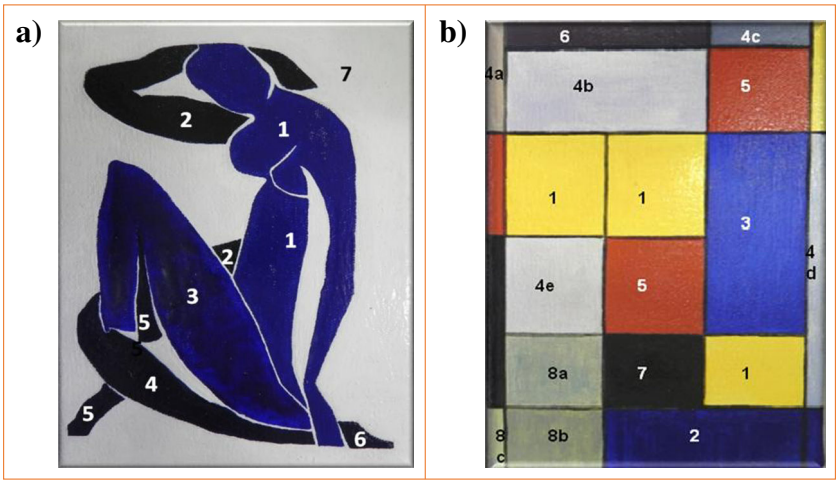

Fig. 2 Shows the painting reproductions: (**a**) blue nude, and (**b**) composition with red, blue, and yellowish-green, in which each area has been labeled with a number depending on the color and artist description. The initial of the original artist: M = Matisse and Mo = Mondrian have been used to distinguish among the different areas of the paintings in the text

discrimination, but could be considered by the multivariate model and, thus, cause misleading results.

The standard normal variate (SNV) algorithm was applied to minimize the multiplicative interferences of scatter and the change of light distance [33]. SNV pretreatment permits normalizing the spectra and, consequently, attenuating changes in the intensity coming from changes in the concentration or experimental conditions, conserving relative intensity between the absorption bands of all spectra. The increase of signal intensity that normally is observed when a higher specular component is detected is reduced.

NV corrects both multiplicative and additive scatter effects [34–36]. SNV uses the equation $x_{Snv} = (x_{i,k} - \bar{x})/STD$ [1], where x_{Snv} is the transformed element, $x_{i,k}$ is the original element, *and* $\bar{x}$ is the mean of spectrum *i.* k=1,2,…, m, where m is the number of variables in the spectra, and I=1,2,…, n, where n is the number validation sets.

Lastly, a baseline algorithm was applied to subtract a polynomial baseline offset from the spectra. No mean centering treatment was applied because no improvements in the results were observed.

Table 2 Description of the *blue nude*'s painting layers based on the artist's notes

Area	Pigments
M1	Cobalt blue dark
M2	Prussian Blue
M3	Ultramarine Blue, dark (linseed oil in excess)
M4	Cobalt blue, dark (1:3)+Prussian Blue (1:3)+Ultramarine Blue, dark (1:3)
M5	Cobalt blue, dark (1:4)+Prussian Blue (1:4)+Ultramarine Blue, dark (2:4)
M6	Cobalt blue, dark (2:4)+Prussian Blue (1:4)+Ultramarine Blue, dark (1:4)
M7	Zinc White

Results and discussion

To reach the objective of predicting the mapping composition of a painting, this work was organized in two sections: the uniform areas discrimination, including the study of the roughness influence and the pigment mapping capabilities of the suggested method. The first step was the identification of areas that present similar physico-chemical properties (uniform areas) as common procedure in artwork characterization, by classifying all acquired spectra in different clusters using PCA.

Table 3 Description of the *composition with red, blue, and yellowish-green* painting layers based on the artist's notes

Area	Pigments
Mo1	Cadmium yellow (lower layer)
	Cadmium yellow+zinc white (superficial layer)
Mo2	Cobalt blue, dark (one layer)
Mo 3	Cobalt blue, dark+zinc white (lower layer – paint very diluted)
	Cobalt blue, dark+zinc white (superficial layer – scratched surface)
Mo 4	Zinc white+cadmium red+cobalt cerulean blue+cadmium yellow in different proportion (lower layer)
	a) Cobalt cerulean blue+low quantity of cadmium red+cadmium yellow (superficial layer – paint very diluted)
	b) Zinc white+cadmium yellow+cadmium red (superficial layer – paint very diluted)
Mo 5	Cadmium red (lower layer)
	Cadmium red+low quantity of cadmium yellow (superficial layer)
Mo 6	Cadmium yellow+cadmium red+cobalt cerulean blue+zinc white (lower layer)
	Cadmium red+cobalt cerulean blue+zinc white (superficial layer)
Mo 7	Ivory black
Mo 8	a) Cobalt cerulean blue+zinc white+cadmium red+cobalt blue, dark+cadmium yellow in different proportion (two layers)
	b) more cobalt cerulean blue (superficial layer)

Once the painting was split in uniform areas and the different data sets were organized, the second step of pigment content prediction was undertaken. Simplified models of pure reference pigments divided by colors were used to predict the composition of the different spots analyzed by applying PLS-DA. The results were finally validated using the notes of the artist and a screening technique. The methods and the analytical technique limitations will be investigated and discussed.

Uniform area discrimination

For artwork characterization purposes, it is important to non-destructively identify uniform areas of equivalent composition, surface texture, and conservation conditions. The selection of areas with similar appearance is a common procedure before any sampling or measurements point election. The similar appearance occasionally does not allow the delimitation of these zones. If used for interpretation, this can lead to changes in the spectra in areas identified as uniform. On the other side, these variations can be advantageous in the application of multivariate methods to discriminate between physical changes across a painting surface, such as retouching, differences in brushstrokes, or alteration phenomena. These factors may lead to an in-depth examination of the history of the object in terms of conservation condition, restoration work, and the presence of additional (not-original) materials [37]. Hence, the first step of the work was to test the capability to determine the different uniform areas presents on the paintings.

A previous step was the evaluation of the capability of mid-IR FORS and multivariate methods to establish whether different pigments mixed with linseed oil (palette 1) are classified as different in the space of the new components using a palette of pure pigments. Next, the uniform areas establishment was tested on the paintings. As a consequence of the results obtained, the influence of the surface roughness on the spectra was investigated.

Single pigment areas

To evaluate the capability of the procedure to discriminate between pure pigments, five spectra were recorded for each of the 17 different oil paints on palette 1. A PCA model was created, and four components (PCs) were considered. The total percentages of variance captured by the PCs were 91.80 %, 3.61 %, 1.43 %, and 1.06 %. The first two PCs mainly take into account a series of bands that are not easily assignable (PC1) and the strong band at 1450–1420 cm^{-1} related to the antisymmetric CO_3^{2-} stretching inverted by the Restrahlen effect [4, 7, 23].The Restrahlen effect could be attributed to the presence of white lead and/or related to the calcium carbonate of the preparation layer common to all the spectra (PC2). PCs 3 and 4 take into account information that is useful for the discrimination of the different pigments. It is possible to identify some of the bands related to silicates, carbonates, and phosphate, although weak signals attributable to the combination bands are more difficult to assign. In the score plot of PCs 3 versus 4 (Fig. 3), the presence of different clusters can be observed. Some of these clusters include more than one pigment because of the absence of characteristic bands of the corresponding compounds or the similarities between their spectra. Despite these difficulties, discrimination can be achieved based on the color of the paint layer. Thus, the model allows the differentiation of the different pigments.

Uniform areas identification

After the establishment of the model to distinguish between pure pigments, PCA using the spectra obtained by analyzing **BN II** was applied with the aim of discriminating between different uniform areas. This painting includes some areas in which a single pigment was used (areas M1, 2, 3, and 7) and others in which pigment mixtures were included (areas M4, 5, and 6).

For this purpose, first an unsupervised PCA model was created using 10 spectra acquired on the same point at seven different uniform areas across the painting. The total percentages of variance captured by the first four PCs were 61.56 %, 25.52 %, 5.12 %, and 1.13 %. PC1 and PC3 were chosen because they include the most relevant information for discrimination purposes.

Figure 4 shows the score plot of PC1 versus PC3. It is possible to observe that uniform areas are separated in different clusters, although it is important to note that the spectra from paint layers that include mixtures of the three blue pigments (cobalt blue dark, ultramarine, Prussian blue) appear as an independent clusters (areas 4, 5 and 6).

Next, the study focused on the capability to discriminate between uniform areas, even when those are not visually different, and on the capability to assign them to the previously established clusters. With this aim, all the measurements conducted on different points across the painting surfaces were projected in the previously unsupervised PCA model.

Figure 5 shows the scores plot of PC1 and PC3 including all of the spectra acquired across the painting surface. In the score plot it can be observed that mixtures including all three blue pigments (cobalt blue dark, ultramarine, Prussian blue), but in different proportions (areas 4, 5, and 6), now appear as a single large cluster (SPOTS – blue nude 4, 5, 6). This behavior suggests that the principal component model is not capable of discriminating between uniform areas of pigment mixtures in which the difference is a slight change of the relative concentrations of the components. On the contrary, the pure pigment areas (area 1, 2, 3, 7) continue to appear as separate clusters (SPOTS – blue nude 1, 2, 3, 7). Hence it is possible to distinguish uniform areas with different composition, except

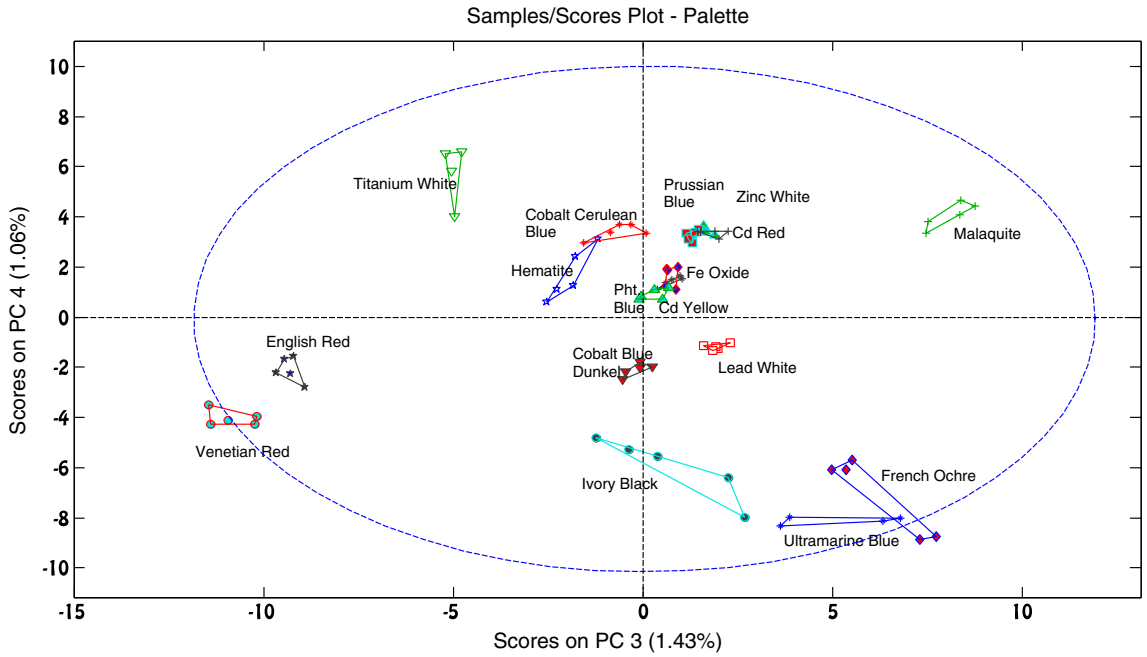

Fig. 3 Score plot of the PC3 versus PC4 for Palette 1 model. Pure pigments discrimination test

among those created with the same pigments but in different proportions.

Influence of surface roughness

Based on the results included in Fig. 5, it is interesting to note the high dispersion of the scores corresponding to the analysis of the different positions (SPOTS – blue nude 3) in the single-pigment area, area 3. This behavior may be related to the roughness variations and even the irregular distribution of the pigment (probably due to the excess of linseed oil highlighted by the artist) with regard to the other single-pigment areas (M1, M2, and M7). Beginning with this evidence, a specific experiment was designed to evaluate the influence of the roughness and morphologic features of the surface on the spectral shape of the mid-IR FORS results.

For this purpose, the 17 pure pigment paints with different textures and thicknesses of palette 2 were studied. The different painting techniques reproduce textures that are commonly found on easel oil paintings.

A data matrix of the 15 spectra was created for each pigment on palette 2 (five spectra×three strips/textures× pigment). The observed behavior was similar for all pigments, and the result for one of them (ultramarine blue) is presented as an example (Fig. 6a and b). The influence of the different textures on the spectra can be observed in Fig. 6b.The spectra obtained from single-pigment layers for the three textures are clearly different. As expected, changes in the texture induce signal distortions in the mid-IR FORS measurement. Especially interesting is the signal of the Si-O mode at 1010 cm^{-1} of the synthetic ultramarine blue, which results as a Restrahlen band [3, 4, 19] that is present only in the spectra acquired on the one-layer paint strip, probably because of the increase of the reflectance. The band detection depends on the concentration of the pigment and the penetration of the radiation in this specific area [3, 38].

The score plot of the model created with the measurements carried out on the three textures shows different clusters (Fig. 6b). It is clear that the dispersion assigned to each cluster increases with the roughness and thickness of the paint layers. The capability of the model to discriminate between different textures demonstrates that the spectral changes depend not only on the composition but also on the morphology of the paint layers. The results also corroborate the critical need to improve the capability of composition prediction using a calibration palette with features as similar to the texture of the original painting layers as possible. It can be point out that a high grade of surface roughness could be a critical factor that may limit the success of the prediction step. The results also show that the differentiation of uniform areas by the model depends on both pigment composition and texture.

Concerning the binder, it can be remarked, based on previous experiment, that mid-IR FORS is not very sensitive to the changes that are normally observed in aged oil. In fact, the band at about 3010 cm^{-1} of the C–H stretching of aliphatic CH=CH, which identifies

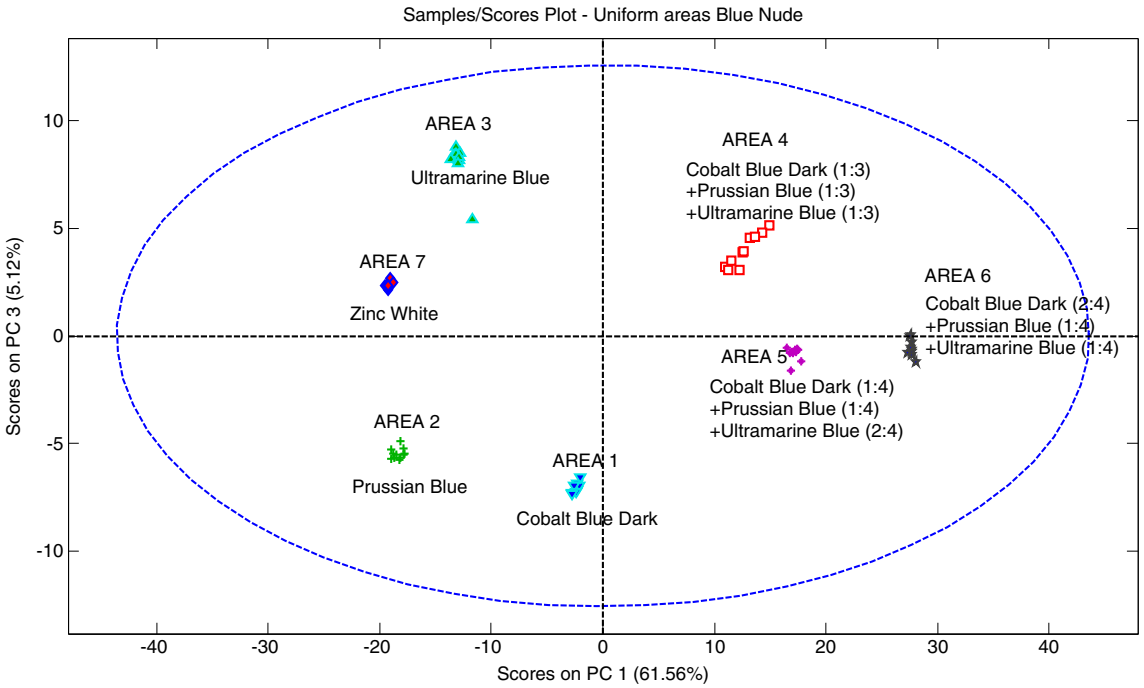

Fig. 4 Score plot of the PC1 versus PC3 for the *BN II* uniform areas model. Unsupervised PCA model for uniform areas selection

unsaturated oil [39], is almost not visible. Thus, the calibration model will not be influenced in a relevant manner. For practical application it should be considered using some fast-aging mock-up as calibration palette model.

Pigment mapping using multivariate calibration

The second part of the study was focused on the pigment discrimination of the different uniform areas to obtain a mapping composition. The noninvasiveness of the mid-IR FORS

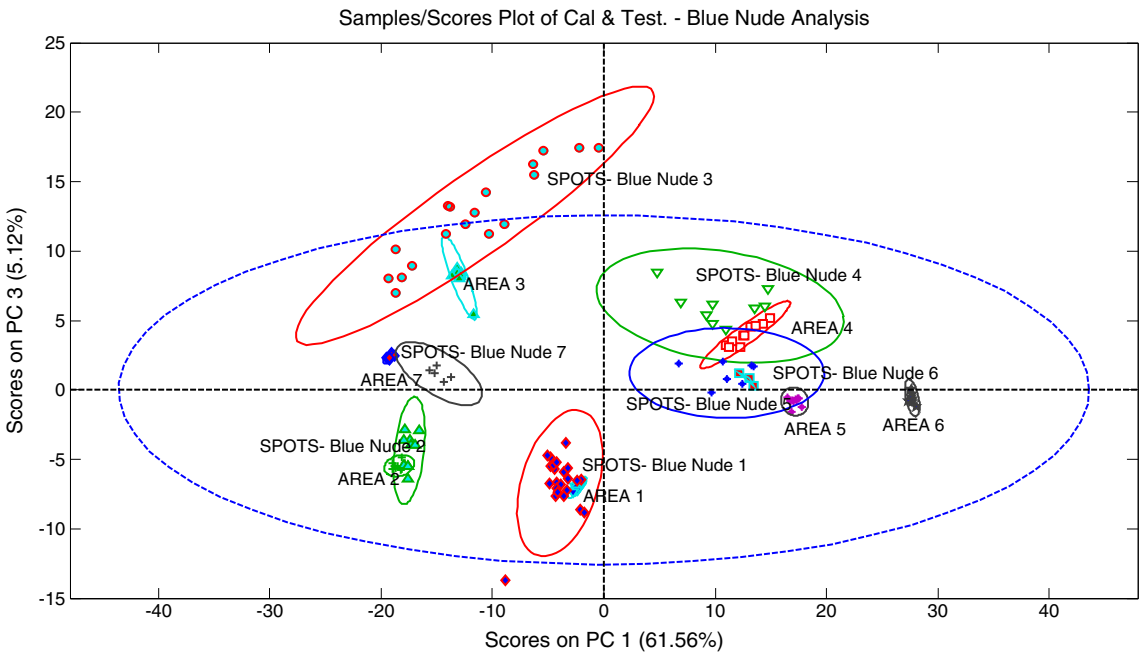

Fig. 5 Score plot of the PC1 versus PC3 of the *BN II* model. The figure shows how the spectra of the different spots analyzed across the painting could be attributed to a specific area. The scores that correspond to the 10-measurement carry-out on the same point are labeled with *AREA*, whereas those corresponding to the different spots are labeled with SPOTS – *blue nude*. The numbers correspond to the zone defined in the diagram presented in Fig. 2

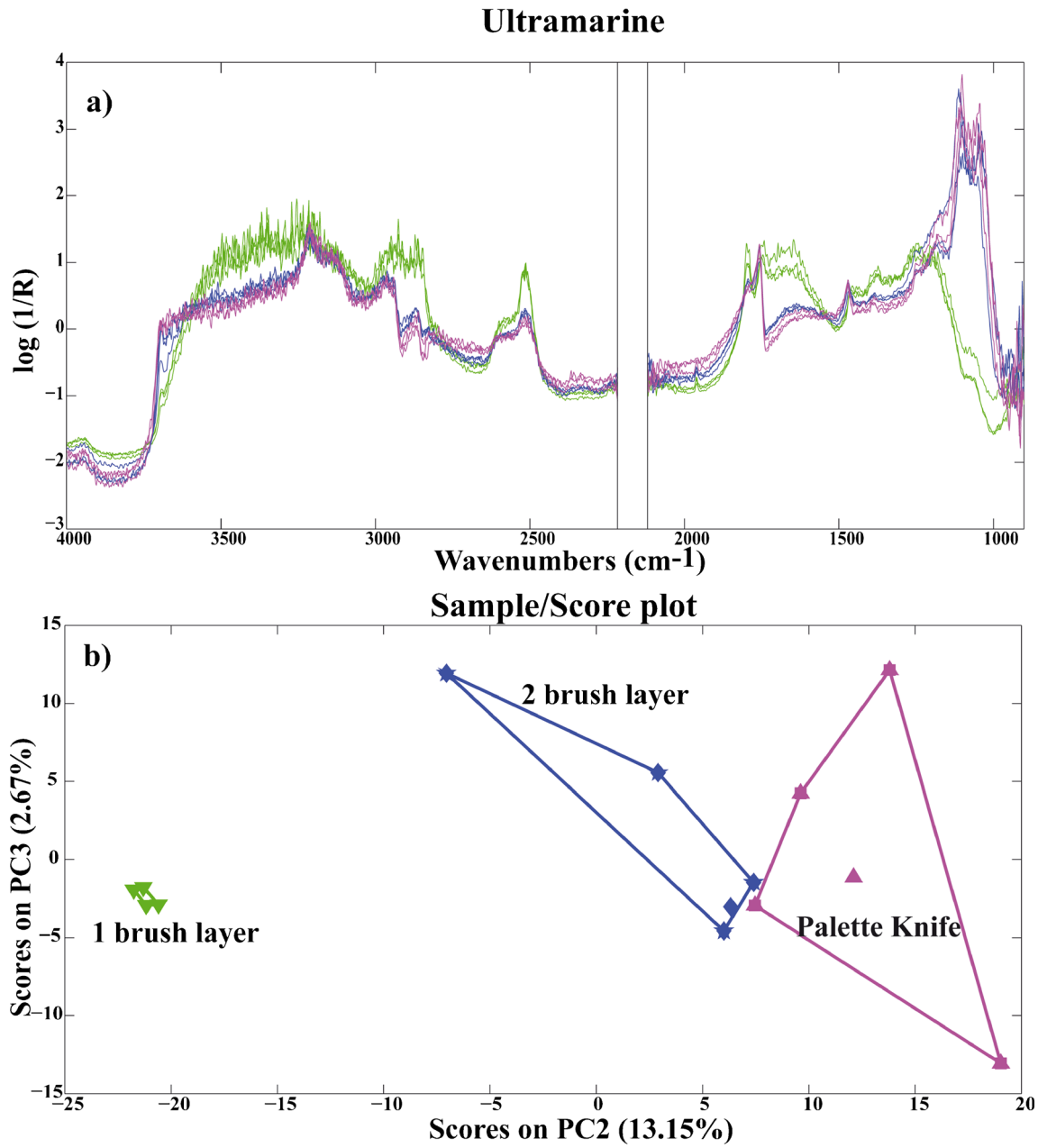

Fig. 6 (**a**) Spectra ultramarine blue, dark measurements (trace: green = one layer; blue = two layers; magenta = palette knife); (**b**) score plot of thePC2 versus PC3 using the spectra matrix acquired on different texture (five spectra three textures)

allows recording a large amount of spectral data which, acquired systematically across the artwork surface, could be used to create a mapping of the composition. Multivariate methods can be helpful in managing and interpreting large numbers of spectra. In particular, PCA and PLS facilitated the discrimination of significant information from noise or other meaningless signals contained in the original data.

PCA, as shown above, considers each mixture as an independent cluster, but is not capable of distinguishing between the pigments that constitute a mixture. This drawback can be overcome using PLS-DA. This technique permits having information of the content of each pigment individually. This data analysis method has been used in several studies for class discrimination [27, 28] because of its capability of predicting the presence of each pigment in a mixtures of them. Consequently, the size of the calibration set necessary for the study is reduced to only the single pigments mock-up.

PLS calibration step

The use of a complex calibration model that considers simultaneously all pigments and textures included in the palette

Table 4 Details of the PLS calibration models (blue, red, and white/yellow) are listed: the spectral range and the PCs considered in the model with the corresponding variance accounted for each PC

Models			PLS	
Data matrix	IR spectral region (cm^{-1})	PC	Variance account X (%)	Variance account Y (%)
White/yellow model samples	3500 - 900 (except 2200 -2050)	1	80.96	19.99
		2	14.47	20.73
		3	3.05	20.60
		4	0.60	18.76
		5	0.58	14.29
Blue model samples		1	79.79	19.95
		2	10.94	19.76
		3	6.23	19.42
		4	1.52	16.79
		5	0.57	15.43
Red model samples		1	4.42	24.51
		2	75.42	4.61
		3	18.24	17.31
		4	1.07	22.61
		5	0.32	21.53

may be difficult in the prediction of the pigment used in the different paint layers. To avoid misleading results, a supervised model was prepared for each color with a reduced number of pigments (blue, red, and white/yellow). These models contain the spectra acquired on palette 2 (10 spectra per pigment/class) with the same ground as the paintings.

In all of the PLS models and cases, the class assignment is presented as a bar chart which shows, for each pigment in the model, the mean of the class assignment values (<0.2 not being in the class, >0.2 being in the class) obtained for each uniform area (spots analyzed following the coordinate stencil). The selection of the number of PCs has been done considering a total variance captured higher than 90 % with a model root-mean-square error of cross-validation (RMSECV) with maximum values of 0.2. Details about the models are presented in Table 4.

Prediction step

Once the uniform areas of the painting were identified and the data was reorganized, the analysis of the spectra using the calibration models could be undertaken. The results of all the spectra acquired following the coordinate stencil on 88 positions across the surface of the two paintings will be presented and discussed. The predicted pigments without characteristic bands in the mid-infrared were later confirmed or discarded by using X-ray fluorescence analysis based on measurements on few positions of the same area. Finally, the results were validated with the real composition described in the artist's notes.

BN II

The results using the PLS-DA model for white area M7 are shown in Fig. 7. The bar chart confirms the presence of the white zinc pigment in the white area of the paintings.

The prediction of the blue areas (areas M1, M2, and M3), where a single pigment was used, is shown in the PLS bar chart Figure S1 (see Electronic Supplementary Material, ESM). The model reports that the Prussian blue is present in M2 as well as in M1 and M3 in significant quantities, which does not agree with the artist's description. The mistake concerning M1 and M3 can be related to the fact that the characteristic band of Prussian blue at 2085 cm^{-1} is partially overlapped by the fiber absorption, which is a significant drawback for the use of chalcogenide fibers. Thus, the spectrum of the Prussian blue standard, once the fiber bands have been cut off, is very similar to the binder spectrum (linseed oil), which is common in all of the paints. In this case, the screening XRF measurements deny the presence of the Prussian blue in M1 and M3 and confirm the use of the same pigment in M2.This result was used to correct the prediction. For M1, the model identifies the presence of cobalt blue, whereas for area M3, the class with the higher value is ultramarine.

Concerning the painting areas that include mixtures (areas M4, 5, 6) (see ESM Figure S2), the results indicate that the paint does not contain phtalocyanine blue or cobalt cerulean blue, as expected. The proportions of cobalt dark blue and ultramarine are almost the same as the proportion of the pigment used by the artist in the M4 and M6 areas, whereas in M5, cobalt blue is underestimated. The Prussian blue prediction was discarded by XRF screening. Considering all the

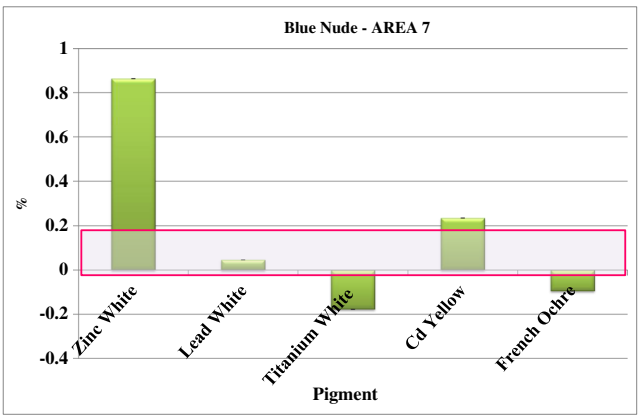

Fig. 7 PLS bar chart of the *BN II*. Pigment prediction: area M7

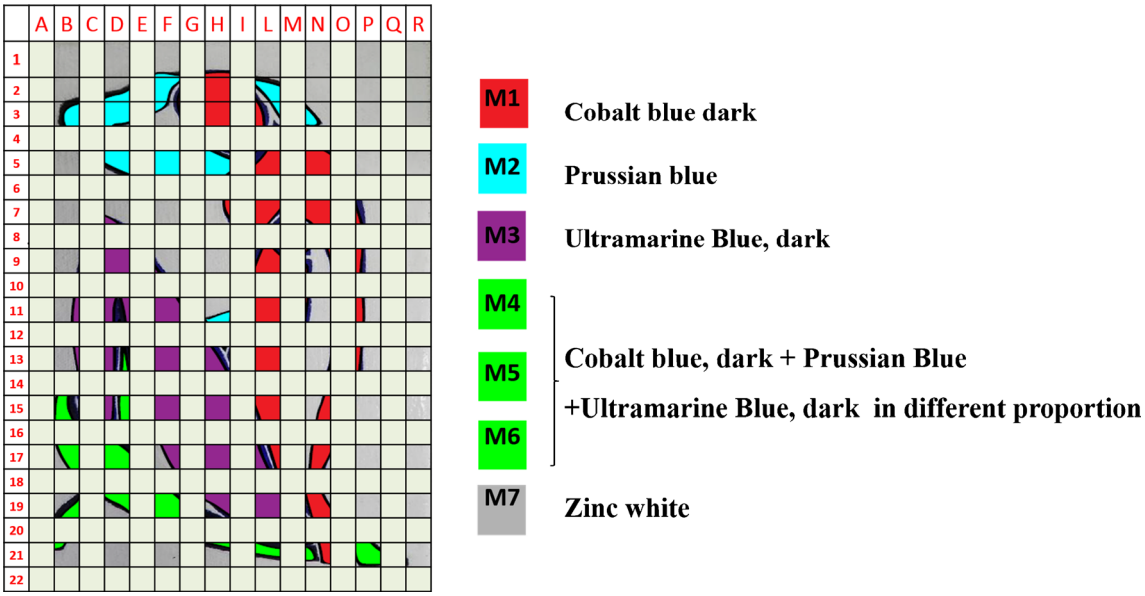

Fig. 8 *BN II* composition mapping based on prediction results

predictions, it is possible to create a composition map of the painting (Fig. 8).

The composition predicted by the PLS model was closer to the composition provided by the artist, showing that this model can be used for the prediction of the composition of uniform areas as long as the pigments present absorption in the considered wavelength range.

RBY

Finally, the whole procedure was tested by applying it to the more complex case of RBY. The unsupervised PCA model was applied to the different points measured obtaining the distribution of uniform areas. Next, the three supervised models were applied to predict the pigments used for all of the uniform areas identified across the RBY surface. The spectral matrix was created using the 88 spectra recorded following the coordinate stencil. The PLS bar chart for all of the areas is presented in ESM Fig. S3.

According to the results, the compositions of areas Mo1, Mo2, Mo3, Mo5, and Mo6 are fully identified and those of areas Mo4 and Mo8 are characterized with some difficulty. The presence of the cadmium red, cerulean

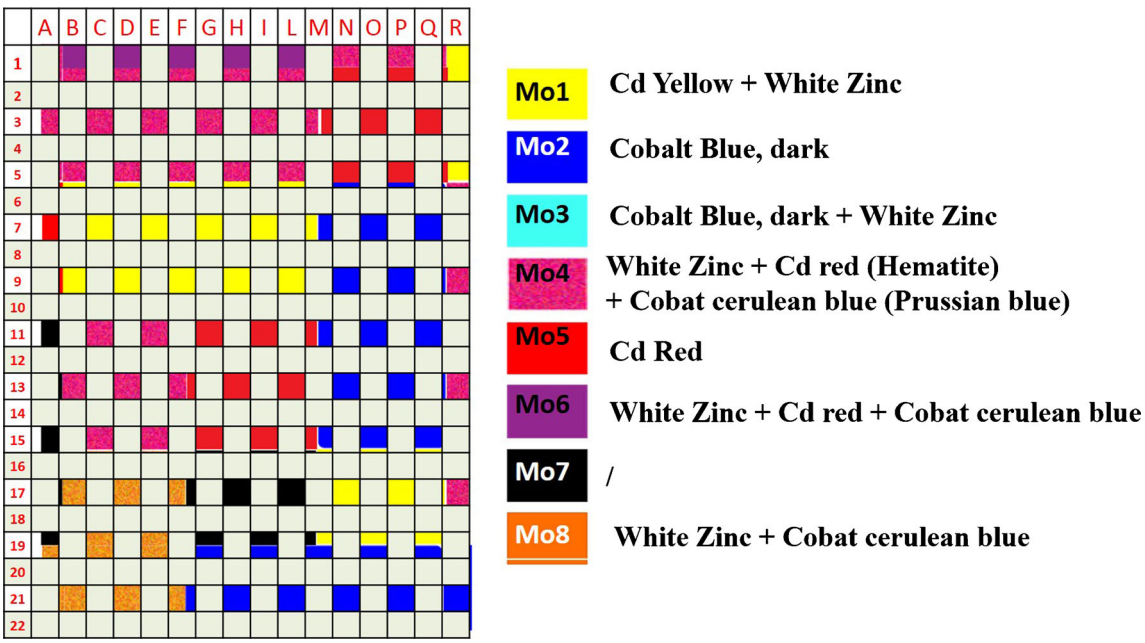

Fig. 9 *RBY* composition mapping based on prediction results

blue, and Prussian blue in area Mo4 has been confirmed, whereas hematite was discarded by XRF. For the black area (Mo7) no prediction was performed because a model for black pigment was not available in the calibration data matrix.

For areas with layers including one or two pigments, the predictions confirm the information provided by the artist. For areas with three or four components, it is more difficult to identify all the pigments included in the mixture. The difficulties in some of the areas could be due to the prediction problems related to the pigments without strong characteristic bands or with bands partially overlapped by the fiber absorption, the detection limit of the technique [3, 38] or the limitations of the PLS method applied.

Despite these problems, even with this more difficult scenario, the composition map shown in Fig. 9 is similar to that provided by the artist, showing that the model may facilitate the identification of the pigments also in this case.

In summary, the procedure suggested obtaining pigment mapping for easel painting implies the procedure explained below:

Create an x/y coordinate stencil, which permits each spectrum to be mapped on the painting surface. Then, acquire spectra on several spots across the surface recording the x/y coordinates. Before using multivariate methods, optimize the spectra data set applying pretreatments. Then, project the data on an unsupervised PCA model for a fast spectra clustering and determination of uniform areas. Finally, create PLS-DA models with reference paint that should be selected based on epoch, color, and texture of the investigated paint layers. Once the prediction has been performed, XRF could be used as a complementary screening technique to confirm or discard the presence of those pigments that do not show strong absorption in the mid-infrared range.

Conclusions

It can be affirmed as follows:

- The results prove that PCA and PLS-DA multivariate methods are capable of modeling the distortions of the mid-IR FORS reflectance spectra and allow the delimitation and discrimination between uniform composition zones on painting.
- The method studied can be applied for the prediction of pigment mappings of different paintings for single pigments or mixtures, if they absorb in the mid-infrared, their concentration are above the detection limit, and they are included in the calibration data matrix.
- The main limitation of the method is the necessity to create a database that includes the features of the artwork studied, taking into account the generic type of binder and the potential pigments present, as well as the roughness surface of the uniform area analyzed. These details can possibly be assessed through the direct observation of the paint layers and the previous knowledge about the epoch of the artwork, although this information is not clear in all cases.
- The removal of varnish will be necessary to avoid interferences in the spectra.

Finally, the analysis of pigments without characteristic bands, which may lead to false positives, requires the use of a screening complementary analytical technique to correct the prediction results.

Acknowledgments The authors thank N. Ferrer (SCT-UB) for her kind advice regarding the use of the infrared spectrometer and interpretation of the resulting spectra, as well as Romà Tauler of the Institute for Chemical and Environmental Research (CID-CSIC) for his support during the data treatment phase.

They thank Silvia Centeno and the Scientific Department of the Metropolitan Museum of Art for the permission to perform the XRF measurements.

The authors are grateful for financial support to the Spanish *Ministerio de Educación y Ciencia* (HAR2011-29654 2011–2013 and PhD Grant FPU/AP2009-2575).

References

1. Rosi F, Burnstock A, Van den Berg KJ et al (2009) Spectrochim Acta A Mol Biomol Spectrosc 71:1655–1662
2. Miliani C, Rosi F, Brunetti BG, Sgamellotti A (2010) Acc Chem Res 43:728–738
3. Sessa C, Bagán H, García JF (2013) Spectrochim Acta A Mol Biomol Spectrosc 115:617–628
4. Miliani C, Rosi F, Daveri A, Brunetti B (2012) Appl Phys A Mater Sci Process 106:295–307
5. Milosevic MSLB (2002) Appl Spectrosc Rev 37:347–364
6. Price BA, Boris P, (eds) (2007) Infrared and Raman Users Group Spectral Database. 2007 ed. Vol. 1 & 2. Philadelphia: IRUG, 2009. Infrared and Raman Users Group Spectral Database. Web. 20 June 2014. <www.irug.org>
7. Ricci C, Miliani C, Brunetti BG, Sgamellotti A (2006) Talanta 69: 1221–1226
8. Poli T, Alice E, Chiantore O (2009) e-Preserv Sci 6:174–179
9. Rosi F, Daveri A, Miliani C et al (2009) Anal Bioanal Chem 395: 2097–2106
10. Poli T, Chiantore O, Nervo M, Piccirillo A (2011) Anal Bioanal Chem 400:1161–1171
11. Wu C, Jacobson AR, Laba M, Baveye PC (2009) Geoderma 152: 171–180
12. Dupuis G, Menu M (2006) Appl Phys A 83:469–474. doi:10.1007/s00339-006-3522-3
13. Dupuis G, Elias M, Simonot L (2002) Appl Spectrosc 56:1329–1336
14. Fabbri M, Picollo M, Porcinai S, Bacci M (2001) Appl Spectrosc 55: 428–433

15. Bacci M, Chiari R, Porcinai S, Radicati B (1997) Chemom Intell Lab Syst 39:115–121
16. Sarmiento A, Pérez-Alonso M, Olivares M et al (2011) Anal Bioanal Chem 399:3601–3611
17. Fabbri M, Picollo M, Porcinai S, Bacci M (2001) Appl Spectrosc 55: 420–427
18. Marengo E, Cristina Liparota M, Robotti E, Bobba M (2005) Anal Chim Acta 553:111–122
19. Rosi F, Federici A, Brunetti BG et al (2011) Anal Bioanal Chem 399: 3133–3145
20. Bouchard M, Rivenc R, Menke C, Learner T (2009) Sect Title Hist Educ Doc 6:27–37
21. Montagner C, Sanches D, Pedroso J et al (2013) Spectrochim Acta A Mol Biomol Spectrosc 103:409–416
22. Giaccai J (2008) Sect Title Hist Educ Doc:1047
23. Miliani C, Rosi F, Burnstock A et al (2007) Appl Phys A Mater Sci Process 89:849–856
24. Melling PJ, Thomson M (2002) Handbook Vib Spectrosc
25. Geladi P, Kowalski BR (1986) Anal Chim Acta 185:1–17
26. Barker M, Rayens W (2003) J Chemom 17:166–173
27. Westerhuis J, Hoefsloot HJ, Smit S et al (2008) Metabolomics 4:81–89
28. Manuel P, Ruis I, Andrikopoulos KS et al (2008) Talanta 75:926–936
29. Ramos PM, Ruisánchez I (2006) Anal Chim Acta 558:274–282
30. Van Den Berg F, Engelsen SB (2009) Trends Anal Chem 28:1201–1222
31. Bromba M, Ziegler H (1981) Anal Chem 1:1583–1586
32. Seah MP, Dench WA (1989) Sect Title Opt Electron Mass Spectrosc Other Relat Prop 48:43–54
33. Azzouz T, Puigdomenech A, Aragay M, Tauler R (2003) Anal Chim Acta 484:121–134
34. Muehlethaler C, Massonnet G, Esseiva P (2011) Forensic Sci Int 209: 173–182
35. Fearn T, Riccioli C, Garrido-Varo A, Guerrero-Ginel JE (2009) Chemom Intell Lab Syst 96:22–26
36. Rinnan Å, Nørgaard L, Berg F van den et al (2009) Infrared Spectrosc Food Qual Anal Control 29–50
37. Baronti S, Casini A, Lotti F, Porcinai S (1997) Chem Intel Lab Syst 39:103–114
38. Sessa C, Vila A, García JF (2011) Anal Bioanal Chem 400:2241–2251
39. Berg JDJ van den (2002) Analytical chemical studies on traditional linseed oil paints. Univ Amst 6:291

Analytical and Bioanalytical Chemistry

Electronic Supplementary Material

Influence of composition and roughness on the pigment mapping of paintings using mid-infrared fiberoptics reflectance spectroscopy (mid-IR FORS) and multivariate calibration

Clarimma Sessa, Héctor Bagán, Jose Francisco García

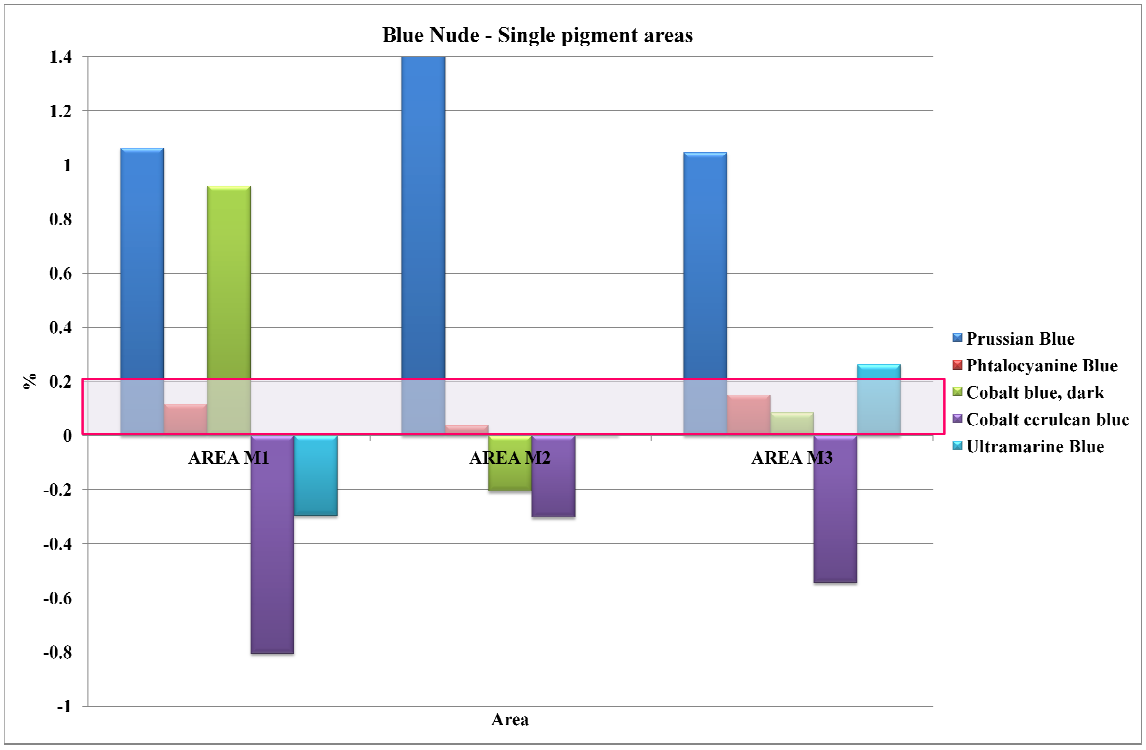

Fig. S1 PLS bar chart of the *BN II*. Pigment prediction: Areas M1, M2, M3

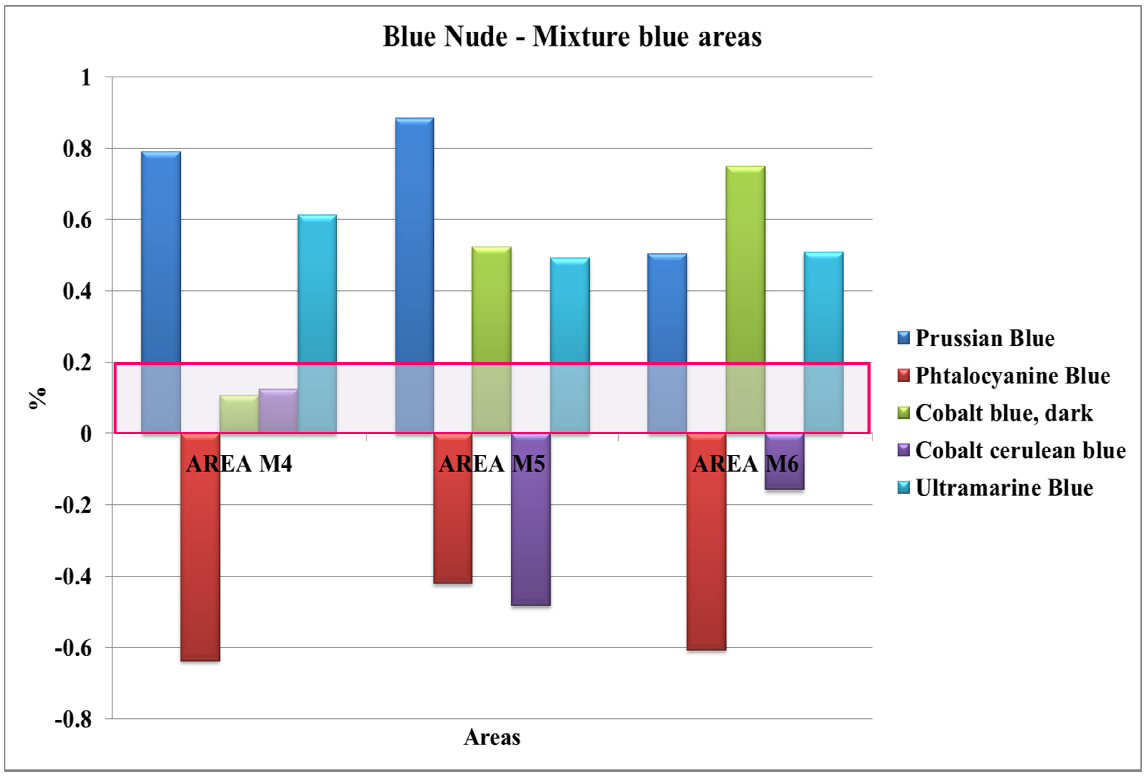

Fig. S2 PLS bar chart of the BN II. Pigment prediction: Area M4, M5, M6

Composition with Red, Blue and Yellowish-Green - Mixtures Prediction

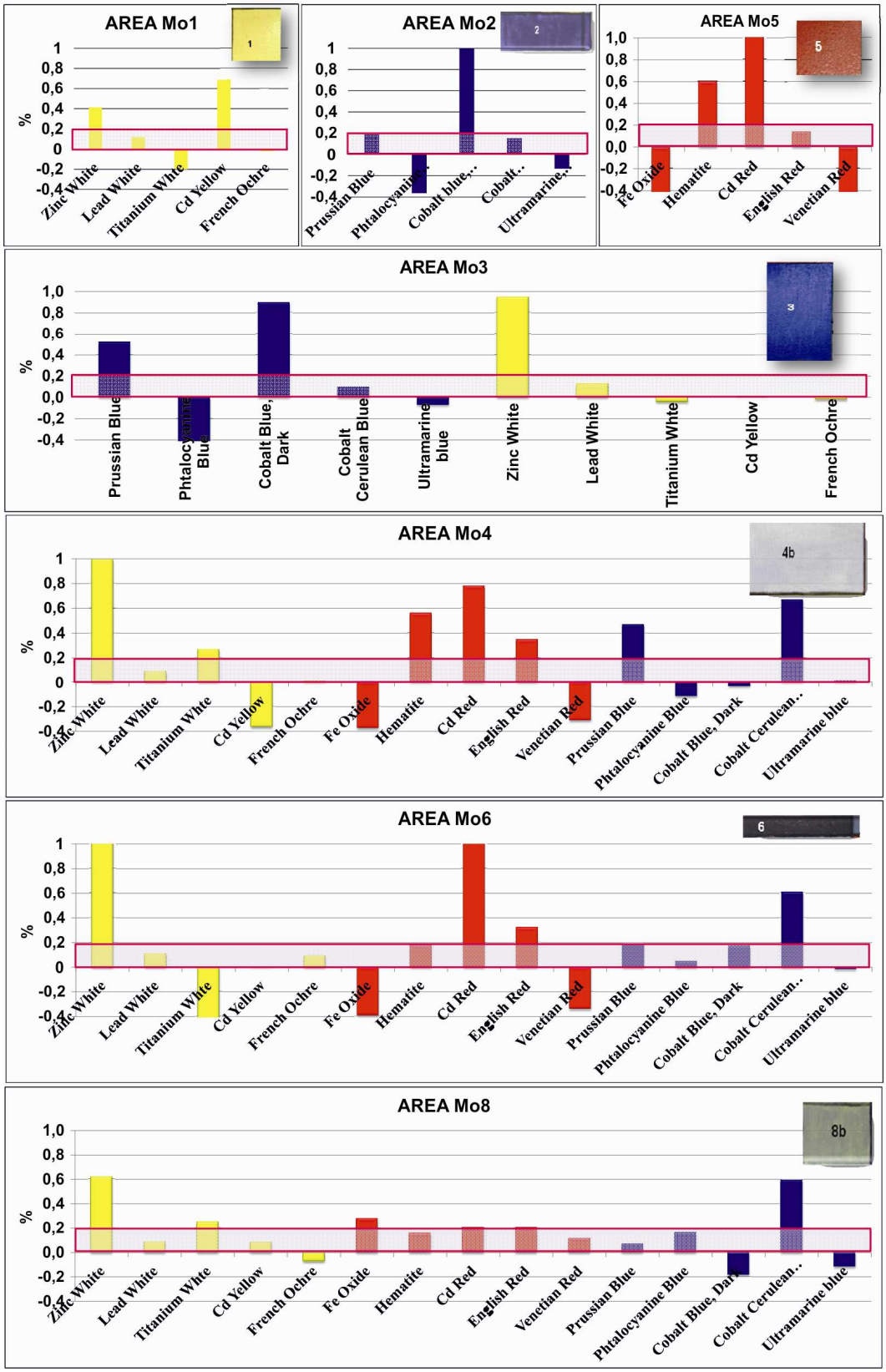

Fig. S3 PLS bar chart for *RBY*. Pigment prediction: Area Mo1, 2, 3, 4, 5, 6, and 8

2.4 Discussion

The results obtained with the SEM-EDS, micro-FTIR, and midIR-FORS contribute to better know the advantages and limitations of both micro- and non-destructive technique when used for artwork characterization purposes.

For **SEM-EDS** analysis, it was proposed a protocol for artwork analysis including: identification peak using expert evaluation and measurement replicates performing areas of 100x100μm^2. The spot analysis should be considered only in specific cases. The detection limit of SEM in the case considered shows lower values when an expert evaluation is executed. The values obtained depend on the stoichiometric relation, rather than the areas investigated. The detections limits determined by the automatic system are elevated and correspond to pigments ratio that could imply chromatic changes and/or intentional admix of pigment during the artistic process without being detected.

About the study of the heterogeneity, it is interesting to notice that value of mRSD for EDS and micro-FTIR are similar due to the punctual feature of the analysis and the probability to found the analyte in the specimen.

In case of **micro-FTIR** measurements, replicates are suggested to improve the representativity of the results. The expert evaluation is proposed, although the detection limit decrease for this technique it is not so evident as in EDS results.

The detection limits established based on **midIR-FORS** measurements are high because it is slightly influenced by the physical distortion of the spectra, which may hinder some important bands detection.

Table 1. Summary of detection limits for pigment in SEM-EDS, micro-FTIR and midIR-FORS.

	SEM-EDS		**micro-FTIR**		**midIR-FORS**	
	Automatic	**Expert**	**Automatic**	**Expert**	**Automatic**	**Expert**
Phtalocyanine blue	**6.2 – 10.2%** (80:20/67:33)	**0.9 – 1.5%** (97:3/95:5)	**2.4 – 3.4%** (93:7/89:11)	**0.9 – 1.5%** (97:3/95:5)	/	**6.2 – 10.2%** (80:20/67:33)
Prussian blue	**6.5 - 15.5%** (80:20/67:33)	**0.8 – 1.3%** (97:3/95:5)	**≤ 0.24 %** (99:1)	**≤ 0.24 %** (99:1)	/	**2.1 – 6.5%** (80:20/67:33)
Ultramarine blue	**1.6 – 2.5%** (95:5/93:7)	**0.3 – 1%** (99:1/97:3)	**≥19 %** (50:50)	**≥19 %** (50:50)	/	**12.1%** (67:33)

The study of instrumental repetitivity, reproducibility and material distribution heterogeneity in paints when the analysis is performed by midIR-FORS demonstrated that the repetitivity for measurement on linseed oil is approximately 3%, whereas values increase up to 18% for the pigments. The reproducibility along time, across surface, and changings both condition is about 4% for oil and 25% for pigments. These values suggest that the instrumental stability just increase the dispersion of the measurement around 1%, whereas the heterogeneity/distribution of the pigment in/on the painting layer increases the lack of reproducibility in 7%. For the pigments studied, the reproducibility improves depending on the intensity of the marker band selected and decreases when the particle size is smaller.

Based on the mRSD for measurement acquired at the same time but changing the point analysed, it is relevant to observe that the midIR-FORS shows higher reproducibility across the surface compared with micro-FTIR values. This phenomenon could be explain considering the higher integrated area investigated by means of the fibre probe. This result implies an improved reproducibility of the non-destructive technique with respect to micro-destructive technique, which results depend on the focus beam.

It has been demonstrated that **PCA** and **PLS** are useful tools for **midIR-FORS** spectra management. PCA in particular helps to perform a first survey of the data and understand data pattern. It can be used for spectra pigment discrimination and even for mixture differentiation, but not for pigment prediction purposes. This limitation has been overcame with the creation of PLS calibration models using a reference palette. Pre-processing algorithms for FORS data treatment and a protocol for pigment prediction mappings have been proposed.

The global evaluation of midIR-FORS, based on statistical and multivariate results, highlighted the influence of the surface roughness on the spectra features. This observation demonstrates the importance of artwork physical features on reflectance spectra quality.

Chapter 3

"Early Stages of Picasso through material characterization of different portraits"

Context

The collaboration between the University of Barcelona and the Museum Picasso of Barcelona, by means of the resources of CHARISMA program [1] and the MOLAB (Mobil facilities for in situ no-invasive measurement) [2], allowed an extensive study of six portraits created by Pablo Ruiz Picasso between 1895 and 1900 by remote analytical techniques. MOLAB is a mobile laboratory that includes a portable set of advanced analytical equipment, for in-situ non-invasive measurements on artworks provided by the Center SMAArt (Scientific Methodologies applied to Archaeology and Art) of the University of Perugia and the CNR-INO (Istituto Nazionale di Ottica Art Diagnostic Group, Florence). The use of the facilities is part of the activities included in the European project CHARISMA, which approved the proposal of the University of Barcelona and the Picasso Museum of Barcelona "*Early Stages of Picasso through material characterization of different portraits*". CHARISMA is an integrating activity project that offers an access free of costs to advanced scientific instrumentation, allowing scientist, conservators-restorers and curators to enhance their research. This project was a unique opportunity to discover the palette and *modus operandi* of the artist in his early production. It was also a great opportunity to test the capability and limitation of non-destructive techniques applied to real artworks. This chapter presents a compendium of the results obtained during the analysis campaign and their interpretation, a discussion on the personality of each portrait, and a global comparison of all the artworks focusing on the obtained information and the possible enigma not solved.

[The authors of the future publication rising from this study will be Clarimma Sessa[1], Reyes Jiménez de Garnica[2], Jose Francisco Garcia[1]
[1] Analytical Chemistry Department, University of Barcelona, Spain
[2] Conservació Preventiva i Restauracio, Fundació Museu Picasso Barcelona, Spain]

3.1 Introduction

Pablo Ruiz Picasso (1881-1973) is considered one of the most important artist of the 20th century. The artist was born in Malaga in 1881. He moved with his family to A Coruña in 1891, where they remain until 1895. In September of this year, they arrived to Barcelona. Between 1897 and 1898 he took an academic course in Madrid, but before the end of this year, his friend Pallarés invited him to travel to Horta de Ebro for a stay to recover after a debilitating disease. Afterwards, in January 1899 he returns to Barcelona. He stayed in the city, although he travels in some occasion to Paris until 1904 when he left Barcelona to definitely establish his residence in Paris. From this point, he starts the part of his career that is commonly known by the large public[3].

Each stage of his life before Paris, was key in Picasso's artistic formation. He grow up in a family with a great devotion to art, which fulcrum was the father José Luis Blasco. Blasco was a painter and professor at the School of Fine Arts in A Coruña (Escuela Eusebio de Guardia) and then in Barcelona (Escuela de Bellas Artes de la Llotjia). In both schools, with a brief parenthesis at the San Fernando Royal Academy of Fine Arts in Madrid, Picasso received his academic formation. When he was only teenager, Picasso boasts of painting of large format such as *La Primera Comunión* (First Communion, 1896) and *Ciencia y Caridad* (Science and Charity, 1897). Although, his inclination towards the Modernism and the avantgardes were clear since his first contact with the active and vibrant cultural atmosphere of Barcelona[4]. It is in the capital of Catalonia that Picasso starts to keep distance from the academic style. On the other hand, despite the new style, he never forgot the great Masters of the past (Velázquez, El Greco, Goya etc.) that he knew from the *Museo del Prado* in Madrid.

Due to the notable influences that these years had on his artistic practice, the study of the palette that Picasso used in this period, between the epoch of his academic formation and the moment of his encounter – clash with the modernism and the bohemian life, is an important information to establish his expressive evolution. Indeed, the information available about the artworks done by Picasso in these early years[5], especially about the material used, is less extended than the existing for other period (see literature comparison section 3.4).

The "Early Picasso project", presented in this chapter, was focused on the material characterization of six portrait of Picasso's early period, selected by the Museum Picasso of Barcelona, as representatives of his fervent artistic production between 1895 and 1900.

The series is composed by two of the works painted in A Coruña. These two works are titled *Home amb boina* (Man in a beret, MPB110058) and *Retrat d'un vell* (Potrait of an old man, MPB110014). The other three portraits *Retrat de Carles Casagemas* (Portrait of Carles Casagemas, MPB 110022), *Retrat d'un desconegut al estil d'El Greco* (Portrait of an unknown man in the style of Greco, MPB 110034) and *Retrat d'un desconegut* (Portrait of an unknown man, MPB 110026) are dated between 1899 and 1900. However, the master piece of this series is the *Autoretrat amb perruca* (Self-portrait with a wig, MPB 110053). Its temporal context is still under investigation. Dated at first 1898-9, it is now considered, based on the catalogue "Yo Picasso", one of his works of the 1900.[6]

One of the main feature of most of the paintings is the evident multilayers structure. Thus, this study is a journey in the studio practice of the artist at his debut throughout material and structure of the artwork investigated.

The complexity and the unicity of each works give the opportunity to test the capacity of the non-destructive analytical technique for the investigation in situ of real artworks.

First, a systematic analysis based on both global and punctual analysis techniques, of each portrait will be presented. Afterwards it will be discussed the information obtained and some issue that remain open. A collection of bibliographic sources on the material characterization of Picassos' artworks will used to highlights possible continuities and/or changes of his palette along time.

3.2 Experimental

The paintings were examined in the restoration studio of the Picasso Museum of Barcelona. Several areas were investigated using complementary analytical techniques, such as XRF, mid-FTIR and NIR-FTIR, UV-Vis and Raman depending on the cases and the material target. Furthermore, IR reflectography images have been acquired at twelve wavelengths (952 – 2265 nm). In some little areas the varnish was removed by the restorer to permit mid-FTIR measurements without the possible interference of the superficial resin. During the measurements the canvases were simply placed on an easel in front of the equipment.

The specialist participants of the analysis campaign were Francesca Rosi, Federica Presciutti, Aldo Romani, Bruno Brunetti, David Buti, Francesca Gabrieli and Chiara Grazia of the University of Perugia (Center SMAArt); Raffaella Fontana and Mattia Patti of the CNR-INO; Reyes Jiménez de Garnica and Anna Vélez of the Museu Picasso Fundation

(Preventive Conservation and restoration department), and Àngels Miquel Vilanova, Héctor Bagán Navarro, Eva Marín Aznar, Clarimma Sessa, Jose Francisco Garcia of the University of Barcelona.

3.2.1 Instruments

Portable Mid-FTIR

Reflection mode spectra collected by a compact ALPHA Bruker Optics spectrometer from spot of ca. 5 mm in diameter. Wavenumbers ranged from 6000-375 cm^{-1}, at 4 cm^{-1} resolution, using 100 scans[2]. The spectrometer was maintained parallel to the surface at a distance of about 5 mm.

Portable NIR-FTIR

Reflectance FT-NIR spectra were recorded using a compact portable JASCO VIR 9600 spectrophotometer equipped with a near-infrared fiber optic sampling probe[7]. The optical bench was made up of a halogen lamp as source, a Michelson interferometer equipped with a CaF_2 beam splitter and a non-cooled InGaAs detector. The spectrophotometer is equipped with a Y-shaped silica-glass fiber-optic probe containing 14 fibres, seven of which carry infrared radiation from the source to the sample, while the other seven collect the radiation reflected off the surface. Correction for background absorption was performed by recording the reflectance spectrum of a metal mirror plate as reference. The fiber optic probe was kept perpendicular to the sample surface. The spatial resolution is determined by the probe diameter and is about 12 mm. In this work, the spectra were collected by 400 interferograms covering a spectral range from 12,000 to 4000 cm^{-1}, at a resolution of 4 cm^{-1}.

Portable XRF

Spectra were recorded using portable equipment made with a miniaturized X-ray generator EIS P/N 9910, equipped with a tungsten anode and a silicon drift detector (SDD) cooled with a Peltier element[8]. The SDD had a resolution of about 160 eV at 5.9 keV. The portable instrument allowed the detection of elements with atomic number higher than silicon ($Z > 14$). The excitation parameters used during the investigations were voltage of 38 kV and current of 0.05 mA. The acquisition time was 60 s. The distance sample-detector was fixed at 2 cm. The beam diameter under these conditions was 4 mm.

Raman

The portable micro-Raman instrumentation is equipped with a diode laser emitting at 785 nm. The laser radiation is focused through an optical fiber, with a core diameter of 100 μm, into a JASCO RMP-100 micro-probe equipped with an Olympus objective (50× or 20×)[2]. In the probe, a beam splitter co-axially focused the radiation into the objective and the image of the irradiated sample was visualized by a CCD camera. The laser beam passed through a cut filter and a notch filter, which eliminates the Rayleigh scattering of the excitation line. The probe is also equipped with an attenuator, which allows for the laser power tuning at the sample. The backscattered Raman light is collected (at 180°) by a 2-m-long optical fiber of 200 μm diameter, and directed to the polychromator and to a Peltier-cooled CCD detector. The portable setup had a spectral resolution of about 8 cm^{-1}. The measurements are contact free and the maximum laser power kept at the surface was 10 mW.

Scanning multispectral IR reflectography (SMIRR)

Scanning multispectral IR reflectography (SMIRR) was performed by using the multi-NIR scanner developed by the National Institute of Optics; IT (CNR-INO). The scanner has 16 bands: 13 in the near IR covering the range 800-2265 nm, and 3 for acquiring a colour RGB image of the painting. The scanning system has a speed of acquisition of about 3 hours per square meter. The instrument software was designed and is maintained at INO[9]. It allows the recording of the multi-spectral images with real-time monitoring of the acquisition through a user-friendly GUI (Graphic User Interface).

3.2.2 Data treatment

The software used for the data treatment was MATLAB® from Eigenvector RI employed for graphic representation and peak evaluation (script by Jordi Fons of the University of Barcelona), MOVIDA® used for on-the-spot data documentation and analysis data management[10], and Ampek PMCA® for XRF spectra examination.

A procedure for high peak calculation was employed for calculating the net counts for each element X-ray, applying a baseline subtraction algorithm. The contribution of mercury was estimated by subtracting the signal of tungsten (from X-ray source). In fact, Lβ emission of tungsten shows a band shape with a shoulder that falls at the same energy of mercury. The spectra not containing mercury were employed for determining the contribution of the shoulder to the Lβ emission of tungsten. The presence of cobalt was evaluated by subtracting the contribution of Kβ emission of iron.

The interpretation of the obtained spectra was done based on the literature [2,8,10–41] and available reference materials.

3.3 Results and discussion

The results obtained for each painting will be presented separately to better describe composition and technical details specific and unique for each work, followed by a global discussion on similarities, studio practice of the artist, questions arisen from the literature available will be exposed. The study of each portrait will be divided inon three main sections. First, a surface and subsurface survey performed by means of VIS, NIR images and XR images (courtesy of the Picasso Museum of Barcelona) will be presented. The second part will be centred on the results obtained with the punctual techniques analysis, mid-FTIR, XRF, complemented with the other techniques when required. The last and summary section is dedicated to the discussion of material identified, in terms of distribution on surface (x/y dimension) and in depth (z dimension, stratigraphy), with the aim to reconstruct mappings that may help the understanding of the artwork structure. The knowledge achieved were partly restricted by the non-destructive techniques' limitations and, in most of the cases, improved by additional information such XRR images or literature contribution.

3.3.1 Home amb boina

Artwork's interest

Picasso painted the "***Home amb boina***" (***Men in a Beret***) [50.5 x 36 cm, MPB110.058] when he was only fourteen years old. He marked this work in the right-hand upper corner with the name "P. Ruiz" and he wrote also the date ´95 below his signature. Even in the early childhood, the talent of Picasso was evident, although almost obfuscated by the academic style and father influences. His academic formation began in the Eusebio de Guarda School of Art and Craft in La Coruña in 1892 and reached its culmination between 1895 and 1897 in the la Llotja School of Fines Art in Barcelona[4]. Particularly during the last months that he spent in La Coruña (first months of 1895), the young Picasso began an intense period of portrait-painting centered mostly on his family, his father, his mother and the sister Lola, although he enlarged the focus of his works with a series of portraits of anonymous Galicians.[3] These portraits are simple but intense. Picasso used a modest palette and focused

his attention on the drawing line and the traits of the characters. The result were sad, sharp or hesitant looks of anonymous people, which seem to hide a large and entangling backward past. In this context, the teenager Picasso created the portrait ***Home amb boina***.[4]

Description and interpretation of the structure of the painting layers

According to the documentation provided by the conservator Sra. Reyes Jiménez, the portrait experienced a relining, although the documentation about this intervention is not conserved and no information about the year of the intervention is available. The original support is described as an irregular fragment, and the dark areas apparently contained some cracks. A protective varnish was probably applied in 1970. Furthermore, the canvas shows evident folds. The artwork is labelled as an academic painting that can be assigned to the Spanish portrait tradition.

The discussion of the results will be organized in three parts: the first based on the description of the artwork structure through the information obtained with the techniques of global analysis (VIS, XR, IR reflectography); the second part will be centred on the results obtained with the punctual techniques analysis (mid-FTIR, XRF); finally, the global discussion will focus on the description of the composition of the different areas and the reconstruction of the stratigraphy.

Direct observation – VIS

Observation of the visible underneath layers

Through the more superficial paint strokes, it is possible to identify the underlying paint layers, although the composition highlighted by the NIR images (see reflectography section below) is hidden under a thick paint layer applied to create the visage of the man. Inspecting the upper edges of the painting some yellow-orange shade (Figure 1a – green dot line) and white areas (Figure 1a - yellow dot line) can be detected. This suggests a layer lying underneath, barely deducible only with a visual inspection. Furthermore, vertical lines that do not correspond to the original composition are visible. In the area of the painting corresponding to the beard a very intense blue can be observed throughout the craquelure (Figure 1b). Little changes of the beret are also apparent.

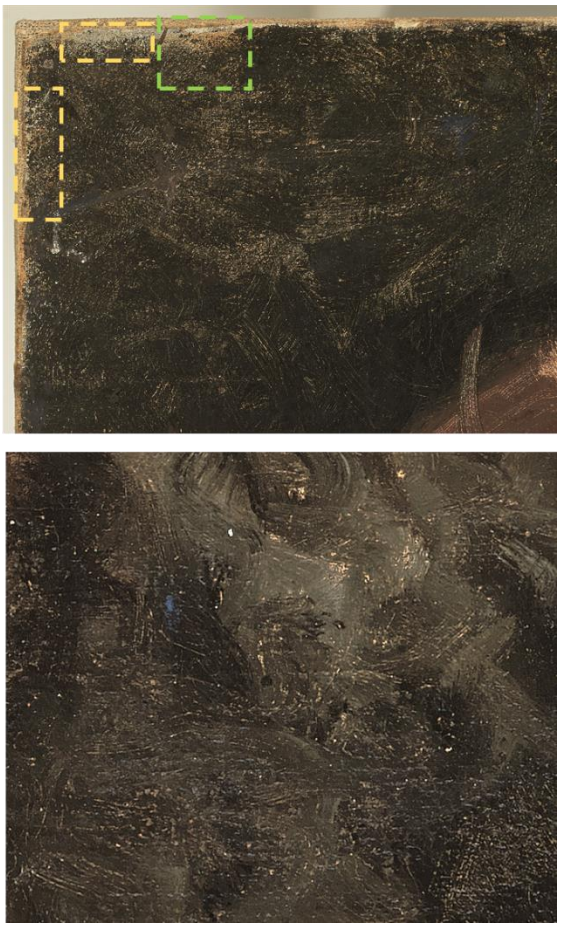

Figure 1.VIS Image: a) upper-left hand corner of the painting with coloured marker lines that highlight the underneath composition, b) zoom on the area located near the beard where a blue area of the underneath layer is visible.

Observation of the superficial layers

Background

The background is not homogeneous. It presents, over the ochre colour of the layer underneath, a black-brown area painted with circularly shaped strokes on the left-hand side. This is a semi dark zone that progressively becomes lighter in the opposite side of the painting due to a light grey-blue paint following the profile of the man's right hand. Picasso applied short and fast strokes around the central subject. The overlapping of the grey-blue paint that can be observed on the beret (Figure 2 – magenta dot line) suggests that first Picasso painted the character in the centre of the canvas. It is interesting to notice that Picasso modified the beret at least in one occasion using the paint of the light perimetral background. It seems that he corrected the profile when the paint was still wet, causing a mixture of the different colours in the back part of the beret. The craquelure is confused with the texture and scratches intentionally created by brush (Figure 2 - violet dot line). The narrow brush stroke that goes down from the top of the painting up to the beret seems to cover a fold

caused by the roll up of the canvas (Figure 2 - orange dot line). Other similar lines are observed on the corners and the right-hand side of the canvas. Furthermore, the brush strokes that are suddenly interrupted on the edges and their direction are an indication that the canvas was cut off after Picasso painted the composition on the surface. The signature "P. Ruiz" and the date "95" are located in the upper right-hand corner (Figure 2 - blue dot line).

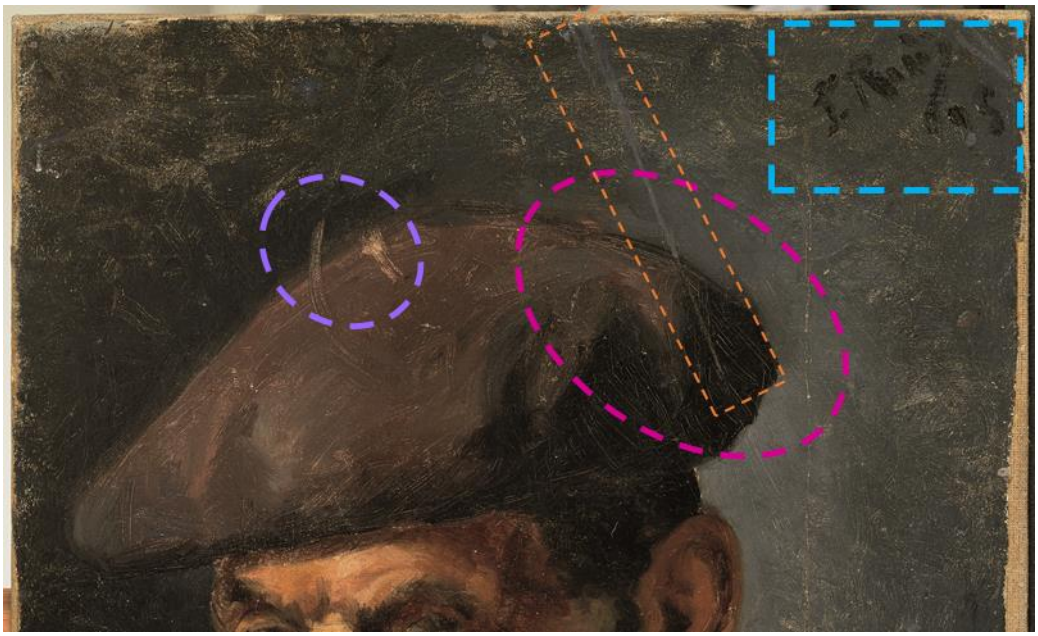

Figure 2. Detail of the face of the old man in a beret. Blended paint of the back part of the beret with the background. Subject

Subject

The character depicted in this painting is the half-length of an old man in a beret turned slightly to the left side, but looking direct to the observer. The young Picasso used a very simple palette ranging from black to reddish brown-ochre and grey-blue shades. The round volumes of the face are moulded with a system of light and shadows created with short and modulated brush strokes of different hues, dark pink, yellow-ochre, grey and white. Moreover, the round perimeter is marked with black brush strokes, the most visible being the one at the lower side of the beret. The expression wrinkles are rendered with a faint dark grey-black paint. The eyes are particularly opaque, especially the right one, typical of old and ill crystalline lenses. The curly beard is painted with light white, dark-grey and ochre brush strokes, probably a mixture of different colours that in some point get lost in the dark colour of the jacket. The man is wearing a black jacket and a brown beret with some violet toques.

Observation with no visible radiation - Underneath layers (XRR, IRR)

Radiography

Unfortunately, no RX images are available. A radiography, in this case, would be extremely important to assess the composition partially visible in the NIR images discussed below.

IR Reflectography

Several NIR images were acquired. Figure 3 shows a contrast-enhanced IR reflectography at 2265 nm wave length. The NIR image suggests the presence of another composition. Vertical lines that pass through the face of the subject (Figure 3 – green lines) became visible, and areas where different textures of the paint layer are highlighted suggest the presence of different materials distributed across the surface with creative intention (Figure 3 – blue lines). The vertical line on the right side and in the right corner indicate that the canvas has been bent when the representation was already there (Figure 3 - magenta line).

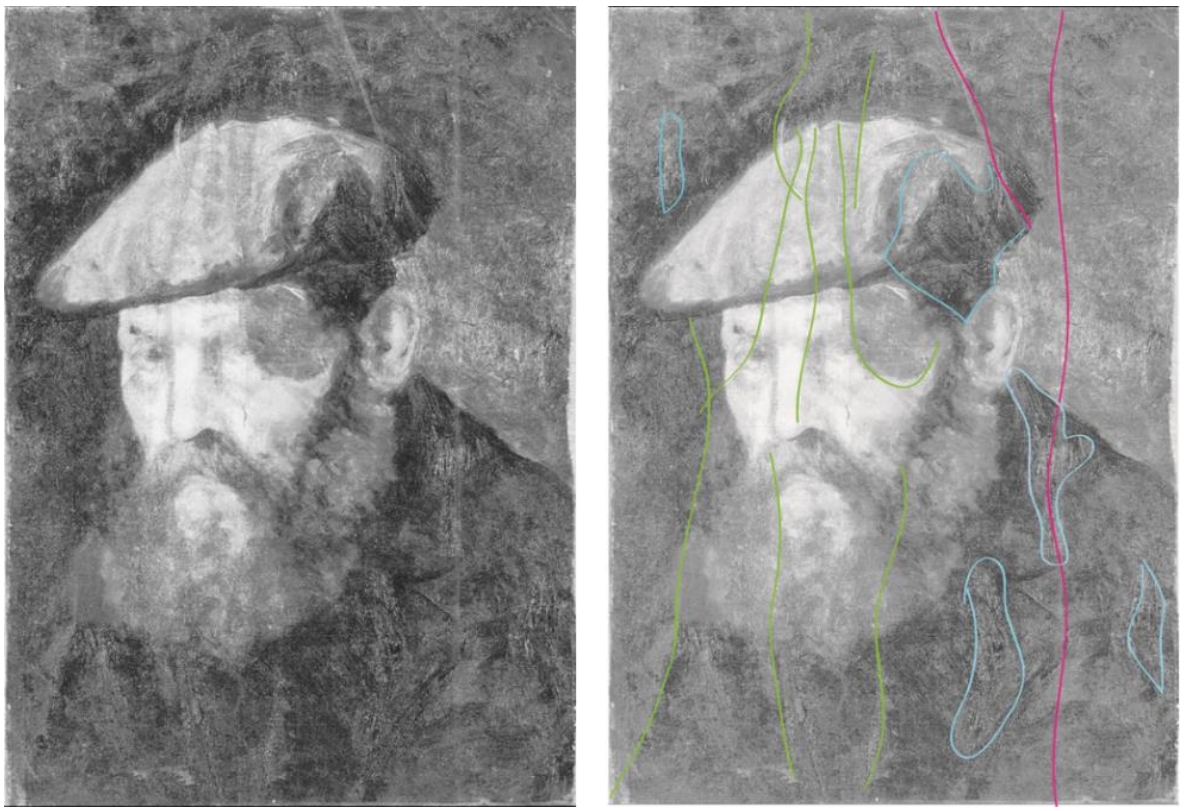

Figure 3. NIR image acquired at 2265 nm - high contrast.

Description and interpretation of the materials

In Figure 4 are presented the XRF (a) and mid-FTIR (b) measurements spot distribution are presented and the corresponding file names are reported in Table 1.

XRF MID-IR

Figure 4. XRF (a) and mid-FTIR (b) measurements spot distribution.

Table 1. Spectrum/spot label for a) XRF and b) mid-FTIR are reported.

a) XRF spectrum/point label	b) mid-FTIR spectrum/point label
P58_X_01_black	P058_M_03_black
P58_X_02_black	P058_M_01_black
P58_X_03_black	P058_M_04_black
	P058_M_05_black
P58_X_04_white	P058_M_07_preparation
P58_X_05_black	
P58_X_06_black	P058_M_02_black
P58_X_07_white	P058_M_11_brown
P58_X_08_brown	
P58_X_09_violet	
P58_X_10_brown	
P58_X_11_violet	P058_M_08_brown
P58_X_12_ochre	P058_M_09_ochre
P58_X_13_flesh	P058_M_10_flesh
P58_X_14_brown	
P58_X_15_black	
	P058_M_14_red
P58_X_16_red	
P58_X_17_flesh	
P58_X_18_flesh	
P58_X_19_flesh	
P58_X_20_flesh	

P58_X_21_flesh	
P58_X_22_grey	P058_M_13_white
P58_X_24_ground	P058_M_06_preparation
P58_X_23_grey	P058_M_15_blue
P58_X_25_black	
P58_X_26_black	
P58_X_27_black	
P58_X_28_black	
P58_X_29_black	P058_M_12_black

Description

Results are discussed in terms of chromatic areas using the complementary information obtained by XRF and mid-FTIR results. The interpretation of the obtained spectra was done based on the literature [2,8,10–41] and reference materials available. It is important to mention that the material distribution across the surface and in depth is not easily interpretable because no XR image is available and because the layer underneath is totally hidden, except on few points on the edges of the painting.

White Areas

The mid-infrared spectrum **M_06_preparation** (Figure 5), acquired on the subjacent layer exposed on the upper left-hand side, shows mainly the presence of Lead Carbonate ($PbCO_3$ and $2PbCO_3 \cdot Pb(OH)_2$ – Lead White) and kaolin ($Al_4[Si_4O_{10}](OH)_8$). The signals that correspond to the Lead Carbonate (mainly hydrocerussite - $Pb(OH)_2$) are the signals of CO_3^{-2} at about 675 cm^{-1} (in-plane bending) and about 1390 cm^{-1} (ν_3 antisymmetric stretching), 3540 cm^{-1} (fundamental OH stretching) and doublet at about 4300 cm^{-1} ($\nu+\delta$ OH). The kaolin is identified by the OH stretching at 3600 cm^{-1}. The spectrum is quite noisy, which is why no other signals could be assigned. In the XRF spectrum **X_24_ground** acquired in the same point, Pb (152 cps), Ca (5 cps) and Fe (7 cps) have been detected. The Pb could be related to the Lead white and Ca to Calcium carbonate of a possible, preparation layer, while Fe could be an indication of the presence of natural earths.

The mid-infrared spectrum **M_07_preparation** (Figure 5) has been acquired on a white spot located on the left-hand side of the painting. The presence of Lead carbonate and kaolin are confirmed and weak signals of Iron hexacyanoferrate ($KFe[Fe(CN)_6]$ or $Fe_4[Fe(CN)_6]_3$ – Prussian Blue) and Hydroxyapatite ($C+Ca_3(PO4)_2$ - Ivory/Bone black) could be also identified with the signal at 2090 and 2012 cm^{-1}, respectively. The spectrum **X_04_white** acquired on the same white paint shows the presence of Pb (148 cps), Fe (30 cps), Ca (11

cps) and Ba/Ti (5 cps), Ca and Fe possibly due to the black paint (Prussian blue + Ivory/Bone black). The notes taken during the experiment indicate that the beam spot of the source was bigger than the area of interest. Thus, the increase of calcium and iron, with respect to point **X_24_ground**, could be due to the Ivory/bone pigment and the Prussian blue of the background. Thus, the preparation or/and subjacent layer applied was Lead carbonate and kaolin, whereas the background was Ivory/bone black plus Prussian blue.

The white used to paint the beard is Lead Carbonate (IR spectrum **M_13_white,** Figure 5). A very weak signal of Hydroxyapatite and iron Hexacyanoferrate have been detected. At about 1620 cm^{-1} can be identified the C=O stretching of amide (amide I) that is an indication of the presence of proteinaceous components, which may be the results of the relining process. The elements detected (**X_22_grey**) were Pb (137 cps), Zn (77 cps), Fe (8 cps) and Ca (2 cps). The presence of Zn could be an indication of the use of Zinc oxide (ZnO - Zinc white). The signal of Fe can be attributed to Prussian blue and Ca probably to the subjacent layer.

The elements detected on XRF spectrum **X_07_white** were Pb (157 cps), Zn (27 cps), Fe (25 cps), Ca (4 cps), Co (12 cps) and traces of Cr. This point corresponds to a scratch on the paint layer that Picasso made to create a detail of the beret, and permits the access to the subjacent layer. Thus, the Co, Cr and Zn belongs possibly to the composition lying underneath. The summary results of the XRF height peaks evaluation are presented in Table 2.

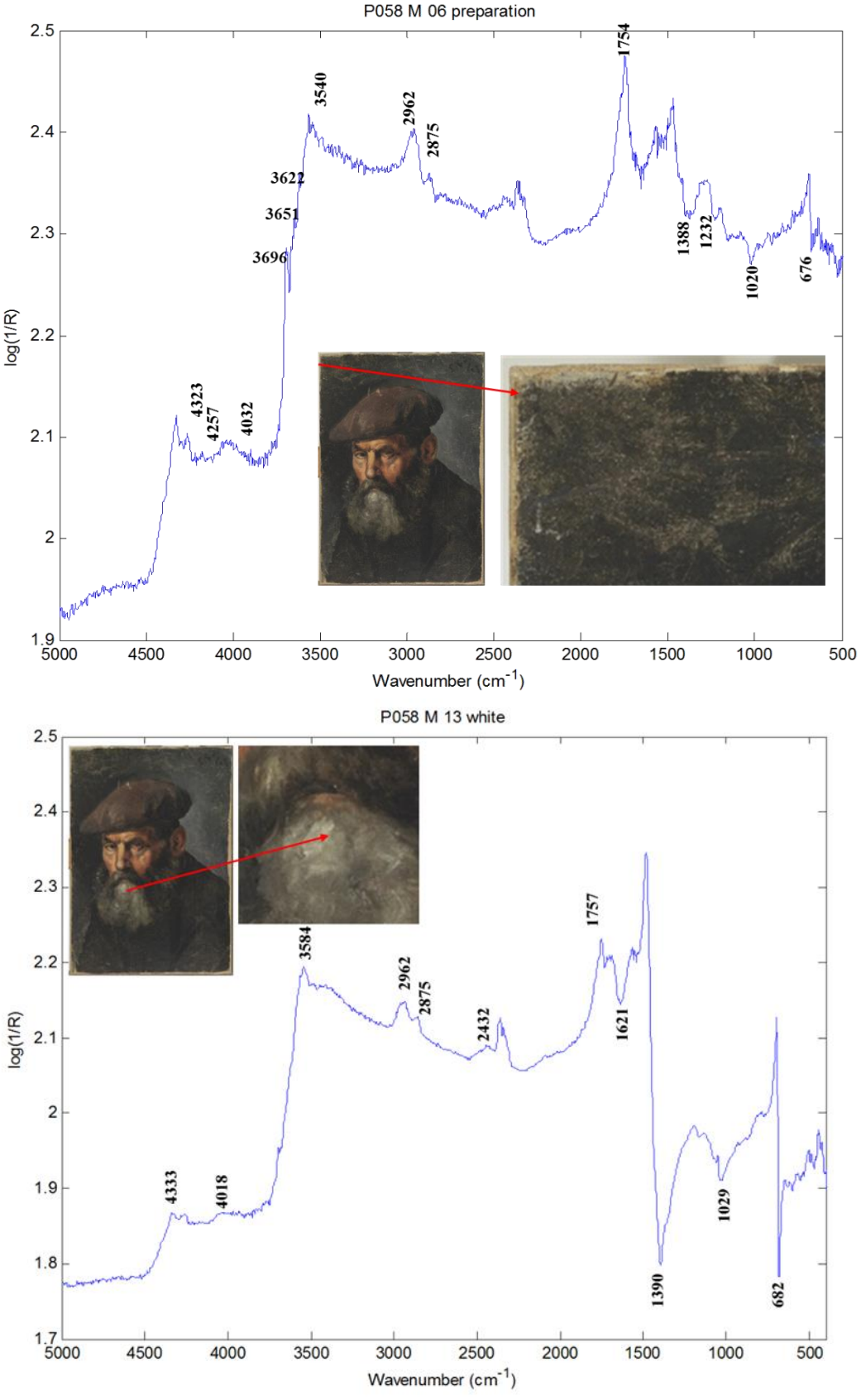

Figure 5. IR spectra M_07_preparation and M_13_white

Table 2. Summary of XRF results for white/ground areas.

cps	P	Ca	Pb	As	Hg	Zn	Cu	Fe	Co	Cr	Ba/Ti	Mn
E (keV)	**2.00**	**3.71**	**10.55**	**11.74**	**9.97**	**8.65**	**8.04**	**6.4**	**6,97**	**5.44**	**4.52**	**5.95**
X_04_white	/	11	148	/	/	/	/	30	/	/	5	traces
X_07_white	/	4	157	/	/	27	/	25	12	1	/	/
X_24_ground	/	5	152	/	/	/	/	7	/	/	/	/
X_22_grey	/	2	137	/	/	77	/	8	/	/	/	/

Grey/Blue Areas

In the mid-infrared spectrum **M_15_blue** (Figure 6) acquired on the dark grey/blue background on the right side of the painting, Prussian blue, Ivory/bone black and a weak signal of Lead white have been detected. The only XRF spectrum that corresponds just to this paint layer is the **X_23_grey** that, unfortunately, was not recorded. On the notes, taken during the analysis Pb, Fe and Ca are indicated (Table 3). Furthermore, in other black points located on the same background no other elements have been detected. Pb and Fe could suggest the use of a mixture of black (Prussian blue and Ivory/bone black) and Lead white to obtain the grey colour of the background.

The same interpretation of the spectrum above is valid for the mid-infrared spectrum **M_05_black** although the signals of Lead white, Prussian blue and Ivory/bone black are stronger and the bands better defined.

Table 3. Summary of XRF results for blue areas.

	P	Ca	Pb	As	Hg	Zn	Cu	Fe	Co	Cr	Ba/Ti
E (keV)	**2.00**	**3.71**	**10.55**	**11.74**	**9.97**	**8.65**	**8.04**	**6.4**		**5.44**	**4.52**
X_23_grey		Present	Present	---	---	---	---	Present	---	---	---

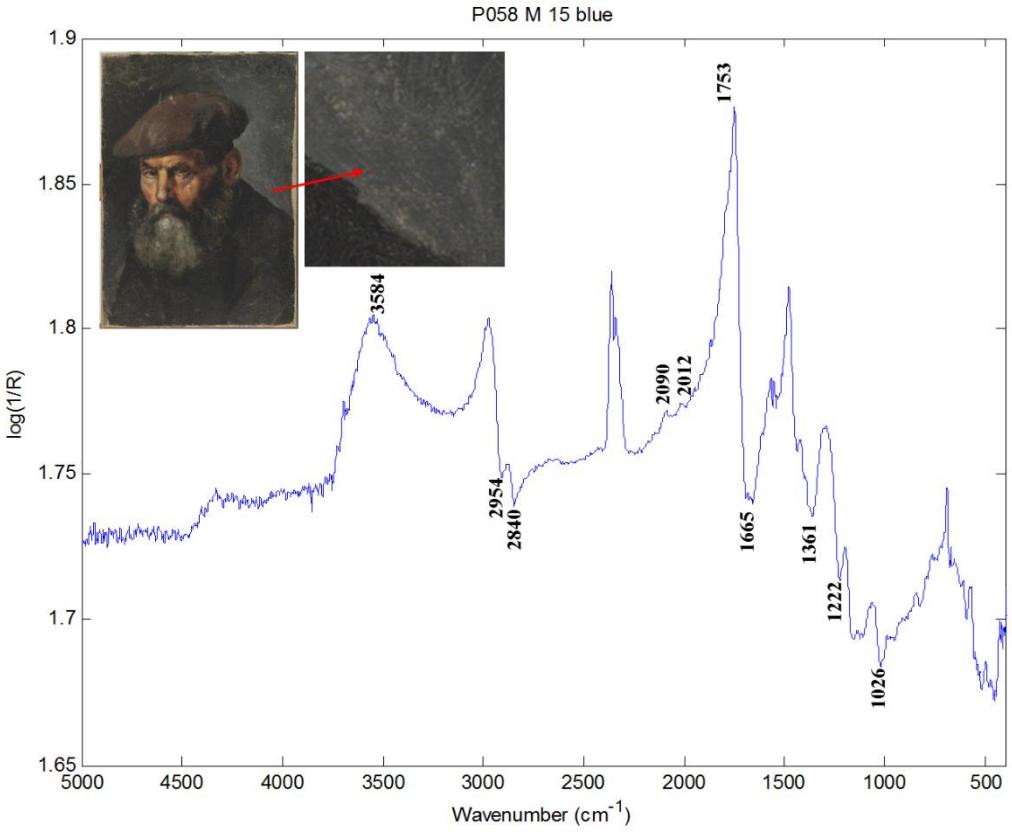

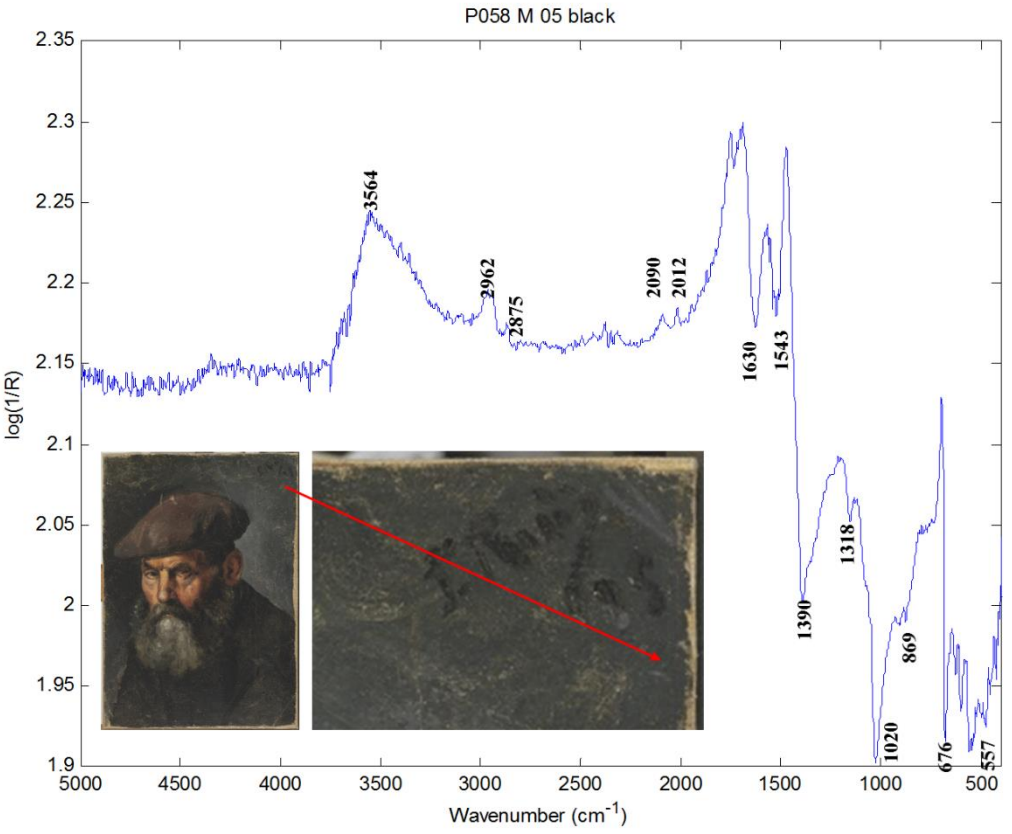

Figure 6. IR spectra M_15_blue and M_5_black.

Signature/black areas

On the upper corner on the left side of the painting Picasso signed the artwork with a black paint. Three mid-infrared spectra were acquired (**M_01/03/04_black,** Figure 7).

The black used is principally Ivory/bone black. The spectra show a C=O stretching of amide (amide I at 1640 cm^{-1}), a N-H bending of amide (amide II at 1540 cm^{-1}). These bands suggest the presence of proteinaceous components. The XRF spectrum acquired on the signature (**X_01/02/03/06_black**) are comparable. In these points Pb, high content of Ca, Fe and traces of P have been detected. The increase of Ca may be related to the Ivory black, while the Fe signal is probably due to the Prussian blue. Comparing the spectra acquired on the signature (**M_01//03/04_black**) and the one acquired on the black of the jacket (**M_12_black**, Figure 7) it is possible to state that Picasso used the same black. Weak signals of Lead Carbonate are also detected. Some of the not assigned bands are present at lower wavenumber that could be related to some oxides. The spectra on the signature are similar to **M_5_black** (background nearby the signature).

Observing the results obtained in the points on the jacket (**X25/26/27/28_black**) the main difference is the lower signal for the Pb, with regard to the rest of the spots, due probably to the thicker black layer. The higher content in Fe could be due to Prussian blue. Indeed, a very high signal is detected on point **X_28_black**. The jacket could also include Cu (green/blue colour) and Zn (white), although the distribution in depth of these elements could not be measured/cannot be confirmed. Thus, they could be related to the composition underneath. A further discussion on the distribution of the different elements across the surface and in depth will be presented in the stratigraphic section. The summary of the results of the XRF height peaks evaluation are presented in Table 4.

Table 4. XRF results for signature.

cps	P	Ca	Pb	As	Hg	Zn	Cu	Fe	Co	Cr	Ba/Ti
E (keV)	**2.00**	**3.71**	**10.55**	**11.74**	**9.97**	**8.65**	**8.04**	**6.4**	**6,97**	**5.44**	**4.52**
P58_X_01_black	traces	39	127	/	/	/	/	14	/	/	/
P58_X_02_black	/	6	162	/	/	/	/	5	/	/	/
P58_X_03_black	traces	25	142	/	/	/	/	17	/	/	/
P58_X_06_black	/	11	148	/	/	/	/	30	/	/	5
P58_X_05_black	/	14	155	/	/	/	2	11	/	/	/
P58_X_15_black	/	14	159	/	1	/	/	13	/	/	/
P58_X_25_black	traces	53	114	/	/	/	4	46	/	/	/
P58_X_26_black	/	12	132	/	/	/	/	99	/	/	/
P58_X_27_black	traces	76	104	/	/	2	3	55	/	1	/
P58_X_28_black	traces	36	115	/	/	/	2	111	/	/	/
P58_X_29_black	traces	25	115	/	/	25	/	79	/	1	/

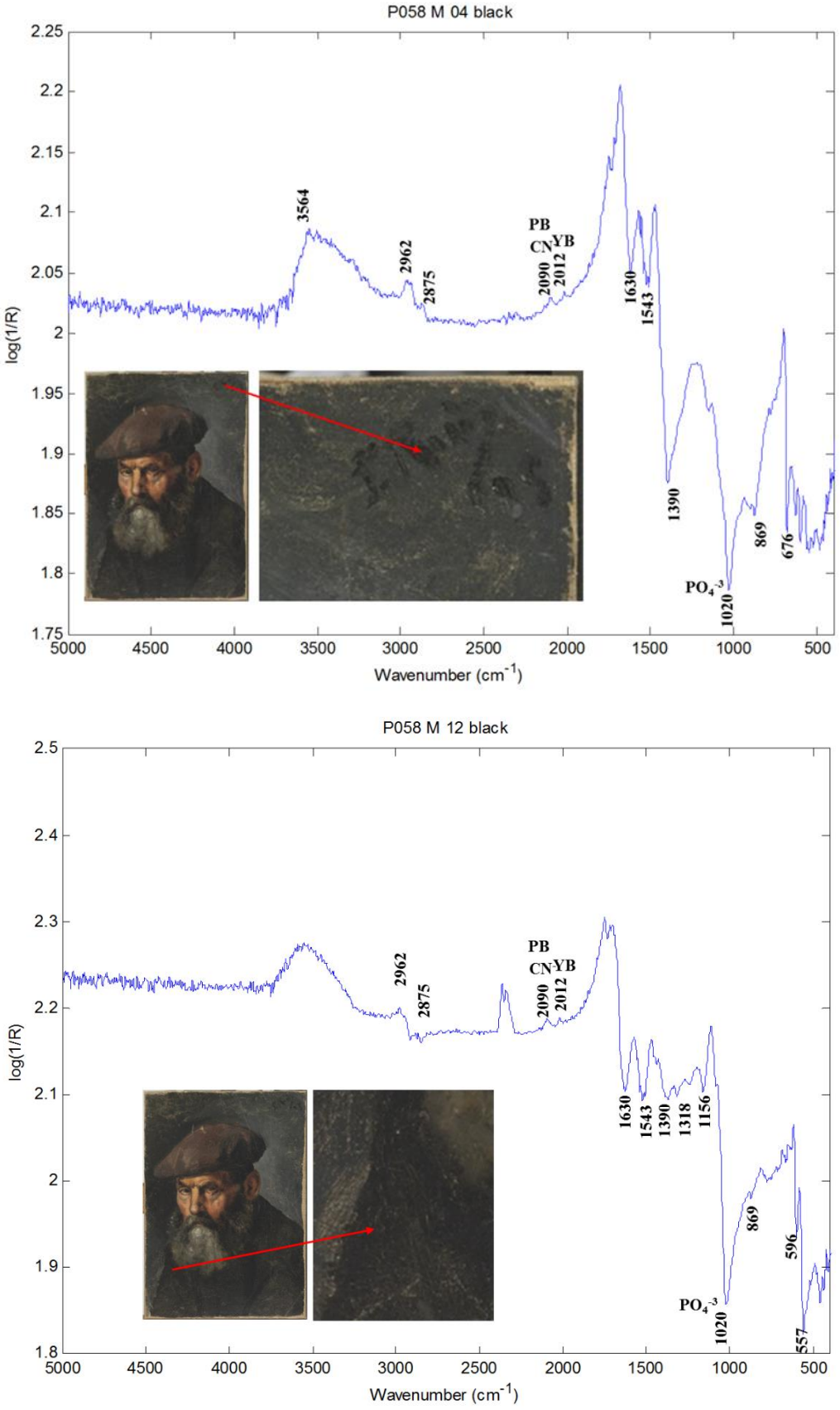

Figure 7. IR spectra M_04_black and M_12_black

Brown areas

Signals of Ivory/bone black, Lead white and Prussian blue have been detected on the beret (**M_08_brown**, Figure 8) of the character. Inverted signals at about 450 cm^{-1} are not assigned. The inverted sharp band at 1320 cm^{-1} suggests the presence of oxalate. The signal between 1600 and 1540 cm^{-1} can be attributed to a proteinaceous material.

The mid-infrared spectra acquired on the top of the beret **M_11_brown** (Figure 8), where Picasso created a detail reducing the painting layer/scratch, suggests the presence of kaolin, lead carbonate and proteinaceous compounds. The XRF spectrum acquired in the same point (**X_07_white**) indicate the presence of Pb (possible preparation), Ca (preparation or/and black), Fe (Prussian blue of the black), Co (violet or cobalt blue), Zn (position not assigned) with traces of Cr (possible green/yellow pigment). The first three elements are rather uniformly distributed across the entire surface, while a Co based pigment seems to be used only to create the violet shade of the hat. In fact, all the other points investigated by XRF in these areas show a high signal of Co (**X_08/09/10/11**) that it is not present in any other area. Zn is detected only in points **X_07** and **X_08**, but its relation with areas and different layers (depth) is difficult to establish (see stratigraphic section).

Point **X_14 brown**, the XRF spectrum acquired on the old man's temple, shows the presence of Cu, As, traces of Cr and a very high signal of Fe. In this point, the brown shade is very dark, that means that a major quantity of a Fe oxide based pigment, such as natural earths could be used or some of the signal belongs to the composition underneath, which is visible in the NIR image in this area as a very dark circular area. The composition on point **X_17** located nearby on the flesh/skin is similar, but the Fe signal is much lower. The results of the XRF height peaks evaluation are summarized in Table 5.

Table 5. Summary of XRF results for brown/beige areas.

cps	P	Ca	Pb	As	Hg	Zn	Cu	Fe	Co	Cr	Ba/Ti
E (keV)	**2.00**	**3.71**	**10.55**	**11.74**	**9.97**	**8.65**	**8.04**	**6.4**	**6.97**	**5.44**	**4.52**
P58_X_07_white	/	4	157	/	/	27	/	25	12	1	/
P58_X_08_brown	/	5	153	/	/	5	/	57	53	/	/
P58_X_09_violet	/	5	136	/	/	/	/	30	25	/	/
P58_X_10_brown	/	4	137	/	/	/	/	54	44	/	/
P58_X_11_violet	/	6	148	/	/	/	/	30	29	/	/
P58_X_14_brown	/	4	138	1	1	/	7	169	/	1	/
P58_X_17_flesh	/	3	141	/	/	/	4	79	/	traces	/

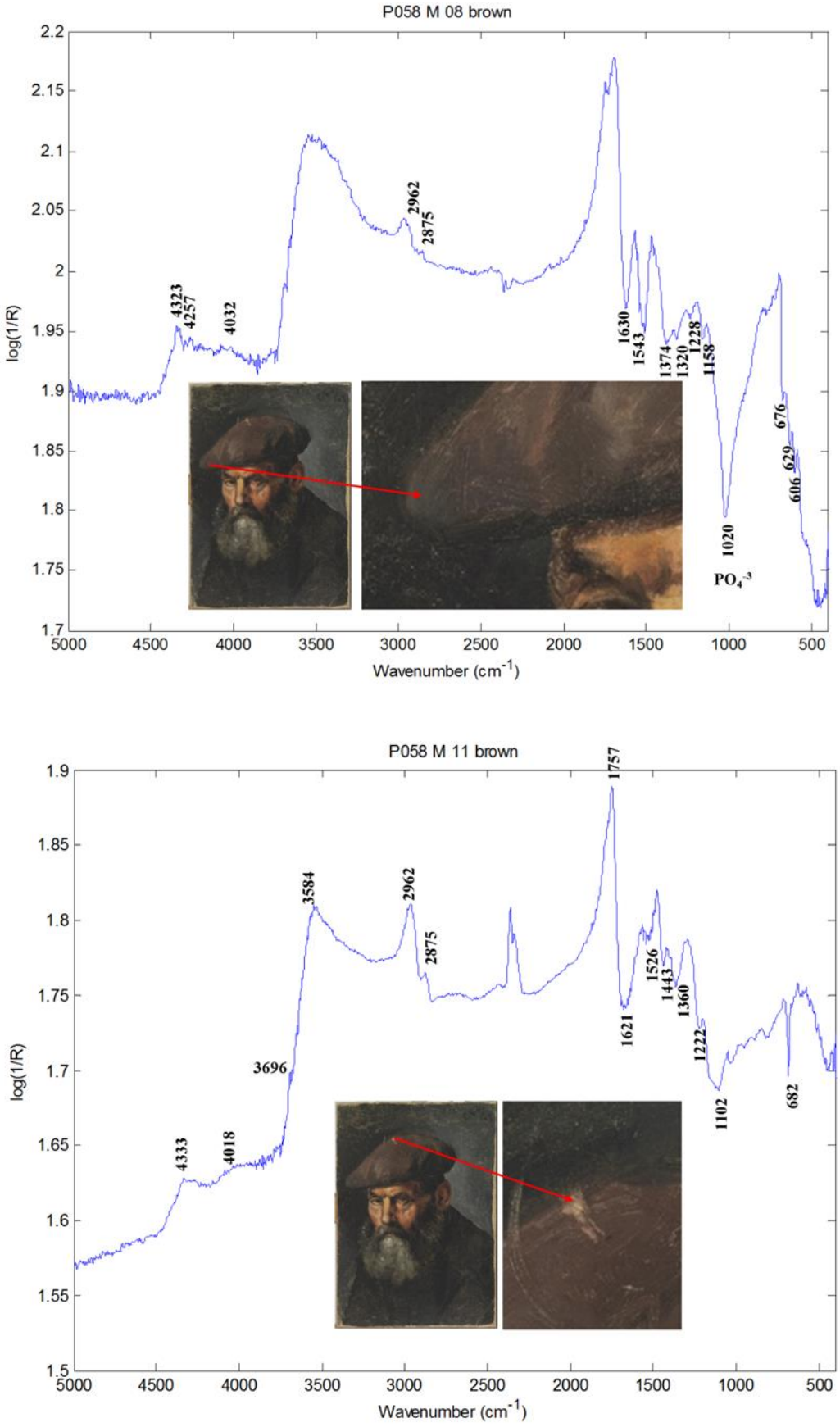

Figure 8. IR spectra M_08_brown

Near-infrared spectra recorded on three points of the hat, the cobalt blue used for the violet shade of the hat could be identified as Cobalt blue, commonly named Thenard's blue, due to the absorption in the range 6500–8500 cm^{-1}. According to the literature the spectral features of the near-infrared electronic absorption allows to characterize the chemical structure of cobalt compounds, as it permits to distinguish smalt (alkali glass containing Co^{2+}), cobalt blue ($CoAl_2O_4$), cerulean blue ($CoSnO_3$), cobalt violet ($Co_2(PO_4)_2$) and cobalt green ($CoZnO_2$) [8,42]. The spectra acquired **(N_01/02_brown**, Figure 9) show three broad bands at about 6596, 7230 and 8150 cm^{-1} and the comparison with a reference spectrum suggests the cobalt blue as possible pigment detected ($CoAl_2O_4$). In this case, the violet colour should be related to a mixture of blue with some red pigment. However, due to the low quality of the spectra, the colour observed, and the phosphate band often detected, the use of cobalt violet is not discarded.

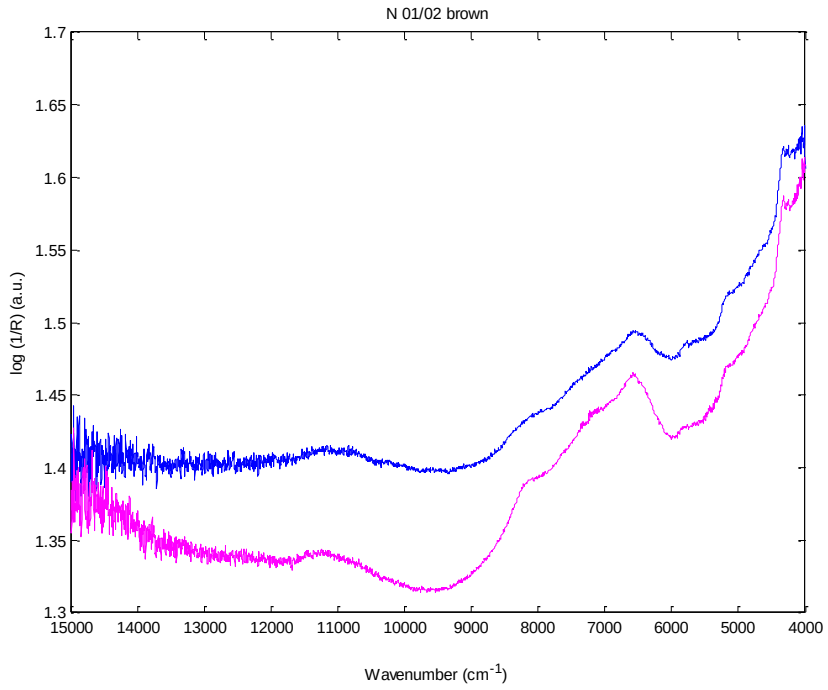

Figure 9. IR spectra N01 and N02_brown

Red/pink areas

The mid-infrared spectrum **M_14_red was measured** on the lips of the old man. The main compound identified is the Lead white. The same could be commented about the mid-infrared spectrum **M_10_flesh** (Figure 10) acquired on the front of the man. In these two points, the XRF spectrums revealed a high presence of Fe that is an indication of the use of Fe oxide based red pigments. The Vermilion could be only confirmed in point **X_16 red**. The results obtained on the other investigated points are comparable **17/18/19/20/21_flesh**. The elements that were detected are Pb, Fe, Ca and traces of Cr. The presence of Zn and Cu in some points (**X_12/13/21**) is probably due to the composition underneath. Finally, due to the high content of Pb the presence of Lead red cannot be discarded.

The mid-infrared spectrum **M_09_ochre** (Figure 10) has been recorded on a yellow-ochre area on the forehead of the old man. In this case, based on the bibliography and the comparison with a reference pigment the use yellow ochre ($Fe_2O.3H_2O$+clay+silica - Natural yellow earth colour + kaolin) mixed with linseed oil could be assumed. The bands at about 1030, 1003 (Si-O) and 906, 775, 536 and 468 cm^{-1} are characteristic of the yellow ochre [43]. The signal at about 3600 cm^{-1} are due to the OH stretching of kaolin - ($AlSi_3$, Si_4)$O_{10}(OH)_2$ - clay mineral). The XRF spectrum **X_12_ochre** shows the presence of Pb, Fe, Ca, Zn and traces of Cr and Ba/Ti. The results of the XRF height peaks evaluation are summarized in Table 6.

Table 6. XRF results for red areas.

cps	P	Ca	Pb	As	Hg	Zn	Cu	Fe	Co	Cr	Ba/Ti
E (keV)	**2.00**	**3.71**	**10.55**	**11.74**	**9.97**	**8.65**	**8.04**	**6.4**	**6.97**	**5.44**	**4.52**
P58_X_12_ochre	/	2	148	/	/	8	/	90	/	traces	traces
P58_X_13_flesh	/	traces	153	/	/	21	/	25	/	/	/
P58_X_16_red	/	2	153	/	3	/	/	43	/	traces	/
P58_X_17_flesh	/	3	141	/	/	/	4	79	/	traces	/
P58_X_18_flesh	/	3	162	/	/	/	/	62	/	traces	/
P58_X_19_flesh	/	3	160	/	/	/	/	35	/	/	/
P58_X_20_flesh	/	2	115	/	/	/	/	106	/	traces	/
P58_X_21_flesh	/	2	149	/	/	15	/	38	/	traces	/

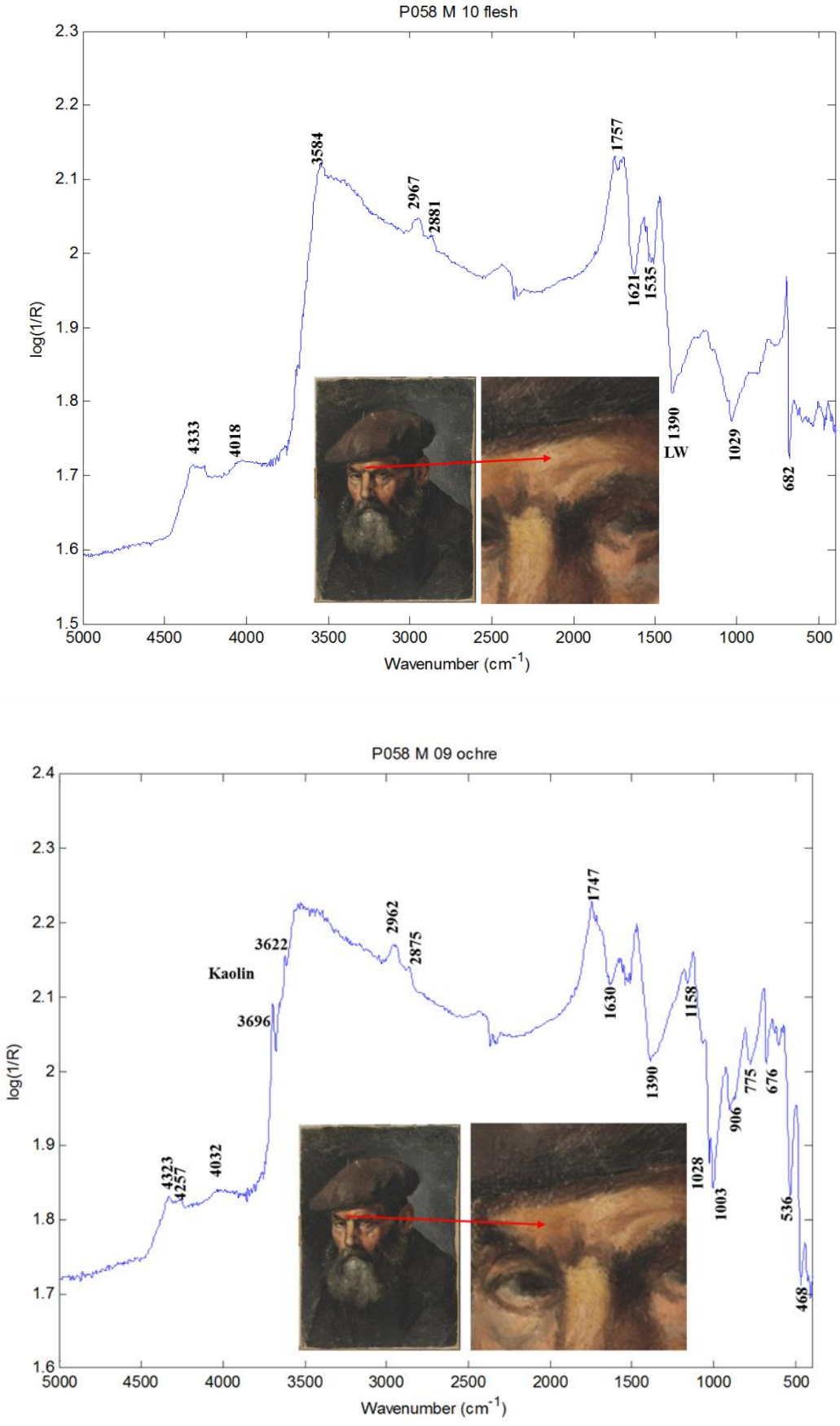

Figure 10. IR spectra M_10_flesh and M_09_ochre

Summary

Figure 11 shows a mapping of the detected elements and compounds.

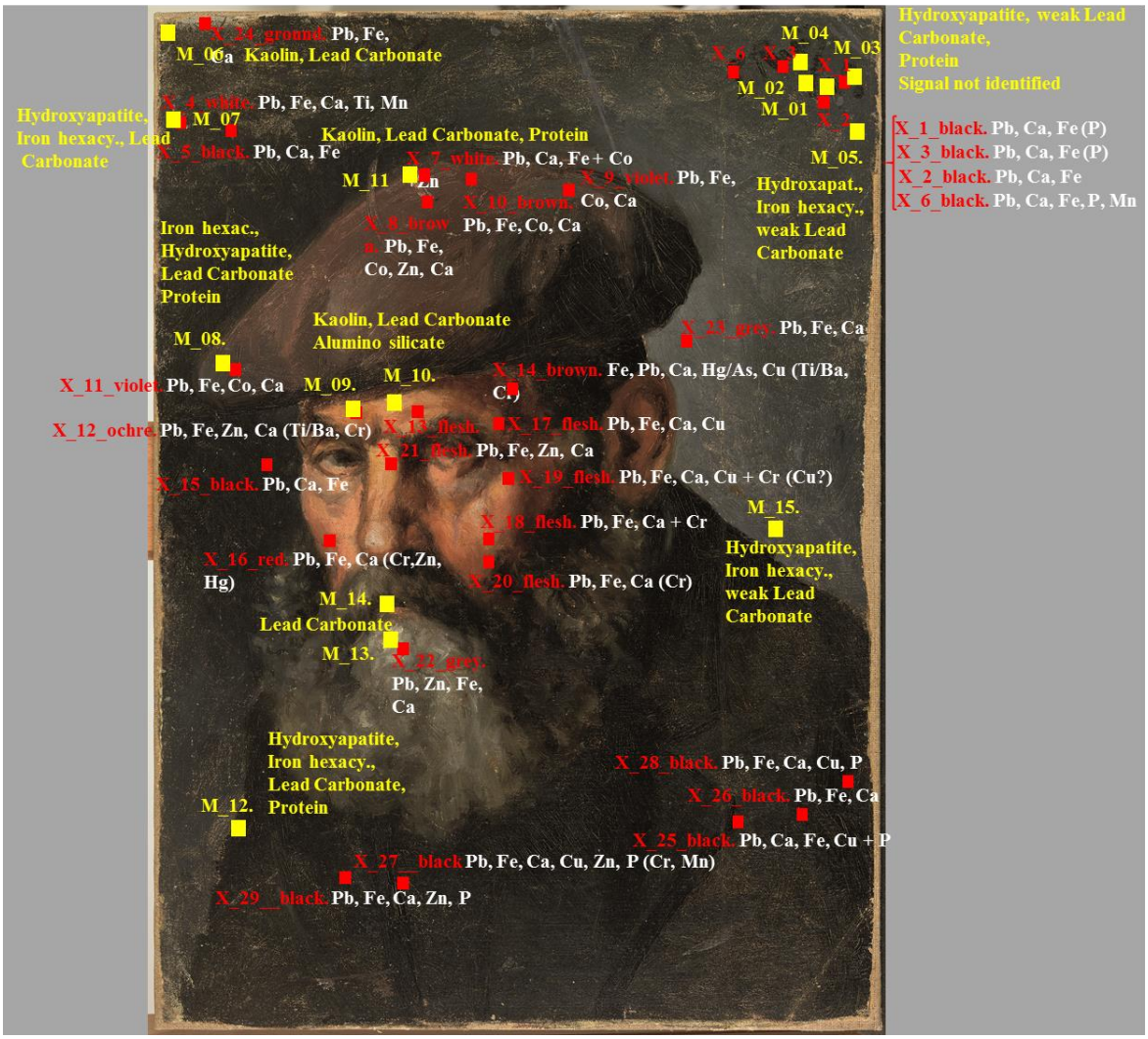

Figure 11. Mapping of the results obtained.

Interpretation

Pigments

White pigments

The Lead white is confirmed by the mid-infrared and XRF measurements, where the main signal originates from the Hydrocerussite component (Figure13 a). The presence of Zinc white (Zinc oxide) has been confirmed and its distribution in depth is not assigned, thus it could be attributed to the layer underneath or/and superficial composition. Its presence has been confirmed by XRF and its distribution is presented in Figure 13b. The O-H stretching characteristic of the Kaolin has been detected in areas with an ochre shade. The Kaolin is

usually a filler of natural pigment such as yellow or brown earth or Fe-oxide based pigments. The presence of low content of Ba/Ti suggests the presence as an accessory compound of some pigment (Figure 13c).

Black pigments

The main black pigment detected is the Ivory/bone black used for the jacket of the old man and for the signature. In this case, the presence of this pigment can be confirmed because of the detection of P (Figure 13d) and the high signal of Ca (Figure 13e). Fe based black pigments and carbon black should not be discarded.

Red – brown pigments

In this painting the main red colours seem to be the Fe based pigments – natural earths. This theory is based on the high signal of Fe on the red and brown areas (Figure 13f). The Hg/Vermilion was detected only in one point (X_16_red). The use of Red lead cannot be excluded. Mn, often associated with brown earth pigments, has also been detected (Figure 13g).

Blue pigment

Picasso, in this case, used Prussian blue (Fe distribution, Figure 13f) and Cobalt blue. The NIR spectra acquired on the beret suggest the presence of the commonly named Thenard's blue ($CoAl_2O_4$). However, the violet tone, the signal of phosphate generally encountered, and the quality of the spectra do not permit to exclude the use of cobalt violet (Figure 13h). In one of his handwritten journals dated 1893 Picasso presents his paint tubes, thus, involuntarily, declaring the use of a cobalt blue = "Azul Cobalto" and a white "Blanco Plata", which is one of the names used for Lead white (Figure 12).

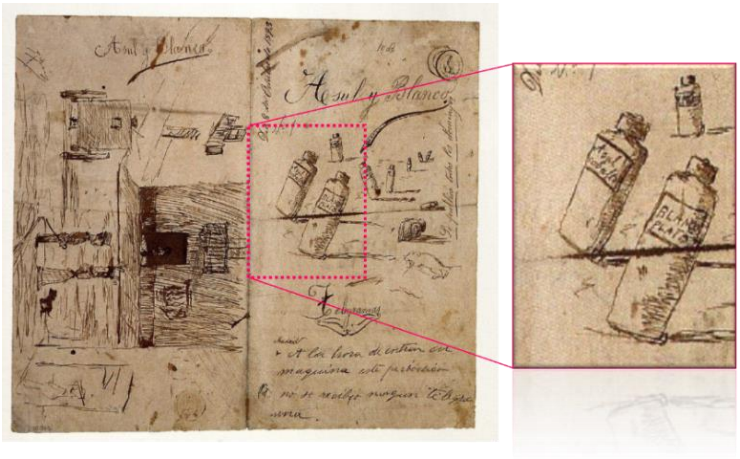

Figure 12. "Azul y blanco", Picasso's handwritten journal, La Coruña, 8 October 1893, Pen&sepia on paper, 20.2x26.3 cm [44].

Yellow/Green pigments

The presence of kaolin and signal of alumina silicate suggests as the presence of natural earths, such as yellow ochre. This pigment is part of the natural tone that Picasso uses for the brown, yellow and red shades. The detection of Cr and Cu may suggest the presence of other green or/and yellow pigments (Figure 13i and l).

Other inorganic compounds

Some products that could be an indication of a degradation process, such as **oxalate** were found in some points of the painting.

Organic compounds

The presence of proteinaceous compounds has been detected. The animal glue used for the reeling treatment has penetrated the paint layer throughout the portrait. This treatment could be the cause of the stiffening of the paint layer, which became more brittle.

It has not been possible to identify exactly the bands corresponding to the agglutinant because the principal signal that could be an indication of the presence of an oil are quite distorted or partially overlapped with other bands.

The summary of the material found is presented in Table 7.

Table 7. Pigments and Binding Media/organic compound Analysis Results

Colours	**Materials/Pigments**	**Binding medium/ organic compounds**
Preparation	Lead carbonate [a,b)], Kaolin [b)]	Animal glue [b)]
White	Lead carbonate [a,b)], Zinc white a)	
Black	Ivory/bone black [a,b)], (Fe oxide based black pigment, carbon black)	
Blue	Prussian blue [a,b)], Cobalt blue [c)], Cu based pigment	
Yellow	Natural earths/Yellow ochre [a, b)]	
Green	Cr based pigments [a)]	
Red – brown	Natural earths/Fe oxide based red pigment [a)], Vermilion [a)], (Red lead)	

a) XRF; b) mid-FTIR spectroscopy; c) NIR.

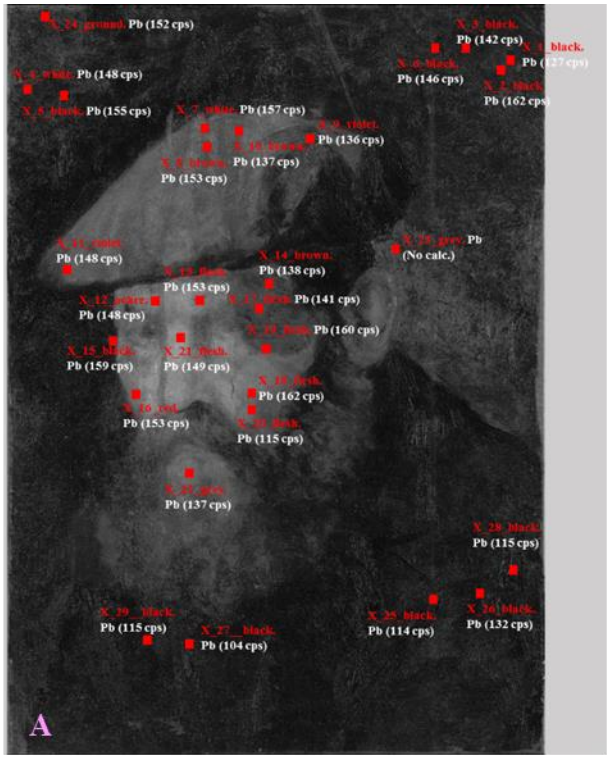
X_24_ground. Pb (152 cps)
X_3_black. Pb (142 cps)
X_6_black. Pb (146 cps)
X_5_black. Pb (155 cps)
X_7_white. Pb (157 cps)
X_9_violet. Pb (136 cps)
X_8_brown. Pb (137 cps)
Pb (153 cps)
X_11_violet. Pb (148 cps)
X_14_brown. Pb (138 cps)
X_13_flesh. Pb (153 cps)
X_12_ochre. Pb (148 cps)
Pb (141 cps)
Pb (160 cps)
X_15_black. Pb (159 cps)
X_21_flesh. Pb (149 cps)
X_18_flesh. Pb (162 cps)
X_16_red. Pb (153 cps)
Pb (115 cps)
X_23_grey. Pb (137 cps)
X_28_black. Pb (115 cps)
X_19_black. Pb (115 cps)
X_27_black. Pb (104 cps)
X_25_black. Pb (114 cps)
X_26_black. Pb (132 cps)
A

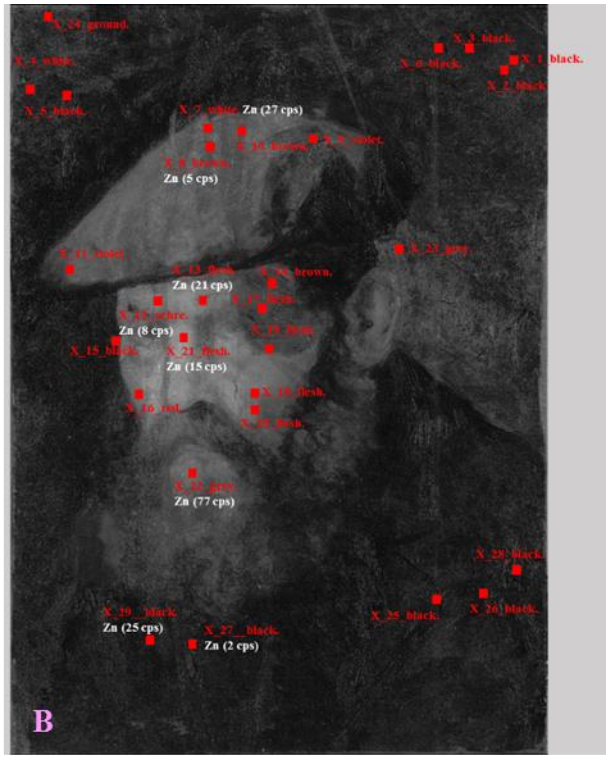
X_24_ground.
X_3_black.
X_6_black.
X_1_black.
X_2_black.
X_5_black.
X_7_white. Zn (27 cps)
X_8_brown. Zn (5 cps)
X_11_violet.
X_23_grey.
X_13_flesh. Zn (21 cps)
X_14_brown.
X_12_ochre. Zn (8 cps)
X_15_black.
X_21_flesh. Zn (15 cps)
X_18_flesh.
X_16_red.
X_23_grey. Zn (77 cps)
X_28_black.
X_19_black. Zn (25 cps)
X_27_black. Zn (2 cps)
X_25_black.
X_26_black.
B

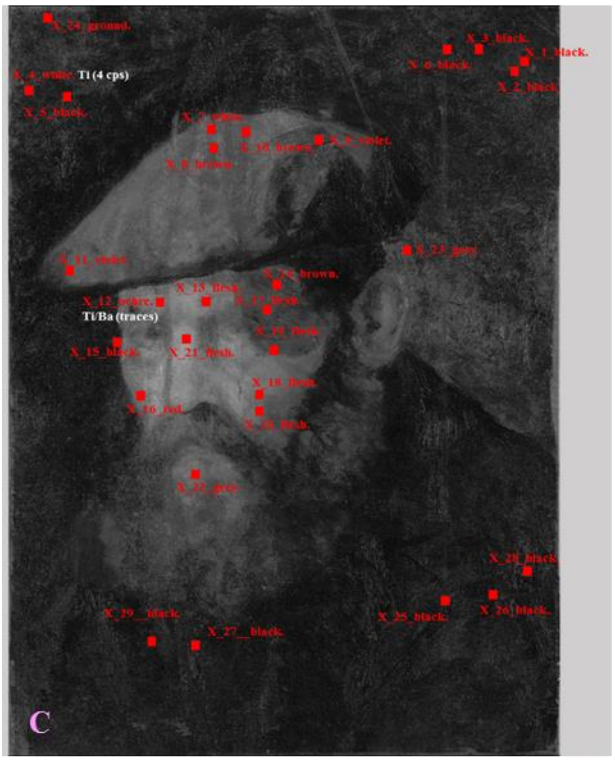
X_24_ground.
X_3_black.
X_6_black.
X_1_black.
X_4_white. Tl (4 cps)
X_2_black.
X_5_black.
X_11_violet.
X_23_grey.
X_14_brown.
X_13_flesh.
X_12_ochre. Ti/Ba (traces)
X_15_black.
X_21_flesh.
X_18_flesh.
X_16_red.
X_23_grey.
X_28_black.
X_29_black.
X_25_black.
X_26_black.
X_27_black.
C

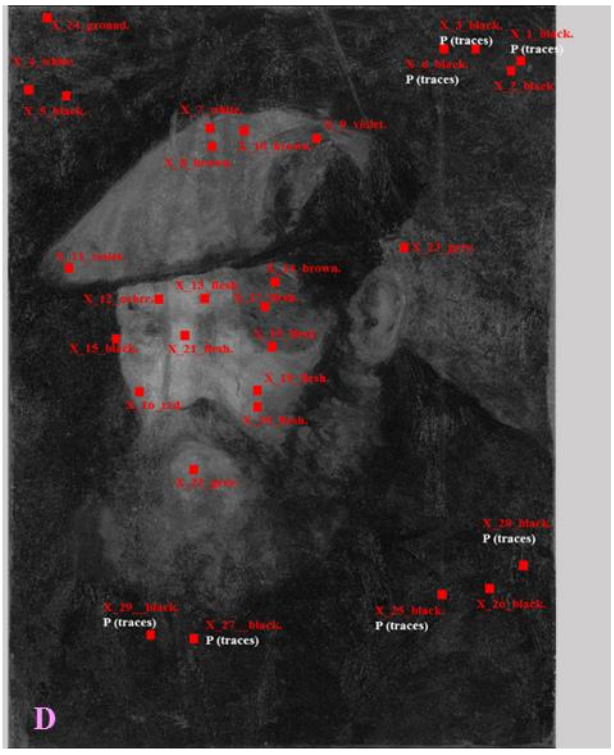
X_24_ground.
X_3_black. P (traces)
X_1_black. P (traces)
X_6_black. P (traces)
X_2_black.
X_5_black.
X_7_white.
X_9_violet.
X_11_violet.
X_23_grey.
X_14_brown.
X_13_flesh.
X_12_ochre.
X_15_black.
X_21_flesh.
X_18_flesh.
X_16_red.
X_23_grey.
X_28_black. P (traces)
X_29_black. P (traces)
X_27_black. P (traces)
X_25_black. P (traces)
X_26_black.
D

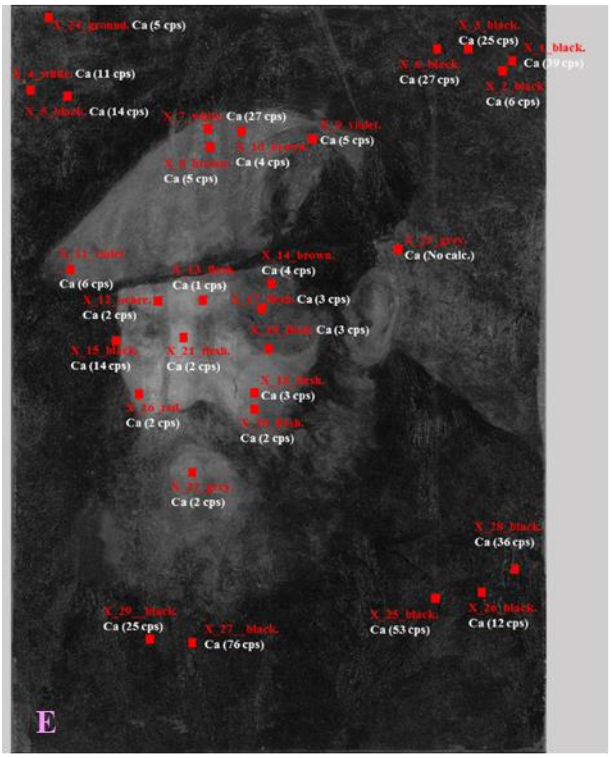
X_24_ground Ca (5 cps)
X_3_black Ca (25 cps)
X_1_black
X_4_white Ca (11 cps)
X_6_black Ca (27 cps)
X_2_black Ca (6 cps)
X_5_black Ca (14 cps)
X_7_violet Ca (27 cps)
X_9_violet Ca (5 cps)
X_10_brown Ca (4 cps)
X_8_brown Ca (5 cps)
X_11_violet Ca (6 cps)
X_25_grey Ca (No calc.)
X_13_flesh Ca (1 cps)
X_14_brown Ca (4 cps)
X_12_ochre Ca (2 cps)
X_17_flesh Ca (3 cps)
X_15_black Ca (14 cps)
X_21_flesh Ca (2 cps)
X_22_flesh Ca (3 cps)
X_18_flesh Ca (3 cps)
X_16_red Ca (2 cps)
X_20_flesh Ca (2 cps)
X_23_grey Ca (2 cps)
X_28_black Ca (36 cps)
X_29_black Ca (25 cps)
X_27_black Ca (76 cps)
X_25_black Ca (53 cps)
X_26_black Ca (12 cps)
E

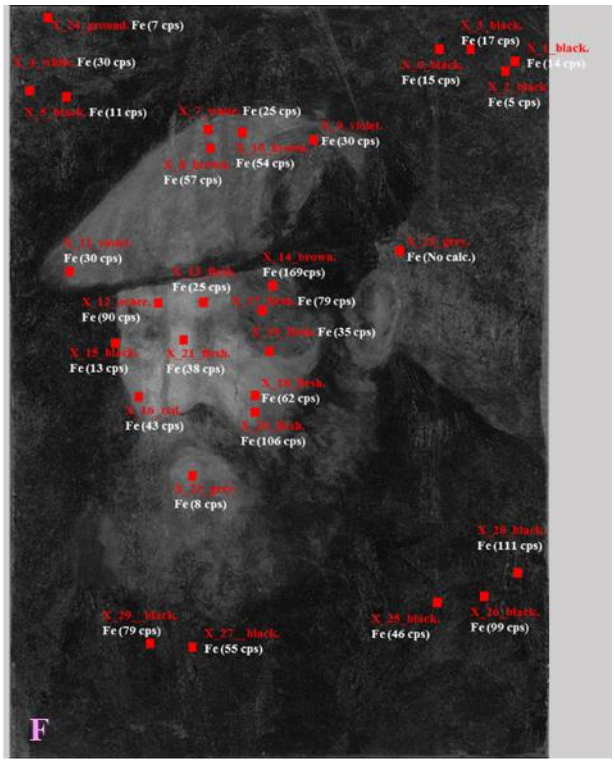
X_24_ground Fe (7 cps)
X_3_black Fe (17 cps)
X_4_white Fe (30 cps)
X_6_black Fe (15 cps)
X_2_black Fe (5 cps)
X_5_black Fe (11 cps)
X_7_white Fe (25 cps)
X_9_violet Fe (30 cps)
X_10_brown Fe (54 cps)
X_8_brown Fe (57 cps)
X_11_violet Fe (30 cps)
X_25_grey Fe (No calc.)
X_14_brown Fe (169cps)
X_13_flesh Fe (25 cps)
X_12_ochre Fe (90 cps)
X_17_flesh Fe (79 cps)
X_22_flesh Fe (35 cps)
X_15_black Fe (13 cps)
X_21_flesh Fe (38 cps)
X_18_flesh Fe (62 cps)
X_16_red Fe (43 cps)
X_20_flesh Fe (106 cps)
X_23_grey Fe (8 cps)
X_28_black Fe (111 cps)
X_29_black Fe (79 cps)
X_27_black Fe (55 cps)
X_25_black Fe (46 cps)
X_26_black Fe (99 cps)
F

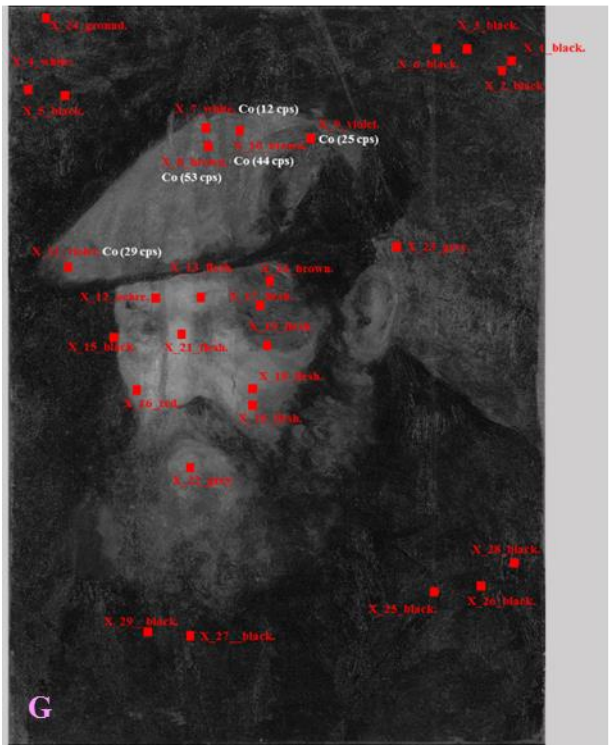
X_24_ground
X_3_black
X_1_black
X_4_white
X_6_black
X_2_black
X_5_black
X_7_white Co (12 cps)
X_9_violet Co (25 cps)
X_10_brown Co (44 cps)
X_8_brown Co (53 cps)
X_11_violet Co (29 cps)
X_25_grey
X_14_brown
X_13_flesh
X_12_ochre
X_17_flesh
X_15_black
X_21_flesh
X_22_flesh
X_18_flesh
X_16_red
X_20_flesh
X_23_grey
X_28_black
X_29_black
X_27_black
X_25_black
X_26_black
G

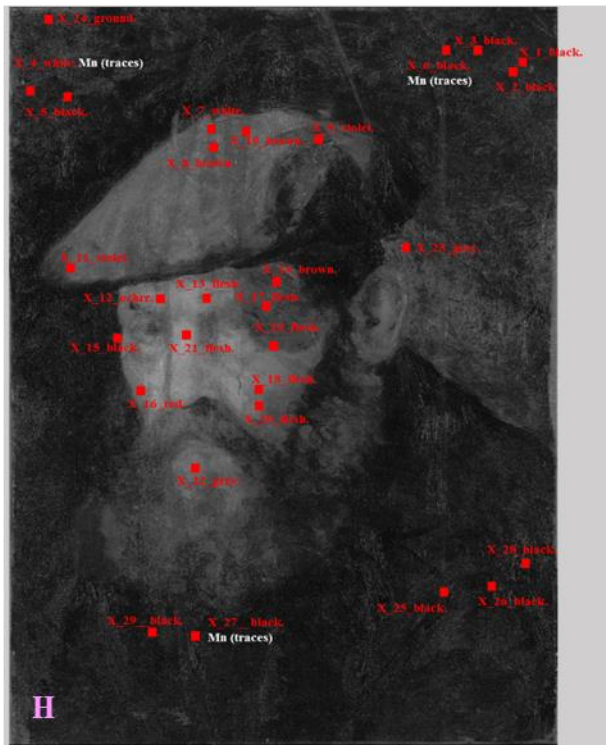
X_24_ground
X_3_black
X_4_white Mn (traces)
X_1_black
X_6_black Mn (traces)
X_2_black
X_5_black
X_7_white
X_9_violet
X_10_brown
X_8_brown
X_11_violet
X_25_grey
X_14_brown
X_13_flesh
X_12_ochre
X_17_flesh
X_15_black
X_21_flesh
X_22_flesh
X_18_flesh
X_16_red
X_20_flesh
X_23_grey
X_28_black
X_29_black
X_27_black Mn (traces)
X_25_black
X_26_black
H

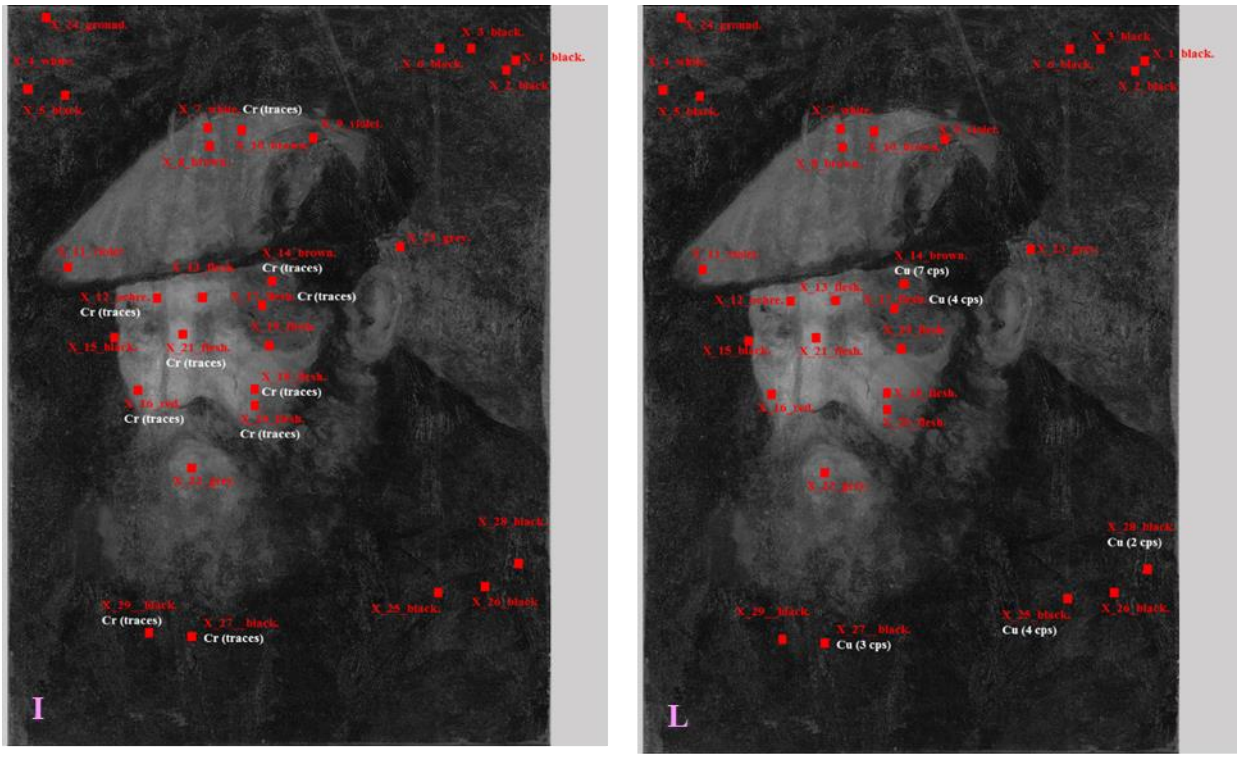

Figure 13. XRF mapping- element distribution and cps obtained: a) Pb, b) Zn, c) Ba/Ti, d) P, e) Ca, f) Fe, g) Mn, h) Co, i) Cr, l) Cu.

Global discussion of the painting

Composition vs. Areas

Area related to the subjacent layer (composition/preparation)

The superficial composition almost completely hides the subjacent layer, which complicates the access to the preparation or/and composition underneath.

The yellow-orange shade and white areas that are visible though out the more superficial paint layer correspond to natural earths with kaolin and lead white. The element that could be attributed to the layer underneath are Fe, Cr, Cu, Zn. Zn and Cr. The Cu has been detected in the circular dark area that corresponds to the man's eye visible on the NIR image (Figure 3) and some other points located in the lower part of the painting. It is difficult to attribute the Zn/White zinc distribution to a specific layer. It follows some of the trends of the composition underneath but also is found on the light part of the old man's face (superficial composition).

Superficial composition

Background II

The dark side on the left-hand side of the background was painted with Ivory/bone black, Prussian blue. Signal attribute to Lead white are also found. It is not clear if this pigment belongs to the superficial layer or to the paint underneath. On the right-hand side of the painting Picasso applied a light grey-blue paint. It is not clear if he used only Prussian blue as blue pigment. For example the presence of ultramarine should not be excluded, although UV-VIS, the technique generally used to detect the pigment, was not able to confirm its presence. The signature "P. Ruiz" and the date "95", located in the upper right-hand corner has been written using the same Ivory/bone black plus Prussian blue as for the jacket.

Subject

The different pigments used to mould the volumes of the face were Fe based red pigments – natural earths (e.g. Yellow ochre), some touches of Vermilion and Lead white. The Vermilion (Hg by XRF) has been detected only on the left cheek. The curly beard is principally Lead white with some black used to create the grey shade (Ivory/bone black + Prussian blue). The dark jacket was painted with a mixture of Lead White with Ivory/bone black plus Prussian blue and possibly Cu based pigment and White zinc (spatial distribution no clear) and the brown/violet beret was painted with natural earths (Fe based pigments), Cobalt blue (or cobalt violet), Ivory/bone black, Prussian blue and Lead white.

A summary of the pigments found is presented in Table 8.

Table 8. Pigments and organic compounds organised by areas.

Areas	Pigments	Binder/organic compound
Area related to the layer underneath (composition/preparation)	Fe based pigment – natural earths + kaolin, Lead white, (Cu/Cr based pigment, Zinc white)	
Background	Ivory/bone black, Prussian blue, Lead white (Fe based black pigments, Carbon black,)	Animal glue
Face (Front/Lips, Cheek)	Fe based pigment – natural earths + Kaolin, Vermilion, Lead white (Red lead)	
Beard	Lead white (Red lead)	
Beret	Natural earths (Fe based pigments), Cobalt blue (Cobalt violet), Ivory/bone black, Prussian blue and Lead white	
Jacket	Ivory/bone black + Prussian blue, Lead white (Fe based black pigments, Carbon black)	
Signature	Ivory/bone black + Prussian blue, Lead white (Fe based black pigments, Carbon black)	

Figure 14. Material distribution mapping.

Stratigraphy

The limitations of the surface techniques do not permit to obtain spatial distribution information. Thus, a clear assignment of a compound to a determined layer (depth) is not possible.

Despite those limitations, an attempt to reconstruct the stratigraphy can be done crossing all the complementary data obtained. Starting from the support, based on the observation of the

edges of the painting layer it can be hypothesizes that a preparation layer possibly applied with a mixture of Lead white and Calcium carbonate is present. The XR image could be a key tool to clear this doubt. Directly on the possible preparation layer, a composition with broad areas characterized by yellow-orange shade (natural earths + kaolin), white (Lead white) and blue (Prussian blue/Co based pigment) depending on the position across the painting can be presumed. It is possible to detect changes on the texture of the subjacent layer where the paint became thicker. No intermediate layer is present between the first composition underneath and the portrait. At a later stage, probably when the paint below was completely dry, he applied the last layers to create the visible composition. The frequent changes of the surface texture, with scratched appearance, could be evidence that the artist scraped away the first composition before starting the portrait, a habit noticed in other Picasso's paintings[45]. This observation is based on the type of craquelure that seems to follow the brush lines and venations of the paint due to the lack of cohesion between the paint below and the superficial layer (Figure 14). Because these specific areas seem to be thicker, it is possible that there was the intention to level it. First, Picasso painted the old man with the beret. According to the NIR images, the position and shape of the beret has been modified in at least one occasion and its profile corrected with the paint applied to create the background. Based on the smears that are visible along the man's profile, the background was the last step of the creation process.

Figure 15. Details of the jacket, where it is possible to observe the craquelure.

3.3.2 Retrat d'un vell

Artwork's interest

The "***Retrat d'un vell***" (**Portrait of an old man**) [58.5 x 42.8, MPB110.058] is part of the series of the anonymous Galicians that Picasso realized in 1895 during the last years in A Coruña, when he was only fourteen. It is commonly presented in literature, together with the *Home amb boina*, as examples of portraits in which Picasso discovers and studied the elderly people. It is with these works that Picasso practiced and matured his style[4].

Description and interpretation of the painting layers structure

The technical notes of the Picasso Museum of Barcelona described the artwork as an irregular fragment relined. No documentation about the date of the intervention is available. The report assesses the good conservation condition of the work, although it points out that the painting layer shows some detachment. A varnish was applied in 1970 and a superficial cleaning was done in 2003. According to the notes of the file the portrait is contextualized in the Spanish academic tradition painted with a simple palette. It is described that Picasso painted the head of the character starting from a layer with ochre hue on which he applied faint brushstrokes.

Direct observation – VIS

Observation of the visible layers lying underneath

In this case, it seems to appear a rather homogeneous ochre shade layer throughout the superficial paint (Figure 16). The canvas pattern is clearly visible, which leads to the assumption that the painting and/or the preparation are very thin. In very few points it is possible to view the subjacent layer.

Observation of the superficial layers

Background

Picasso frames the figure in a greenish-blue-black background painted with fast and multidirectional brushstrokes, especially in the right-hand upper corner where the strokes follow a weaving side-to-side. In the area on the right-hand side, which marks the profile of the face and the shoulder, the artist applied a grey paint, which possibly is related to a mixture of blue/black with white paint. Clearly, Picasso intended to create light and shadow areas. With the same grey the artist marks the profile of the head and the jacket. Here, the light is coming simply from one source located on the back. The paint layer seems very thin and

each stroke has its own edges. It can be assumed that Picasso used the subjacent layer as integral part of the portrait. Inspecting the edges of the canvas it is possible to deduce that it was cut off accurately, after Picasso painted the composition on the surface. On the right-hand side, top corner, Picasso marked his work using the signature "P. Ruiz" followed by a narrow line and the data "95". Interestingly, the signature is located extremely close to the painting edge.

Subject

Picasso depicted an old man with greyish-white hair, wearing a brown-black-bluish jacket and a white shirt. The expression lines/wrinkles of the face are skilfully created playing with different shades of few basic colours – white, black, brown - ochre. The same can be commented about the neck. The source of light come from the left-hand side. It is interesting to observe that the illuminated part of the figure is the left-hand side, whereas in the background is the right - hand side. It seems a rather unbalanced use of the light that can be considered a naivety of a fourteen years old painter or simply an attempt to create a complex light space.

Figure 16. VIS Image of *Retrat d'un vell*.

Observation with no visible radiation - subjacent layers (XRR, IRR)

Radiography

An XR image is not available. The museum planned a radiography campaign in the next months.

IR Reflectography

Several NIR images were acquired. Figure 17 shows a contrast-enhanced IR reflectography at 2265 nm. The image unveils some shapes lying underneath (magenta line), mostly located in the central part of the canvas. A central, roundly shaped element can be observed (exp. Orange line). According to these areas the texture is changing across the surface (exp. Green line). Even though the presence of a subjacent layer is an interesting discovery about the painting, the more relevant information given by the NIR image is the possibility to really analyse the brushstrokes and the *modus operandi* of the young Picasso. The NIR image highlights the fast and inaccurate brushstrokes, which Picasso applied on the external part of the background. These traits suggest that the artist had the intention to quickly fill up the most peripheral areas of the painting. With a more accurate manner he applied the paint that has the aim to define the profile of the man (head and shoulders). These strokes are vertical and surround the man, whereas the traits of the extreme background have a horizontal trend and show weaving side-to-side movement. Narrow black strokes, as for example the black line in the blue rectangle, seem to mark a rough outline of the portrait, the cheeks, the mouth, the eyes, the perimeter of the head and the edge of the shirt. The numerous traits of the collar of the jacket (right-hand side) suggest some insecurity and maybe some changes in the composition. The dotted yellow line marks the area of the ear that Picasso changed/moved and finally refined with the same paint of the background. Most of the dark shades of the face disappear; in fact just part of the right-hand eyebrow is still visible in the reflectography. It seems that black was applied by using two different materials. This becomes quite evident by the different appearance of the two eyebrows in the reflectography image.

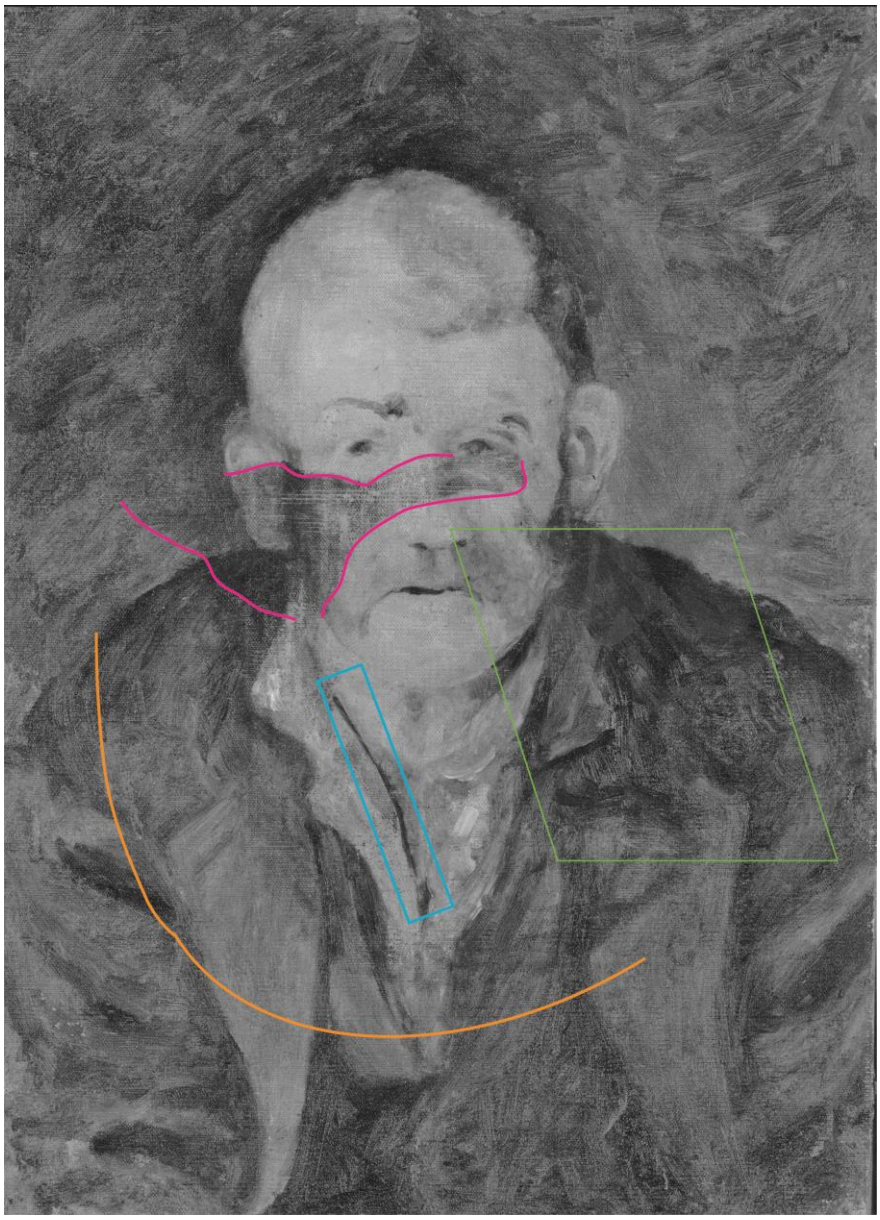

Figure 17. NIR image acquired at 2265 nm high contrasted.

Description and interpretation of the materials

Figure 18 shows the XRF (a) and mid-FTIR (b) measurements spot distribution and the corresponding file names (Table 18) are reported. In this case, the superficial layer completely hides the paint layers underneath, which makes direct access impossible. Indeed, due to the limitation of the surface techniques, the information about the nature of the underneath material is difficult to establish.

XRF MID-IR

Figure 18. XRF (a) and mid-FTIR (b) measurements spot distribution.

Table 8. Spectrum/spot label for a) XRF and mid-FTIR are reported.

a) XRF spectrum/point label	b) mid-FTIR spectrum/point label
P014_X_01_black	P014_M_06_black
P014_X_02_black	P014_M_07_black
P014_X_03_flesh	P014_M_02_flesh
P014_X_04_brown	P014_M_03_ochre
P014_X_05_black	P014_M_01_black
P014_X_06_black	P014_M_08_black
P014_X_07_black	P014_M_13_black
P014_X_08_red	P014_M_05_flesh
P014_X_09_red	P014_M_04_flesh
P014_X_10_brown	P014_M_14_ochre
P014_X_11_black	P014_M_09_black
P014_X_12_black	P014_M_11_black
	P014_M_10_black
P014_X_13_white	P014_M_12_white
P014_X_14_brown	P014_M_16_preparation
P014_X_15_white	
P014_X_16_brown	P014_M_15_preparation

Description

Results are discussed by chromatic areas using the complementary information obtained by XRF and mid-FTIR results. The interpretation of the spectrum obtained has been done based on the literature [2,8,10–41] and reference materials available.

White Areas

The areas investigated is the white of the collar of the character depicted. The bands identified in mid-infrared spectrum **M_12_white (**Figure 19**)** may be assigned to the Basic lead Carbonate (Lead white – characteristic bands 3575, 1399, 676 cm^{-1}). The signals in the near infrared range between 4263 - 5785 cm^{-1} can be attributed to the lipid binder. The major element detected by XRF is Pb (186 cps) and a weak signal of Fe (2 cps); thus, the presence of Lead white can be confirmed (**X_12_white**, Table 9).

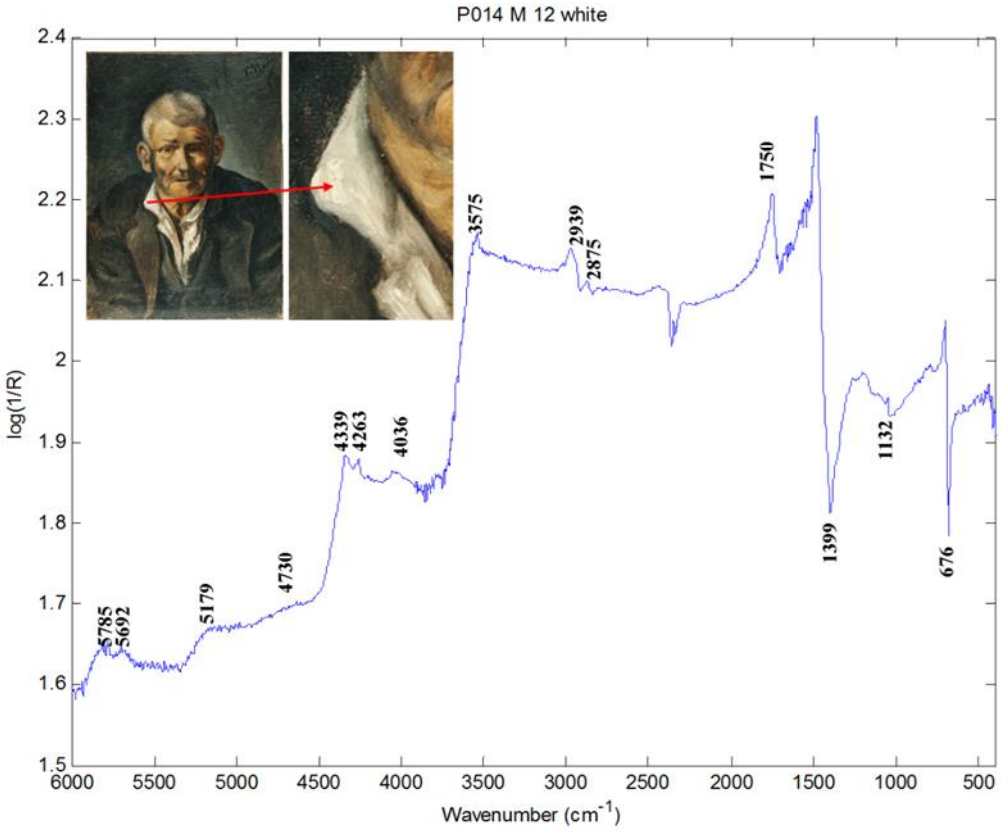

Figure 19. IR spectrum M_12_white

Table 9. Summary of XRF results for white/ground areas.

cps	Ca	K	Ti/Ba	Cr	Mn	Fe	Pb	Hg	Zn
E (keV)	**3.71**	**3.00**	**4.52**	**5.44**	**5.95**	**6.4**	**10.55**	**9.97**	**8.65**
P014_X_13_white	Traces	/	Traces	/	Traces	2	186	/	/

Black/Signature areas

The mid-infrared spectrum **M_01_black**, acquired on the background, is very noisy and distorted, and therefore is not useful for compounds identification. This behaviour may be consequence of the roughness of the surface due to the varnish applied in 1970 and the fineness of the paint layer. Another point that was investigated lies in the background (**M_13_black**), near the left-hand side ear of the man. The identified signal can be attributed to the Iron hexacyanoferrate (Prussian blue), Hydroxyapatite (Ivory/bone black), protein (1600-1400 cm^{-1}) and sulphate (about 600 cm^{-1}). The XRF spectra of spots **X_06** and **X_07** show similar compositions, as the high counts of Ca could be related with the ivory/bone black. The signal of Fe is rather low (about 5 cps) and could be associated to Prussia blue or a natural earth from the layer underneath. The Pb signal is important and can be related to Lead white. Point **X_05** results are different. The high signal of Ti together with Fe (19 cps) and Mn (2cps) could suggest a retouch. P traces are also detected.

The black that Picasso used to sign his work has been investigated. The main signals identified in the mid-infrared spectra **M_06_black, M_07_black** (trace of the signature) **M_08_black** (background nearby) are attributed to iron Hexacyanoferrate - Prussian blue (2090 cm^{-1}), Hydroxyapatite - Ivory/bone black (2012, 1020 cm^{-1}), sulphate (600-570 cm^{-1}) and a proteinaceous compound (1600-1400 cm^{-1}). According to the XRF spectra acquired on the signature (**X_01_black, X_02_black**) the content of Ca may be the component of the ivory/bone black (15, 13 cps, respectively). The high signal of Pb is probably due to the preparation layer. The high content of Fe in point **X_01** could be an indication of the presence of Fe based black pigments or Prussian blue, although together with a high content of Mn it could be evidence of natural earths. The Mn detected also on the jacket has not been detected in other points on the background.

Three spots on the jacket were analysed. The mid-infrared spectrum **M_09_black** shows very weak signals of Prussian blue and Ivory/bone black. The inverted signal with minimum at about 1000 cm^{-1} is a possible sign of silicate. The signal of silicate is not specific to a determined pigment, thus its presence does not permit to exclude other compounds such as Ultramarine blue. In the mid-infrared spectrum **M_10_black** the signal of ivory/bone black is stronger and the signal of sulphate is also present in the mid-infrared spectrum **M_11_black**. The XRF spectra **X_11** and **X_12** were acquired close to points **M_09** and **M_10**. Here the elements detected were Pb (140 and 135 cps respectively), Fe (49 and 27 cps), Ca (18 and 34 cps), Mn (8 and 2 cps) and traces of Cr and P. Fe and Ca can be attributed

to the black paint (Prussian blue + Ivory black), although Mn content together with Fe also indicates the presence of earth pigments. A Cr-based pigment is also probable.

According to the elemental composition found, the presence of two black pigments can be deduced, one of which has Ca, Fe and Mn (black brush strokes added with the signature) and one with content of Ca and lower signal of Fe without Mn used on the background. A different case is the **X_5** with evident signal of Ti. The results of the XRF height peaks evaluation are summarized in Table 10.

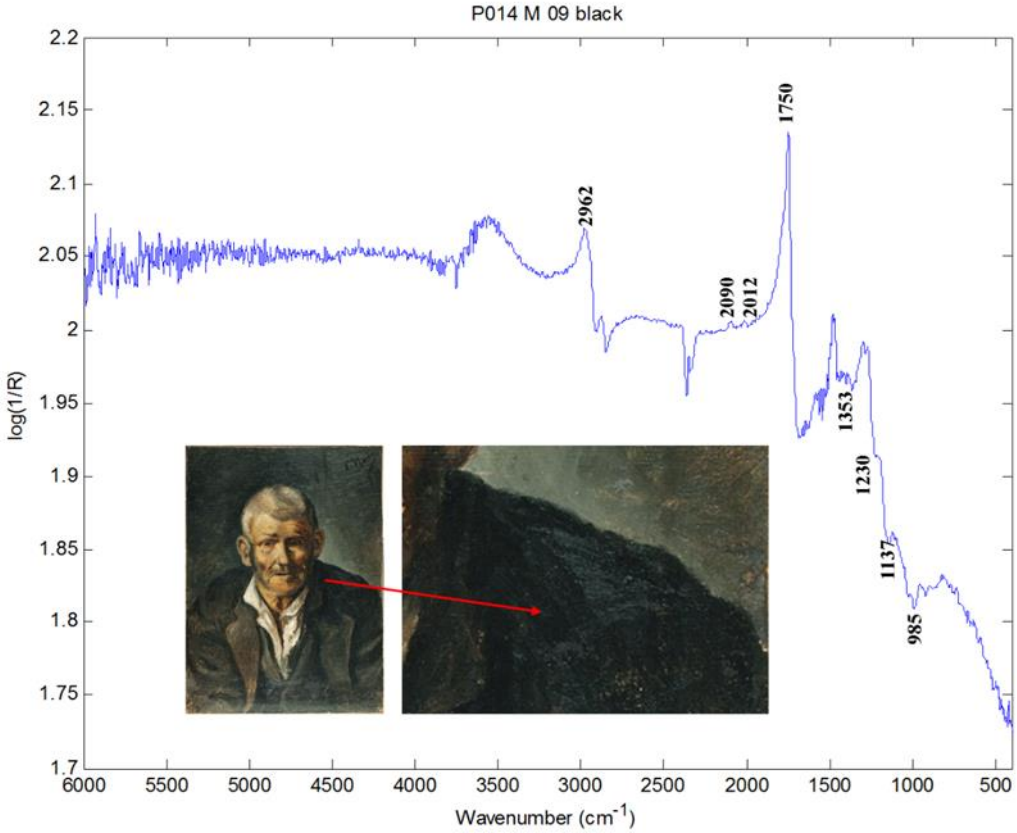

Figure 20. IR spectrum M_09_black

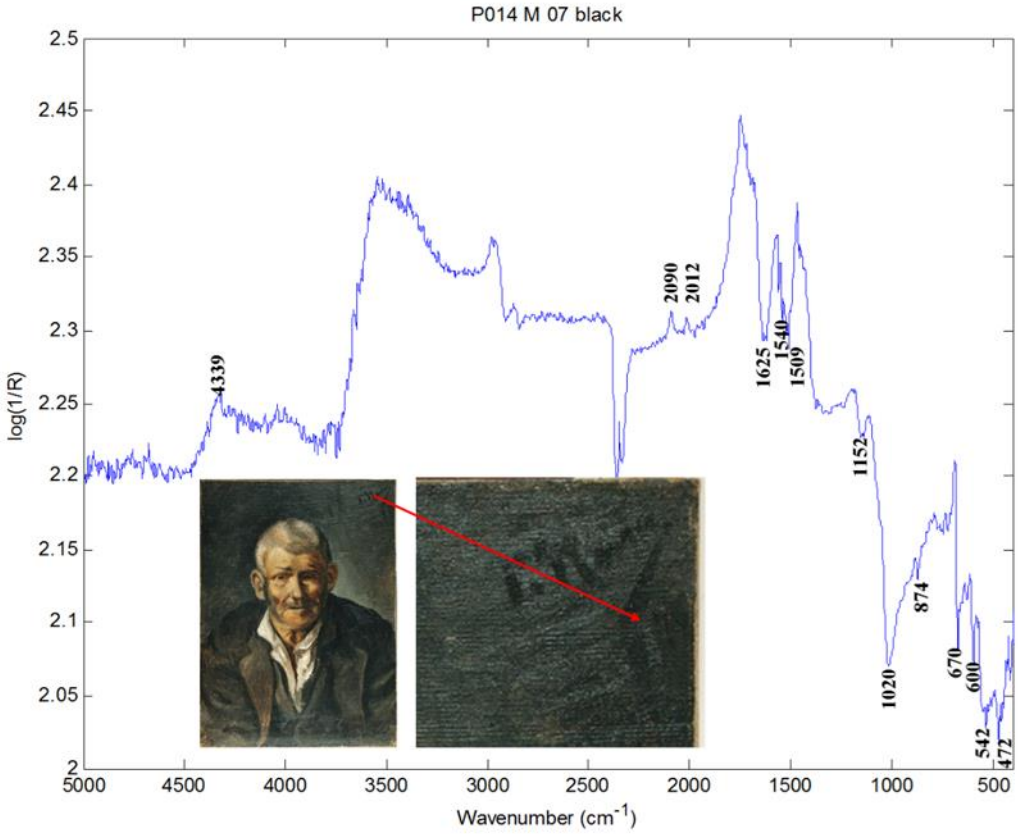

Figure 21. IR spectrum M_07_black

Table 10. Summary of XRF results for black areas.

cps	Ca	K	Ti	Cr	Mn	Fe	Pb	Hg	Zn
E (keV)	**3.71**	**3.00**	**4.52**	**5.44**	**5.95**	**6.4**	**10.55**	**9.97**	**8.65**
P014_X_01_black	15	/	/	Traces	6	30	145	/	/
P014_X_02_black	13	/	/	/	Traces	8	163	Traces	/
P014_X_06_black	12	/	Traces	/	/	5	145	/	/
P014_X_07_black	10	/	/	/	/	6	151	/	/
P014_X_05_black	35	/	18	Traces	2	19	126	/	/
P014_X_11_black	18	/	/	/	8	49	140	/	/
P014_X_12_black	34	/	/	/	2	27	135	/	/

Brown/Preparation/Red/flesh-ochre areas

Two spots of the flesh of the man have been analysed (**M_02_flesh**/**M_03_ochre**). The signals detected are mainly related to the basic lead carbonate and the lipid. The inverted band with minimum at 1030 and 998 cm^{-1} may be an indication of a silicate pigment – natural

earths, e.g. yellow ochre. Due to the low resolution of the bands is not possible to confirm kaolin. The results obtained by XRF in two points that correspond to the flesh **X_03_flesh** (clear area) and a darker brown shade on the front (**X_04_brown**) show an increase of Fe (8 and 27 cps, respectively) that suggest the use of a Natural earth - Fe-based red-brown pigment. The other elements detected were Pb (about 160 cps) and traces of Ca and Mn. In mid-infrared spectra **M_04_flesh** and **M_05_flesh** the signal of the lipid binder may be recognized. It is not clear if Lead white and sulphates are present. The compounds detected in mid-infrared spectrum **M_14_ochre** could be attributed to the lipid of the binder (very noisy spectrum). Furthermore, the inverted band at about 1000 cm^{-1} suggests the presence of a silicate-based pigment. Weak bands of Prussian blue and Ivory/bone black were detected. The XRF spectrum that correspond to this area (**X_10_brown**) shows a high content of Fe (32 cps) that suggests the use of natural earth, a Fe-based pigment. The other elements detected were Pb (139 cps) and Ca (8 cps). This area includes a thick black line, which is the mouth. As these points do not contain Mn, their composition will be different from the signature and other black areas.

Two reddish spots were investigated on the right-hand eye. The elements detected on point **X_08_red**, located in a brown dark area, were Pb (147 cps), Fe (35 cps), Ca (2 cps) and traces of Cr. On point **X_09_red** a similar elemental composition was found, the only point where Hg (6 cps) has been detected. These values could be an indication of the use of Vermilion on the flesh areas together with Fe-based red pigments. The increase of the lead signal will not permit to exclude the presence of Red lead.

Due to the loss of painting layer it was possible to achieve the layer underneath. Based on the mid-infrared spectrum **M_15_preparation** it is possible to assess the presence of silicate and lipid binder. The elements found (**X_16_brown**) were Pb (157 cps), Fe (26 cps), Ca (7 cps), Mn (4 cps), Ti (2 cps) and traces of K. In spot **M_16_preparation** ivory/bone black, Prussian blue and sulphate have been detected. The spectrum **X_14_brown** shows a high backscattered signal typical of low-density material. This fact and the drastic decrease of Pb suggest that in this point, there was a loss of material and the canvas was finally analysed. Despite the decrease of Pb, the composition is quite similar to point **X_15_white** were the elements detected were Fe (8 cps), Ca (7 cps), Mn (2 cps) and traces of Ti. The interpretation of these points is difficult for two main reasons: the presence of Ti, found previously at black point X_05 and the presence of Mn, found at black areas of the signature and two points on the jacket. The results of the XRF height peaks evaluation are summarized in Table 11.

Table 11. XRF results for brown/preparation areas.

cps	Ca	K	Ti	Cr	Mn	Fe	Pb	Hg	Cu	Zn
E (keV)	**3.71**	**3.00**	**4.52**	**5.44**	**5.95**	**6.4**	**10.55**	**9.97**	**8.65**	**3.71**
P014_X_03_flesh	Traces	/	/	/	Traces	8	157	Traces	N. Q.	/
P014_X_04_brown	Traces	/	/	/	/	27	162	Traces	N-Q.	/
P014_X_10_brown	8	/	/	/	/	32	139	/	/	/
P014_X_08_red	2	/	/	Traces	/	35	147	/	/	/
P014_X_09_red	Traces	/	/	/	/	58	165	6	/	/
P014_X_14_brown	7	3	Traces	/	Traces	9	41	/	/	/
P014_X_15_white	7	Traces	/	/	2	8	131	/	/	/
P014_X_16_brown	7	Traces	2	/	4	26	137	/	/	/

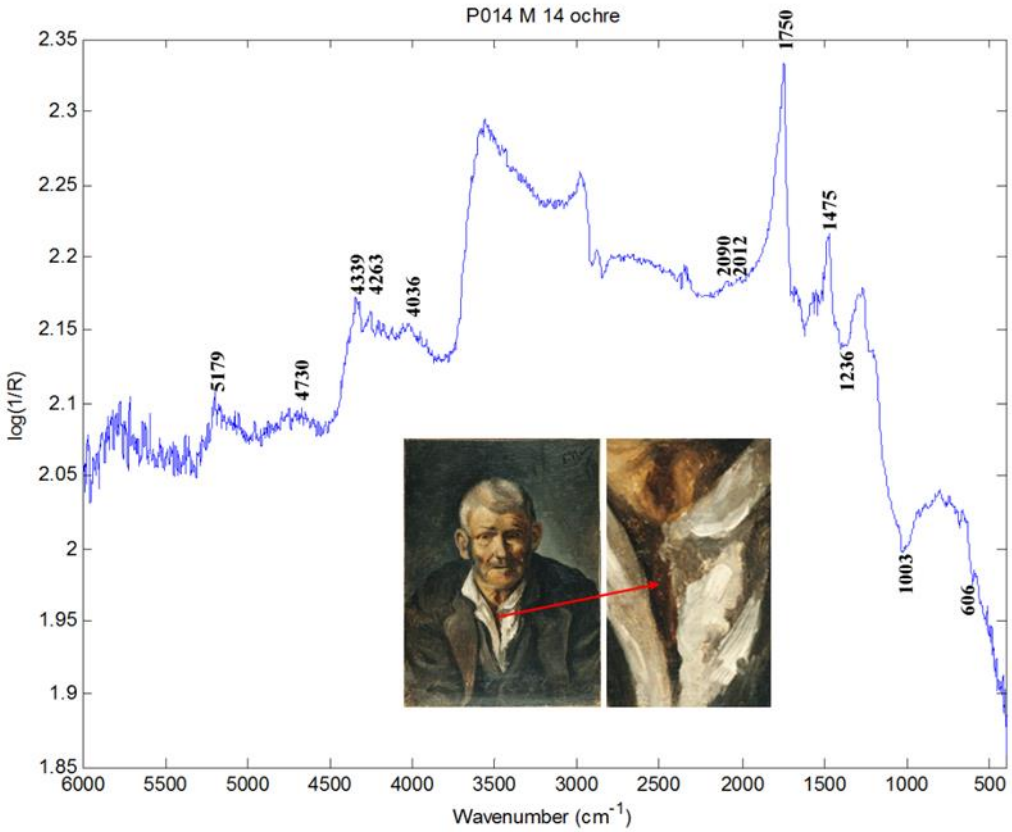

Figure 22. M_14_ochre

Summary

Figure 11 shows a mapping of the elements and compounds detected.

Figure 23. Mapping of the results obtained.

Interpretation

Pigments

White pigments

The main white pigment encountered is the Lead white (Figure 24a). Other compounds that are generally of this colour are the silicate and sulphates detected which could be considered fillers.

Black pigments

Based on the infrared spectra and the detection of high signals of Ca by XRF (Figure 24b), Ivory/bone black can be confirmed. On the other hand, according to the elemental

composition it could be hypothesized that another type of black containing Mn/MnO was used. Observing the mapping in Figure 24c it is clear that this element plays an important role for black areas discrimination. Point X_5 should be considered an outlier due to the singular high content of Ti (Figure 24d).

Red – brown pigments

Fe based red pigments – natural earths with a possible silicate matrix can be hypotized based on the content of Fe and silicate signals on the red-brown areas. Vermilion/Hg (Figure 24g) has been detected only on one point located on the face of the man. Further explication of the possible origin are exposed in the stratigraphy section.

Blue pigments

The Prussian blue has been confirmed by infrared spectra and signal of Fe by XRF (Figure 24e). It is often associated with the ivory black in black paint.

Yellow/Green pigments

Signal of Cr was identified (Figure 24f). Therefore, the possibility of the presence of yellow/green pigment should not be discarded.

Other inorganic compounds

No other inorganic compounds were detected.

Organic compounds

Signal of lipid, protein and resin were found. These compounds could be related respectively to the binder, relining and coating of varnish.

The summary of the material found is presented in Table 12.

Table 12. Pigments and Binding Media/organic compound Analysis Results

Colours	**Materials/Pigments**	**Binding medium/ organic compounds**
Preparation	Lead white [a, b)]	
White	Lead white [a, b)],	Lipid, protein, resin [b)]
Black	Ivory/bone black [b)], Mn oxides [a)] (Fe based black pigments, Carbon black)	
Blue	Prussian blue [b)] (Ultramarine)	
Green	Cr based pigment [a)]	
Red – brown - orange	Brown – ochre natural earths [a)] + silicate matrix [b)], Vermillion [a)]	
Others	Silicate based pigment [b)], sulphate [b)]	

a) XRF; b) mid-FTIR spectroscopy.

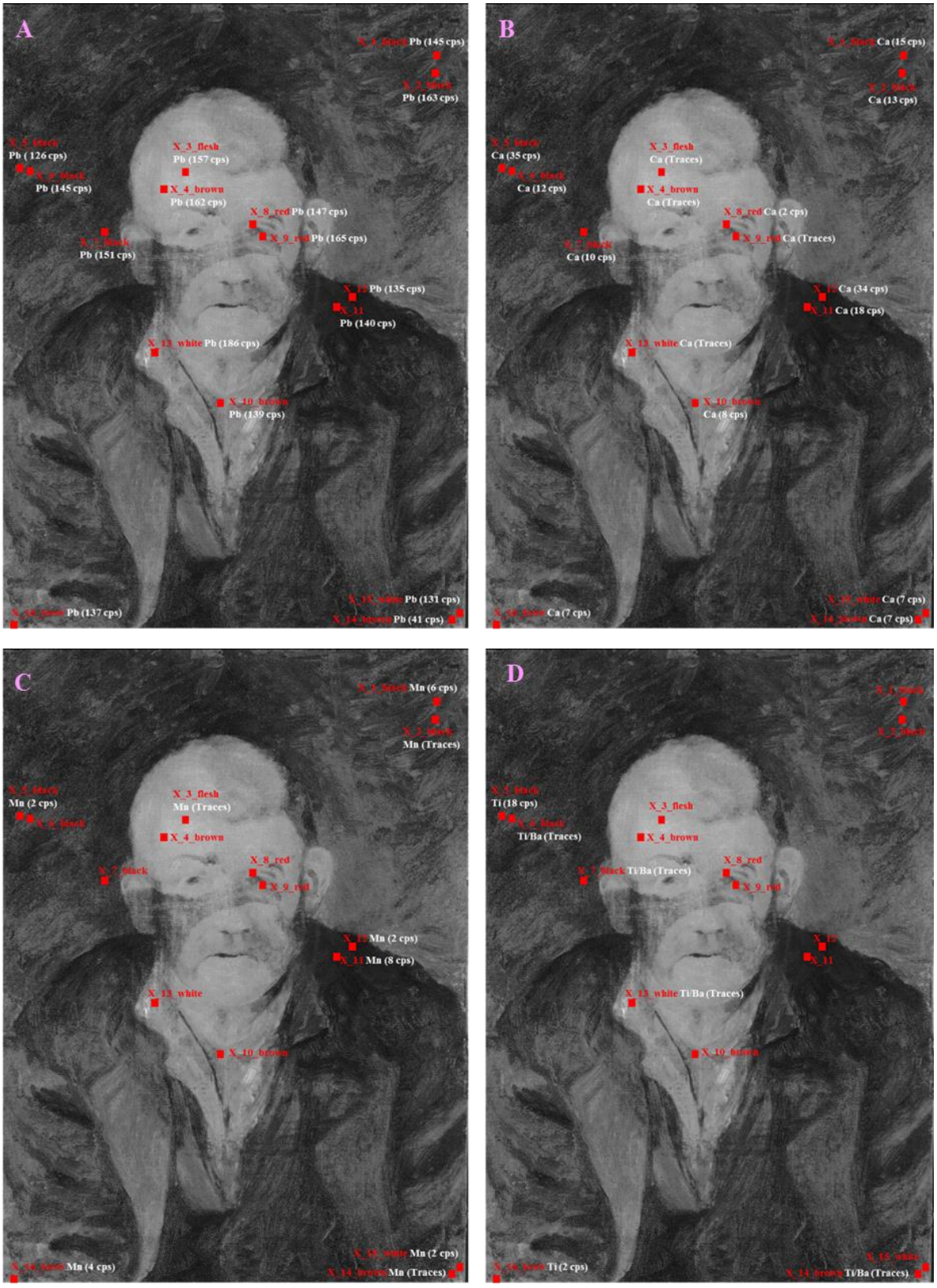

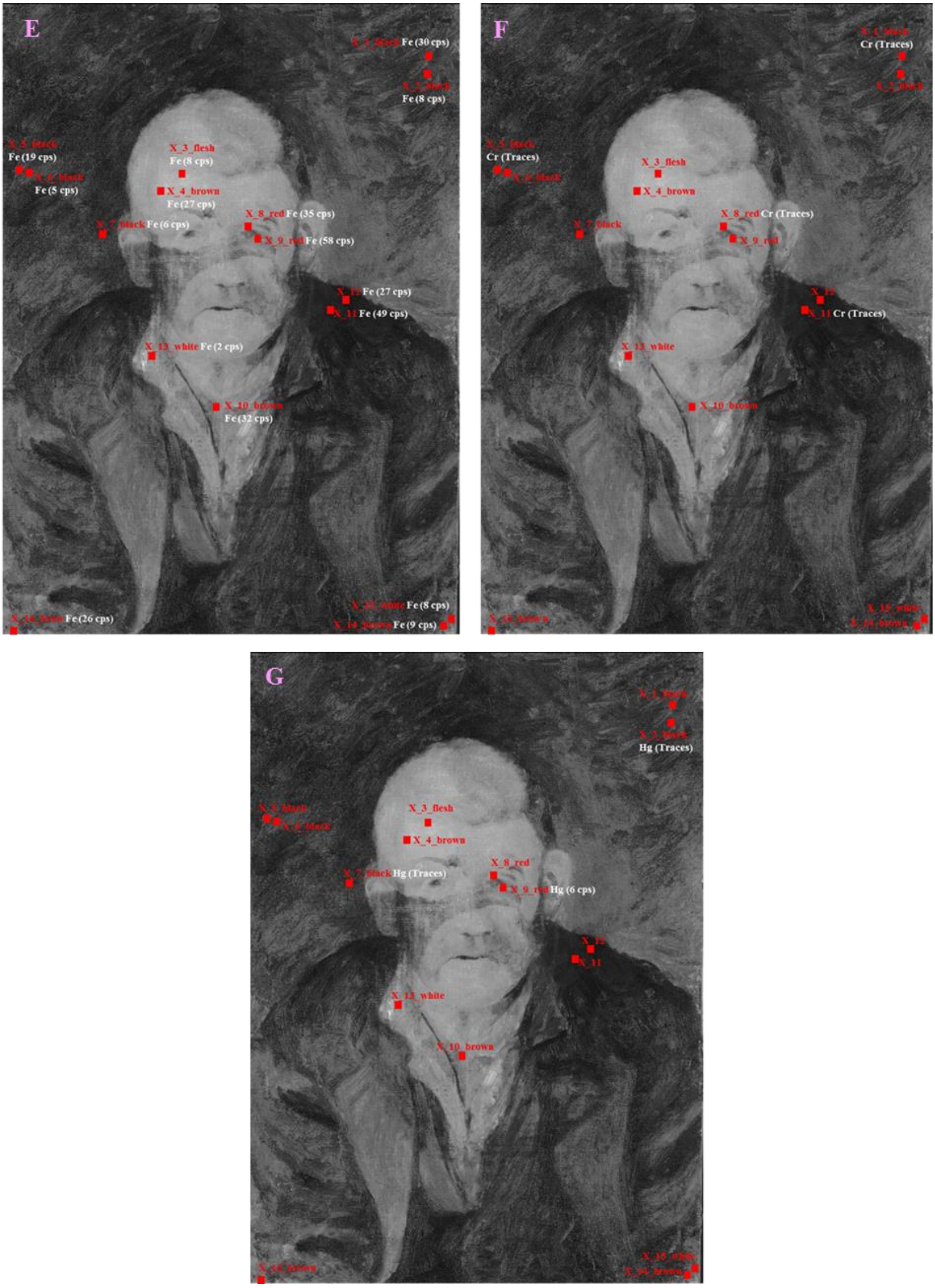

Figure 24. XRF mapping- element distribution and cps obtained: a) Pb, b) Ca, c) Fe, d) Hg, e) Mn, f) Cr, g) Ti/Ba.

Global discussion of the painting

Composition vs. Areas

Background

The spectra obtained were rather noisy and not always easily interpretable. The greenish-blue-black background was painted with ivory/bone black mixed with Prussian blue. The use of carbon black or Fe-based black pigment could not be excluded. The detected sulphates are probably a filler. This paint layer hides a layer of ochre colour painted with natural earths with a silicate matrix. In some points Mn has been detected, among those the signature and jacket spots with some traces on the background. Thus, Picasso probably signs his work using the same black, but more concentrated, or a black pigment that could not be identified with the employed techniques. Cr-based pigment can be assumed.

Subject

The dark jacket was painted with the same pigment used in the background plus a Cr-based pigment. The white shirt has been created with thick brushstrokes of Lead white. The basic colours used to create the expression lines/wrinkles of the face were Lead white, Ivory/bone black, brown-ochre/natural earths with Vermilion and possibly red lead. The same is true for the neck. Sulphates possibly are fillers of those pigments. The light areas behind the head were not analysed. There is some problem related to the presence of Ti in some perimetral points of the painting. These points seem to be related with the detection of Mn, element that has been found in some characteristic black areas such as the signature trace.

A summary of the pigments found is presented in Table 13.

Table 13. Pigments and organic compounds organised by areas.

Areas	Pigments	Binder/organic compound
Subjacent layer	Natural earth – Fe based pigments + Silicates, Lead white	Oil, Animal glue, Varnish
Background	Ivory/bone black + Prussian blue, Sulphates	
Face (Front/Lips, Cheek)	Natural earth – Fe based pigments + Silicates, Lead white (Red lead, Vermilion)	
Hair	/	
nightshirt / neckerchief	Lead white	
Jacket	Natural earth – Fe based pigments + Silicates + Mn oxides, Ivory/bone black + Prussian blue, Sulphates, Cr based pigment	
Signature	Ivory/bone black + Prussian blue, Sulphates, Mn oxides	

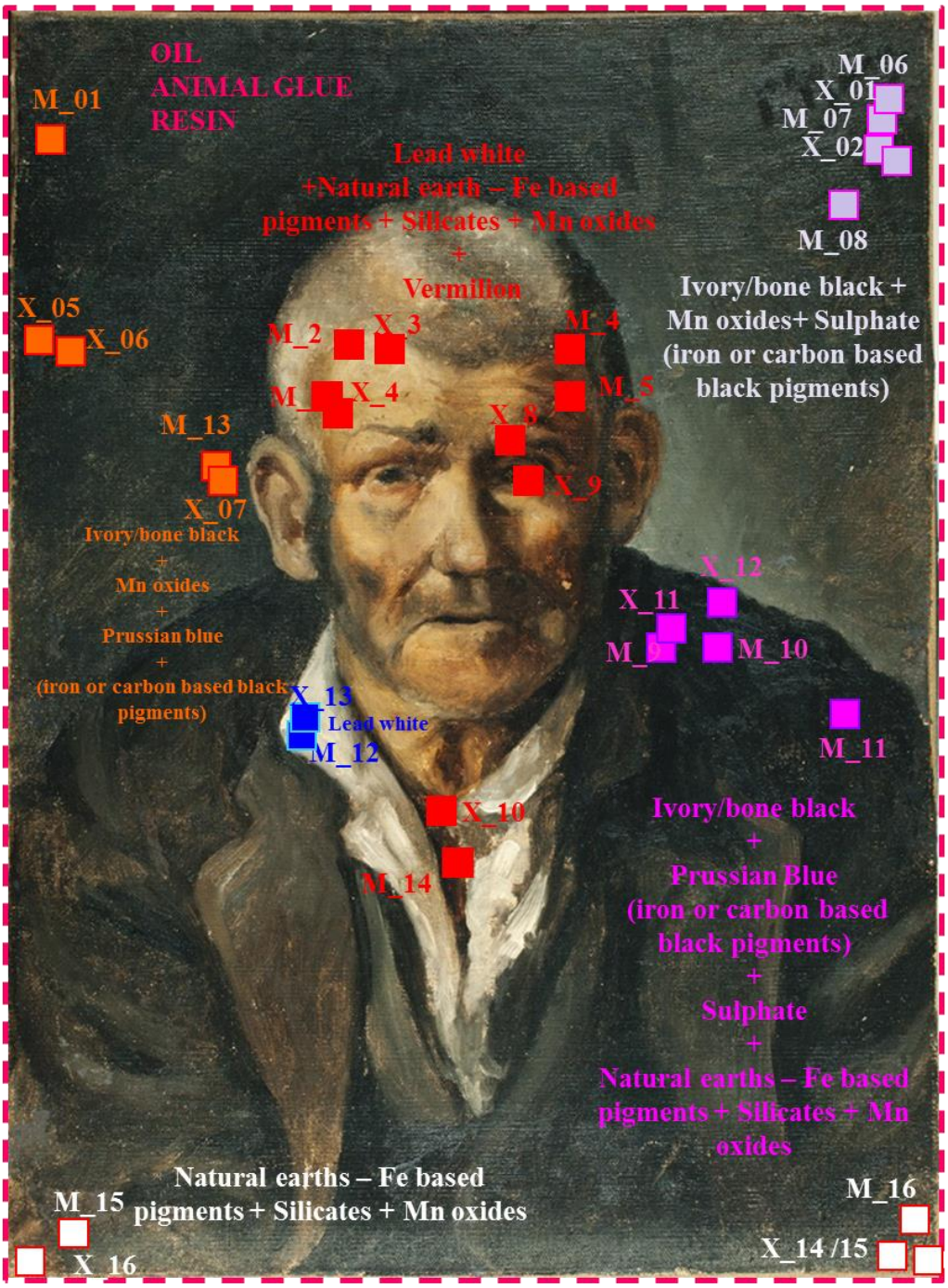

Figure 25. Material distribution mapping.

Stratigraphy

The stratigraphy, starting from the support to the superficial layer, is composed possibly by a very thin preparation layer, probably coloured or covered with a layer of natural earths. Overlapping this layer the sketches that are visible in the NIR image may be located, which could not be fully clarified. The high signal of Fe (X_09) and the presence of silicates and Cr-based compounds may be attributed to these layers. A radiography might enable the

interpretation of these irregular shapes. Then, Picasso applied the brown-black of the background (Ivory/bone black plus Prussian blue). Afterwards, he created the face/head and the jacket using the natural earth pigments plus the black of the background with some Mn oxides. With the same black he signed the painting and applied the last black strokes to the face (mouth, eyebrows), the neck, collar, and the jacket of the character. Finally, he filled up the background, applied the light area trying not to blur the paint over the man's profile. At last, Picasso painted his signature. This observation is based on the fact that the vertical strokes of the "P" and "R" of his name interrupt the horizontal layer below (Figure 26).

Figure 26. NIR image. Detail of the signature.

3.3.3 Autoretrat amb perruca

Artwork's interest

The painting ***Autoretrat amb perruca*** (**Self-portrait with a Wig**) [55 x 46, MPB110.553] is the fulcrum of the project "Early Stages of Picasso through material characterization of different portraits". The painting is, at the moment, dated between 1897 and 1898, although lately a debate arose about its chronology and a possible later dating is considered. Indeed, in the catalogue of the last exposition at the Picasso Museum of Barcelona "Yo Picasso" [6], the self-portrait appears dated 1900. The painting is a portrait were Picasso depicts himself as an 18th century gentleman in a puffed wig, in the style of Old Masters like Goya or Rembrandt. Evidently, even at these early stages, Picasso was already confident to take from the masters of the past.[46] The painting was part of the important exhibition "*Picasso et le portrait"* hosted to the Museum of modern art (New York, 28th April-17th September 1996) and later to the Galeries Nationales du Grand Palais (Paris, 15th October 1996 - 20th January 1997).

Description and interpretation of the structure of the painting layers

According to the documentation provided by the conservator Sra. Reyes Jimenez, the painting was subject to relining in the past, but no documents about this intervention are available. In 1970 a protective varnish has been applied and in 2003 a superficial cleaning has been carried out. The frame has been changed in 2011. It was produced with the aim to conserve the original stretcher frame of the artwork. As explained in the report of the museum, it is clearly visible that Picasso reused a canvas on which a previous composition appears. Considering the comments of the conservators, this composition was completely dry when he started to paint the more superficial portrait. This interpretation is based on the fact that the different paints across the surface appear almost pure and not mixed together. At the moment of the analysis the entire surface was varnished. It was possible to localize some retouches by using a Wood-lamp (UV), as it is described in the notes taken during the investigation.

Direct observation – VIS

Observation of the visible underneath layers

As mentioned above, it is possible to distinguish, in some areas, the layer lying underneath due to the thin superficial paint strokes. In the upper part of the painting it is possible to

observe the first black ground and the lines that mark a contour of a hat (Figure 27 - green line). The colour of the hat seems to have green and ochre hues. In the lower part, the shape of a dark jacket (magenta line) is clearly visible, which does not match proportionally with the face of the character visible on the surface. The position of the white-grey collar/shirt on the right side suggests that the character painted underneath is represented in profile and looks toward the right-hand side (white dashed line). In the area marked with the red dashed line it is possible to observe part of the beard of the character revealed by IR reflectography as discussed below.

Figure 27. VIS Image with coloured marker lines that highlight the composition underneath.

Observation of the superficial layers

Background

In the upper part, the artist creates a dark background covering the composition underneath with fast and faint strokes of a diluted brown paint. On the left-hand side, and particularly in the right-hand side, he applied narrow red-white and brown strokes. In the documentation provided, these strokes are described as tests of the colour used for the flesh. It is clear that Picasso did not care to uniformly cover the previous representation. However, he tried to include some of the pre-existing traits in his new work.

Subject

In the centre of the artwork, Picasso portrays himself rotated partially towards the left, but his severe and inquisitive look is directed to the viewer. The face shows the physiognomy of a young man, confirmed by the similarity with other self-portraits of his childhood. The artist painted his face with dense paint strokes, which have been applied in an accurate manner, almost vertically. The shades and shadows of the flesh have been created with the skilful use of different colours - red, white, green, ochre and black. Finally, the wig has been painted with broad strokes using a white-grey paint and applying few yellow touches.

Observation with no visible radiation - Subjacent layers (XR, IR)

Radiography

The Radiography (supplied by the conservator Reyes Jimenez, Figure 28a) allows a clearer identification of the traits of the composition underneath. It shows the hat, the jacket, but most important, it highlights the collar of the jacket of the first composition that is not clearly distinguishable on the VIS image (Figure 27). A preparation layer is present as indicated by the pattern of the canvas visible on the XR radiography. The radiography shows a distribution of heavy elements on the entire painting, concentrated in the central part of the image. The paint, including heavy metals is probably White lead mixed with other pigments. The image permits to recognize the hat, the beard and the jacket. Of special interest and not clear in the VIS image is the lapel of the jacket of the first composition (Figure 28a, dotted blue line), which includes a material radio-opaque to the XR radiation concentrated mainly in one corner. Moreover, it is possible to observe better a triangular-shaped stripe that corresponds to the shirt of the character painted underneath (element present also in the VIS image). It is possible to observe the change between the light strokes of the *Home amb barret* (*Man with the hat*) and the dense and thick paint applied to create the face of the *Autoretrat* (Figure 27 , dotted white line). The interpretation of the XR image, with the important contribution of the complementary IR reflectography, provides useful information about the creation process of the face of the *Autoretrat*. In the XR image the intensity of the visage brush strokes that define his expression, probably created with the application of White lead, become visible. Moreover, it is possible to observe changes in the definition of the face perimeter close to the left-hand side eye. The eye is correct and the entire profile of the face is moved towards the interior. In this manner, the face became thinner and the expression more penetrating and tough. On the other hand, it is clear how in the flesh areas, especially

on the cheek, the XR opaque features decrease, which indicates that the pigment used should have a lower Z number compared to lead, for example Fe-based colours. The element that is particularly interesting and improves the knowledge about the creation of the face/head of the *Autoretrat* is the hair. The XR image shows the hair completely painted and finished. The material present is a weak XR absorber, although at some point the XR image became clear/white due to the introduction of some white pigment to create the highlights. The coiffure with the part of the hair is characteristic of other portraits of the same period [6]. This interpretation suggests that the portrait was already finished. Apparently, Picasso decided later to superimpose the wig. The artist hide the hair with the wig's paint. The brush strokes of the wig with broad and not dense that present low XR absorption. Throughout these strokes, a black line is visible even in the VIS image corresponding to the superior right-hand side limit of the hair (Figure 27, dotted yellow line). It is possible that the faint strokes at the end of the white collar were applied at the same time as the wig (Figure 28b, solid orange line). The collar shows two different textures in the XR image, one that seems very similar to collars found in other Picasso's self-portraits, created with dense paint strokes, while the last part was applied later with diluted paintbrush strokes similar to those of the wig. The wig and the last part of the collar almost disappeared in the XR image (Figure 28a). It is difficult to verify the moment when Picasso painted/superposed the wig. The white/grey parts of the wig could be due to a mixture of the white with a still wet darker paint of the subjacent layer or/and the effect of the faint and thin layer that permits to see the layer underneath, or a simple mixture of white and blue/black pigment. Another possibility is that the wig paint was applied a rather large time after, when the underneath layer was completely dry. This theory is based on the inspection of the texture of the paint layer in the face region that has not been modified by the later application of the paint of the wig (Figure 28, zoom in dotted red line). In this case, also the grey shade could originate from the mixture of a blue/black paint and a white, or the partial transparency of the superficial layer.

a)

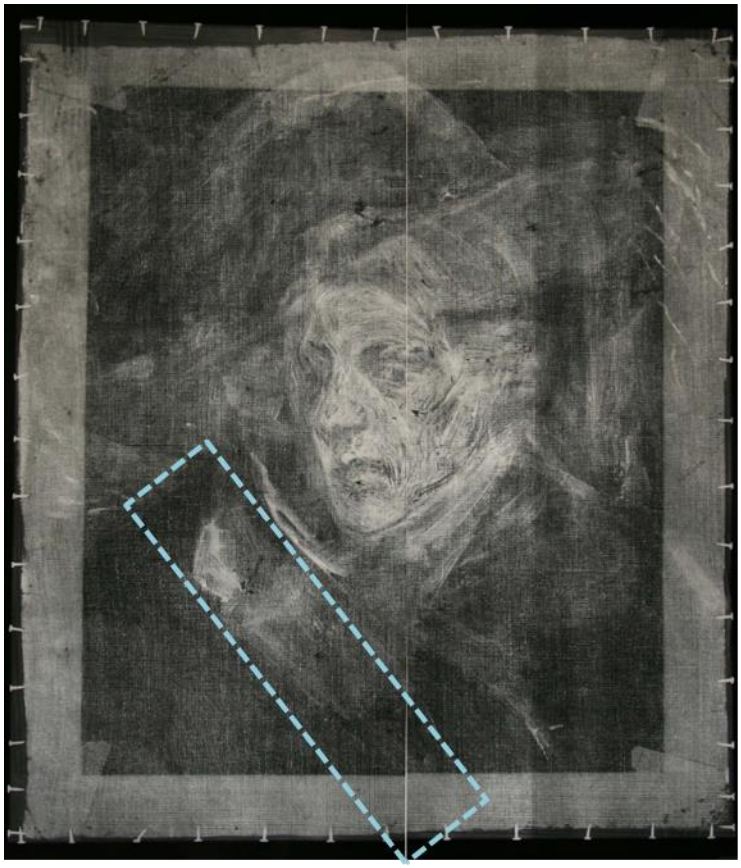

b)

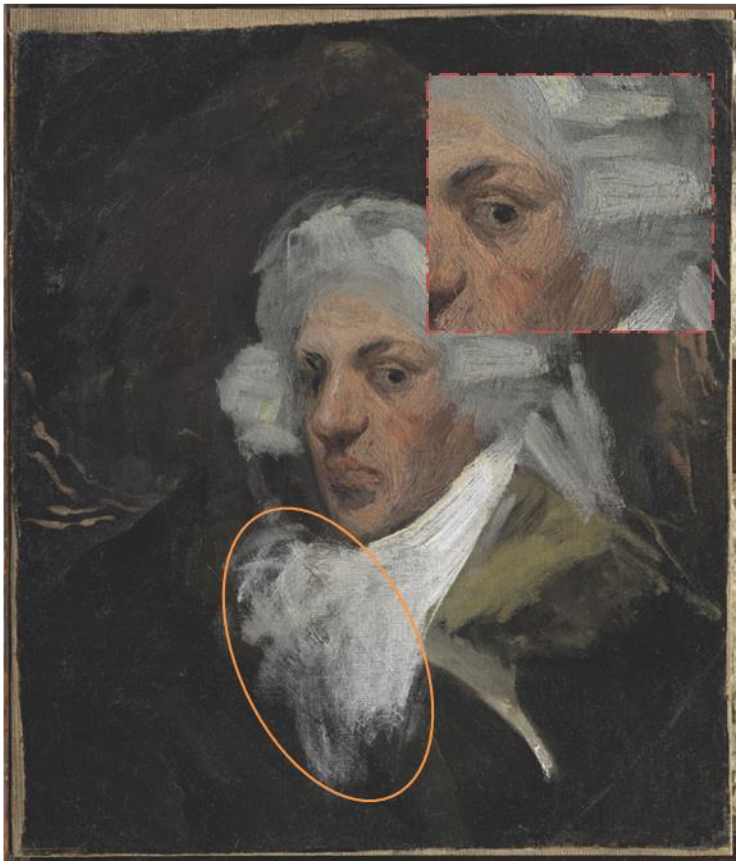

Figure 28. a) XR image; b) VIS Image.

IR Reflectography

Several NIR images were acquired. Figure 29a shows a contrast-enhanced IR reflectography at 2265 nm. The relevant information obtained with this technique is the face with a beard of the character of the first composition. The NIR image was a perfect guide for the interpretation of the radiography.

The image permits to clearly identify the hat, the beard and the jacket of the composition underneath. This type of representation is typical of several Picasso portraits. Some similarities can be observed in the portrait of his father (Figure 29b). This is one of the favourite subjects of his painting attributed to the first years of his artistic career. However, based on the literature available, Picasso has never depicted his father wearing hats. Another possibility is that the composition underneath is one of the numerous portraits of the friends that he frequently met at the famous bar "Els Quatre Gats" (Figure 29c). Furthermore, it is possible to observe how the white diagonal line towards the lower corner agrees with the end of the beard, which could be evidence that it is part of the shirt of the character underneath. Regarding the superficial composition, the IR reflectography permits a clear vision of the subject/Picasso without wig. The visage is accurately outlined (jaw, beard, eyebrows). One can see the aforementioned changes of the eye and the left-hand side perimeter of the visage. The hair profile/limits are marked with lines and the triangular-shaped sideburn.

Furthermore, at this side, some lines come out from the front. These lines could correspond to the hair fringe similar to the one showed in Figure 29d. Based on the high and low absorption in the IR reflectography and XR radiography, respectively, it can be hypotized that the hair presents probably a dark/black colour. Thus, the reflectography shows a finished portrait, on which Picasso superposed the wig in a later moment.

In the IR image, the wig is barely visible, in spite of its white colour. The reason for that is that its diluted and thin paint does not permit reflection of the IR radiation. It is deducible because it hides the forehead and it appears in the hair area, the back of the neck and the end of the shirt collar. As observed with XR, the collar of the shirt and the material applied at the end show a completely different behavior.

In summary, the artwork is composed by three subjects: one underneath "**Home amb Barret**" (Man with a hat) and two on the superior layer "**Autoretrat**" (Self-portrait) and "**Autoretrat amb Perruca**" (Self-portrait with a wig).

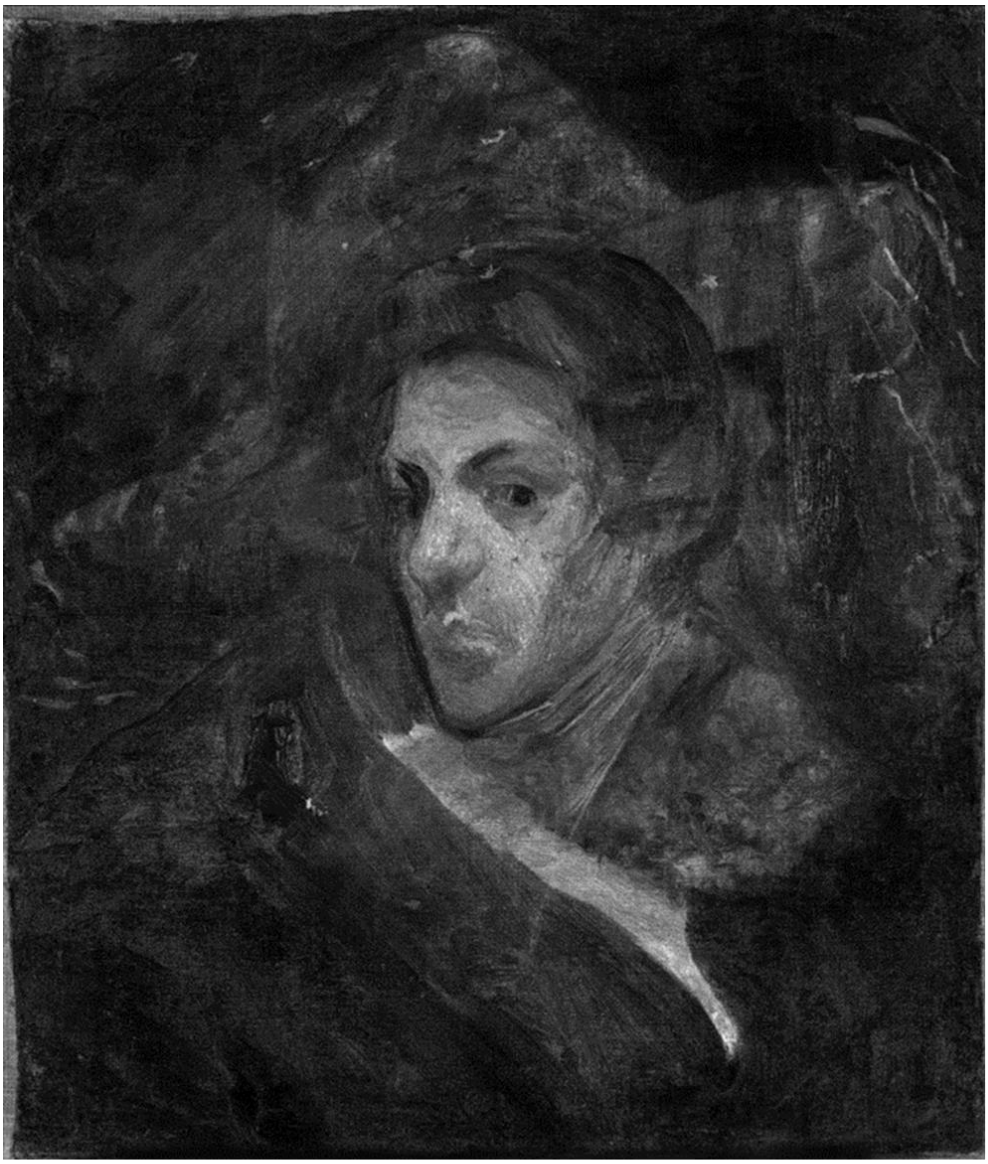

Pablo Picasso.
Retrato de Santiago Rusiñol.
Barcelona,
1899-1900

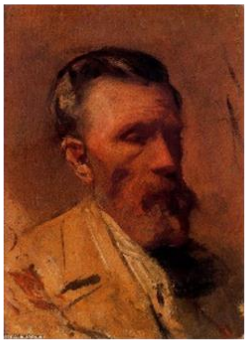

Pablo Picasso.
Retrato del padre.
Barcelona,
1896

Picasso. Autoretrat.
Barcelona,
1896 (Specular version of the original).

Figure 29. a) Contrasted IR radiography image acquired at 2265 nm. b) Portraits of Santiago Rusiñol ; c) Portrait of his father; d) Self-portrait[3].

Description and interpretation of the materials

In Figure 30 the XRF (a) and mid-FTIR (b) measurements spot distribution are presented and the corresponding file names are reported in Table 14.

XRF MID-IR

Figure 30. XRF (a) and mid-FTIR (b) measurements spot distribution.

Table 14. Spectrum/spot label for a) XRF and mid-FTIR are reported.

a) XRF spectrum/point label	b) mid-FTIR spectrum/point label
P553_X_01_pink	P553_M_03_flesh
P553_X_02_dark pink	
P553_X_03_black	P553_M_04_black
P553_X_04_brown	P553_M_05_brown
P553_X_05_brown	P553_M_01_brown
P553_X_06_brown	
P553_X_07_black	P553_M_02_black
P553_X_08_black	
P553_X_09_red	
P553_X_10_lips	
P553_X_11_lipsdark	
P553_X_12_white	P553_M_09_white
P553_X_13_green	P553_M_06_green; P553_M_08_green
P553_X_14_brown	
P553_X_15_grey	
P553_X_16_dark grey	
P553_X_17_black	P553_M_10_black
P553_X_18_black	P553_M_11_black
P553_X_19_grey	P553_M_07_grey

Description

The results are discussed by chromatic areas using the complementary information obtained by XRF and mid-FTIR measurements.

White Areas

The mid-IR spectrum **M_07_grey** acquired on the shirt of the "Home amb Barret" (Figure 5) mainly shows the signals of Basic Lead Carbonate ($PbCO_3$ and $2PbCO_3 \cdot Pb(OH)_2$ – White lead) (Figure 31). The signals that correspond to the Lead Carbonate are the signals of CO_3^{-2} at 680 cm^{-1} (in-plane bending) and about 1390 cm^{-1} (ν_3 asymmetric stretching), 3540 cm^{-1} (fundamental OH stretching). The signal in the NIR range at 4300 cm^{-1} is mainly due to the Hydrocerussite (ν (OH)+deformation modes (Pb+OH)). Weak signals of the organic binder can be observed (C-H stretching at 2958 and 2873 cm^{-1} and the C=O stretching at 1750 cm^{-1}). The XRF spectrum **X_19_grey** acquired on the same point shows the presence of Pb (153 cps), Fe (7 cps), low content of Ca (2 cps), Co (3 cps) and traces of Mn. The presence of Co could be related to the dark layer that probably is present under the white collar. Detailed discussion on the distribution of the elements in depth will be presented in the stratigraphy section.

Observing spectrum **M_09_white** it is possible to identify the Basic Lead Carbonate. The weak band at 2085 cm^{-1} is attributed to the CN^- stretching characteristic of Iron hexacyanoferrate ($KFe[Fe(CN)_6]$ or $Fe_4[Fe(CN)_6]_3$ – Prussian Blue). Signals of the lipid binder have been detected. The XRF spectrum **X_12_white** acquired on the same area shows the presence of Pb (157 cps), Hg (4 cps) and traces of Fe and Ca. Other two measurements on grey areas have been carried out by using XRF. On point **X_15_grey** Pb (156 cps), Hg (4 cps), Fe (3 cps) and traces of Ba have been detected.

Point **X_16_darkgrey** is quite different from the other three analysed point. The XRF spectrum shows a high level of Fe (31 cps) together with slightly lower content of Pb (137 cps), slightly higher amount of Hg (6 cps), Ca (6 cps), Ba (3 cps), Cr (2 cps) and Cu (1 cps). This point corresponds to a "window" that permits the access to the subjacent composition, probably the visage of the subject. This characteristic could justify the different elemental compositions. The Fe increases probably due to the use of natural earths in the first composition or as consequence of the presence Fe-based black pigments.

More difficult is the interpretation of the Hg signal observed on point **X_12/15/16**, which could be related to the flesh of the inferior composition. Alternatively, the presence of Hg in

other areas (**X_05/06/14**) could also be associated to a layer that Picasso used to cover/hide the first representation.

The results of the XRF height peaks evaluation are summarized in Table 15.

Table 15. Summary of XRF results for white/grey areas.

	Ca	Ba	Cr	Mn	Fe	Co	Pb	Hg
E (keV)	**3.71**	**4.52**	**5.44**	**5.95**	**6.4**	**6.97**	**10.55**	**9.97**
P553_X_12_white	Trace	/	/	/	Trace	/	157	4
P553_X_15_grey	2	Trace	/	/	3	/	156	4
P553_X_16_dark grey	6	3	2	/	31	/	137	6
P553_X_19_grey	2	/	/	Trace	7	3	153	/

Figure 31. IR spectrum M_07_grey.

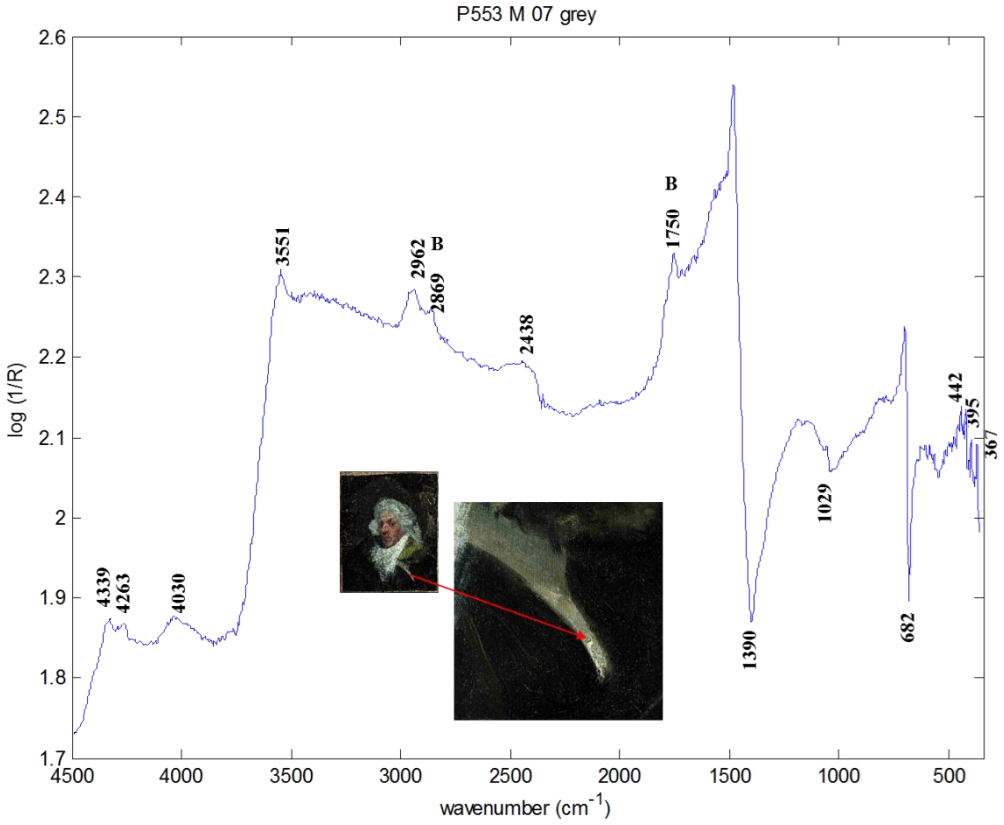

Green Areas

In mid-infrared spectrum **M_06_green** (Figure 32) the signal of Basic Lead Carbonate is predominant. Moreover, a weak signal is present at 2085 cm^{-1} of the CN^- stretching characteristic of the Iron Hexacyanoferrate. The strong inverted signal at 1000 cm^{-1} (Si-O stretching) and a weak band at 3694 cm^{-1} (OH stretching) are characteristic of the Kaolin

(clay mineral, Phyllosilicates ($AlSi_3$, Si_4) O_{10} $(OH)_2$). Signals of the lipid binder are also present. A weak signal at about 800 cm^{-1} could be an indication of the presence of Lead Chromate ($PbCrO_4$ – Chrome yellow). Signals of proteins (signal between - 1559 and 1540 cm^{-1}) and varnish (at about 1470 and 1380 cm^{-1}) were detected. The XRF spectrum **X_13_green** acquired on the green area of the shoulder of the subject demonstrates the presence of Pb (141 cps), Fe (9 cps), Cr (4 cps), Hg (3 cps), Cu (3 cps), Ca (2 cps) and traces of Ba.

The mid-infrared spectrum **M_08_green** shows an inverted band at about 1020 cm^{-1}, which it is attributed to Hydroxyapatite ($C+Ca_3(PO_4)_2$ – Ivory black). The combination band at about 2000 cm^{-1} confirms its presence. The characteristic bands of Basic Lead Carbonate and a weak inverted signal at about 800 cm^{-1}, as observed for the spectrum **M_06_green**, were detected. The band at 2090 cm^{-1} of the Iron hexacyanoferrate is also present. On the point **X_14_brown**, close to the point where the spectrum M_08 was acquired, shows the presence of Pb (146 cps), Hg (11 cps), Fe (8 cps), Ca (3 cps), Ti/Ba (2 cps) and traces of Cr and K. The intensity of Hg at this point could be related to the flesh of the composition underneath or/and to the layer used to cover it. The XRF results are presented in Table 16.

Table 16. Summary of XRF results for green areas.

cps	Ca	Ba	Cr	Mn	Fe	Co	Pb	Hg
E (keV)	**3.71**	**4.52**	**5.44**	**5.95**	**6.4**	**6.97**	**10.55**	**9.97**
P553_X_13_green	2	Trace	4	Trace	9	/	141	3
P553_X_14_brown	3	2	Trace	/	8	/	146	11

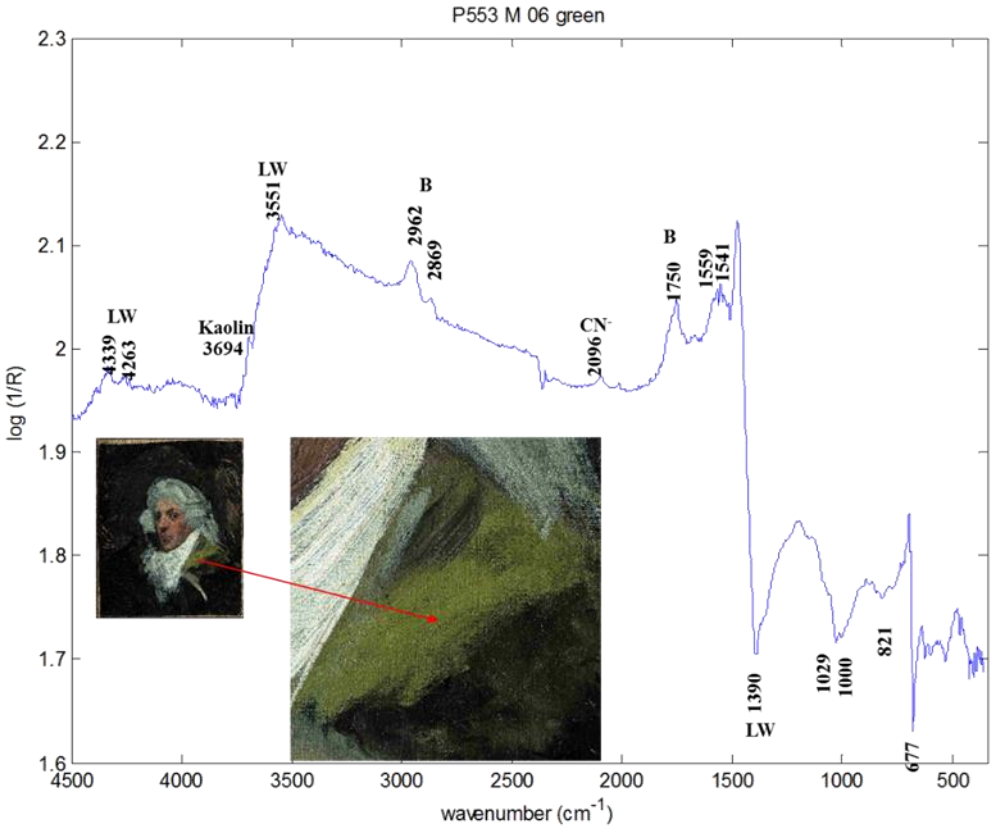

Figure 32. IR spectrum_06_green.

Brown-beige areas

The mid-infrared spectrum **M_01_brown** shows the presence of Hydroxyapatite (band at about 2017 cm^{-1}), Iron hexacyanoferrate (CN^- - 2090 cm^{-1}) and Kaolin (Si-O stretching mode at 1000 cm^{-1}, OH stretching at 3600 cm^{-1}). The signals of lipid, varnish and protein were detected. The attribution of the bands at 679, 625, 532, 420, 395, 385 cm^{-1} at lower wavenumber cannot clearly be assigned, although could be explained, based on the literature, by the use of a Fawn ochre pigment [48].

The XRF spectra **X_05_brown** (no hat under the brown layer) and **X_06_brown** (brown over the hat, more reddish than point 05) were acquired on the brown paint that covers the hat and part of the background area. Pb (130 cps), Fe (28 cps), Hg (12 cps), Ca (4 cps), trace of Ba and K have been detected.

The mid-infrared spectrum **M_05_brown**, very similar to point M_01 and M_04, shows the strong inverted signal of the Si-O stretching and the OH stretching characteristic of Kaolin (3692, 3694, and 3622 cm^{-1}). Moreover, it is possible to identify a clear signal of the Iron

Hexacyanoferrate at 2090 cm^{-1} and a very low presence of Hydroxyapatite. Some weak signals can be assigned to Basic Lead Carbonate. Protein, resin and lipid compound were detected.

The **X_04_brown** has been acquired on the same area that corresponds to the brown/black colour under the hat. The elements detected were Pb (188 cps), Fe (31 cps), Ca (5 cps), Hg (4 cps), Cr (2 cps) and Ba (2 cps).

Another XRF (**X_20_beige)** measurement has been acquired on a beige area that corresponds to the paint layer of the hat that is visible between the more superficial strokes. The elements identified are Fe (27 cps), Pb (145 cps), Ca (3 cps) and traces of Ba. The high signal of Hg on point **X_05/06/14** could be related to the reddish shade of the dark area of the background and could be associated with higher probability to the layer used to the cover/hide the first composition, instead of the flesh of the "Home amb Barret". Considering point **X_14** the more difficult to interpret. The XRF results are presented in Table 17.

Table 17. Summary of XRF results for brown/beige areas.

	Ca	**Ba**	**Cr**	**Mn**	**Fe**	**Co**	**Pb**	**Hg**
E (keV)	**3.71**	**4.52**	**5.44**	**5.95**	**6.4**	**6.97**	**10.55**	**9.97**
P553_X_04_brown	5	2	2	/	31	/	188	4
P553_X_20_beige	3	Trace	/	/	27	/	143	/
P553_X_05_brown	4	Trace	/	/	28	/	130	12
P553_X_06_brown	6	Trace	/	/	16	/	128	8
P553_X_14_brown	3	2	Trace	/	8	/	146	11

Black Areas

The mid-infrared **M_02_black** spectrum shows the signals of the lipid binder, a resin (varnish), and a protein (animal glue used for the relining). As compounds of the pigments used the characteristic band at 2090 cm^{-1} of the Hexacyanoferrate (Prussian Blue) can be identified as well as the strong inverted band at 1020 cm^{-1} of the ion PO_4^{-3} and the combination band at about 2000 cm^{-1} that are characteristic of the Hydroxyapatite (Ivory/Bone black). The doublet at 379-395 cm^{-1} cannot clearly be assigned, although based on the literature it could be an indication of the presence of Fawn ochre. The signal at 562 cm^{-1} could be attributed to Cobalt violet light ($NH_4CoPO_4*H_2O$).[49] The XRF spectrum **X_07_black** was acquired in the area close to point M_02 where there was no hat under the black layer. The elements detected were Pb (124 cps), Ca (30 cps), Fe (26 cps), Ti (11 cps), Mn (3 cps) and traces of P. It is the only point where high signal of Titanium have been detected. This could be an indication of a restoration or the application of some other paint on the original layer.

The mid-infrared **M_04_black** was acquired on the area of the wig covered by a thin black layer and it is very similar to point M_01. Thus, the cover layer of the dark areas and the hair of the "*Autoretrat*" belong to the same representation. The main compounds detected were Iron hexacyanoferrate, Kaolin, Basic Lead Carbonate, protein and a resin. The XRF spectrum **X_03_black**, which corresponds to the same area as point M_04, shows the presence of Pb (152 cps), Fe (18 cps), Ca (12 cps), Hg (10 cps) and traces of Ba and Cr.

The mid-infrared spectrum **M_10_black** is similar to those acquired on point M_02. Furthermore, it proves the presence of heavy metal carboxylates (ν_s (CO) signal between 1364 and 1320 cm^{-1}) [16]. Heavy metal carboxylates (soaps) are compounds formed by heavy metal ions, such as lead, zinc, or copper, and fatty acids. In a dried and aged paint film, these compounds result from the reaction of the ions in the inorganic pigments with the fatty acids of the binder. Metal carboxylates can form during the aging process of the paint or can be deliberately added to the original formulation of the paint as driers.[50]

In the XRF spectrum **X_17_black** (this area corresponds to the shoulder of the "Home amb Barret" the detected elements were Pb (123 cps), Co (41 cps), Fe (25 cps), Ca (29 cps), Cu (1cps) and traces of P and Mn.

The detection of Kaolin in spectra **M01/M04** is the main factor that differentiate these points from points **M02/M10**.

According to the mid-infrared spectrum **M_11_black**, the Lead Carbonate is predominant. Signals of an organic binder and a resin are present. The signal of Prussian blue can be identified at 2090 cm^{-1} and the Ivory black is confirmed by the bands at 1026 cm^{-1} and 2017 cm^{-1}. The spectrum is quite noisy and it is not possible to confirm the presence of the Kaolin, Calcium Carbonate (Signal at 2594 and 2518 cm^{-1} corresponding to the overtone $\nu_1+\nu_3$). In XRF spectrum **X_18_black** the elements detected were Pb (140 cps), Fe (5 cps), Ca (11 cps) and traces of Mn.

The presence of Hg can be related with points **X_05**, **X_06** and **X_14,** the same areas in which Kaolin was detected, and **X_07**, but it cannot be associated with points **X_19/20** or **X_17**, **X_18**, **X_08** and **X_09.** According to the results, there seems to be evidence for the assumption that Hg/Vermilion and Kaolin/natural earth pigments are present in the paint used to cover the hat.

The XRF results are presented in Table 18.

Table 18. XRF results for black areas.

cps	Ca	Ba	Ti	Cr	Mn	Fe	Co	Pb	Hg
E (keV)	**3.71**	**4.52**		**5.44**	**5.95**	**6.4**	**6.97**	**10.55**	**9.97**
P553_X_03_black	12	Trace		Trace	Trace	18	/	152	10
P553_X_07_black	30	/	11	/	3	26	/	124	/
P553_X_08_black	15	/		/	Trace	9	/	141	/
P553_X_17_black	29	/		/	Trace	25	41	123	/
P553_X_18_black	11	/		/	/	5	/	140	/

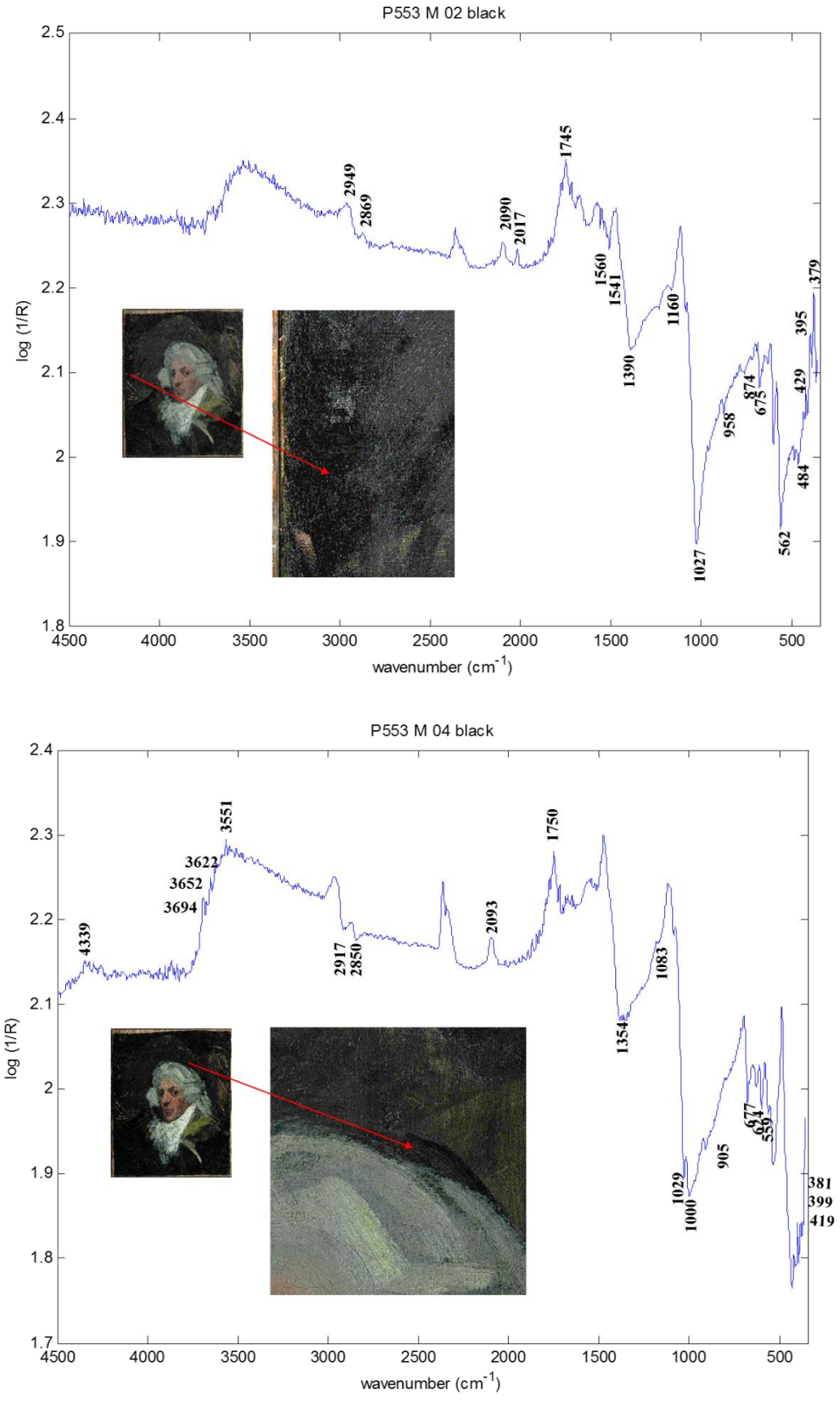

Figure 33. IR spectrum M_02_black and M_04_black

Red Areas

The mid-infrared spectrum **M_03_flash** presents mainly the characteristic signal of the Basic Lead Carbonate and Kaolin. The bands of the lipid binder and the resin of the varnish can also be assigned. It is possible to see only a very weak peak at 2090 cm^{-1} of the Iron hexacyanoferrate. The XRF spectrum **X_01_pink** was acquired on the flesh of the forehead, and the elements detected were Pb (149 cps), Hg (5 cps), Fe (4 cps), Ca (2 cps) and traces of Ba. In a point nearby, corresponding to a more dark shade around the eye (**X_02_darkpink**), the signal obtained for Pb is lower (121 cps), but we can observe an increase of the signals of Hg (17 cps), Ba (3 cps) and Fe (6 cps). Traces of Mn were also detected.

Two points positioned on the lips (**X_10_lips** and **X_11_lipsdark)** have been analysed: one corresponding to the lighter part and another on the more dark side. The difference observed is a slight decrease of the Pb and Hg in the dark area. The signals of Ca, Ba, Cu and Fe remain are comparable.

A spot (**X_09_red**) on the red lines, described in the introduction as tests of colour for the flesh, has been analysed. The elements detected were the same founded in the other red areas. More specifically, the cps counted are similar to those obtained for the peaks of spectrum **X_02_dark pink** acquired on the dark shadow on the eye. The signal of Cu (3 cps) has been detected in both points.

The micro-Raman spectrum **Rm_01_red** of the lower part of the lips shows bands at about 337, 287 and 250 cm^{-1} that confirm the presence of Vermilion (HgS). A small shift of the band has been observed based on the comparison with the reference FT-Raman spectrum of Cinnabar. The spectrum is part of the RRUFF Project/data base[51].

The XRF results are presented in Table 19.

Table 19. XRF results for red areas.

	Ca	Ba	Cr	Mn	Fe	Co	Cu	Pb	Hg
E (keV)	**3.71**	**4.52**	**5.44**	**5.95**	**6.4**	**6.97**	**8.1**	**10.55**	**9.97**
P553_X_01_pink	2	Trace	/	/	4	/		149	5
P553_X_02_dark pink	3	3	/	Trace	6	/		121	17
P553_X_09_red	3	3	Trace	/	8	/		131	16
P553_X_10_lips	2	1	/	/	3	/		126	25
P553_X_11_lipsdark	3	1	/	/	4	/		120	18

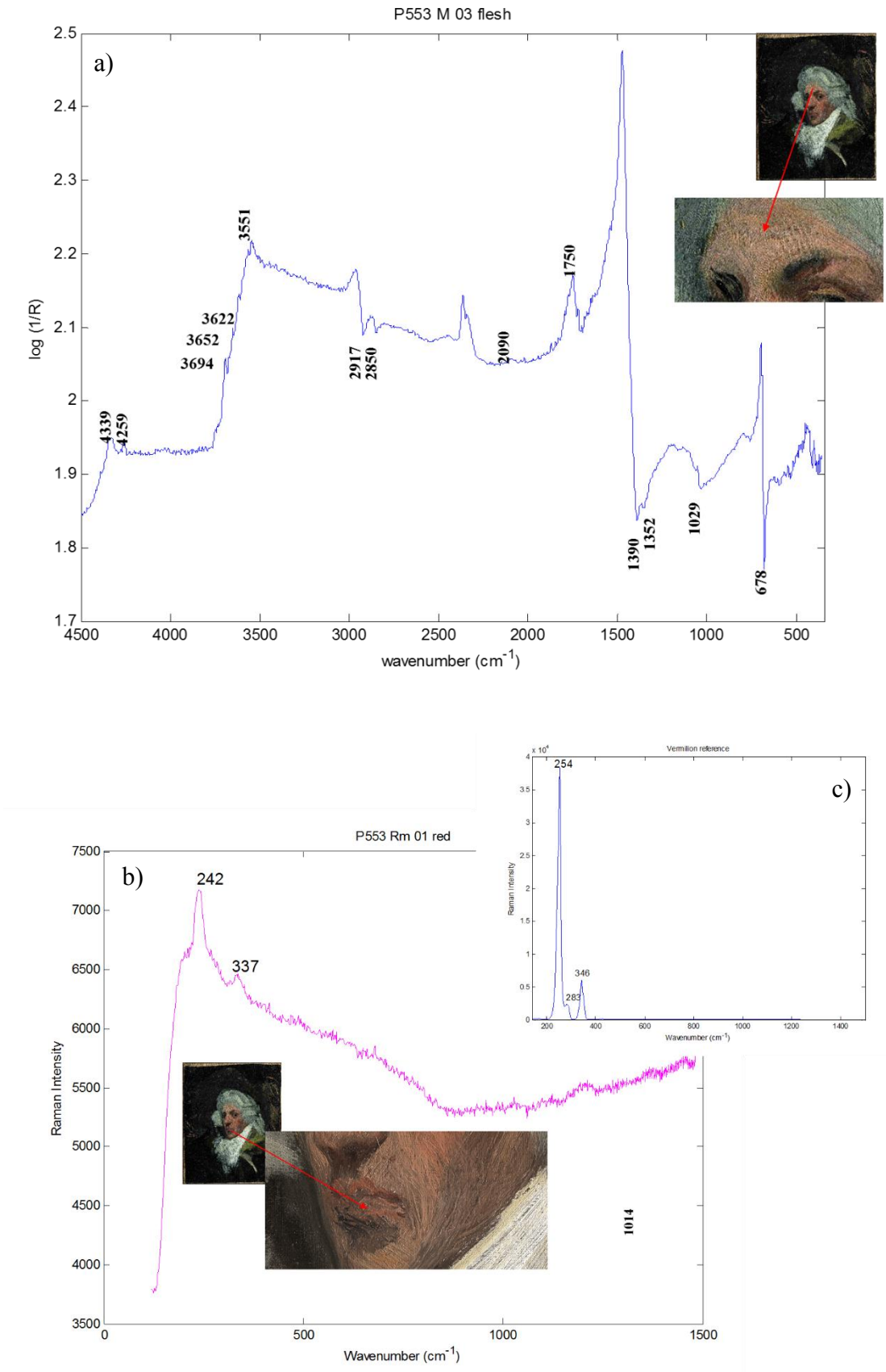

Figure 34. a) IR spectrum M_03_flesh; b) Raman spectrum 01_red; c) Cinnabar reference (R050072, 780 nm)

Summary

Figure 11 shows a mapping of the elements and compounds detected.

Figure 35. Mapping of the results obtained.

Interpretation

Pigments

White pigments

The main white pigment used by the artist is Lead White. The mid-infrared measurements have detected manly Hydrocerussite. This pigment has been confirmed based on XRF results by a strong signal of Pb (mean 140 cps – Figure 36a) all across the painting. The signals that could be assigned to Calcium Carbonate were not confirmed by infrared spectroscopy. The O-H stretching characteristic of the Kaolin have been detected in brown and red areas (not confirmed in the green/yellow area of the shoulder). The Kaolin is usually a filler of natural pigment such as Fe-based red pigments with colours from yellow to brown. The presence of low content of Ba could suggest the presence of an accessory compound of some pigment (Figure 36b).

Black pigments

The black, dark-red and grey areas also showed the presence of Ivory/bone black identified by the presence of a sharp band at 2010 cm^{-1}, which can be related to the phosphate content of the pigment as illustrated in the infrared spectra. On some dark areas, traces of manganese were detected by XRF, possibly due to addition of MnO_2, which is normally a component of the brown earths. The Ivory/bone black contains commonly about 10% carbon, 84% calcium phosphate and 6 % calcium carbonate. Thus part of the signal detected for Ca is due to its presence (Figure 36c). It can be confirmed by the increased on the spots of the dark background analysed. However, another explanation could be the thinner layer at these points that could permit the access of the X-rays to the preparation layer possibly made with a mix of Calcium Carbonate and White lead as found in other Picasso paintings that have been investigated. As the signal of Fe is rather high in some black points, Fe-based (Figure 36d) and Carbon black pigments cannot be excluded.

Red – brown pigments

The XRF signal of the Hg (Figure 36e) and the peaks assigned in the Raman spectrum are an indication of the use of Vermilion. On the other hand, the use of Red lead, based on the XRF results obtained for Pb, cannot be excluded. The use of the Fe-oxides-based earth can be confirmed by the increase of the Fe counts on red/pink and brown points. Kaolin has been detected in some of the analysed areas, a fact that suggests the use of some Natural Earth pigments. In the case of red and yellow iron earth pigments, the colour is produced by Fe

(III) oxides and hydroxides whose infrared bands fall in a range where other absorptions are present and a clear assignment is not possible. Generally, the infrared study provides information for the identification of the accessory minerals such as quartz, clays, carbonates, sulphates [26].

Blue pigments

A Cobalt-based pigment has been found in some of the spots analysed on the lower part of the painting (Figure 36f). As no other elements that could be associated to a cobalt pigment were detected, it is possible to speculate about the presence of the commonly named Thénards blue. It is a cobalt (II) oxide-aluminium oxide, or cobalt (II) aluminate, $CoAl_2O_4$. However, cobalt violet cannot be excluded. The Prussian blue has been confirmed as pigment used mixed with yellow pigments to obtain green hues or with the Ivory/bone black to modulate the dark shade of the background.

Cu-based compounds (Figure 36g) were also found but the specific kind of pigment could be not identified because the signal detected by XRF probably originates from the subjacent layers and no other technique had access to the layer of interest. The Cu-based pigments could present a colour range from blue to green.

Yellow/Green pigments

Cr has been detected mostly in the right side of the painting, as can be seen on the XRF mapping in Figure 36h. The pigments used for the green shade could be a mixture of Lead Chromate with Prussian blue or Chrome oxides. As explained above, the detected Cu could be attributed also to a green compound.

Chrome Yellow, better defined as Lead chromate, could have been used, based on the characteristic bands at about 830 cm^{-1} assigned in the mid-infrared spectrum on the yellow-green area, the XRF signal of the Pb, that slightly increases in this area, and the Cr. The presence of Yellow ochre is also possible due to the high signal of Fe and the detection of Kaolin, which generally is a filler of natural earths.

Other inorganic compounds

Some product that could be an indication of a degradation process, such as Carboxylates were found in the lower area of the painting.

Organic compounds

The mid-infrared results suggest the presence of a Lipid binder. Moreover, signals of a resin attributed to the presence of a varnish have been detected. Finally, signals of Proteins suggest that the animal glue used during the restoration process has migrated from the verso directly on the surface of the painting.

Table 20. Pigments and Binding Media/organic compound Analysis Results

Colours	**Materials/Pigments**	**Binding medium/ organic compounds**
Preparation	/	Oil, Resin, Animal glue [b)]
White	White Lead [a,b)], Calcium Carbonate[a,b)], Kaolin [b)]	
Black	Bone/Ivory black [b)], (Iron oxide based pigments, carbon black)	
Blue	Cobalt blue/Thènards blue [a,b)], Prussian Blue [b)] , Cu based pigment*	
Yellow	Chrome Yellow [a,b)], Natural earths + Kaolin [b)]	
Green	Mixture Prussian blue + Chrome yellow [a,b)], Cu based pigment* (Chrome oxides [a,b)])	
Red – brown	Vermilion [a,b,c)], Brown Earth/ Iron oxide based pigments with Kaolin [b)] (Red lead)	

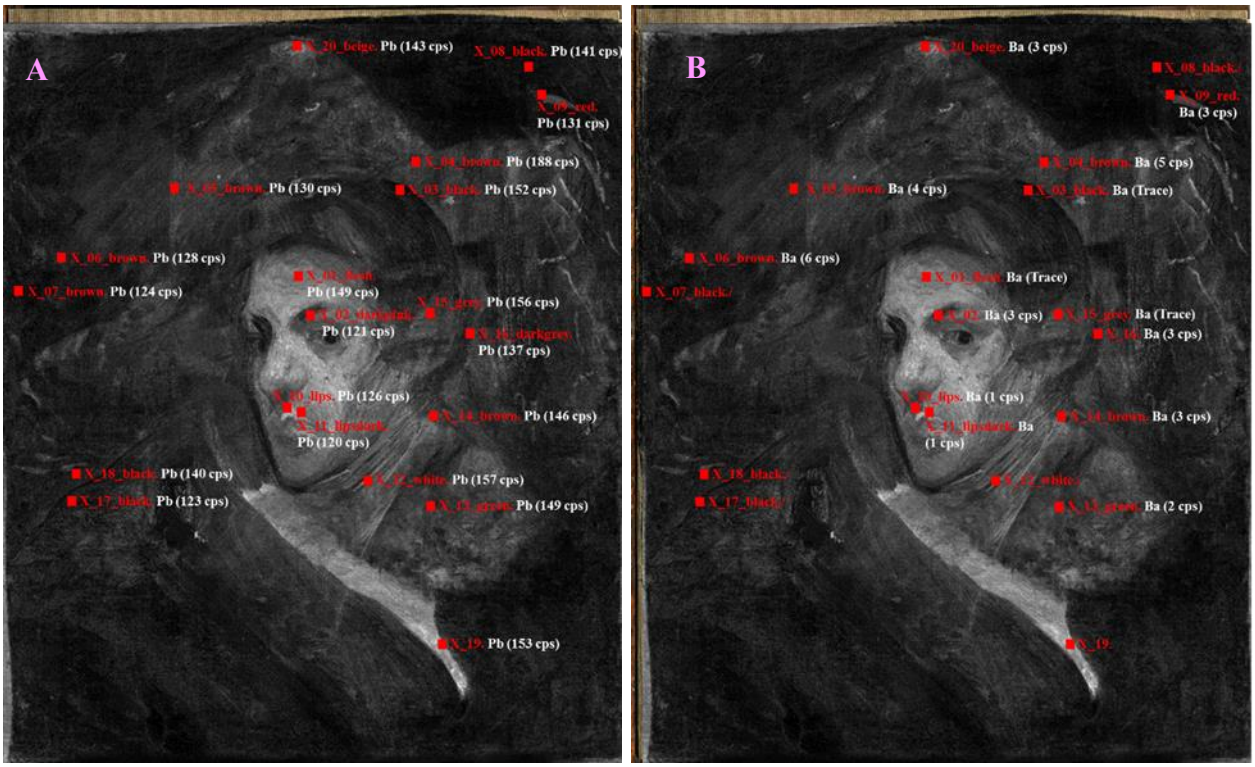


C
X_20_beige Ca (3 cps)
X_08 Ca (15 cps)
X_09_red Ca (3 cps)
X_04_brown Ca (5 cps)
X_05_brown Ca (4 cps)
X_03_black Ca (12 cps)
X_06_brown Ca (6 cps)
X_01_pink Ca (2 cps)
X_07_black Ca (30 cps)
X_02_darkpink Ca (3 cps)
X_15_grey Ca (2 cps)
X_16_darkgrey Ca (6 cps)
X_10_lips Ca (2 cps)
X_11_lipsdark Ca (3 cps)
X_14_brown Ca (3 cps)
X_18_black Ca (11 cps)
X_12_white Ca (Trace)
X_17_black Ca (29 cps)
X_13_white Ca (2 cps)
X_19_grey Ca (2 cps)

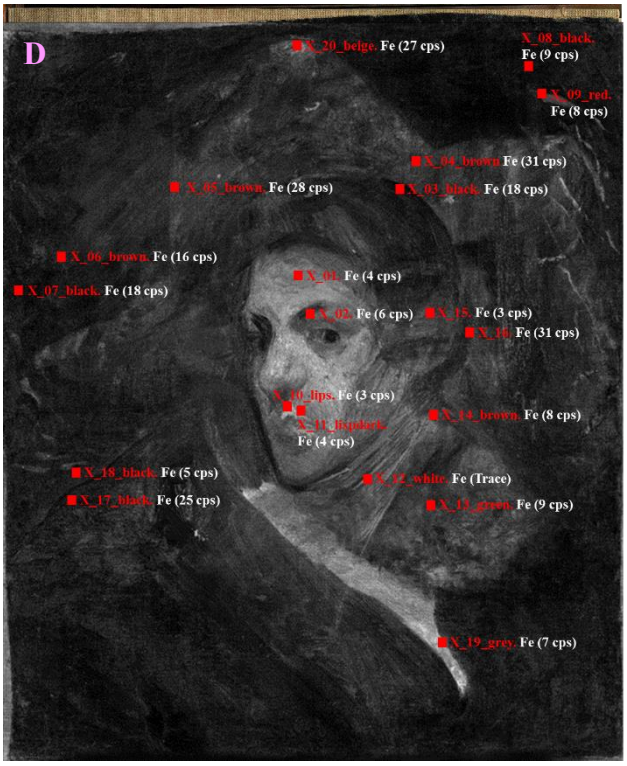
D
X_20_beige Fe (27 cps)
X_08_black Fe (9 cps)
X_09_red Fe (8 cps)
X_04_brown Fe (31 cps)
X_05_brown Fe (28 cps)
X_03_black Fe (18 cps)
X_06_brown Fe (16 cps)
X_01 Fe (4 cps)
X_07_black Fe (18 cps)
X_02 Fe (6 cps)
X_15 Fe (3 cps)
X_16 Fe (31 cps)
X_10_lips Fe (3 cps)
X_14_brown Fe (8 cps)
X_11_lipsdark Fe (4 cps)
X_18_black Fe (5 cps)
X_12_white Fe (Trace)
X_17_black Fe (25 cps)
X_13_green Fe (9 cps)
X_19_grey Fe (7 cps)


E
X_20_beige
X_08_black
X_09_red Hg (16 cps)
X_04_brown Hg (4 cps)
X_05_brown Hg (12 cps)
X_03_black Hg (10 cps)
X_06_brown Hg (8 cps)
X_01_flesh Hg (5 cps)
X_07_black
X_02 Hg (17 cps)
X_15_grey Hg (4 cps)
X_16 Hg (6 cps)
X_10_lips Hg (25 cps)
X_14_brown Hg (11 cps)
X_11_lipsdark Hg (18 cps)
X_18_black
X_12_white Hg (4 cps)
X_17_black
X_13_green Hg (3 cps)
X_19_grey

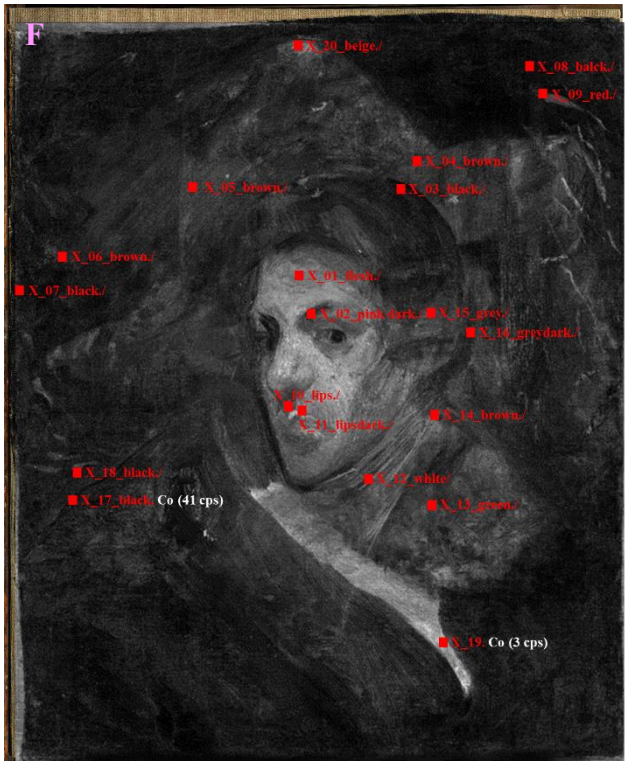
F
X_20_beige
X_08_balck
X_09_red
X_04_brown
X_05_brown
X_03_black
X_06_brown
X_01_flesh
X_07_black
X_02_pink dark
X_15_grey
X_16_grydark
X_10_lips
X_14_brown
X_11_lipsdark
X_18_black
X_12_white
X_17_black Co (41 cps)
X_13_green
X_19 Co (3 cps)

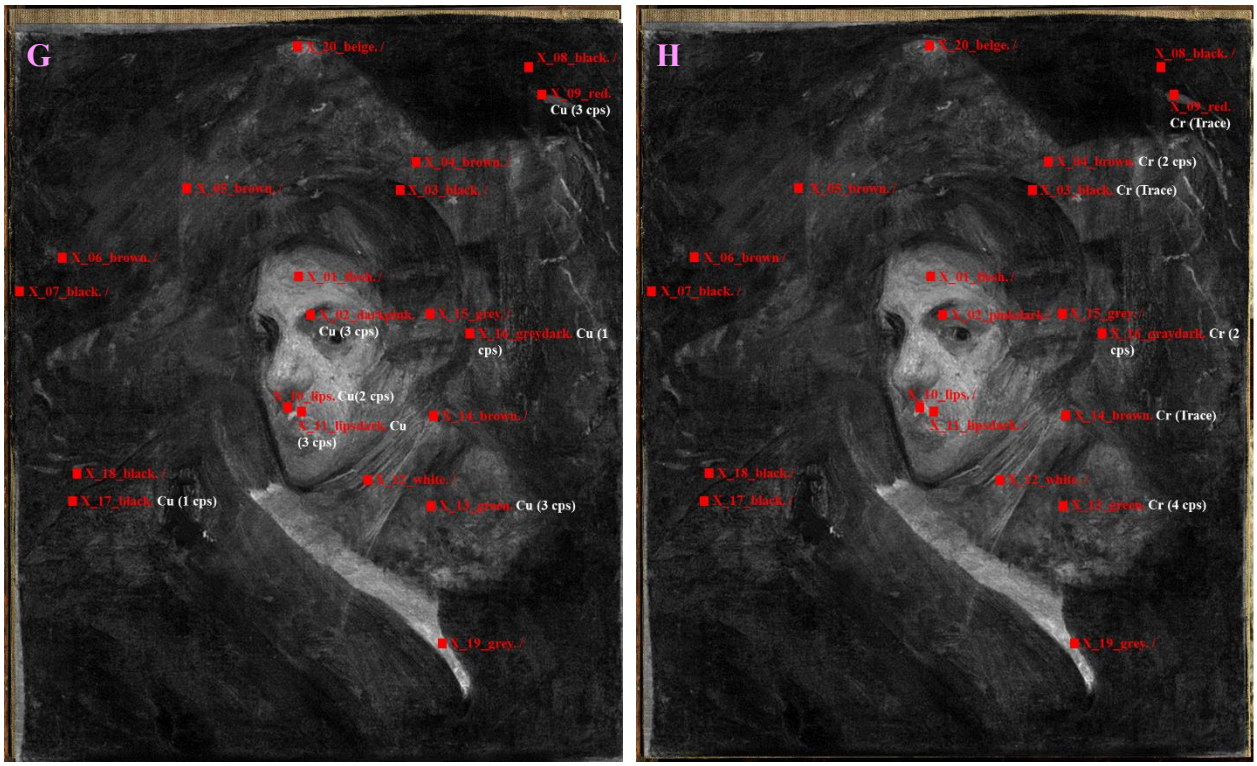

Figure 36. XRF mapping- element distribution and cps obtained: a) Pb, b) Ba, c) Ca, d) Fe, e) Hg, f) Co, g) Cu, h) Cr.

Global discussion of the painting

Composition vs. Areas

First of all, the painting analysed could be divided in two layers with two overlapped compositions. (*Home amb barret*, underneath; *Autoretrat* and *Autoretrat amb Perruca*, superficial). The two layers include compositions that follow the same structure: characters depicted in the centre of the canvas surrounded by the background.

Background

Home amb barret

The dark background created to frame the face of the subject has been painted with a mixture of Ivory/bone black with a content of Mn oxides and Prussian blue. Unconfirmed, but possible pigments used are iron or carbon based black pigments.

Autoretrat/Autoretrat amb perruca

To the above mentioned compounds Vermilion and Natural earths have to be added, with content of kaolin and a Ba-based compound, which were applied to cover the hat and possibly the visage of the character underneath.

Subject

Home amb barret

The hat that Picasso clumsily tried to cover could been painted with a Yellow ochre mixed with Lead White, based on XRF results and the light yellow hue that can be seen.

Although the face of the subject is totally hidden, the detection of the Hg in the area, which is not due to the superficial paint layer, could suggest the use of Vermilion for the pink and red of the flesh and to obtain the reddish shadow of the beard. The shirt has been painted with Lead White and Calcium Carbonate. Finally, for the jacket Picasso used a Cobalt blue, commonly named Thènards blue, and a black paint containing Prussian blue plus Ivory/bone black.

Autoretrat

For the colour of the visage Picasso used Vermilion, probably Fe-based red pigments/natural earths. Also on the lips Vermilion has been detected, although based on the XRF results (Fe signal) Fe-based red pigments and Red lead cannot be excluded.

The artist applied thick stokes of Lead White for the shirt and a Lead Chromate mixed with Prussian blue for the jacket. The presence of green Chrome oxides cannot be excluded. Indeed, it is reasonable to assume the use of Fe-based red pigment based on the low absorption areas in the XR image and the more reddish left-side hand cheek.

The original hair of the Autoretrat was dark/black. The composition is difficult to separate from the materials that correspond to the layer applied to cover the two other compositions and paint the superficial background. It is likely that the difference is on the higher signal of Ca, which could be an indication of Ivory/bone black. Other possible component of the dark paint are the Mn oxides/brown natural earths, Prussian blue, Fe based black pigments and Carbon black.

Autoretrat amb Perruca

The main difference according to the previous representation is the superposition of the wig and the area at the end of the collar. It is difficult to assess when these strokes were added. Two possibilities can be hypothesized:

- A modification made short time after the visage and head of the Autoretrat. Thus, the grey shadow should be due to the mixture of the superficial black of the hair;
- A change made considerable time after, when the paint of the visage was dry. Consequently, the grey should be considered a mixture of a white with a dark colour. This behaviour could explain the intact rheology of the first composition layer;

The white is not completely identified. Among the candidates, based on the XRF results the most probable possibility is the white lead.

Table 21. Pigments and organic compounds organised by areas (I. Home amb barret; II. Autoretrat; III. Autoretrat amb perruca).

Areas	Pigments	Binder/organic compound
Background	I. Ivory/bone black + Mn oxides + Prussian blue, (Iron or carbon based black pigments) II. Vermilion + Natural earths + Prussian blue	Oil, Varnish, Animal glue
Face (Front/Lips, Cheek)	I/II. Lead White + Vermilion + Natural earths/Fe based red pigments (Red lead) II. Cu based pigment	
Hat	I. Yellow ochre + White lead	
Hair	III. Ivory/bone black (Mn oxides + Prussian blue, Iron or carbon based black pigments)	
Jacket	I. Cobalt blue /violet II. Lead Chromate (Cr oxides) + Prussian Blue + White lead + Ivory/bone black	
Shirt	I/II/III. Lead White + Calcium Carbonate + Prussian blue	
Wig	III. Lead White (Calcium carbonate) + Prussian Blue	

Figure 37. Material distribution mapping.

Stratigraphy

The painting is composed of two compositions, the *Home amb Barret* lying underneath and the superior that could be split in two, *Autoretrat* and *Autoretrat amb perruca*. Taking advantage of the possibility of XRF to obtain signal from the layers underneath, an approximate stratigraphic distribution could be deduced complemented, as guide, with the XR and IR images. Starting from the support, it is possible to assume the presence of a preparation layer, based on the regular pattern highlighted by the XR image. Afterwards, Picasso painted the *Home amb Barret.* Probably, when this layer was completely dry, he

created the *Autoretrat.* Finally, he modified the latter superposing the wig. Inspecting the XR and IR images it can be deduced that the *Autoretrat* was created directly on the first composition. However, the XRF results suggest that before the execution, the hat and the visage were covered by a layer containing natural earths with Kaolin, Vermilion and a Ba-based compound. This structure allowed both types of radiation to access the composition underneath, except to the visage of the *Home amb barret*, whose observation is hindered by the presence of thick brush strokes of a pigment with a high Z number (e.g White lead), which absorb the XR and, as white, reflect the NIR radiations. After finishing the first composition *Home amb barret* and covering the hat and possibly the visage, Picasso superposed the face of the *Autoretrat* and the corresponding hair. Then, he applied the tick paint layer to represent the more plain and uniform white collar, which in some points hides the paint of the cheek. It seems that Picasso has no intention to change the background of the first composition. Probably completely finished, the portrait was again partially changed to create the *Autoretrat amb perruca*. It is not possible to determine when Picasso painted the *Autoretrat*, although the intact rheology of the paint located on the visage in correspondence of the wig limits suggests that the paint was dry when Picasso made this change. The composition was probably, finished, when it was modified to create the *Autoretrat amb perruca*. The possibility that the second superficial composition was applied when the first layer was still wet, could explain the grey/white colour of the wig. Finally, Picasso painted the wig and the final part of the collar.

3.3.4 Retrat de Carles Casagemas

Artworks' interest

The portraits ***Retrat de Carles Casagemas*** (**Portrait of Carles Casagemas**) [55 x 46 cm MPB_110.022] is part of the paintings and drawings, which Picasso creates between 1899 and 1904, which are remarkable for the combination of conventional art of portraiture that, as young artist, he was developing.[52] In this period, he supported himself with the few profits coming from the occasional publications of his drawings on the local press. He developed a particular inclination for a graphic style and his figures assume appearance of portrait /caricature. In almost all cases his characters are dunked in a dark background.[53,54] The portrait of Casagemas is described as a very interesting mix of graphic style and the gloomy palette that Picasso used in his oil paintings. This portrait, theatrically dark and dim, suggests some qualities of the caricatures (the clearly accentuated jacket and the facial strokes).

This work is part of the numerous drawings and oils of Casagemas that Picasso realized in the period of 1900 when he and his friend were always together.[55] The painting is a portrait dated, by different sources, between 1899/1900.[52,53,55,56]

In the late 1800s, Barcelona, Spain's second largest city and capital of Catalonia, was the centre of Spanish modernism. Pierre Daix, Picasso's friend and biographer, referred to the city as "a seething brew of ideas and experiences".[57] At the epicentre of this creativity was a meeting place founded in 1897, The Four Cats, or *Els Quatre Gats* in Catalan. Located in a modernist building, the Casa Marti, Els Quatre Gats, was at once a tavern, and forum for performers, poets and theatre productions. Ad most important, it was a place for exchange and conversation[57]. It was at Els Quatre Gats were the 17-year-old Pablo Picasso left behind the academia of Madrid. From February 1899 until the end of 1900 he met modernist artists that will be key figure and influences on his artistic career. In this effervescent cultural ambient he was growing while he was developing his artistic skills. The Quatre Gats was the "showcase" where Picasso installed his first two exhibitions. Here Picasso get closer to the young artist, Carles Casagemas I Coll. Painter and poet (1880-1901), he was son of the United States consul general in Barcelona.[57]

Between January and September 1900 they were sharing a studio in Barcelona. In the autumn of that year, Casagemas accompanied Picasso on his trip to Paris, where they visited the Exposition *Universelle* together with several other Catalan artists. As *David J. Chalif* wrote,

"*While in Paris, Casagemas developed an obsession with Laure Gargallo, known as Germaine, the future wife of Ramon Pichot, another Quattre Gats friend. Due to some love issues, Casagemas committed suicide in Café de L'Hippodrome on the Boulevard de Clichy in Montmarte, on February 17, 1901, after first attempting to kill Germaine*". Picasso was not in Paris at the time of friend's death; Picasso later insisted that it was because of Casagemas's suicide that he began painting in blue, announcing his "Blue period" [57,58]. At that time, Picasso worked frenetically on the portraits of the friends of his art league, which were part of his first exhibition at *Els Quatre Gats*.

Description and interpretation of the painting layers structure

In the last forty years, it has been subject to three restorations. According to the documentation provided by the conservator Sra. Reyes Jimenez, it has been relined and the painting layers have been consolidated in 1970. In 2004 it has again been consolidated with animal glue and submitted to an intervention of colour reintegration. As the documentation says, the use of animal glue has caused detachments of the paint layer. The retouches are clear and are not coherent with the substrate in terms of texture. In 2008 the frame has been changed.During the analysis campaign the entire surface. With the help of the conservators' expertise, the points for the analysis were chosen trying to avoid the reintegrated areas, localized mostly in the lower part and along the edge.

Direct observation – VIS

Observation of the visible subjacent layers

Recently, the painting has been under restoration. Thanks to the removal of the varnish and the retouches, the painting layers lying underneath have become visible. A very bright palette can be seen. Blue, green and yellow-ochre colours characterized by pastel shades have been hidden by the artist with darker and gloomier colours. Figure 38 shows a picture taken during the restoration process.

Figure 38. VIS image of the painting during the restoration process.

Observation of the superficial layers

Background

The character depicted on the surface, comes out from a dark background. Black and brown paint are mixed together and surround the subject, while a dark gray-blue create a shadow on his shoulder and large brilliant brush of green light the two opposite sides up.

Subject

The subject is dressed with a brown, yellow-ochre and green jacket which Picasso defines with vibrant and rapid black brush strokes. A white shirt and a black pullover complete his formal clothing.

The attention, however, is centred on the expressive elongated face of the subject. A faint rosy complexion and the green shadows on the cheeks contribute to express, in conjunction with the cold white of the forehead, the nature of the character. The black eyes and the brown eye sockets make the look very intense.

Observation with no visible radiation - subjacent layers (XRR, IRR)

Radiography

The reproduction of the radiography (photo taken in the restoration studio of the museum Picasso with courtesy of the conservator Reyes Jimenez) shows a distribution of heavy elements on the entire painting, almost concentrated in the lower part of the image (white-grey areas). The paint, including heavy metals (probably lead white), seems to be applied with long and broad brush strokes. The information obtained does not permit to locate the strokes in the stratigraphy, which could be part of the superficial composition, the inferior or the intermediate layer.

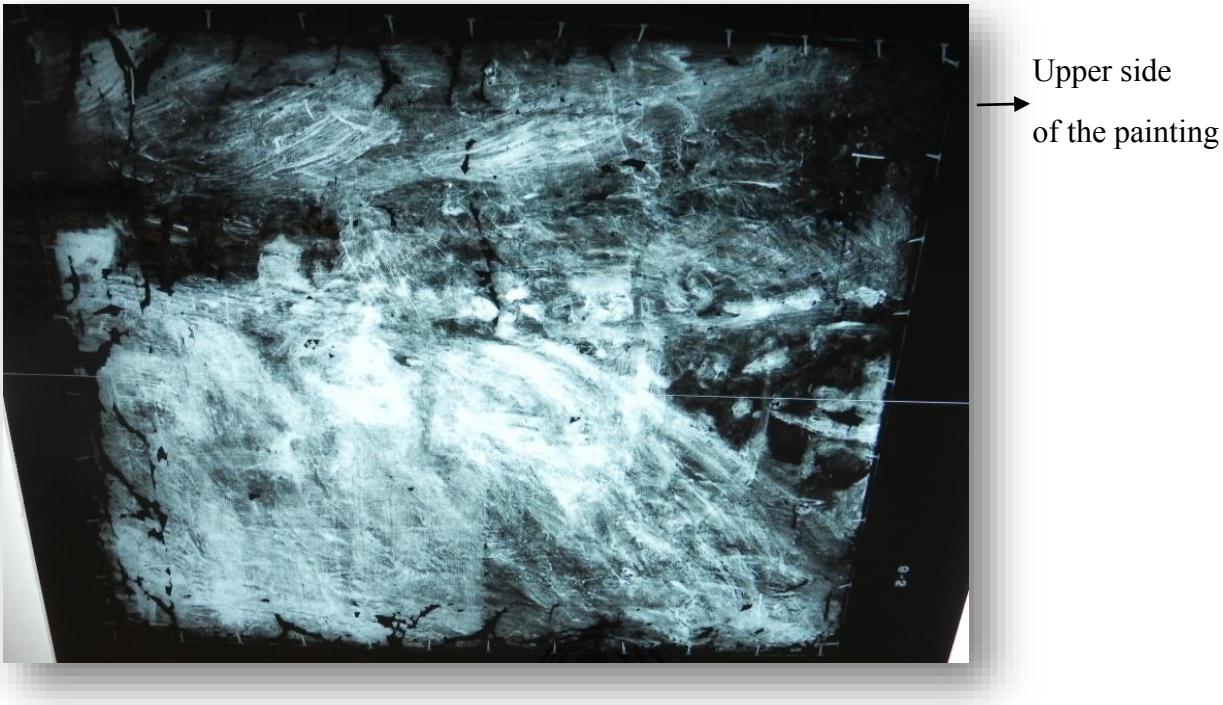

Figure 39. Reproduction of the X-ray image of the painting, rotated by 180º (courtesy of the conservator Reyes Jimenez).

IR Reflectography

In Figure 40 the image aquired at 2265 nm is presented. Due to the features of the painting, such as the presence of the varnish on the surface or/and the above described heavy metal based paint, no information about hidden compositions has been achieved. A layer of lead white, for example, did not allow to obtain signal from the layers underneath. On the image, it is possible to perceive the discontinuity of the painting layer due to the presence of several retouches, mostly concentrated on the edges of the painting. It is important to notice that the areas, where the composition is clearly visible, are regions where the varnish was removed before the analysis campaign. The discontinuity of the painting surface and non-original material can be identified. Those materials were removed during the restoration process and are clearly visible in Figure 38.

Figure 40. IR radiography image acquired at 2265 nm.

Description and interpretation of the materials

In Figure 41 the XRF (a) and mid-FTIR (b) measurement spot distribution are presented and the corresponding file names are reported in Table 1.

XRF MID-IR

Figure 41. XRF (a) and mid-FTIR (b) measurements spot distribution.

Table 22. Spectrum/spot label for a) XRF and mid-FTIR are reported.

a) XRF spectrum/point label	b) mid-FTIR spectrum/point label
P022_X_01_white	P022_M_11_white
P022_X_02_black	
P022_X_03_brown	P022_M_05_black
P022_X_04_green	P022_M_01_green
P022_X_05_black	
P022_X_06_white	P022_M_06_flesh
P022_X_07_red	
P022_X_08_pink	
P022_X_09_black	P022_M_04_black
P022_X_10_red	
P022_X_11_white	P022_M_09_white
P022_X_12_grey	P022_M_08_green
P022_X_13_brown	P022_M_07_green
P022_X_14_green	

P022_X_15_green	
P022_X_16_brown	
P022_X_17_black	P022_M_10_black
P022_X_18_blue	P022_M_02_blue
P022_X_19_canvas	P022_M_03_preparation

Description

White Areas

The mid-infrared spectrum **M_02_blue_ under painting** acquired on the ground exposed on the left side of the painting (Figure 42) is essentially based on Calcium carbonate. Unfortunately, this point is located in an area that could be not representative of the original composition. The sharpness and intensity of the C-H stretching, (2910 and 2846 cm^{-1}) and the very weak sharp doublet in the NIR range at about 4300 cm^{-1} could be an indication of the presence of wax. The signal of the carbonyl stretching (C=O) at 1745 cm^{-1} is contained in a large number of different compound classes e.g. carboxylic acids, esters, amide etc. Thus, it could be related to the presence of wax or other organic binders. At lower wavenumbers the signals are in good correlation with iron oxides, although this range is common to other oxides. The band at 2085 cm^{-1} is attributed to the CN^- stretching characteristic of the Iron hexacyanoferrate ($KFe[Fe(CN)_6]$ or $Fe_4[Fe(CN)_6]_3$ – Prussian Blue). The signal of Calcium Carbonate ($CaCO_3$) at 2594 and 2518 cm^{-1} corresponds to the overtone $\nu_1+\nu_3$. The XRF measurement on point 18 (**X_18_blue**) on the left side, but in the lower edge of the painting, is comparable with the spectrum described above in terms of appearance/colour/texture. It shows a high content of Pb (111 cps) that seems to be the major element across the entire artwork (no information about the location in depth of the layer). The signal of the Pb could be related to the presence of other compounds, such as Lead Chromate ($PbCrO_4$ – Yellow chrome) or Lead Oxide (Pb_3O_4) in other areas of the painting. The Fe (14 cps) is detected as component of the Prussian blue. The presence of Ca (68 cps) is also detected. The Ca seems to be particularly located in high concentration in some points on the edge of the painting.

The mid-infrared spectrum **M_03_preparation** acquired from the ground exposed on the left side of the painting showed that, probably, the priming layer is based on Neutral and Basic Lead Carbonate ($PbCO_3$ and $2PbCO_3 \cdot Pb(OH)_2$ – Lead White) mixed with Calcium Carbonate. The band that correspond to the Lead Carbonate (meanly hydrocerussite - $Pb(OH)_2$) is the signal of the CO_3^{-2} at 675 cm^{-1} (in-plane bending) and about 1390 cm^{-1} (ν_3 asymmetric stretching), 3540 cm^{-1} (fundamental OH stretching) and doublet at about

4300 cm^{-1} (ν+δ OH). Signal of Calcium Carbonate is observable as weak signal at 2518 cm^{-1} corresponding to the overtone $\nu_1+\nu_3$ [13,26]. The presence of bands at 1670 and 1580 cm^{-1} may indicate some proteinaceous material [28]. The carbonyl (C=O) at 1745 cm^{-1}, doublet at about 4300 cm^{-1} can be ascribed to the ν+δ (CH) mode of aliphatic chains (partially overlapped with the ν+δ (OH) of lead white) and a weak signal at about 5800 cm^{-1} (ν_1 CH) are due to the lipid binder. The XRF spectrum acquired on point 19 (**X_19_canvas**) shows the presence of Pb (108 cps), a low content of Ca (20 cps) and Fe (7 cps) and traces of Cr and Ba.

The mid-infrared spectrum (**M_06_flesh - forehead/dark side - cleaned area,** Figure 43) mainly shows the signals of lead white (also the signals in the NIR range at 4300 cm^{-1} are mainly due to the hydrocerussite). The weak band at 2085 cm^{-1} is attributed to the CN^- stretching characteristic of the iron Hexacyanoferrate (Prussian Blue).[20,26] The signals (C-H stretching) at 2958 and 2873 cm^{-1} are due to the organic binder. The indication of protein arises from the two weak bands at about 1670 and 1580 cm^{-1}, combined with weaker CH stretching. The doublet at 600-630 cm^{-1} could be due to Barium Sulphate (BaSO4 – Barium White). The XRF spectrum (**X_06_white**) gives evidence for a high level of Pb (173 cps).

The bands present in this mid-infrared spectrum **M_09_white** indicate that this area is based on lead white (mainly Hydrocerussite) (Figure 43). Weak signals of the organic binder can be observed (C-H stretching at 2958 and 2873 cm^{-1} and the C=O stretching at 1745 cm^{-1}). The XRF results (**X_11_white**) confirm the high presence of Pb.

As observed for point M_03_preparation, in mid-infrared spectrum **M_11_white**, located on the left-hand side edge of the painting, lead white is the main compound. Calcium carbonate is also present. Bands at low wavenumbers range are not assigned, although silicates are possible. Weak oxalates and weak wax can be identified with the sharp peak at 1460 cm^{-1} and sharp CH combination at 4300 cm^{-1} overlapped with the lead white bands. The XRF (**X_01_white**) results show a high signal of Ca (293 cps). It is the only point that shows high content of Ca. It could be beneficial to observe the IR reflectography, because this measurement corresponds to be very bright and unique area of the painting that could be identified as a restoration or different preparation layer. One should bear in mind that, in the notes, this point is defined as a "*lacuna"* (loss of material). Other elements detected are Fe (12 cps) and Pb (10 cps). Traces of Cr and Ba are present. This point shows some features also found in the FTIR spectrum of point **M_02_blue**. In Table 23 a summary of the XRF results obtained for white/preparation areas is presented.

Table 23. Summary of XRF results for white/preparation areas.

cps	Ca	Fe	Pb	Ba	Cr
E (keV)	**3.71**	**6.4**	**10.55**	**4.52**	**5.44**
P22_X_01_white	293	12	10	Trace	2
P22_X_18_blue	68	14	111	Trace	3
P22_X_19_canvas	20	7	108	Trace	2
P22_X_06_white	3	5	173	Trace	Trace
P22_X_11_white	2	2	154	/	0

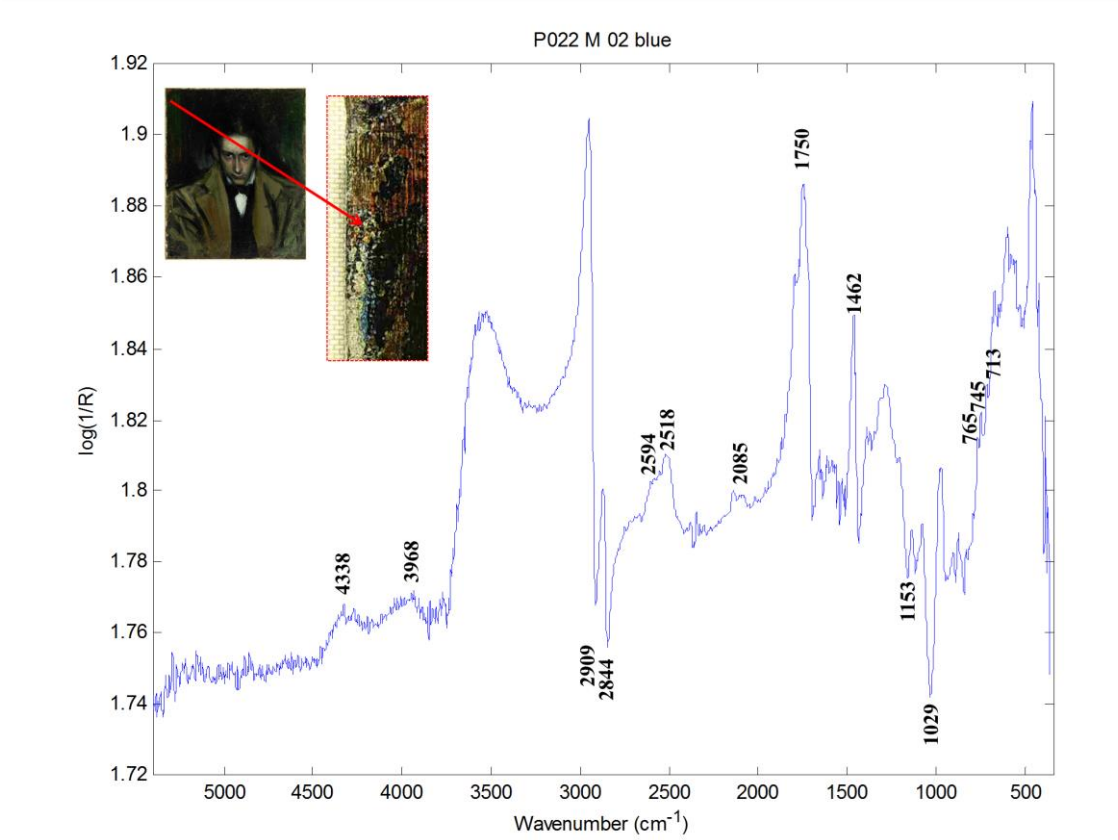

Figure 42. IR spectrum M_02_blue

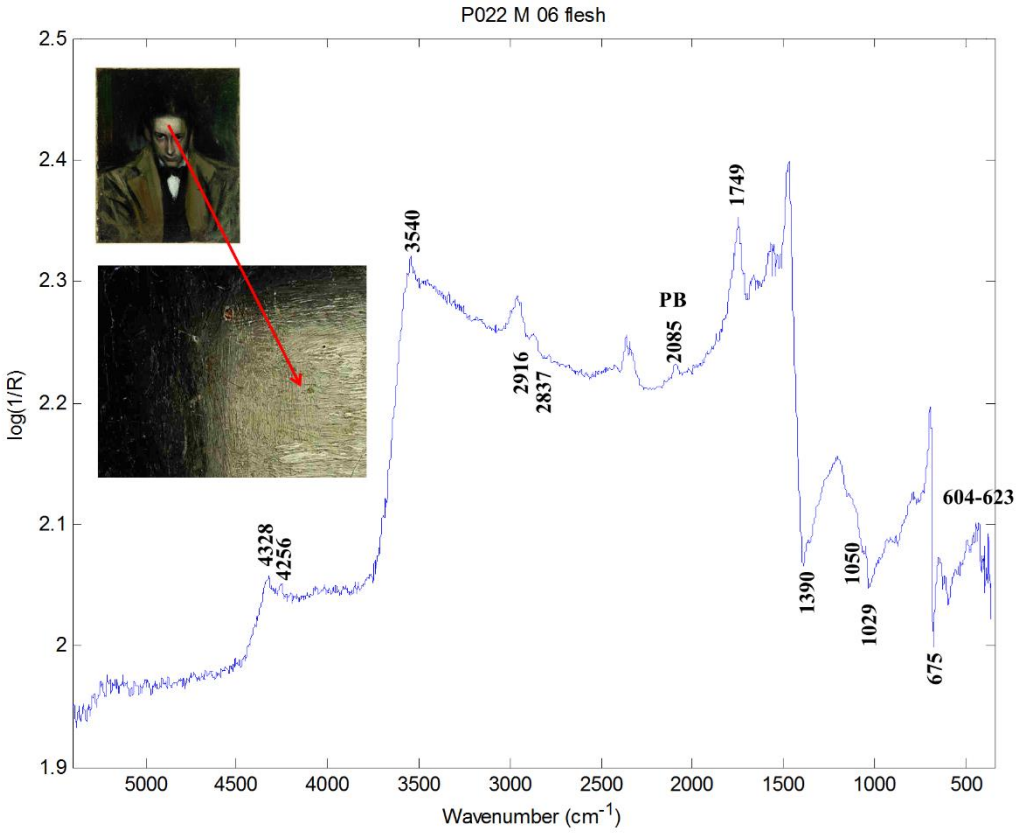

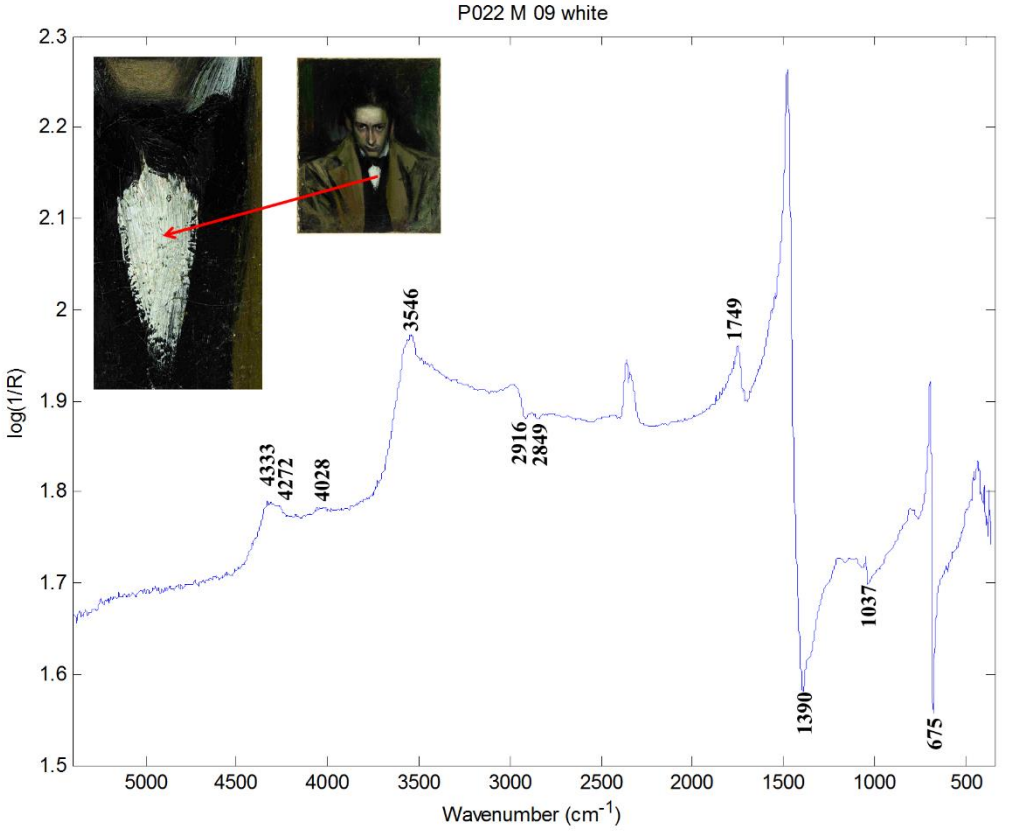

Figure 43. M_06_flesh and M_09_white

Green-Brown Areas

The mid-infrared spectrum **M_01_green** shows the signals of the varnish, that are present in more or less all the spectrum, which in some cases was not removed or remained as residue on the surface when the analysis were performed. In this measurement, acquired on the green brush stroke that characterized the left side of the background, it is possible to see the signal of iron Hexacyanoferrate at 2085 cm^{-1} partially overlapped with the combination band (2064, 2132 and 2190 cm^{-1} - $\nu_1+\nu_3$) of Barium Sulphate. Other signal attributed to the Barium Sulphate are located at 1965 cm^{-1} (2 ν_1), at 604 and 632 cm^{-1} (bending ν_4)[11]. The signals located in the range between 350 and 428 cm^{-1} are in good correlation with chrome oxides. According with the XRF results (**X_04_green**) the signal of the Ba is comparable to the signal of the Cr (about 14 and 12 cps), which can be an indication probably of the presence of Barium Chromate ($BaCrO_4$ - Barium Yellow) with some impurity of Strontium Chromate ($SrCrO_4$ - Strontium Yellow). In the XRF spectrum, the high signal for Fe (118 cps) and the presence of K (Kα 3.32 keV) are due to the Prussian blue. Pb (about 102) and Ca (10 cps) were also detected.

According to the mid-infrared spectrum **M_07_green**, the lead carbonate is predominant. Signals of an organic binder are present. A weak signal of Prussian blue can be identified at 2085 cm^{-1}. The signal of weak oxalates at 1320 cm^{-1} and the bands of sulphate at 630-600 cm^{-1} are present. The additional bands in the 1200-900 cm^{-1} range are not assigned (this is valid for most of the spectra). This spectral range is full of absorption signals and it is generally difficult to separate the different contributions [48]. The XRF results (**X_13_brown**) confirm Pb (164 cps) as major element, rather high content in Fe (63 cps) can be an indication of some based Fe-oxide pigment. Cr (4 cps) and traces of Ca and Ba have been identified. A low content in Hg can be justified by the presence of Mercury Sulphide (HgS - Vermilion), which the artist used to enhance the reddish shade. The measurement XRF on point **X_16_brown** (on the right edge of the painting) shows the presence of Pb (125 cps), Fe (53 cps), Ca (8 cps) and traces of Ba and Hg. Although it is a point located near the edge, its composition is comparable with point **X_13_brown** described above. Point **X_03_brown** (at the end of the bright green brush stroke on the left side) contains Pb (124 cps) and Ca (5 cps). A high signal of Fe (214 cps) was detected. Its content is similar to point **X_2_black** and is higher than in all the other analysed spots. On **X_2_black** – near to the "*lacuna"* of point X_1_white – Pb (135 cps), Fe (210 cps), Ca (about 9 cps) and Cr (3 cps) and traces of Ba were detected. The mid-infrared spectrum **M_08_green** acquired is similar to mid-infrared spectrum **M_07_green**, but without oxalates. The signal of Prussian blue is higher.

According to the XRF results point **12_grey** contains Pb (150 cps), Fe (30 cps), Cr (3 cps) and traces of Ba. Other two green (more dark shade) points have been analysed by XRF. The XRF spectrum acquired on points **X_15_green** and **X_14_green** show a moderate content in Fe (a mean of 50 cps) similar to the results for the green areas described above, a low signal of Cr (about 5 cps), Ca (about 5 cps) and Ba (about 4 cps). Hg is also confirmed as indication of the presence of Vermilion.

Table 24. XRF results for green-grey areas.

cps	Ca	Fe	Pb	Ba	Cr	Hg
E (keV)	**3.71**	**6.4**	**10.55**	**4.52**	**5.44**	**10.01**
P22_X_04_green	10	118	102	14	12	0
P22_X_12_grey	3	30	150	2	3	/
P22_X_13_brown	2	63	164	2	4	2
P22_X_14_green	6	48	141	3	4	2
P22_X_15_green	4	55	136	4	6	3
P22_X_16_brown	8	53	125	3	/	2
P22_X_03_brown	5	214	124	/	/	/
P22_X_02_black	9	210	135	/	3	/

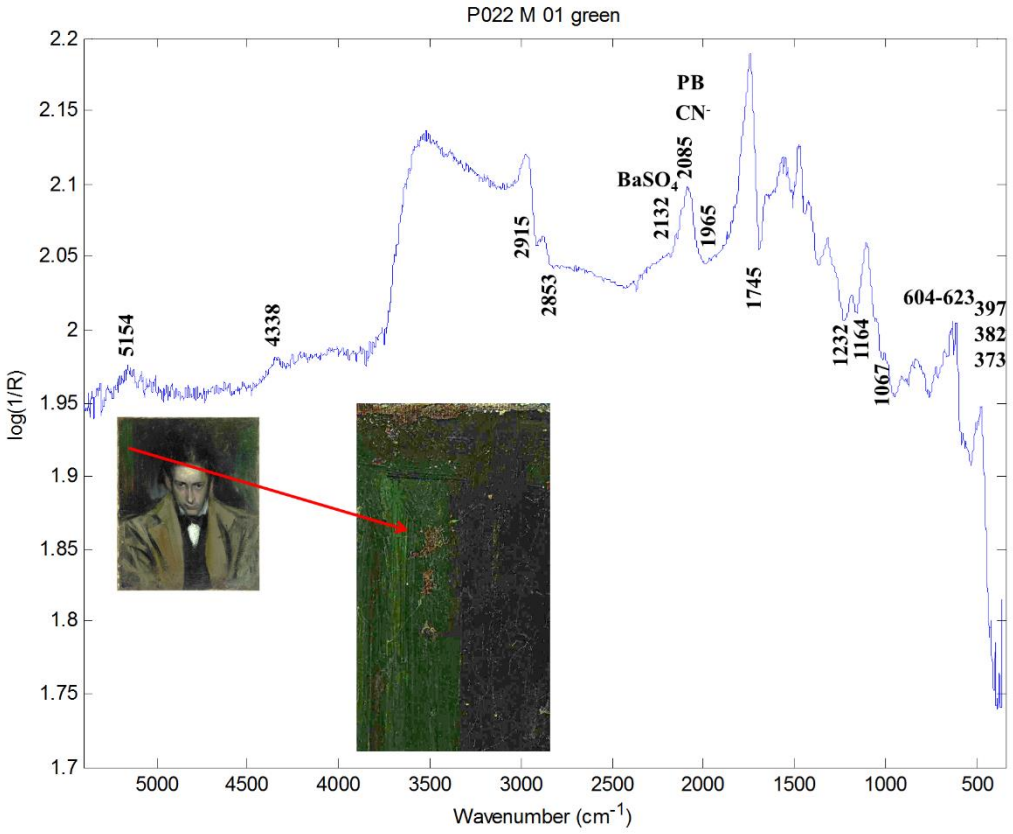

Figure 44. IR_spectrum_M01_green

Black Areas

In general, the spectra acquired in black areas are very noisy and difficult to interpret. In the mid-infrared spectrum **M_04_black** (Figure 45) the inverted band at about 1000 cm^{-1} is very difficult to assign to any element or compound. It could be related to a silicate-based pigment (Si-O stretching), or also to a phosphate indicating the possible presence of ivory black ($C+Ca_3(PO4)_2$), which normally is identified by a signal in the small band at about 2000cm^{-1} not visible in this case possibly due to the presence of the varnish. The further signals at lower wavenumbers may be assigned to Fe-oxides indicating the possible presence of a black iron based pigment, although the signal of Fe is not higher than those obtained in the brown-green area. All these possibilities cannot be excluded and finally no identification is achieved. The weak band at about 1320 cm^{-1} indicates oxalates. On XRF spectrum **X_09_black**, Pb (136 cps), Fe (47 cps), Ca (4 cps) and traces of Ba and Cr have been identified. The mid-infrared spectrum **M_05_black** is similar to the previous but with weaker signals at about 1000 cm^{-1}. The presence of Lead Carbonate and also oxalates is found[16]. The peak at 876 cm^{-1} indicates Calcium Carbonate. Looking at the elemental composition Fe appears as first or second element (counts values). This could support the hypothesis of a Fe-based black.

Different to the other black colours, the spectral signatures in spectrum **M_10_black** (on the waistcoat) are more similar to those of spectra acquired on the greens. Oxalates, Lead Carbonate and unidentified sharp bands at 560-600 cm^{-1} can be observed. The XRF results (**X_17_black**) indicate Pb (about 142 cps), Fe (27 cps), and traces of Ba, Cr. The signal of Ca (13 cps) is slightly higher than in the other black areas. On the other hand, the signal of Fe is lower and comparable with measurement on point **X_05_black** (Fe 32 cps) – near point **X_6_white** (forehead/dark side).

Table 25. XRF results for green-grey areas.

cps	Ca	Fe	Pb	Ba	Cr	Hg
E (keV)	**3.71**	**6.4**	Trace	**4.52**	**5.44**	**10.01**
P22_X_02_black	9	210	Trace	/	3	0
P22_X_05_black	5	32	128	Trace		2
P22_X_09_black	4	47	136	Trace		0
P22_X_17_black	13	27	142	Trace	/	2

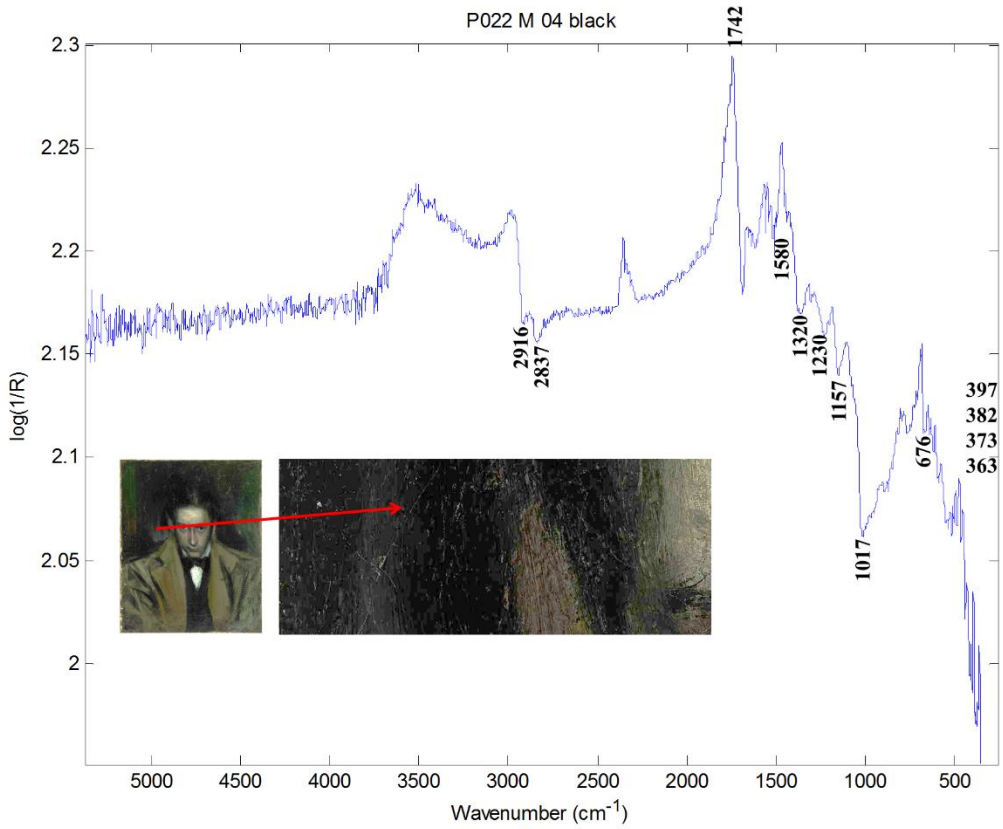

Figure 45. IR spectrum_M_04_black

Red Areas

The main elements found in the XRF spectra, which characterize the red/pink points (**X_07_red**, **X_08_pink**, **X_10_red**), are the Pb, Fe, Ca and Hg. No FTIR measurements were acquired on red areas because normally red pigments do not exhibit strong or characteristic absorption in the range of the mid IR. The signal of Fe is lower than other points across the painting. The signal seems to change on the pink point where the red is less intense. Traces of Cr, Ba and K are identified. The higher signal of mercury is an indication of Mercury Sulphide (HgS - Vermilion). The presence of Vermilion has been confirmed by UV-VIS reflectance measurements [8].

Table 26. XRF results for black areas.

cps	Ca	Fe	Pb	Hg	Hg
E (keV)	**3.71**	**6.4**	**10.55**	**10.01**	**11.86**
P22_X_07_red	5	19	152	6	3
P22_X_08_pink	3	6	150	3	0
P22_X_10_red	6	17	149	7	2

Summary

Figure 11 shows a mapping of the detected elements and compounds.

Figure 46. Mapping of the results obtained.

Interpretation

Pigments

White pigments

The white used is Lead white (mainly hydrocerussite). High signal of Pb (Figure 47a) has been obtained all across the painting, which suggest that it is also caused a layer lying underneath. Barium sulphate was also detected in the IR spectrum but a low concentration

found across the painting of the Ba (Figure 47b) and the punctual increase in a green area can be an indication of a component of different pigments (for example barium yellow). Calcium carbonate (Figure 47c) was detected mostly in the point localized near the edge of the painting; thus, it could be part of the original paint layer/preparation or is due to a possible restoration.

Black pigments

The results obtained with XRF and FTIR on the black areas have not been significant enough to identify the black pigment used. The absorption band of ivory black and bone black, which belong to calcium phosphate [$C + Ca_3(PO_4)_2$] appear in a IR spectrum acquired in reflectance mode as an inverted band at about 1000 cm^{-1}. However, the signal could also be related to a silicate-based pigment (Si-O stretching). The presence of ivory black is normally identified by observing the small band at about 2000 cm^{-1}, which does not appear in this case. It is important to bear in mind that its detection could be hindered by the presence of varnish on the painting surface. Fe-oxides indicating the possible use of a black iron based pigment and carbon black should not be excluded (Figure 47d). Finally, no identification has been achieved.

Red – brown pigments

Detection of Hg (Figure 47e) on the red areas (lips, eye and flesh on the cheek) indicates the use of Vermilion. Furthermore, this red pigment is used also in brown areas to obtain a more reddish shade. Considering the counts obtained for Fe (mean results 50 cps) on XRF spectra, Fe-based red pigments cannot be excluded in the brown areas.

Blue pigments

The presence of Prussian blue has been demonstrated.

Yellow/Green pigments

Barium and/or Strontium yellow and natural earths (e.g. Ochre) are pigments that could have been used to create the brown-grey-green colours. Considering the result of the spectrum acquired on the upper left side, the green shade was probably obtained with a mixture of Prussian blue, some barium sulphate and yellow pigment yellow (strontium yellow - $SrCrO_4$ or barium yellow - $BaCrO_4$ or Chrome yellow - $PbCrO_4$). Other green Cr-oxides based pigments could have been used on the green-brown areas. Chrome yellow and yellow ochre could be the reason for the brown-grey-green hue (Figure 47f).

Other inorganic compounds

Very weak signal of possible oxalate have been detected.

Organic compounds

A specific identification of the organic compound found is not possible due to the limitations of the technique, although the presence of lipid, proteins and wax seems possible.

Table 27. Pigments and Binding Media/organic compound analysis Results

Paint colour	Pigments	Binding medium/ organic compounds
White/ Preparation	White lead [a), b)], Barium sulphate [a), b)], Calcium carbonate* [a), b)]	lipid binder, wax*, proteins*[b)]
Black	(Ivory/bone black, Carbon black or Fe-based black pigment)	
Red - brown	Vermilion [a)], (Fe-based pigments – natural earths, Red lead)	
Blue	Prussian blue [a), b)]	
Yellow	(Barium yellow/Strontium, Fe-based pigment - Ochre, Chrome yellow)	
Green	Barium sulphate + Prussian blue + Chromates: Barium yellow/Strontium (Chrome oxides)	

a) XRF; b) mid-FTIR spectroscopy; *probably material used in previous restoration

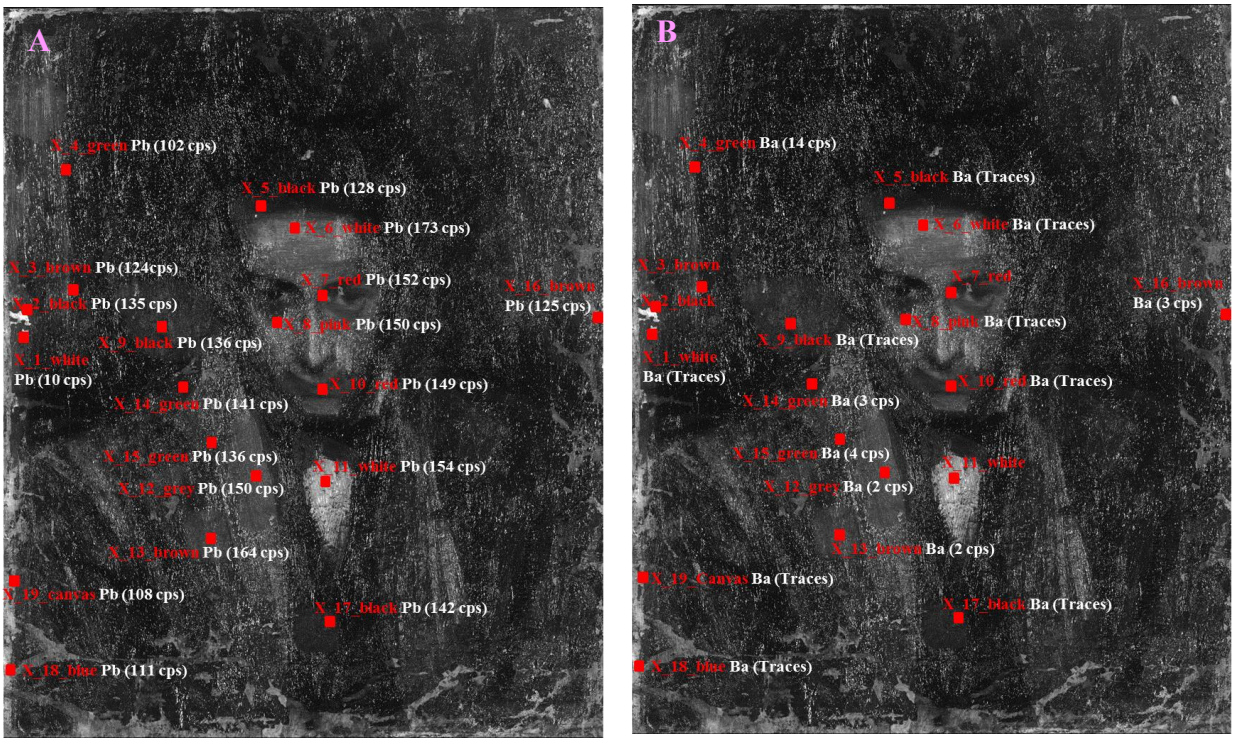

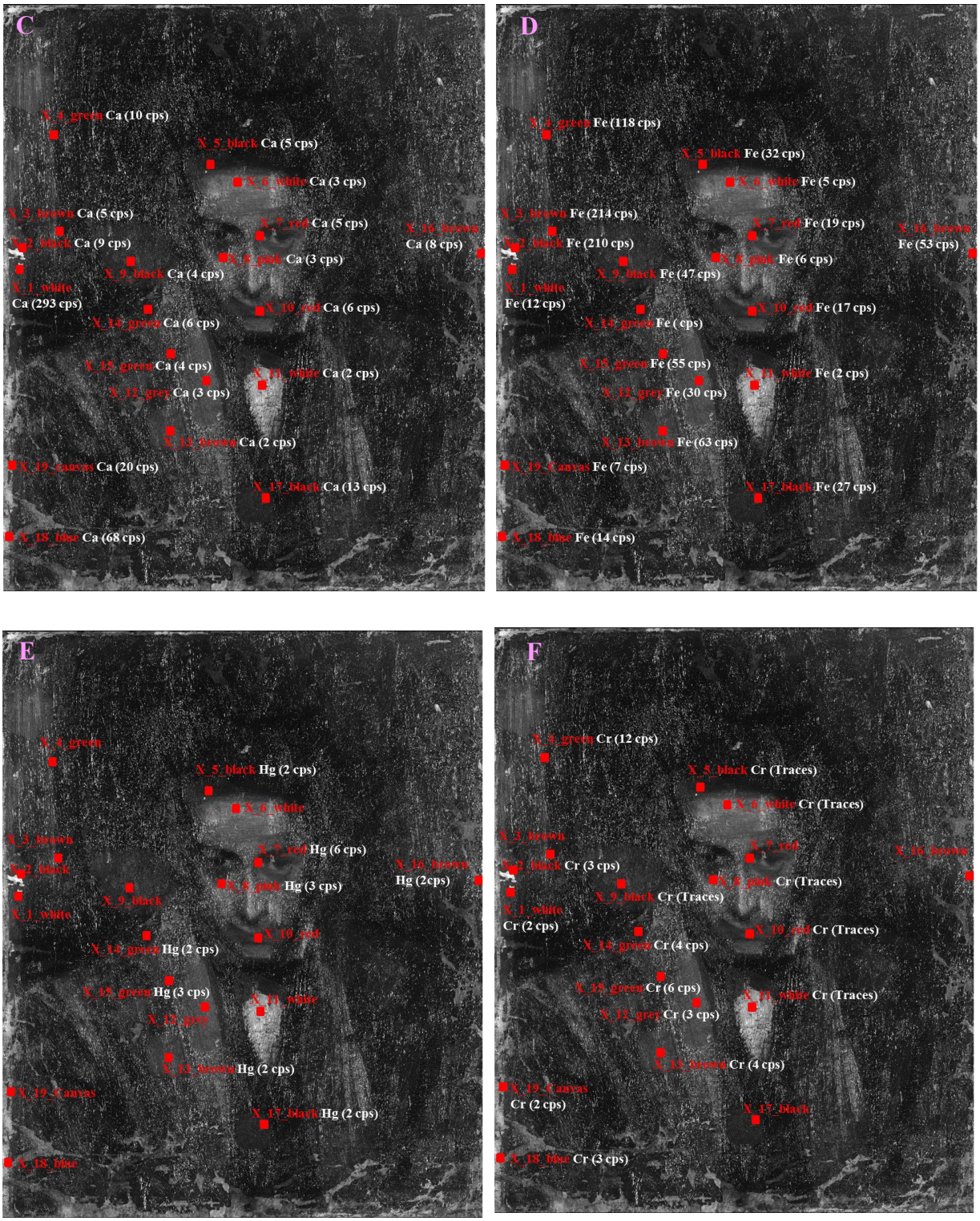

Figure 47. XRF mapping- element distribution and cps obtained: a) Pb, b) Ba, c) Ca, d) Fe, e) Hg, f) Cr.

Global discussion of the painting

Composition vs. Areas

Background

The dark area of the background includes White lead and Barium sulphate, which can be part of the subjacent layer, although it was not possible to identify the black/dark pigment/s used. The pigments comparable with the results obtained are Ivory/bone black, Carbon black and/or Fe-based black pigment with possible Chrome oxides or/and Chromates. The bright green areas on the left-hand side include Barium sulphate plus Prussian blue and a yellow pigment that could be Barium, Strontium and Chrome yellow

Subject

The brown-ochre-green jacket was painted with the same white compounds aforementioned plus Prussian blue and Vermilion and other pigments in accordance with the data obtained, such as Chrome/barium yellow, Fe-based pigments – natural-earth pigments or/and Chrome oxides. The visage of Casagemas includes also White lead and Barium sulphate plus Prussian blue, which is responsible of the cold colour/feeling, and Vermilion used for the reddish shade of the cheeks and lips. The presence of Fe-based red pigment and Red lead could not be excluded. The shirt was painted mainly with White lead, while the waistcoat presents black pigment/s, none of which could be identified. The possible candidates have been listed above.

Table 28. Pigments and organic compounds organised by areas. * possible restoration material.

Areas	Pigments	Binder/organic compound
Area related to the underneath layer (composition/preparation)	White lead + Calcium carbonate	
Dark background	White lead + Barium sulphate + Black pigm. (Ivory/bone black, Carbon black, Fe based black pigment) + (Cr oxides or Chromate)	Lipid, Animal glue, wax*
Green background (brush stroked near the edges)	White lead + Prussian blue + Barium sulphate Vermilion (Fe based pigments, Red lead)	
Face (Front/Lips, Cheek)	White lead + Prussian blue + Barium sulphate Vermilion (Fe based pigment, Red lead)	
Waistcoat	White lead + (Ivory/bone black, Carbon black, Fe based black pigment)	
Shirt	White lead	
Jacket	White lead + Barium sulphate + Prussian blue + Vermilion. (Barium/Strontium yellow, Fe based pigments – natural earths and/or Chrome oides)	

Stratigraphy

The limitation of the surface non-destructive techniques hinder the reconstruction of the stratigraphy. However, the information provided by the XR radiography, the reflectography and the XRF allows an approximation of the distribution of the materials in depth. It is interesting to focus on the relation between the XR, NIR and VIS images shown in Figure 48. These images present a "lacuna"/loss of material from the superficial layer of the upper part of the artwork. It was covered with dark material at the moment of the analysis campaign, probably applied during one of the three interventions in the past, and removed during the recent restoration. This fact permitted to get access to the layer underneath, i.e. to the first composition, which in this area presents an ochre shade. Comparing the VIS image with the radiography, one can see that in the XR image the area of the *lacuna* appears as a black area in the centre of well-defined brush strokes that present high XR absorption and a bright/white colour. These strokes are part of the strongly absorbing material (white areas) that cover a large part of the radiograph and are probably caused by White lead. This behaviour suggests that the white lead layer is overlying the composition underneath. The presence of this layer between the two compositions could be explained by the intention to separate them, is part of an intermediate composition or has to be considered as material of the portrait. The IR image shows the almost complete absorption of the IR radiation in both areas, *lacuna* and superficial paint layer. This behaviour means that there is no reflection of the radiation and could have two explanations. On the areas that surround the *lacuna,* the presence of the lead white layer as part of the superficial composition or as base may cause the absorption of the radiation before it could even be reflected by the material underneath. On the other hand, the areas of the lacuna appear black because the material of the first composition strongly absorb or because there is no preparation layer that permits reflection.

Based on this hypothetic structure, the stratigraphy, starting from the canvas, is composed by a first composition, which may or may not present a preparation layer. In this case the application of white lead plus calcium carbonate can be assumed. This composition is followed by a very thin layer of yellow-ochre, green and light blue hues, depending on the zone of the painting. Then, the presence of a heavy-metal-based paint layer (probably lead white according to the high concentration of Pb detected by XRF) has been identified. As mentioned before, this layer could be a separation between the first and the superficial compositions with the intention to hide the first or/and to prepare the surface to start a new painting, or it is part of the materials of the portrait.

This structure suggests that the detected elements might be part of the superficial composition and no information about the first composition has been achieved.

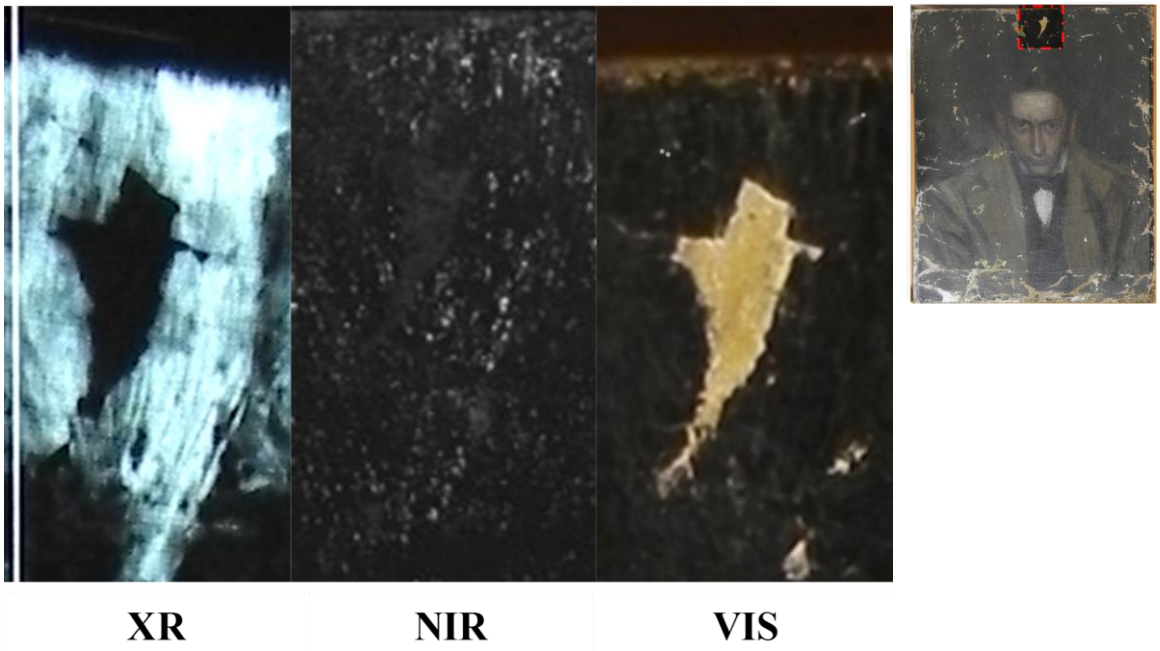

Figure 48. XR, NIR and VIS images of a detail/"lacuna" (upper part of the painting).

3.3.5 Retrat d'un desconegut a l'estil d'El Greco

Artwork's interest

The painting "***Retrat d'un desconegut a l'estil d'El Greco***" (**Portrait of an unknown man in the style of El Greco**) [MPB110.034] is an enigmatic representation of an unknown man in the centre of a dark background. The painting is portrait dated 1899 [52,53,55,56]. In the literature, it is one of the main artworks used to explain the importance of the influence that the painter Doménikus Theokópoulos, named "El Greco", had on Picasso's artistic style. Although Picasso had the chance to admire El Greco's works on several occasions, above all in Madrid during his visits to the Museo Nacional del Prado with his father, the main connection between him and the Greek artist is the friendship with Santiago Rusiñol[56]. Rusiñol, one of the artists of the *Els Quatre Gats,* had a strong passion for El Greco as precursor of the "Modernity", which he was able to spread to the nineteenth century unrest of Barcelona's artistic atmosphere.

The physiognomy of the character depicted in the *Retrat d'un desconegut a l'estil d'El Greco* is often presented as a revisit/reproduction of the "*El caballero de la mano en el pecho*" de El Greco dated ca. 1580 conserved at the Museo Nacional del Prado (Figure 49)[53,59]. The elongated and static face of the gentleman in El Greco's painting is presented in the Picasso version as a dynamic portrait where the paint strokes seem to stretch the visage of the character. As a matter of fact, the tuft of hair that in the *Gentleman* is short and has round limits, "melt" (extended) up to the half of the front head of the *Desconegut* ending with a triangular shape. All the features of the face are created with concave and light but precise brush strokes that make the portrait more dramatic. The proud and noble look of the El Greco gentleman seems to be lost in the Picasso subject, which is partially hidden in the dark background. Both are looking directly at the observer but the El Greco's original seems calm, while the man's look in Picasso portrait is focused and penetrating. Finally, the white collars, although completely different because of the artists' different epoch, fulfil the function to bring out the visages of both characters. In both cases, they appear as evanescent figures. The influence of the *El Greco*'s style is evident until Picasso's late production, although the interest in his art decreased over time and the references to his artworks acquired a caricature appearance[56].

Figure 49. Duelista, identificación de Doménikus Theokópoulos el Greco, focalización de Pablo Picasso (http://museosvirtuales.azc.uam.mx/picasso/index.php).

The Portrait of an *Unknown man in the style of El Greco* is dated 1899 and it is strictly connected with the *"Pablo Picasso. Retrato de Santiago Rusiñol caracterizado como El caballero de la mano en el pecho de El Greco, retratos de Josep Rocarol, algunos apuntes de Miquel Utrillo y otros croquis"* (Barcelona, 1899 - 1900, drawings on paper with mixed techniques, Museum Picasso of Barcelona – MPB110.683) (Figure 50a) and "*Personaje estilizado al estilo de El Greco*" (Barcelona, 1899, drawings on paper, private collection) where it is possible to observe different sketches of the same subject (Figure 50b - red dotted line). The artist marked this work with the signature "P. Ruiz Picasso", the signature used by the artist throughout 1900.

a)

b)

Figure 50. Pablo Picasso. a) "Personaje estilizado al estilo de El Greco", b) "Retrato de Santiago Rusiñol caracterizado como El caballero de la mano en el pecho de El Greco, retratos de Josep Rocarol, algunos apuntes de Miquel Utrillo y otros croquis" [58].

Description and interpretation of the painting layers structure

According to the documentation provided by the conservator Sra. Reyes Jimenez, relining was conducted at the Montjuïc studio in 1970. In July 2008, in some regions the paint has been consolidated and fixed, and the main retouches have been removed.

As described in the documentation, the canvas seems to be cut leaving irregular edges. Observing the upper corner on the right side of the painting it becomes clear that another composition lies underneath. The report of MPB highlights that the artist used broad and thin brush strokes to paint the superficial composition. The entire surface was varnished during the analysis campaign, but in some small areas the varnish was removed by the restorers to permit mid-FTIR measurements.

Direct observation – VIS

The composition underneath is clearly observable on the upper and lower corners of the right-hand side of the painting. Uniform areas of colours, with shades from white, ochre, light reddish to dark brown, were applied following a diagonal direction (Figure 51a - green dotted lines). Other irregular shapes are hidden in the dark background, and the colour of the subjacent layer can be observed through the decaying/crumbling paint or the transparency of the superficial layer. However, the subject of the underlying composition cannot be identified. The irregular but defined edges of the canvas suggest that the portrait was cut out and thus imply the possibility that it is a fragment of a larger work, which could hinder the interpretation of the composition underneath. It is not clear when the painting was cut. A detail that proves the minimal thickness of the composition underneath is the possibility to observe the canvas through the beard of the subject (Figure 51a- dotted yellow line).

Background

It is ambiguous if in this composition the character is coming out from the dark background or is sinking into it. The effect of the darkness is so strong that the right ear is not clearly visible. Instead, at the position of the ear one can see red strokes (Figure 51b) that are visible behind the black of the background: they could be part of the portrait hinting at the ear or simply belong to the composition underneath. Further details that are difficult to explain are the white brush stokes that continue from the original canvas to the new one.

a)

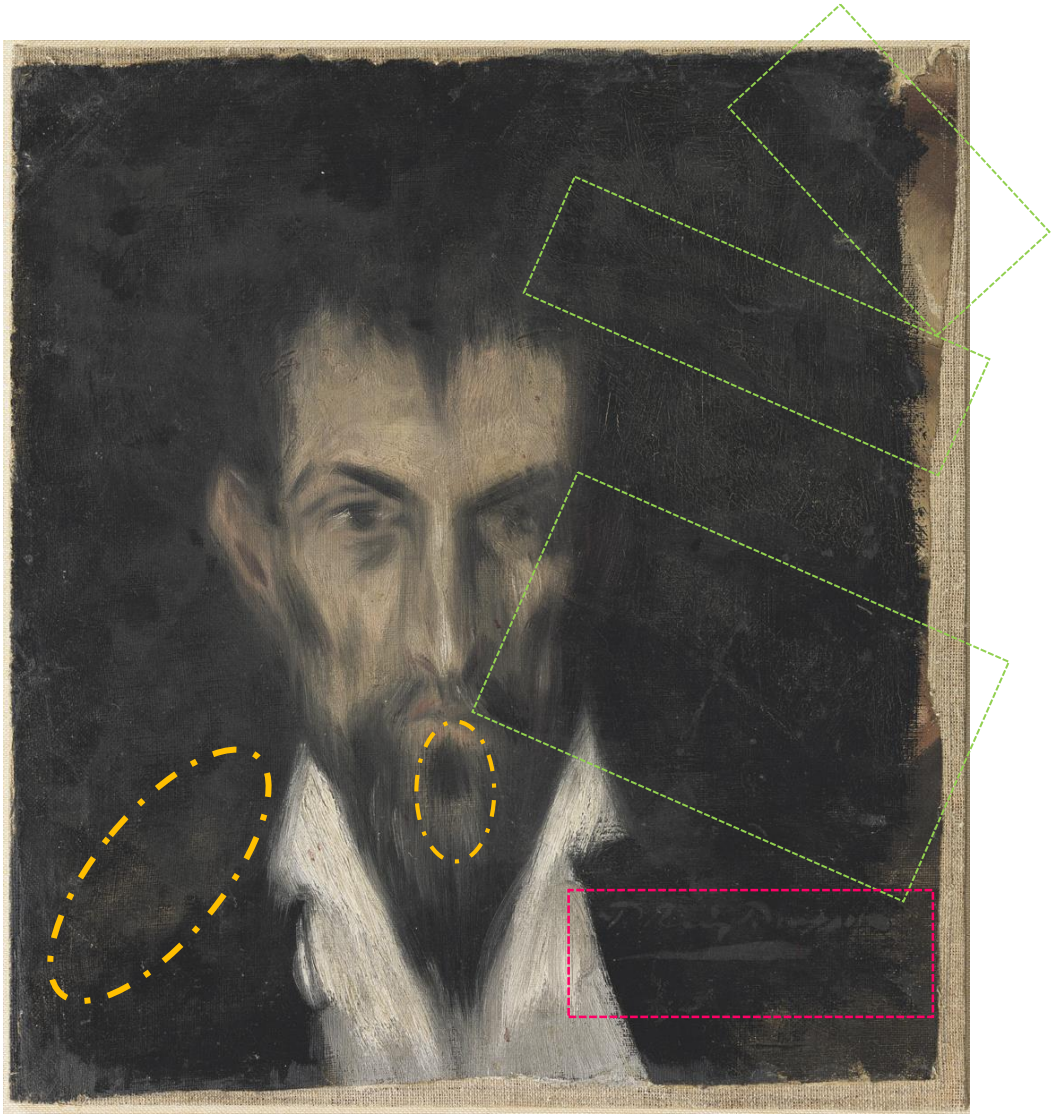

b)

Figure 51. a) VIS Image with marker lines that highlight the underneath composition; b) Details of the face of the character.

Picasso did not achieve a uniform background, and probably he was not trying to. In fact, the background shows patches of different shades. It seems as if these differences in colour could be related to the areas of the subjacent composition, which the black diluted paint is not able to cover uniformly, or they could simply be caused by the heterogeneity of the varnish used to cover and protect the painting at a later point of time.

Picasso signed this work in the inferior corner on the right side of the painting. The signature "*P. Ruiz Picasso*", a star-shape sign, the stripe, which underlines the signature, and other marks appear in a dark green-black hue, which can be observed in other areas of the background.

Subject

The artist depicts a man with a very expressive face in the centre of the canvas. He is dressed with a brilliant white shirt and a black jacket visible only in outlines/hardly distinguishable from the also black background. The elongated face of subject seems to be melting down. The paints used are not pure and tend to be smeared into each other. The hair, the face and the beard are painted with broad and faint strokes, while narrow touches are applied to mark the details of the face, such as eyebrows, eyelid, eye socket, lips, nose and the lines applied to sketch the left ear.

A more detailed/further study would be necessary to check the origin of the white strokes at the margin between shirt and jacket that come out from the original canvas and have left some marks on the relined canvas (Figure 51a, red box?). It is possible that the canvas was painted after it was cut off or simply retouched after being fixed on the canvas used for the relining.

Observation with no visible radiation - subjacent layers (XRR, IRR)

Radiography

As written in the documentation of the piece, two radiographies were done in July 1970, probably when the painting was relined, and one in June 2009 by SGS. Only a copy of one of the radiographies is available. It is a partial negative, not including the upper and lower parts, and its quality is not optimal.

In the RX image (Figure 52a), it is possible to distinguish the back side of a nude, probably a man, whose nape corresponds to the face of the unknown man depicted on the surface of the painting. The lack of parts of the arms and back suggests that the canvas is a fragment of a larger composition. The features of the body are well defined. The traits that the artist uses to represent the back of the man are very similar to those in the sketch titled "*Woman from the back*" dated 1902 (Figure 52b). This demonstrates the continuity between his later productions with the works of his early years. Despite this similarity, the subject seems to be part of the several academic drawings and sketches that Picasso created between 1894 and 1895 to study the human anatomy (Figure 52c).

It is interesting to notice that the absorption of the areas of the face observed in the XR image has a higher signal/absorption signal is more pronounced in the highlighted areas, e.g. the part of the beard close to the nose, than to the flesh zones.

Figure 52. a) RX image compared with b) Woman from the back, c/d) Nude study from Life and e) Oriental scene (image from *Picasso development of a genius* 1890-1904)[44].

IR Reflectography

Several NIR images were acquired. Figure 53 shows a contrasted IR reflectography at 2265 nm. The NIR images do not provide much information about the composition underneath, which may be because of the varnish on the surface and/or due to the presence of material that absorbs IR radiation in the black areas and highly reflecting materials on the white zones of the superficial composition. Only few lines/areas behind the face of the character are highlighted by the reflectography (Figure 53 – green dotted lines).

However, some of the traits not clearly observable in the VIS image are better visible, in particular, the lines that pass under the right eye and come out from the right side of the collar of the white shirt (Figure 53 – yellow dotted lines). The signature almost disappeared.

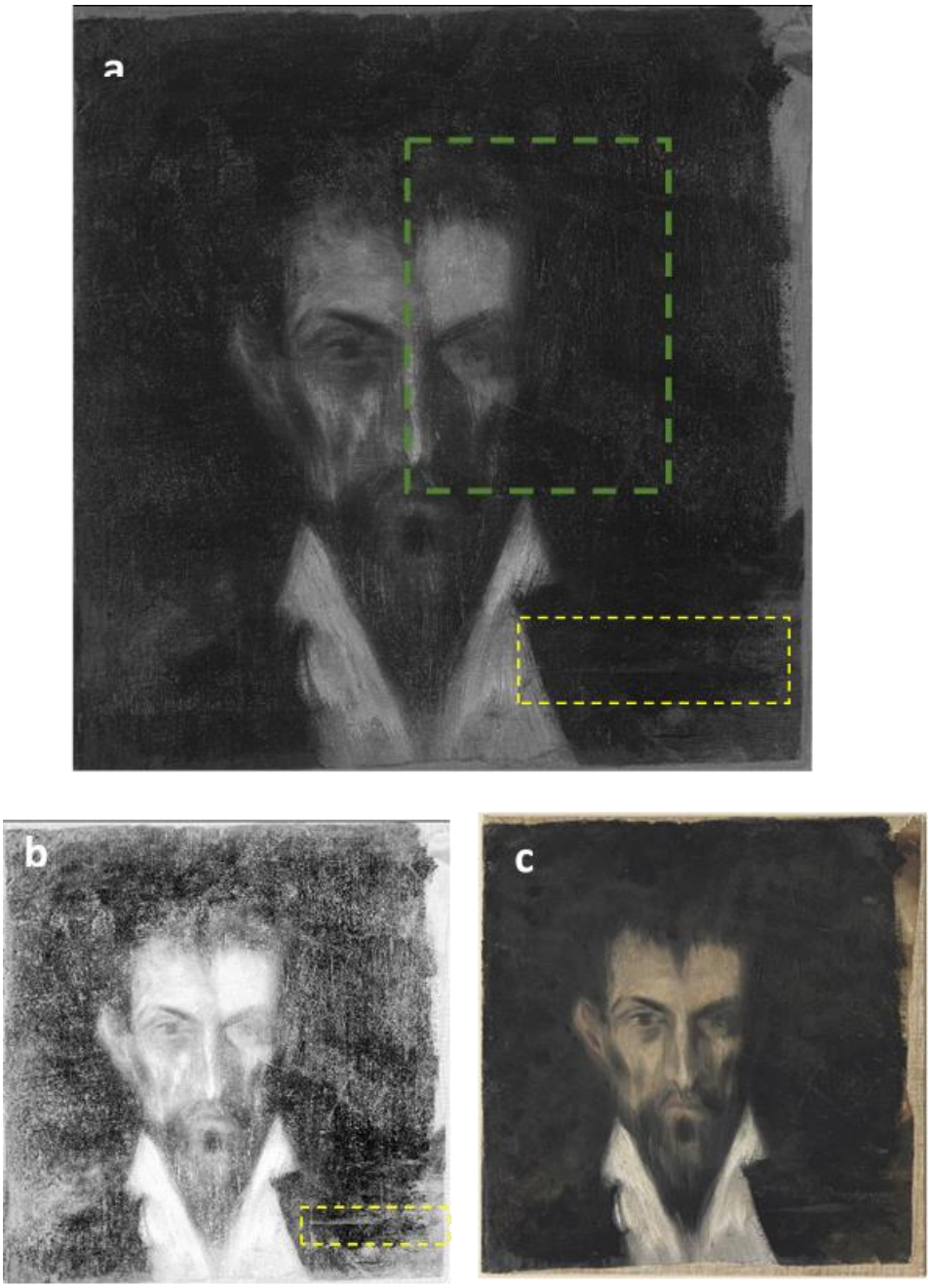

Figure 53. IR reflectography image acquired at 2265 nm a) NIR original b) NIR with contrast-enhanced and c) VIS image.

Description and interpretation of the materials

In Figure 54 the XRF (a) and mid-FTIR (b) measurement spot distributions are presented and the corresponding file names are reported in Table 29.

XRF MID-IR

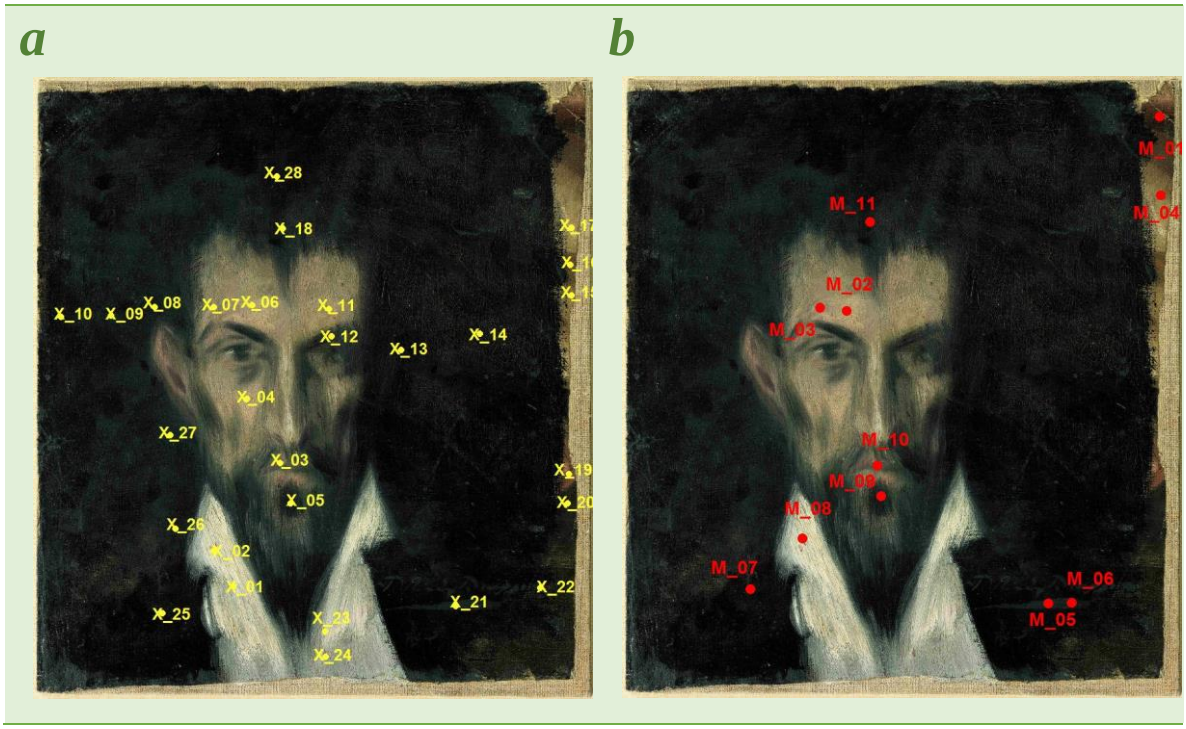

Figure 54. XRF (a) and mid-FTIR (b) measurements spot distribution.

Table 29. Spectrum/spot label for a) XRF and mid-FTIR are reported.

a) XRF spectrum/point label	b) mid-FTIR spectrum/point label
P034_X_01_white	P034_M_08_white
P034_X_02_red	
P034_X_03_red	P034_M_10_red
P034_X_04_flesh	
P034_X_05_black	P034_M_09_black
P034_X_06_flesh	P034_M_03_flesh
P034_X_07_flesh	P034_M_02_flesh
P034_X_08_black	
P034_X_09_black	
P034_X_10_black	
P034_X_11_flesh	
P034_X_12_black	
P034_X_13_black	
P034_X_14_black	
P034_X_15_black	
P034_X_16_brown	
P034_X_17_white	P034_M_04_beige
P034_X_18_black	P034_M_11_black
P034_X_19_red	P034_M_01_brown
P034_X_20_brown	
P034_X_21_signature	P034_M_05_black
P034_X_22_signature	P034_M_06_black
P034_X_23_white	
P034_X_24_red	
P034_X_25_black	P034_M_07_black
P034_X_26_black	
P034_X_27_black	
P034_X_28_black	

Description

White Areas

The mid-infrared spectrum **M_08_white** (Figure 55) has been acquired on the white-collar of the nightshirt of the subject. In the spectrum, it is possible to identify the inverted bands between 1200 and 1050 cm^{-1}, which correspond to the asymmetric stretching of SO_4^{2-}. The minimum at about 1054 cm^{-1} and the signals at 965, 626 and 596 cm^{-1} (ν4 sulphate asymmetric bending) reveal the presence of Lead Sulphate ($PbSO_4$ – *Anglesite* mineral). The Lead Carbonate has been detected (meanly hydrocerussite - $Pb(OH)_2$) due to the signal of the CO_3^{-2} at 665 (in-plane bending), 3534 (fundamental OH stretching) and doublet at about 4300 cm^{-1} (ν+δ OH). This signal is confirmed by the high Pb signal obtained by XRF on this area. The signals of a lipid binder can be observed at 1454 ,1630, 2954 and 2861 cm^{-1} that are due to the C–H bending of CH_2, C=C stretching of cis –CH=CH–, CH_3, C–H stretching of CH_3 and CH_2, respectively[60]. It is important to note that the carbonyl asymmetric stretching band of the lipid binder at 1745 cm^{-1} could be mistaken with the $\nu_1+\nu_3$ combination mode of the hydrocerussite. Thus, the presence of both compounds hinder the assignation of this band to a particular mode[26]. Four XRF measurements have been performed on the same area (Table 30). Two directly on the white paint (**X_01/X_23**) and the other two on the red spots/drops that are clearly observable on the collar (**X_02/X_24**). In this section we will focus on the elements that are of interest for identification of white pigments. The results obtained for these two measurements will be further discussed in the *red areas* section. The XRF spectra **X_ 01_white** and **X_23_white** are comparable. On both spots Pb (about 160 cps), Fe (2 cps) and traces of Ca and Mn have been detected. These results suggest the presence of White lead. Furthermore, the spectra **X_02_red** and **X_24_red** are very similar. It is interesting to observe that the signal of Ca increases and the Pb content slightly decreases in the points previously described. Also Ba has been detected in both spots. The **X_24_white** is the only point on the collar where a Zn signal has been detected. This limits the sensitivity of the instrument to this element and, thus, the signal could be under the detection limit of the technique. Otherwise, the low signal could be also attributed to the paint layer underneath. The elemental composition assessed on **X_17_white** spot is clearly different compared to the other white points. The spectrum has been recorded on the right-hand side of the painting, where the underneath composition comes out, in particular on a thin white brush stroke that was applied on a beige/ochre area. In this case, the Pb signal decreases drastically (23 cps), the Ca (75 cps) and Fe (14 cps) content increase and a very strong presence of Zn (252 cps) is detected. The Ca can probably be attributed to

the preparation layer and the presence of Fe to the ochre shade of the Fe oxide pigments under the stroke. Finally, the Zn signal it is probably caused by the use of a Zn oxide commonly labelled as Zinc White (ZnO). Traces of Ba, Mn and Cr have also been found. XRF results are presented in Table 30.

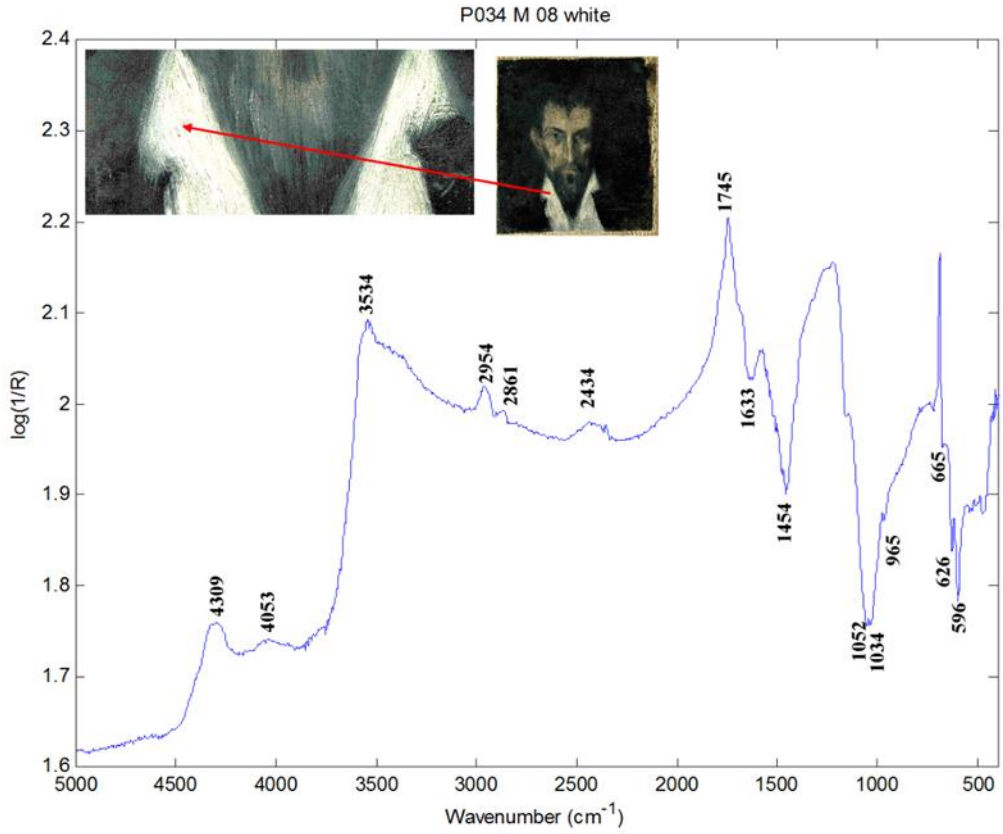

Figure 55. IR spectrum M_08_white.

Table 30. Summary of XRF results for white/grey areas. *Not Quatified.

cps	Ca	Pb	As	Hg	Zn	Cu	Fe	Cr	Ba	Mn
E (keV)	**3.71**	**10.55**	**11.74**	**9.97**	**8.65**	**8.04**	**6.4**	**5.44**	**4.52**	**5.95**
P034_X_01_white	1	165	/	/	/	/	2	/	/	/
P034_X_23_white	1	161	/	/	/	/	2	/	/	Traces
P034_X_02_red	3	151	/	/	/	/	2	/	2	/
P034_X_24_red	4	154	/	/	N.Q.*	/	4	/	4	/
P034_X_17_white	75	23	/	/	252	/	14	1	1	Traces

Signature areas

The spectra acquired on the signature on the right corner of the painting will be discussed in this separate section. Although the label assigned to the four points analysed suggest a black colour, after a more accurate exam of the paint layer, this can be described as dark green-

black. The mid-IR spectrum **M_05_black** (Figure 56) and **M_06_black** show a weak signal at 2015 cm^{-1} and a signal at about 1030 cm^{-1} (PO_4^{-3}) characteristic of the Hydroxyapatite ($C+Ca_3(PO4)_2$ - Ivory Black). A weak signal of Lead Carbonate at about 1370 cm^{-1} can be identified. The inverted bands in the range between 1740 and 1450 cm^{-1} could be attributed to a protein. The bands detected can be assigned to C=O stretching due to a lipid component (1735 cm^{-1}), a C=O stretching of amide (amide I at 1668 cm^{-1}); N–H bending of amide (amide II at 1563 cm^{-1}); C–H bending (1469 cm^{-1}) and C–O bending of an esteric bond of the proteinaceous material [10]. It is important to keep in mind that the IR bands here described are affected by distortions and some of the assignation can be difficult due to slightly shifted wavenumbers. The presence of a proteinaceous material could be related to the relining process, which involved animal glue. The bands at low wavenumbers are the same as found in spectrum **M_08_white** and can be attributed to Lead Sulphate. Thus, it seems possible that the signature was white at first and was then coloured with the black of the background. Both spectra (**M_05/06**) have been recorded close to each other on the trace/brush stroke that Picasso used often to underline his signature/name. Two XRF measurements have been performed on the signature, one on the trace near to point **M_05/M_6** (**X_21_signature**) and the second one on the "*o*", the last character of the name (**X_22_signature).** The elemental compositions encountered on both spots are comparable and the detected elements are Pb (84/72 cps), Zn (61/77 cps), Fe (54/50 cps), Ca (9/8 cps) and traces of Mn (Table 31).

Black Areas

In mid-infrared spectrum **M_07_Black** (**Errore. L'autoriferimento non è valido per un segnalibro.**), recorded on the black shoulder of the subject's jacket, bands characteristic of Hydroxyapatite have been detected. The weak signal at 2085 cm^{-1} could be attributed to the CN^- stretching characteristic of Iron hexacyanoferrate (Prussian blue), although the assignation is not clear. The two signals at 626−627 and 597 cm^{-1} suggest the presence of Lead Sulphate as in the spectra **M_08_white** [11]. A weak band at 2518 cm^{-1} permits to identify Calcium Carbonate ($CaCO_3$ - Signal at 2594 and 2518 cm^{-1} corresponds to the overtone $\nu_1+\nu_3$). The XRF spectrum **X_25_black** corresponds to the area of the jacket. On this point Zn (168 cps), Pb (39 cps), Ca (59 cps), Fe (24 cps) and traces of Cr and Ba have been detected. The same interpretation of the spectrum **M_07** can be considered for spectrum **M_11_black.**

The mid-infrared **M_09_black** was acquired on the beard of the subject, below the lower lip. The signal of Hydroxyapatite is clear while the presence of Hexacyanoferrate cannot be confirmed. The weak band at about 1360 cm^{-1} could be related to Lead Carbonate. The XRF

spectrum **X_05_black** was acquired on the same area as point **M_09**. The detected elements are Pb (92 cps), Zn (68 cps), Fe (12 cps) and Ca (11 cps). The investigated spot is located on the hair of the subject, close to his front. These two spectra suggest the use of the same black paint to finish the face details. The corresponding XRF spectrum **X_18_black** shows the presence of Zn (399 cps), Pb (68 cps), Fe (20 cps), Ca (11 cps) and traces of Cr.

These signals could be related with the presence of Prussian blue in the black paint together with the information coming from the composition underneath. Fe is a possible indication of Natural earths and Pb of the White lead. The Zn signal may possibly originate from the white located in the upper layer. The other measurements on the background were performed with the intention to trace the distribution of the Zinc across the painting associated with greyish areas. Detailed discussion on the distribution across the surface and in depth of the elements will be presented in the stratigraphy section. The Ca detected in high concentrations could be attributed to the preparation layer, or could be part of the Ivory/bone black pigment. The high count values for Pb in spectra **X_12/X_13, X_8/X_9** and **X_27/X_28** suggest the presence of Lead White, probably of the subjacent layer based on the XR image inspection, although the same element is part of the Lead Sulphate compound also detected by mid-infrared spectroscopy. As very high concentrations of Zn have been detected the use of Zinc White can be confirmed. In particular, it interesting to mention that this type of white frequently occurs in oil paints mixed with lead white, barium sulphate, or titanium dioxide to improve the hiding power or as a lightening agent in colour tube pigments added by the manufacturers [12]. The drastic decrease of Pb when Zn signal increases suggests a relation of the two elements. One of the possible explanations for this behaviour is a difference in the distribution in depth of the two elements.

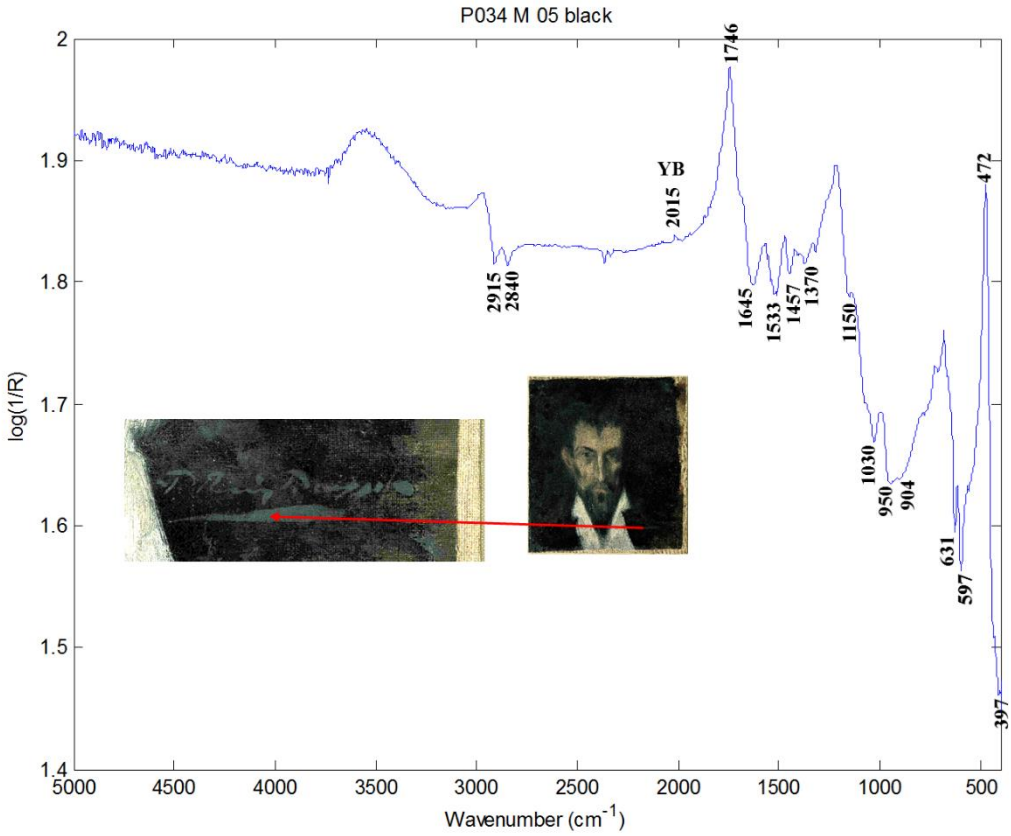

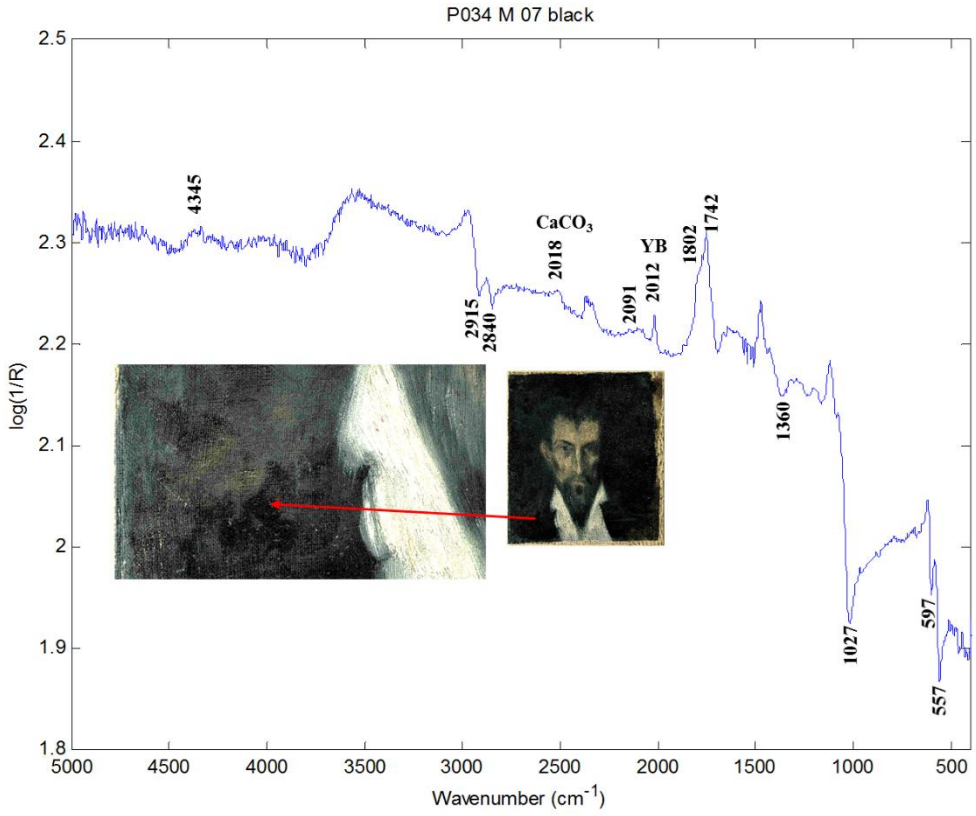

Figure 56. IR spectra M_05_black and M_07_black.

Table 31. XRF results for black/signature areas.

cps	Ca	Pb	As	Hg	Zn	Cu	Fe	Cr	Ba	Mn
E (keV)	**3.71**	**10.55**	**11.74**	**9.97**	**8.65**	**8.04**	**6.4**	**5.44**	**4.52**	**5.95**
P034_X_21_signature	9	84	/	/	61	/	54	/	/	Traces
P034_X_22_signature	8	72	/	/	77	/	50	/	/	Traces
P034_X_05_black	11	92	/	/	68	/	12	/	/	/
P034_X_18_black	11	68	/	/	399	/	20	Traces	/	/
P034_X_25_black	59	39	/	/	168	/	24	Traces	Traces	/
P034_X_08_black	16	125	/	3	34	N.Q.	18	Traces	/	Traces
P034_X_09_black	15	118	/	2	34	N.Q.	18	Traces	/	Traces
P034_X_10_black	23	99	/	/	73	/	29	Traces	/	Traces
P034_X_12_black	8	164	/	/	/	/	6	Traces	/	Traces
P034_X_13_black	8	152	/	2	N.Q.	/	6	/	/	/
P034_X_14_black	31	37	/	/	427	/	23	Traces	Traces	Traces
P034_X_26_black	31	49	/	/	139	/	22	Traces	Traces	/
P034_X_27_black	17	101	/	2	80	/	29	Traces	Traces	Traces
P034_X_28_black	30	131	/	/	25	6	17	Traces	/	Traces

Brown-beige areas

The brown-beige area belongs to the first composition that is not covered by the portrait. The mid-infrared spectrum **M_01_brown** shows the presence Kaolin (Si-O stretching mode at 1000 cm^{-1}, OH stretching at 3600 cm^{-1}), Lead carbonate and a weak signal of Calcium Carbonate. The signals of lipid and protein are detected. The same bands are present in the mid-infrared spectrum **M_04_beige (**Figure 57), apart from stronger signals of Lead carbonate. The content of more Lead white explains the lighter hue of the colour. The XRF spectra **X_15_brown**, **X_16_brown** and **X_20_brown** acquired on the first composition on the right-hand side of the painting, show a similar composition. Differences can be found in the increase of the Zn count values and the decrease of the Pb signal. The high values of Fe suggest the presence of Fe oxide, which together with the Kaolin was detected by mid-infrared, and thus indicates the presence of Natural earths. The signal of Ca and Ba could be related with the preparation layer. Cr-based pigment can also be confirmed. The Zn present in these areas can possibly be related to the paint that the artist seems to have applied extensively on the background of the portrait, which was smeared over the first composition.

Table 4. Summary of XRF results for brown/beige areas.

cps	Ca	Pb	As	Hg	Zn	Cu	Fe	Cr	Ba	Mn
E (keV)	**3.71**	**10.55**	**11.74**	**9.97**	**8.65**	**8.04**	**6.4**	**5.44**	**4.52**	**5.95**
P034_X_15_brown	11	66	/	/	419	0	19	1	1	/
P034_X_16_brown	8	11	/	/	468	0	51	8	2	/
P034_X_20_brown	8	54	/	/	246	0	78	11	4	/

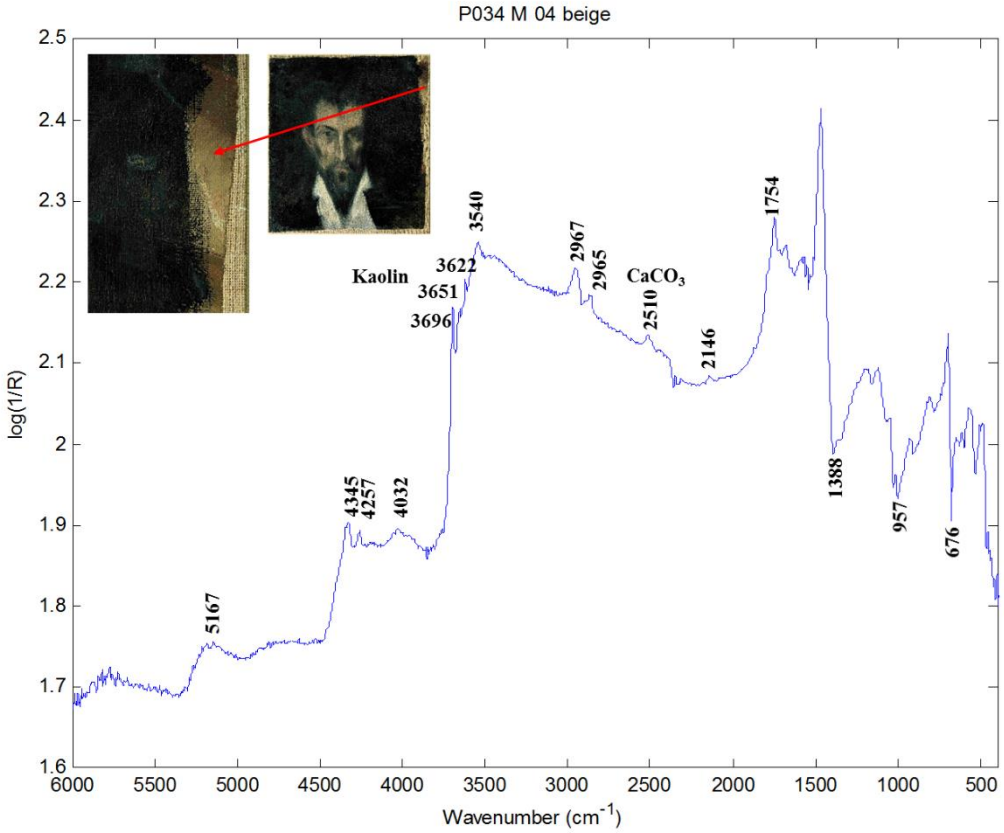

Figure 57. IR spectrum M_04_beige

Red/pink areas

The mid-infrared spectrum **M_02_flesh** has been acquired on the forehead of the character. The spectra present mostly the signals of Lead Carbonate and a weak signal of Hydroxyapatite. The signals detected for **M_03_flesh** are same as of **M_02**, although Hydroxyapatite is stronger.

Thus, the black pigment used for the shadows of the face is possibly Ivory black. The XRF spectra **X_06_flesh/07_flesh/11_flesh/02_red/03_red/04_flesh** and **24_red** acquired on the face and the collar present comparable compositions.

The signal of Ca and traces of Mn are probably related to the Ivory black pigment. The discrete presence of Fe is an indication of Fe oxide due to the use of some Natural earths,

and the Hg is an evidence of the use of Vermilion for the red shades of the flesh. The high signal of Pb is related to the Lead White and the probable presence of Red lead. The mid-infrared spectrum **M_10_red** shows the signals characteristic of Lead Carbonate and Hydroxyapatite. The detection of Hg and Fe (**X_3_red**) permits to confirm the use of Vermilion and a Fe-based pigment to obtain the reddish colors of the lips. The presence of Red lead cannot be excluded. Although, due to the variable concentration of Fe and the low signal for Hg (red areas) it is probable that another red compatible with the elemental composition, e. g. Red lead, was used.

Table 4. XRF results for red areas.

	Ca	**Pb**	**As**	**Hg**	**Zn**	**Cu**	**Fe**	**Cr**	**Ba**	**Mn**
E (keV)	**3.71**	**10.55**	**11.74**	**9.97**	**8.65**	**8.04**	**6.4**	**5.44**	**4.52**	**5.95**
P034_X_06_flesh	2	135	/	3	79	/	6	1	/	traces
P034_X_07_flesh	3	159	/	4	29	/	6	/	/	traces
P034_X_11_flesh	3	166	/	4	/	/	5	traces	/	traces
P034_X_02_red	3	151	/	/	/	/	2	/	2	/
P034_X_03_red	4	119	/	4	51	/	9	/	/	/
P034_X_04_flesh	2	150	/	3	/	/	4	/	/	/
P034_X_24_red	4	154	/	/	N.Q.	/	4	/	4	/
P034_X_19_red	7	117	6	4	60	52	56	/	/	/

Summary

Figure 58 shows a mapping of the elements and compounds detected.

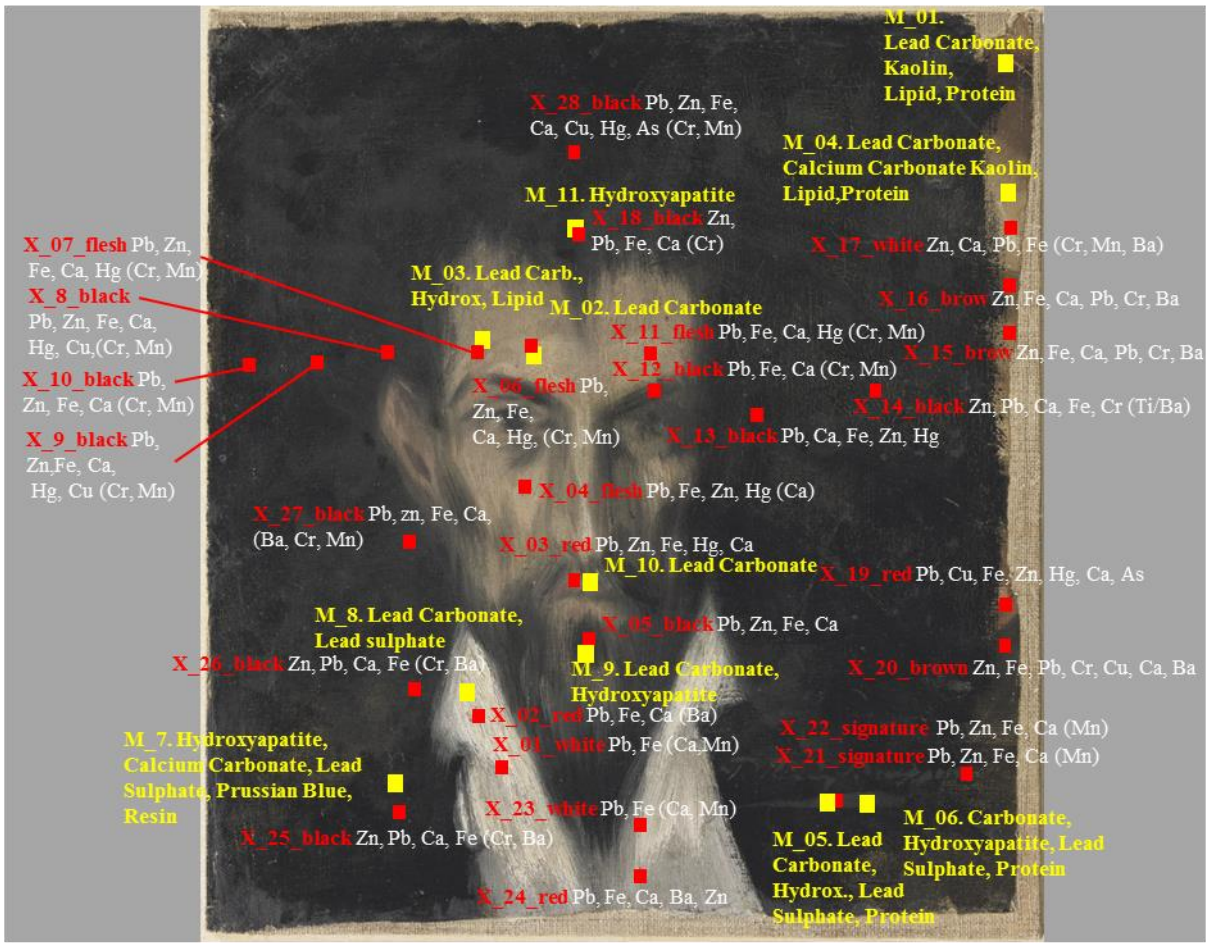

Figure 58. Mapping of the results obtained.

Interpretation

Pigments

White pigments

The use of Lead white has been confirmed by the mid-infrared measurements where the main signal was due to the Hydrocerrussite component (Figure 59a). Lead sulphate has been also found on the jacket, collar and signature but its origin could not be established. It could be a filler or impurity of the Zinc white used [61]. Its presence has been confirmed by XRF and its distribution is presented in Figure 59b. In particular, it frequently occurs in oil paints mixed with lead white, barium sulphate, or titanium dioxide to improve the hiding power or as a lightening agent in coloured tube pigments added by the manufacturers[22]. The use of zinc white in paintings is known to date not before the end of the 18th century. After the

industrial production based on the process elaborated by Leclaire (also known as the French – or indirect – process), the use of this pigment increased and it rapidly replaced the poisonous lead white [62].

The signals of Calcium Carbonate could be considered part of the Ivory black or/and the preparation layer (Figure 59c), if present. The O-H stretching characteristic of the Kaolin has been detected in brown and beige areas. The Kaolin is usually a filler of natural pigment such as yellow or brown earth or Fe-oxide based pigments. The presence of low content of Ba could suggest the presence of an accessory compound of some pigment (Figure 59d).

Black pigments

Ivory/bone black has been detected in the black areas by IR and corroborate with high Ca signal by XRF. On some dark areas, traces of Mn were detected by XRF, possibly due to addition of MnO_2 to some other pigment (Figure 59e). The Ivory/bone black contains commonly about 10% carbon, 84% calcium phosphate and 6% calcium carbonate, that means the part of the signal detected for Ca are due to its presence The high signal of Fe on the black areas could be related to Fe-based black pigment (Figure 59f). The presence of Carbon black pigments cannot be excluded.

Red – brown pigments

Detection of Hg (Figure 59g) on the red/pink areas of the face indicates the use of Vermilion (HgS). This element has been found in other areas but a clear relation with the paint layer could not be established. This red pigment is used also in brown areas to obtain a more reddish shade. Considering the counts obtained for Fe element (mean results 60 cps) on XRF spectra, the use of red pigments based on Fe-oxide should not in the brown areas. Ochres are variably coloured roks and soils primarly composed of oxides and hydroxides of iron. Such ochres can be very pure, but more typically contain other minerals such as quarz, clays, gypsum, micas, and kaolin. Thus, due to the strong signal of Fe on the brown-beige areas and the detection by mid-infrared of Kaolin in the same areas the use of yellow/brown ochre can be confirmed[63]. Based on the high Pb signal the presence of Red lead seems possible.

Blue pigment

Very weak signals of Prussian blue have been detected by mid-infrared measurements on the black areas.

Green pigments

The presence of As associated with Cu (Figure 59h) suggests the use of a copper arsenate pigment, namely Scheele's green or emerald green[20], although its presence is not confirmed. Due to the numerous possible formula to which those names can be associated, only a vague identification of the compounds can be offered based solely on XRF results.

Yellow pigments

As explained in red-brown section, yellow ochre may be present. The presence of traces of Cr (Figure 59i) could be an indication for the use of some Cr oxide.

Organic compounds

Based on the mid-infrared results a Lipid binder can be confirmed. Moreover, signals of a Resin attributed to the presence of varnish have been detected. Finally, signals of Proteins suggest that the animal glue used during the restoration process has migrate from the verso directly on the surface of the painting.

A summary of the pigment and organic compounds is presented in Table 32.

Table 32. Pigments and Binding Media/organic compound.

Colours	**Materials/Pigments**	**Binding medium/ organic compounds**
Preparation	Calcium carbonate + Lead White (Barium sulphate)	Lipid, Resin, Animal glue [b)]
White	Zinc White [a)], Lead Carbonate [a,b)], Lead Sulphate [b)], Calcium Carbonate [a,b)]	
Black	Bone/Ivory black [b)], (Iron oxide based pigments, Carbon black, Mn oxides)	
Blue	Prussian Blue [b)]	
Yellow	Yellow ochre with Kaolin [b)]	
Green	Cu based pigment (Chrome oxides)	
Red – brown	Vermilion [a,b,c)], Brown Earth/ Iron oxide based pigments + Kaolin [b)] (Red lead)	

a) XRF; b) mid-FTIR spectroscopy; c) Raman.

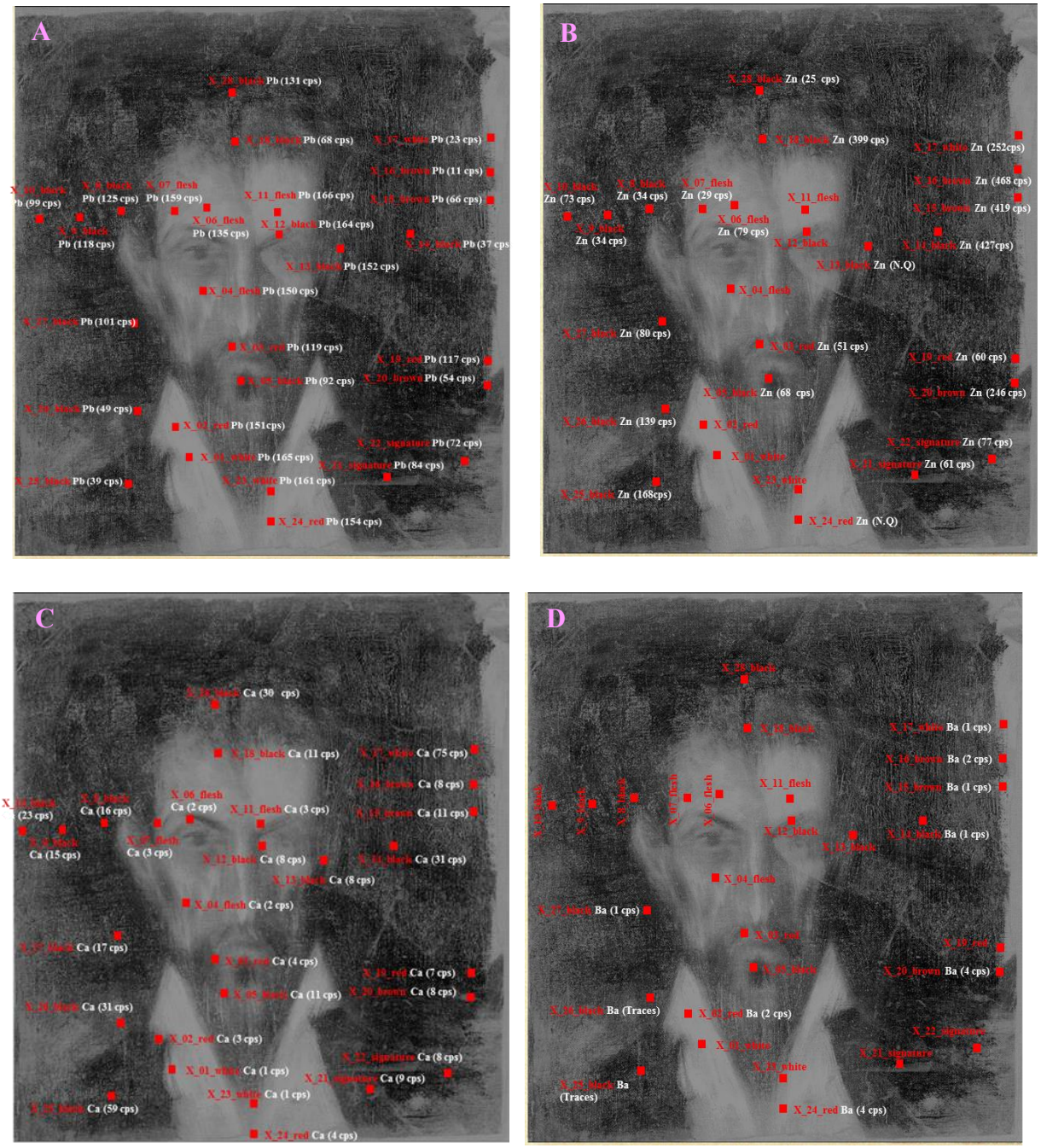
A
X_28_black Pb (131 cps)
X_18_black Pb (68 cps)
X_27_white Pb (23 cps)
X_16_brown Pb (11 cps)
X_07_flesh Pb (159 cps)
X_11_flesh Pb (166 cps)
X_15_brown Pb (66 cps)
X_06_flesh Pb (135 cps)
X_12_black Pb (164 cps)
X_09_black Pb (118 cps)
X_13_black Pb (152 cps)
X_04_flesh Pb (150 cps)
X_03_red Pb (119 cps)
X_19_red Pb (117 cps)
X_20_brown Pb (54 cps)
X_02_red Pb (151cps)
X_22_signature Pb (72 cps)
X_01_white Pb (165 cps)
X_21_signature Pb (84 cps)
X_25_black Pb (39 cps)
X_23_white Pb (161 cps)
X_24_red Pb (154 cps)
B
X_28_black Zn (25 cps)
X_18_black Zn (399 cps)
X_27_white Zn (252cps)
X_16_brown Zn (468 cps)
X_15_brown Zn (419 cps)
X_07_flesh Zn (29 cps)
X_11_flesh
X_06_flesh Zn (79 cps)
X_13_black Zn (N.Q)
X_14_black Zn (427cps)
X_04_flesh
X_03_red Zn (51 cps)
X_19_red Zn (60 cps)
X_20_brown Zn (246 cps)
X_02_red
X_01_white
X_22_signature Zn (77 cps)
X_21_signature Zn (61 cps)
X_23_white
X_24_red Zn (N.Q)
C
X_28_black Ca (30 cps)
X_18_black Ca (11 cps)
X_27_white Ca (75 cps)
X_16_brown Ca (8 cps)
X_09_black Ca (16 cps)
X_06_flesh Ca (2 cps)
X_11_flesh Ca (3 cps)
X_15_brown Ca (11 cps)
X_07_flesh Ca (3 cps)
X_12_black Ca (8 cps)
X_14_black Ca (31 cps)
X_13_black Ca (8 cps)
X_04_flesh Ca (2 cps)
X_03_red Ca (4 cps)
X_19_red Ca (7 cps)
X_05_black Ca (11 cps)
X_20_brown Ca (8 cps)
X_02_red Ca (3 cps)
X_22_signature Ca (8 cps)
X_01_white Ca (1 cps)
X_21_signature Ca (9 cps)
X_23_white Ca (1 cps)
X_24_red Ca (4 cps)
D
X_28_black
X_18_black
X_27_white Ba (1 cps)
X_16_brown Ba (2 cps)
X_15_brown Ba (1 cps)
X_11_flesh
X_12_black
X_14_black Ba (1 cps)
X_04_flesh
X_03_red
X_19_red
X_05_black
X_20_brown Ba (4 cps)
X_02_red Ba (2 cps)
X_01_white
X_22_signature
X_21_signature
X_23_white
X_24_red Ba (4 cps)

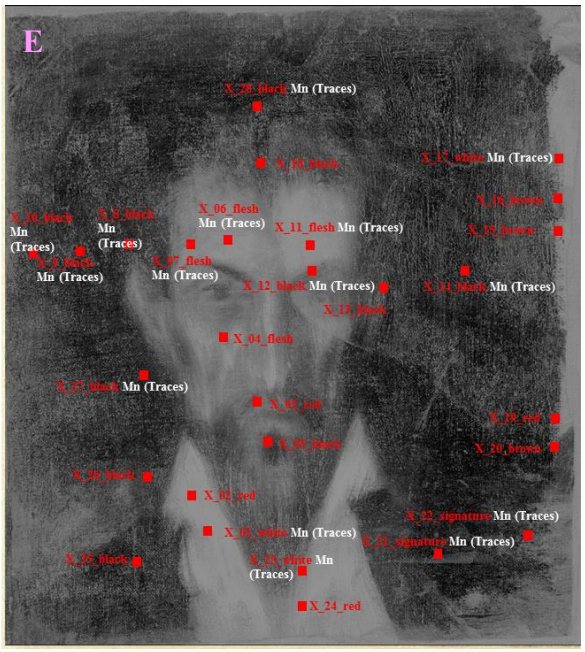
E
X_28_black Mn (Traces)
X_18_black
X_17_white Mn (Traces)
X_16_brown
X_10_black Mn (Traces)
X_9_black Mn (Traces)
X_06_flesh Mn (Traces)
X_11_flesh Mn (Traces)
X_15_brown
X_8_black Mn (Traces)
X_07_flesh Mn (Traces)
X_12_black Mn (Traces)
X_14_black Mn (Traces)
X_13_black
X_04_flesh
X_27_black Mn (Traces)
X_03_red
X_19_red
X_05_black
X_20_brown
X_26_black
X_02_red
X_22_signature Mn (Traces)
X_01_white Mn (Traces)
X_21_signature Mn (Traces)
X_25_black
X_23_white Mn (Traces)
X_24_red


F
X_28_black Fe (17 cps)
X_18_black Fe (20 cps)
X_17_white Fe (14 cps)
X_16_brown Fe (51 cps)
X_10_black Fe (29 cps)
X_9_black Fe (18 cps)
X_8_black Fe (18 cps)
X_07_flesh Fe (6 cps)
X_06_flesh Fe (6 cps)
X_11_flesh Fe (5 cps)
X_15_brown Fe (19 cps)
X_12_black Fe (6 cps)
X_14_black Fe (23 cps)
X_13_black Fe (6 cps)
X_04_flesh Fe (4 cps)
X_27_black Fe (29 cps)
X_03_red Fe (9 cps)
X_19_red Fe (56 cps)
X_05_black Fe (12 cps)
X_20_brown Fe (78 cps)
X_26_black Fe (22 cps)
X_02_red Fe (2 cps)
X_22_signature Fe (50 cps)
X_01_white Fe (2 cps)
X_21_signature Fe (54 cps)
X_25_black Fe (24 cps)
X_23_white Fe (2 cps)
X_24_red Fe (4 cps)


G
X_28_black Hg (N.Q)
X_18_black
X_17_white
X_16_brown
X_8_black Hg (3 cps)
X_06_flesh Hg (3 cps)
X_11_flesh Hg (4 cps)
X_15_brown
X_9_black Hg (2 cps)
X_07_flesh Hg (4 cps)
X_12_black
X_14_black
X_13_black Hg (2 cps)
X_04_flesh Hg (3 cps)
X_27_black Hg (2 cps)
X_03_red Hg (4 cps)
X_19_red Hg (4 cps)
X_05_black
X_20_brown
X_26_black
X_02_red
X_22_signature
X_01_white
X_21_signature
X_25_black
X_23_white
X_24_red Hg (N.Q.)


H
X_28_black Cu (6 cps)
X_18_black
X_17_white
X_16_brown
X_8_black Cu (N.Q.)
X_9_black Cu (N.Q.)
X_07_flesh
X_06_flesh
X_11_flesh
X_15_brown
X_12_black
X_14_black
X_13_black
X_04_flesh
X_27_black
X_03_red
X_19_red Cu (52 cps)
X_05_black
X_20_brown
X_26_black
X_02_red
X_22_signature
X_01_white
X_21_signature
X_25_white
X_24_red

Figure 59. XRF mapping- element distribution and cps obtained: a) Pb, b) Zn, c) Ca, d) Ba, e) Mn, f) Fe, g) Hg, h), Cu, i) Cr.

Global discussion of the painting

Composition vs. Areas

First, the analysed painting could be divided into two layer with two overlapped compositions. As the composition of the first/subjacent layers is not readable we will divide the areas of the background in two parts: composition I, and the portraits with subject and background.

Composition I

This composition is visible on the edge of the right-hand side, starting from the lower corner up to the top. To paint the uniform areas, with shades from white, ochre, light reddish to dark brown of the composition underneath, Lead white, natural earths from brown to yellow shades (high signal of Fe), and Ivory/bone black mixed with a Cr-based pigment were used. These are the pigments used to paint the anatomy visible in the XR image.

In the more reddish-dark area corresponding to measurement **X_19_red**, Vermilion and a Cu-based pigment have been identified. Common Cu-based pigments found in Picasso paintings are Scheele's green or emerald green. Other irregular shapes are hidden by the dark background, and based on the colours that can be observed through the decayed paint or the transparency of the superficial layer the same aforementioned pigments can be considered.

Background

The dark background created to frame the face of the subject was painted with a mixture of Bone/Ivory black containing traces of Mn oxides and Lead white. Not confirmed, but possible pigments used are iron or carbon based black pigments. Vermilion has also been found but its relation with paint layer and its distribution are not clear. Finally, Zinc white has been applied on the surface to create the filmy (semi-opaque) effect that surround the face of the subject.

Subject

The black jacket was painted or covered with the same black pigment aforementioned plus Prussian blue in a small quantity. Picasso painted the complexion/face and the unknown man's lips with white Lead and Vermilion. The use of Fe-oxide-based pigments and Lead Red cannot be excluded. The white paint layer of the nightshirt includes Lead sulphate and Lead White. The shadows and features of the visage are marked with Ivory/Bone black. The use of Fe-based black pigment and carbon black seems probable/possible. The presence of a Fe-based black pigment has to be considered due to the high signal of Fe. A summary of the pigments and organic compounds found is presented in Table 33.

Table 33. Pigments and organic compounds organised by areas.

Areas	Pigments	Binder/organic compound
Preparation layer	Calcium carbonate, Lead white and barium sulphate	
Background	I. Lead White, Natural earths from brown to yellow shades, Ivory/Bone black + Cr based pigments, Vermilion, Cu based pigment II. Bone/Ivory black + Mn oxides, Lead white (iron or carbon based black pigments)	Oil, Animal glue, Varnish
Face (Front/Lips, Cheek)	White Lead + Vermilion, Ivory/Bone black (iron based red pigments and Lead red)	
Jacket	Bone/Ivory black, Lead sulphate, Lead white, Prussian Blue (iron or carbon based black pigments)	
Shirt	Zinc White + Lead White + Lead Sulphate	
Signature	Bone/Ivory black + Mn oxides, (Zinc White) (Fe or carbon based black pigments)	
Semi-opaque effect	Zinc White	

I. First composition; II. Portrait of an Unknown man

Stratigraphy

As mentioned before, the presence of a composition lying underneath is clearly observable both, on the lower and right-hand side of the painting, where the artist did not apply the dark paint of the background of the portrait and where the same black paint was too diluted to hide completely the first painting layers. The composition with a man from behind is clearly visible in the XR image. The presence of Ba, Pb and Ca in higher concentration, where the paint layer on the surface becomes thinner, permits to speculate about a possible preparation layer. Thus, it is deducible that the paint contains/consists of a mixture of Calcium Carbonate, Lead White and Barium White. These are common elements found in the preparation layers of Picasso's paintings.

Picasso painted a composition with broad uniform areas. The part that we are able to observe is probably a fragment of a larger composition. The creation of the original composition could be divided in different phases. First, the artist painted the dark background. Afterwards, he applied the brushstrokes of the subject/figure. Then, he completed the background and the details of the face, such as hair, shadows, and the eyebrows using the same black used to create the dark background.

He applied a thicker and more opaque layer, achieved by the use of small quantities of a blue component (Prussian blue as explained above), to paint the jacket. Finally, he applied an extensive layer of Zn white that has a greyish hue and creates a "filmy/milky" (semi-opaque) effect. The white paint is partly mixed/blurred with the still wet black paint. To finish it he applied other final black retouches to add the right-hand side part of the moustache and the goatee

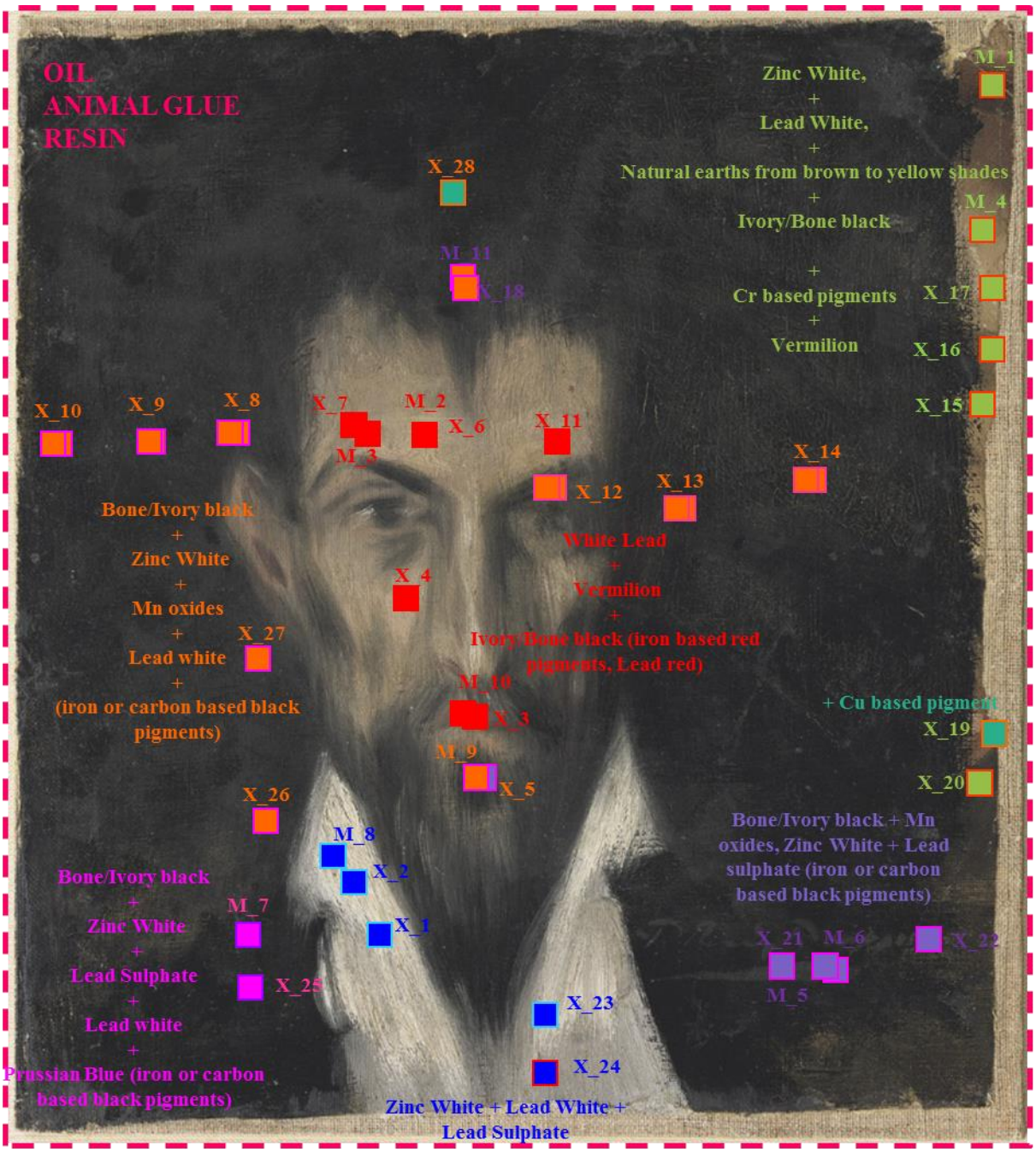

Figure 60. Material distribution mapping.

3.3.6 Retrat d'un desconegut

Artwork's interest

The painting "**Retrat d'un desconegut**" (**Portrait of an unknown man**) [47.5 x 35.2 cm, MPB110.026] is part of a series of numerous portraits that Picasso painted between 1899 and 1900, whose subjects' identities remain a mystery. For his first exhibition at "Els 4Gats" Picasso created a number of portraits taking inspiration from the persons who he knew in Barcelona during his "modernist" years. Unfortunately, a catalogue of this exhibition does not exist, but based on the well-known artworks that have been conserved, press-critics, and comments by his entourage researchers are is confident about knowing at least/several/most of the subjects depicted. They were his friends, from Jaume Sabartés and Carles Casagemas to Manuel Pallarés and Mateu Fernández de Soto etc. as well as some unidentified persons[52]. In the publication "Picasso i els 4Gats" (1995, Museum Picasso of Barcelona), Francesc Fontbona wrote:

" *....Uns quants d'aquestes retrats són considerats avui personatges desconeguts, i altres que han estat publicats (per Zervos, per Palau i Fabres o per altres associats a personatges concrets no sempre semblen tenir identificacions* del tot convincents.

Com és sabut, Picasso tenia en aquells anys vinculacions amb el catalanisme radical. La revista *"**La llustració llevantina**" publicà el 1901 la foto dels detinguts a la manifestació de l'11 de Setembre, on hi havia com a minim cinc persones del cercle de Picasso: Josep Maria Folch I Torres,]……[aleshores molt amics del pintor, seria logic que també haguessin estat retratats per ell.].....[no sería gens estrany que alguns altres dels trenta detinguts que surten a la fotografia esmendada fossin també del grup de Picasso i que haguessin estat retratats per ell l'any anterior, quan preparava la seva famosa exposició d'Els Quatre Gats."*

Fontbona explains that it is realistic that most of the unknown portraits probably represent persons close to Picasso and he makes reference to a photograph that appears in the magazine named "***La llustració llevantina***" (Figure 61). It is a photograph taken in occasion of the public performance on September 11th, 1901[I] when thirty demonstrator were jailed. As Picasso was part of the Catalan nationalism, most of the people in the photographs were his friends and it is proved that some of those was subjects of his portraits. As Fontbona wrote, it is possible that some of them are the characters depicted in the already unknown portraits.

The subject of the portrait has a very characteristic head/face; striking details are the asymmetric chin, the ears that adhere to the face, the moustache, and the round bulb. Looking

at the men of the magazine cover in detail one can identify one person that could possibly match the man of the portrait. It is the second man to the left in the back row of the image (Figure 61). His name is reported at the bottom of the magazine page as *Manel Ribas Carreras*. However, this is only an unconfirmed, personal hypothesis unrelated with the main scope of this study, as it is focused on the material characterization of the paintings.

Figure 61. Image of "Ilustració llevantina, La. Any 02, 2a època. Núm. 23" (1 oct. 1901), Barcelona 1901 @ 2005 Biblioteca de Catalunya.

Note

[1] September 11th is the celebration of the "Diada", day of Catalonia. It commemorates the defeat of *Catalonia* during the War of the Spanish Succession in 1714. © Enciclopèdia Catalana

Description and interpretation structure of the painting layers

According to the documentation provided by the conservator Sra. Reyes Jimenez, the painting is dated 1899 and identified as a work created in Barcelona. As the documentation reports, it was relined at the taller de Montjuïc in 1970. The canvas is an irregular fragment positioned on a regular frame during a undated intervention. It has been identified an industrial preparation layer. The report sad that the painting presents some retouches. On July 23th 2008, some areas of the paint layer were fixed and the most evident retouches were removed.

According to the report, this work is a cut-off canvas fragment on which Picasso applied tree compositions. The first one is visible at the edges: in the right-hand side, in the upper corner it is possible to recognise a window. The composition is probably an urban landscape. The second composition is described as more "colourist" and rather visible throughout the superficial layers. The third composition is described as a portrait of an unknown man that Picasso painted with broad brushstrokes and diluted oil paint. The RX images were acquired on July 16th 1970.

Direct observation – VIS

The portrait has a very complex structure with multiple layers. Observing in detail the brush strokes, the paint used, and its borders/boundaries, it is possible to identify three different compositions, which will be named first composition (composition I), second composition (composition II) and portrait, starting from the canvas to the more superficial layer. The first composition is visible in the upper part and right-hand side of the painting. The palette used seems to be very simple. On a large brown-beige area Picasso applied faint black brush strokes. The only elements recognizable are two black crossed lines in a rectangular shape located in the upper corner on the right-hand side of the canvas. On the left side of the window there is a black area that seems to have a triangular shape on which a narrow vertical white stripe is visible. Looking at the left side of the artwork one can see a light green area. The borders/boundaries of this composition are irregular and sharp, which means that the canvas was cut off and that it was probably a part of a larger painting. It is not clear when the framework has been changed.

The black brush strokes and the little white touch on the upper right-hand side appear suddenly interrupted. The second composition and the portrait present defined borders/boundaries. It seems that Picasso painted both compositions on the canvas with the first representation mounted on a smaller framework whose dimensions are probably those

marked with magenta dotted line in Figure 62. When the painting was relined the entire fragment was ironed and pasted on larger canvas, so that all paint layers became visible. The representation is not perfectly vertical but is slightly tilted.

.

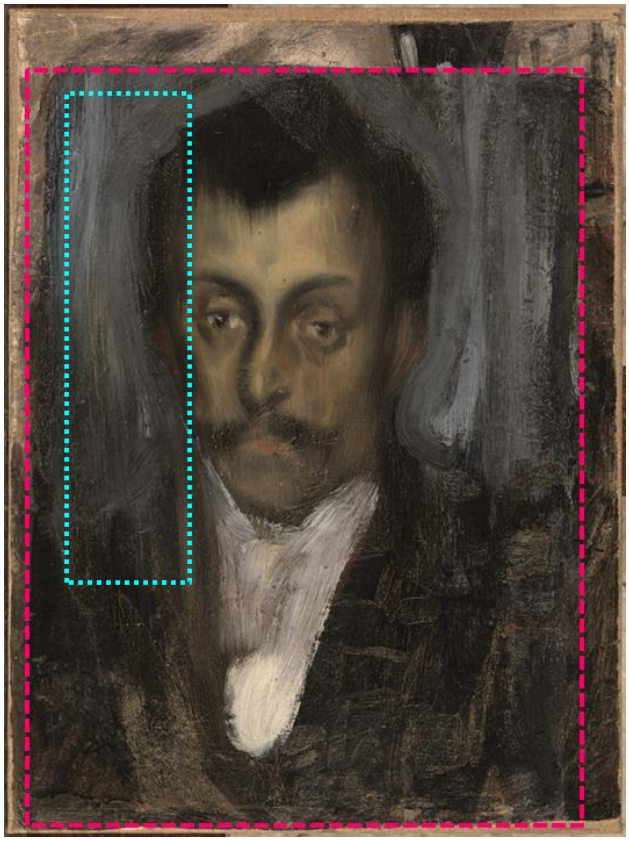

Figure 62. VIS Image.

Concerning the second composition it is possible to perceive brush strokes of very bright colours throughout the paint layer of the portrait, located principally in the lower part of the painting. Purple areas can be found behind the white collar. Orange, yellow and white-beige brush marks are visible, which delimitate small rectangular areas and, thus, create a pattern comparable with an urban landscape, a recurring subject of Picasso's artistic production [4,64].

Figure 63. a) Casa en Hora, Horta de San Joan, summer 1898 (Private collection)[53]; b) Els Terrats de Barcelona, Barcelona, 1902/3 (©Museo Picasso Barcelona).

Observation of the visible layers underneath

Observation of the superficial layers

Background

In this painting, Picasso frames the subject of the portrait in bright dense, although fluid, broad brush strokes using a grey-white-bluish paint. The paint is rather opaque and completely hides the subjacent layers in this area. The light colours permit to brighten up the painting and to bring out the unknown character's face. The thick brush strokes were applied when the second composition was already dry, thus no mixture between the paint layers can be observed. From the blue-white brush strokes it is possible to see how a blue brushstroke interrupts the vertically oriented paint to emphasize the shoulder with a horizontal line (Figure 62 – dotted blue line).

Subject

The subject depicted by Picasso is a man with black hair, moustache and sketchy beard. His skin tone is ranging from ochre-green, blue-black to orange-red shades. Picasso achieved a cold effect that match the haughty and thoughtful look of the subject. The fluid brush strokes of the face and the hair were applied vertically and in an accurate manner. The black lines that delineate the eyebrows, the spherical eyeballs and the nose are faint continuous brush strokes. The ears appear just outlined. The subject is wearing a white nightshirt or a neckerchief painted with white broad strokes, which end with round edges. The same shape can be observed on the blue strokes of the background that define the profile the character's face located in the left-hand side of the painting.

Observation with no visible radiation – subjacent layers (XRR, IRR)

Radiography

The only image available was a negative of the radiography campaign in 1970 (Figure 64). The museum has planned to acquire new images. The XR image was probably taken before the change of the frame and the relining. In fact, the edges of the negative correspond only to the well-defined boundaries of the superficial composition. The painting is rather small (47.5 x 35.2 cm) and it is likely that only one plate was enough to cover the entire artwork during the radiography. It is important to keep in mind that the radiography is not complete. It is important to keep in mind that radiography may show superposed layers (3D structure) on images (2D representation). In this case the Figure 64 is a mix of the three overlapped

compositions. First, the regular pattern visible in the XR image suggests the presence of a preparation layer. Furthermore, some thick overlapped brush strokes can be perceived (intense white, high Z number material), mainly located in the centre and on the right-hand side. Also on the left-hand side of the painting white areas can be observed, which seem to follow the border of the first composition and present fast and diagonally oriented paint application from the portrait boundaries towards the edges (upper corner). Areas of low XR absorption are distributed across the painting. The broad white strokes of the man's shirt are visible because they were applied with a heavy-metal-based paint. In the same area the strokes of the second composition are barely visible.

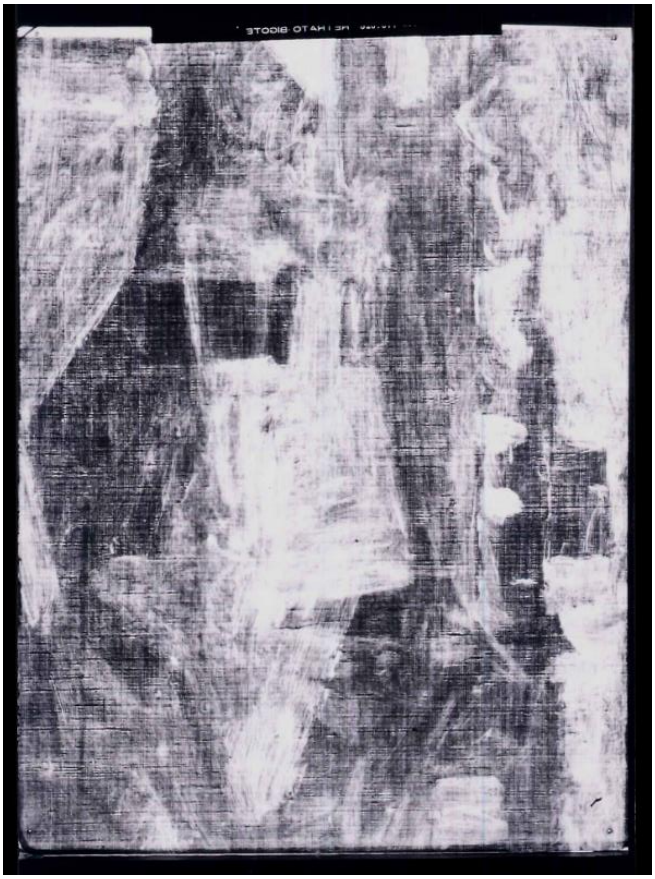

Figure 64. This is the negative with iinverted colour of the XR image.

IR Reflectography

Several NIR images were acquired. Figure 65 shows an IR reflectography at 2265 nm. The first relevant consideration is that the NIR image traces more evident edges between the superficial layers and the first composition, especially on the right-hand side and the base of the work, which are rather blurry in the VIS image. In particular, drops of black paint in the left-hand side lower corner are better visible. This supports the suggestion that the paint was diluted, a fact that would explain the low grade of hiding capacity. Consequently, the black paint does not cover the reddish-orange-ochre areas of the layer underneath. In the image the

presence of the varnish is evident by the brilliant interferences possibly related to the roughness of the paint layer. One can see the difference to the areas above the right-hand side eyebrow where the varnish has been removed (Figure 65 – dotted magenta lines). Interesting, though, is that this brilliant glare is located only where the paint layer is very rough and the texture changes with respect to the rest of the painting (a kind of grazing angle (?) effect). The rest of the areas that correspond to the first composition that surround the portrait appear opaque. The black lines that define the edges of the jacket are more evident. In particular, the line that marking the left-hand side shoulder, which is partially hidden by the dense blue-white paint in the VIS image, is clearly observable in the NIR image. The greyish-white filmy/"milky" effect and "*sfumato"* was applied when the portrait was finished. This theory is based on the observation of the subject's right-hand shoulder, the visage, and in particular the forehead.

Figure 65. NIR image acquired at 2265 nm high contrasted.

Description and interpretation of the materials

In Figure 66 the XRF (a) and mid-FTIR (b) measurement spot distributions are reported and the corresponding file names are given in Table 34.

XRF	MID-IR
a	*b*

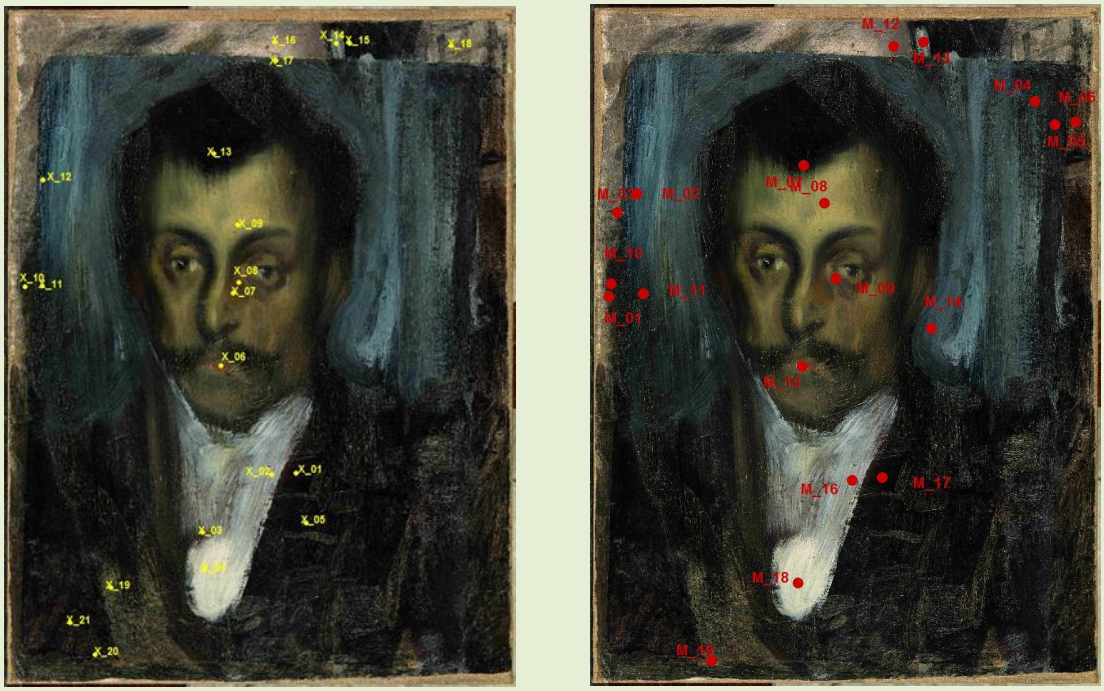

Figure 66. XRF (a) and mid-FTIR (b) measurement spot distribution.

Table 34. Spectrum/spot label for a) XRF and mid-FTIR are reported.

a) XRF spectrum/point label	b) mid-FTIR spectrum/point label
P026_X_01_purple	P026_M_17_black
P026_X_02_white	P026_M_16_white
P026_X_03_purple	
P026_X_04_white	P026_M_18_white
P026_X_05_black	
P026_X_06_red	P026_M_15_red
P026_X_07_brown	P026_M_09_flesh
P026_X_08_green	
P026_X_09_flesh	P026_M_08_flesh
P026_X_10_brown	P026_M_01_brown
	P026_M_10_brown
P026_X_11_blue	P026_M_11_blue
P026_X_12_blue	P026_M_02_blue
	P026_M_03_blue
P026_X_13_black	P026_M_07_black
P026_X_14_white	P026_M_13_white
P026_X_15_black	
P026_X_16_beige	P026_M_12_brown
P026_X_17_blue	
P026_X_18_beige	
P026_X_19_yellow	
P026_X_20_orange	P026_M_19_red
P026_X_21_orange	
	P026_M_04_blue
	P026_M_05_blue
	P026_M_06_brown
	P026_M_14_blue

Description

White Areas

The mid-infrared spectrum **M_13_white** has been acquired on a white brush stroke located in the upper right-hand side of the painting that belongs to the first composition, starting from the canvas. The main signals indicate the presence of Lead Carbonate ($PbCO_3$ and $2PbCO_3 \cdot Pb(OH)_2$ – White lead). The signals can mainly be attributed to Hydrocerrussite - $Pb(OH)_2$. The band centred at 1073 and the shoulders at 982 cm^{-1} and 1192 cm^{-1} correspond to the symmetrical vibration of SO_2^{4-}, while the peaks at about 600 and 630 cm^{-1} are assigned to the out-of-plane bending vibration[5]. The weak signal between 2140 and 2064 cm^{-1} and the high signal of Ba (12 cps) detected by XRF (**X_14_white**) suggest the presence of Barium sulphate ($BaSO_4$ – White filler). The inverted signal at 1630 cm^{-1} indicates the presence of a proteinaceous compound. It is possible to confirm the presence of Hydroxyapatite ($C+Ca_3(PO4)_2$ - Ivory/Bone black) due to the bands at 2012 cm^{-1}. The black pigment identified is probably due to the underlying paint layer. The other elements detected in this area were Pb (145 cps), Co (2 cps), Fe (2 cps), Ca (2 cps) and traces of Mn. On the other hand, the mid-infrared spectrum **M_16_white** has been recorded on the white of the collar of the character depicted on the surface. In this case the spectrum shows Lead Carbonate as main component. The characteristic bands of the compound are well defined. The elements detected based on XRF results (**X_2_white**) were Pb (135 cps), Zn (46 cps), Co (6 cps), Hg (3 cps) and traces of Ca, Ba, Mn and Fe. In this case, the Co could be attributed to the blue pigment that creates the grey shade of the collar. The same could be commented about the mid-infrared spectrum **M_18_white** (same white of the collar). It also presents as main compound Lead Carbonate. No proteinaceous compounds were detected. This could be due to the fact that the white paint layer is thicker than in point **M_16** and the animal glue used during the relining process did not penetrate the paint layer. The elements detected in the XRF spectrum acquired approximately in the same position (**X_04_white**) were Pb (150 cps), Zn (36 cps) and traces of Ca, Co, Hg and Fe. The distribution of Zn and (?) will be discussed in the stratigraphy section.

Table 35. Summary of XRF results for white/ground areas.

cps	Ca	Ba	Mn	Fe	Co	Zn	Pb	Hg
E (keV)	**3.71**	**5.52**	**5.95**	**6.4**	**6.97**	**8.65**	**10.55**	**9.97**
P026_X_02_white	Traces	Traces	Traces	Traces	6	46	135	3
P026_X_04_white	Traces	/	/	Traces	Traces	36	150	/
P026_X_14_white	2	12	Traces	2	2	/	145	/

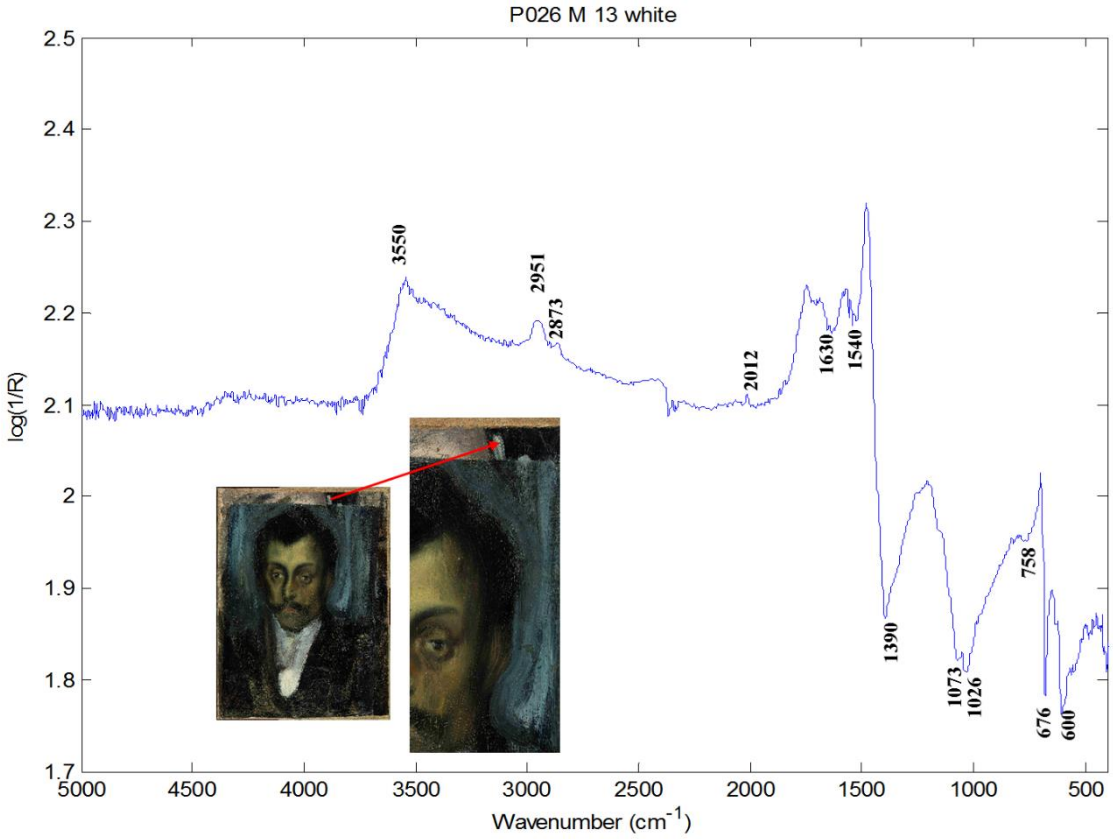

Figure 67. IR spectrum

Blue Areas

The mid-infrared spectrum **M_02_blue** has been recorded on the broad light blue brush strokes located on the left-hand side of the painting. In spite of the darker shade of point **M_03_blue**, the mid-infrared spectrum is very similar. The signals detected at about 1750 cm^{-1} and the sharp doublet at about 4330 cm^{-1} suggest the presence of lipids. The inverted band at about 1000 cm^{-1} could be attributed to a silicate; based on the blue colour for example Ultramarine ($3Na_2O.3Al_2O_3.6SiO_2.2Na_2S$) cannot be excluded. All silicates absorb strongly in the range of 1100-800 cm^{-1} with intense Si–O asymmetric stretching modes. Thus, a certain identification of the silica-based pigment only on the basis of infrared

very often is not feasible since in reflection mode the strong silicate mode is distorted by the surface reflection generating reststrahlen bands [26]. The elements detected based on XRF results (**X_12_blue**) were Zn (151 cps), Pb (93 cps), Co (39 cps), Fe (4 cps) and traces of Ca, Ba and Hg. The mid-infrared spectrum **M_11_blue** shows also the characteristic bands of silicates at about 1000 cm^{-1} as well as lipid and Lead Carbonate. Some signals at low wavenumber remain unidentified. According to the XRF spectrum **X_11_blue** the elements detected in this area were Zn (447 cps), Pb (41 cps), Co (44 cps), Fe (5 cps), Ca (2 cps) and traces of Ba.

The mid-infrared spectra **M_04_blue** and **M_05_blue** suggest the presence of Lead carbonate and proteins. Furthermore, the signal with the minimum at about 1520 cm^{-1} can be attributed to zinc carboxylate ($ZnC_2O_4.2H_2O$). It is a metal soap formed from the reaction of a simple metal salt – present as a drier or pigment – with an organic medium[7]. The elemental composition concluded from the XRF spectrum **X_17_blue,** acquired on the top of the painting, is comparable to the other blue spots analysed on the left-hand side, although the signal of Pb is considerably higher (136 cps). The mid-infrared spectrum **M_14_blue** shows mainly the presence of Lead Carbonate.

Table 36. Summary of XRF results for blue areas.

cps	Ca	Ba	Mn	Fe	Co	Zn	Pb	Hg
E (keV)	**3.71**	**5.52**	**5.95**	**6.4**	**6.97**	**8.65**	**10.55**	**9.97**
P026_X_11_blue	2	Traces	/	5	44	447	41	/
P026_X_12_blue	Traces	Traces	/	4	39	151	93	Traces
P026_X_17_blue	Traces	Traces	/	4	51	144	136	/

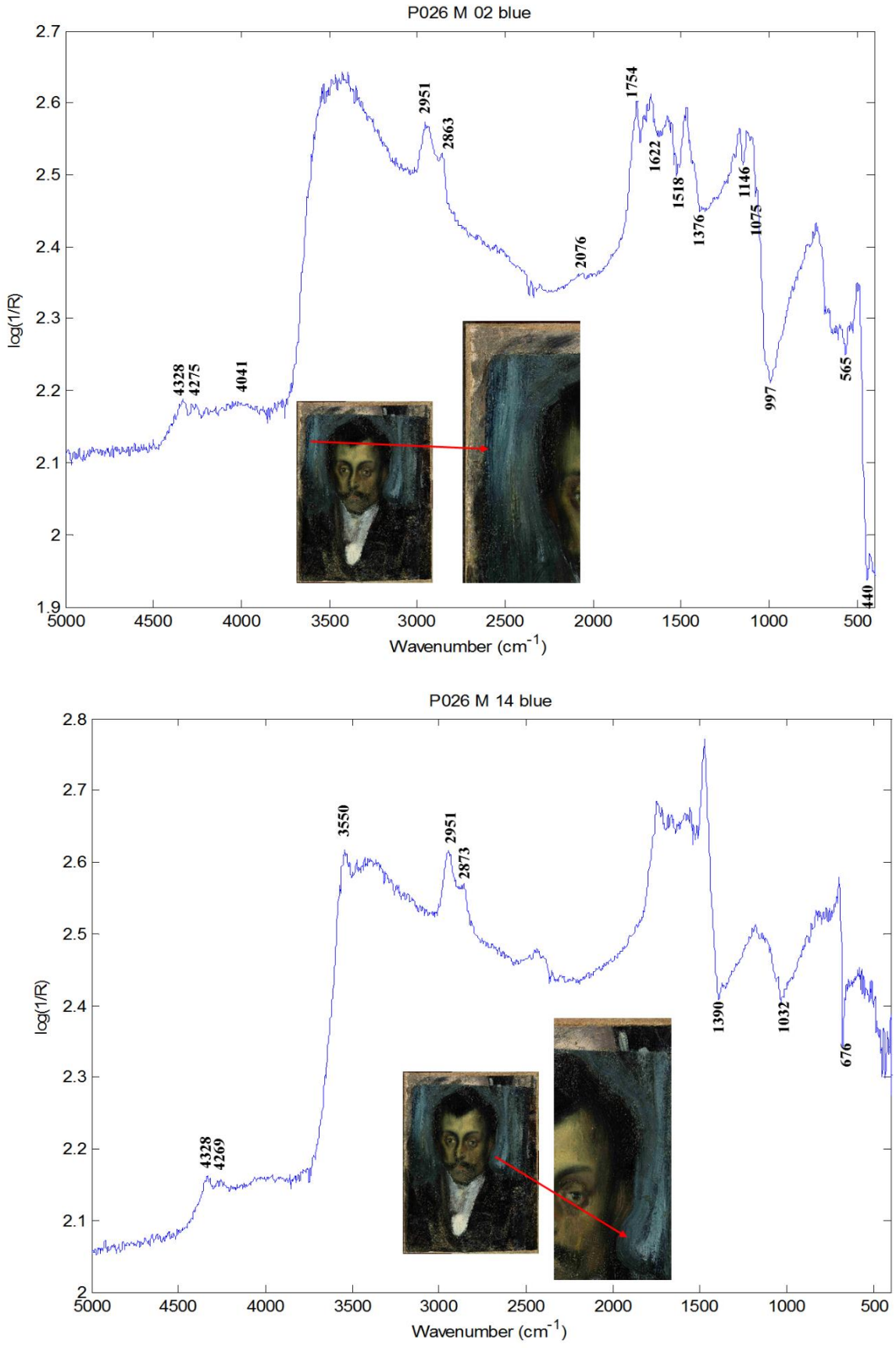

Figure 68. IR spectra M_02_blue and M_14_blue

According to the XRF results, a Co-based pigment has been identified, while silicate signals could be an indication of the presence of Ultramarine blue, although it cannot be confirmed. Measurements in the near infrared range were performed. Studies of Bacci *et al*. and Miliani [8,67] affirm the possibility to distinguish between different types of cobalt blue based on the near infrared reflectance spectra. In this case, the NIR spectrum **N_01** (Figure 69) shows three sub-bands at about 6610, 7230 and 8150 cm^{-1} that indicate the presence of Cobalt blue - $CoAl_2O_4$, commonly named Thenard's blue.

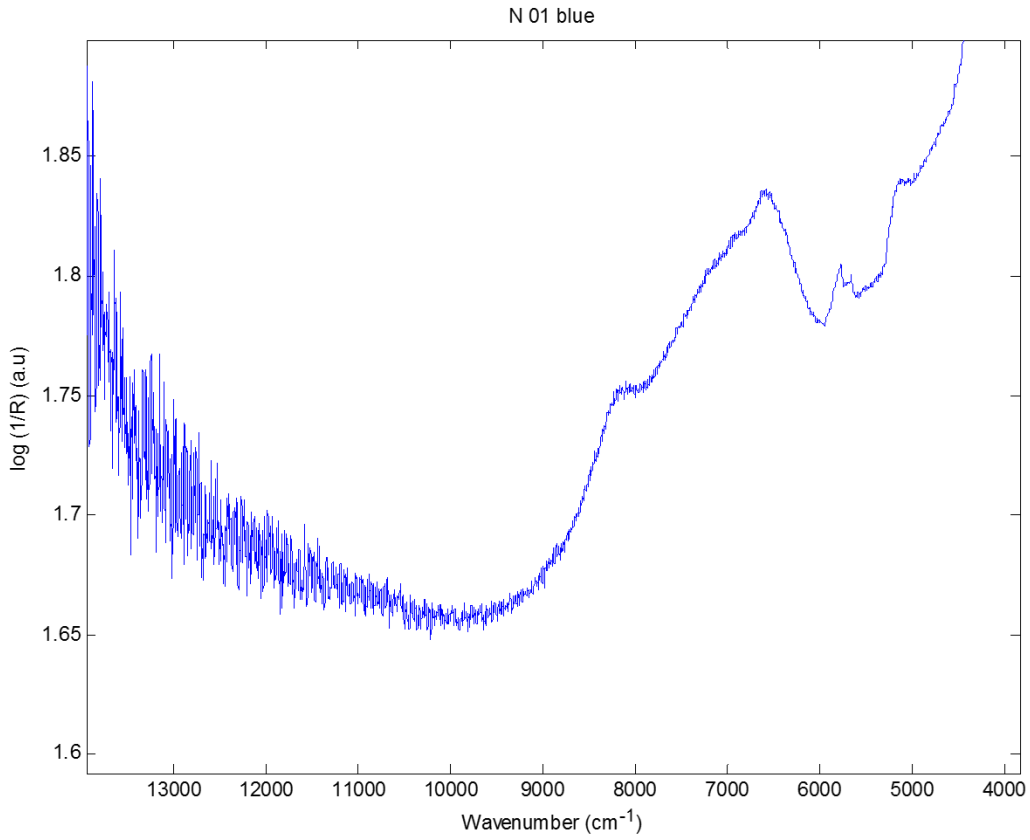

Figure 69. NIR spectrum N_01_blue

Black areas

The mid-infrared spectrum **M_07_black** is very noisy, although it possible to deduce that the black used for the hair of the man represented in the portrait is probably not Ivory/Bone black. The elements detected in this area (**X_13_black**) were Pb (127 cps), Zn (77 cps), Co (21 cps), Fe (9 cps), Hg (4 cps), Ca (2 cps) and Ba (2 cps). The black colour could be an iron-based black pigment, interpreting the signal of Fe or a carbon black. The mid-infrared spectrum **M_17_Black** presents the signal of White lead, Barium sulphate (600 cm^{-1}) and proteins. The presence of Zn carboxylate can be assumed due to the signal at about 1520 cm^{-1}.

The elements detected in this area (**X_01_purple**) were Pb (131 cps), Zn (30 cps), Co (11 cps), Fe (10 cps) and Ca (2 cps), Ba (3 cps), Hg (6 cps) and traces of Mn. The XRF spectrum **X_05_black** was acquired in the area next to point X_01. Both points show similar elemental composition. The detected elements were Pb (135 cps), Zn (25 cps), Co (14 cps), Fe (4 cps) and Ca (2 cps), Hg (6 cps) and traces of Mn and Ba.

The XRF spectrum **X_03_purple** has been acquired on a brown-purple point located between the white brush strokes of the collar. On this point, the spectrum showed very high signals of Zn (265 cps). Further elements are Pb (67 cps), Co (10 cps), Ba (4 cps), Fe (2 cps), Hg (8 cps) and traces of Ca. The signal of Zn increases drastically. Its distribution will be discussed in the next section.

The XRF spectrum **X_15_black** has been acquired on the black in the upper right-hand corner of the first composition, and shows the presence of Pb (147 cps), Ca (10 cps), Ba (8 cps), Fe (2 cps) and traces of Hg. The high content of Ca and the results obtained on point **M_13** suggest the use of Ivory/bone black. The black paint used in the two compositions is clearly different.

Figure 70. Detail of the purple areas behid the white collar.

Table 37. XRF results for black/purple areas.

cps	Ca	Ba	Mn	Fe	Co	Zn	Pb	Hg
E (keV)	**3.71**	**5.52**	**5.95**	**6.4**	**6.97**	**8.65**	**10.55**	**9.97**
P026_X_01_purple	2	3	Traces	10	11	30	131	6
P026_X_05_black	2	Traces	Traces	4	14	25	135	6
P026_X_13_black	2	2	/	9	21	77	127	4
P026_X_03_purple	Traces	4	/	2	10	265	67	8
P026_X_15_black	10	8	Traces	2	/	/	147	Traces

Brown areas

The mid-infrared spectra **M_01** and **M_10_brown** have been acquired on the left-hand side of the painting, on a layer that could be attributed to the first composition.

In both spectra signals of Lead white, Barium sulphate and Silicate have been identified. Additionally, in point **M_01** also Zn carboxylate, protein and Hydroxyapatite (Ivory/bone black) have been found. Unfortunately, spectrum **M_10** is too noisy to confirm the presence of Kaolin. In this area, the following elements have been detected: Pb (147 cps), Ba (9 cps), Fe (7 cps), Ca (5 cps), Hg (3 cps) and traces of Mn and Co (**X_10_brown).** Pb and Ba confirm Lead white and Barium sulphate, respectively, and Hg indicates the presence of Vermilion, while the Ca can be related to the Ivory/bone black or/and the preparation layer.

The mid-infrared spectrum **M_06_brown** was acquired on the first composition, but on the visible part on the right-hand side of the painting. The main signals correspond to Lead Carbonate, Zn carboxylate, Iron Hexacyanoferrate at 2090 cm^{-1} ($KFe[Fe(CN)_6]$ or $Fe_4[Fe(CN)_6]_3$ – Prussian Blue) and Silicate. Weak signals of Barium sulphate are also present. The infrared measurement **M_12_brown** was acquired on the light brown of the first composition (upper part, right-hand side). The compounds detected are principally barium sulphate, lipid and Lead carbonate. As mentioned before, in **M_10** the presence of Kaolin cannot be confirmed due to the noisy signal. The XRF spectra **X_16_beige** and **X_18_beige** acquired on the same light brown areas are similar. The only difference is a slightly higher signal of Fe on point **X_18,** which is actually darker. This can be an indication of the use of some natural earths (Fe-based brown pigments).

Table 38. XRF results for brown/red/yellow areas.

cps	Ca	Ba	Mn	Fe	Co	Zn	Pb	Hg
E (keV)	**3.71**	**5.52**	**5.95**	**6.4**	**6.97**	**8.65**	**10.55**	**9.97**
P026_X_10_brown	5	9	Traces	7	Traces	/	147	/
P026_X_16_beige	2	10	/	Traces	Traces	/	148	3
P026_X_18_beige	2	8	Traces	3	Traces	/	147	2

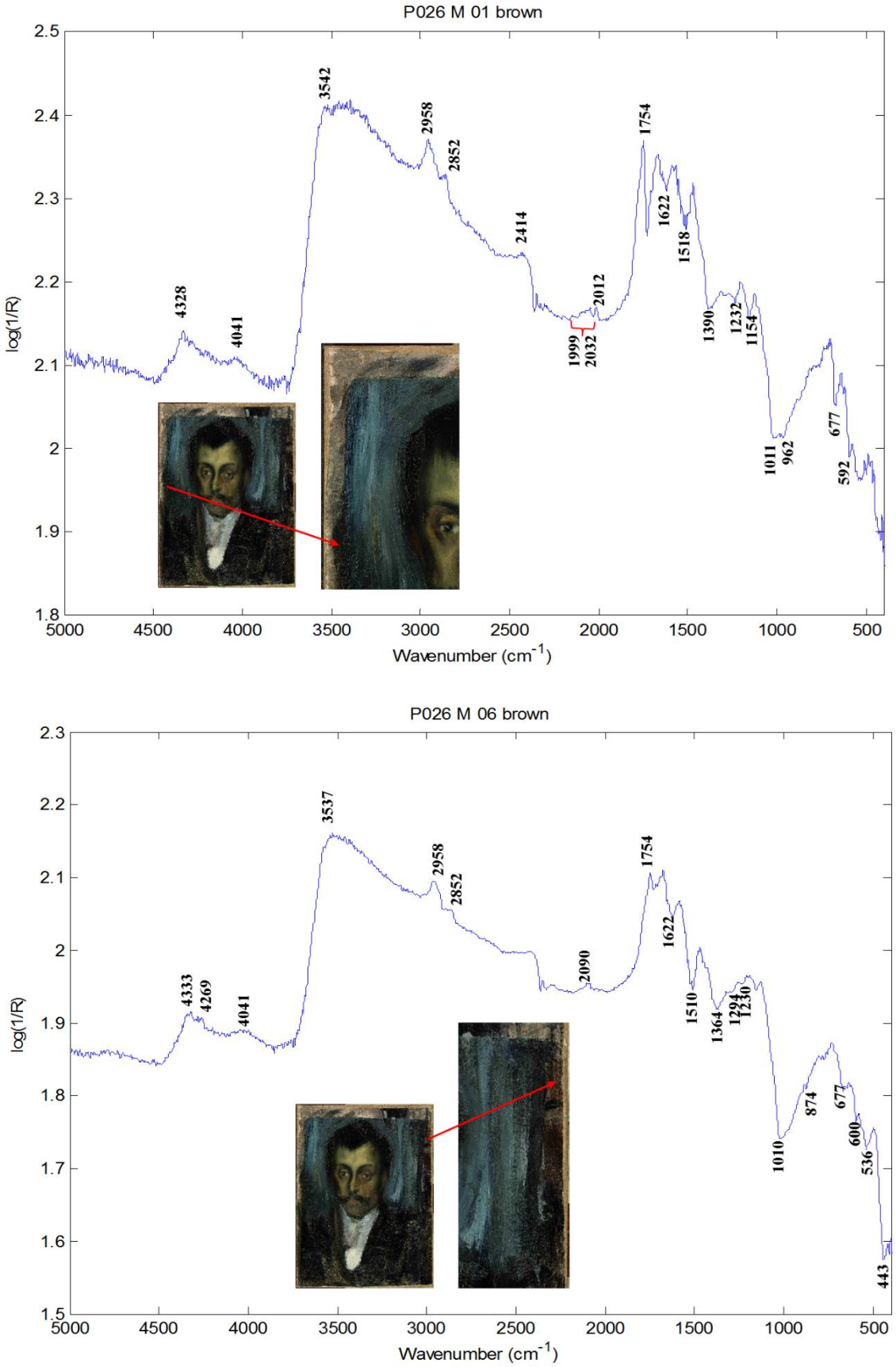

Figure 71. IR spectra M_01_brown and M_06_brown.

Red/orange areas

On the front of the subject the spectrum **M_08_flesh** shows Lead Carbonate and a strong inverted band with minimum at 1530 cm^{-1} (ν_a COO asymmetric mode) characteristic of Zn metal soap [7]. The elements detected nearby (**X_09_flesh)** were Pb (152 cps), Zn (40 cps), Co (2 cps), Hg (2 cps) and traces of Ca, Ba and Fe. These results suggest the use of Lead white, Vermilion and a Co-based pigment for the complexion, while the distribution of Zn/Zinc white will be discussed in the next sections.

The mid-infrared spectrum **M_09_flesh** has been acquired on a dark shadows of the face, close to the right-hand eye. The compounds detected are principally Lead Carbonate and Silicate. The spectrum is quite noisy and the signal of oxalate cannot be confirmed. The corresponding XRF spectrum is **X_07_brown**, which was recorded on the same shadow, where Picasso created an orange shade. The presence of Hg (6 cps) and Fe (23 cps) suggests the use of Vermilion mixed with a Fe-based red pigment - Natural earth. On the other hand, the XRF spectrum **X_8_green** has been acquired on the same area, but in a green-brown shade brush stroke (Figure 72). The elements detected were Zn (276 cps), Pb (68 cps), Co (39 cps), Hg (4 cps), Ba (3 cps), Fe (2 cps) and Ca (2 cps). It is possible to observe an increase of Co probably responsible for the darker shade, a decrease of Fe and Pb. The mid-infrared spectrum **M_15_red**, recorded on a point located on the lips, shows strong signal of Lead Carbonate, Barium sulphate and lipids. The XRF spectrum that corresponds to the same area is **X_6_red**. Here, a high signal of Zn (401 cps) was detected as well as signals of Pb (43 cps), Ba (10 cps), Hg (10 cps), Co (5 cps), Fe (2 cps) and traces of Ca and Mn. An significant increase of Hg suggests the use of Vermilion. On the other hand, the signal of Pb, although lower than in the other point, does not permit to exclude the use of Red lead.

The mid-infrared spectrum **M_19_red** was acquired in a point located in a lower area of the artwork that corresponds to the red-orange paint layer that is visible throughout the faint black paint of the jacket, and probably corresponds to the first composition. Here the main compound is Lead carbonate with a strong inverted band of oxalate. The elements detected in this area (**X_20_orange**) were Pb (136 cps), Fe (34 cps), Ca (10 cps), Hg (8 cps), Co (5 cps), Ba (4 cps) and Mn (4 cps). The spectrum **X_21_orange** corresponds to the same area, although the elemental composition is quite different. The elements detected were Pb (139 cps), Hg (12 cps), Co (11 cps), Zn (18 cps) Fe (9 cps), Ca (3 cps) and traces of Ti/Ba and Cr. On point **X_19_yellow** the XRF spectrum indicates the presence of Zn (336 cps), Pb (78 cps), Co (6 cps), Fe (4 cps), Ca (2 cps) and traces of Ba. The most relevant difference is the

absence of Zn in point **X_20_orange**. The signal of Zn is related to the presence of White zinc, whose relation with the paint layer is difficult to assess.

Table 39. XRF results for red/yellow areas.

cps	Ca	Ba	Mn	Fe	Co	Zn	Pb	Hg
E (keV)	**3.71**	**5.52**	**5.95**	**6.4**	**6.97**	**8.65**	**10.55**	**9.97**
P026_X_06_red	Traces	10	Traces	2	5	401	43	10
P026_X_07_brown	3	4	/	23	13	86	113	6
P026_X_08_green	2	3	/	2	39	276	68	4
P026_X_09_flesh	Traces	Traces	/	Traces	2	40	152	2
P026_X_19_yellow	2	Traces	/	4	6	336	78	/
P026_X_20_orange	11	4	4	34	5	/	136	8
P026_X_21_orange	3	Traces (Ti/Ba)	/	9	11	18	139	12

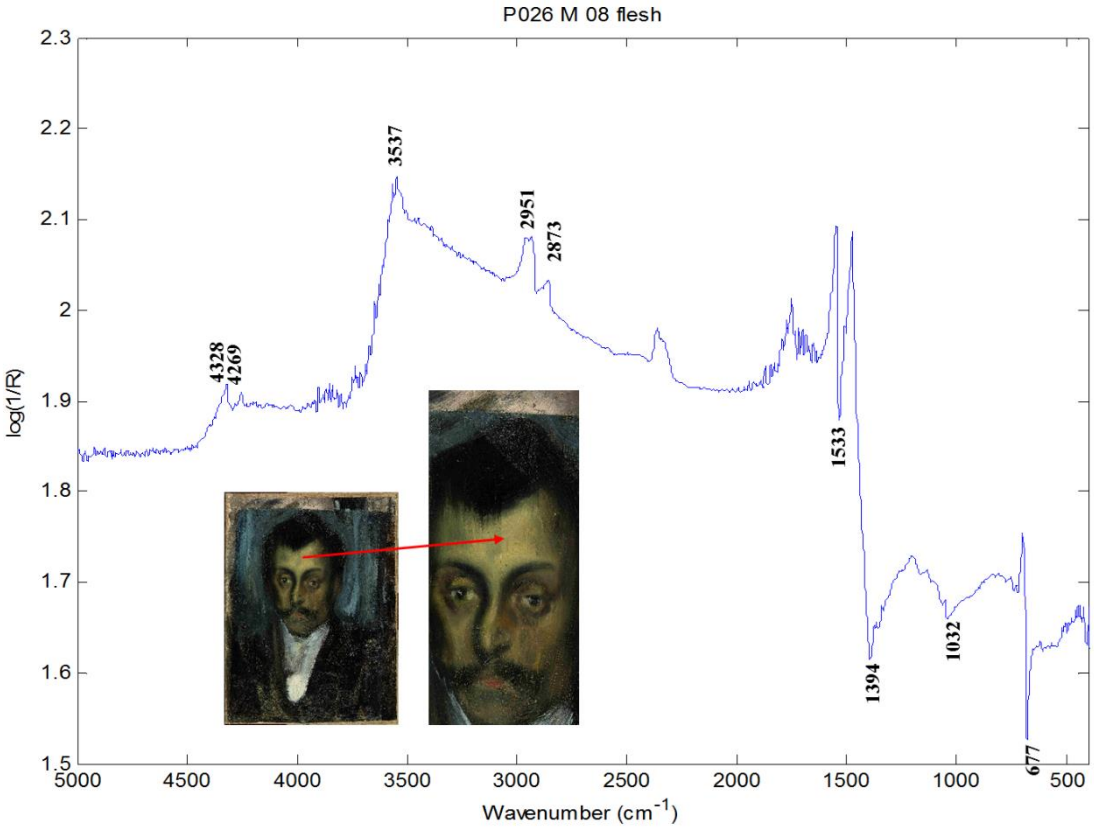

Figure 72. IR spectrum M_09_flesh.

Summary

Figure 73 shows a mapping of the elements and compounds detected.

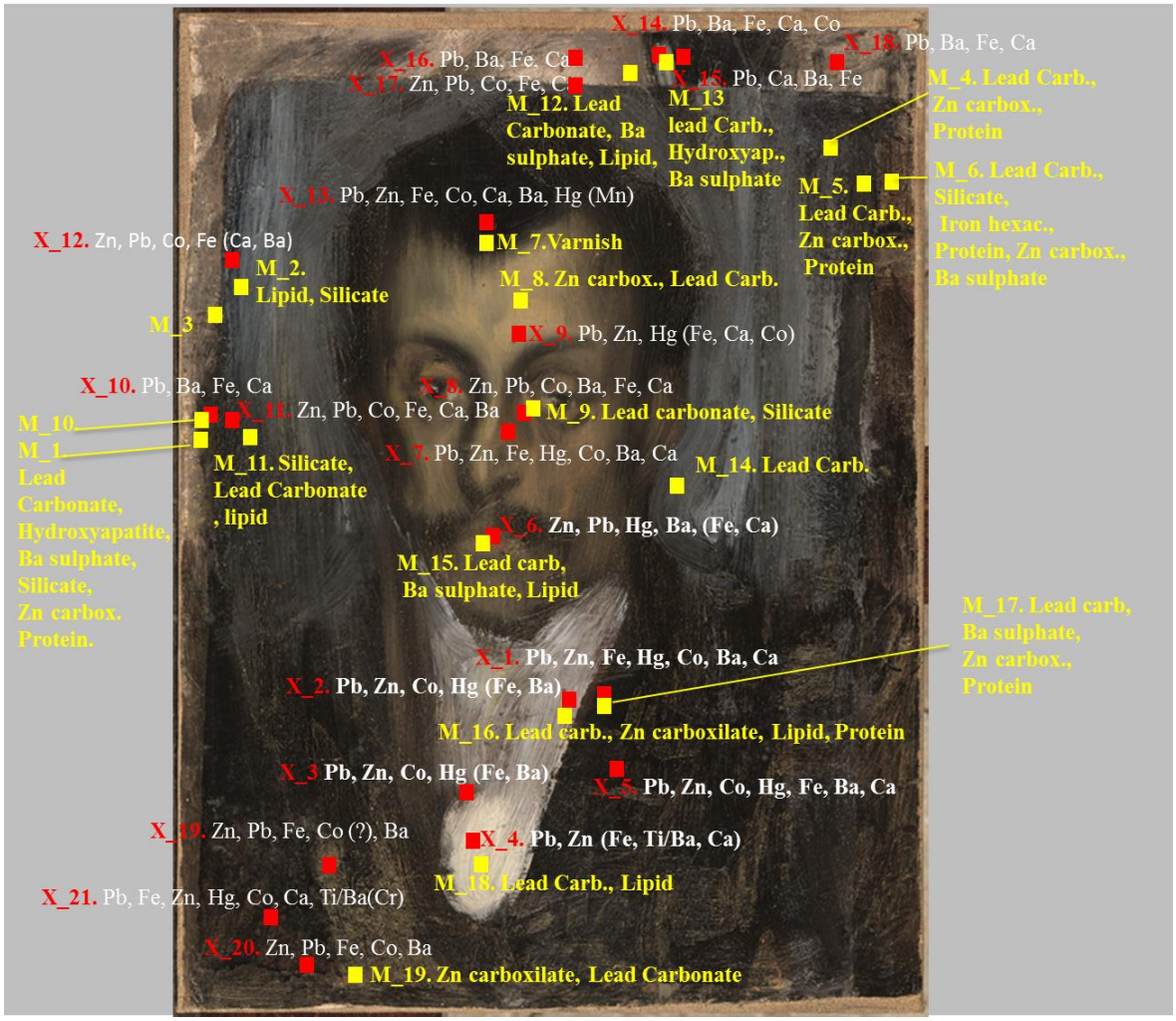

Figure 73. Mapping of the results obtained.

Interpretation

Pigments

White pigments

The use of White lead is confirmed by both mid-infrared and XRF measurements (Figure 75a) and it was detected in across the entire composition. It cannot be excluded that part of the signal is due to the preparation layer. Barium sulphate has been detected in different points of the painting not connected with a particular composition (Figure 75b). This pigment is probably a filler.

The most important evidence is the high signal of zinc/ zinc white clearly is not present on the first painting layers (Figure 75c).

It is no clear if Zinc white is used directly as white pigment or was mixed in other commercial paints[68]. Even so, it is interesting to notice that when zinc counts increase the lead counts decrease and *vice-versa*. The low XRF signal of Ca distributed across the entire work is an indication of the presence of calcium carbonate, not detected by mid-infrared, and probably due to the preparation layer (Figure 75d).

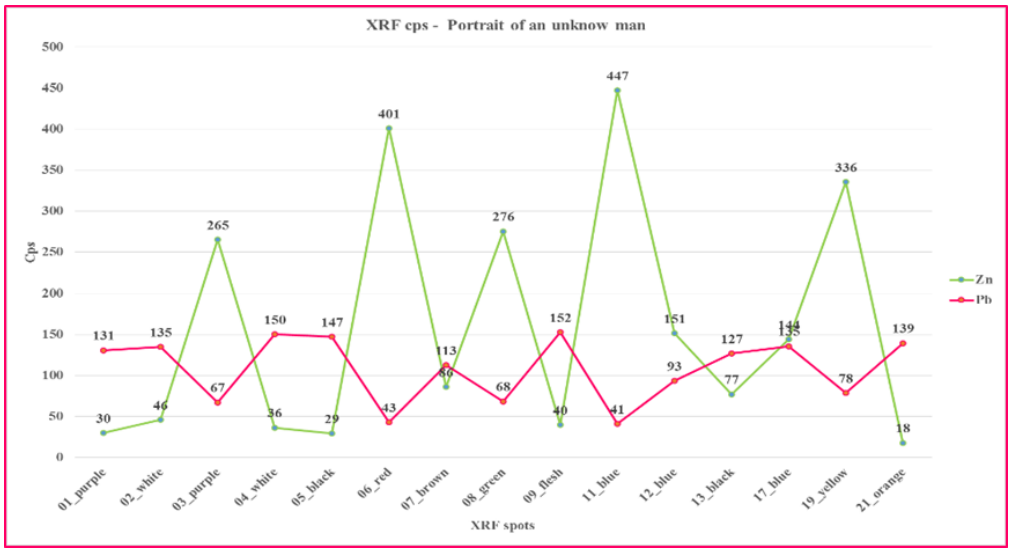

Figure 74. XRF data. Pb/Zn signal relation.

Black pigments

The Ivory/bone black has been detected only on the first composition by both, IR and XRF techniques. In presence of Ivory/bone pigment normally an increase of the Ca signal in XRF spectra is observed. However, the black used for the portrait has not been identified. Based on the signal of Fe it seems possible that Fe-based black pigments (Figure 75e) were used, or Carbon black pigments, due to the fact that neither infrared spectroscopy nor XRF are sensible to these compound classes. Traces of Mn have been detected by XRF. It has been reported that the brown shade of natural earths is in some cases caused by manganese oxides (MnO_2) [69,70] (Figure 75f).

Red – brown pigments

The increase of Fe signal in red-brown and orange spots suggests the presence of Fe-based red pigments - Natural earth. The detection of Hg is evidence that Picasso used Vermilion. It is not located in a specific area (Figure 75g), although its signal increases significantly in the spectrum acquired on the red spot on the lips, in the purple spots, and the orange layer underneath. The use of Red lead cannot be excluded due to the high signal of lead, although it is interesting to notice that in the red spot on the lips and generally across the face of the character the counts of lead decrease.

Blue pigments

The blue is the most prevalent colour on the painting. The presence of Cobalt blue (Thenard's blue) has been demonstrated (Figure 75h). The detection of silicates in the blue areas investigated are possible related to Ultramarine blue. Prussian blue has been detected only in a black spot of the first composition, and it is normally accompanied by ivory black. The mixture of these two pigments is a constant of this series of portraits and the Prussian blue is probably added to the black paint because of its high hiding and tinting power

Other inorganic compounds

Zn oxalate due to the creation of soap is normally an indication of the reaction between the fatty acids of the linseed oil and metals, such as zinc, lead etc.

Organic compounds

Based on the mid-infrared results a Lipid binder can be confirmed. Moreover, signals of a Resin attributed to the presence of varnish have been detected. Finally, signals of Proteins suggest that the animal glue used during the restoration process has migrate from the verso directly on the surface of the painting.

Table 40. Pigments and Binding Media/organic compound Analysis Results

Colours	**Materials/Pigments**	**Binding medium/ organic compounds**
Preparation	Calcium carbonate [a)]	Lipid, protein, resin [b)]
White	White Lead [a,b)], Barium sulphate [a,b)], Zinc oxide [a)]	
Black	Bone/Ivory black [b)] + Calcium carbonate, (Iron oxide based pigments, Carbon black), Mn oxides	
Blue	Prussian Blue [b)], Cobalt blue/Thènards blue [a,b)] (Ultramarine blue [b)])	
Red – brown - orange	Vermilion [a,b], Brown Earth/ Iron oxide based pigments, (Red lead)	

a) XRF; b) mid-FTIR spectroscopy; c) NIR.

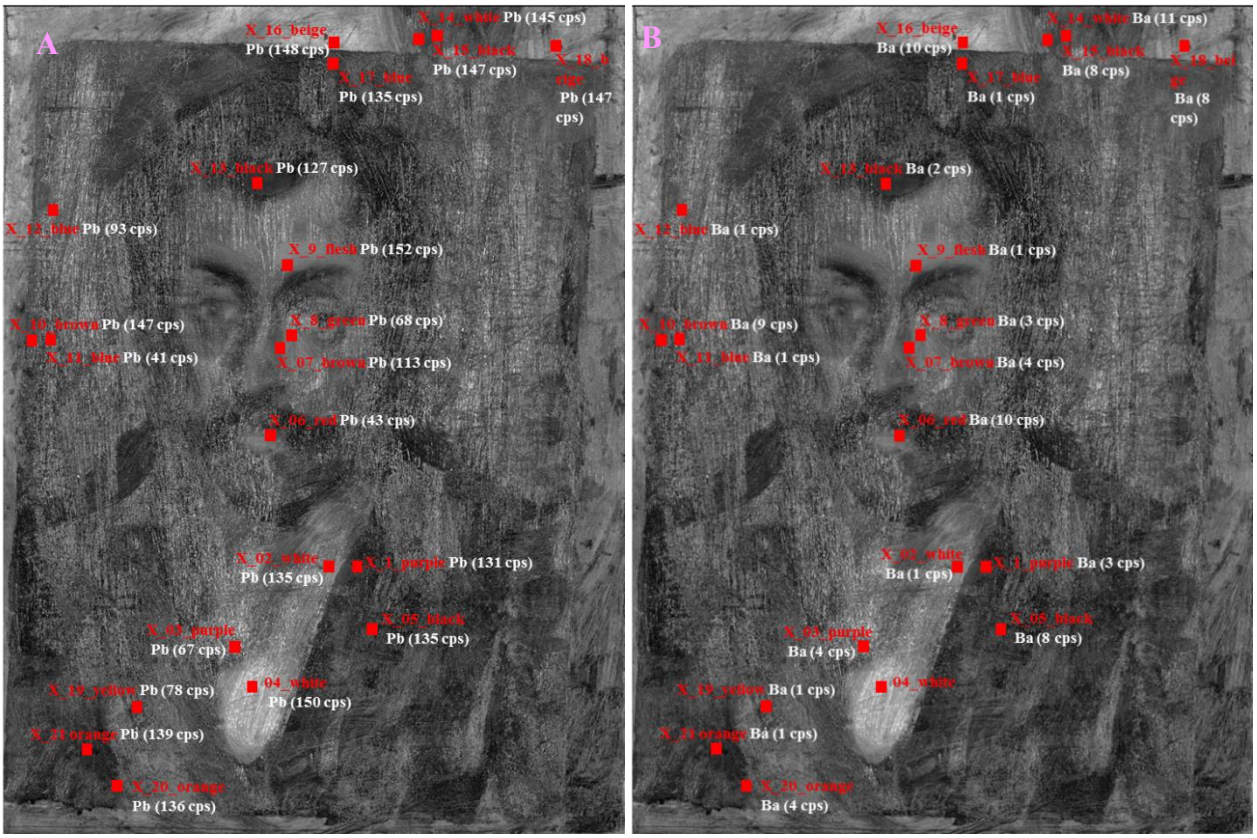
A
X_16_beige Pb (148 cps)
X_14_white Pb (145 cps)
X_15_black Pb (147 cps)
X_18_b ege Pb (147 cps)
X_17_blue Pb (135 cps)
X_13_black Pb (127 cps)
X_12_blue Pb (93 cps)
X_9_flesh Pb (152 cps)
X_10_brown Pb (147 cps)
X_8_green Pb (68 cps)
X_11_blue Pb (41 cps)
X_07_brown Pb (113 cps)
X_06_red Pb (43 cps)
X_02_white Pb (135 cps)
X_1_purple Pb (131 cps)
X_05_black Pb (135 cps)
X_03_purple Pb (67 cps)
X_19_yellow Pb (78 cps)
04_white Pb (150 cps)
X_21 orange Pb (139 cps)
X_20_orange Pb (136 cps)
B
X_16_beige Ba (10 cps)
X_14_white Ba (11 cps)
X_15_black Ba (8 cps)
X_18_bei ge Ba (8 cps)
X_17_blue Ba (1 cps)
X_13_black Ba (2 cps)
X_12_blue Ba (1 cps)
X_9_flesh Ba (1 cps)
X_10_brown Ba (9 cps)
X_8_green Ba (3 cps)
X_11_blue Ba (1 cps)
X_07_brown Ba (4 cps)
X_06_red Ba (10 cps)
X_02_white Ba (1 cps)
X_1_purple Ba (3 cps)
X_05_black Ba (8 cps)
X_03_purple Ba (4 cps)
X_19_yellow Ba (1 cps)
04_white
X_21 orange Ba (1 cps)
X_20_orange Ba (4 cps)

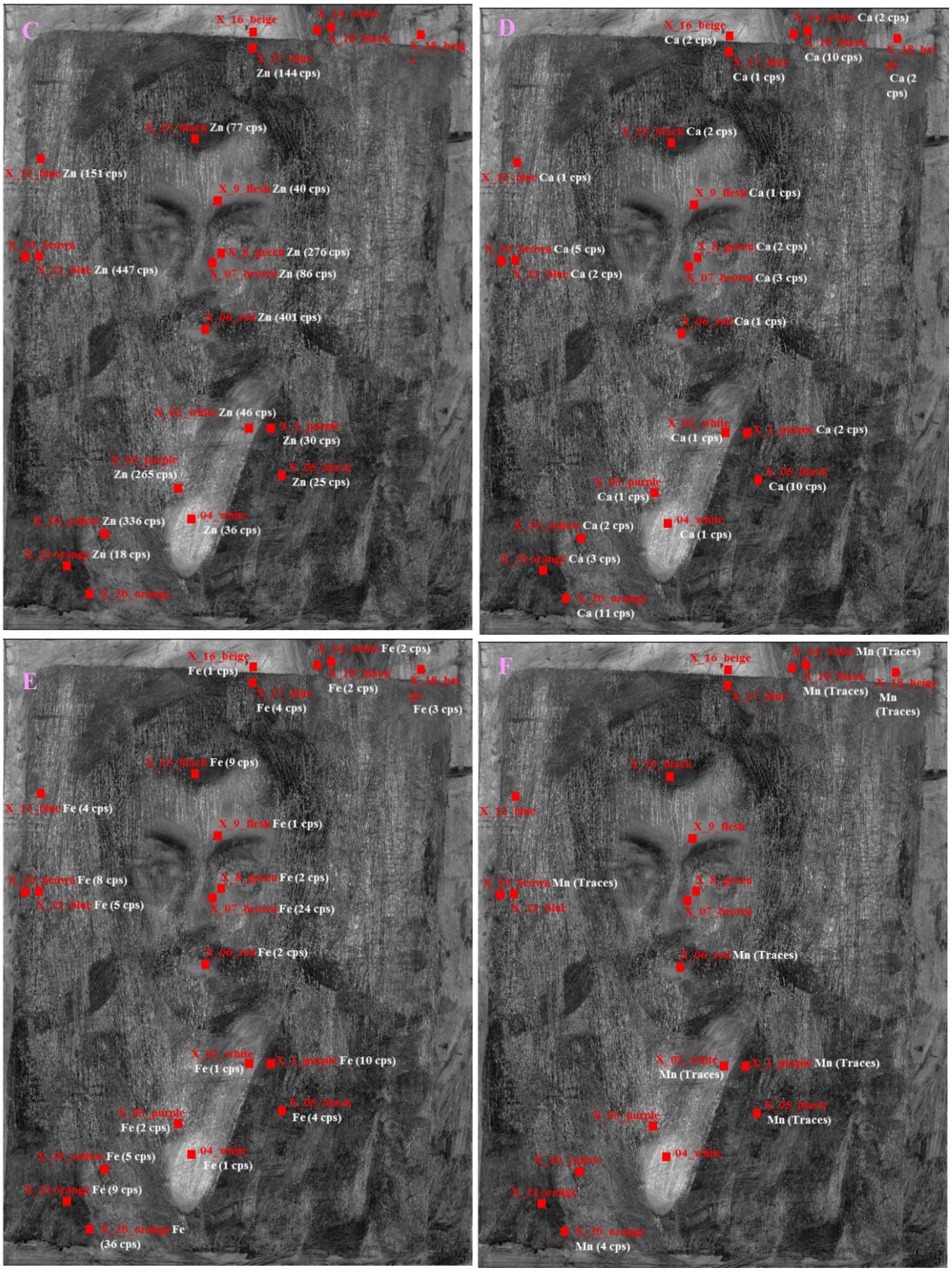
C
X_16_beige
X_14_white
X_15_black
X_18_beig e
X_17_blue
Zn (144 cps)
X_13_black Zn (77 cps)
X_12_blue Zn (151 cps)
X_9_flesh Zn (40 cps)
X_10_brown
X_8_green Zn (276 cps)
X_11_blue Zn (447 cps)
X_07_brown Zn (86 cps)
X_06_red Zn (401 cps)
X_02_white Zn (46 cps)
X_1_purple Zn (30 cps)
X_03_purple Zn (265 cps)
X_05_black Zn (25 cps)
X_15_yellow Zn (336 cps)
X_04_white Zn (36 cps)
X_21_orange Zn (18 cps)
X_20_orange
D
X_16_beige Ca (2 cps)
X_14_white Ca (2 cps)
X_15_black Ca (10 cps)
X_18_bei ge Ca (2 cps)
X_17_blue Ca (1 cps)
X_13_black Ca (2 cps)
X_12_blue Ca (1 cps)
X_9_flesh Ca (1 cps)
X_10_brown Ca (5 cps)
X_8_green Ca (2 cps)
X_11_blue Ca (2 cps)
X_07_brown Ca (3 cps)
X_06_red Ca (1 cps)
X_02_white Ca (1 cps)
X_1_purple Ca (2 cps)
X_05_black Ca (10 cps)
X_03_purple Ca (1 cps)
X_15_yellow Ca (2 cps)
X_04_white Ca (1 cps)
X_21_orange Ca (3 cps)
X_20_orange Ca (11 cps)
E
X_16_beige Fe (1 cps)
X_14_white Fe (2 cps)
X_15_black Fe (2 cps)
X_17_blue Fe (4 cps)
X_18_bei ge Fe (3 cps)
X_13_black Fe (9 cps)
X_12_blue Fe (4 cps)
X_9_flesh Fe (1 cps)
X_10_brown Fe (8 cps)
X_8_green Fe (2 cps)
X_11_blue Fe (5 cps)
X_07_brown Fe (24 cps)
X_06_red Fe (2 cps)
X_02_white Fe (1 cps)
X_1_purple Fe (10 cps)
X_05_black Fe (4 cps)
X_03_purple Fe (2 cps)
X_15_yellow Fe (5 cps)
X_04_white Fe (1 cps)
X_21_orange Fe (9 cps)
X_20_orange Fe (36 cps)
F
X_16_beige
X_14_white Mn (Traces)
X_15_black Mn (Traces)
X_18_beige Mn (Traces)
X_17_blue
X_13_black
X_12_blue
X_9_flesh
X_10_brown Mn (Traces)
X_8_green
X_11_blue
X_07_brown
X_06_red Mn (Traces)
X_02_white Mn (Traces)
X_1_purple Mn (Traces)
X_05_black Mn (Traces)
X_03_purple
X_04_white
X_15_yellow
X_21_orange
X_20_orange Mn (4 cps)

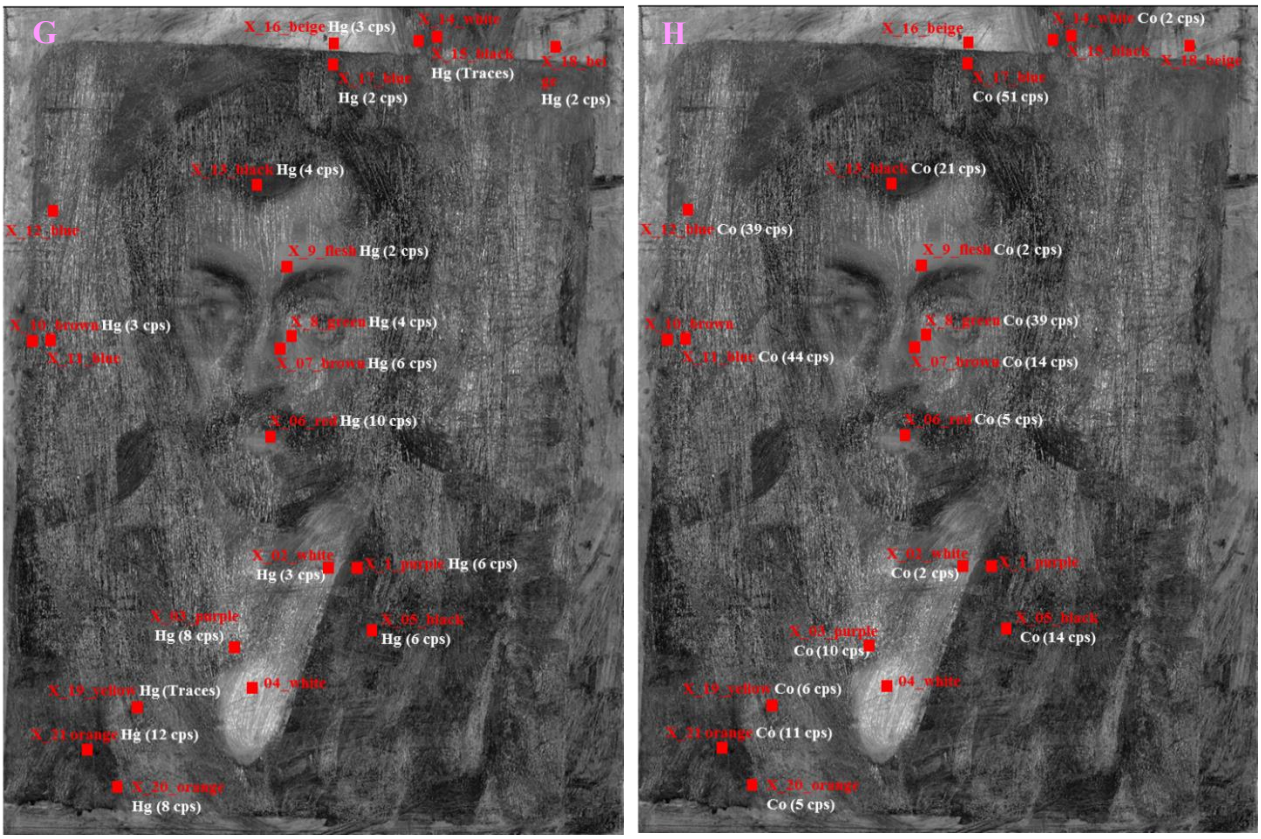

Figure 75. XRF mapping- element distribution and cps obtained: a) Pb, b) Ba, c) Zn, d) Ca, e) Fe, f) Mn, g) Hg, h) Co.

Global discussion of the painting

Composition vs. Areas

Composition I

On the large brown-beige area, Picasso used White lead on which creates a brown shade with some natural earths with silicate matrix. He painted the black areas using ivory/bone black plus Prussian blue and the narrow vertical white trait using white lead. Barium sulphate has been detected, probably due to the underneath layer. It can be considered a filler of a not identified pigment.

Composition II

The Orange is a mixture of white lead, vermilion and red Fe based pigments. The yellow colour has been obtained white lead with a not identified yellow pigment. Use of yellow ochre cannot be discarded. The purple areas contain vermillion and probably Fe based red

pigments – natural earths. Unfortunatly, the green areas on the left side of the painting were not analysed.

Background portrait

The bright brush strokes were painted with a mixture of white lead, white zinc and cobalt blue. Based on the blue colour and the detection of silicate the presence of Ultramarine cannot be excluded.

Subject

The black of the hair is not ivory/bone black, although another but not identified black pigment. A Co based pigment is part of the paint layer. Based on Fe content should be hypotized the use of Fe based black pigments. Carbon black is also possible.

His skin tone was created with Natural earths – silicate matrix, the not identified black, Cobalt blue with touches of vermilion. Red lead cannot be discarded. The nightshirt (or neckerchief) was painted with White lead and White zinc mixed.

Table 41. Pigments and organic compounds organised by areas.

Areas	Pigments	Binder/organic compound
Composition I	White lead, natural earths + silicate matrix, ivory/bone black + Prussian blue, Barium sulphate.	Oil, Animal glue, Varnish
Composition II	White lead, Vermilion + red Fe based pigments/natural earths, White zinc + barium sulphate (Yellow ochre, Cr based pigment*)	
Background	White lead, White zinc, Cobalt blue/Thenard's blue, (Ultramarine blue/silicate base pigment)	
Face (Front/Lips, Cheek)	Vermillion, natural earths – silicate matrix (Red lead), cobalt blue, not identified black	
Hair	Not identified, Cobalt blue (Fe based black pigments, Carbon black)	
nightshirt / neckerchief	White lead, white zinc + barium sulphate.	
Jacket	Not identified (Fe based black pigments, Carbon black)	

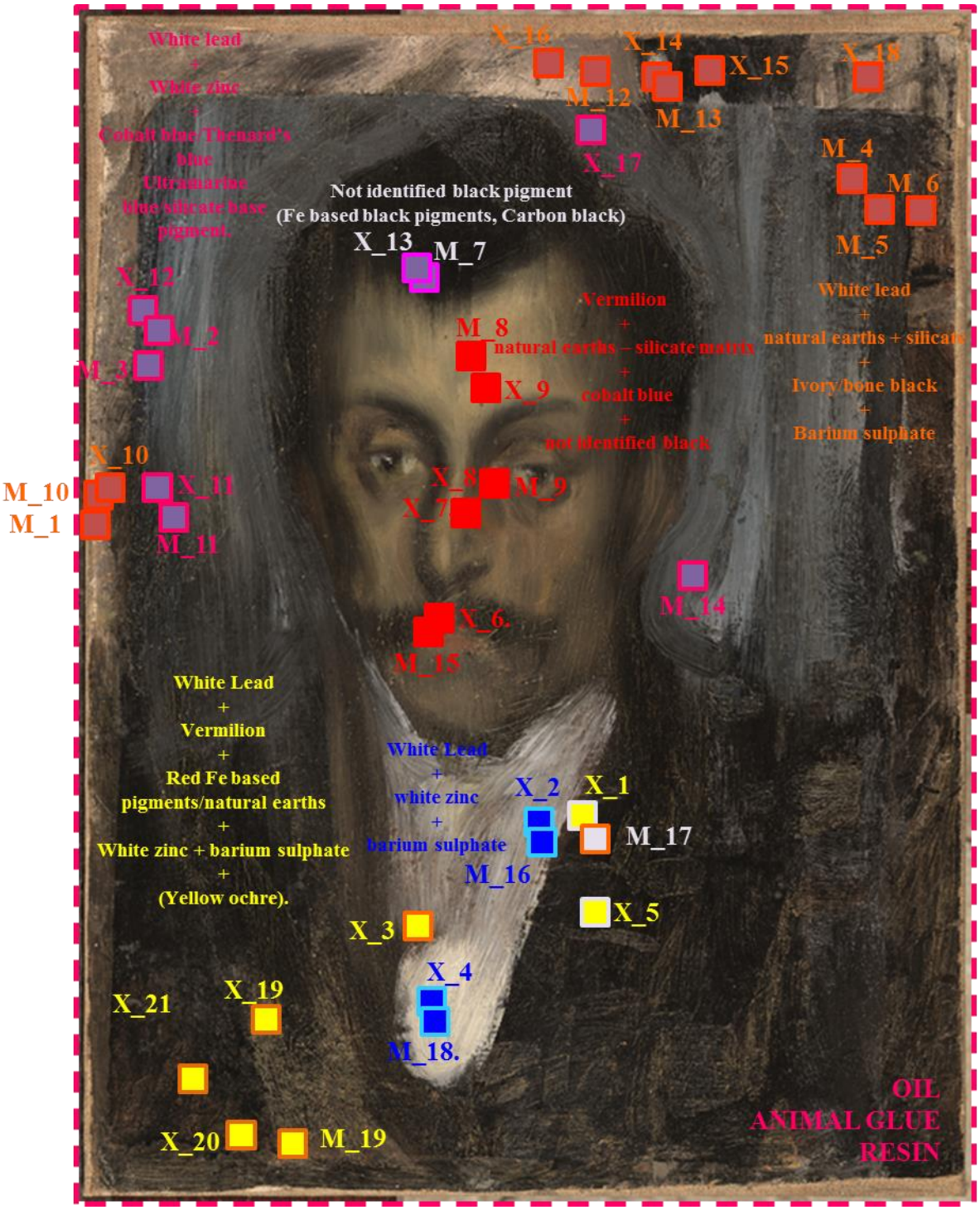

Figure 76. Material distribution mapping

Stratigraphy

The painting could be divided in three compositions. It was possible to directly access the subjacent layers, which belong to the first composition, as well as the portrait layers. We considered mainly the results obtained by XRF, as it is the only technique that reaches also the layers underneath. The stratigraphy of the painting will be reconstructed starting from the support to the superficial layer.

The distribution of Pb, Ca and Ba across the painting surface suggests that the artist used Lead white, Calcium carbonate, and Barium sulphate to prepare the substrate for the first composition. The presence of the preparation layer is clearly visible in the regular pattern highlighted by the XR radiography. After that, Picasso created the first painting, applying white lead with shadows of brown natural earths with silicate matrix. He painted the black areas with ivory/bone black mixed with small amounts of Prussian blue, a pigment used to obtain a deeper colour. It is not clear if Picasso himself used to mix these two colours or if it was a result of the mixture practice of the industrial paint production.

Then, Picasso decided to cover the first picture/painting with the second, more colourful composition. It can be seen through the diluted paint of the portrait, but just on the lower part of the canvas. Lead white, Zinc white and Vermilion with a Fe-based pigment were applied in short and narrow strokes creating a geometric pattern.

The signal of Hg, despite its increase on the flesh and lips of the character, seems to be related also to the composition underneath. Table 42 presents the XRF results obtained in spots corresponding to white areas (high Z number) vs. spots on grey areas (lower Z number) of the XR radiography. The most relevant difference between the spots is the high signal of Hg in correspondence with the central white bright areas.

The Hg signals probably related to the composition underneath seem to be related to the radio-opaque areas highlighted by the XR radiography. The extensive use of Vermilion has been observed also in the *Autoretrat amb Perruca*, described in section 3.3.3, with the probable aim to cover a precedent composition. Point

Following that, Picasso superposed the portrait starting with the face. The skin is a mixture of Lead white with Vermilion and touches of Cobalt blue and Fe-based red pigments. The black of the hair could not be identified although a carbon black or Fe-based black pigment may be assumed. With the same black colour, Picasso painted the jacket. He marked the shoulders simply with two broad lines. In a second moment, when he created the background with Lead white and Cobalt mixed with some silicate matrix pigment – probably Ultramarine – he hid the black line of the shoulders (clearly visible in the NIR image) and modelling the

shape of the head. The white filmy (semi-opaque) effect on the face of the subject and generally on the superficial layer seems related to the distribution of the Zn/Zinc white.

Table 42. XRF results. Comparison between measurements corresponding to white /high Z number areas vs. spots on grey/lower Z number areas in XR radiography.

	cps	Ca	Ba	Mn	Fe	Co	Zn	Pb	Hg
	E (keV)	**3.71**	**5.52**	**5.95**	**6.4**	**6.97**	**8.65**	**10.55**	**9.97**
XR image Bright areas	P026_X_06_red	Traces	10	Traces	2	5	401	43	10
	P026_X_08_green	2	3	/	2	39	276	68	4
	P026_X_09_flesh	Traces	Traces	/	Traces	2	40	152	2
	P026_X_02_white	Traces	Traces	Traces	Traces	6	46	135	3
	P026_X_01_purple	2	3	Traces	10	11	30	131	6
	P026_X_13_black	2	2	/	9	21	77	127	4
	P026_X_05_black	2	Traces	Traces	4	14	25	135	6
	P026_X_13_black	2	2	/	9	21	77	127	4
	P026_X_20_orange	11	4	4	34	5	/	136	8
	P026_X_21_orange	3	Traces (Ti/Ba)	/	9	11	18	139	12
XR image Darker areas	P026_X_19_yellow	2	Traces	/	4	6	336	78	/
	P026_X_04_white	Traces	/	/	Traces	Traces	36	150	/
	P026_X_11_blue	2	Traces	/	5	44	447	41	/
	P026_X_12_blue	Traces	Traces	/	4	39	151	93	Traces
	P026_X_10_brown	5	9	Traces	7	Traces	/	147	/

3.4 Global discussion

The study combines the information obtained with different analytical techniques and documentary researches to investigate Picasso's early palette and his studio practice during the first years of his artistic career.

The global discussion will be organized in three sections. First, a comparison of the results obtained with the bibliography available will be presented. After that, the singularities of each portrait and the common features will be discussed, focusing on some specific topics that need further investigation. Finally, the limitations and capacities of non-destructive techniques employed will be critically analysed.

Comparison with literature

The studies published in the last years about material investigation of Picasso's artworks and his palette are mainly based on his mature production/later works. The main interest found in the different references available was his use of enamel paints, presumably Ripolin® brand. These studies, which investigated a large assortment of artworks, have collected an exhaustive information about Picasso's palette of the years between 1900 and 1946 [1–14]. Furthermore, few sources of information about the materials characteristic of artworks of the first years of the 1900s/20th century could be found, which are not even available as scientific publications. The correlation between these years and his first steps as non-academic artist is not directly possible. The artistic and personal growth of the artist, the evolution of his technique, the different circumstances, places and material suppliers are factors that could totally change the material identity of an artist's palette. Even so, it is possible to find some common points of the *modus operandi* and the material used.

Ripolin® was the most popular house paint during the 20th century. Photographs of Picasso's studio showing cans, from a correspondence with his friend Roland Penrose, and receipts are the evidence that the artist used this kind of enamel paints. Despite of his preference for these new products, the most relevant detail related with the present study is the fact that Picasso never stopped using artist's tube paints. It has been demonstrated that Picasso used both, artist's and no traditional artist's paints in the 1920s and 1930s, and as early as the 1910s[2]. Indeed, the house paint brand provided only a limited selection of pigments, among which the most common tube paint's pigments were notably absent[82]. Thus, Picasso enlarged the color chart including his favorite pigments/paints. Table 43 shows a compendium of the pigments found on Picassos' artworks of the years between 1900 and 1946 (literature

sources) compared with those found on the six portraits dated between 1895 and 1900. It is interesting that the materials found in the present study are comparable to those encountered in other works of the artist. Moreover, there was continuity, in terms of pigments, during his entire career. The artwork considered for comparison are: *Ciència i caritat* (1897)[15]; *Portraits of Hermen Anglada-Camarasa, Santiago Rusiñol and Juli Vallmitjana* (aprox. 1900)[10]; *Life* (1903)[16]; *Les Demoiselles d'Avignon* (1907)[17]; *Head of Harlequin* (1917)[3]; *Still life* (1922)[8]; *Harlequin musician* (1924)[7]; *Harlequin* (1927)[2]; *The Red Armchair* (1931)[8]; *The Dreamer* (1932)[2]; *Reading at Table* (1934); *Woman Asleep at a Table* (1936) [2]; *Femme au chapeau assise sur une chaise* (1938) [8] and a large corpus of paintings conserved at the Picasso Museum of Antibes (1946)[1].

The use of different pigments at the different periods should be discussed carefully, because the variability can be related to different factors, such as the unique features of the artwork, the availability of materials, different artistic techniques and the sensitivity of the analytical techniques used for the investigation. However, an attempt to observe some consistency in the choices made by Picasso can be done.

Prussian blue, for example, has been found very often and on different works. It was used mostly as primary colour in mixtures. Some of the studies highlighted the use of this pigment admixed with yellow chrome or other yellow pigments. This is a common industrial practice documented in the literature[18]. On the *Autoretrat amb perruca* the same mixture has been found in the green areas located on the shoulder of the subject. Moreover, Prussian blue has been found in dark areas[15]. According with the results obtained in this study, the detection of this pigment is strictly limited to the dark/Ivory black areas. It is not clear if this is an intentional admixing by the artist or if it is related to the commercial paint tubes' composition. However, its use permits to improve the hiding power and to obtain more intense dark shades. The **Cobalt-based pi**gments (Cobalt phosphate or Cobalt arsenate) have been detected, mostly in the purple areas, on several paintings with different formulation, depending on the shades desired. Its use has been documented based in the notebooks of his childhoods until his late works created in Antibes in 1946.

The use of **Fe-based pigments**, such as natural brown/red and yellow earths, has been documented and the presence of **Kaolin** as filler of this kind of pigments has been demonstrated. The traces of manganese have been identified as accessory element of the Umber (brown earth). Natural earth pigments are present in several paintings, although based on the variability of the accessory compounds, such as kaolin, silicates and **Mn oxides**, it could be speculated that different materials and/or suppliers, and thus different formulations,

were used. A characteristic specific to the composition of the six portraits is the detection of a high content of Mn and kaolin, not commonly found in other works. **Black pigments** of different chemical composition have been documented, pure or mixed together. Fe-based black pigment has been found only in few works. It is interesting that starting from 1932 the carbon black is predominant. Both Fe-based black pigments and carbon black were not detected in the series of portraits due to the limitation of the techniques. As *Muir et al.* wrote that the black supplied by Ripolin was composed by carbon black. This is only a hypothesis for the reason of the (possible) change in the artist's practice. The green areas generally present mixtures of blue and a yellow paint (e.g. **Chrome green**= Prussian blue + Yellow chrome), although in some cases the detection of Cr could be potentially related to the green Chrome oxide has been also detected. The commonly used yellow pigments were **Yellow ochre** and/or different Cr based pigments, such as **Yellow chrome** (Lead Chromate).

Lead white seems to be a constant of the artist palette and was mainly used to paint the shirt and the face of the subject of the portraits. However, it has been detected in noticeable amounts across the entire surface of the paintings. In the *Retrat de Carles Casagemas* Picasso seems to use the Lead white to apply the intermediate layer between two compositions. This practice was also found in *The Still life* (1922). According to Picasso's correspondence, he was very enthusiastic about how fast the Ripolin was drying and how it permitted him to apply the last touches without any consequence for the first paint layers of his composition[8]. As the practice of the later changes in his paintings and the reuse of canvases has also been observed in the six portraits, it can be speculated that he used white lead as siccative agent. In fact, lead is known for its excellent siccative properties[19]. Picasso probably knew the fast drying of the paint since his academic formation and/or based on empiric observation. The **Barium sulphate** and **calcium carbonate** have also been identified, mainly attributed to filler or/and preparation layers. The **White zinc** has been detected in several others of Picasso's artworks as common artistic paint or as component of the commercial enamel paints. Its presence and its impurities have been specially investigated, mainly because it was used as white pigment or bulking compound admixed in Ripolin paints[5]. On the other hand, its use as artistic pigment is important because this pigment emerges only in the second quarter of the 19th century[2]. A very important evidence of Zn has been found on the two portraits *Retrat d'un desconegut* and *Retrat d'un desconegut a l'estil d'El Greco.* Although a low Zn signal has been detected also on the portrait *Home amb boina* dated 1895, the considerable content of Zn based pigments in the two later portraits of the series seems relevant and should be studied further.

Table 1. Compendium of the pigments founds on Picasso's artworks between 1900 and 1946: literature sources (pink) vs. six portraits of early Picasso project (green). N.C.= (no confirmed).

		Calcium Carbonate	White lead	Lead sulphate	Barium sulphate	Sulphate	Kaolin	Silicate	Zinc White	Cr based pigm.	Chrome green (Y. chrome+ Prussian b.)	Strontium yellow	Naples yellow
Early Picasso*	**1895**												
	1895												
	1897/8 (1900)												
	1899/ 1900												
	1899				N.C								
	1899-1900												
Literature	**1897**												
	1900												
	1903												
	1907												
	1917												
	1922												
	1924												
	1927												
	1931												
	1932												
	1934												
	1936												
	1938												
	1946												

**Early Picasso: 1. Home amb boina (1895); 2. Retrat d'un vell (1895); 3. Autoretrat amb perruca (1897/1898 or/and 1900); 4. Retrat de Casagemas (1899/1900); 5. Retrat d'un desconegut a l'estil de El Greco (1899); 6. Retrat d'un desconegut (1899/1900)*

Table 1 (continued)

		Cd Yellow/red	Vermilion	Mn oxides	Natural earths	Fe based black pigment	Carbon black	Ivory/bone black	Prussian Blue	Ultramarine	Co based pigment	Cu based pigments	Red lead
Early Picasso*	**1895**					**N.C.**	**N.C.**						**N.C.**
	1895					**N.C.**	**N.C.**			**N.C.**			**N.C.**
	1897/8 (1900)					**N.C.**	**N.C.**						**N.C.**
	1899/ 1900				**N.C.**	**N.C.**	**N.C.**	**N.C**					**N.C.**
	1899		**N.C.**			**N.C.**	**N.C.**			**N.C.**			**N.C.**
	1899-1900					**N.C.**	**N.C.**						**N.C.**
Literature	**1897**												
	1900												
	1903					-	-						-
	1907												
	1917												
	1922												
	1924												
	1927												
	1931												
	1932												
	1934												
	1936												
	1938												
	1946												

**Early Picasso: 1. Home amb boina (1895); 2. Retrat d'un vell (1895); 3. Autoretrat amb perruca (1897/1898 or/and 1900); 4. Retrat de Casagemas (1899/1900); 5. Retrat d'un desconegut a l'estil de El Greco (1899); 6. Retrat d'un desconegut (1899/1900)*

Portrait highlights

Each portrait results to be a unique piece with own personality and structure. With a simple palette Picasso was able to play with the colours to create different shades and tones. Despite his undeniable talent since the beginning of his career, an evolution can be noticed from his portraits of A Coruña and the later works of this series of portraits. The meticulous inspection of the brush strokes and material distribution helps to notice important details, which allow an understanding of the *modus operandi* of the young artist.

For example the **role of the background**, in which Picasso framed the subjects, changes. In the two Galician portraits, dated 1895, *Retrat d'un vell* and *Home amb boina*, Picasso applied lighter brush strokes on the dark area creating different light focuses. These elements seem to manifest the intention to create a complex light space. Furthermore, the use of the background paint to crop/mark the profile of the subject seems to be applied with rather hesitant brush strokes. This observation is based on the smears of the paint observed on the profile of both portraits, and evident on the backside of the beret of the *Home amb boina*. Instead, in *Autoretrat amb perruca* the background seems to lose its importance. Confused brushstrokes cover the previous composition and few red-white lines brighten up the background with unclear intention. In *Retrat de Carles Casagemas* the green areas and few grey strokes on the left-side shoulder of the subject seem to be a reminiscence of his first works. On the other hand, in the two paintings *Retrat d'un desconegut* and *Retrat d'un desconegut a l'estil d'El Greco* the background shows an important role in the composition. The brushstrokes were applied in a confident manner and are used to mould/shape the subjects.

The **non-destructive techniques** used in this study permitted to obtain useful information about the paintings, in terms of composition and structure. A meticulous evaluation and comparison between all the complementary data available is important to reconstruct and identify the materials and their distribution. Key tools employed as guidelines for data interpretation were the subsurface images (XR radiography and NIR reflectography). Indeed, the absence of the radiography during the analysis of *Home amb boina* and *Retrat d'un vell* was a rather important issue. However, thanks to the NIR images, it was possible to demonstrate that the well-documented practice of the artist to reuse the canvas is not limited only to his later works of this period but was common even during the first years of his career. All the works present a complex layer structure with overlapped compositions.

The NIR images were very important to better understand the fulcrum of the series, *Autoretrat amb Peluca.* The observation of a well-defined profile of the hair under the wig

permits to split the paintings in three different artistic creations: the already known *Home amb Barret* and *Autoretrat amb perruca,* and the intermediate step of the *Autoretrat*. Picasso modified his self-portrait superposing a wig on his head and applied probably few black brushstrokes, mainly changing the left-hand side eye, which gives the feeling of more mature vision of himself. It is important to remark that the possibility to access to the subjacent layer strongly depends on the physicochemical nature of the materials and their distribution. This is the reason why not all the hidden compositions of the portraits were clearly visible.

The non-destructive punctual analysis techniques allowed achieving the elemental and molecular composition of a high number of spots of the surface layers accessible. Mappings of the compounds detected across the entire surface were created and it was possible to develop a rather complete idea of all the different areas of the artworks. The important limitation of this kind of techniques is the lack of information about the in depth composition and materials distribution. Indeed, the attribution of the compound and elements encountered to a specific layer is a complex problem. The sequence of the painting layer was not clear especially for the *Retrat d'un desconegut* and some doubts about the use and location of the Hg/Vermilion layer arose in the *Autoretrat amb perruca* and the same *Retrat d'un desconegut.* The same can be commented about the distribution of Zn in *Retrat d'un desconegut a l'estil de El Greco.* In these cases, the XRF spectra were complex combinations of all paint layers. Many interferences and overlapped peaks hindered the interpretation. The determination of elements such as Zn, Cu and Hg was thwarted by the signal of the tungsten X-ray source. Moreover, the interpretation and assignment of the characteristic bands in the reflectance infrared spectra was difficult and laborious. A large number of inorganic compounds were identified, but only general information about the organic binder and restoration material was achieved. The information of both techniques and some complementary measurements of NIR reflectance spectra and Raman were essential to understand the palette used to paint the different works, although the low sensitivity of these techniques did not permit to answer all the questions about the composition. For example, the presence of a Strontium signal encountered on the *Retrat de Carles Casagemas*, which suggests the possible use of Strontium yellow, should be investigated further. In the same painting, some doubts remain about the kind of black paint used. Moreover, it was not possible to confirm or exclude the use of Ultramarine blue on the *Home amb boina* and the *Retrat d'un desconegut*. Moreover, the use and distribution of White zinc is also an other topic to be investigate in the future.

3.5 References

1. *www.charismaproject.eu*.

2. Miliani, C., Rosi, F., Brunetti, B. G. & Sgamellotti, A. In situ noninvasive study of artworks: the MOLAB multitechnique approach. *Acc. Chem. Res.* **43,** 728–738 (2010).

3. Palau i Fabre, J. *Picasso The early years 1881-1907*. 558 (Rizzoli New York, 1980).

4. Ocaña, M. T., Gual, M., Léal, B. & Torras, M. *Young Picasso/Picasso Joven*. 339

5. Delbourgo, S. Etude de la matière picturale de Pablo Picasso. in *Icom Comm. Conserv. 6th Trienn. Meet.* 9 (ICOM, 1981).

6. Vallès, E. & Cendoya, I. *Yo Picasso, Autoretrats*. 175 (Museo Picasso, 2013).

7. Vagnini, M. *et al.* FT-NIR spectroscopy for non-invasive identification of natural polymers and resins in easel paintings. *Anal. Bioanal. Chem.* **395,** 2107–18 (2009).

8. Miliani, C., Rosi, F., Burnstock, A., Brunetti, B. G. G. & Sgamellotti, A. Non-invasive in-situ investigations versus micro-sampling: a comparative study on a Renoirs painting. *Appl. Phys. A* **89,** 849–856 (2007).

9. Daffara, C., Pampaloni, E., PEZZATI, L., Barucci, M. & FONTANA, R. Scanning multispectral IR reflectography SMIRR: an advanced tool for art diagnostics. *Acc. Chem. Res.* **43,** 847–56 (2010).

10. Amat, A., Miliani, C. & Brunetti, B. G. Non-invasive multi-technique investigation of artworks: A new tool for on-the-spot data documentation and analysis. *J. Cult. Herit.* **14,** 23–30 (2013).

11. Rosi, F. *et al.* On the use of overtone and combination bands for the analysis of the CaSO4-H2O system by mid-infrared reflection spectroscopy. *Appl. Spectrosc.* **64,** 956–963 (2010).

12. Ricci, C. *et al.* The Perugino's palette: integration of an extendedin situ XRF study by Raman spectroscopy. *J. Raman Spectrosc.* **35,** 616–621 (2004).

13. Rosi, F. *et al.* An integrated spectroscopic approach for the non-invasive study of modern art materials and techniques. *Appl. Phys. A Mater. Sci. Process.* **100,** 613–624 (2010).

14. Rosi, F. *et al.* A non-invasive XRF study supported by multivariate statistical analysis and reflectance FTIR to assess the composition of modern painting materials. *Spectrochim. Acta Part A Mol. Biomol. Spectrosc.* **71,** 1655–1662 (2009).

15. Miliani, C. *et al.* In situ non-invasive investigation on the painting techniques of early Meissen Stoneware. *Spectrochim. Acta Part A Mol. Biomol. Spectrosc.* **73,** 587–592 (2009).

16. Monico, L., Rosi, F., Miliani, C., Daveri, A. & Brunetti, B. G. Non-invasive identification of metal-oxalate complexes on polychrome artwork surfaces by reflection mid-infrared spectroscopy. *Spectrochim. Acta. A. Mol. Biomol. Spectrosc.* **116,** 270–80 (2013).

17. Casadio, F. *et al.* Scientific Investigation of an Important Corpus of Picasso Paintings in Antibes : New Insights into Technique , Condition , and Chronological Sequence. *J. Am. Inst. Conserv.* **52,** 184–204 (2013).

18. Ricci, C., Miliani, C., Brunetti, B. G. & Sgamellotti, A. Non-invasive identification of surface materials on marble artifacts with fiber optic mid-FTIR reflectance spectroscopy. *Talanta* **69,** 1221–1226 (2006).

19. Brunetti, B. G., Matteini, M., Miliani, C., Pezzati, L. & Pinna, D. MOLAB, a mobile laboratory for in situ non-invasive studies in arts and archaeology. *Sect. Title Hist. Educ. Doc.* **116,** 453–462 (2007).

20. Rosi, F., Miliani, C., Borgia, I., Brunetti, B. & Sgamellotti, A. Identification of nineteenth century blue and green pigments by in situ x-ray fluorescence and micro-Raman spectroscopy. *J. Raman Spectrosc.* **35,** 610–615 (2004).

21. Rosi, F. *et al.* Multivariate chemical mapping of pigments and binders in easel painting cross-sections by micro IR reflection spectroscopy. *Anal. Bioanal. Chem.* **399,** 3133–3145 (2011).

22. Clementi, C. *et al.* Photoluminescence properties of zinc oxide in paints: a study of the effect of self-absorption and passivation. *Appl. Spectrosc.* **66,** 1233–41 (2012).

23. Monico, L., Janssens, K., Miliani, C. & Brunetti, G. Supporting Information The Degradation Process of Lead Chromate in paintings by Vincent van Gogh studied by means of Spectromicroscopic methods . Part III : Synthesis , characterization and detection of different crystal forms of the chrome yellow pigment. 1–13

24. Monico, L. *et al.* Degradation Process of Lead Chromate in Paintings by Vincent van Gogh Studied by Means of Spectromicroscopic Methods. 4. Arti fi cial Aging of Model Samples of Co-Precipitates of Lead Chromate and Lead Sulfate. **4,** (2013).

25. Miliani, C. *et al.* Original and fake blue pigments from the church of S. Francesco in Montefalco painted by Benozzo Gozzoli: a spectroscopic approach. *Proc. IRUG6 Conf.* (2004).

26. Miliani, C., Rosi, F., Daveri, A. & Brunetti, B. Reflection infrared spectroscopy for the non-invasive in situ study of artists' pigments. *Appl. Phys. A Mater. Sci. Process.* **106,** 295–307 (2012).

27. Romani, A., Clementi, C., Miliani, C. & Favaro, G. Fluorescence spectroscopy: a powerful technique for the noninvasive characterization of artwork. *Acc. Chem. Res.* **43,** 837–846 (2010).

28. Vagnini, M. *et al.* FT-NIR spectroscopy for non-invasive identification of natural polymers and resins in easel paintings. *Anal. Bioanal. Chem.* **395,** 2107–2118 (2009).

29. Miliani, C. *et al.* Fiber-optic Fourier transform mid-infrared reflectance spectroscopy: A suitable technique for in situ studies of mural paintings. *Appl. Spectrosc.* **61,** 293–299 (2007).

30. Monico, L. *et al.* Degradation process of lead chromate in paintings by Vincent van Gogh studied by means of spectromicroscopic methods. 3. Synthesis, characterization, and detection of different crystal forms of the chrome yellow pigment. *Anal. Chem.* **85,** 851–9 (2013).

31. Buti, D., Rosi, F., Brunetti, B. G. & Miliani, C. In-situ identification of copper-based green pigments on paintings and manuscripts by reflection FTIR. *Anal. Bioanal. Chem.* **405,** 2699–711 (2013).

32. Muehlethaler, C., Massonnet, G. & Esseiva, P. The application of chemometrics on Infrared and Raman spectra as a tool for the forensic analysis of paints. *Forensic Sci Int* **209,** 10 (2011).

33. Sessa, C., Bagán, H. & García, J. F. Evaluation of MidIR fibre optic reflectance: detection limit, reproducibility and binary mixture discrimination. *Spectrochim. Acta. A. Mol. Biomol. Spectrosc.* **115,** 617–28 (2013).

34. Poli, T., Chiantore, O., Nervo, M. & Piccirillo, A. Mid-IR fiber-optic reflectance spectroscopy for identifying the finish on wooden furniture. *Anal Bioanal Chem* **400,** 1161–1171 (2011).

35. Castro, K., Pérez-Alonso, M., Rodríguez-Laso, M. D., Fernández, L. a & Madariaga, J. M. On-line FT-Raman and dispersive Raman spectra database of artists' materials (e-VISART database). *Anal. Bioanal. Chem.* **382,** 248–58 (2005).

36. Identification of nineteenth century blue and green pigments by in situ x-ray fluorescence and micro-Raman spectroscopy - Rosi - 2004 - Journal of Raman Spectroscopy - Wiley Online Library.

37. Sessa, C., Vila, A. & Garcia, J. F. Determination of detection limits for SEM-EDS and m-FTIR analysis of artwork. - *Anal. Bioanal. Chem.* - *Anal. Bioanal. Chem.* **400,** 2241–2251 (2011).

38. Sawczak, M. *et al.* Complementary use of the Raman and XRF techniques for non-destructive analysis of historical paint layers. *Appl. Surf. Sci.* **255,** 5542–5545 (2009).

39. Burnstock, A., Reissner, E., Richardson, C. & Berg, K. J. Van Den. Inorganic Materials from Paintings and Watercolours By Paul Cézanne from The Courtauld Gallery Using two Methods of Non-Invasive Portable XRF with Light Microscopy and SEM / EDX Spectroscopy. in *9th Int. Conf. NDT Art, Jerusalem Isr. 25-30 May 2008* 25–30 (2008).

40. Trentelman, K. *et al.* The examination of works of art using in situ XRF line and area scans. *X-Ray Spectrom.* **39,** 159–166 (2010).

41. Miguel, C., Lopes, J. A. J. A., Clarke, M., Melo, M. J. & João, M. Combining infrared spectroscopy with chemometric analysis for the characterization of proteinaceous binders in medieval paints. *Chemom. Intell. Lab. Syst.* **119,** 32–38 (2012).

42. Bacci, M. & Picollo, M. Non-Destructive Spectroscopic Detection of Cobalt(II) in Paintings and Glass. *Stud. Conserv.* **41,** 136–144 (1996).

43. Vahur, S., Teearu, A. & Leito, I. ATR-FT-IR spectroscopy in the region of 550-230 cm-1 for identification of inorganic pigments. *Spectrochim. Acta. A. Mol. Biomol. Spectrosc.* **75,** 1061–72 (2010).

44. Ocaña, M. T., Bonet, J. M. & Vives, R. *Picasso The development of a genius 1890-1904*. (1997).

45. Tel, B., Sra, L., Jim, R. & Picasso, M. *Els Terrats de Barcelona*. 1–11 (1903).

46. Picasso, P. *Picasso et les maîtres*. (Éditions de la Réunion des musées nationaux, 2008). at <http://cataleg.ub.edu/record=b1912650~S1*cat>

47. Barrie, P. *Picasso Joven*.

48. Vahur, S., Knuutinen, U. & Leito, I. ATR-FT-IR spectroscopy in the region of 500-230 cm-1 for identification of inorganic red pigments. *Spectrochim. Acta. A. Mol. Biomol. Spectrosc.* **73,** 764–71 (2009).

49. Casadio, F. *et al.* Pablo Picasso to Jasper Johns: a Raman study of cobalt-based synthetic inorganic pigments. *Sect. Title Hist. Educ. Doc.* **43,** Ahead of Print (2012).

50. Arslanoglu, J., Centeno, S. a., Digney-Peer, S. & Duvernois, I. "Picasso in The Metropolitan Museum of Art": An Investigation of Materials and Techniques. *J. Am. Inst. Conserv.* **52,** 140–155 (2013).

51. R T, D. The RRUFF Project: an integrated study of the chemistry, crystallography, Raman and infrared spectroscopy of minerals. in *Progr. Abstr. 19th Gen. Meet. Int. Mineral. Assoc. Kobe* (2006). at <http://rruff.info/cinnabar/display=default/R050072>

52. Ocaña, M.Teresa; Fontbona, Francesc; Mendoza,Cristina; Gual, Malén; Bagunyà, Lluis; McCully, Marylin; Rafat i Planas, Claustre; Doñate, Mercè; Panyella, Vinyet; Palau i Frabres, J. *Picasso i Els 4Gats*. 322 (1995).

53. McCully Natasha, M. S. Picasso: the early years, 1892-1906. 374 (1997).

54. Washington, N. G. of art. Exhibition Picasso The Early Years 1892–1906 . (1997).

55. Fabre, J. P. i. *Picasso i els seus amics catalans*. 63–131 (2006).

56. Vallès, Eduard;Casacubertas, Margarida; Panyella, Vinyet; Trenc, E. *Picasso versus Rusiñol*. 421 (2010).

57. David Chalif, M.D., J. & Chalif, D. J. The Death of Casagemas: Early Picasso, The Blue Period, Mortality and Redemption. *Neurosurgery* **61,** 404–417 (2007).

58. *Picasso in the Metropolitan Museum of Art*. 364 (Yale University Press, 2010).

59. Picasso, P., Baldassari, A. & Rubin, W. S. *Picasso et le portrait*. (Flammarion, 1996). at <http://cataleg.ub.edu/record=b1309810~S1*cat>

60. Berg, J. D. J. van den. Analytical chemical studies on traditional linseed oil paints. *Univ. Amsterdam* (2002).

61. Brostoff, L. B., Maynor, C. I. & Speakman, R. J. Preliminary Study of a Georgia O ' Keeffe Pastel Drawing Using XRF and μXRD. 154–166 (2009).

62. Burkhardt, J. & Grillo-Werke., A. G. in *Ind. Inorg. Pigment.* (Buxbaum, G. & Pfaff, G.) 88–94 (2005).

63. Eastaugh, N., Siddall, RuthWalsh, V. & Chaplin, T. *Pigment Compendium: A Dictionary of Historical Pigments*. 202 (Elsevier, 2006).

64. Sessa, C., Miquel, À., Marín, E. & García-Martínez, J. *Informe sobre l ' obra " Els Terrats de Barcelona " de Picasso a partir de les imatges obtingudes mitjançant reflectometria de infraroig Índex*. 1–20 (2013).

65. Shen, Y. *et al.* Study on the preparation and formation mechanism of barium sulphate nanoparticles modified by different organic acids. *J. Chem. Sci.* **119,** 319–324 (2007).

66. Robinet, L. & Corbeil, M. The Characterization of Metal Soaps. *Stud. Conserv.* **48,** 23–40 (2003).

67. Bacci, M. & Picollo, M. Non-Destructive Spectroscopic Detection of Cobalt (II) In Paintings and Glass. *Stud. Conserv.* **41,** 136–144 (1996).

68. Moezzi, A., McDonagh, A. M. & Cortie, M. B. Zinc oxide particles: Synthesis, properties and applications. *Chem. Eng. J.* **185-186,** 1–22 (2012).

69. Mayer, R. *The Artist's handbook of Materials&Techniques*. 1–761 (1991).

70. Hradil, D., Grygar, T., Hradilová, J. & Bezdička, P. Clay and iron oxide pigments in the history of painting. *Appl. Clay Sci.* **22,** 223–236 (2003).

Chapter 4

A procedure for faded silver image recovery by means of X-Ray fluorescence spectroscopy

Context

This chapter is focused on the optimisation of XRF technique for trace elements determination on salt print images and its application for the recovery of faded cases.

* This study was accomplished during a three months fellowship at the Department of Scientific Research of the Metropolitan Museum of Art (MET, NY).

[The authors of the future publication rising from this study will be Clarimma Sessa[1], Lisa Barro[2], Silvia A. Centeno[3], Federico Caro[3], Héctor Bagán[1], Jose Francisco Garcia[1]*
[1] Analytical Chemistry Department, University of Barcelona, Spain
[2] Department of Photograph Conservation, The Metropolitan Museum of Art, New York, NY
[3] Department of Scientific Research, The Metropolitan Museum of Art, New York, NY]

4.1 Introduction

Since the first attempts to produce salt print photographs (1839), there was concern about the phenomena of fading that alter this type of images[1]. Indeed, in 1855 the Photographic Society of London appointed a committee of chemists and photographers to investigate the causes of the degradation with the aim to establish a conservation protocol. Many experiments were performed, but the specific causes were not identified and are still under investigation, although the influence of factors such as temperature, humidity and moisture on aging and discoloration has been demonstrated[2].

The salt print photographs have a very thin image layer without organic binder. The image-forming layer is deposited directly on the top layer of the paper fibres or on a thin layer of sealant, which prevents deeper penetration of the reagent. In this case, the image-forming substance is metallic silver, which is the main element encountered. However, the chemical composition of such images may change depending on the support, processing and toning. A photographic silver image is made permanent (fixed), after development, by bathing it in a solution containing, in the most of the cases, thiosulfate, which forms a soluble thiosulfate complex with the residual silver halide[3]. Then, the residues are removed by means of water baths. The improper execution of the fixing and washing steps may result in residues of sulphur or undeveloped silver. In particular, the presence of sulphur (retained Hypo) is described as a very important cause of deterioration, mostly manifested as fading of the images. Thus, the identification of sulphur is crucial in the investigation of photographic images. The detection of traces of this element and its relation with the image-forming silver are extremely valuable to understand the processes and photographic techniques specific to particular artists, or to assess possible contaminations in the presence of moisture and adequate temperature[4–7]. The residual thiosulfate, because of its labile sulphur, reacts with the silver in the image to form silver sulphide[8], especially at high relative humidity. The effect of excessive sulfiding of the silver image first appears in the areas of low silver density, the highlights, causing the image surface to become brownish. Despite this change on colour tone, not all the silver salt print photographs present the same degradation status. The colour change/fading is clearly complex and there is considerable variation between different images with the same chemistry and even between different areas of the same image. Two artistic salt print photographs, part of the Metropolitan Museum of Art's collection, were analysed with the aim to compare two different cases: the Gustave Le Gray's old-hypo image '*View from Photographer's Studio'* (1850s) that does not appear deteriorated and the "*Lady Elizabeth (Rigby) Eastlake*" (1843-1847) by the photographers

Robert Adamson and David Octavius Hill, which shows an evident fading phenomenon. Both images were selected by the conservator of photographs L. Barro and the research scientist S. Centeno, as representatives of two different real cases, in which the detection of the sulphur and its relation with silver could be crucial to better understand degradation mechanisms and print-out processes. The objective of this study is twofold: first, to optimize the sulphur determination in salt silver photographs by means of X-ray fluorescence (XRF), and second to apply this technique to investigate a procedure for fade image recovery in this type of photographs. For this purpose, standards created by the Analytical Sciences Division of Kodak's Technology Centre and facsimile photographs realized by Lisa Barro were analysed.

4.2 Experimental

The XRF has been extensively employed to perform elemental analysis on photographs [9–11]. It is non-destructive, fast and easy to apply, although it has some limitations on the detection of low-Z elements [12].

4.2.1 Materials/samples

The following samples were analysed in the study:

- Retained hypo standards created by the Analytical Sciences Division of Kodak's Technology Center;
- Two no-art silver print photographs processed with an old-hypo thiosulfate bath that will be named A1 and B1;
- Two gray scales corresponding to the images A1 and B1;
- A silver print photograph "*View from Photographer's Studio*" by Gustave Le Gray (19th century, Gilman Collection, Acc. 2005.100.190, ©The Metropolitian Museum of Art);
- A silver print photograph "*Lady Elizabeth (Rigby) Eastlake*" by the photographers Hill and Adamson (1843-1847, Acc. 2013.159.12, ©The Metropolitian Museum of Art).

The specificities of these cases are described below.

Standards and Photographic facsimiles description

To prepare the *retained hypo* standards, strips of Kodak Edge-7 paper were processed to cover a wide range of "retained hypo" on the surface. They were characterized by ICP-OES (Figure 1) by the Analytical Sciences Division of Kodak's Technology Centre. The labels

and the concentrations obtained for each standard are showed in Table 1. The sample at 2µg [S]/cm^2 is a row stock non-processed paper with the emulsion layer removed with bleach. This standard has to be considered as a "blank "or zero level of hypo deposition. The paper contains TiO_2 and ZnO as brightener components.

Table 1. Standard labels and corresponding concentration ICP-AES values (µg/cm^2)

Labels	µg [S] /cm^2
A	2
B	20
C	23
D	30
E	38
F	56
G	60
H	72

Figure 1. Standards of "Hypo retained" created by the Kodak's Technology Centre.

Two accelerated ageing no-art photographs have also been characterized. They are part of the series of facsimiles created by the photographs conservator Lisa Barro during a large and exhaustive research about image tonality in Gustave Le Gray's salted paper prints published in 2005[14]. The two reproductions were salt for three minutes with 5% ammonium chloride and sensitized with 15% silver nitrate. The image "*A1*" was put in an old hypo bath for 60 hours, whereas the image "B1" was only immersed for 15 hours to simulate some of the procedure used by Le Gray and described in his treatises (Figure 2).

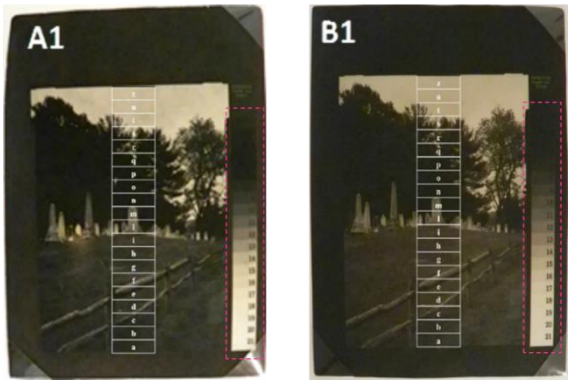

Figure 2. Facsimiles A1 and B1 (the magenta dotted line indicate the grey scale).

Art Photographs

The *"View from Photographer's Studio"* (1851–54) of the nineteenth century French photographer Gustav Le Gray is a salted paper print from paper negative (Figure 3). *Barro et al*. wrote about this image that *"...The immediate assumption is that the silver image has deteriorated to a yellow/ochre tone. It does, however, resemble freshly made experimental samples when left for an extended immersion in the old hypo bath"*[15]. Thus, the photograph is of interest for the study because according to the procedure of Le Gray to intentionally used an 'artificially aged' sodium thiosulfate bath to fix his prints, this should be a case of high hypo retention that it is not affected by fading phenomena[14]. The spots marked with red and violet stars were analysed in two different moments and permit to verify the reproducibility of the method.

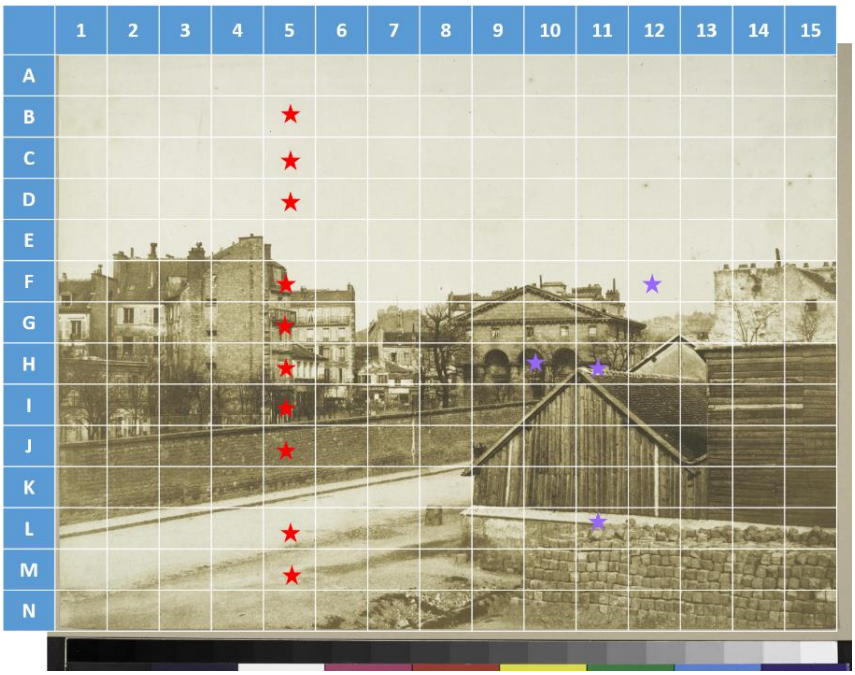

Figure 3 'View from Photographer's Studio'. The Metropolitan Museum of Art, Gilman Collection, (2005.100.190) Photograph ©The Metropolitian Museum of Art

The salt print photograph that depicts the British author, art critic and art historian "*Lady Elizabeth (Rigby) Eastlake*" (1843-1847) is a work of the artists Robert Adamson (British, Scotland 1821–1848) and David Octavius Hill (British, Scotland 1802–1870) (Figure 4). The two photographers produced several bodies of work from 1843 to 1847, including genre portraits and architectural views[16]. Many of these images are now seriously faded and damaged. Several examples can be viewed on the web site of the Metropolitan Museum of Art (NY), J. P. Getty Museum and other famous collections. Among the, the image

collections of the Edinburgh University is particularly interesting for this investigation. In fact, in the museum of this institution is conserved a reproduction of the photograph "*Lady Elizabeth (Rigby) Eastlake*", which the artists Hill and Adamson created using the same negative. The two images with the same subject present different grade of conservation.

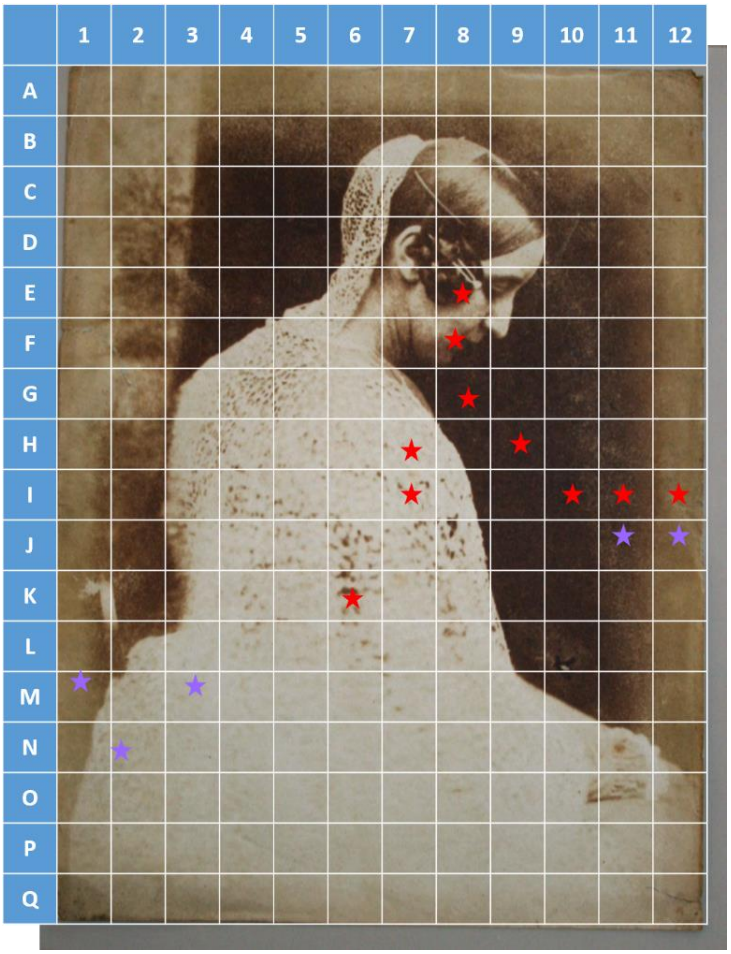

Figure 4. 'Lady Elizabeth (Rigby) Eastlake'. The Metropolitan Museum of Art, 2013. (2013.159.12) Photograph ©The Metropolitian Museum of Art.

4.2.2 Instrumentation

X-ray fluorescence (XRF) measurements were performed using a Bruker ARTAX 400 instrument equipped with an Rh tube and a Si drift detector. The instrument comprises with a CCD camera, used for visualizing the sample, which serves two main purposes in the measuring process: firstly, it is used for the optical analysis of the sample and the selection of the measuring point. Secondly, and in conjunction with a laser spot and crosshairs on the video display, it allows the reproducible setting of the measuring distance.

4.2.3 Experiment set-up and data treatment

For the optimization of the method, a series of ten measurements was performed by XRF on a single spot for each standard on the same central location (coordinate F4) and on different points following a stencil. This permits each spectrum to be mapped to an x/y coordinate and to evaluate the distribution of the element considered. The measurements were performed with no mat-paper support and with air beneath (Figure 5) to avoid noise and possible signal not related to the specimen.

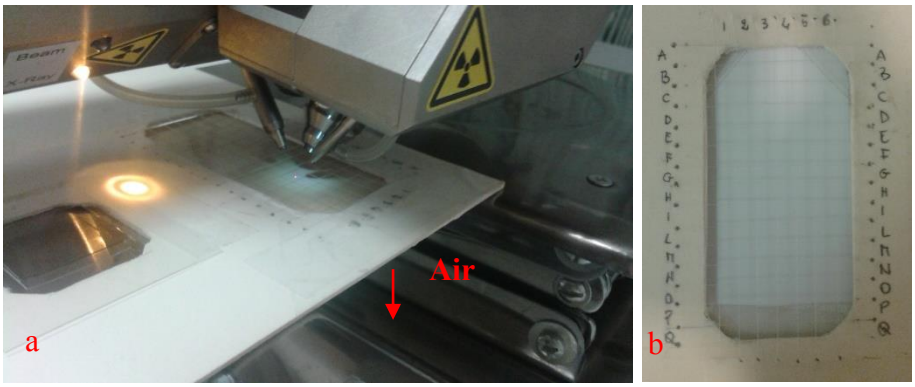

Figure 5. a) Measurement set-up, b) x/y coordinate stencil.

Six spots were analysed on the photographs A1 and B1, and ten on each reference grey scales. A total of fourteen and fifteen spots have been analysed for the Le Gray and H&A image, respectively (Figure 3 and 4). The points have been accurately selected to allow an evaluation of different grades of fading and different density areas across the image. We were not able to place the star for spectrum DmaxB on the H&A photograph. However, micro-photographs indicate to establish that the point was very similar to point I12.

The variables used were the net integrated areas of Kα of sulphur at 2.309 keV (energy range between 2.16 to 2.45 keV) and the Lα of Silver at 2.983 keV (energy range between 2.88 to 3.09 keV). The software Spectra ARTAX 5.3.18.0, available with the instruments, has been used for calculation. Further information about algorithm used is available in the manuals of the Bruker AXS Microanalysis GmbH[17]. The Ag signal has been estimated by subtracting the signal of Rh (from X-ray source). In fact, Lβ emission of Rh shows a band shape with a shoulder that falls at the same energy of Ag. The spectra not containing Ag have been used for determining the contribution of the shoulder to the Lβ emission of Rh [18]. All the intensity showed below, if not otherwise specified, are mean values of three measurement replicates. Since the signal intensities were normalized considering the signal of the Rh (emission line Kα1 20.216 keV)[19,20].These relative intensities allowed comparison within and between prints[11].

4.3 Results and discussion

First of all the optimization of the analysis procedure will be discussed, in terms of setting selection and physical factors that may influence signal intensity of the target elements. Once the procedure is established, the results obtained for the hypo-standard will be presented. Then, the calibration curve will be used to determine the level of sulphur on both, facsimiles and art-photographs. Finally, the relation between sulphur/silver signals obtained on the artefact will be examinated, and a procedure for faded image recovery will be proposed.

4.3.1 Analytical method optimization

As aforementioned, the determination of sulphur is important to understand the degradation of photographs. The first step is the optimization of the analytical procedure to increase the sensitivity for the elements to be determined.

The experimental conditions considered, and discussed below, are the atmosphere, the collimator pinhole diameter, the voltage, the amperage and the direct or filtered radiation source.

Air/He atmosphere and Collimators

According to the literature, air readily absorbs low energy X-rays emitted, particularly by elements with $Z \geq 22$ (titanium). It is common when analysing low Z elements to purge the atmosphere with helium. It is necessary for low Z elements but is useful in their work for all elements of interest, even for those with an atomic number larger than 41.

Collimators are another option in XRF instruments. Collimators are usually used when a small spot size is needed either because the sample or a specific point of interest on a sample is small. Normally, the photographs present large uniform areas defined by its density grade, based on different grades of exposition. Thus, the use of a collimator with a bigger pinhole diameter is suggested. In this case, a 1.5 mm diameter collimator was employed.

Voltage and amperage settings

The optimal high voltage setting is usually 1.5 to 2 times the absorption edge energy of the highest energy element of interest[21]. Although sulphur has a very low energy edge (2.471 keV), higher voltage has been considered in order to evaluate the limit conditions that permit multi-elements detection[13], e.g. for Ag or other elements of interest for photographs characterization purposes. In this case, different combination of voltage (between 10 and 50 kV), and amperage/intensity settings have been tested, within the instrument limit conditions

specified by the manufacturers (Figure 6a). As can be seen in Figure 6b the highest counts values for sulphur K line are obtained using a voltage of 30 kV and an amperage/intensity of 1300 µA, as consequence these conditions were selected for the analysis.

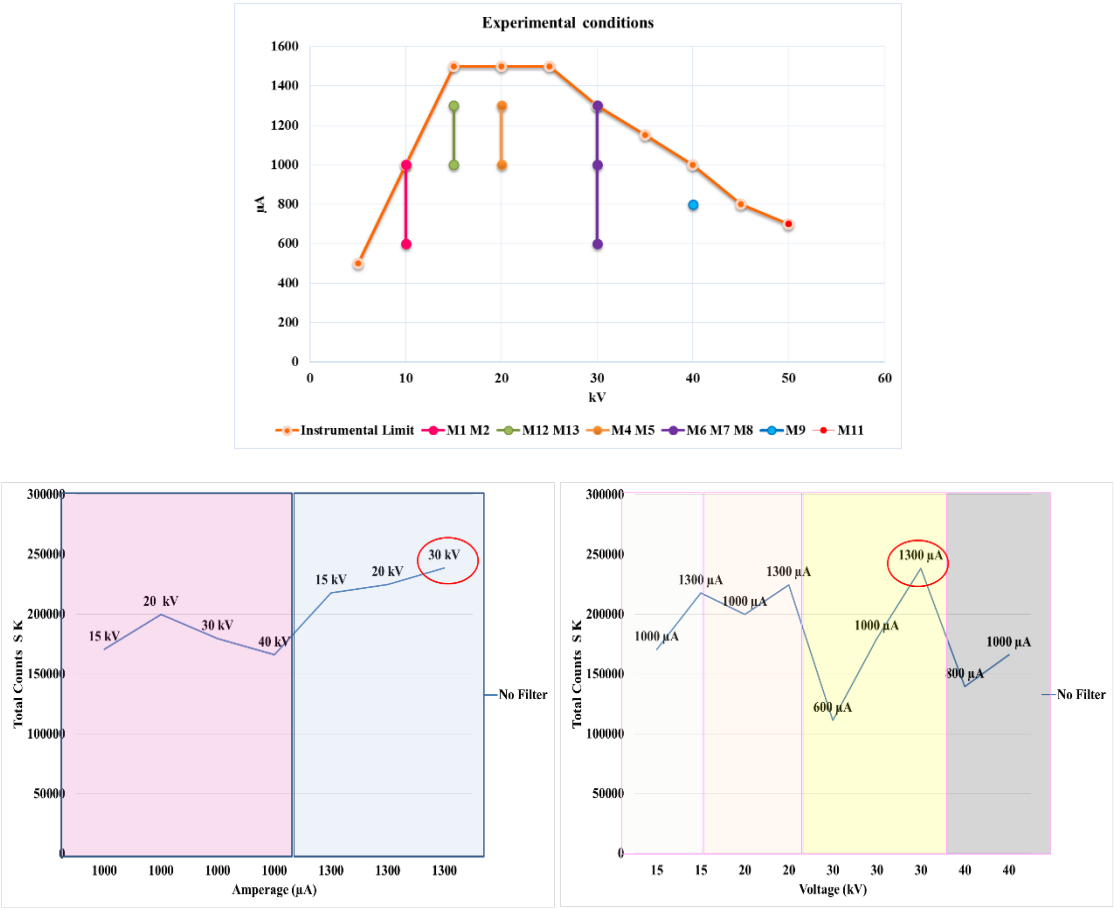

Figure 6. a) Instrument manufacturer's specification curve and Voltage and Amperage condition considered; b) S K integrated values for Voltage and Amperage condition considered.

Direct or filtered Rh source radiation

The tested filters consisted of titanium (1 mil/25.4 µm), molybdenum (Mo1 1 mil/24 µm) and zirconium (15 µm). Interference of tube spectral lines with a number of analyte elements is unavoidable in most cases. Fortunately, this contribution to analyte intensity is almost constant[19].

The use of a Ti filter reduces the counts obtained for the sulphur by more than 50%. For all the other filters, the effect is even stronger. On the other hand, the Ti filter is useful to improve the detection of the L lines of Ag, as can be seen in the example in Figure 7. It shows two spectra acquired on the same point of a high-density area of image A1. Comparing the spectrum acquired using a titanium filter (magenta trace) to one recorded without any

filter (green trace) it is possible to see how the L lines of the rhodium tube are filtered, but also how the other element peaks nearby are drastically reduced.

However, because Rh has no interferences in the S measurements and the contribution of silver signal could be subtracted, the use of a filter was discarded.

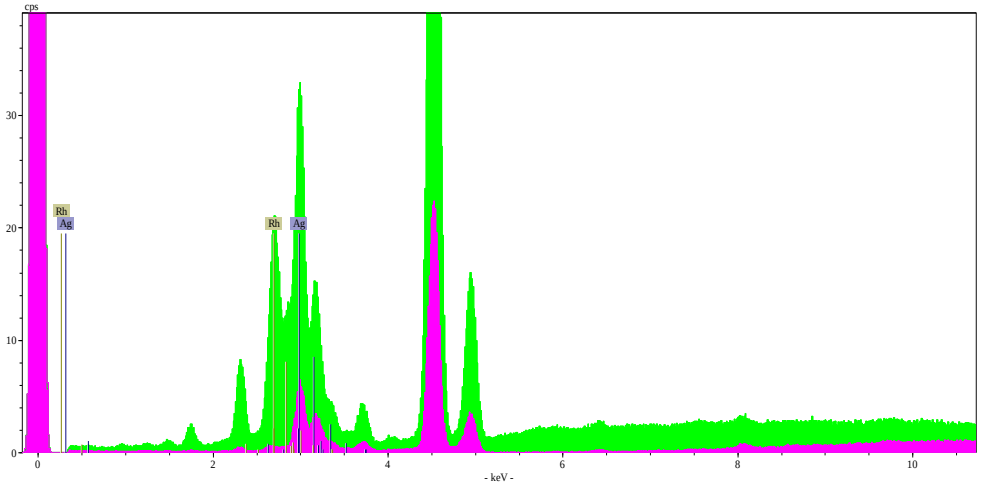

Figure 7. Dmax spectrums of a Le Gray reproduction acquired without filter (green trace) and with a Ti filter (magenta trace).

In Figure 8 shows the values of the integrated area of the sulphur K line for the standard with the higher hypo deposition for all the filters tested using different amperage and voltage settings. The different colours of the areas indicate that one of the conditions was kept constant. Observing the results, the optimum conditions previously established are valid even when filters are used.

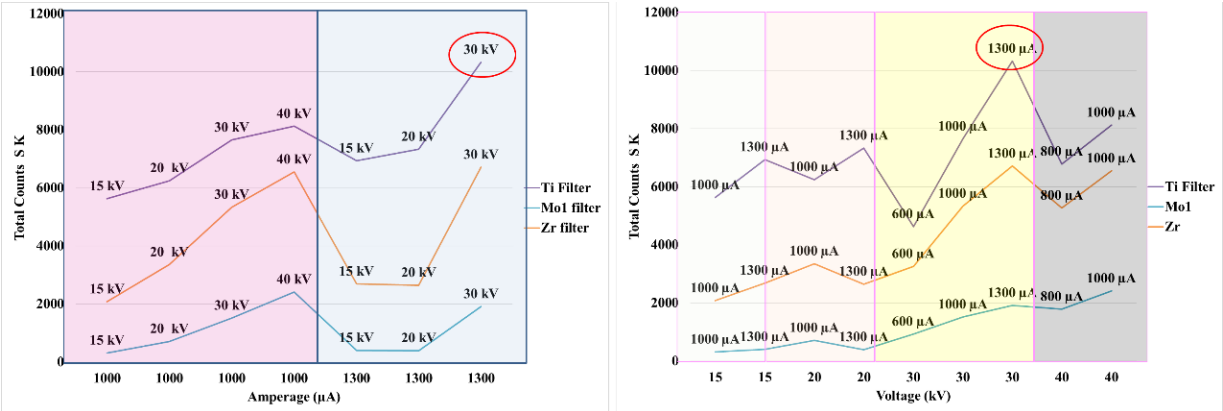

Figure 8. Total net counts for S K of the 72 [S] µg/cm^2 standard. Filters, amperage and voltage tests.

Acquisition time/Live time

The standard criteria for selecting count times are a compromise between available time, number of measurements needed and precision. We did not considered time spans less than

200s because the element of interest is a light element and is generally found in very low concentration. Measurements with increased acquisition time of 200 to 700 seconds have been recorded. As expected, the total counts obtained with higher time acquisition increase proportionally. However, the signal-to-noise ratio does not improve significantly between 200s and 700s. Thus, 200s was considered the optimal time.

In summary, the optimal conditions established for sulphur detection on salted paper photographs by XRF are an acquisition time of 200 s, voltage of 30 kV and amperage of 1300 μA in a He atmosphere, without using filters. It is important to keep in mind that during the measurements no support behind the specimen has to be present.

Calibration and interferences

Matrix effect and Thickness influence

The main advantage of x-rays fluorescent methods applied to trace element analysis is that the relations governing elemental and instrumental effects follow simple expressions. The effects of signal enhancement may usually be disregarded in the analysis of trace elements. If the matrix is similar, a linear relation can be found between the concentration of a given element (ppm) and the intensity of the radiation (I). Considering the elements present in images and standard matrix, the characteristics lines of the Zn (support) are higher than the absorption edge of the sulphur, which means that the probability that enhanced effect of the signal may happen is negligible [20]. The silver is an important element present in salt print images. Its L lines are near to the K lines of sulphur, although it is important to considerer that L lines are less energetic than K line and an influence on the sulphur emission should be minimum. When matrix effects are either negligible or constant, the linear relationship between radiation intensity and weight fraction of analyte is expected.

The transmission of X-ray is generally not affected by the matrix, however for lower energy X-rays, the transmission is more like UV rays and it can be stopped even by lightweight materials like paper. So for elements like S, the signal detected by XRF is higher for the compounds located on the surface of the sample[22,23]. In case of “hypo retained on paper” we are evaluating a deposition of the sulphur on surface (thin film approximation) and we considered no sub-estimation of the analyte signal [9,22].

Heterogeneity

The heterogeneity of the standards may be evaluated by comparing the dispersion (mRSD) obtained for the sulphur signal under constant analysis conditions on the same point - repetitivity values (P=, five measurement replicates) with those obtained for reproducibility across the standard's surface (P≠, five spot replicates). The heterogeneity clearly increases in all the cases when different points were analysed with a mean value of 4% (Figure 9). In Figure 10 it is possible to see that the dispersion decreases from the lower concentration to the standard S [56], then a slightly increase can be observed for the standards with highest Hypo values, S [72]. The dispersion for the higher sulphur concentration standard may be due to the saturation and the creation of cluster of hypo crystals on the surface. While for the no-processed standard S [2] µg/cm^2 is due to the not uniform distribution and fixation of the Hypo deposition on the surface. Furthermore, the concentration is probably near to the detection limit that means that higher error in signal evaluation is expected.

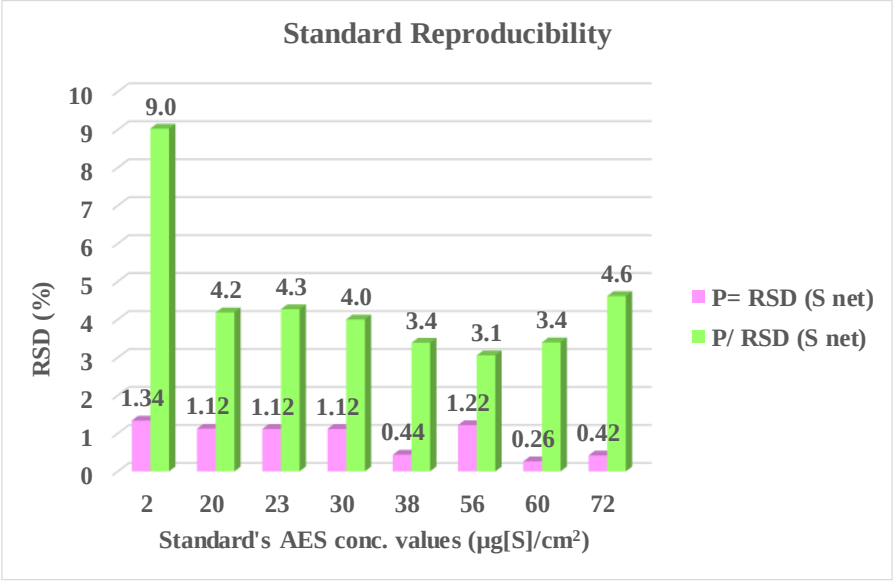

Figure 9. Standards reproducibility. RSD values for Same Point (P=) vs. Different Point (P≠).

Finally, we evaluate the calibration model. The linear equation obtained will be used for the determination of the sulphur content on the salt print image created with similar processing procedure (Figure 10).

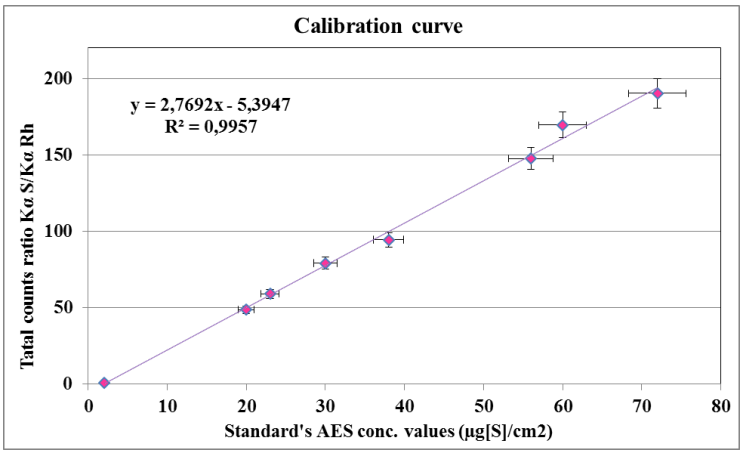

Figure 10. Calibration curve obtained with XRF counts results vs. AES concentrations values obtained for [S] analysing the "Hypo standards".

Photographic Facsimiles evaluation

The two greys scale of the image A1 and B1 were analysed with the aim to evaluate the sulphur and silver content depending on the density of the areas. Figure 11 shows the signal of the sulphur and silver values (total counts Sulphur K line – red line and Ag L line – magenta line) obtained. The sulphur shows no dependence on the image densities, while, as expected, the silver decreases from high to low density grade. In the range between grades 1 up to 7 the two elements seems not be related, whereas from grades 9 up to 21 they shows a similar behaviour. The counts values for Ag signals are slightly higher in the image A1, which was treated with an old-hypo bath for more hours (60h), with respect to the B1 image (15h).

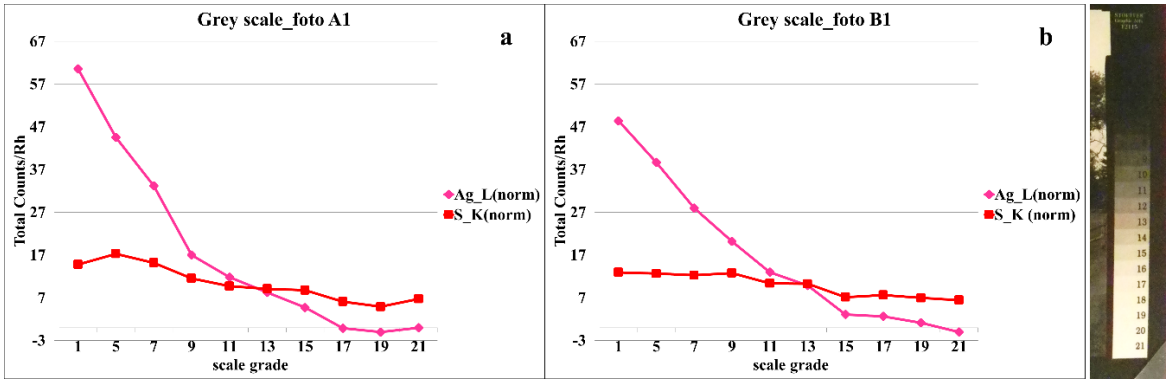

Figure 11. Signal counts for S k and Ag L lines obtained for the grey scale analysis. I/IIa) no filter I/II b) Ti filter for image A1 and B1.

On the other hand, the results obtained on the image A1 and B1 on different spots across the surface show that the sulfur and silver follow the same behavior, comparable with the range from 9 to 27 of the grey scale (Figure 12).

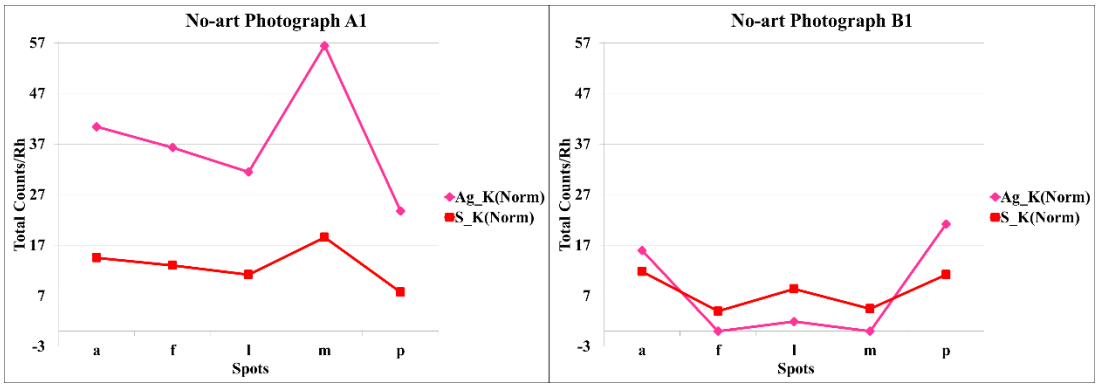

Figure 12. Signal counts for S k and Ag L lines obtained for different spots across the surface of no-art photographs A1 and B1.

The fact that the signal of sulphur are almost constant suggests that the element may be attributed to the paper support or/and to a low level of hypo retained or silver sulphide[8]. To verify this hypothesis, the content of sulphur has been calculate applying the equation obtained with the standards' calibration curve. The results are presented in the bar chart in Figure 13. The nominal concentration values are slightly higher than the S concentration of the row stock non-processed paper standard (2µg [S]/cm^2). Comparing the concentrations of the two images, it is possible to comment that the sulphur signal values do not shows significant differences depending on the hours that the image was let in the old-hypo bath.

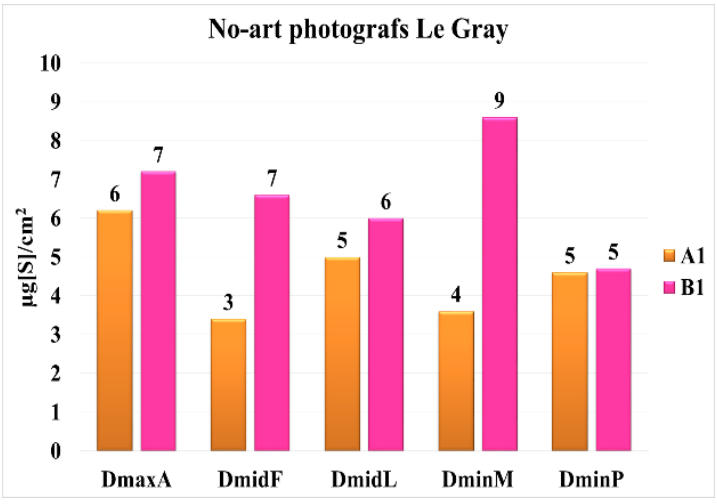

Figure 13. [S] values calculated for five points on images A1/B1.

4.3.2 Photographs characterization and recovery procedure proposal

The first step of the comparison between the two artistic photographs will be the evaluation of sulphur content to verify the possible correlation with the phenomenon of fading. Then, the sulphur/silver relation will be discussed for both cases to further evaluate differences or similarities that may help to explain the different condition of conservation.

Retained hypo evaluation

The sulphur concentrations values calculated for both Le Gray and Hill and Adamson images are much higher than those obtained on the facsimiles. This is an evidence that the reproductions cannot be considered alike the aged art photographs, although an important approximation. The comparison between the two art-photographs reveals that the content of sulphur of the not-faded image are only slightly lower than those calculated for the degraded image. Moreover, considering the variability within the photograph spots it is not possible to exclude a high dependence on the point analysed. However, the higher value has been found in the faded areas (Figure 14).

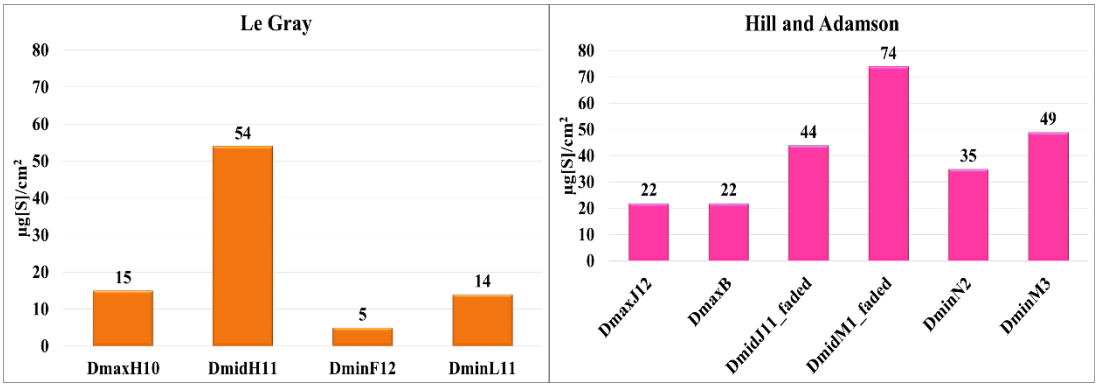

Figure 14. Concentration values calculated for each points analysed on "View from Photographer's Studio" and "Lady Elizabeth Eastlake".

Silver/sulphur relation

Le Gray "View from Photographer's Studio"

The first real photograph analysed is a case of brownish colour image no degraded. The elements detected on the Le Gray image were Al, Si, P, S, K, Ca, Fe, Zn, and Ag. In Figure 16 are presented two graphics (two different experiments) that show the relation of the signal detected for sulphur and silver on different spots (for spots location see Figure 3) and some

microphotographs of the spots acquired by means of the CCD camera. As expected, the silver content decrease drastically in the measurement of low-density areas. The high difference between the silver detected on the two max density can be explain with the micro heterogeneity of the Ag deposition on the surface, as can be observed in the spot microphotographs of the high density areas (Figure 15a/b – DmaxH10/11 and I5). The measurements in some cases show spectra with a high backscatter effect. This effect is typical of low-density matrix (physic structure) such as basic paper and therefore, it is an indication of the absence of the homogenous salt layer. The sulphur signal is rather constant in the areas of low density that presents more brownish colour (Figure 15a/b – DminF10/L11/L5/M5). This suggest that a minimum level of hypo retained is present on the image. It is interesting to notice the strict relation between the two elements in the high-density areas (DmaxH10/11, F5, G5, I5 and H5). Based on this observation, the presence of a complex between silver and sulphur could be speculate. The measurement performed in two different days assure the reproducibility of the procedure and the data pattern. It can be hypotized the presence of silver sulphide (Ag_2S) on the high-density areas. It is a compound commonly found on photographs. Indeed, the publication of *Pope*[8] largely explains the phenomenon of its formation. It is attributed to three different possibilities/moments of the revelation process: fixation or/and bleaching/washing, and/or during the storage of the piece. The cause is identified in the residues of thiosulfate that may react with silver and then decompose to form silver sulphide. Further explanation about the reaction mechanisms are presented elsewhere[24].

Two trends can be extracted from the data behaviour. First, that the image shows a ground signal of S in the low-density areas (S min) and second, that when the S>Smin, the signal is comparable to the signal of the silver and it can be identified as high-density area.

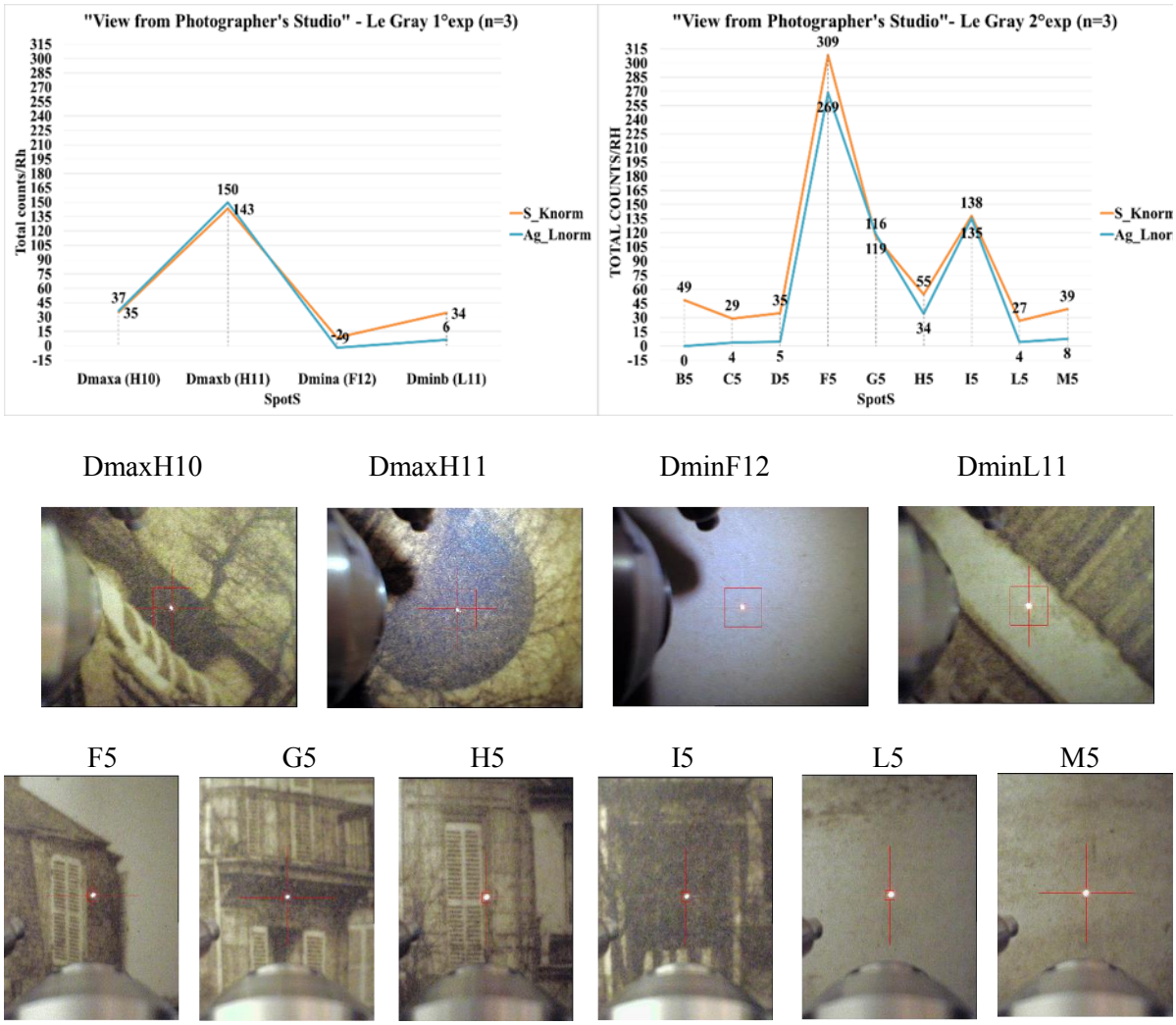

Figure 15. a) Signal counts for S k and Ag L lines obtained for "View from Photographer's Studio", b) micro-photographs of the different points analysed.

"Lady Elizabeth Eastlake"

The second photograph analysed is a case of degradation manifested with fading. In this case the elements detected were Al, Si, P, S, K, Ca, Ti, Fe, Co, As and Ag. Many of these elements could be ascribed to the paper used, rather than to the photographic process itself [15,25] , as it was demonstrated in other studies of salt image of the same photographers[26]. The presence of cobalt, associated with arsenic, iron and occasionally bismuth are described as related with the presence of smalt, a blue cobalt glass added to rags during 19th-century paper manufacture to produce a "corrected white paper". The manual wrote by Herring in 1859 report that "*Until very recently the fine bluish tinge given to many writing paper was derived from the admixture of that expensive mineral blue, the oxide of cobalt, generally termed smalts, and which has still the advantage over the ultramarine of imparting a colour which*

will endure for a much longer period"[25]. This mean the choice to use a fine quality paper, which will have a defining influence on the final appearance of the image[27]. The three graphics in Figure 16 show the counts results obtained in three different experiments (graphic c n=1).

The spots M3, O2, M1, DmaxB, J11 and J12 selected during the first experiment show very low values of silver, while sulphur maintains values comparable with those obtained in high-density areas of Le Gray image (between 150-300 counts). These spots are all located on faded areas of the background/edges (M1, J11/12) and of Lady Elisabeth's dress (M1, M3 and O2).

During the second experiment the spots were selected trying to analyzed areas that seems unaltered, part on the face (E8, F8) and part located on the background (G8, H9, I10). The counts values of sulfur and silver detected in each spots are comparable and show the same pattern observed on the high-density areas of the Le Gray image.

On the contrary, the measurements acquired on spots of faded area present high level of sulphur, especially on spot I11 and I12, while the silver is much lower and the correlation is no more appreciable. Spots H7 and I7 that are completely white show levels of sulfur comparable with the no degraded areas, although the silver level are much lower. The spot K6 shows an intermediate situation. It is a high-density point (see microphotograph K6) and shows the sulphur values similar to point H9 (no-faded), although the signal of silver is much lower.

Comparing graphics b and c, the relation between sulfur and silver are maintained in all spots, except in point I12 affected by sample heterogeneity.

The higher level of density on the faded areas have been confirmed by a comparison of the photograph of the Metropolitan Museum with a reproduction taken in 2010 of another image produce by the same negative conserved at the Edinburg university museum (Figure 17). The causes of the degradation are not clear, but if the complex presents is silver sulphide, it is possible that acids compounds may had a role in the process[28]. According with the results, during the process of fading the image has been affected by loss of silver (forming-image material), while the sulphur, which was forming the complex with silver, is retained in the photographs support. Thus, the sulphur may be used as record of the silver counts values and it could be used to establish the presence of higher density areas where the image is completely or partially vanished. According to this behavior, a procedure for recovery faded silver images may be proposed. The procedure will includes: establish the ground level of sulphur according with the signal obtained on low-density areas; evaluate the calibration

between signal counts and density level creating a grey scale reference; reconstruct the subject of the photograph using an image manipulation software according with the grey level calibration.

In is important to consider that for the procedure suggested is required a high spatial resolution, as consequence of the high heterogeneity of the silver/sulfur deposition. Hence, new XRF imaging scanner could be used to acquire an adequate number of spectra[29].

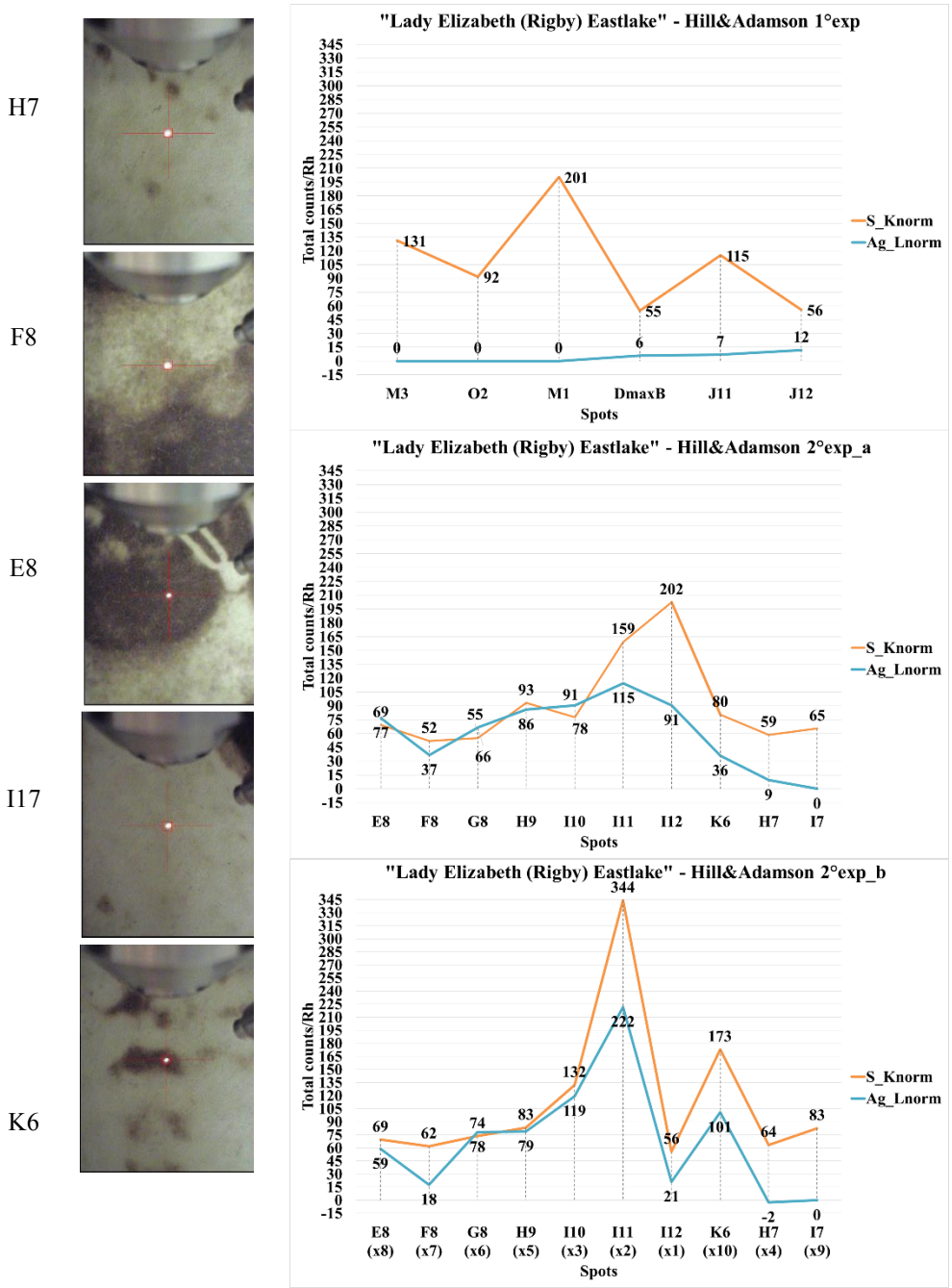

Figure 16. a/b/c) Signal counts for S k and Ag L lines obtained for “Lady Elizabeth Eastlake”; b) micro-photographs of the different points analysed.

University of Edinburg's image The Metropolitan museum' image

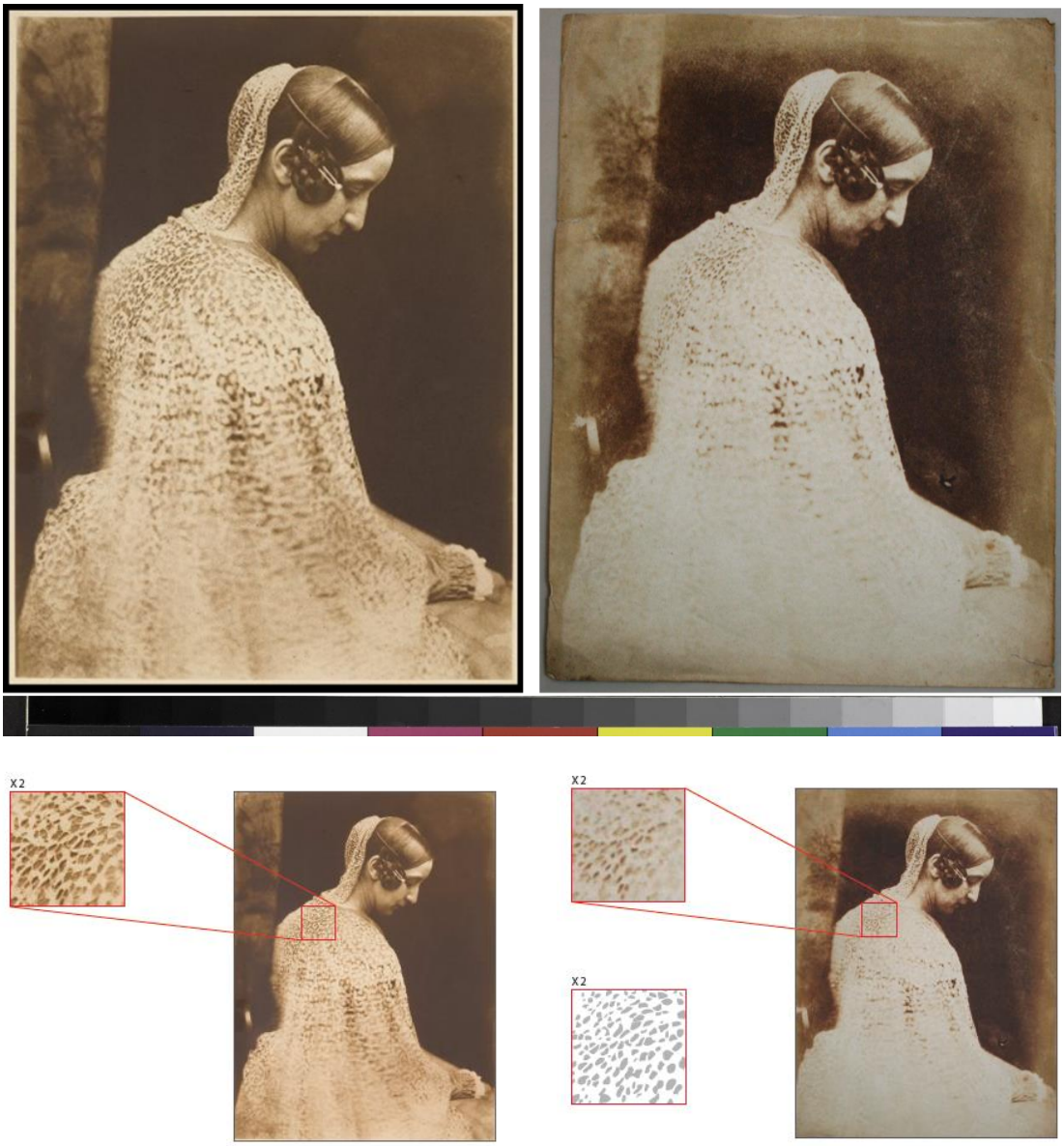

Figure 17. Reproduction of 'Lady Elizabeth (Rigby) Eastlake'. a) Photograph ©**2010** Edinburg University; b) Photograph ©2013 The Metropolitian Museum of Art; c) comparison of details of the dress in the two images that show the fading during the years.

4.4 Conclusions

- The results suggest that the optimal conditions for sulfur detection by XRF are an acquisition time of 200 s, 30 kV and 1300 µA in a He atmosphere, without using filters.
- The use of a titanium filter could be useful to improve the detection limit of L lines of the silver in photographs, although imply the loss of 50% percent of sulfur signal counts.

- The standards evaluated in this study can be used for a sulfur content evaluation of salt print photographs.
- The analysis of reproduction and real salt print photographs of Le Gray show a linear relation between sulfur and silver signal that could be an indication of the formation of a complex with the two elements, probably silver sulfide.
- The results obtained on the Hill and Adamson faded photographs suggest that the degradation is due to the possible loss of the silver being its relation with sulphur indicative of degradation phenomena.
- The sulphur signal is indicative of original level of silver in faded areas.
- Based on the relation between sulphur and silver, a procedure for image recovery has been suggested. This procedure includes the calibration between signal counts and density image level with the aim to create a grey scale reference. Based on the grey level calibration the subject depicted in the photograph can be reconstruct using a software of image manipulation.

4.5 References

1. Eaton, G. T. in *Issues Conserv. Photogr.* (Norris, D. H. & Gutierrez, J. J.) (Getty Conservation Institute, 2010).

2. Feldman, L. H. Discoloration of black-and-white photographic prints. *J. Appl. Photogr. Eng.* **7,** 1–19 (1981).

3. Haist, G. *Modern Photographic Processing*. (2000).

4. Weaver, G. A Guide to Fiber-Base Gelatin Silver Print Condition and Deterioration.

5. Grzywacz, C. M. *Monitoring for Gaseous Pollutants in Museum Environments*. 1–176 (Getty Publications, 2006).

6. Outline, S. Fundamentals of the Conservation of Photographs.

7. Centeno, S. a., Schulte, F., Kennedy, N. W. & Schrott, A. G. The formation of chlorine-induced alterations in daguerreotype image particles: a high resolution SEM-EDS study. *Appl. Phys. A* **105,** 55–63 (2011).

8. Pope, C. I. Formation of silver sulfide in the photographic image during fixation. *J. Res. Natl. Bur. Stand. Sect. C Eng. Instrum.* **64C,** 65 (1960).

9. Stulik, D. C. & Herant P. Khanjian. in *Conserv. Sci.* (Joyce H. Townsend, Katherine Eremin, A. A. (eds)) 188–194 (2003).

10. Vila, A. & Centeno, S. A. FTIR , Raman and XRF identi fi cation of the image materials in turn of the 20th century pigment-based photographs. **106,** 255–262 (2013).

11. Eremin, K., Tate, J. & Berry, J. in *Conserv. Sci.* (Townsend, J. H., Eremin, K. & Adriaens, A.) (2003).

12. Namowicz, C., Trentelman, K. & Mcglinchey, C. XRF of Cultural Heritage Materials: Round-Robin IV - Paint On Canvas. 144–153

13. Shackley, M. S. *X-Ray Fluorescence Spectrometry (XRF) in Geoarchaeology*. *X-Ray Fluoresc. Spectrom. Geoarchaeology* 231 (Springer New York, 2011). doi:10.1007/978-1-4419-6886-9

14. Barro, L. & Kennedy, N. W. Gustave Le Gray's Salted Paper Prints. in *Trienn. Meet. ICOM Comm. Conserv.* **2,** 533–540 (2005).

15. Stulik, D. C. & Kaplan, A. The Atlas of Analytical Signatures of Photographic Processes SALT PRINT. *Getty Conserv. Inst.* 1–19 (2013).

16. *Focal Encyclopedia of Photography*. 30–36 (2007).

17. Bruker AXS Microanalysis GmbH. ARTAX^{TM} USER MANUAL. 96 (2006).

18. Miliani, C., Rosi, F., Burnstock, A., Brunetti, B. G. G. & Sgamellotti, A. Non-invasive in-situ investigations versus micro-sampling: a comparative study on a Renoirs painting. *Appl. Phys. A* **89,** 849–856 (2007).

19. Feret, F. R., Hamouche, H. & Boissonneault, Y. in *JCPDS - Int. Cent. Diffr. Data 2003, Adv. X-ray Anal. Vol.46* **46,** 381–387 (2003).

20. Reynolds, J. Matrix corrections in trace element analysis by X-Ray fluorescence : estimation of the mass absorption coefficient by compton scattering. *Am. Mineral.* **48,** (1963).

21. Moore, M. D. & Reynolds Jr., R. C. *X-ray Diffraction and the Identification and Analysis of Clay minerals.* (1997).

22. Barrett, T., Shannon, R., Wade, J. & Lang, J. in *Stud. Archaeol. Sci. Handheld XRF Art Archaeol.* (Shugar, A. N. & L. Mass, J.) 191 – 214 (2012).

23. Sitko, R. Quantitative X-ray fluorescence analysis of samples of less than "infinite thickness": Difficulties and possibilities. *Spectrochim. Acta Part B At. Spectrosc.* **64,** 1161–1172 (2009).

24. Haist, G. *Modern Photographic Processing: v. 1*. 559–663 (2000).

25. Herring, R. *Paper & paper making, ancient and modern.* 100 (1856).

26. Eremin, K., Tate, J., Morrison-Low, A., Berry, J. & Stevenson, S. Non-destructive analysis of Nineteenth century Scottish calotype negatives and salt prints. *MRS Online Proc. Libr.* **712,** (2002).

27. Vila, A. *et al.* Understanding the gum dichromate process in pictorialist photographs : A literature review and technical study. *Stud. Conserv.* **58,** (2013).

28. Ezenwa, I. A., Okereke, N. A. & Egwunyenga, N. J. Optical Properties of Chemical Bath Deposited Ag2S Thin Films. **2,** 101–106 (2012).

29. Alfeld, M., Pedroso, V., Hommes, V. E. & Van, G. TECHNICAL NOTE A mobile instrument for in situ scanning macro-XRF investigation of historical paintings. *Anal. At. Spectrosc.* **28,** 760–767 (2013).

Chapter 5

Optimization, evaluation and application of an analytical method for ancient bronze characterization: "Resurrection Pulpit of San Lorenzo"

Context

The restoration process of the Resurrection Pulpit conserved in the church of San Lorenzo in Florence (Italy), which lasted from July 2010 to October 2013, was the occasion of a further study of one of the most famous works of the last years of Donatello (Donato di Niccolò di Betto Bardi, 1386-1466). The *Opificio delle Pietre Dure* (Florence) undertook a complex investigation project in which we collaborated in the task of the metal alloys characterization. The presented study is focused on the optimization of a specific analytical methodology from sampling procedure to ICP-OES/MS determination. Finally, principal component analysis was tested as useful multivariate method for elemental compositions discrimination. The obtained results will be used by the OPD as complementary information to better understand the object and the studio practice of the artist and/or collaborators. Detailed information about the pulpit is available on the web site of the institute (http://www.opificiodellepietredure.it/index.php?it/822/donatello-pulpito-della-resurrezione-firenze-basilica-di-san-lorenzo).

[The authors of the future publication rising from this study will be Clarimma Sessa[1], Simone Porcinai[2], Jose Francisco Garcia[1]
[1] Analytical Chemistry Department, University of Barcelona, Spain
[2] Istituto di Ricerca sulle Onde Elettromagnetiche "Nello Carrara" - CNR, Italy]

5.1. Introduction

On the conservation and historic side, the investigation of a metal alloy of an ancient object means to contribute to the understanding of the technologies of metal production[1] and permit to reconstruct the moment of genesis of the artwork, which means a travel to the creative approach of the artist towards the matter. From the analytical point of view, it means a challenge and compromise between the minimal impact of the process on the object and the quality of the results.

The main objective of this study was to establish the composition of the metal alloys used to cast the different parts of the pulpit, and their comparison. A secondary objective, which helped to achieve the main scope, was to evaluate the influence of the different sources of dispersion in the concentration determination of the constitutive elements of the samples. Furthermore, we aimed at finding an optimum procedure for determination of concentration of major and minor components of the metal alloy.

In this study, ICP-OES and ICP-MS were employed for the detection of major and trace elements detection respectively. The use of these techniques is preferred when the non-destructive techniques, such as XRF, are not able to provide results of sufficient quality, in terms of detection limit, calibration (matrix effect) and sensitivity, and only a limited quantity of material can be extracted from the object. These techniques permit the simultaneous determination of a large number of elements with high accuracy even at low concentrations. The method is well developed and only a small amount of material is needed for performing an analysis[2].

The entire analytical process begins with a sampling campaign performed in-situ where arduous decisions have to be made about the location of the points to be analyzed. Obviously, the aesthetic appearance of the object has to be respected and a limited number of samples can be taken[3]. Moreover, the extracted material has to be able to answer artistic and historic queries proposed by the conservators, to which the obtained information is directed.

The Resurrection pulpit, which was analysed in this study, is a large metallic parallelepiped artefact (length 292 cm, height 123 cm, thickness about 10 or more cm). It has a structure that includes six different metallic panels on which decorative frames are mounted that follow its entire perimeter. From the analytical point of view, the analysis of the composition of such large and complex structures needs an elaborate sampling plan. At the beginning, an effective method for material extraction, taking into account the physical features of the object, had to be optimized to maximize the material recovery while at the same time

minimizing the damage and ensuring representative results[4]. Once the material is available it has to be pre-treated depending on the analytical technique used. In this case, the sample has to be weighted, digested by acids, diluted and finally analyzed by ICP. The manipulation and analysis of the material includes several steps, each one a possible source of errors and contamination that may influence the results and cause variability not directly correlated with the metal composition. A meticulous study of the dispersion due to all the aforementioned sources has to be performed with the aim to discern this variability from the proper differences within and between the samples.

The heterogeneity of the bulk samples hinders the accurate interpretation of the results. In fact, it is important bearing in mind that the homogeneity of metal alloy is influenced by the combination of diverse factors: physical properties of the elements included (melting point, density), their proportions and solubility and finally the cooling of a melt in the mould[5], determined by the technology involved [6–8]. The complex system that may arise from a casting procedure and the need to know the dispersion of the results obtained, before to proceed to any comparison, are the reasons why the characterization of a metal object needs a well-established and robust procedure specifically designed for the investigated artefact.

This chapter is divided into two main blocks. In the first part, all the steps of the analytical process will be discussed, the source of variability statistically evaluate and finally a protocol for metal alloys analysis will be proposed. The second block will be dedicated to the application of this procedure to the analysis and comparison of the elemental compositions of all samples extracted from the different part of the Pulpit. Since the amount of the collected data was considerable, a multivariate method, such as PCA has been tested as useful tool for simultaneous evaluation of differences and similarities among samples and a practical method for data visualization[9]. Different models were created considering minor and major elements, separately or together.

5.2. Experimental

5.2.1 Materials/samples

Fifty samples taken from the Resurrection Pulpit, artwork in restoration under the direction of OPD, in three sampling campaigns (2010, 2012, 2013), were analysed. Moreover, the composition of new and used drill bits employed for the sampling procedure were examined.

Additional reference samples from a control material (control bronze (PL) samples) with similar compositions to the ancient alloys were analysed. Description of the samples is presented in Table 1. A simplified schema of the Pulpit and the approximate location of the samples is presented in Figure 1.

Table 1. Samples description.

Samples		
Campaign	**Label**	**Description**
July/September 2013	Icp1	Panel "Pie donne al sepolcro" - **F**
	i1	
	Icp2	Frame above the panel "Pie donne"
	i2	
	Icp3	Panel "Discesa al limbo" - **E**
	i3	
	Icp4	Panel "Resurrezione" - **D**
	i4	
	Icp5	Panel "Ascensione"- **C**
	i5	
	Icp6	Lower frame above the panel "Ascensione"
	i6	
	Icp7	Lower frame above the panel "Discesa al limbo"
	i7	
	Icp8	Intermediate frame above the panel "Resurrezione". IN decorative rectangle decorative element
	i8	
	Icp9	Intermediate frame above the panel "Resurrezione". ON the border of the decorative rectangle
	i9	
	Icp10	Intermediate frame above the panel "Resurrezione". OUT/NEARBY the decorative rectangle
	Icp11	Upper frame above the panel "Discesa al limbo"
	i11	
	Icp12	Upper frame above the panel "Ascensione"
	i12	
	Icp13	Fame above the panel "Pentecoste"
	i13	
	Icp14	Panel "Pentecoste" - B
	C3*	Fame above the panel "Martirio di San Lorenzo"
	C3a	

***Sampling campaign July 2010**

Table 1 (continued). Samples description.

Jan. 2012	**m20**	Panel “Martirio di San Lorenzo” (depth max.7mm) - **A**

May 2013	**m21**	Panel “Martirio di San Lorenzo” (ext. depth 2-3 mm) - 40 cm from m20
	m22	Panel “Martirio di San Lorenzo” (ext. depth 2-3 /4-5 mm)- 40 cm from m20
	m23	Panel “Martirio di San Lorenzo” (int. depth 4-5 /6-7 mm) - 40 cm from m20
	m24	Panel “Martirio di San Lorenzo” (ext. depth 2-3 mm) - 40 cm from m20
	m25	Panel “Martirio di San Lorenzo” (ext. depth 2 -3 /4-5 mm) - 40 cm from m20
	m26	Panel “Martirio di San Lorenzo” (int. depth 4-5 /6-7 mm) - 40 cm from m20

Jan. 2012	**m1**	“New white drill” (steel)	
	m2	“New white drill” (steel)	
	m3	“White drill” used for sample 11/12	
	m4	“White drill” used for sample 13/14/15	
	m5	“New red drill” (ELA-Carbide 1/025)	
	m6	“New red drill” (ELA-Carbide 1/025)	
	m11	re-melting (external)	Junction area between “Martirio di San Lorenzo” and “Pentecoste”
	m12	re-melting (internal)	
	m13	re-melting (external)	
	m14	re-melting (intermediate)	
	m15	re-melting (internal)	
	m16	re-melting (external)	
	m17	re-melting (internal)	

Sampling 2010	**m3**	“New red drill” (ELA-Carbide 1/025)
	m4	
Sampling 2012/3	**m1**	“New white drill” (Dentsply - steel)
	m2	
	m5	“white drill” used for sample 11/12
	m6	“white drill” used for sample 13/14/15

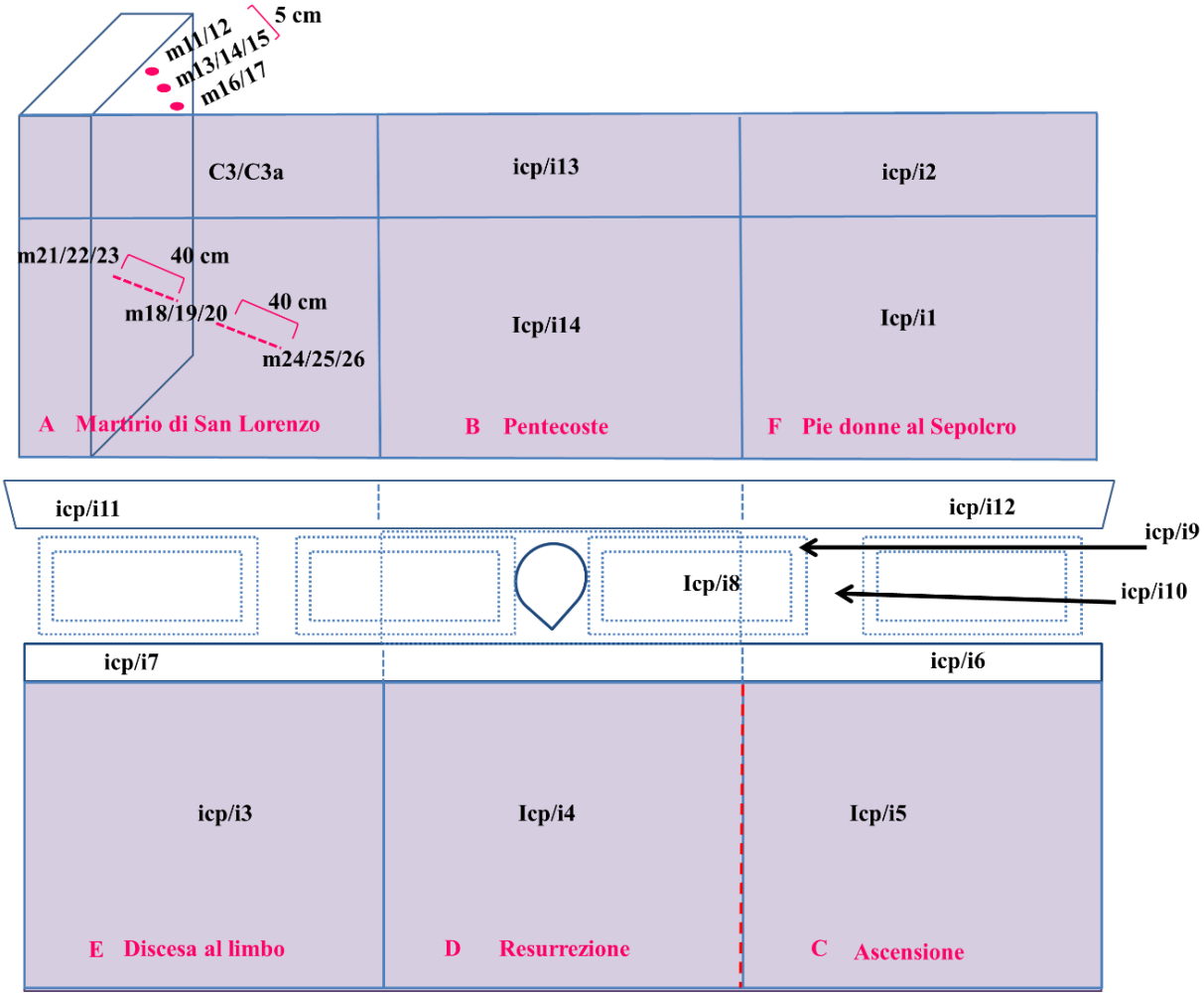

Figure 1. Approximate schema of samples distribution. The "icp" and "i" series were extracted at the same points.

5.2.2 Procedure/Samples treatment

Sampling

The sample material was extracted by the OPD specialized staff and co-workers. Specimens were obtained by drilling small holes (1.6 mm diameter) with drill bit in discreet and hidden areas of the backside of the pulpit. An Adhesive Plastic Bag (APB) fixed on the surface and held around the drill was used to avoid loss of sample material (Figure 2a). The holes were drilled in two or three steps, respectively, depending on the point features, i.e. that it was possible to obtain material belonging to different depths (Figure 2b).

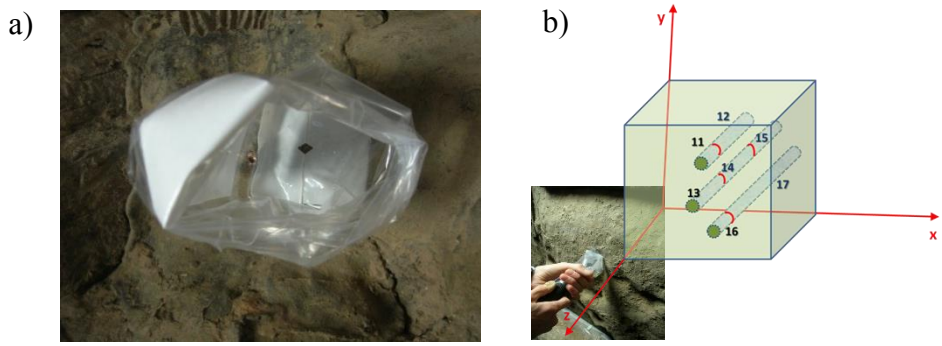

Figure 2. a) Documental pictures taken during sampling campaign 2012; b) scheme of the sampling procedure – samples extracted from different depth.

Sub-sampling

Each inner sample was subdivided in three equivalent parts. For this purpose, the total material taken was mechanically homogenate on a glossy paper surface and then divided in three parts that will be named a), b) and c). The three parts were digested and analysed independently (Figure 3). The sub-sampling protocol was not followed for material coming from the surface due to the small quantity recovered.

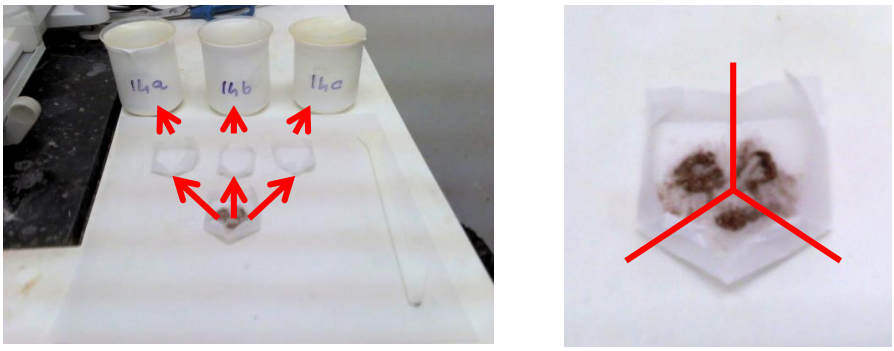

Figure 3. Images of the Sub sampling procedure.

Sample digestion

Each sample was weighted (measuring on average 20 mg) and different mixtures of acids were added following three methods.

Method 1. The sample was placed in a Teflon glass with 1 ml HNO_3, 0.25 ml HF and 1 ml of double deionised water for 12 hours for complete dissolution. After dissolution, the samples were diluted with a 1% HNO3 solution to a 50ml volumetric plastic flask and filled up to the reference volume.

Method 2. The sample was placed in a Teflon glass with a mixture of 1 ml HNO_3, 0.25 ml HF and 1 ml of double deionised water. The Teflon glass was heated in a sand bath for 30 min to aid the attack reaction. 1 ml of $HClO_4$ was added to the Teflon glass and let in a sand

bath until the evaporation of $HClO_4$ (avoiding the complete dryness). The residue was dissolved in 1ml of the HNO_3 and 5 ml of double deionised water. Finally, the solution was diluted to a volumetric plastic flask of 50ml and filled up to the reference volume using HNO_3 (1%).

Method 3. The sample was placed in a Pyrex glass with a mixture of 6.25g tartaric, 6.25 ml HNO3, 12.5 ml of double deionised water, let at room temperature for 12 hours. Then, the solutions were diluted with a 1% HNO_3 to a volumetric plastic flask of 50ml and filled up to the reference volume.

5.2.3 Instrumentation

Inductively coupled plasma optical emission spectroscopy (ICP-OES)

The major and trace elements were determined in the aqueous solution using a Perkin-Elmer Model OPTIMA 3200RL ICP-OES spectrometer equipped with a Perkin-Elmer AS-90 Plus auto sampler. This equipment consists of a radiofrequency source (working at 1150 W and a frequency of 40 MHz), a cross-flow nebulizer and an SCD (segmented-array charge coupled device) detector. The following emission lines were used for each element determined (nm) Cu: 324.752; Pb: 220.353; Sn 189.927; Sb 206.836; As 188.979; Fe 259.939; Ni: 231.604; Cr 267.716; Ag 328.068. The detection limits of the ICP-OES are 0.01 mg l^{-1} for Cu; 0.2 mg l^{-1} for Pb; 0.1 mg l^{-1} for Sn; 0.1 mg l^{-1} for Sb; 0.5 mg l^{-1} for As; 0.02 mg l^{-1} for Fe; 0.1 mg l^{-1} for Ni; 0.01 mg l^{-1} for Cr; 0.1 mg l^{-1} for Ag**.**

Inductively coupled plasma mass spectrometer (ICP-MS)

A Perkin-Elmer ELAN 6000 ICP-MS spectrometer equipped with a PerkinElmer AS-91 auto sampler was used for the trace element concentration determination. Several element isotopes (^{121}Sb; ^{107}Ag; ^{75}As; ^{60}Ni; ^{197}Au; ^{209}Bi; ^{135}Ba; ^{59}Co) were measured. With the aim to correct the instabilities in the ICP-MS measurements, Ir was used as an internal standard with a concentration of 200 µg L^{-1} in all of the samples. The detection limits of the ICP-MS measurements are 0.1 µg l^{-1} of ^{121}Sb; 0.1 µg l^{-1} of ^{107}Ag; 0.2 µg l^{-1} of ^{75}As; 0.2 µg l^{-1} of ^{60}Ni; 0.5 µg l^{-1} of ^{197}Au; 0.5 µg l^{-1} of ^{209}Bi; 0.05 µg l^{-1} of ^{135}Ba; 0.1 µg l^{-1} of ^{59}Co**.**

Three measurements for each sample/solution were acquired with both techniques.

5.2.4 Data treatment

Principal Component Analysis (PCA)

To facilitate the comparison between the different alloys, PCA was applied to the concentration values obtained. PCA was implemented in Matlab PLS_toolbox_652 from Eigenvector RI. In some models an autoscale pre-treatment was applied (Eq.11). This pre-treatment consist in subtracting the mean to every variable with the aim to remove the constant part of the data (mean centering) with the additional step of dividing the entire data set by their standard deviation to give the same weight to all variables regardless of its concentration magnitude. [9,10]

5.3. Results and discussion

5.2.5 Sample dissolution procedure optimization

The ratio of the sample weight to the volume of the acids and their composition is an important factor, particularly in the analysis of complex matrices, such as copper alloys. Incomplete wetting of the samples or occlusion of the analytes within the grains can result in a non-quantitative recovery of the metals. The potential presence of certain metals may yield to precipitation phenomena depending on the chemical attack conditions[11]. Thus, three digestion methods have been evaluated to optimize the metal alloy samples analysis. Due to the limited amount of the available material an average of 20 mg of bulk sample were used for each attack.

In **Method 1** each sample was weighted and placed in a Teflon glass with a mixture of 1 ml HNO3, 0.25 ml HF and 1 ml H_2O and let stand for 12 hours for complete dissolution. Complete dissolution was achieved in almost all of the cases, although some remains were observed in few solution containing superficial samples.

Method 2 was applied to the samples taken in the 2012 campaign because some insoluble remains appeared after application of method 1. For this reason, after the use of HNO_3 and HF, a strong and oxidant acid, such as $HClO_4$, was added to the solution, trying to totally dissolve the samples. Unfortunately, the procedure did not help to dissolve the residue, but only to break up the particles and, furthermore, a white precipitate appeared. The results

indicate that the use of $HClO_4$ was not an optimal choice for the study of metal samples. The addition of the acid caused the partial or complete loss of the signal of some elements, such as Sb, As, Sn, Ag and Bi. In the case of the As the problem was the interference of the Cl (Ar+Cl=75≈As, OES meas.), whereas the other elements precipitated as salts of Sb, As, Sn and Bi, as confirmed by SEM-EDX determinations (Figure 4) on the residue separated from the solution.

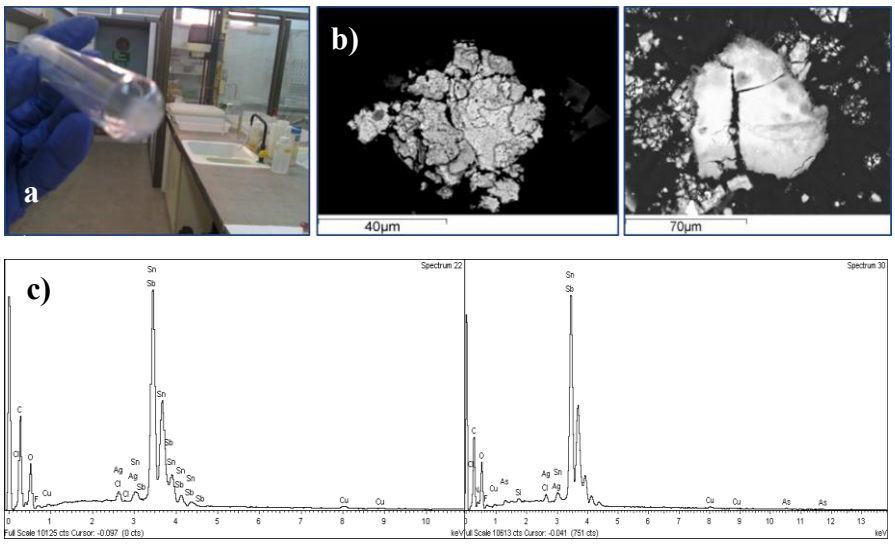

Figure 4 SEM a) White residue; b) back-scattered electrons images of the residue; c) spectra of sample 17a/b.

The problems encountered were attributed to the nature of the samples. As highlighted in the sampling paragraph below, the material coming from the superficial part of the panel has to be avoid because is not representative of the alloy composition because it may includes alteration products and remains of the mould material. Its chemical behaviour is completely distinct and the chemical attack optimum for metals does not permit its complete dissolution.

For the **Method 3** a mixture of 6.25 g tartaric, 6.25 ml HNO_3 and 12.5 ml H_2O was used for dissolution of the metals at room temperature. This method also achieved the total dissolution of the sample, but the amount of the involved reagents induces several problems of interferences in some determination cases. It could be observed that the signal of Cr-52 was magnified due to the interference produced by Ar+C (the latter coming from the organic matter) and Al also leads to interferences.

The results show that Method 2 (HF) was the most suitable attack procedure for the alloy samples

5.2.6 Sampling

The establishment of an effective and practical sampling procedure is an important step along the complex analytical path of an art object [6]. In this case two aspect of the sampling strategy were considered: the sample point election and the set-up of a reproducible sample's extraction procedure. Both aspects contribute to obtain representative and comparable information. The analysed points were chosen by agreement with the conservators and scientific staff of the OPD according with the structure of the Pulpit. Concerning the extraction of the samples, due to the results of the material analysed after the first exploratory sampling campaign in 2010, it was decided to take from each point two samples: the first corresponding to the more external part (surface and limited depth) and the second corresponding to the inner part. The drills used during sampling campaign 2010 were ELA-Carbide bur 1/025 while in campaign 2012/2013 were Steel bit 23/20 Dentsply. To optimize the retrieval of the material and to achieve a separation between the samples coming from the two different depths, an Adhesive Plastic Bag was designed and used to recover the material during the drilling process. The procedure includes fixing the bag on the surface by a sticking part located on its base; to introduce the bit by a hole created in the centre of the sticky side, holding and closing manually the open side of the bag around the drill (Figure 2). This was a simple but rather important improvement of the procedure.

5.2.7 Evaluation of drill contamination

The possibility of contamination caused by the use of the drill for samples extraction was considered. For this purpose fragment of the drill bits used in the different sampling campaigns were analysed.

Sampling Campaign 2010

The material of the working part of the drills used for sampling 2010 was Tungsten Carbide (WC). WC is an inorganic chemical compound containing equal parts of tungsten and carbon atoms. In this case, the other elements found were Fe, Ni, Au, traces of Sb and Ag and a high content of Co (Table 2).

The elements that could be used as marker of the attrition rate of the drills for the ELA-Carbide 1/025 are Ni, Au and Co. Due to the absence of Cu, Pb and Sn no contamination for the major components of the samples is possible. Observing the results obtained for the analysis of the samples taken with those drills it is possible to assert that there was no contamination.

Sampling Campaign 2012/2013

The material that composes the working part of the drills used during sampling campaign in 2012/13 was steel. If we compare the results obtained analysing two new drills (m1 and m2) and two drills that were used to extract the samples m11/12 and m13/14/15, it is possible to observe that the concentration of the major element does not change. On the other hand, a slight contamination with Co for the drill used can be observed (Table 2b).

The element that could be used as marker of the attrition rate for the "new white drill (steel)" is Fe. Thus, for the major components (Cu, Pb and Sn) no contamination of samples was expected. For the minor components (Ni and Co), it is difficult to establish if part of the concentration found comes from the drills. However, observing the results of the analysis of samples taken with this drill type it is possible to assess that there was no contamination, except for the samples m12 and i13, which present a higher amount of Fe with respect to the others; afact that could explain the different values obtained for the major elements.

Although necessary for sampling, it should be noted that the use of drill bits may result in a slight increase in the measured weight percentage (w%) of the Fe or Co, which contributes to a constant background and does not create differences from sample to sample[12]. Some high contamination is easily detectable by the unusual behaviour of the major element of the alloy.

Table 2. Concentrations of the main elements found in drill composition – a) OES results for Cu; Pb; Fe; b) MS results for ^{60}Ni;^{121}Sb; ^{107}Ag;^{197}Au;^{59}Co - ELA-Carbide 1/025 and Steel bit 23/20 Dentsply

a) w% OES	**Description**		**Cu**	**Pb**	**Fe**
Sampling 2010	**label**	**λ**	**327.393**	**220.353**	**238.204**
	m3	"New red drill" (ELA-Carbide 1/025)	0.14	-0.73	9.54
	m4		0.21	-0.74	7.29
Sampling 2012/3	**m1**	"New white drill" (Dentsply - steel)	0.09	-0.01	94.87
	m2		0.08	-0.02	94.68
	m5	"white drill" used for sample 11/12	0.28	0.04	96.24
	m6	"white drill" used for sample 13/14/15	0.15	0.03	96.34

Table 2 (continued)

b) ppm MS		Description	Ni	Sb	Ag	Au	Co
	label	isotope	60	121	107	197	59
Sampling 2010	m3	"New red drill" (ELA-Carbide 1/025)	3915.7	8.9	31.2	1784.4	473694.5
	m4		3585.0	6.6	24.2	1462.7	405928.8
Sampling 2012/3	m1	"New white drill" (Dentsply - steel)	787.2	23.3	4.2	1.1	80.6
	m2		797.6	23.7	1.8	0.7	81.9
	m5	" white drill" used for sample 11/12	764.6	21.4	1.1	0.9	94.5
	m6	"white drill" used for sample 13/14/15	765.5	21.4	0.9	0.6	85.7

5.2.8 Evaluation of the different sources of dispersion

The contributions of the different sources of dispersion in the analysis process for element concentration determination were evaluated. The aim of this stage of the study was establish the maximum uncertainty associated with the elements concentration, which will determine the discrimination capabilities when different objects or parts of them are compared. The results of the samples extracted from the Martirio di San Lorenzo panel, the re-melting and the control bronze were presented below as representative of the whole sample set available.

Reproducibility of measurement, sample treatment and subsample selection

Reproducibility of the measurement step

The reproducibility of the measurement step was determined by measuring the same solution (dilution 1:10) three independent times in the ICP/OES (among measurements 1, 2, 3) samples/solutions were analysed). After a specific experiment on dilution factor, a ratio of 1:10 seemed to be the optimal choice to obtain representative concentration values and is probably the dilution that better match the matrix of the standards used for calibration in ICP-OES. The concentrations of all elements and samples are included in the Annex A. The relative standard deviations for the re-melting, the Martirio di San Lorenzo panel, and the control bronze plate (PL) samples, arranged based on measurements/replicates and their values range, are reported in Table 3. The RSD values obtained range between 0.13 – 1.63 % for Cu; 0.03 – 0.89% for Pb and 0.25 and 2.25% for Sn. The higher values correspond to the lower concentrated element Sn. The average of RSD of measurement, treatment and subsampling for this series of determination were 0.74% for Cu. 0.50% for Pb and 1.07% for Sn (Table 4).

Table 3. OES results for Cu, Pb and Sn of the measurement/replicates– samples I) m12/15/17, II) m20/23/26 and control material – III) PL 1/2/3, 5/6/7 and 11/12/13.

I. w% Labels		meas. 1			meas. 2			meas. 3		
		Cu			Pb			Sn		
		a	b	c	a	b	c	a	b	c
		327.393	327.393	327.393	220.353	220.353	220.353	189.927	189.927	189.927
Re-melting		85.14	87.36	87.31	9.23	9.46	9.03	3.56	3.76	3.49
	m12	84.22	86.42	85.15	9.24	9.48	9.01	3.70	3.79	3.59
		83.37	85.82	84.69	9.15	9.40	8.96	3.66	3.69	3.49
	x	**84.24**	**86.53**	**85.72**	**9.21**	**9.45**	**9.00**	**3.64**	**3.75**	**3.53**
	S(x)	0.88	0.78	1.40	0.05	0.04	0.04	0.07	0.05	0.06
	RSD	1.05	0.90	1.63	0.52	0.41	0.41	1.97	1.32	1.63
		86.61	85.71	86.32	8.37	8.69	8.71	3.42	3.41	3.45
	m15	85.09	84.11	84.50	8.30	8.64	8.71	3.54	3.50	3.57
		84.43	84.40	84.34	8.28	8.63	8.67	3.44	3.49	3.42
	x	**85.38**	**84.74**	**85.06**	**8.32**	**8.65**	**8.70**	**3.47**	**3.47**	**3.48**
	S(x)	1.12	0.85	1.10	0.05	0.03	0.02	0.06	0.05	0.08
	RSD	1.31	1.01	1.29	0.59	0.39	0.23	1.86	1.52	2.25
		86.83	85.55	85.48	8.55	8.47	8.70	3.48	3.49	3.50
	m17	85.11	84.06	83.86	8.57	8.45	8.70	3.58	3.51	3.51
		84.67	83.98	83.99	8.57	8.43	8.70	3.57	3.48	3.43
	x	**85.54**	**84.53**	**84.45**	**8.56**	**8.45**	**8.70**	**3.54**	**3.49**	**3.48**
	S(x)	1.14	0.88	0.90	0.01	0.02	0.00	0.06	0.02	0.04
	RSD	1.33	1.04	1.07	0.13	0.28	0.03	1.61	0.51	1.23

Table 3. (Continued)

II. w% Labels		meas. 1			meas. 2			meas. 3		
		Cu			Pb			Sn		
		a	b	c	a	b	c	a	b	c
		327.393	327.393	327.393	220.353	220.353	220.353	189.927	189.927	189.927
Martirio di San Lorenzo		83.39	81.71	82.24	6.49	6.46	6.49	6.13	6.07	6.11
	m20	84.12	82.32	81.68	6.59	6.54	6.55	6.22	6.13	6.15
		83.55	82.42	82.86	6.59	6.51	6.58	6.25	6.16	6.19
	x	**83.69**	**82.15**	**82.26**	**6.56**	**6.50**	**6.54**	**6.20**	**6.12**	**6.15**
	S(x)	0.38	0.38	0.59	0.06	0.04	0.05	0.06	0.05	0.04
	RSD	0.45	0.47	0.72	0.89	0.62	0.74	1.04	0.78	0.71
		84.32	82.28	81.83	7.76	7.52	7.99	5.37	5.25	5.21
	m23	83.98	82.33	81.47	7.85	7.59	8.05	5.44	5.33	5.25
		84.58	82.57	82.17	7.83	7.59	8.03	5.37	5.32	5.26
	x	**84.29**	**82.39**	**81.82**	**7.81**	**7.57**	**8.02**	**5.39**	**5.30**	**5.24**
	S(x)	0.30	0.15	0.35	0.05	0.04	0.03	0.04	0.04	0.03
	RSD	0.36	0.18	0.43	0.62	0.52	0.39	0.76	0.75	0.48
		82.87	82.60	85.86	7.56	7.46	8.09	4.89	4.91	5.06
	m26	82.83	81.64	84.34	7.65	7.46	8.15	4.96	4.93	5.04
		83.11	82.63	85.30	7.64	7.49	8.15	4.99	4.90	5.10
	x	**82.94**	**82.29**	**85.17**	**7.62**	**7.47**	**8.13**	**4.95**	**4.91**	**5.07**
	S(x)	0.15	0.57	0.77	0.05	0.02	0.04	0.05	0.01	0.03
	RSD	0.18	0.69	0.90	0.63	0.28	0.45	1.03	0.25	0.62

Table 3. (Continued)

		meas. 1			meas. 2			meas. 3			
III.	**w%**	**a**	**b**	**c**	**a**	**b**	**c**	**a**	**b**	**c**	
	Label	**Cu**	**Cu**	**Cu**	**Pb**	**Pb**	**Pb**	**Sn**	**Sn**	**Sn**	
		327.393	**327.393**	**327.393**	**220.353**	**220.353**	**220.353**	**189.927**	**189.927**	**189.927**	
Bronze plate		83.59	83.76	85.24	4.19	4.26	4.39	5.06	5.12	5.39	attack 1
	PL1/2/3	83.76	83.27	84.71	4.25	4.29	4.43	5.18	5.26	5.53	
		83.79	84.35	85.35	4.19	4.26	4.43	5.16	5.31	5.46	
	x	**83.71**	**83.79**	**85.10**	**4.21**	**4.27**	**4.42**	**5.13**	**5.23**	**5.46**	
	S(x)	0.11	0.54	0.35	0.04	0.01	0.02	0.06	0.10	0.07	
	RSD	0.13	0.65	0.41	0.88	0.34	0.55	1.19	1.94	1.31	
		5	**6**	**7**	**5**	**6**	**7**	**5**	**6**	**7**	
		82.38	84.18	83.07	4.32	4.40	4.33	5.35	5.42	5.34	attack2
	PL5/6/7	81.78	84.72	83.37	4.35	4.45	4.39	5.34	5.44	5.43	
		83.00	85.04	83.71	4.33	4.42	4.35	5.38	5.47	5.43	
	x	**82.39**	**84.65**	**83.39**	**4.33**	**4.42**	**4.35**	**5.35**	**5.44**	**5.40**	
	S(x)	0.61	0.43	0.32	0.02	0.03	0.03	0.02	0.02	0.05	
	RSD	0.74	0.51	0.38	0.43	0.59	0.68	0.37	0.41	0.97	
		11	**12**	**13**	**11**	**12**	**13**	**11**	**12**	**13**	
		84.99	87.16	85.39	4.18	4.35	4.07	5.18	5.36	5.10	attack 3
	PL11/12/13	86.43	85.79	85.73	4.20	4.39	4.09	5.24	5.38	5.05	
		85.44	85.97	86.21	4.22	4.42	4.12	5.16	5.45	5.11	
	x	**85.62**	**86.30**	**85.78**	**4.20**	**4.39**	**4.09**	**5.19**	**5.40**	**5.09**	
	S(x)	0.73	0.75	0.41	0.02	0.03	0.03	0.04	0.05	0.03	
	RSD	0.86	0.87	0.48	0.47	0.78	0.61	0.82	0.85	0.60	

Table 4. Summary - Max and min values of RDS and mRSD for Cu. Pb. Sn – measurement step

Measurement step		Cu 327.393	Pb 220.353	Sn 189.927
Range	max	**1.63**	**0.89**	**2.25**
	min	**0.13**	**0.03**	**0.25**
Re-melting	mRSD (n=9)	1.18	0.33	1.55
Martirio		0.49	0.57	0.71
Control		0.56	0.59	0.94
mRSD (n=27)		**0.74**	**0.50**	**1.07**

Reproducibility of samples treatment and subsample selection (+ measurement)

The reproducibility of the measurement + sample treatment (chemical attack) + subsample selection was determined by analysing three subsamples (a, b, c) of the material available for each point. In order to enable the comparison of these values with those corresponding just to the measurement step, only one ICP/OES measurement of each subsample was used. Thus, each series is composed by three values (Table 5/6). The standard deviations obtained for the inner samples depend on the element and seems to show a little dependence on the sample. The sample m26 seems to not have been properly homogenized. The values of relative standard deviations range between 0.05 - 2.16 for Cu, 0.29 – 4.61 for Pb and 0.34 – 3.82 for Sn (Table 5).

The higher values correspond to the lower concentrations. However, apparently there is a trend that shows a higher RSD for Pb than for Sn (except for m12). The average of RSD of measurement, treatment and subsampling for this series of determination are 1.12% for Cu. 2.27% for Pb and 1.80% for Sn (Table 5/6).

Table 5. Summary - Max and min values of RDS and mRSD for Cu. Pb. Sn – measurement, treatment and subsampling.

Measurement + subsampling + chemical attack		Cu 327.393	Pb 220.353	Sn 189.927
Range	max	**2.16**	**4.16**	**3.82**
	min	**0.05**	**0.29**	**0.34**
Remelting	mRSD (n=9)	0.84	2.11	1.75
Martirio		1.49	2.36	1.26
Control		1.03	2.35	2.39
mRSD (n=27)		**1.12**	**2.27**	**1.80**

Table 6. OES results for Cu. Pb and Sn organized for subsamples – samples a) m12/15/17.b) m20/23/26 and c) control material – PL 1/2/3/5/6/7/11/12/13.

I.	w%	meas. 1 Cu 327.39	meas. 2 Cu 327.39	meas. 3 Cu 328.39	meas. 1 Pb 220.35	meas. 2 Pb 220.35	meas. 3 Pb 221.35	meas. 1 Sn 189.93	meas. 2 Sn 189.93	meas. 3 Sn 189.93
Re-melting	**m12a**	85.14	84.22	83.37	9.23	9.24	9.15	3.56	3.70	3.66
	m12b	87.36	86.42	85.82	9.46	9.48	9.40	3.76	3.79	3.69
	m12c	87.31	85.15	84.69	9.03	9.01	8.96	3.49	3.59	3.49
	x	**86.60**	**85.26**	**84.63**	**9.24**	**9.24**	**9.17**	**3.61**	**3.70**	**3.61**
	S(x)	1.27	1.10	1.23	0.22	0.24	0.22	0.14	0.10	0.11
	RSD	1.47	1.30	1.45	2.36	2.55	2.44	3.82	2.67	2.97
	m15a	86.61	85.09	84.43	8.37	8.30	8.28	3.42	3.54	3.44
	m15b	85.71	84.11	84.40	8.69	8.64	8.63	3.41	3.50	3.49
	m15c	86.32	84.50	84.34	8.71	8.71	8.67	3.45	3.57	3.42
	x	**86.21**	**84.57**	**84.39**	**8.59**	**8.55**	**8.53**	**3.43**	**3.54**	**3.45**
	S(x)	0.46	0.50	0.04	0.19	0.22	0.21	0.03	0.04	0.04
	RSD	0.53	0.59	0.05	2.19	2.56	2.51	0.74	1.02	1.02
	m17a	86.83	85.11	84.67	8.55	8.57	8.57	3.48	3.58	3.57
	m17b	85.55	84.06	83.98	8.47	8.45	8.43	3.49	3.51	3.48
	m17c	85.48	83.86	83.99	8.70	8.70	8.70	3.50	3.51	3.43
	x	**85.95**	**84.34**	**84.22**	**8.57**	**8.57**	**8.57**	**3.49**	**3.53**	**3.49**
	S(x)	0.76	0.67	0.40	0.11	0.13	0.14	0.01	0.04	0.07
	RSD	0.88	0.79	0.47	1.33	1.46	1.60	0.34	1.12	2.02

Table 6 (Continued)

II.	w%	meas. 1 Cu 327.39	meas. 2 Cu 327.39	meas. 3 Cu 328.39	meas. 1 Pb 220.35	meas. 2 Pb 220.35	meas. 3 Pb 221.35	meas. 1 Sn 189.93	meas. 2 Sn 189.93	meas. 3 Sn 189.93
Martirio di San Lorenzo	**m20a**	83.39	84.12	83.55	6.49	6.59	6.59	6.13	6.22	6.25
	m20b	81.71	82.32	82.42	6.46	6.54	6.51	6.07	6.13	6.16
	m20c	82.24	81.68	82.86	6.49	6.55	6.58	6.11	6.15	6.19
	x	**82.45**	**82.71**	**82.94**	**6.48**	**6.56**	**6.56**	**6.10**	**6.17**	**6.20**
	S(x)	0.86	1.26	0.57	0.02	0.03	0.05	0.03	0.05	0.04
	RSD	1.04	1.53	0.69	0.29	0.45	0.69	0.47	0.76	0.70
	m23a	84.32	83.98	84.58	7.76	7.85	7.83	5.37	5.44	5.37
	m23b	82.28	82.33	82.57	7.52	7.59	7.59	5.25	5.33	5.32
	m23c	81.83	81.47	82.17	7.99	8.05	8.03	5.21	5.25	5.26
	x	**82.81**	**82.59**	**83.10**	**7.76**	**7.83**	**7.82**	**5.28**	**5.34**	**5.32**
	S(x)	1.32	1.27	1.29	0.23	0.23	0.22	0.08	0.10	0.05
	RSD	1.60	1.54	1.56	3.00	2.92	2.85	1.55	1.81	1.01
	m26a	82.87	82.83	83.11	7.56	7.65	7.64	4.89	4.96	4.99
	m26b	82.60	81.64	82.63	7.46	7.46	7.49	4.91	4.93	4.90
	m26c	85.86	84.34	85.30	8.09	8.15	8.15	5.06	5.04	5.10
	x	**83.78**	**82.93**	**83.68**	**7.70**	**7.75**	**7.76**	**4.95**	**4.98**	**5.00**
	S(x)	1.81	1.35	1.42	0.34	0.36	0.34	0.09	0.06	0.10
	RSD	2.16	1.63	1.70	4.38	4.61	4.42	1.84	1.21	2.01

Table 6 (Continued)

III.	w%	meas. 1 Cu	meas. 2 Cu	meas. 3 Cu	meas. 1 Pb	meas. 2 Pb	meas. 3 Pb	meas. 1 Sn	meas. 2 Sn	meas. 3 Sn
		327.39	**327.39**	**328.39**	**220.35**	**220.35**	**221.35**	**189.93**	**189.93**	**189.93**
Control Material	**PL1**	83.59	83.76	83.79	4.19	4.25	4.19	5.06	5.18	5.16
	PL2	83.76	83.27	84.35	4.26	4.29	4.26	5.12	5.26	5.31
	PL3	85.24	84.71	85.35	4.39	4.43	4.43	5.39	5.53	5.46
	x	**84.19**	**83.91**	**84.50**	**4.28**	**4.32**	**4.30**	**5.19**	**5.32**	**5.31**
	S(x)	0.91	0.73	0.79	0.10	0.09	0.13	0.17	0.18	0.15
	RSD	**1.08**	**0.87**	**0.94**	**2.36**	**2.12**	**2.93**	**3.33**	**3.46**	**2.81**
	PL5	82.38	81.78	83.00	4.32	4.35	4.33	5.35	5.34	5.38
	PL6	84.18	84.72	85.04	4.40	4.45	4.42	5.42	5.44	5.47
	PL7	83.07	83.37	83.71	4.33	4.39	4.35	5.34	5.43	5.43
	x	**83.21**	**83.29**	**83.92**	**4.35**	**4.40**	**4.37**	**5.37**	**5.40**	**5.43**
	S(x)	0.91	1.47	1.04	0.04	0.05	0.05	0.05	0.06	0.05
	RSD	**1.09**	**1.77**	**1.24**	**0.99**	**1.09**	**1.10**	**0.85**	**1.04**	**0.85**
	PL11	84.99	86.43	85.44	4.18	4.20	4.22	5.18	5.24	5.16
	PL12	87.16	85.79	85.97	4.35	4.39	4.42	5.36	5.38	5.45
	PL13	85.39	85.73	86.21	4.07	4.09	4.12	5.10	5.05	5.11
	x	**85.85**	**85.98**	**85.87**	**4.20**	**4.23**	**4.25**	**5.22**	**5.22**	**5.24**
	S(x)	1.15	0.39	0.39	0.14	0.15	0.15	0.13	0.16	0.18
	RSD	**1.35**	**0.45**	**0.46**	**3.32**	**3.66**	**3.54**	**2.52**	**3.15**	**3.52**

Comparison of the dispersion produced the measurement step vs. subsampling +sample treatment (chemical attack) + measurement step

According to the dispersion ranges quoted in Table 7, it is clear that for Cu the dispersions of the entire process (subsampling, sample treatment (chemical attack) and measurement) are similar to the dispersions produced by the measurement steps. Therefore, we conclude that the subsampling and sample treatment do not increase the dispersion of the results obtained as consequence of the measurement step.

This means that sample material is quite homogeneous in terms of Cu particles distribution. For Sn, a slight increase can be observed. Pb shows a significant increase in the dispersion as consequence of the subsampling and sample treatment steps. Taking into account that the chemical treatment dissolves the sample completely, this behaviour will probably indicates that the Pb particles have a physical behaviour that hinder the homogenization and causes an irregular distribution in the material of the sample. On the other side, the expected dispersion of the concentration determined in terms of RSD are < 2% for Cu and < 4% for Sn, Pb for <5%.

Table 7. Min and Max RSD values of the dispersion produced by the measurement step vs. subsampling +sample treatment (chemical attack) + measurement step

Elements						
	Cu		**Pb**		**Sn**	
%	**Meas.**	**Subsampling +Treatment + Meas.**	**Meas.**	**Subsampling +Treatment + Meas.**	**Meas.**	**Subsampling +Treatment + Meas.**
Min	0.13	0.05	0.03	0.29	0.25	0.34
Max	1.63	2.16	0.89	4.16	2.25	3.82
mRSD (n=27)	**0.74**	**1.12**	**0.50**	**2.27**	**1.07**	**1.80**

Effect of depth on the dispersion and concentration

Two aspects have been considered: the relation between the external and the internal samples and the effect of the depth on the set of the inner samples. External samples are those that include the superficial material.

Effect of depth on the concentration - External vs. internal samples

Observing the results shown in Table 8, it becomes clear that there is a significant difference between the values of concentration obtained for the different elements of the surface samples with regard to the internal ones. The concentration of the elements is probably decreased due to the inclusions of components not belonging to the alloys such as residues of patina[13], clay, dust or alteration materials. These results indicate that superficial material must be avoided during the sampling process[3,14–18]. In case of casted metal object, the segregation behaviour of lead in copper alloy is extensively documented [6,19–24]. For an alloy of a given lead content the distribution of lead is governed by the cooling rate of the original casting [21]. Different types of segregation have been demonstrated [6] and one or more of these could be the cause of the high variability of Pb concentration in alloy samples.

It can be seen in Figure 5 that the ratio Cu/Pb is higher for inner samples respect the external ones. Thus, Pb seems to be present in higher concentrations in the first mm of the alloy.

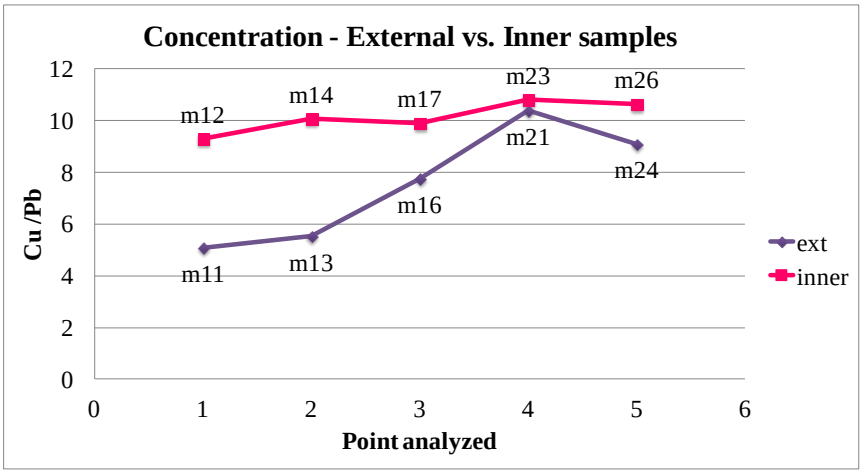

Figure 5. Graphical representation of Cu/Pb ratio for external samples (blue line - m11/13/16 - 21/24) and inner samples (magenta line - m12/14/17 – 23/26).

Table 8. Comparison of the concentration obtained for Cu and Pb - external samples (m11/13/16) and inner samples (m12/14-15/17), for three different sampling points.

w%		Cu 327.393	Pb 220.353	Cu+Pb	Cu/Pb
Re-melting	**m11 (n=1)**	59.54	11.71	71.25	5.08
	m12a (n=3)	84.24	9.21	93.45	9.15
	m12b (n=3)	86.53	9.45	95.98	9.16
	m12c (n=3)	85.72	9.00	94.71	9.53
	x (n=9)	85.50	9.22	94.72	9.28
	S(x)	1.16	0.23	1.27	0.22
	RSD	1.36	2.45	1.34	2.32
	m13 (n=1)	76.75	13.90	90.65	5.52
	m14a (n=2)	87.96	8.76	96.73	10.04
	m14b (n=2)	85.92	8.48	94.40	10.14
	m14c (n=2)	87.80	8.76	96.56	10.03
	x (n=6)	87.23	8.67	95.90	10.07
	S(x)	1.13	0.16	1.30	0.06
	RSD	1.30	1.89	1.35	0.60
	m15a (n=3)	85.38	8.32	93.70	10.26
	m15b (n=3)	84.74	8.65	93.39	9.79
	m15c (n=3)	85.06	8.70	93.75	9.78
	x (n=9)	85.06	8.56	93.61	9.95
	S(x)	0.32	0.21	0.20	0.28
	RSD	0.38	2.41	0.21	2.77
	m16 (n=1)	76.67	9.91	86.58	7.74
	m17 (n=3)	85.54	8.56	94.10	9.99
	m17b (n=3)	84.53	8.45	92.98	10.00
	m17c (n=3)	84.45	8.70	93.15	9.71
	x (n=9)	84.84	8.57	93.41	9.90
	S(x)	0.61	0.13	0.61	0.17
	RSD	0.72	1.46	0.65	1.69

Effect of the depth on the concentration of detected elements for internal samples

The effect of the penetration depth on the concentration of elements in the internal samples has been studied by using two sampling points of the same alloy where the extraction was performed in three steps. Thus, six samples, from three depths, were taken – samples m21/m24 coming from the first 2-3 mm (Figure 6 – part/depth 1), samples m22/m25 from 2-3 up to 4-5 mm (Figure 6 – part/depth 2) and samples m26/m23 coming from 4-5 up to 6-7 mm (Figure 6 – part/depth 3). The values are reported in Table 9.

Table 9. Comparison of the concentration obtained for Cu and Pb- external samples (m21/24 - pink). intermediate samples (m22/25- ochre) and inner samples (m23/26 - blue).

	w%	Cu 327.393	Pb 220.353	Sn 189.927	Cu+Pb	Cu/Pb	Cu/Sn
Martirio di San Lorenzo	**m21**	80.66	7.77	5.19	88.43	10.38	15.53
	m22	84.03	7.89	5.43	91.92	10.65	15.49
	m23a	84.29	7.81	5.39	92.10	10.79	15.63
	m23b	82.39	7.57	5.30	89.96	10.89	15.55
	m23c	81.82	8.02	5.24	89.85	10.20	15.62
	x	**82.84**	**7.80**	**5.31**	**90.64**	**10.63**	**15.60**
	s(x)	1.29	0.23	0.08	1.27	0.37	0.04
	RSD	1.56	2.92	1.45	1.40	3.50	0.29
	m24	81.22	8.94	3.53	90.17	9.08	23.03
	m25	81.64	8.50	5.03	90.14	9.60	16.22
	m26a	82.94	7.62	4.95	90.55	10.89	16.77
	m26b	82.29	7.47	4.91	89.76	11.02	16.74
	m26c	85.17	8.13	5.07	93.29	10.48	16.80
	x	**83.46**	**7.74**	**4.98**	**91.20**	**10.79**	**16.77**
	s(x)	1.51	0.35	0.08	1.85	0.28	0.03
	RSD	1.81	4.46	1.64	2.03	2.60	0.18

An important dispersion of values can be observed in the two first parts, whereas the internal samples – part/depth 3 - shows the much more similar compositions with differences that agree with the dispersion determined in the previous sections.

The gradient of concentration from surface towards the inner part of the casted object could be justified with phenomena of inverse segregation often associated, as described in literature [6], with alloys of copper containing arsenic, antimony or tin – that can push the alloying element to the exterior of the mould surface. The inverse segregation is observed in

a cast metal in which an excess of lower-melting metal occurs in the earlier-freezing portions because liquid metal enters cavities developed in the earlier-solidified metal. In any case, to demonstrate these phenomena deeper studies should be done.

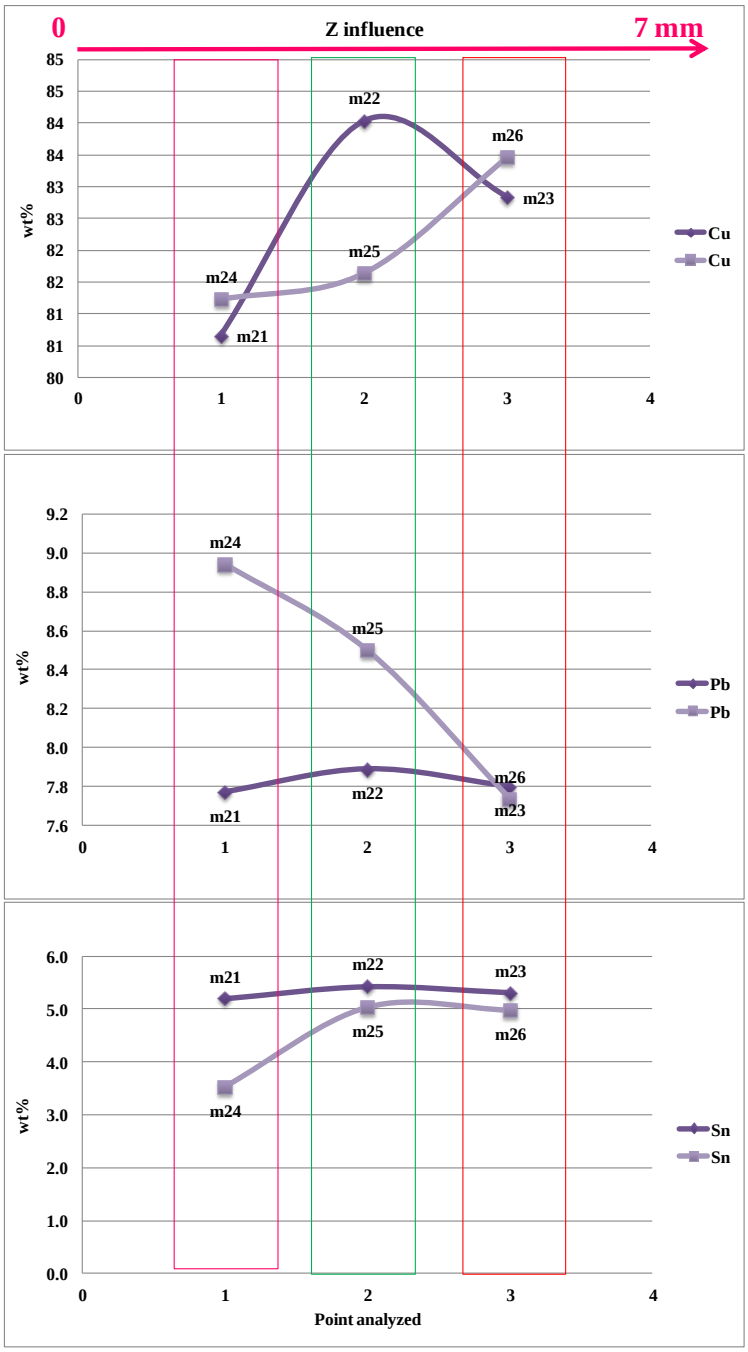

Figure 6. Graphical representation of the concentration of Cu. Pb and Sn at different sampling depth.

Effect of the distance (X/Y sampling point position) on the dispersion and concentration

The effect of the distance on the dispersion and concentration for the same object has been studied at two levels: short (micro – 5 cm) and large (macro – 40 cm) distance between sampling points.

Effect of the micro X/Y distance on the dispersion

With the aim to evaluate the effect of the micro X/Y distance, we considered the inner samples m12, m15 and m17 that were taken at a distance of 5 cm one from each other. Three different series, each including one subsample of every sample, were examined (Table 10). In this way, we get series of n=3 and the dispersion obtained will be comparable to the values obtained for measurement and subsampling + sample treatment (chemical attack) + measurement step.

These results indicate that the Cu concentrations for the three inner samples are equivalent. Thus, there is no influence of the micro X/Y distance on the concentration obtained for the re-melting. For Pb, there are differences between the positions that could be caused by the depth (in accordance with the previous discussion) or both depth and x/y position. According to the sampling description, samples m12 it is more superficial with respect to the others samples. Pb and Sn seem to have a heterogeneous distribution in the material for the proposed procedure of analysis.

Table 10. I) OES results for Cu Pb and Sn divided between points analysed; II) Weighted mean values of concentrations are reported for samples m12/15/17 taken with 5 cm distance.

I. w%		Cu 327.393			Pb 220.353			Sn 189.927		
		meas. 1								
		a)	b)	c)	a)	b)	c)	a)	b)	c)
Re-melting	m12 (n=1)	85.14	87.36	87.31	9.23	9.46	9.03	3.56	3.76	3.49
	m15 (n=1)	86.61	85.71	86.32	8.37	8.69	8.47	3.42	3.41	3.45
	m17 (n=1)	86.83	85.55	85.48	9.03	8.71	8.70	3.48	3.49	3.50
	x (n=3)	**86.19**	**86.21**	**86.37**	**8.88**	**8.95**	**8.73**	**3.49**	**3.55**	**3.48**
	S(x)	0.92	1.00	0.91	0.45	0.44	0.28	0.07	0.18	0.02
	RSD	1.07	1.17	1.06	5.05	4.93	3.19	2.07	5.18	0.71
	meas. 2									
	m12 (n=1)	84.22	86.42	85.15	9.24	9.48	9.01	3.70	3.79	3.59
	m15 (n=1)	85.09	84.11	84.50	8.30	8.64	8.71	3.54	3.50	3.57
	m17 (n=1)	85.11	84.06	83.86	8.57	8.45	8.70	3.58	3.51	3.51
	x (n=3)	**84.81**	**84.86**	**84.51**	**8.70**	**8.85**	**8.80**	**3.61**	**3.60**	**3.56**
	S(x)	0.51	1.35	0.64	0.48	0.55	0.17	0.08	0.16	0.04
	RSD	0.60	1.59	0.76	5.55	6.19	1.98	2.34	4.55	1.17
	meas. 3									
	m12 (n=1)	83.37	85.82	84.69	9.15	9.40	8.96	3.66	3.69	3.49
	m15 (n=1)	84.43	84.40	84.34	8.28	8.63	8.67	3.44	3.49	3.42
	m17 (n=1)	84.67	83.98	83.99	8.57	8.43	8.70	3.57	3.48	3.43
	x (n=3)	**84.16**	**84.73**	**84.34**	**8.67**	**8.82**	**8.78**	**3.56**	**3.55**	**3.45**
	S(x)	0.69	0.96	0.35	0.44	0.52	0.16	0.11	0.12	0.04
	RSD	0.82	1.14	0.41	5.11	5.84	1.77	3.02	3.40	1.07

Table 10 (continued)

	II. Micro X-Y distance (5 cm)											
	OES	**Cu**	**Pb**	**Sn**	**Cu+Pb+Sn**	**Cu/Pb**	**Cu/Sn**	**Weight (g)**	**Weighted mean**				
	w%	**327.393**	**220.353**	**189.927**					**Cu**	**Pb**	**Sn**	**Cu/Pb**	**Cu/Sn**
Re-melting	**m12a (n=3)**	84.24	9.21	3.64	97.09	9	23	0.01761					
	m12b (n=3)	86.53	9.45	3.75	99.73	9	23	0.02118					
	m12c (n=3)	85.72	9.01	3.53	98.26	10	24	0.01709					
	x (n=9)	**85.5**	**9.22**	**3.64**	**98.36**	**9.27**	**23.50**		**85.56**	**9.23**	**3.65**	**9**	**23**
	S(x)	1.16	0.23	0.11	1.32	0.21	0.68						
	RSD	1.36	2.45	3.04	1.34	2.26	2.89						
	m15a (n=3)	85.38	8.32	3.47	97.17	10	25	0.02168					
	m15b (n=3)	84.74	8.65	3.47	96.86	10	24	0.02503					
	m15c (n=3)	85.06	8.7	3.48	97.24	10	24	0.02883					
	x (n=9)	**85.06**	**8.56**	**3.47**	**97.09**	**9.95**	**24.49**		**85.04**	**8.57**	**3.47**	**9.9**	**25**
	S(x)	0.32	0.21	0.01	0.20	0.27	0.10						
	RSD	0.38	2.41	0.27	0.21	2.76	0.41						
	m17a (n=3)	85.54	8.56	3.54	97.64	10	24	0.02745					
	m17b (n=3)	84.53	8.45	3.49	96.47	10	24	0.02666					
	m17c (n=3)	84.45	8.7	3.48	96.63	10	24	0.02131					
	x (n=9)	**84.84**	**8.57**	**3.51**	**96.91**	**9.90**	**24.22**		**84.87**	**8.56**	**3.51**	**9.9**	**24**
	S(x)	0.61	0.13	0.03	0.63	0.17	0.1						
	RSD	0.72	1.46	0.92	0.65	1.70	0.2	**x**	**85.16**	**8.79**	**3.54**	**9.70**	**24.04**
								S(x)	0.4	0.4	0.1	0.37	0.5
								RSD	0.4	4.4	2.7	3.86	2

Effect of the macro X/Y distance on the dispersion and the concentration

The samples considered for this case were samples m20, m23 and m26, inner samples extracted at three points with a distance of 40 cm one from each other. The dispersion increases for Pb (10%) and Sn (11%) (Table 11).

Table 10. I) OES results for Cu Pb and Sn divided between points analysed. On part II) weighted mean values of concentrations for Samples m20/23/26, taken with 40 cm distance are reported.

I. w%		Cu 327.393			Pb 220.353			Sn 189.927		
		meas. 1								
		a)	b)	c)	a)	b)	c)	a)	b)	c)
Martirio di San Lorenzo	m20(n=1)	83.39	81.71	82.24	6.49	6.46	6.49	6.13	6.07	6.11
	m23(n=1)	84.32	82.28	81.83	7.76	7.52	7.99	5.37	5.25	5.21
	m26(n=1)	82.87	82.60	85.86	7.56	7.46	8.09	4.89	4.91	5.06
	x (n=3)	**83.53**	**82.20**	**83.31**	**7.27**	**7.15**	**7.52**	**5.46**	**5.41**	**5.46**
	S(x)	0.73	0.45	2.22	0.68	0.60	0.90	0.62	0.59	0.57
	RSD	0.88	0.55	2.66	9.39	8.36	11.90	11.42	10.98	10.37
		meas. 2								
	m20(n=1)	84.12	82.32	81.68	6.59	6.54	6.55	6.22	6.13	6.15
	m23(n=1)	83.98	82.33	81.47	7.85	7.59	8.05	5.44	5.33	5.25
	m26(n=1)	82.83	81.64	84.34	7.65	7.46	8.15	4.96	4.93	5.04
	x (n=3)	**83.64**	**82.10**	**82.50**	**7.36**	**7.20**	**7.58**	**5.54**	**5.46**	**5.48**
	S(x)	0.71	0.40	1.60	0.68	0.58	0.90	0.64	0.61	0.59
	RSD	0.84	0.48	1.94	9.17	8.00	11.81	11.49	11.26	10.78
		meas. 3								
	m20(n=1)	83.55	82.42	82.86	6.59	6.51	6.58	6.25	6.16	6.19
	m23(n=1)	84.58	82.57	82.17	7.83	7.59	8.03	5.37	5.32	5.26
	m26(n=1)	83.11	82.63	85.30	7.65	7.46	8.15	4.99	4.90	5.10
	x (n=3)	**83.75**	**82.54**	**83.44**	**7.36**	**7.19**	**7.59**	**5.53**	**5.46**	**5.52**
	S(x)	0.75	0.11	1.65	0.67	0.59	0.87	0.65	0.64	0.59
	RSD	0.90	0.14	1.97	9.13	8.22	11.50	11.68	11.73	10.66

Table 11 (continued).

Martirio di San Lorenzo	**II. Macro X-Y distance (40 cm)**												
	OES	**Cu**	**Pb**	**Sn**	**Cu+Pb+Sn**	**Cu/Pb**	**Cu/Sn**	**Weight (g)**	**Weighted mean**				
	w%	**327.393**	**220.353**	**189.927**					**Cu**	**Pb**	**Sn**	**Cu/Pb**	**Cu/Sn**
	m20a (n=3)	83.69	6.56	6.20	96.44	13	14	0.04433					
	m20b (n=3)	82.15	6.50	6.12	94.77	13	13	0.05037					
	m20c (n=3)	82.26	6.54	6.15	94.95	13	13	0.05812					
	x (n=27)	**82.70**	**6.53**	**6.16**	**95.39**	**12.66**	**13.43**		**82.64**	**6.53**	**6.15**	**13**	**13**
	S(x)	0.86	0.03	0.0		0.09	0.06						
	RSD	1.04	0.45	0.6		0.75	0.48						
	m23a (n=3)	84.29	7.81	5.39	97.50	11	16	0.03631					
	m23b (n=3)	82.39	7.57	5.30	95.26	11	16	0.03550					
	m23c (n=3)	81.82	8.02	5.24	95.09	10	16	0.03948					
	x (n=27)	**82.84**	**7.80**	**5.31**	**95.95**	**10.63**	**15.60**		**82.81**	**7.81**	**5.31**	**11**	**16**
	S(x)	1.29	0.23	0.1		0.37	0.04						
	RSD	1.56	2.92	1.4		3.50	0.29						
	m26a (n=3)	82.94	7.62	4.95	95.50	11	17	0.02944					
	m26b (n=3)	82.29	7.47	4.91	94.68	11	17	0.03493					
	m26c (n=3)	85.17	8.13	5.07	98.36	10	17	0.03596					
	x (n=27)	**83.46**	**7.74**	**4.98**	**96.18**	**10.79**	**16.77**		**83.51**	**7.75**	**4.98**	**11**	**17**
	S(x)	1.51	0.35	0.1		0.28	0.0						
	RSD	1.81	4.46	1.6		2.60	0.2	**x**	**82.99**	**7.36**	**5.48**	**11.34**	**15.27**
								S(x)	0.5	0.7	0.6	1.13	1.7
								RSD	0.6	9.8	11.1	10.00	11

The comparison between micro X/Y and macro X/Y distance (Table 12) permits to highlighting an important increase of RSD values for Sn (≈Δ7%) and Pb (Δ6%). The Cu seems to maintain a desirable reproducibility of <1%.

Table 11. Min and Max RSD values of the dispersion produced by the micro X/Y distance and the macro X/Y distance.

X/Y micro distance		**Cu 327.393**	**Pb 220.353**	**Sn 189.927**
Range	**max**	**1.59**	**6.19**	**5.18**
	min	0.41	1.77	0.71
Remelting - mRSD (n=9)		0.96	4.40	2.61
X/Y macro distance				
Range	**max**	**2.66**	**11.90**	**11.68**
	min	0.13	0.02	8.37
Martirio- mRSD (n=9)		1.15	9.72	11.15

Total reproducibility

The maximum dispersions in terms of RSD obtained following this procedure are for Cu < 3%, for Pb < 12% and for Sn <12% and the average RSD values, being slightly lower, are for Cu < 1.5%, for Pb< 10% and for Sn <11%. These values are the consequence of the dispersion introduced by the macro X/Y distance for the three elements (Table 13).

The X/Y distance in large objects produces an important heterogeneity on the elements distribution, e. g. of Pb and Sn that increases dramatically the dispersion of the results (from 4.4 % to 9.7 % for Pb and from 2.6 to 11.1% for Sn). This behavior is probably related to the process of solidification of the alloy and it will depend on the form of the object and the material of the mould[25]. In addition, it is important to bear in mind that the variation of the concentration of some elements, such as Pb, Sn or Sb, introduces changes on the malleability and hardness of the objects[23]. This fact should be taken into account when trying to establish a relationship between different objects based on the composition of the samples. In the case of the Pulpit, these facts will be important in the discussion of the relationship between panels and frames.

Table 12. Summary- Min and Max RSD and mRSD values for all the factors considered.

Elements												
RSD	**Cu**				**Pb**				**Sn**			
%	**Meas.**	**Subsampl. + Treatm. + Meas.**	**X/Y micro**	**X/Y macro**	**Meas.**	**Subsampl. + Treatm. + Meas.**	**X/Y micro**	**X/Y macro**	**Meas.**	**Subsampl. + Treatm. + Meas.**	**X/Y micro**	**X/Y macro**
Min	0.13	0.05	1.59	0.13	0.03	0.29	1.77	0.02	0.25	0.34	0.71	8.37
Max	**1.63**	**2.16**	**0.41**	**2.66**	**0.89**	**4.16**	**6.19**	**11.90**	**2.25**	**3.82**	**5.18**	**11.68**
mean	0.74	1.12	0.96	1.15	0.50	2.27	4.40	9.72	1.07	1.80	2.61	11.15

Proposed procedure

Once the effects of measurement, sample treatment and subsampling have been understood, the procedure suggested for the analysis includes, for each sample taken, the chemical dissolution of three different subsamples and the acquisition of three independent measurements of the different solution by ICP. Thus, the concentration value obtained for each sample will be the average of three determinations (n=9). All the results presented below were obtained following the proposed procedure. As summary, a scheme of the different steps and the related sources of dispersion is presented in Figure 7.

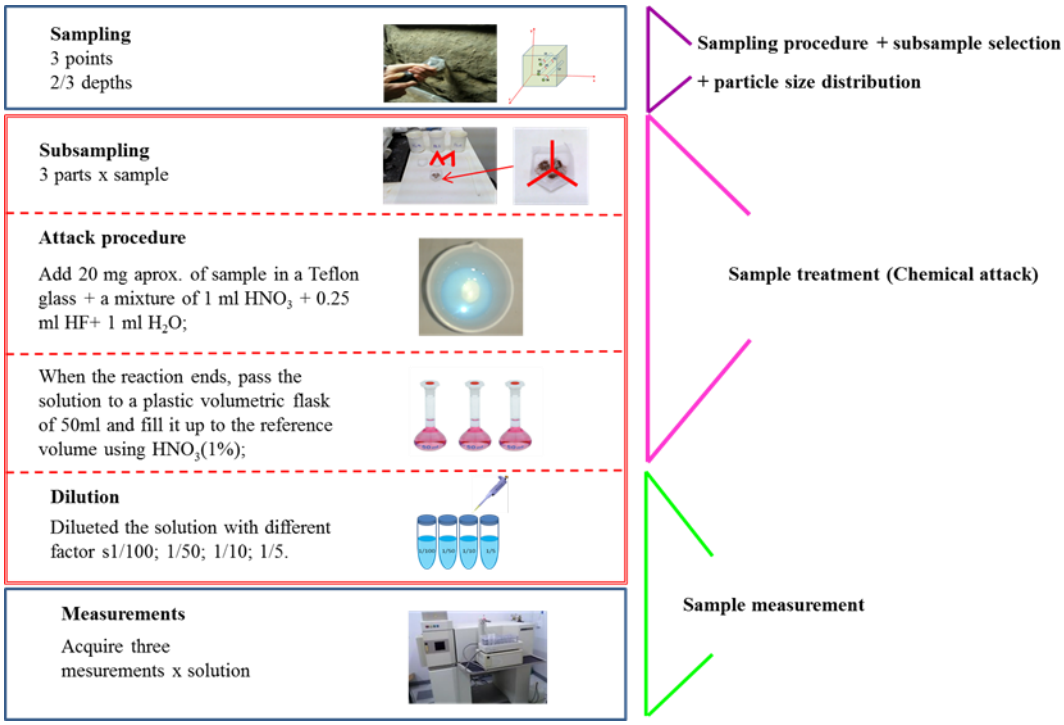

Figure 7. Scheme of the analytical procedure and the source of dispersion related to each steps.

Reproducibility along time

To evaluate the reproducibility of the result along time, samples C3 (sampling campaign 2010) and C3a (sampling campaign 2012) have been compared because the samples had been extracted from the same point of the Pulpit but in two different sampling campaigns. The mean concentrations of both series of analysis are comparable (Table 14). The dispersion values observed for the major elements are included in the maximum dispersion values presented above (Table 13). Furthermore, dispersion improved for minor element.

Table 13. Reproducibility of the analytical method along time. Comparison of results obtained for sample C3/C3a taken at the same point in campaign 2010 or 2012, respectively.

		Martirio di San Lorenzo								
		Frame above the panel "Martirio di San Lorenzo"								
		OES	**Cu**	**Pb**	**Sn**	**Cu+Pb+Sn**	**MS**	**Ni**	**Sb**	**As**	**Co**
			w%					**ppm**			
UPPER PART	**Sampling 2010**	**C3(m3)**	80.05	10.92	5.72	**97**		1840.0	2776.0	1442.0	16.6
		C3(m3.2)	79.06	10.86	5.93	**96**		1726.0	2405.0	1257.0	13.6
		C3 (m8.1)	79.96	10.73	5.98	**97**		1713.0	2386.0	1247.0	13.5
		x (n=9)	**79.69**	**10.84**	**5.88**	**96**		**1759.7**	**2522.5**	**1349.5**	**14.6**
		s(x)	0.55	0.10	0.14			69.9	219.9	109.8	1.8
		RSD	0.69	0.90	2.35			4.0	8.7	8.3	12.1
	Sampling 2012	**C3a1**	81.15	11.70	5.76	**99**		1743.7	2536.0	1160.2	15.4
		C3a2	79.83	11.48	5.64	**97**		1735.7	2516.2	1118.2	15.1
		C3a3	79.17	11.30	5.59	**96**		1725.4	2501.2	981.4	15.0
		x (n=9)	**80.05**	**11.49**	**5.66**	**97**		**1734.9**	**2517.8**	**1086.6**	**15.2**
		s(x)	1.01	0.20	0.09			9.2	17.4	93.5	0.2
		RSD	1.26	1.75	1.54			0.5	0.7	8.6	1.4
		x(n=18)	**79.87**	**11.16**	**5.77**	**97**					
		s(x)	0.75	0.39	0.16						
		RSD	0.94	3.45	2.72						

5.2.9 Composition and metal alloy discrimination

Once the source of variability and the analytical procedure to be followed for the analysis have been established, we proceed with the analysis of the different samples taken in different places of the different parts of the Pulpit and to discuss the similarities between them in terms of composition.

The major elements identified for all the samples analysed are Cu, Pb and Sn. Due to the high content of these elements the alloys founded can be defined as tin bronzes and leaded-tin bronzes. In addition to the concentration of these elements, the concentrations of Ni, Sb, As, Ag, Bi and Co were determined by ICP-MS. The results show the presence, as main elements, of Ni and Sb, As and Co. The high dispersion obtained for the concentration values of Ag, Au and Bi does not permit to use these elements as factor of discrimination between alloys.

It is important to highlight that the presence of Pb in renaissance bronze has been reported to be a key element for the discrimination of casting procedure in studies published by the OPD[26] and others institutions[1,27]. Thus, a greater amount of Pb increases castability and it is typical, during the period considered, as a characteristic of old technology. On the other hand, higher content of Sn, which increases the hardness of the resulting alloy, improves its metallurgical properties and lowers the melting point[23], is characteristic of later, though chronologically close manufactures and casting techniques[26].

The comparison of the different parts of the Pulpit will be done by a classical approach, namely by direct comparison of the concentration determined for the different constitutive elements, and by applying multivariate methods, as an attempt to reveal patterns that could not be easily deduced in the direct approach.

Classical approach

In this section, the similarities and differences between alloys will be discussed by comparing the concentrations of the elements on the different samples.

Procedure A. Concentration comparison

A scheme of the Pulpit parts with the approximate location of samples is presented in Figure 1. In this first part, the criterion used in this first part to determine the differences between concentration values is to investigate if they differ more than approx. 3 times the uncertainty values associated to each element. These uncertainty values were established in the previous study: 3% for Cu and 12% for Pb and Sn. This criterion is chosen because the quoted

uncertainty values present the worst case established and also, because the variability introduced by X/Y distance may hide some similarities. As it was mentioned previously, this second aspect has been evaluated for panel size objects but it is partially unknown for thinner and smaller objects such as frame parts. The dispersion values established for panels are considered as an approximation.

This section includes panels' comparison, frames comparison and a comparison among panels and frames. For practical reasons each panel was labelled with a capital letter e.g. "*A"* for Martirio di San Lorenzo. Furthermore, the different samples/frames will be labelled with a capital letter that denote the corresponding panel (A-F), an abbreviation that indicate the level of the decoration. Starting from the top of the Pulpit, the frames was classed with "*above panel*" (ab) when the decoration includes only one piece, *upper/intermediate/lower* when the decoration includes three levels (low, int and up) plus the sample labels (e.g. icp/i1) (Table 15).

Table 14. Legend of frame label that will be used in the next sections.

	Panels		**Frames**	
Letter	**Relief**	**samples**	**Level**	**samples**
A	Martirio di San Lorenzo	m20, 21/22/23, 24/ 25/26	above panel*(**ab**)	**C3a**
B	Pentecoste	icp/i 14	above panel*(**ab**)	**icp/i 13**
C	Ascensione	icp/i 5	lower (**low**) upper (**up**)	**icp/i 6** **icp/i 12**
D	Resurrezione	icp/i 4	intermediate (**int**)	**icp/i 8 - IN** **icp/i 9 - ON** **icp/i 10 – OUT/NEARBY**
E	Discesa al Limbo	icp/i 3	lower (**low**) upper (**up**)	**icp/i 7** **icp/i 11**
F	Pie donne	icp/i 1	above panel*(**ab**)	**icp/i 2**

*no physical separation between the panel and frames is present.

Composition and comparison of the panels

In the discussion, each panel will be compared with the remaining ones in terms of major and minor elements. A binary (CuSn) and a ternary (CuPbSn) alloys were identified. Minor elements, such as Ni, Sb, As, Bi and Co were found. The mean results are shown in the bar charts in Figure 8 (panels) and Figure 9 (frames) are represented with the corresponding dispersion established in the previous part.

Martirio di San Lorenzo

Three replicates of each sample m20, m23 and m26 have been analysed (Table 1). As it can be observed, the results are quite reproducible, most for Cu with a RSD $_{[n=9]}$ of 0.5%, but also for Pb with RSD 9.7% and Sn with 11.1%. The values are useful evidence of the limitations related to the Pb and Sn determination. On the other hand, the alloy can be defined as ternary alloy (element proportion - Cu83Pb7Sn6).

Pie donne

The results show RSD $_{[n=9]}$ 0.87% for Cu, 2.42% for Pb and 0.25% for Sn. The alloy can be defined as ternary alloy (Cu85Pb7Sn5).

Pentecoste

The RSD $_{[n=9]}$ values are 2.3% for Cu, than 1.73% for Pb and 2.33% for Sn. The alloy can be defined as ternary alloy (Cu89Pb5Sn3).

Discesa, Resurrezione, Ascensione

There are several interesting characteristics of these panels. The sum of the major elements concentration is close to 100% and the most important is the very small amount of Pb. As a matter of fact these alloys can be defined as binary (Discesa Cu89Sn5, Resurrezione Cu87Sn6, Ascensione Cu94Sn5).

In summary, it can be established that Martirio di San Lorenzo (A) are similar to Pie donne (F) and different from all the other panels. Pentecoste (B) is slightly different from Martirio di San Lorenzo and Pie donne and completely different to Discesa (E), Resurrezione (D) and Ascensione (C), which are similar among each other

a)

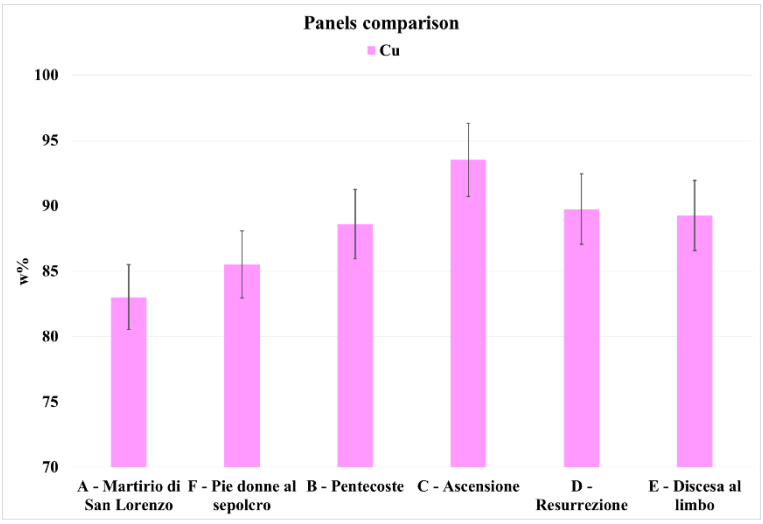

b)

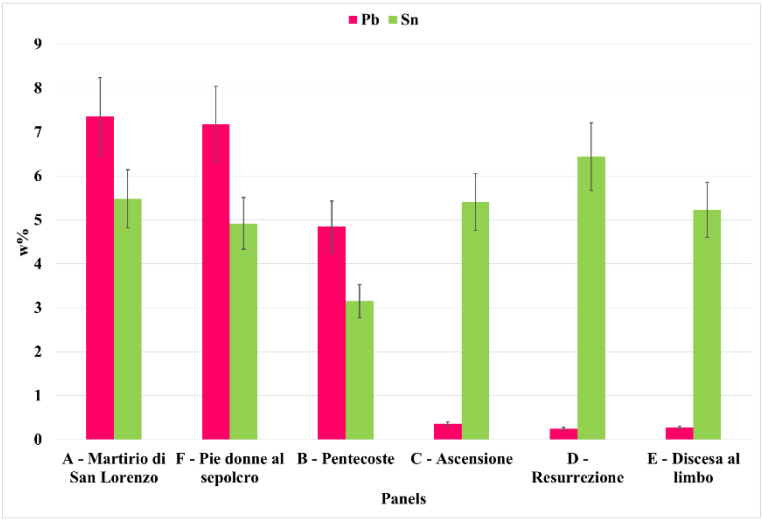

c)

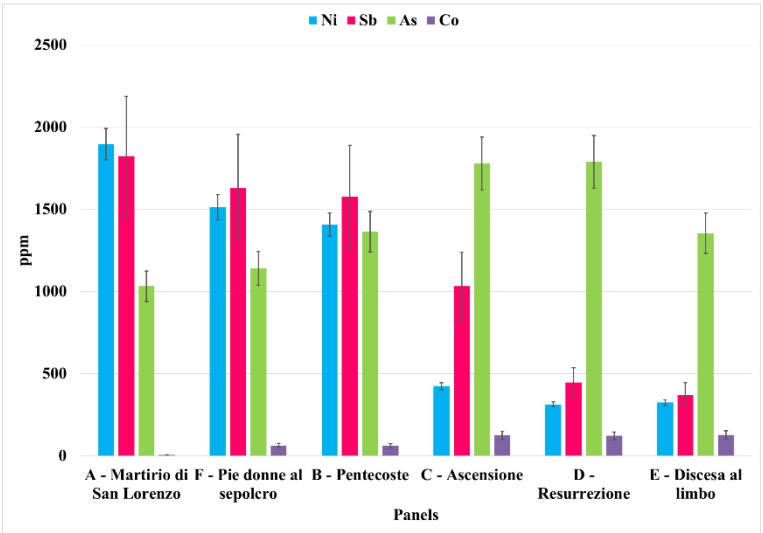

Figure 8. Bar charts of the mean of the concentration of major and minor elements for all the panels' samples (a - Cu, b - Pb and Sn; c - Ni, Sb, As and Co).

Composition and comparison of the Frames

As observed for the panels, the frames' alloys may be classified as binary (CuSn) and a ternary (CuPbSn), although high content of Sb and As have been detected.

ABOVE THE PANELS The Frames of *Martirio di San Lorenzo* and *Pie donne* are similar, while the frame of *Pentecoste* is slightly different, due to the lower amount of Sn (AabC3≈Fabi2~Babi13).

UPPER PARTS. Discesa (Eupi11) is different to *Ascensione* (Cupi12). Sample i11 has a unique composition, with high amount of Pb and very high of Sb.

INTERMEDIATE PART. (*IN, ON and OUT/NEARBY the central decorative element)*. All samples correspond to the part above the *Resurrezione*. The samples DintONi9 and DintOUTi10 of the frieze are similar. The sample DintINi8 is different from the others.

LOWER PARTS. *Ascensione* (Clowi6) is similar to *Discesa* (Elowi7).

TOTAL COMPARISON. Comparing single upper parts of *Martirio di San Lorenzo*, *Pie donne*, *Pentecoste* are different from Upper, Intermediate and Lower parts of *Discesa*, *Resurrezione* and *Ascensione* due to the different amount of Pb.

Panels and frame's comparison

The composition of the *Martirio di San Lorenzo* and *Pie donne* panels is similar to their frames although the composition of frames shows a higher amount of Pb (A≈AabC3; F≈Fabi2). The *Pentecoste* panel and frame are different based in the Pb and Cu concentration (B≠Babi13). The *Discesa* panel seems similar to lower part of its frame despite of difference in the amount of Sn. The panel and the lower part of the frame are different to the upper part judging from the concentrations of Cu, Pb and especially Sb (E≈Elowi7≠Eupi11).

The composition of the *Resurrezione* panel could be similar to the ON and OUT/NEARBY parts of the frame, but in the frame samples, the amount of Sb is clearly higher. On the other hand, panel and these two parts of the frame are different from the IN sample in terms of the lower amount of Sn and, especially, the higher amount of Sb (D≈DintOUTi10/DintONi9≠DintINi8). The *Ascensione* panel and the lower and the upper parts of the frame seem similar (C≈Clowi6≈Cupi12).

a)

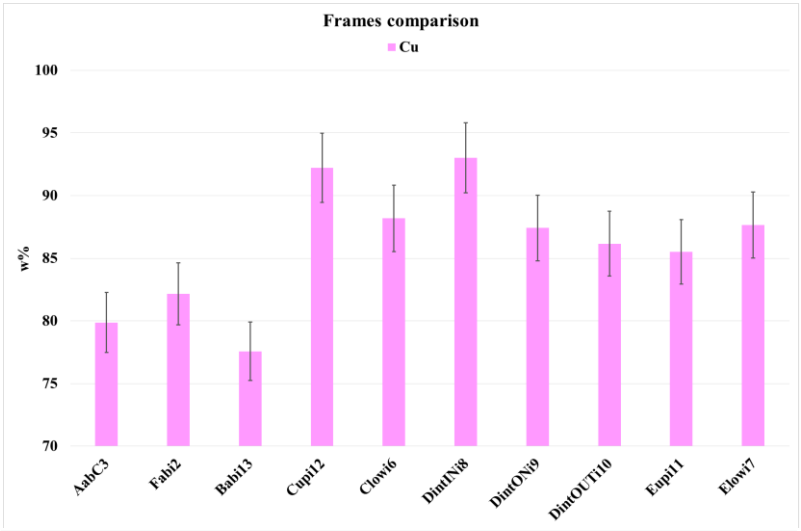

b)

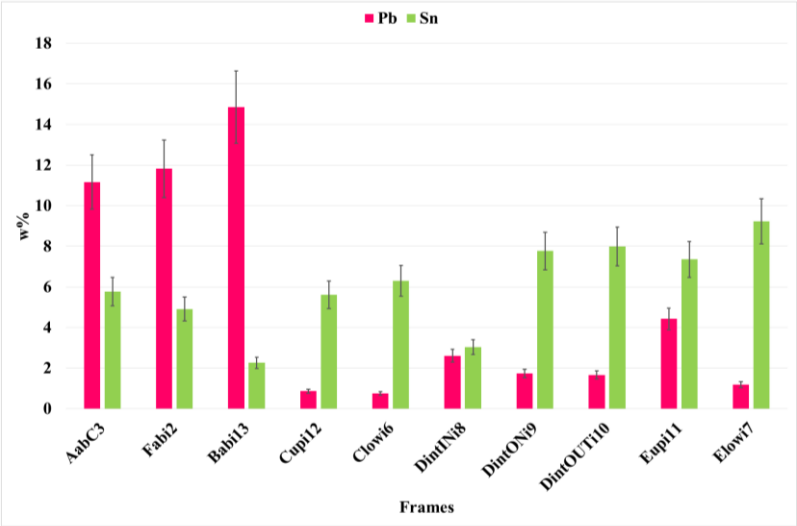

c)

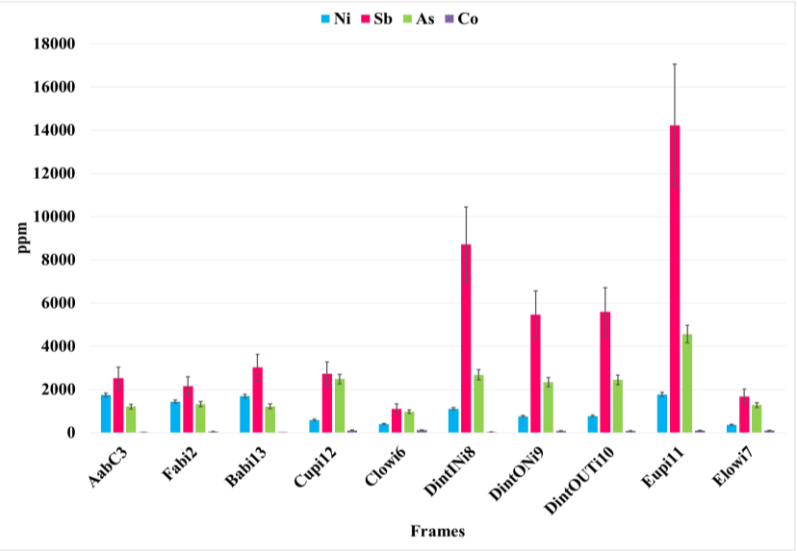

Figure 9. Bar charts of the mean of the concentration of major and minor elements for all the frames' samples (a-Cu; b-Pb and Sn; c-Ni, Sb, As and Co.

Procedure B. Ranges comparison

It has been discussed that the differences of the concentration values may be caused by several factors that can be summarized as those related to the heterogeneity depending on the casting procedure, those related to the original composition of the alloys, to obtain different properties, and the uncertainty introduced by the analysis process. In the ranges procedure, first a list of concentrations for the different elements on the samples analysed is defined and arranged in ascending order. Then, the discontinuities in the concentration series were defined and the ranges that could be related to different original compositions were established. It was defined a colour scale to indicate the increase of the concentration and distribution mappings were created. Finally, looking at the distribution of concentrations, some elements were established as relevant for discrimination purposes. In this case, the key elements selected for this purpose were Pb, Sb, Co and Ni (Figure 10). The samples were classified according to these ranges and the results were plotted in order to facilitate the interpretation of the different compositions.

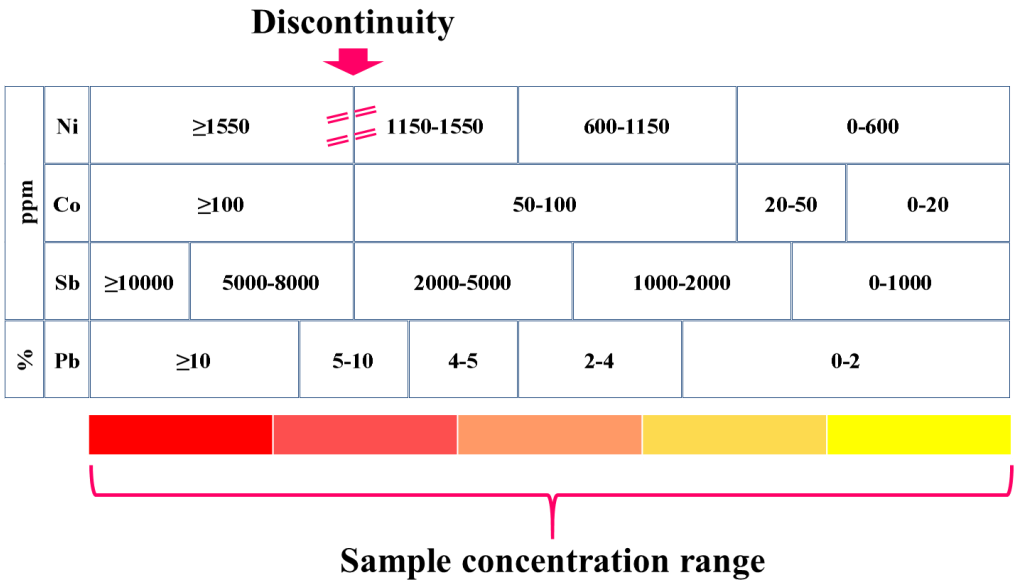

Figure 10. Scheme of the concentration range established for Ni, Co, Sb, and Pb.

Pb clearly separates the *Martirio*, *Pie donne* and *Pentencoste* panels (A, F, B) and frames from the other three panels (E, D, C) and frames (with lower concentration) (Figure 11). In the first group, *Pentecoste* also appears slightly different from *Martirio* and *Pie donne*. According to the relationship between panels and frames, this element also separates the panels from their corresponding frames (with higher concentration), except for Ascensione where panel and frames are similar.

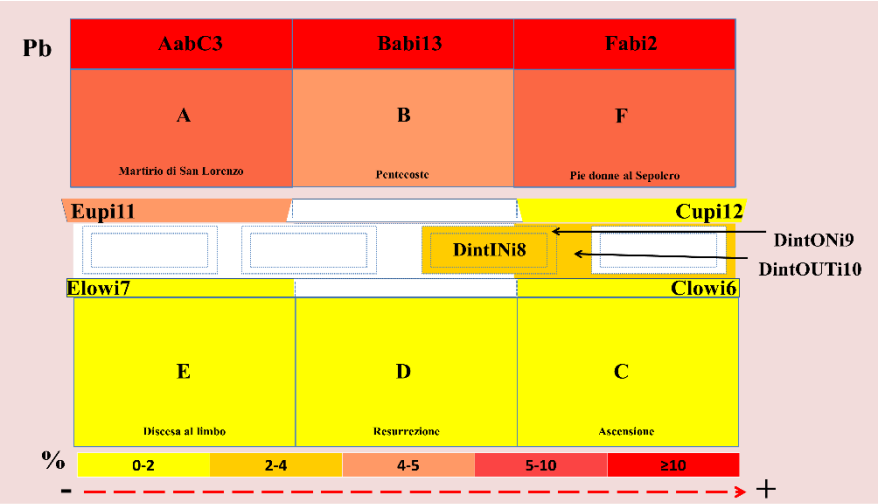

Figure 11. Schema of the range distribution of Pb across the panels and frames.

Sb confirms the distribution recognized by the Pb, *Martirio*, *Pie donne* and *Pentecoste* panels and frames are different from the other three panels and frames (Figure 12). In all cases, Sb concentration in frames is higher than in panels, except for the lower frame of *Ascensione*. Sb also discriminates the upper frame of *Discesa al limbo* and sample IN taken from the intermediate frame of *Resurrezione* from the other parts.

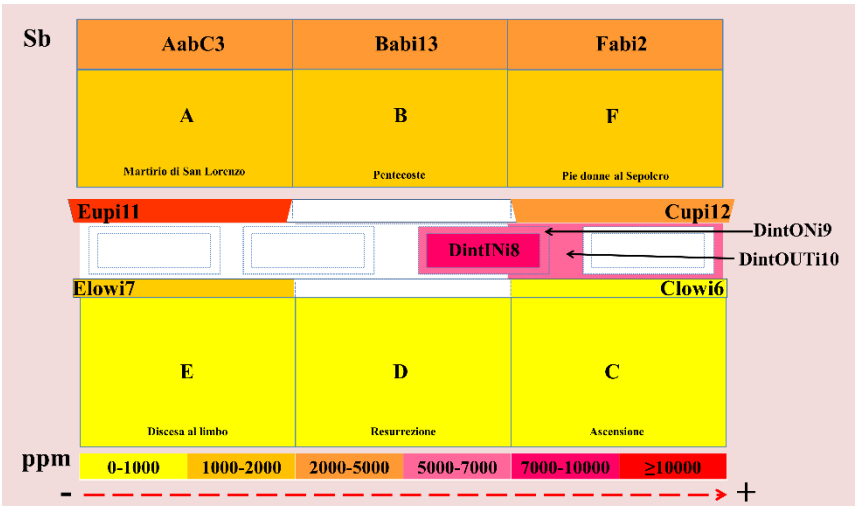

Figure 12. Schema of the range distribution of Sb across the panels and frames.

Co also points out the difference between Martirio, Pie donne and Pentecoste panels and the other three panels (Figure 13). In the case of Discesa, Resurrezione and Ascensione, Co also separates panels (higher concentration) from frames.

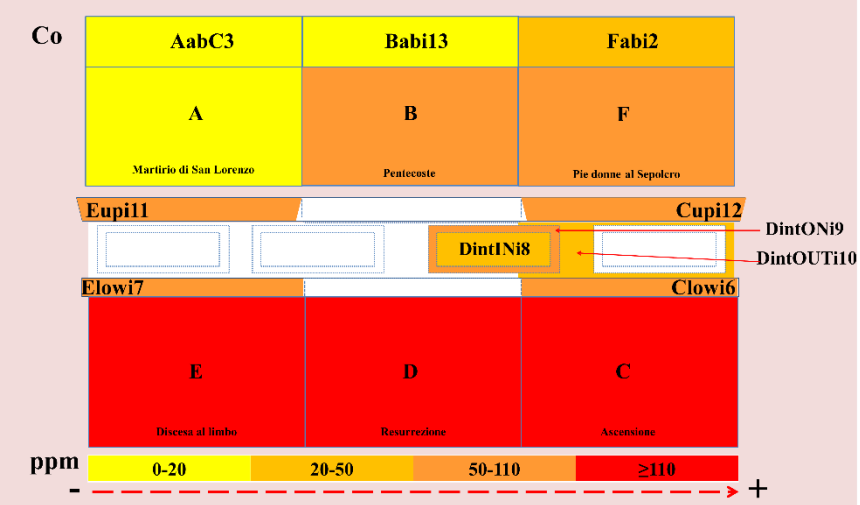

Figure 13. Schema of the range distribution of Co across the panels and frames.

Ni distribution corroborates the previous distributions and clearly separates *Martirio*, *Pie donne* and *Pentecoste* panels from the other three panels (Figure 14).

It is interesting to notice that *Ascensione* panel and frames are similar and that the Upper part of the frame of *Discesa* and sample IN taken from intermediate frame of *Resurrezione* are different from the other frame samples of this area.

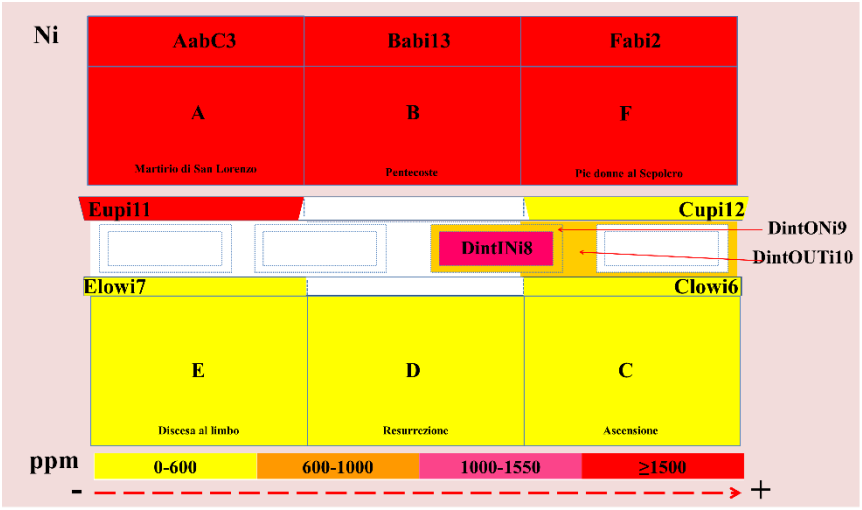

Figure 14. Schema of the range distribution of Ni across the panels and frames.

Principal Component Analysis

As the number of factors to be considered for the interpretation is elevated, the comparison of the composition obtained for the different panels and frames were performed by using a multivariate method. Principal Component Analysis (PCA) has been employed as tool to manage the data set available. Different models that include the concentrations of the major and minor elements of the samples coming from the panels and the frame have been analysed with the PCA method.

PANELS

First of all, the relationship between panels has been studied. The first part of the PCA analysis was performed with the panels using only the concentration of the major elements present in the alloy.

MODEL 1a (Major elements)

The percentages of variance captured by 3 PCs were 99.83%, 0.16% and 0.01% respectively (Figure 15). As no treatment has been applied, this model differentiates between alloys giving more importance to the elements with higher concentration.

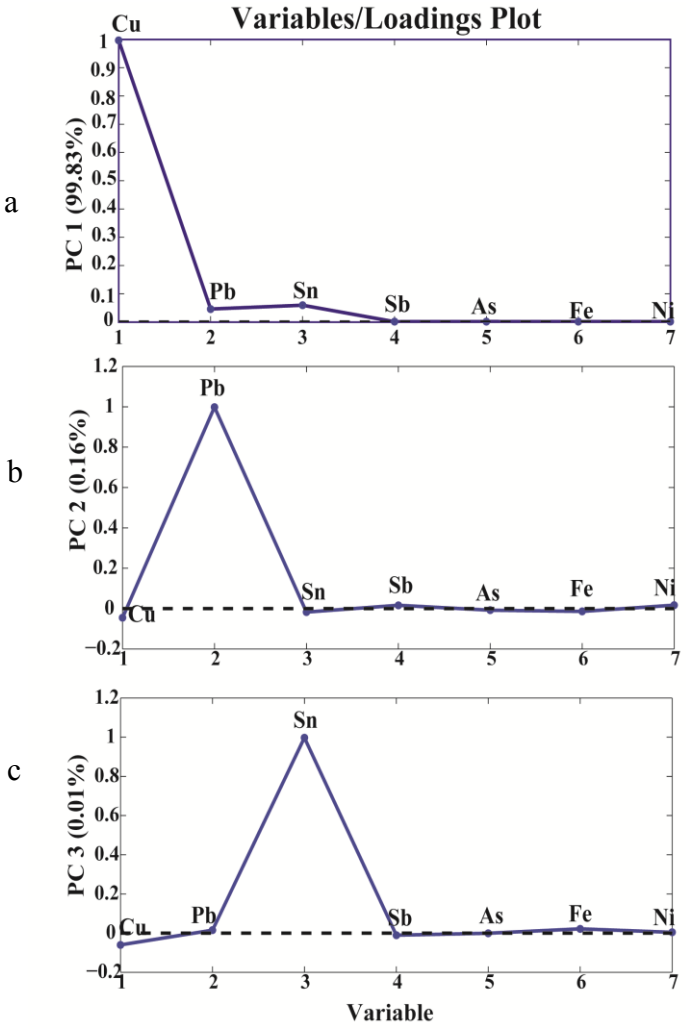

Figure 15. Model 1a - Loadings a) PC1. b) PC2. c) PC3.

In the score plot of PCs 1 vs. 2 (Figure 16a) the presence of two different clusters can be observed. The alloys of the panels *Martirio*, *Pentecoste* and *Pie donne* are different from panels *Ascensione*, *Resurrezione* and *Discesa al limbo*. This separation is due to PC2 that permits to discriminate the alloy because of the concentration of Pb. The PC1 that is related to Cu has no discrimination capability. Observing score plot PCs 2 vs. 3 (Figure 16b) it is possible to distinguish *Pentecoste* from the others by PC3 due to the importance that Sn has in this PC. In this panel the concentration of Sn is lower than in any other panel. Similarities can be observed among *Martirio*, *Pie donne*, *Pentecoste*, *Ascensione*, *Resurrezione* and *Discesa al limbo,* although the concentration of Sn of the latter is slightly different.

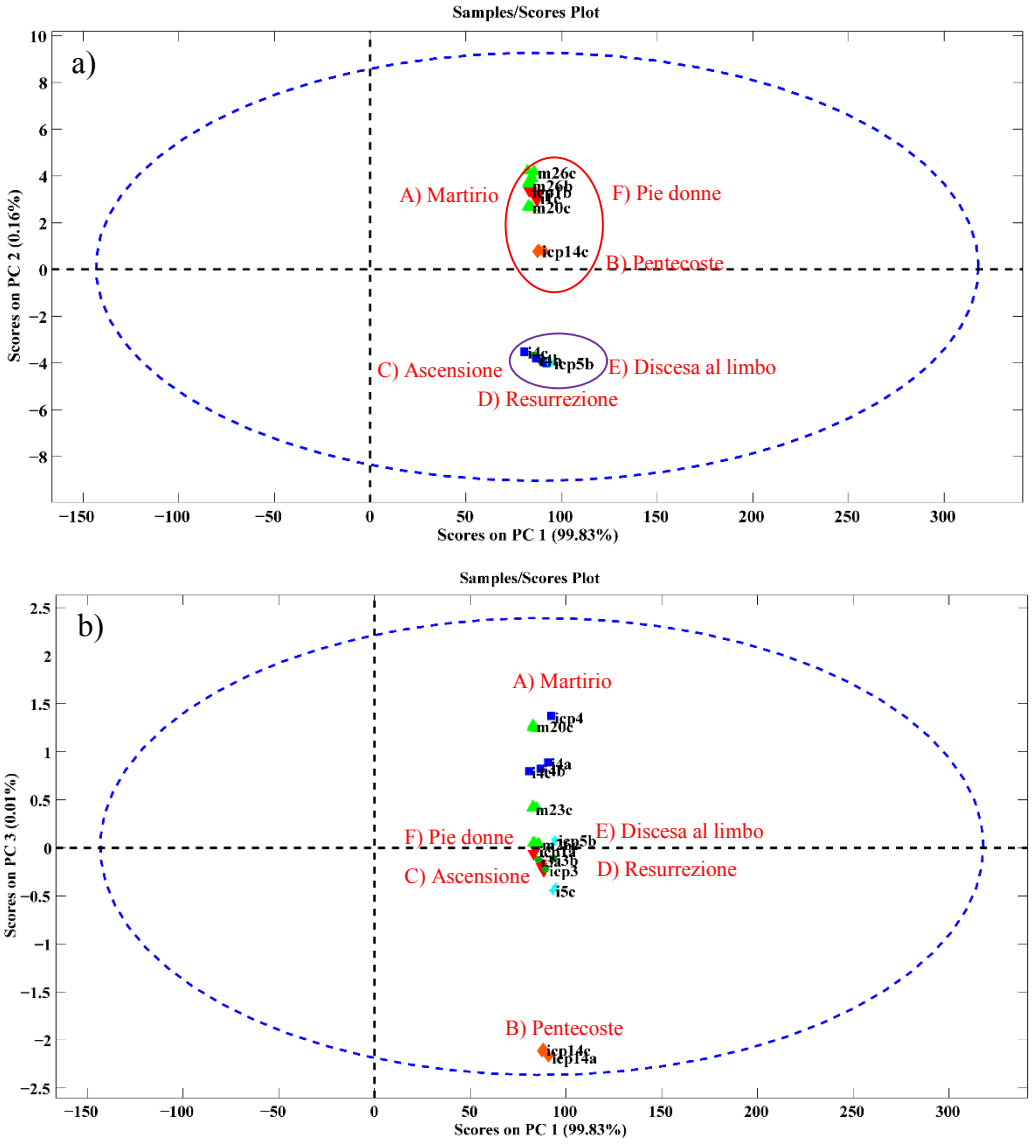

Figure 16. Model 1a – a) Score plot of PC1 vs. PC2; b) PC1 vs. PC3.

MODEL 1b autoscale (Major elements)

With the aim to maximize the differences among elements without taking into account the magnitude of their concentrations,an autoscale pre-treatment was applied to the data. The percentages of variance calculated by the first three PCs were 60.54%, 18.16%, and 11.65%, respectively (Figure 17).

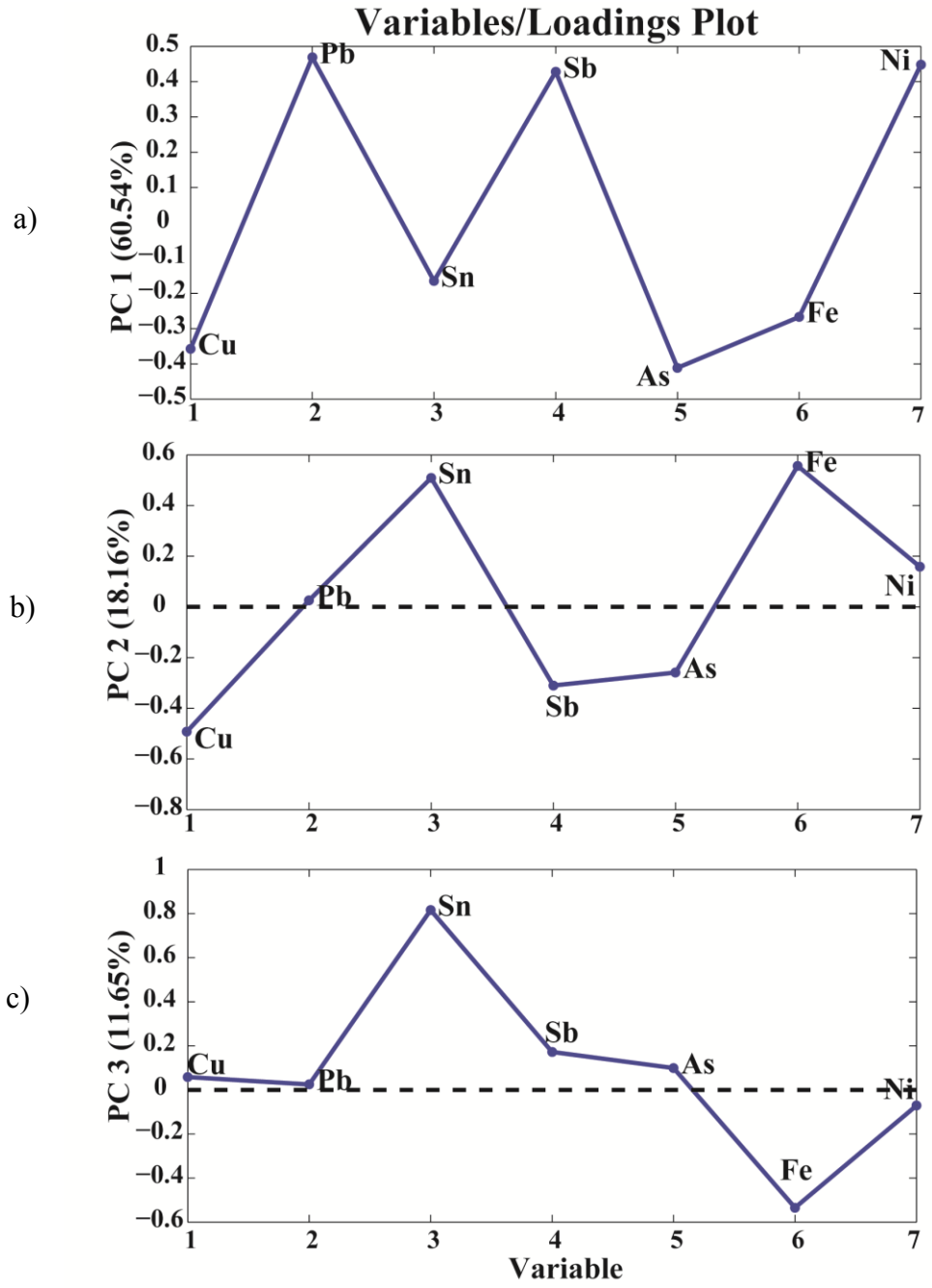

Figure 17. Model 1b - Loadings a) PC1. b) PC2. c) PC3.

In the score plot of PCs 1 vs. 2 (Figure 18) it is possible to see the separation in four clusters. Considering PC1 the separation between panels leads to the same results obtained with Model 1a, which was not scaled. Separation between panels *Martirio*, *Pie donne* and *Pentecoste* from panels *Ascensione*, *Resurrezione* and *Discesa al limbo* has been confirmed by the comparison of Pb, Sb and Ni versus Cu, Sn, As and Fe (PC1). Furthermore, PC2, which assigns positive contribution to Sn and Fe and negative to Cu, Sb and As, discriminates between panel *Ascensione* from *Resurrezione* and *Discesa* and also between panel *Pentecoste* from *Martirio* and *Pie donne*.

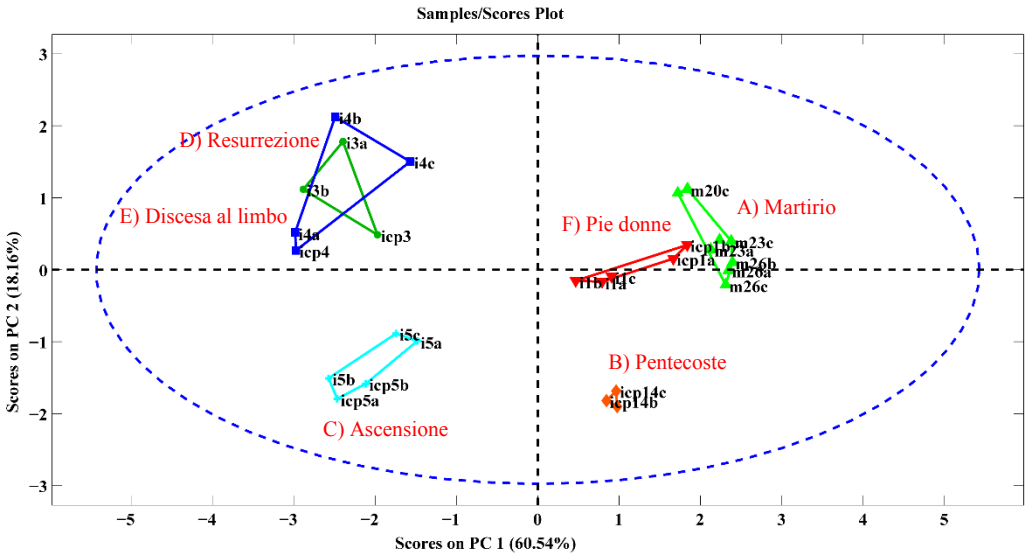

Figure 18. Model 1b - Score plot of PC1 vs. PC2.

MODEL 2 (Minor elements)

The next step of the study was to verify the possibility to discriminate among the samples based on the concentration of minor elements. The percentages of variance captured for the first three PCs were 89.64%, 10.01% and 0.34% respectively (Figure 19). As no treatment were applied, this model takes into account mostly the elements with higher concentration. Observing the score plot PCs 1 vs. 2 (Figure 20) the same clustering obtained with major elements can be identified. The alloys of panels *Martirio*, *Pie donne* and *Pentecoste* are separated from panels *Ascensione*, *Resurrezione* and *Discesa al limbo* by PC2 because of the different concentrations of As (positive contribution) and Ni (negative contribution). In this case, PC1 was not useful for alloy discrimination purposes.

a)

b)

c)

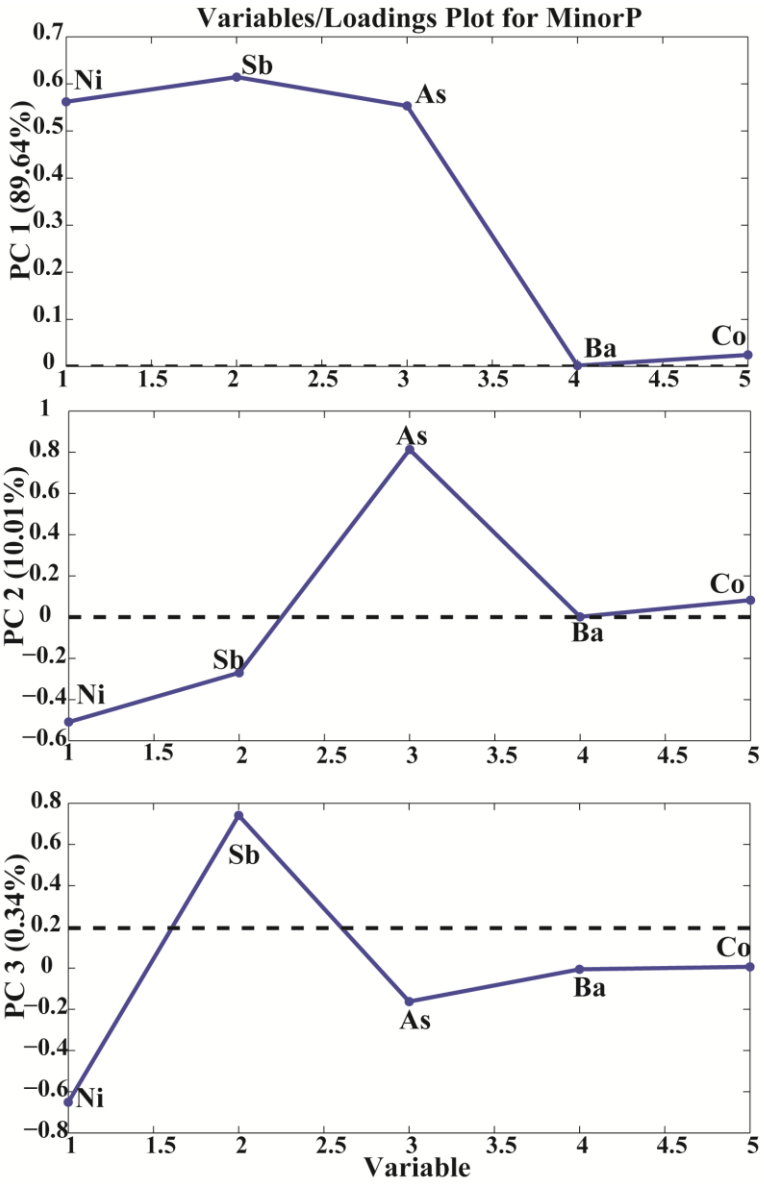

Figure 19. Model 2 - Loadings a) PC1. b) PC2. c) PC3.

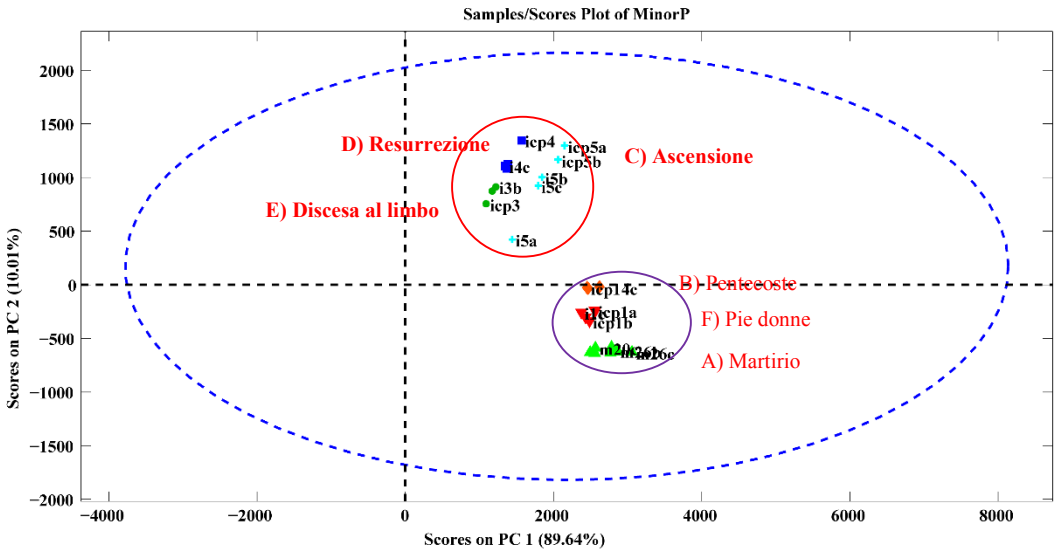

Figure 20. Model 2 - Score plot of PC1 vs. PC2.

Summary Panels' models results

It is possible to conclude, in terms of alloy composition, that *Martirio di San Lorenzo* (A) is similar to *Pie donne* (F), and *Pentecoste* (B), although the latter presents a unique composition. Because of the slightly difference it could be hypothesize that its creation process was differed from the before mentioned panels, even if their possible contemporaneity or common studio provenance cannot be excluded.

The *Ascensione* is slightly different from the panels *Resurrezione* and *Discesa al Limbo*, although their composition can be considered similar.

Based on this PCA analysis the elements that have been considered useful for alloy discrimination purposes are Pb (major), Ni and As (minor).

The three models show similar results and permit a clear differentiation among panels. Moreover, the autoscale pre-treatment in model 1b (major element) allowed to highlight slight variations not appreciable with the others models. The use of PCA method permitted to achieve the same conclusions of the classical method, although with more clear graphic representation.

FRAMES

The next step of the study is to analyse the relationship between the samples coming from the different part of the structure (*frames)*. The system used to label the frames' samples is reported in Table 15.

MODEL 3a (Major element)

Following the same procedure used above, major elements of the samples coming from the frames have been considered. The percentages of variance captured by the first three PCs were 99.56%, 0.39% and 0.04% respectively (Figure 21).

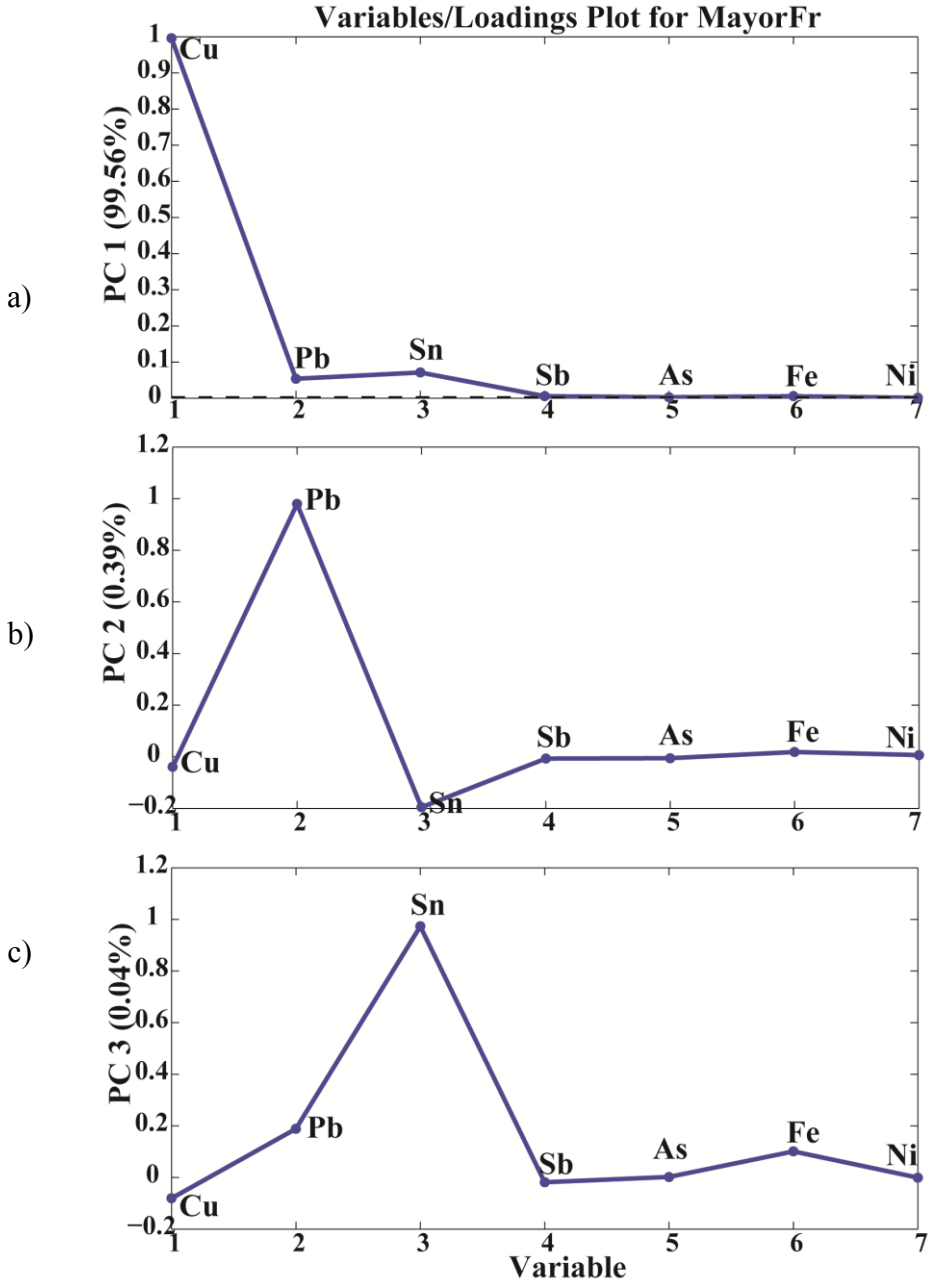

Figure 21. Model 3a - Loadings a) PC1. b) PC2. c) PC3.

In the score plot of PCs 1 vs. 2 and PCs 2 vs. 3 (Figure 22a/b), the presence of different clusters can be observed. The PC2 considers the different concentration of Pb. On the other hand, the concentration of Cu (PC1) is not useful for cluster discrimination. Thus, the alloys of frames AabC3a, Babi13 and Fabi2 are different from frames Clowi6, Cupi12, DintINi8, DintONi9, DintOUTi10 and Elowi7, Eupi11. Observing the score plot PCs 2 vs. 3 it is possible to distinguish sample D2i8 from the others based on PC3 due to the concentration of Sn.

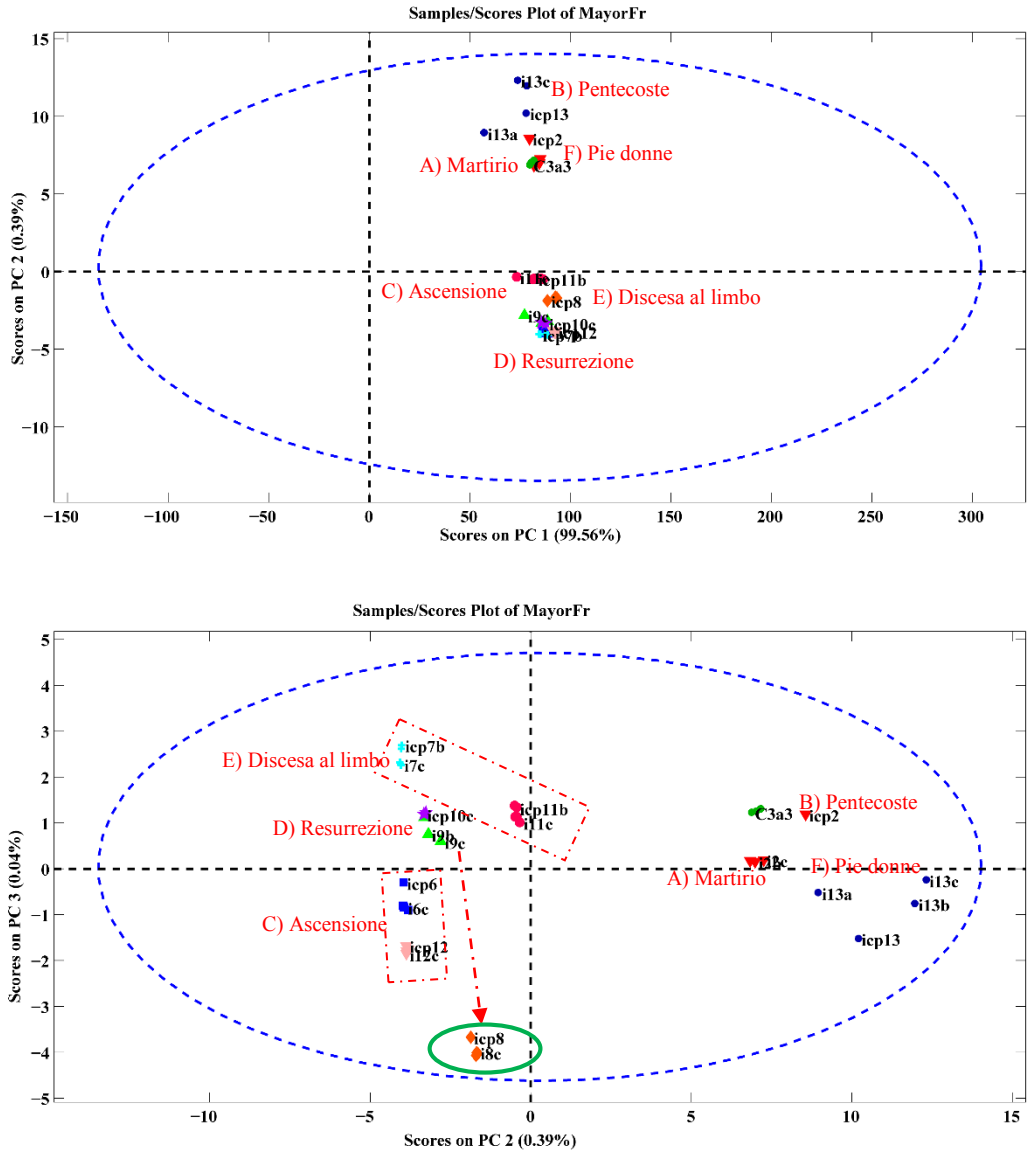

Figure 22. Model 3a - Score plot of a) PC1 vs. PC2; b) PC2 vs. PC3.

MODEL 3b autoscale (Major element)

An autoscale pre-treatment was applied to the data matrix created with the concentration obtained for the frames samples. The percentages of variance captured by three PCs were 36.63%, 35.66% and 13.43% respectively (Figure 23).

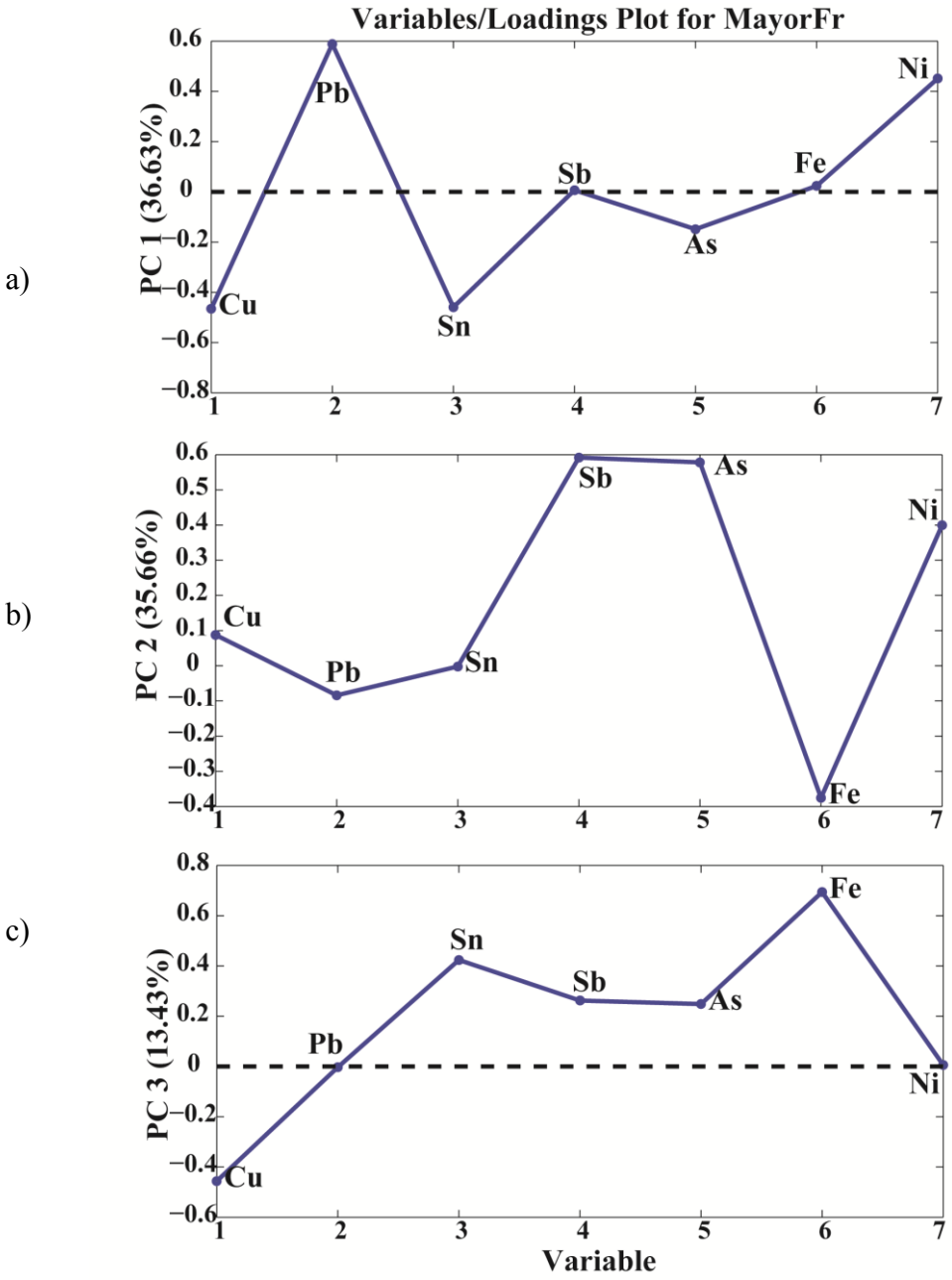

Figure 23. Model 3b - Loadings a) PC1. b) PC2. c) PC3.

In the score plot of PCs 1 vs. 2 (Figure 24) one can see the separation of three groups of samples Babi13, AabC3a, DintINi8 and DintINi8 from the others by PC1 due to the different concentration of Pb and Ni versus Cu and Sn. It is also possible to observe the separation of the frames' alloys AabC3a, Babi13 and Fabi2 are different from frames Clowi6, Cupi12, DintONi9, DintOUTi10 and Elowi7 by PC2, because of the different concentration of Sb, As and Ni vs. Fe. The dispersion obtained for sample i13 is a consequence of its contamination with the drill material (major component Fe). Thus, as one of the main variables considered in loading PC2 is Fe (negative contribution) i13 appears slightly separated from the other samples.

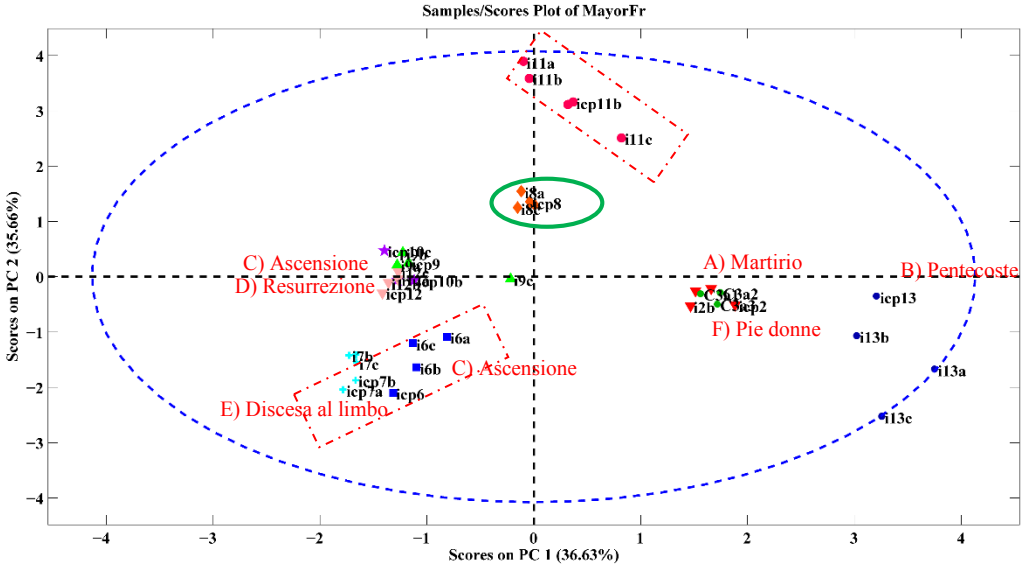

Figure 24. Model 3b - Score plot of PC1 vs. PC2.

MODEL 4 (Minor element)

Next, minor elements of the samples coming from the frames have been considered. The percentages of variance captured by three PCs were 98.23%, 1.20% and 0.57% respectively (Figure 25).

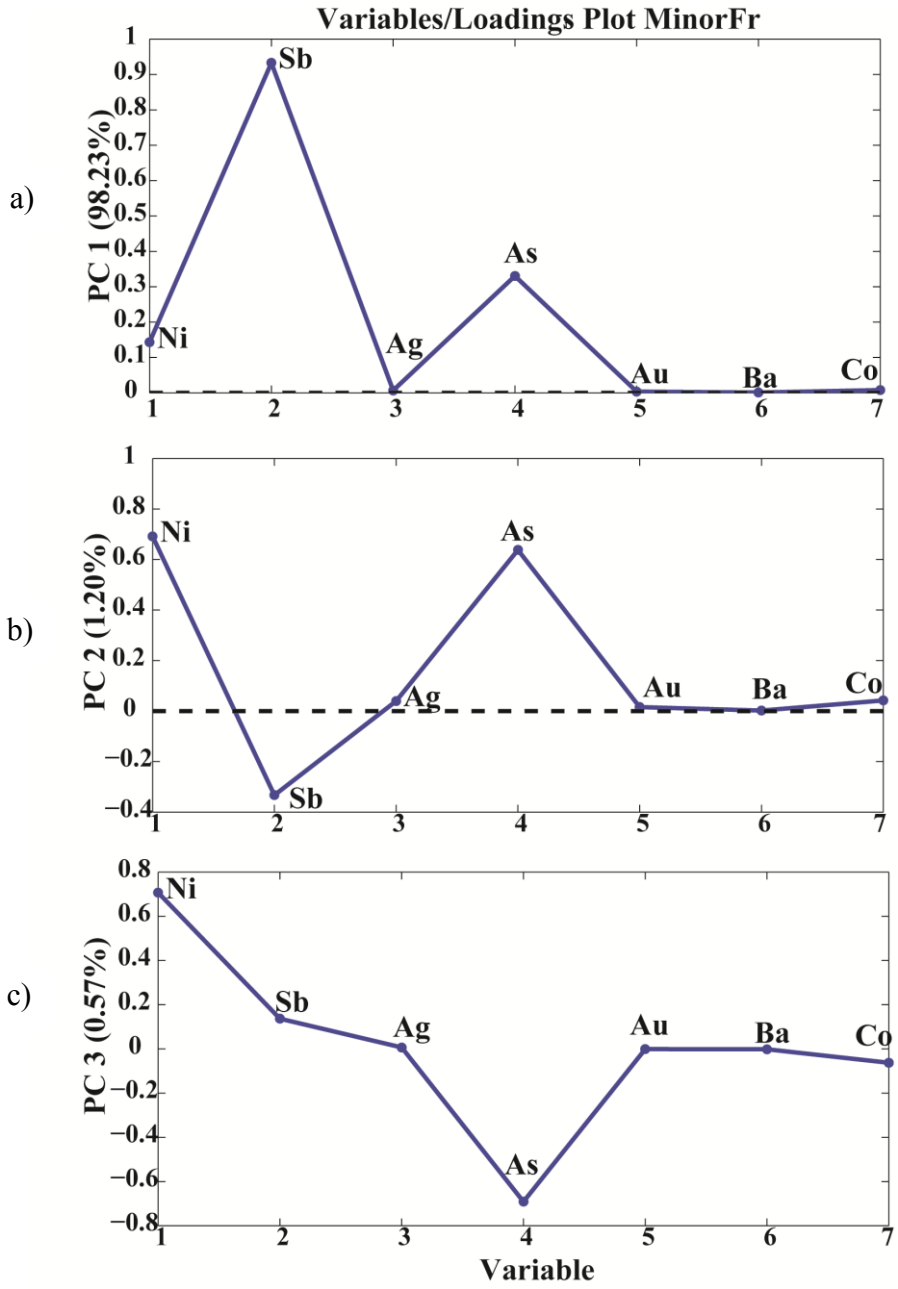

Figure 25. Model 4 - Loadings a) PC1, b) PC2. c) PC3

The score plot of PCs 1 vs. 2 (Figure 26) shows the separation of the frames' alloys AabC3a, Babi13, Fabi2 and Cupi12 from frames DintONi9, DintOUTi10, DintINi8, and Eupi11 based on PC1, for the concentration of Sb and As.

DintINi8 and Eupi11 are separated from all the others samples by PC2 due to the concentration of Ni, As and Sb. Clowm6 and Elowm7 form an independent cluster due to PC2.

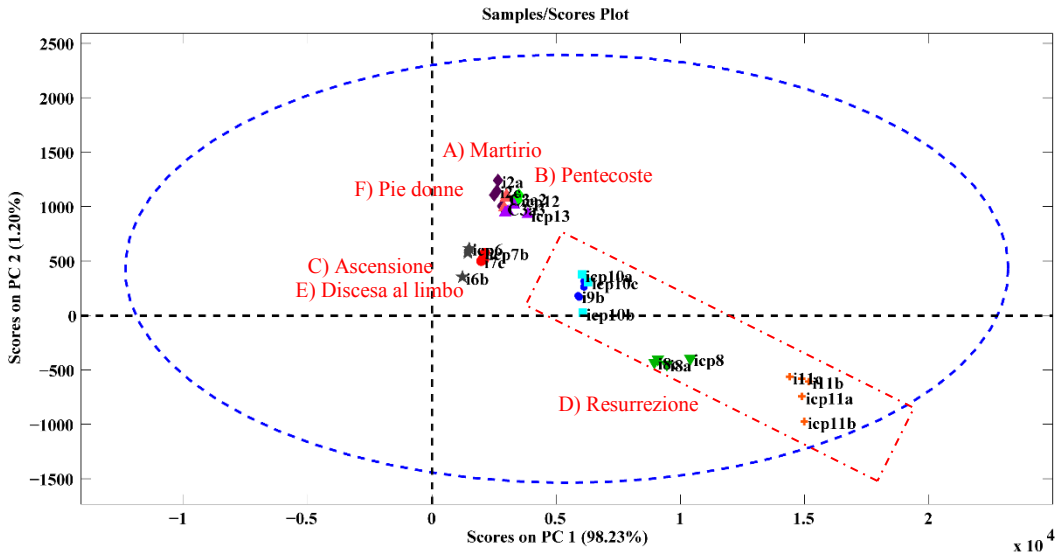

Figure 26. Model 4 - Score plot of PC1 vs. PC2.

Summary of Frame's models results

It is possible to conclude, in terms of alloy composition that samples AabC3a, Babi13 and Fabi2 are similar. Clowi6 and Elowi7, despite of some doubt about their relation expressed above, seem to follow a similar behaviour in all analysed models and can be considered to resemble each other. Cupi12, DintONi9 and DintOUTi10 have comparable composition. Sample Eupi11 and DintINi8, almost related; are almost related and seem to be a unique case compared with all the samples. As also indicated by the PCA models of the panels, the elements that have been considered useful for alloy discrimination purposes are Pb (major), Ni and As (minor).

The three models show similar results and permit a clear differentiation among frames. Moreover, the autoscaled model 3b (major element) allowed to identify a contaminated sample based on the dispersion within its subsamples. The observation is based on to the behaviour observed for sample Babi13 (subsample i13a/b/c) that clearly appeared contaminated by the drill residues during the phase of the sample treatment.

PANELS & FRAMES

The comparison between all samples, panels and frames, is rather difficult to perform with classical statistical methods. Thus, PCA complex models were crated with the aim to evaluate the relationship between them considering the major elements (Cu, Pb, Sn, Fe, Ni determined by OES) and all the elements (major-OES and minor MS).

Model 5TotA Autoscale (Major elements)

The percentages of variance captured by three PCs were 36.57%, 28.46% and 17.69% respectively (Figure 27).

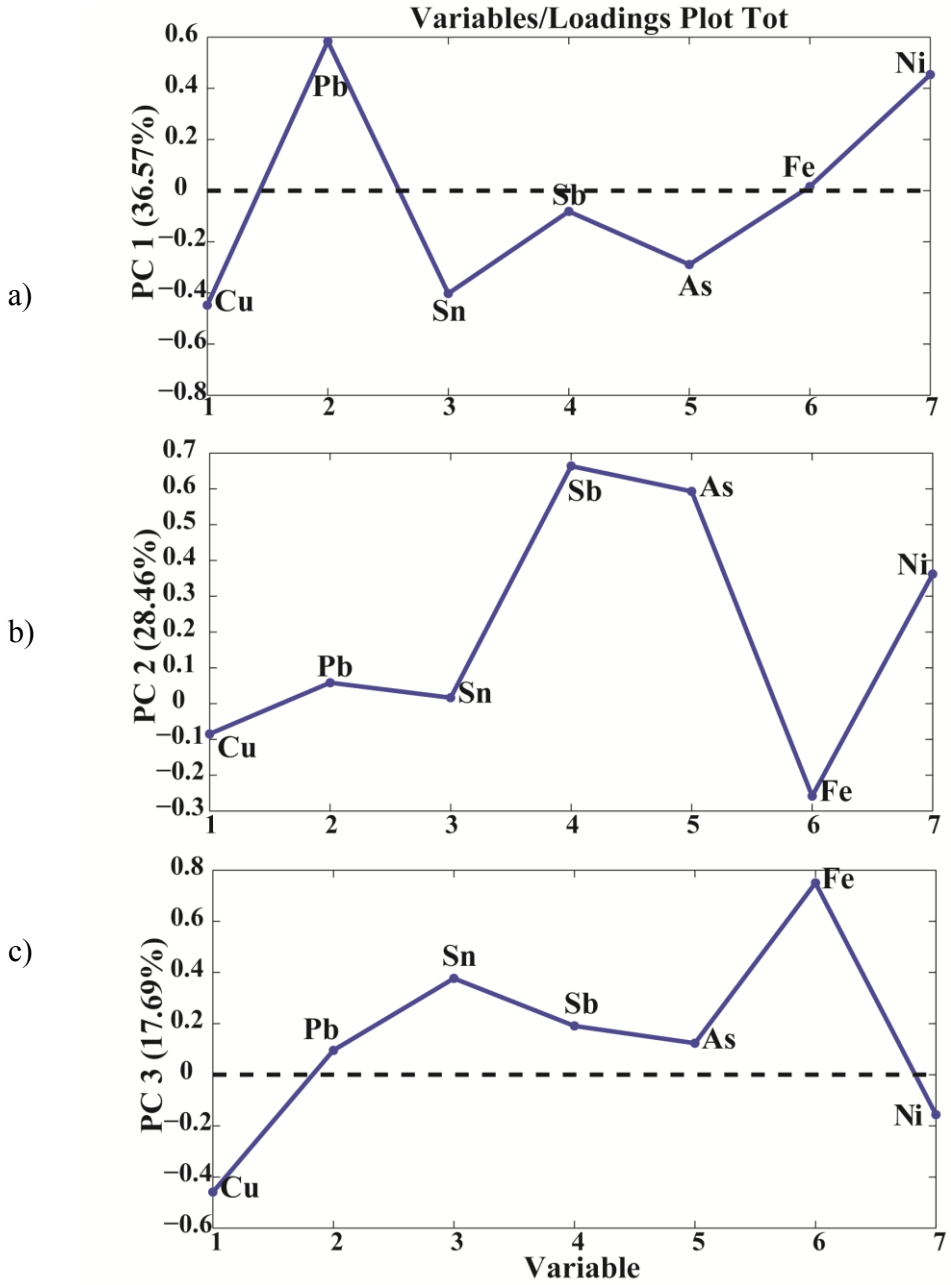

Figure 27. Model 5TotA - Loadings a) PC1, b) PC2. c) PC3

The score plots of this model are similar to the previous autoscaled models. PC1 assigns positive contribution to Pb and Ni and negative to Cu, Sn and As. PC2 assigns positive contribution to Fe and negative to Cu, As and Ni. According with the score plot of PCs 1 vs. 2 (Figure 28), when panels and frames are considered within the same analysis, it is possible to see that panels A, B, F are similar in composition to frames AabC3a, Babi13 and Fabi2. Panels C, D and E are similar to frames Clowi6 and Cupi12, DintONi9, DintOUTi10 and Elowi7, DintINi8. Eupi11 seems to have a composition different from all the others samples, frames and panels.

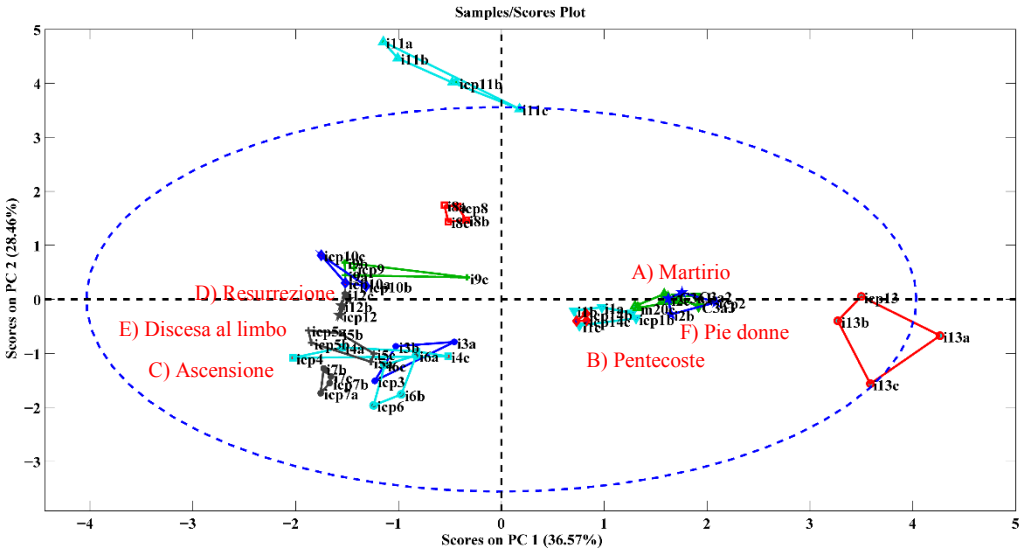

Figure 28. Model 5TotA - Score plot of PC1 vs. PC2.

5Totb Autoscale (All element)

The final PCA analysis had the objective to compare all together the panels and the frame in one analysis and evaluates the relationship between them introducing in the model the entire data set obtained. The percentages of variance captured by three PCs were 38.10%, 24.11% and 13.53%, respectively (Figure 29).

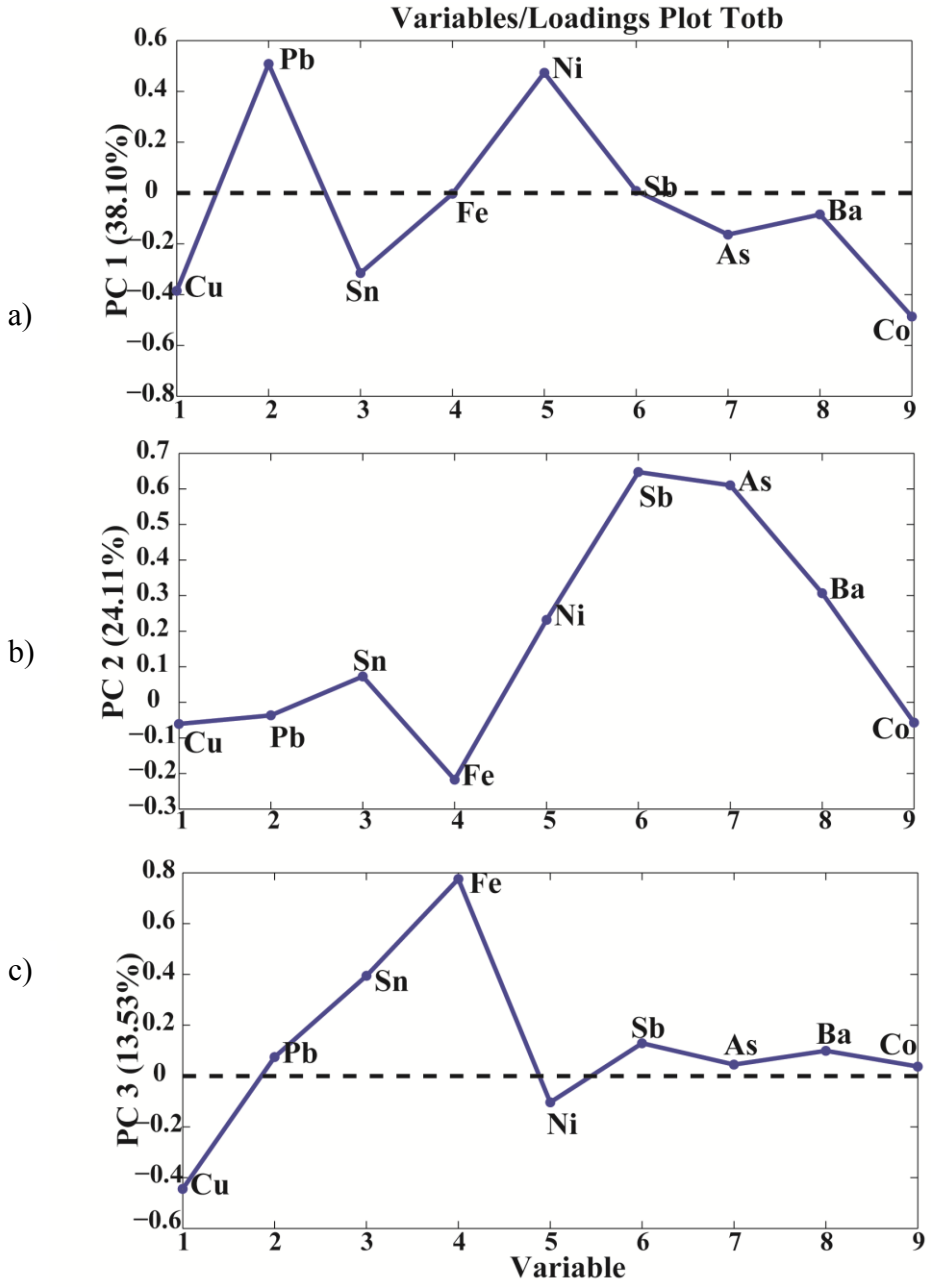

Figure 29. Model 5TotB - Loadings a) PC1, b) PC2, c) PC3.

For the model PC1 assigns positive contribution to Pb and Ni and negative to Cu, Sn and Co, whereas, PC2 assigns positive contribution to Fe and negative to Cu. According to the score plot of PC1 vs. PC2 vs. PC3 (Figure 30), A (*Martirio)*, B (*Pentecoste)* and F (*Pie donne)* belong to the same cluster, all together with the corresponding frame samples (AabC3a, Babi13 and Fabi2). The second cluster is composed by the panels C (*Discesa*), D (*Resurrezione*) and E (*Ascensione*) with three frame samples coming from the lower part (Clowi6 and Elowi7) and one from the upper part (Cupi12). The fourth cluster assembles two samples of the intermediate part (DintONi9 and DintOUTi10), while the samples DintINi8 and Eupi11 seem to be different from all the samples and form separates clusters.

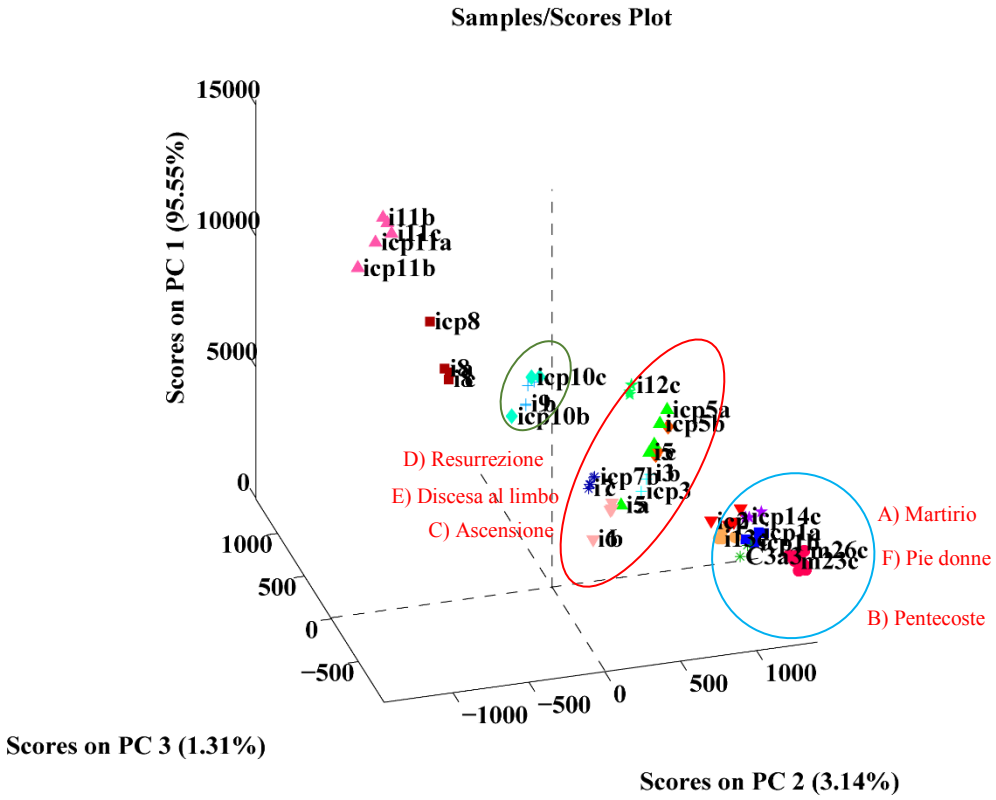

Figure 30. Model 5TotB – Score plot of PC1 vs. PC2.vs. PC3.

Global discussion

Martirio and *Pie donne* panels are equivalent. Their frames are also similar to the panels (except for the amount of Pb, which is higher on the frames) and similar among them.

Pentecoste is more similar to *Pie donne* than to *Martirio* (although Pb and Sn are lower). The frame of Pentecoste is different from the panel (its Pb concentration is higher) and also to the other frames of Martyrdom and Pie donne.

These three panels (Martyrdom, Pie donne and Pentecoste) are different from the other three (Discesa, Resurrezione and Ascensione) by the low amount of Pb in the latters.

Discesa, Resurrezione and Ascensione panels are similar among them.

The Discesa panel is different from its lower and upper panels. In the frames, the amount of Pb, Sn and Sb increase (Sb especially for the upper part of the frame that it is not similar to any other part).

The Resurrezione panel is similar to the intermediate panel (ON and OUT/NEARBY samples) except for the increased concentration of Pb and (again) Sb. The sample corresponding to the square fragment of the intermediate frame (IN samples) shows an increase of Sb also exceptional and, therefore, it is different to the panel and the other frame parts.

The Ascensione panel is similar to its lower and upper frames, which are similar among them. In this case the amount of Pb and Sb do not increase from panel to frames.

The lower and upper frames of Discesa and Ascensione seem different.

5.4. Conclusions

Contribution of different sources to the variability on concentration

For Cu the dispersion obtained by the complete process corresponds to the one observed after the measurement step alone, i.e. the influence of sub-sampling and … is negligible. For Pb and Sn sub-sampling and position (depth and X/Y) significantly increase the dispersion determined in the measurement step.

Following the proposed analytical procedure (n=3x3) the uncertainty associated with the concentration of the different major elements will be approximately < 2% for Cu, < 11% for Sn and < 10% in the case of Pb.

Homogeneity of elements distribution in the alloy

Cu is homogeneously distributed. The amount of Sn presents an strong variation in macro X/Y distance. Pb probably is heterogeneous in depth, with increasing concentration towards the surface. At a certain depth the concentration of Pb starts to be reproducible.

Sampling procedure

External samples show a composition very different from the internal samples. The sampling procedure must avoid the first mm below the surface and start the material extraction at a depth of at least 2-3 mm. A control of sampling depth is recommended to ensure comparable and reproducible results. Ranges of 3-6 mm are recommended if enough material is to be obtained.

Analysis procedure

The proposed procedure will include the sampling strategy described above, the chemical attack following the specification of method 2, separation of the samples in three replicate subsamples and three separate measurements for each solution (n=3x3). At least 20 mg of material are necessary for each replicate. Around 100 mg per sample will be adequate.

Drills influence

The major elements founded in both drill were Fe and Co and some minor, such as Ni and Sb. The contamination of the drills is negligible considering the concentrations obtained for the bronze samples. It is recommended to use drills made of ELA-Carbide because the amount of Co will permit to easily identify their influence on the different samples.
Steel drills have produced contamination in some cases, although easily discernable.

Composition

A binary (CuSn) and a ternary (CuPbSn) alloy were identified. The different panels and frames can be defined as tin and tin-leaded bronzes. Minor elements such as Ni, Sb, As, Bi and Co were found. Pb and Sb concentrations increase on frames with respect to the panels.

Panels and frames comparison

Multi-element comparison between samples was conducted and classification of different alloy composition was established. According to the classical and multivariate methods used to compare the different element concentrations four principal groups of samples/pieces could be identified.

Type 1.

The concentration of Pb is important to identify the two major type of alloy. The panels *Martirio*, *Pie Donne* and *Pentecoste* with the corresponding frames C3, i1 and i13, respectively, show a high concentration of Pb and can be defined as ternary alloy of Cu, Sn and Pb (tin-leaded bronzes). The results have confirmed the expectation, as well as demonstrated a high affinity between these six parts/samples. Even though the panel

Pentecoste is part of this group due to its ternary alloy, its composition should be considered unique. The main factor that leads to this speculation is the content of tin that is lower than all the other samples. This could be an indication that it has been produced with the same casting technology/procedure and alloy proportion but maybe in a different studio or moment. The panel is similar in composition to its corresponding frame, although the latter presents a lower amount of Pb.

Type 2.

The second main group is composed of the panels *Discesa al limbo*, *Resurrezione* and *Ascensione* that can be defined as a binary alloy of Cu and Sn. The content of Pb is very low. As described in literature, this can be an indication of the use of a better casting technology. The concentration of Co and Ni also are characteristic for these three panels.

The model PCA that permits to consider major and minor element simultaneously reveals that the frames belonging to the lower (i6 and i7), intermediate (i9 and i10) and upper part (i12) are similar in composition to the *Discesa al limbo*, *Resurrezione* and *Ascensione* panels. Yet, a more detailed study of the concentrations for Discesa and Resurrezione reveals that the frames present a slightly higher content of Pb and high concentrations of the minor elements (Ni, Sb, As and Co), especially for the samples taken in the intermediate part. Ascensione panel and frames are equivalent, except for the Sb concentration.

Type 3.

The sample i8, extracted in the centre of a decorative tablet located on the intermediate frieze of the Pulpit, as a decorative component, shows a composition different from all the other samples (slightly higher Pb and very high concentration of Sb and As). This could be an indication of a different origin of the piece, maybe mounted later on the Pulpit structure.

Type 4.

The sample i11 (upper part) is the only sample belonging to the frames, that presents a high content of Pb (similar to Pentecoste) and Sn, as well as very high concentration values of Ni and Sb.

Multivariate method

The study has demonstrated that PCA is a very useful method for data set management. The possibility to correlate all variables simultaneously permits to observe data behaviour otherwise not detectable. All presented models have demonstrated results coherent with the conclusion that was achieved by the classical statistic approach, with the advantage of an easy and practical graphic visualization.

5.5. References

1. Van Langh, R. *et al.* New insights into alloy compositions: studying Renaissance bronze statuettes by combined neutron imaging and neutron diffraction techniques. *J. Anal. At. Spectrom.* **26,** 949 (2011).

2. Trampuž Orel, N. & Drglin, T. ICP-AES comparative study of some Late Bronze Age hoards: Evidence for low impurity bronzes in the Eastern Alps. *Nucl. Instruments Methods Phys. Res. Sect. B Beam Interact. with Mater. Atoms* **239,** 44–50 (2005).

3. Šatović, D., Desnica, V. & Fazinić, S. Use of portable X-ray fluorescence instrument for bulk alloy analysis on low corroded indoor bronzes. *Spectrochim. Acta Part B At. Spectrosc.* **89,** 7–13 (2013).

4. Miliani, C., Rosi, F., Burnstock, A., Brunetti, B. G. G. & Sgamellotti, A. Non-invasive in-situ investigations versus micro-sampling: a comparative study on a Renoirs painting. *Appl. Phys. A* **89,** 849–856 (2007).

5. Festa, G. *et al.* Non destructive neutron diffraction measurements of cavities, inhomogeneities, and residual strain in bronzes of Ghiberti's relief from the Gates of Paradise. *J. Appl. Phys.* **109,** 064908 (2011).

6. Scott, D. A. *Metallography and Microstructure of Ancient and Historic Metals*. (1991).

7. Taşliçukur, Z., Altuğ, G. S. ., Polat, Ş., Atapek, Ş. . H. & Türedi, E. A Microstructural Study on CuSn10 Bronze Produced by Sand and Investment Casting Techniques. in *Met. 2012* (2012).

8. Walaszek, D. *et al.* Metallurgical and chemical characterization of copper alloy reference materials within laser ablation inductively coupled plasma mass spectrometry: Method development for minimally-invasive analysis of ancient bronze objects. *Spectrochim. Acta Part B At. Spectrosc.* **79-80,** 17–30 (2013).

9. Massart, L. & Vandeginste, B. *Handbook of Qualimetrics Part A*. 519–556 (1991).

10. *Handbook of Near-Infrared Analysis, Third Edition*. 208–210 (2007).

11. Balcerzak, M. Sample digestion methods for the determination of traces of precious metals by spectrometric techniques. *Anal. Sci.* **18,** 737–50 (2002).

12. Young, M. L. *et al.* Matisse to Picasso: a compositional study of modern bronze sculptures. *Anal. Bioanal. Chem.* **395,** 171–84 (2009).

13. Scott, D. A. The non-destructive investigation of copper alloy patinas. 465–492 (2004).

14. Scott, D. A. *Metallography and Microstructure of Ancient and Historic Metals*. 1–155 (1991).

15. Schrenk, J. L. The Royal Art of Benin: Surfaces, Past and Present. in *Anc. Hist. Met. Conserv. Sci. Res.* (Scott, D., Podany, J. & Brian b., C.) (1991).

16. Wadsak, M. *et al.* Multianalytical Study of Patina Formed on Archaeological Metal Objects from Bliesbruck-Reinheim. *Mikrochim. Acta* **133,** 159–164 (2000).

17. Figueiredo, E., Valério, P., Araújo, M. F. & Senna-Martinez, J. C. Micro-EDXRF surface analyses of a bronze spear head: Lead content in metal and corrosion layers. *Nucl. Instruments Methods Phys. Res. Sect. A Accel. Spectrometers, Detect. Assoc. Equip.* **580,** 725–727 (2007).

18. Young, M. L., Casadio, F., Marvin, J., Chase, W. T. & Dunand, D. C. An Ancient Chinese Bronze Fragment Re-Examined after 50 Years: Contributions from Modern and Traditional Techniques. *Archaeometry* **6,** 1015–1043 (2010).

19. Marabelli, M. The Monument of Marcus Aurelius: Research and Conservation. in *Ancient&Historic Met. Conserv. Sci. Res.* (Scott, David A, Podany, Jerry, Considine, B. B.) 84 (1991).

20. Munnik, F., Sjöland, K. A., Vittiglio, G., Ingelbrecht, C. & Wätjen, U. Nuclear microprobe study of metal segregation in quaternary bronze. *Nucl. Instruments Methods Phys. Res. Sect. B Beam Interact. with Mater. Atoms* **158,** 281–286 (1999).

21. Hughes, M. J., Northover, J. P. & Staniaszek, B. E. P. Problems in the Analysis of Leaded Bronze Alloys In Ancient Artefact. *Oxford J. Archaeol.* **1,** 359–364 (1982).

22. Halvaee, a & Talebi, a. Effect of process variables on microstructure and segregation in centrifugal casting of C92200 alloy. *J. Mater. Process. Technol.* **118,** 122–126 (2001).

23. Bugoi, R., Constantinescu, B., Popescu, A. D. & Munnik, F. Archaeometallurgical Studies of Bronze Age Objects from the Romanian Cultural Heritage. *Rom. Reports Phys.* **65,** 1234–1245 (2013).

24. Munnik, F. & Sj, K. A. Using microprobe distribution maps to determine homogeneity and correlation between elements. **163,** 348–353 (2000).

25. Craddock, P. T. & Picton, J. Medieval Copper Alloy Production and West African Bronze Analyses - PART II. *Archaeometry* **28,** 3–32 (1986).

26. Lanterna, G. Multidisciplinary scientific analysis on restoration of a renaissance masterpiece: Verrocchio " L' Incredulita di San Tommaso ", outdoor bronze group of Orsammichele Church in Florence . A case history. *Thermochim. Acta* **269/270,** 729–742 (1995).

27. Smith, Dylan (National Gallery of Art, Washington, D. The application of alloy analysis to questions of attribution: Giovanni Francesco Susini and the workshop of Gianbologna. in *Met. 2010 -Proceedings Interim Meet. ICOM-CC Met. Work. Gr.* (Mardikian, Paul; Chemello, Claudia; Watters, Christopher; Hull, P.) 256–263 (2010).

Global conclusions

This doctoral thesis aimed at the evaluation of micro- and non-destructive analytical techniques as well as the improvement of specific methods for the analysis of artworks. The investigation of three categories of artistic objects, namely oil paintings, ancient photographs and a large metal alloy structure, has demonstrated the importance to optimize analytical procedures capable of enhancing the knowledge about the pieces by taking into account their heterogeneity, physicochemical features and integrity. On the other side, the application of different analytical techniques permitted broad vision on their capacities and limitations when complex matrices and/or limited sample amounts have to be examined.

The presented research studies allowed achieving:

- the establishment of the detection limits and evaluation of the reproducibility of SEM-EDS and micro-FTIR in the application to paint layer investigation. Despite the good quality of the obtained spectra and the high sensitivity of these techniques, the low amount of material and the distribution of the different compounds across the sample made it difficult to obtain representative results. These problems could partially be overcome by analysing large areas rather than spots for SEM-EDS and performing replicates on different points of the specimen for micro-FTIR.

- the evaluation of the capacities and limitations of midIR-FORS when employed to the examination of oil paintings. It has been proved that the detection limits for this kind of set-up are especially high, although the major areas investigated permit to achieve better reproducibility and more representative information with respect to micro-FTIR. The physical feature/roughness of the analysed surface is a critical factor that may cause distortions in the spectra and be responsible for a decreased signal-to-noise ratio.

- the creation of pigment mapping of oil paintings by means of midIR-FORS and multivariate methods. In a comprehensive study, the optimal data pre-processing methods as well as a protocol for the application of PCA and PLS-DA for FORS spectra modelling have been proposed. Furthermore, these methods were successfully applied to investigate and prove the influence of the surface roughness on the variability of the FORS spectra.

- the assessment of the palette that was used by Pablo Picasso during the first years of his artistic career. The non-destructive punctual-analysis techniques allowed achieving mappings of the elements/compounds detected across the entire surface of six portraits and it was possible to obtain a wide information about all the different regions of the artworks. In this study, it has been confirmed that an important limitation of this kind of techniques is the lack of information about the in depth composition and materials distribution, which has been partially overcome with the simultaneous and accurate evaluation of all available data complemented with NIR reflectography and XR radiography.

- the establishment of a procedure for faded silver image recovery in old photographs using XRF spectroscopy. The optimization of the method for sulphur detection in a first step, and the possibility to investigate two emblematic cases of silver images with this method allowed the demonstration of a relation between sulphur and silver, which is a key to the identification of high density areas that have lost the silver component over time. The study can be considered exemplary the difficulties encountered in the creation of adequate calibration standards to match the matrix of the photographs.

- the optimization and application of an analytical method for the characterization of ancient bronze objects. The unique opportunity to follow the analysis of the Donatello's San Lorenzo Pulpit from the sampling to the ICP determinations allowed the investigation of all the possible sources of data variability. Thus, it was possible to compare the different parts of the structure and establish relations between the compositions of different samples that will be used by the conservator to complement the stylistic and historic study of the artwork. It has been proved that PCA is a very useful method for data management, which provides results in accordance with the conventional statistic methods with the additional advantage of an easy and practical graphic visualization.

Resumen

Introducción

Las obras de arte son el resultado material de un proceso mental. La materialización de una idea implica la elección de la técnica y del suporte más apropiado. La caracterización material de las obras de arte mediante el uso de técnicas analíticas adecuadas a cada problema permite:

- Analizar la naturaleza/composición química y estructuración de los materiales utilizados;
- Investigar las técnicas artísticas empleadas;
- Establecer el estado de alteración superficial o interna del objeto como resultado de la exposición a determinadas condiciones ambientales;
- Estudiar el proceso de envejecimiento de los materiales antiguos y de los productos modernos;
- Estudiar la eficacia de estrategias de restauración y conservación.

Esta información puede contribuir a la resolución de diferentes problemas como el estudio del desarrollo tecnológico en diversas épocas, la datación y evaluación de la autenticidad del objeto y el establecimiento de las condiciones ambientales óptimas para su conservación. Además permite localizar y estudiar las intervenciones de restauración anteriores y planificar adecuadamente las sucesivas, si fueran necesarias.

En la presente tesis se han estudiado tres tipologías de obras de arte: pinturas al óleo sobre tela, fotografías antiguas y un objeto metálico de gran formato. Debido a la especificidad de su composición y estructura, cada una de las obras ha requerido el desarrollo de métodos de análisis optimizados de acuerdo con la problemática de cada caso. Con fin de contextualizar las dificultades y los factores a tener en cuenta a la hora de investigar las diferentes obras, es importante conocer sus principales características.

Pinturas al óleo

Una pintura al óleo se compone de una estructura compleja que incluye diferentes capas, sobrepuestas según criterios de estabilidad y afinidad físico-química. Empezando por la base hacia la superficie se pueden distinguir cuatro estructuras principales: el soporte, la capa de preparación e imprimación, las capas de pintura y finalmente, las capas de protección.

Los soportes sobre los que se ha trabajado a lo largo de la historia han sido variados, desde tablas de maderas hasta cerámica, aunque el más común a partir del siglo XV ha sido la tela, que puede ser de diferentes tipos, como son lino, algodón u otros tipos de fibras. Con el fin

de preparar la superficie de trabajo se aplican sobre el soporte, una o más capas de preparación. Ésta asume la función de amortiguar cambios de temperatura y humedad y/o estímulos mecánicos. Una vez obtenida una superficie apta, se aplican las capas de pintura que finalmente pueden ser tratadas con barniz u otros productos de protección.

Las capas de pintura están constituidas por un medio aglutinante que en los casos investigados es óleo, en el que están dispersados los pigmentos. Estos últimos son substancias colorantes, naturales o sintéticas, normalmente de origen inorgánicas, aunque pueden existir variantes orgánicas. Los pigmentos se distinguen de los tintes por no ser solubles en el medio en que se dispersan.

La aplicación de diferentes capas de pintura, la mezclas de más de un tipo de pigmentos/pintura para obtener una más amplia escala de colores, tienen como efecto la creación de una estructura, muy fina (orden de micras) y muy heterogénea.

Desde el punto de vista analítico, las capas pictóricas se presentan como las partes más complejas de las obras y pueden incluir diferentes niveles de heterogeneidad. Áreas de las mismas superficies de igual color pueden tener composiciones diferentes (nivel macroscópico) o a nivel microscópico, bajo un mismo punto pueden estar presentes capas pictóricas de diferente naturaleza química, o una única capa monocroma puede incluir diferentes pigmentos y substancias.

Entre los componentes de estas capas, los pigmentos son elementos muy importantes. Su concentración y distribución, influencian las características estéticas, regulan las intervenciones de restauración, y determinan, junto con el aglutinante, las condiciones de conservación de la obra.

Las propiedades fundamentales de estas substancias son: el tamaño de partícula, su reactividad, el grado de estabilidad fisicoquímica y las propiedades ópticas.

El tamaño de partícula puede variar de muy fino (ϕ<0.3 μm) hasta tener dimensiones mayores de 40 μm de diámetro. Típicamente, pigmentos de partículas más fina tienen más poder de cubriente, son más opacos, mientras que tamaños más gruesos hacen que las capas pictóricas sean más transparentes.

Los pigmentos interaccionan, según mecanismos complejos, con el aglutinante para la formación de un film plástico en el cual las partículas están suspendidas. El sistema que se crea puede reaccionar con los agentes externos, tal como la humedad, los contaminantes, etc. Su conservación, se ve influenciada por su grado de estabilidad es decir por su reactividad.

Las substancias colorantes usadas en el ámbito artístico abarcan una gran variedad de compuestos, clasificados normalmente por su color. Por ejemplo, uno de los blancos más

usados es el Blanco de plomo, habitualmente encontrado como mezcla de óxido de plomo y carbonato básico de plomo, en proporción diferente según el sistema de producción empleado. Entre los azules el Ultramar (aluminosilicato de sodio) tiene gran importancia, Este es la versión sintética del más costoso lapislázuli. Así, se podrían reseñar amplias listas de compuestos que cubren una extensa escala de colores. El color es una de las propiedades más importante de los pigmentos artísticos y es debida a la absorción y/o transmisión de la luz. Los pigmentos blancos son pigmento que causan un alto grado de reflexión y absorben solo una limitada parte de la radiación. La situación opuesta se manifiesta con los negros, mientras que el color del resto es provocado por la absorción selectiva de la luz, dependiendo esta de la longitud de onda. Los diferentes fenómenos físicos que determinan las propiedades ópticas de estas substancias son la refracción, la reflexión especular y la reflexión difusa (*scattering*). Tales fenómenos regulan el poder de cubrimiento, la luminosidad y la transparencia de las capas pictóricas.

Fotografías antiguas

El campo de la fotografía es muy amplio. Una de las tipologías más importante y antigua es la de las imágenes fotográficas producidas sobre soporte de papel, sensibilizado con nitrato de plata. El inventor de este tipo de fotografía fue Fox Talbot (1800-1877). Tras él, realizaron grandes aportaciones al desarrollo de la técnica fotográfica el fotógrafo/artista francés Gustave Le Gray (1820-1884) y los escoceses Octavius Hill (1802-1870) y Robert Adamson (1821-1848).

El proceso fotográfico, en el caso específico investigado en la presente tesis, se desarrolla en diferentes etapas. La primera es la elección de un papel de buena calidad (sin impurezas) para que pueda ser apto a la aplicación de los agentes químicos necesarios para la formación de la imagen. El papel está normalmente tratado para que pueda ser impermeable y no dejar que los reactivos queden retenidos entre las fibras. En la superficie se aplica una solución salina, normalmente cloruro de sodio y se deja secar. Sobre esta última capa se sobrepone una de nitrato de plata (agente sensibilizante). En esta fase, la hoja se deja secar en un cuarto oscuro. En la fase siguiente se expone la hoja en contacto con un negativo, a la luz directa, para que la capa fotosensible reaccione. Como consecuencia, las áreas en las que el negativo deja pasar la luz se vuelven oscuras. El nitrato de plata en exceso se elimina con baño de agua. Finalmente, la imagen se fija con un baño de tiosulfato de sodio. La imagen estará constituida por partículas de plata reducidas depositadas directamente sobre el soporte de papel. Las imágenes fotográficas de este tipo resultan ser muy sensibles y habitualmente

están afectadas por fenómenos de descoloración, de las que desconocen todavía los mecanismos y causas. No obstante, se ha demostrado que los agentes contaminantes y la humedad tienen un papel importante en la estabilidad de estas obras tan delicadas.

Objetos metálicos

El uso de aleaciones metálicas, definidas como mezclas intencionales de dos o más metales, se remonta a la prehistoria. La posibilidad de variar las propiedades físicas y mecánicas de un material, ha estimulado al hombre a una continua experimentación. Entre la amplia variedad de aleaciones producidas, una de la más importante y encontrada en objetos artísticos es el bronce. Los bronces están formados mayoritariamente por cobre. Los posibles metales añadidos son estaño, plomo, arsénico, plata, oro y antimonio además de cantidades limitadas de níquel, platino y mercurio.

Los objetos metálicos pueden ser producidos principalmente mediante dos técnicas. La fundición y moldeado de la aleación metálica o el modelado manual de la pieza metálica. La primera técnica es la que se usó para la creación del Pulpito de San Lorenzo de Florencia, que será el objeto de investigación de esta tesis.

En el momento de la solidificación, la aleación metálica asume y crea su propia estructura interna. Los metales se distribuyen según sus propiedades físico-químicas y crean un sistema sólido complejo, en el que se pueden manifestar diferentes fenómenos de segregación, tanto a nivel microscópico como también macroscópico. Durante la solidificación el metal con mayor punto de fusión empieza a crear cristales que crecen según lo que se define *dendrita*, cristal metálico caracterizado por una estructura con diferentes ramas que se desarrollan de modo aproximadamente perpendicular. Al crecer, las impurezas o/y otros metales quedan atrapados en los intersticios entre las ramas y causan un gradiente de distribución de los componentes de la aleación (nivel microscópico).

A nivel macroscópico la heterogeneidad de la pieza puede ser influenciada por diferentes fenómenos definidos como segregación normal, inversa o debida a la gravedad. La primera ocurre cuando el metal con punto de fusión más alto solidifica primero y se queda distribuido en la parte externa del objeto, cerca de las paredes del molde – solidificación lenta. La segregación inversa sucede cuando las aleaciones solidifican rápidamente y que el elemento con punto de fusión más alto queda en el interior y el que tiene punto de fusión menor queda al exterior del objeto, creado como en algunos casos una capa externa. Finalmente, la segregación por gravedad es debida a las diferentes densidades de los componentes de la aleación que se distribuye en el fondo en la superficie, dependiendo de cómo está

posicionado el molde. El grado de solubilidad mutua de los diferentes metales y las propiedades físicas, como el punto de fusión, determinan las diferentes fases presentes en el sólido y consecuentemente sus propiedades mecánicas. Todas estas propiedades determinan la resistencia de la obra, su conservación y la tecnología necesaria para su creación.

Técnicas analíticas

Debido a la gran variedad de materiales, a la complejidad y la unicidad de las obras, al valor de las creaciones artísticas, y la necesidad de mantener su integridad para preservar su legibilidad es importante que las técnicas de análisis utilizadas sean no destructivas o cuando menos minimicen las cuantidades de muestra necesarias, respectando la integridad de la obra. Al mismo tiempo es importante obtener resultados representativos de su composición lo que también condiciona la optimización del análisis.

Un primer examen de las obras se realiza a partir de las imágenes adquiridas con técnicas de análisis global, como la reflectografía y el análisis radiográfico. Ambas técnicas se basan en la penetración selectiva de la radiación de diferentes longitudes de onda (NIR y Rayos X) a través de los diversos materiales y la capacidad de estos de reflejarla o absorberla. La reflectografía se usa mayoritariamente para explorar la presencia de dibujos preparatorios y cambios en la ejecución de la obra. En las imágenes obtenidas por reflectografía, zonas oscuras indican materiales que absorben mientras que las claras, capas que reflejan la radiación infrarroja. Contrariamente, en la radiografía, las partes más claras indican materiales con alto número atómico que absorben radiación de longitudes de onda de los rayos X. Las imágenes no son fácilmente interpretables debido a que son representaciones bidimensionales de estructuras tridimensionales.

Este examen global aporta información sobre la estructura de las obras y a partir de él, se utilizan técnicas de análisis puntuales. Estas técnicas nos proporcionan información complementaria sobre la composición molecular y elemental de los materiales utilizados en diferentes puntos de las obras. Según las técnicas utilizadas es posible la adquisición de la información con o sin la necesidad de tomar muestra.

Una técnica ampliamente usada en el análisis puntual es la Microscopia Electrónica de Rastreo (*Scanning electron microscopy with Energy Dispersive X-Ray analysis*, SEM-EDS). Esta técnica permite adquirir imágenes con una magnificación desde 15 hasta 500000X. Las muestras se barren con un haz de electrones primarios que provoca la emisión de electrones secundarios (SE), de baja energía (≥50eV), capaces de suministrar imágenes topográficas útiles para la investigación de superficie, o de electrones de Backscattering (BE) de energía

más alta que proveen información de la morfología y composición de la muestra. El equipo se encuentra comúnmente asociado a una sonda de microanálisis elemental EDS capaz de detectar elementos de Z≥6-8. Requiere muestras compatibles con la condición de vacío y del orden de 1mmx100μmx100μm, una cantidad que aunque mínima, clasifica la técnica como una micro-destructivas.

La Fluorescencia de rayos X (*X-ray fluorescence*, XRF) permite el análisis elemental *in situ*. La técnica XRF se basa en la interacción de la muestra con un haz de fotones X de alta energía que provocan la extracción de electrones de las capas más internas del átomo, y como consecuencia la emisión de rayos X característicos de cada elemento.

La Espectroscopia de infrarrojo (Fourier transform infrared spectroscopy, FTIR) es una técnica de análisis molecular, en la que se miden las transiciones entre los niveles vibracionales activos en la región IR. La radiación infrarroja se refiere a la parte del espectro electromagnético entre la región del visible y de las de microondas (13000-10 cm^{-1}), aunque la zona de mayor interés para la identificación de las estructuras moleculares es la definida del medio infrarrojo (4000-200 cm^{-1}). La técnica de espectroscopia infrarroja es probablemente, junto con la microscopia electrónica, de la más usadas en el campo de la investigación de Patrimonio, sobre todo después del desarrollo de acoplamientos con fibras ópticas (*Near/mid infrared fiberoptics reflectance spectroscopy* NIR/midIR-FORS) que logran espectros en el MidIR o NIR sin toma de muestra.

Los espectros obtenidos dependen del tipo de reflexión registrada. La reflexión especular se presenta cuando el ángulo de emisión es igual al de incidencia y esta puede provocar grandes distorsiones del espectro y generar la presencia de bandas de absorción muy intensas, que aparecen con forma de primera derivada o invertidas por el efecto Restrahlen. Por otra parte la reflexión difusa, obtenida en presencia de cuerpos opacos que dispersan la radiación en todas las direcciones y emiten señales dependientes de la densidad, índice de refracción, dimensiones de las partículas y morfología del material también se registra en los espectros FORS. Los dos tipos de reflexión se pueden corregir con las ecuaciones de Kramers-Kronig y Kubelka-Munk respectivamente. En el caso del análisis de una superficie opaca, en la que se registra la suma de los dos fenómenos, estas ecuaciones no pueden ser aplicadas a los espectros conjuntamente y eso determina la perdida de sensibilidad y una dificultad importante para la interpretación de los espectros que se encuentran muy distorsionados con bandas afectadas por significativos cambio de números de onda.

La Espectrometría de Emisión Óptica con Plasma de Acoplamiento Inductivo (*Inductively coupled plasma optical emission spectroscopy*, ICP-OES) y Espectrometría de masas con

plasma de acoplamiento inductivo (*Inductively coupled plasma mass spectrometry*, ICP-MS) son dos técnicas comúnmente usadas en el ámbito del Patrimonio. Ambas son capaces de proporcionar información cualitativa y cuantitativa acerca de la composición elemental de las muestras. La mayor ventaja, además de la limitada cantidad de muestra necesaria, es la posibilidad de calibrar el equipo y obtener límites de detección muy bajos. El muestreo y el tratamiento de muestra son fases críticas del procedimiento analítico y requieren una planificación y ataque cuidadoso.

La mayor ventaja de las técnicas no destructivas además de la conservación del objeto es la posibilidad de adquirir un alto número de espectros a lo largo de toda la superficie. Esto abre la posibilidad a la obtención de resultados más representativos mediante la realización de series de medidas que incluya tanto valores como sea necesario. En esta situación los métodos multivariantes ayudan en el proceso de evidenciar patrones de comportamiento difícil de reconocer con el simple análisis estadístico. Los métodos más usados son el análisis de componentes principales (PCA) y *Partial Least Square* (PLS). Antes del uso de estos métodos es necesaria la optimización del conjunto de datos mediante la aplicación de pre-tratamientos, como por ejemplo algoritmos de auto-escalado, normalización y corrección de la línea base. La elección de los algoritmos depende de la naturaleza de los datos y la información que se quiera obtener. PCA y PLS son métodos que permiten reducir el número de variables. PCA se usa normalmente como método no supervisado y permite una representación gráfica de los datos en la que es posible discriminar comportamientos similares de las muestras y evaluar los factores que los determinan. PLS funciona de manera similar aunque además puede ser usado como método de calibración.

Objetivos de la tesis

El objetivo principal de la tesis es la evaluación de técnicas micro- y no destructivas para la caracterización material de obras del patrimonio.

Los objetivos específicos han sido:

- la determinación del límite de detección y reproducibilidad de SEM, micro-FTIR y midIR-FORS. Para la gestión de los espectros de esta última técnica se aplicaron métodos multivariantes;
- Estudio de la paleta usada por Pablo Ruiz Picasso durante sus primeros años de producción artística;

- Optimización de un método analítico para la detección de azufre en fotografías antiguas (*silver print image*) mediante XRF y la propuesta de un procedimiento para la recuperación de imágenes que manifiesten fenómenos de descoloración;
- Optimización de un procedimiento analítico para el análisis de muestras metálicas y aplicación a muestras reales extraídas del Pulpito de San Lorenzo de Florencia.

Evaluación de técnicas analíticas de la caracterización de obras de arte

Determinación del límite de detección para SEM-EDS y m-FTIR para el análisis de pintura al óleo

El objetivo central del presente estudio fue la determinación del límite de detección y reproducibilidad de las técnicas SEM-EDS y el micro-FTIR en el caso concreto del análisis de capas de pintura al óleo.

Material

Para el estudio se prepararon 25 simulacros aplicando sobre telas comerciales capas pictóricas al óleo con mezclas binarias de pigmentos (Azul de Prusia-PB, Ftalocianina Azul - Ftl y Ultramar artificial - UM) en diferentes proporciones, desde 1 hasta el 50% .

Equipos y procedimientos

SEM-EDX. Cambridge Instruments Stereoscan 360 con sonda para microanálisis INCA ENERGY 200. Las condiciones de medidas fueron 20 kV, 1 nA y las medidas se adquirieron a 20-35 mm de distancia entre la muestra y el detector. Las muestras fueron extraídas de la superficie de los simulacros con un bisturí y depositadas sobre un soporte especifico de aluminio y recubierta de grafito. Se analizaron tres muestras para cada simulacro y se evaluaron cuatro áreas diferentes para cada una (10 x 10, 20 x 20, 50 x 50 and 100 x 100 μm^2).

Micro-FTIR. Para el estudio se utilizó un espectrómetro de transformada de Fourier BOMEM MB-120 acoplado con un microscopio Spectra-Tech Analytical Plan (KBr beam splitter, fuente Glowbar, detector MCT. Los espectros se registraron en el intervalo entre 4000 y 350 cm^{-1} con una resolución de 4 cm^{-1}. Los resultados se trataron con el programa GRAMS-32 asociado al equipo.

Se analizaron cinco muestras extraídas de diferentes lugares de la superficie de los simulacros con el objetivo de establecer la reproducibilidad de la técnica y la homogeneidad de las capas pictóricas. Sistemáticamente se focalizó el haz de infrarrojo en el centro de la celda de diamante en la que se había depositado y preparado cada muestra.

El parámetro utilizado para la determinación del límite de detección es el DL0.5 que se define como la concentración mínima a la que el compuesto se detecta en el 50% de los espectros.

Resultados

La discusión de las capacidades de detección del SEM y m-FTIR se ha dividido en dos partes: la primera focalizada en la caracterización de los pigmentos empleados y en la determinación del límite de detección utilizando sistemas de detección automática o supervisada. La segunda se centra en la evaluación de la dispersión de los valores obtenidos como indicadores de la heterogeneidad de la distribución de los pigmentos en las capas pictóricas.

Límite de detección

Los límites de detección obtenidos para ambas técnicas son elevados, podrían enmascarar la presencia de componentes intencionalmente añadidos por el artista y también dificultar la obtención de una descripción correcta de la obra. El método supervisado es recomendado para el análisis de los espectros, si bien los LD no disminuyen en micro-FTIR tanto como en SEM. Los límites obtenidos para cada técnica y pigmentos aparecen en la Tabla 1.

Tabla 1. Comparación de los límites de detección de SEM-EDS y micro-FTIR.

DL0.5	**SEM-EDS**		**micro-FTIR**	
	Automático	**Supervisado**	**Automático**	**Supervisado**
	6.2 – 10.2%	**0.9 – 1.5%**	**2.4 – 3.4%**	**0.9 – 1.5%**
Ftalocianina azul	(80:20/67:33)*	(97:3/95:5)*	(93:7/89:11)*	(97:3/95:5)
	6.5 - 15.5%	**0.8 – 1.3%**	**≤ 0.24 %**	**≤ 0.24 %**
Azul de Prusia	(80:20/67:33)*	(97:3/95:5)*	(99:1)*	(99:1)*
	1.6 – 2.5%	**0.3 – 1%**	**≥19 %**	**≥19 %**
Ultramar Azul	(95:5/93:7)*	(99:1/97:3)*	(50:50)*	(50:50)*

* Entre paréntesis se muestra la proporción de pigmentos que supone el límite de detección en las mezclas binarias analizadas.

Reproducibilidad

La reproducibilidad de los resultados de componentes minoritarios ha resultado ser, en el caso del SEM-EDS, dependiente de las áreas analizadas y por esa razón se recomienda la investigación de áreas no menores de 100x100 micras. En el caso del micro-FTIR siendo una técnica puntual en el que el diámetro del haz cubre una área muy limitada, se recomienda adquirir replicados de medidas en más puntos de la muestras.

Evaluación de la espectroscopia remota midIR-FORS: Limite de detección, reproducibilidad y discriminación de mezclas binarias

En este estudio se ha evaluado la capacidad de la Espectroscopia de infrarrojo remota (MidIR-FORS) en tres aspectos: la reproducibilidad de las medidas en relación a la estabilidad instrumental y la distribución de compuestos en las capas pictóricas, el límite de detección para el análisis de pigmentos en pinturas al óleo y la capacidad para la identificación de mezclas.

Material

Para el estudio se prepararon 25 simulacros aplicando sobre telas comerciales capas pictóricas a óleo con mezclas binarias de pigmentos (Azul de Prusia-PB, Ftalocianina Azul - Ftl y Ultramar artificial - UM) en diferentes proporciones a partir de 1 hasta el 50% del uno respecto al otro.

Equipo y procedimiento

El sistema está formado por un espectrómetro de infrarrojo medio con transformada de Fourier BOMEN MB-120 acoplado con una sonda de fibras ópticas de calcogenite Remspec Corporation con cobertura espectral de 4000 cm^{-1} a 900 cm^{-1}. Las determinaciones han incluido series de 5 medidas realizadas en condiciones diferentes en relación a la posición (P) y a los días (D). A partir de los espectros adquiridos con los análisis mediante espectroscopia de infrarrojo medio remota se han identificado los picos característicos de cada compuesto, se han calculado las áreas de las bandas características y a partir de los resultados se ha establecido el límite de detección de la técnica. El parámetro considerado es el DL0.5. En el caso de la reproducibilidad el parámetro considerado es el mRSD (media de las deviaciones estándar relativas).

Límite de detección

Los límites de detección son altos y por tal razón se requiere el uso de técnicas complementarias para poder asegurar una descripción correcta de la obra. El estudio demostró la importancia de la influencia de las características físico-químicas de la superficie en la calidad de los espectros y la consecuente sensibilidad de la técnica. Los límites de detección de midIR-FORS se presentan en la Tabla 2.

Tabla 2. Límites de detección de midIR-FORS.

DL5.0	**midIR-FORS**
	Supervisado
Ftalocianina azul	**6.2 – 10.2%** (80:20/67:33)*
Azul de Prusia	**2.1 – 6.5%** (80:20/67:33)*
Ultramar Azul	**12.1%** (67:33)*

* Entre paréntesis se muestra la proporción de pigmentos que supone el límite de detección en las mezclas binarias analizadas.

Reproducibilidad

A partir de los resultados obtenidos en el estudio de reproducibilidad instrumental y de distribución de la muestra se puede resumir que la repetitividad (mismo día en el mismo punto - D=P=) a partir de la absorción del grupo carbonilo del aceite es de aproximadamente el 3% y para los pigmentos del 18%, mientras que la reproducibilidad a lo largo del tiempo (D≠P=), a lo largo de la superficie de la muestra (D=P≠) o variando ambos factores es del 4% para el aceite y del 25% para los pigmentos. Estos valores indicarían que la inestabilidad instrumental aumenta del orden del 1% la dispersión de las medidas, mientras que la heterogeneidad en la distribución de los pigmentos en la capa pictórica incrementa la falta de reproducibilidad en el 7%. Para los pigmentos estudiados, la falta de reproducibilidad mejora con la intensidad de la señal de la banda característica del pigmento y con la disminución del tamaño de sus partículas. El resultado de este estudio indica que la influencia del día no es significativa a largo o corto plazo así que el protocolo de análisis no tendría que implicar restricciones en el tiempo de las medidas.

Capacidad de identificación de mezclas

Finalmente se quiso evaluar la capacidad del conjunto MidIR-FORS para la identificación de mezclas de pigmentos en capas pictóricas al óleo. Para este tipo de estudio se aplicó el análisis de componentes principales a los espectros adquiridos sobre los simulacros antes descritos. A partir de los resultados se observó que es posible distinguir entre diferentes

mezclas de pinturas al óleo de acuerdo con los intervalos de concentración considerados y según los límites de detección previstos (Figura 1).

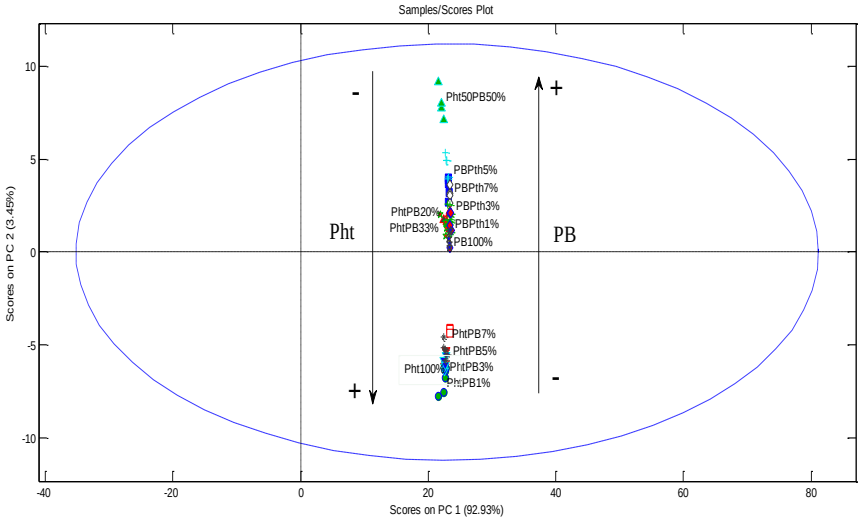

Figura 1. Score plot de las componentes PC1vs. PC2. En el grafico se pueden apreciar dos grupos en el que las muestras se dividen según los límites de detección del componente minoritario.

Creación de mapas de composición de pinturas al óleo mediante el uso de la espectroscopia de infrarrojo remota (midIR-FORS)

El estudio está centrado en la aplicación de midIR-FORS y métodos multivariantes para la investigación de pintura al óleo. Los objetivos eran la evaluación de la influencia de la rugosidad de la superficie analizadas en la calidad de los espectros adquiridos y explorar la capacidad de los métodos multivariantes para la creación de mapas superficiales de distribución de pigmentos en pinturas al óleo.

Material

Para el estudio, se analizaron dos pinturas al óleo, copias en formato reducido de la "Composition with Red, Blue and Yellowish-Green" de Piet Mondrian (1920) y "Blue nude" de Henri Matisse (1952), realizadas por el artista A. Rodriguez, con pigmentos y aglutinante compatibles con la época de los originales, y una paleta de referencia creada con los mismos materiales.

Equipo y procedimiento

El instrumento utilizado fue un espectrómetro de infrarrojo medio con transformada de Fourier BOMEN MB-120 acoplado con una sonda de fibras ópticas de calcogenite Remspec Corporation con cobertura espectral de 4000 cm^{-1} a 900 cm^{-1}. Manteniendo la sonda perpendicular a la superficie se realizaron 10 medidas para cada pintura al óleo de la paleta

de referencia y 88 medidas a lo largo de la superficie de las dos réplicas siguiendo una red fija, que permite reconocer el punto de medida. PCA ha sido aplicado para la discriminación de áreas uniformes y la evaluación de la influencia de la rugosidad de la superficie, mientras que PLS-DA ha sido empleado para la predicción y reconstrucción de mapas de composición. Como fase previa, se aplicaron pre-tratamientos (reducción de la matriz de datos, corrección de la línea base, algoritmo de normalización SNV) con tal de mejorar la calidad de los espectros y reducir las fuentes de ruido. Además se han adquirido 5 medidas sobre paletas de referencias ejecutadas sobre tela con pinturas al óleo de naturaleza variada (17 pigmentos diferentes) y aplicada con diferentes texturas y número de capas pictóricas (5 espectros para cada textura).

Resultados

Los espectros obtenidos mediante espectroscopia remota de infrarrojo medio con fibras ópticas (midIR-FORS) han resultado depender no solo de la composición química del objeto, sino también de las características físicas de la superficie analizada. Esta doble dependencia provoca distorsiones de las bandas de absorción y una baja relación señal/ruido. Los análisis han permitido observar una alta variabilidad en la calidad de los espectros obtenidos. Aplicando PCA ha sido posible apreciar cómo, dependiendo de la superficie analizada, la distancia entre los scores aumenta al aumentar la rugosidad de la superficie y la opacidad de la misma. La dispersión empieza a aumentar una vez que el espesor de la pintura se hace más grande (dos capas) y se vuelve un factor importante en la identificación del clúster cuando la superficie se hace más irregular, rugosa y espesa (aplicación de pintura con espátula) (Figura 2).

Se han creado diferentes modelos PLS basados en las medidas sobre las pinturas de referencia han sido creados para la evaluación de las medidas adquiridas a lo largo de toda la superficie de las obras. Los modelos han permitido predecir satisfactoriamente los pigmentos presentes en las diferentes áreas. Los resultados han sido comparados con las notas en las que el artista describió materiales, el procedimiento de realización de las diferentes áreas, y con la composición elemental determinada mediante un método de control (medidas XRF).

Se puede concluir que la espectroscopia midIR-FORS es una técnica espectroscópica que puede ser usada como técnica de monitorización para detectar pequeños cambios en la morfología de la superficie, lo que abre la posibilidad de su aplicación para la detección de posibles retoques, aspecto importante en la caracterización de las obras de arte. Además el uso de métodos multivariantes puede ser de gran utilidad a la hora de gestionar un volumen

de datos importante permitiendo la extracción de información no fácilmente deducible con una normal evaluación de los espectros.

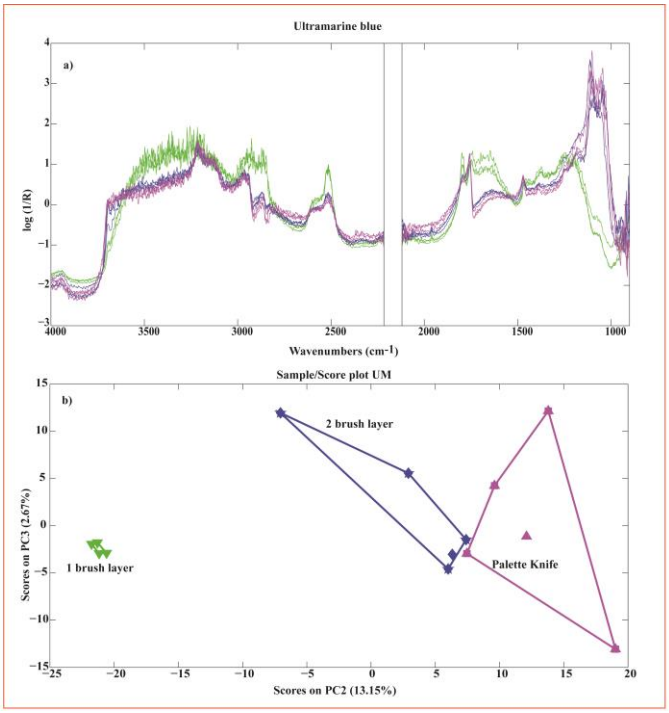

Figura 2. Espectro adquirido sobre la capa de pintura a base de ultramar azul. Los diferentes colores indican el tipo de superficie en que han sido registrados (verde=una capa; azul=dos capas; rosa=espátula). El siguiente *Scoreplot* muestra los mismos espectros en el espacio de las componentes principales, en el que se puede apreciar como la distancia entre scores/espectro aumenta al aumentar la rugosidad de la superficie.

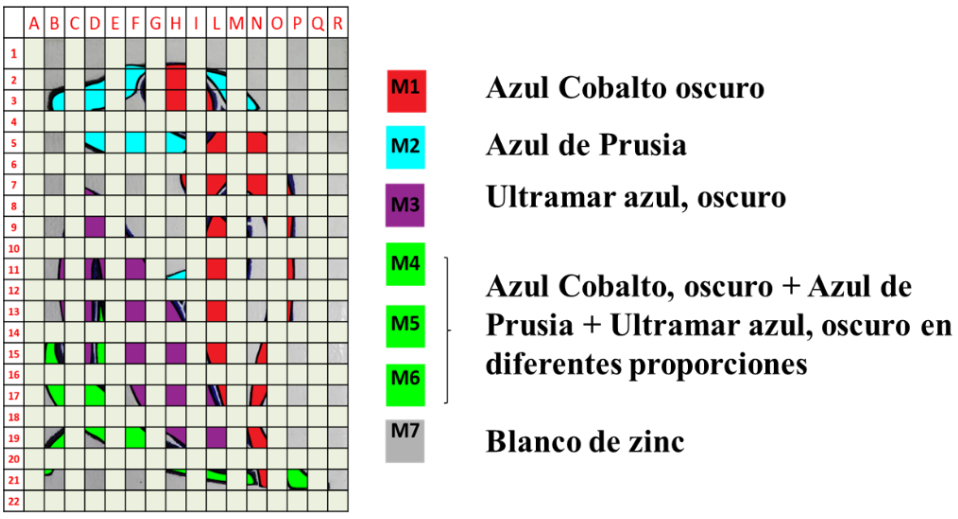

Figura 3. Mapa de composición basado en las predicciones obtenidas de los modelos PLS-DA.

Aplicaciones de técnicas no destructivas para el estudio de la paleta de Picasso en su primera época de producción artística

El estudio ”Early Picasso” ha sido posible gracias a la utilización del MOLAB (laboratorio móvil para el análisis *in situ* de obras de arte), del Center SMAArt (Scientific Methodologies applied to Archaeology and Art) de la Universidad de Perugia (Italia). El proyecto fue concedido en el ámbito del proyecto europeo Charisma (Cultural Heritage Advanced Research Infrastructures). Las obras que se analizaron, seleccionadas en colaboración con el Museo Picasso de Barcelona, son seis retratos realizados por el artista entre aprox. el 1895 y el 1900. El estudio ha permitido reconstruir el proceso creativo del artista en sus primeros años de actividad.

Materiales

Las obras investigadas están conservadas en el Museo Picasso de Barcelona y son el *Autorretrato con Peluca* (MPB 110.053), *Retrato de anciano* (MPB110.014), *Hombre con boina* (MPB110.058), *Retrato de Carles Casagemas* (MPB 110.022), *Retrato de un desconocido* (MPB 110.026) y *Retrato de un desconocido al estilo del Greco* (MPB 110034).

Instrumentos

Se han utilizado diferente técnicas no destructivas incluidas en el MOLAB (Fluorescencia de rayos X, espectroscopia Mid- y Vis-NIR, Espectroscopia UV-Vis, espectroscopia Raman, NIR Imaging y Scanning multispectral IR reflectography - SMIRR). La campaña de análisis se realizó en el Museo Picasso en julio 2013.

Resultados

El estudio de cada obra se desarrolló en tres etapas diferentes: un primer examen basado en imágenes obtenidas gracias a técnicas de análisis global, imágenes en el visible, radiografías RX y reflectografía en el intervalo del infrarrojo cercano; una etapa de interpretación de los resultados obtenidos con técnicas puntuales (XRF y MA-rFTIR) y finalmente una discusión acerca de los materiales usados y sus distribuciones en la estructura de la obra. A continuación se hará una breve descripción por cada uno de los retratos según la información obtenida.

Hombre con boina (50,5 x 36 cm) y Retrato de anciano (58,5 x 42,8 cm)

Ambos son retratos que Picasso realiza a la edad de catorce años (1895). De acuerdo con la documentación del Museo Picasso de Barcelona, las dos pinturas sobre tela están firmadas y datadas en la esquina superior derecha (visión del espectador) con el nombre P. Ruiz y la fecha "95". Forman parte de la serie de retratos de anónimos gallegos que el artista pinta en A Coruña antes de la llegada a Barcelona. El análisis de capas subyacentes basada en las reflectografías adquiridas han revelado la presencia de composiciones subyacentes de temática no identificada. Los materiales encontrados separados por áreas se muestran en la Tabla 3 A/B.

Tabla 3. Pigmentos y compuestos orgánicos encontrados organizados por áreas. A) Hombre con boina; B) Retrato de anciano

A) Hombre con boina

Áreas	Pigmentos	Aglutinantes/compuestos orgánicos
Capas subyacentes	Pigmentos de Fe – Tierras naturales + caolín, Blanco de plomo, (Pigmentos a base de Cu/Cr, Blanco de zinc)	
Fondo	Negro de huesos, Azul de prusia, Blanco de plomo (Negros de Fe, Negro de carbón)	Cola animal
Cara (Frente/Labios, mejillas)	Pigmentos de Fe – Tierras naturales + caolín, , Bermellón, Blanco de plomo (Plomo rojo)	
Barba	Blanco de plomo (Plomo rojo)	
Gorra	Tierras naturales (Pigmentos de Fe), Azul cobalto (Violeta de cobalto), Negro de huesos, Azul de Prusia, Blanco de plomo	
Chaqueta	Negro de hueso + Azul de Prusia, Blanco de plomo (Negros de Fe, Negro de carbón)	
Firma	Negro de hueso + Azul de Prusia, Blanco de plomo (Negros de Fe, Negro de carbón)	

B) Retrato de anciano

Áreas	Pigmentos	Aglutinantes/compuestos orgánicos
Capas subyacentes	Pigmentos a base de Fe – Tierras naturales + Silicatos, Blanco de plomo	Aceite, Cola animal, Barniz
Fondo	Negro de huesos + Azul de Prusia, Sulfatos	
Cara (Frente/Labios, mejillas)	Pigmentos a base de Fe – Tierras naturales + Silicatos, Blanco de plomo (Plomo rojo, Bermellón)	
Pelo	/	
Camisa/pañuelo	Blanco de plomo	
Chaqueta	Pigmentos a base de Fe – Tierras naturales + Silicatos + óxidos de Mn, Negro de hueso + Azul de Prusia, Sulfatos, (Pigmentos de Cr, Negros de Fe, Negro de carbón)	
Firma	Negro de hueso + Azul de Prusia, Sulfatos, óxidos de Mn	

Autorretrato con Peluca (55 x 46 cm)

Es una obra emblemática en la cual Picasso se representa con una peluca a semejanza de los grandes maestros como Goya y Rembrandt. Es comúnmente datada entre el 1897 y el 1898, aunque últimamente, en el catálogo "Yo Picasso" (publicación del Museo Picasso de Barcelona) se encuadra como obra del 1900. Se trata de una estructura compleja de capas superpuestas en la que se han podido apreciar tres composiciones. Un hombre con sombrero y el Autorretrato ya conocidos y una representación intermedia del joven Picasso sin peluca. Tal afirmación se basa en el acabado del pelo visible en la imagen NIR de la Figura 4. Los materiales encontrados se muestran en la Tabla 4.

RX NIR VIS

Figura 4. Imágenes XR, NIR y VIS de Autorretrato con peluca.

Tabla 4. Pigmentos y compuestos orgánicos encontrados organizados por áreas. I primera composición; II segunda composición; III tercera composición.

Áreas	Pigmentos	Aglutinantes/compuestos orgánicos
Fondo	I. Negro de hueso + óxidos de Mn + Azul de prusia, (Negros de Fe, negro de carbón) II. Bermellón + Pigmentos de Fe – Tierras naturales + Azul de prusia	Aceite, Cola animal, Barniz
Cara (Frente/Labios, mejillas)	I/II. Blanco de plomo + Bermellón + Tierras naturales – Rojos de Fe (Plomo rojo) II. Pigmentos de Cu	
Sombrero	I. Ocre amarillo + Blanco de plomo	
Pelo	III. Negro de hueso (Óxidos de Mn + Azul de prusia, Negros de hierro, Negro de carbón)	
Chaqueta	I. Azul de Co/Violeta de Co II. Cromado de plomo (Óxidos de Cr) + Azul de Prusia + Blanco de plomo + Negro de hueso.	
Camisa	I/II/III. Blanco de plomo+ Carbonato de calcio + Azul de prusia	
Peluca	III. Blanco de plomo (Carbonato de calcio) + Azul de prusia	

Retrato de Carles Casagemas (55 x 45 cm)

En esta obra Picasso representa uno de sus mejores amigos, figura que le acompañará en su crecimiento artístico hasta el 1901, año en que Casagemas se suicida. Como en las obras anteriores, también este retrato parece tener una composición subyacente, aunque su visión se ve dificultada por una capa de pintura que aparece altamente absorbente en la radiografía y que impide el acceso a las capas inferiores. La observación de una pérdida de material que aparece de color ocre, la cual interrumpe pinceladas muy bien definidas de esa capa radio-opaca, sugiere su posición intermedia entre las dos composiciones identificadas. Los materiales encontrados se muestran en la Tabla 5.

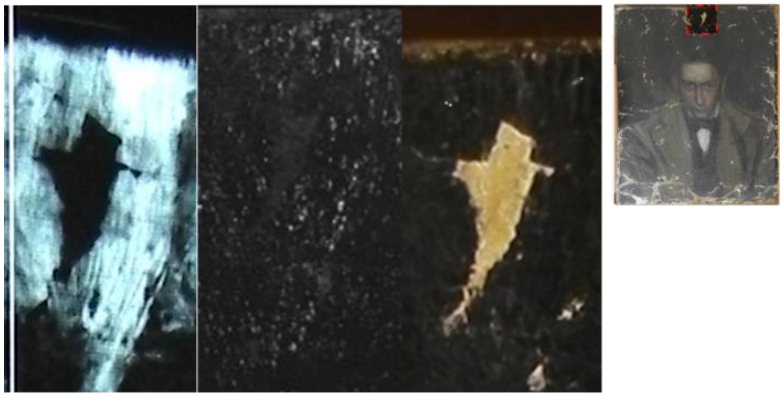

Figura 5. Imágenes XR, NIR y VIS de una pérdida de material localizada en la parte superior de la pintura.

Tabla 5. Pigmentos y compuestos orgánicos encontrados organizados por áreas.

Áreas	Pigmentos	Aglutinantes/compuestos orgánicos
Capas subyacentes	Blanco de plomo + carbonato de calcio	Aceite, cola animal, cera*
Fondo oscuro	Blanco de plomo + Sulfato de bario + Pigmento negro (Negro de hueso, Negros de Fe, Negro de carbón) + (óxidos de Cr o cromatos)	
Fondo verdes (pinceladas a los márgenes)	Blanco de plomo + Azul de prusia + Sulfato de bario Bermellón (Pigmentos rojo de Fe, Plomo rojo)	
Cara (Frente/Labios, mejillas)	Blanco de plomo + Azul de Prusia + Sulfato de bario Bermellón (Pigmentos rojo de Fe, Plomo rojo)	
Chaleco	Blanco de plomo + (Negro de hueso, Negros de Fe, Negro de carbón)	
Camisa	Blanco de plomo	
Chaqueta	Blanco de plomo + Sulfato de bario + Azul de prusia + Bermellón (Amarillo de Ba/ de Sr, Pigmentos de Fe – Tierras naturales y/o óxidos de Cr)	

Retrato de un desconocido (47,5 x 35,2 cm)

Esta obra hace parte de la series de retratos que Picasso realiza entre el 1899 y 1900, el cual sujeto, aún no ha sido identificados. Es una pintura en la que dos o más composiciones se solapan. Parte de estas composiciones son accesibles y visibles en los extremos de la tela. En este caso la interpretación y la asignación de los materiales a las diferentes composiciones han sido particularmente difíciles debido a la complejidad de su estructura. Los materiales encontrados se muestran en la Tabla 6.

Tabla 6. Pigmentos y compuestos orgánicos encontrados organizados por áreas.

Áreas	Pigmentos	Aglutinantes/compuestos orgánicos
Composición I	Blanco de plomo, tierras naturales + silicatos, Negro de hueso + Azul de Prusia, Sulfato de bario.	Aceite, Cola animal, Barniz
Composición II	Blanco de plomo, Bermellón + Pigmentos rojo de Fe/Tierras naturales, Blanco de zinc + Sulfato de bario (Ocre amarillo, Pigmentos de Cr*)	
Fondo	Blanco de plomo, Blanco de zinc, Azul de Co, (Ultramar/silicato)	
Cara (Frente/Labios, mejillas)	Bermellón, Tierras naturales – silicatos (Rojo de plomo), Azul de Co/Violeta de Co, Negro no identificado (Negros de Fe, Negro de carbón)	
Pelo	Negro no identificado (Negros de Fe, Negro de carbón), Azul de cobalto (Negros de Fe, Negro de carbón)	
Camisa/Pañuelo	Blanco de plomo, Blanco de zinc + Sulfato de bario	
Chaqueta	Negro no identificado (Negros de Fe, Negro de carbón)	

Retrato de un desconocido al estilo del Greco (34,7 x 31,2 cm)

Es un misterioso retrato inspirado al *Caballero con la mano en el pecho* de El Greco (Doménikos Theotokópoulos, 1541- 1614) testimonia la gran admiración de Picasso por los grandes maestros del pasado. Los materiales encontrados se muestran en la Tabla 7.

Tabla 7. Pigmentos y compuestos orgánicos encontrados organizados por áreas.

Áreas	Pigmentos	Aglutinantes/compuestos orgánicos
Capas de preparación	Carbonato de calcio, Blanco de plomo, sulfato de bario	
Fondo	I. Blanco de plomo, Tierras naturales marrón y amarillas, Negro de Hueso + Pigmentos de Cr, Bermellón, pigmentos de Cu II. Negro de hueso + Óxidos de Mn, Blanco de plomo (Pigmentos de Fe o/y negro de carbón)	Aceite, Cola animal, Barniz
Cara (Frente/Labios, mejillas)	Blanco de plomo + Bermellón, Negro de hueso (Pigmentos de Fe o/y negro de carbón)	

Tabla 7 (continuación)

Chaqueta	Negro de hueso, Blanco de plomo, Azul de prusia (Pigmentos de Fe o/y negro de carbón)	
Camisa	Blanco de Zn + Blanco de plomo + Sulfato de plomo	
Firma	Negro de hueso + Óxidos de Mn, Blanco de plomo (Pigmentos de Fe o/y negro de carbón) (Blanco de Zn)	
Efecto superficial	Blanco de zinc	

Evaluación de un procedimiento para la recuperación de imágenes fotográficas antiguas

Durante la estancia en el Metropolitan Museum of Art de Nueva York se llevó acabo la optimización de un método de análisis mediante la técnica de Fluorescencia de Rayos X (XRF) para la determinación de azufre en fotografías antiguas. La determinación de azufre en este tipo de obras puede ser clave para entender las técnicas fotográficas características de un determinado artista o los procesos de degradación de estas obras.

Materiales

Para el estudio se analizaron patrones sobre papel realizados con la técnica de "retained hypo" con concentraciones crecientes de S en superficie ([S]= 2, 20, 23, 30, 38, 56, 60, 72 μg/cm2). Los patrones fueron creados y caracterizados previamente mediante ICP-OES por el Analytical Sciences Division of Kodak's Technology Center. Finalmente el método fue aplicado para el estudio de dos fotografías de finales del siglo XIX (Lady Elizabeth (Rigby) Eastlake, 1843-1847. Ref. 2013.159.12, Hill and Adamson, British y View from Photographer's Studio, 1851-54, Ref. 2005.100.190, Gustave Le Gray, French, 1820-1884)

Instrumentos

Bruker ARTAX 400 con tubo de Rh y detector *Si drift.*

Resultados

Los resultados indican que las mejores condiciones son un tiempo de adquisición de 200 s, 30 kV y 1300 μA en atmosfera de helio, sin filtros.

Las fotografías antiguas se analizaron manteniendo las condiciones optimizadas. Se estudiaron dos fotografías reveladas con el mismo procedimiento, la primera de las cuales se encuentra en buenas condiciones de conservación mientras que la segunda está afectada por graves fenómenos de descoloración.

Gracias a la comparación se pudo establecer que la señal detectada de azufre (línea Kα) y plata (línea Lα) manifiestan una relación directamente proporcional en áreas de alta densidad

(áreas con más deposición de plata). En la zona descolorida la plata se pierde, aunque el azufre sigue manteniendo los niveles de señal iniciales. La relación establecida y la utilización del azufre como indicador de la intensidad original de la señal de la plata, han permitido poder restablecer áreas oscuras perdidas.

Optimización de una metodología analítica para el análisis de bronces

En colaboración con el Opificio delle Pietre Dure de Florencia (OPD) se realizó un estudio sobre las aleaciones metálicas del Pulpito di San Lorenzo de Florencia. El objetivo final del estudio es comparar la composición de los diferentes paneles de bronce que conforman el Púlpito y para ello, se ha realizado un primer trabajo de optimización del procedimiento de análisis y evaluación de las diferentes fuentes de dispersión en los resultados.

Materiales

Muestras provenientes de diferentes partes del Púlpito fueron analizadas con ICP-OES e ICP-MS.

Instrumentos

El espectrómetro usado fue un ICP-OES Perkin-Elmer OPTIMA 3200RL acoplado con un sistema de auto-muestreo AS-90 Plus, mientras que las medidas ICP-MS fueron adquiridas con un Perkin-Elmer ELAN 6000.

Resultados

Las etapas consideradas en la evaluación de la dispersión han sido: el muestreo *in situ*, el submuestreo, el ataque químico para la disolución de la muestra y la fase de medida.

Los elementos mayoritarios estudiados en las muestras han sido Cu (≈w% 85,13), Pb (≈w% 8,78), Sn (≈w% 2,51) y como minoritarios Fe, As, Sb, Ni, Ag. Observando los resultados ha sido posible deducir que el Pb es el elemento mayoritario que presenta la mayor variabilidad y dispersión en la concentración ya que en la fase de enfriamiento de la aleación sufre un proceso de segregación que supone una distribución no homogénea en el interior de la pieza de bronce. Cu y Sn resultaron ser más homogéneamente distribuidos.

Los resultados obtenidos indican una dispersión de concentraciones de aproximadamente el ≤1.5 % por el Cu, ≤11% por el Sn y ≤10% por el Pb en el total del proceso y permiten continuar con el estudio comparativo de los diferentes paneles.

La discriminación y comparación ha sido realizada con métodos estadísticos y multivariantes. Se han obtenido mapas de composición y de relaciones entre las diferentes

partes. Los resultados serán utilizados, juntos con los obtenidos con otras técnicas utilizadas por el OPD, para la reconstrucción de la historia de la creación del objeto estudiado.

Conclusiones

La presente tesis doctoral tenía como objetivo principal la evaluación de técnicas micro- y no destructivas para el análisis de obras del Patrimonio. La investigación de tres categorías de obras, pintura al óleo sobre tela, fotografías antiguas y un objeto metálico de grandes dimensiones, ha demostrado la importancia de optimizar procedimientos de análisis específicos para incrementar el conocimiento de las obras teniendo en cuenta su heterogeneidad, características físico-químicas, respetando su integridad física.